Warped Extra Dimensions:
Flavor, Precision Tests and Higgs Physics

Dissertation

zur Erlangung des Grades "Doktor der Naturwissenschaften"

am Fachbereich Physik, Mathematik und Informatik

der Johannes Gutenberg-Universität

in Mainz

Florian Goertz

geboren in Bad Kreuznach

Mainz, 2011

Abstract

In this thesis, the phenomenology of the Randall-Sundrum setup is investigated. In this context models with and without an enlarged $SU(2)_L \times SU(2)_R \times U(1)_X \times P_{LR}$ gauge symmetry, which removes corrections to the T parameter and to the $Zb_L\bar{b}_L$ coupling, are compared with each other. The Kaluza-Klein decomposition is formulated within the mass basis, which allows for a clear understanding of various model-specific features. A complete discussion of tree-level flavor-changing effects is presented. Exact expressions for five dimensional propagators are derived, including Yukawa interactions that mediate flavor-off-diagonal transitions.

The symmetry that reduces the corrections to the left-handed $Zb\bar{b}$ coupling is analyzed in detail. In the literature, Randall-Sundrum models have been used to address the measured anomaly in the $t\bar{t}$ forward-backward asymmetry. However, it will be shown that this is not possible within a natural approach to flavor. The rare decays $t \to cZ$ and $t \to ch$ are investigated, where in particular the latter could be observed at the LHC. A calculation of $\Gamma_{12}^{B_s}$ in the presence of new physics is presented. It is shown that the Randall-Sundrum setup allows for an improved agreement with measurements of A_{SL}^s, $S_{\psi\phi}$, and $\Delta\Gamma_s$. For the first time, a complete one-loop calculation of all relevant Higgs-boson production and decay channels in the custodial Randall-Sundrum setup is performed, revealing a sensitivity to large new-physics scales at the LHC.

Zusammenfassung

Gegenstand dieser Arbeit ist die Untersuchung der Phänomenologie von Randall-Sundrum-Modellen. Es werden Modelle, bei denen Beiträge zum T-Parameter und zur $Zb_L\bar{b}_L$-Kopplung durch eine erweiterte $SU(2)_L \times SU(2)_R \times U(1)_X \times P_{LR}$ Eich-Symmetrie verboten sind und solche ohne diese Symmetrie gegenübergestellt. Die Kaluza-Klein-Zerlegung wird direkt in der Massenbasis vorgenommen, wodurch ein vertieftes Verständnis verschiedener Eigenschaften der Modelle ermöglicht wird. Eine vollständige Analyse flavor-ändernder Prozesse auf Born-Niveau wird präsentiert. Es werden exakte Ausdrücke für fünf-dimensionale Propagatoren hergeleitet, unter Berücksichtigung flavor-ändernder Yukawa Kopplungen.

Die Unterdrückung der Korrekturen zum $Zb_L\bar{b}_L$-Vertex wird detailliert analysiert. Randall-Sundrum-Modelle wurden in der Literatur herangezogen, um die gemessene Erhöhung in der $t\bar{t}$ Vorwärts-Rückwärts-Asymmetrie zu erklären. Es wird gezeigt, dass dies in einem natürlichen Ansatz bezüglich der Flavor-Struktur nicht möglich ist. Die seltenen Zerfälle $t \to cZ$ und $t \to ch$ werden untersucht, wobei insbesondere der letztere eine Größenordnung erreichen kann, die am LHC messbar ist. Es wird eine Berechnung von $\Gamma_{12}^{B_s}$ unter Berücksichtigung von Beiträgen neuer Physik durchgeführt und gezeigt, dass in Randall-Sundrum-Modellen eine bessere Übereinstimmung mit den gemessenen Werten für A_{SL}^s, $S_{\psi\phi}$ und $\Delta\Gamma_s$ erreicht werden kann. In dieser Arbeit wird die erste vollständige Ein-Schleifen-Rechnung für alle relevanten Produktions- und Zerfallskanäle des Higgs-Bosons in Randall-Sundrum-Modellen präsentiert. Dabei wird eine Sensitivität auf große Skalen, jenseits der direkten Reichweite des LHC, festgestellt.

Contents

Preface

The Randall-Sundrum (RS) setup provides promising possibilities to address several puzzles in particle physics. The aim of this thesis is to study the phenomenology of RS models with bulk gauge and matter fields in an anarchic approach to flavor. We formulate the Kaluza-Klein (KK) decomposition of the theory directly in the mass basis. The couplings to a brane-localized Higgs sector are included in an exact way via boundary conditions. This avoids the truncation of the KK towers, which is in contrast to the usual approach of treating these couplings as a perturbation. In consequence, a clear and analytical understanding of important model-specific features is possible. For gauge fields, we present the decomposition in a covariant R_ξ gauge. In the case of the fermion sector, the flavor mixing is included in a completely general way. We show how the hierarchies of the quark sector are generated naturally in warped models, starting from anarchical 5D Yukawa matrices (featuring neither symmetries nor hierarchies). To this end, the analogy to the Froggatt-Nielsen mechanism is demonstrated. We present a detailed discussion of the interactions of the model, including a complete survey of tree-level flavor-changing effects.

A first look at electroweak precision observables reveals that the minimal RS model generically induces sizable contributions to the T parameter. However, we show that a heavy Higgs boson $m_h \lesssim 1$ TeV cancels part of the corrections. This allows for new-physics scales as low as a few TeV. At the same time, this option potentially improves the agreement between theory and experiment in the $Z \to b\bar{b}$ pseudo observables. Nevertheless, the minimal RS model features sizable corrections to these observables. Extending the gauge group to the custodial group $SU(2)_L \times SU(2)_R \times U(1)_X \times P_{LR}$ and including an appropriate embedding of the fermions, allows to remove the problematic contributions. In addition, the T parameter is then protected by a *symmetry*. We explore the custodial RS model in detail. The approach of treating electroweak symmetry breaking exactly allows for a clear analysis of the model specific features and protection mechanisms. As we formulate the KK decomposition of the fermion sector of the minimal model in a general way, allowing for additional fermion representations, the application to the extended fermion sector of the custodial model can be performed conveniently. In turn, it is straightforward to address questions about the model-dependence of the resulting gauge- as well as Higgs-boson interactions with the Standard-Model fermions. We demonstrate explicitly the protection of the T parameter and of the left-handed $Zb\bar{b}$ couplings. In particular, we work out, which contributions are protected and which terms inevitably escape protection. We identify them with the irreducible sources of custodial symmetry breaking.

Due to the presence of the towers of KK excitation one often encounters infinite sums over gauge boson profiles. We show how to perform these complete sums for towers with massless as well as massive zero modes, by using completeness relations for the profiles. As a first application, these results are used to study effective four-quark interactions in both RS variants. We pay special attention to the interactions with the Higgs sector and to the correct inclusion of Yukawa interactions that couple Z_2-odd fermions. In the perturbative approach these contributions would be naively lost. This formal part of the thesis, already including some phenomenological considerations is presented in Chapter 3.

A promising method to treat fields in five dimensions that appear as internal states in Feynman diagrams is to use five dimensional propagators. This avoids the KK decomposition and the need to sum up the contributions afterwards again. Especially for the case of sums

involving several fermion generations, performing the KK sum turns out to be impractical. In Chapter 4, we obtain exact expressions for the five dimensional propagators of massive gauge bosons. Beyond that, analytic results for five-dimensional fermion-propagators, including a generic flavor structure with off-diagonal Yukawa couplings, are presented for the first time. These expressions are useful for studying loop mediated flavor-changing neutral currents, like $B \to X_s \gamma$, in warped extra dimensions.

The phenomenological survey of this thesis in Chapter 5 starts with an analysis of precision tests. After exploring the modification of Standard Model parameters in the presence of warped extra dimensions, aspects of the electroweak precision parameters will be treated again. Since the anarchic RS setup predicts modified couplings especially for the third generation of quarks, the focus will be on this sector. A detailed analysis of the $Z \to b\bar{b}$ pseudo observables is presented. To a great extend, we will pay attention to the comparison of the results in the custodial RS model with those of the minimal model. The $t\bar{t}$ forward-backward asymmetry, measured at Tevatron, shows a deviation from the Standard Model prediction of about $2\,\sigma$. We analyze if this discrepancy could be caused by the Randall-Sundrum setup calculating the corresponding prediction at next-to-leading order in the strong coupling constant. The results presented are valid for a broader class of new physics models. Then we study the flavor (changing) sector of the model. After an analysis of the non-unitarity of the CKM matrix, the flavor-changing rare decays $t \to cZ$ and $t \to ch$ will be examined. We will apply the formalism of five dimensional propagators to study the anomalous magnetic moment of the muon in the RS setup. Another focus is on CP violating observables in the B_s^0-system, where recently some anomalies have been reported. We perform a calculation of the absorptive part of the B_s^0–$\bar{B}_s^0$ mixing amplitude in the presence of new physics and explore, if warped extra dimensions can lead to an improved agreement between theory and experiment in several observables.

One of the main questions which the CERN Large Hadron Collider (LHC) is supposed to answer is how the electroweak symmetry is broken in nature. In consequence, one focus of the phenomenological part is a detailed discussion of Higgs physics at Tevatron and the LHC. For the first time, we present a complete one-loop calculation for all relevant Higgs-boson production and decay channels in the Randall-Sundrum setup, incorporating the effects stemming from the extended electroweak gauge-boson and fermion sectors. We discuss the impact on physics at the LHC and demonstrate that the Higgs sector could be very viable for finding physics beyond the Standard Model.

As this thesis is about extensions of the Standard Model of particle physics, it is mandatory to explore the motivations to go beyond this successful model. Therefore, important aspects of the Standard Model are reviewed in Chapter 1, starting from an effective field theory approach. The fact that this minimal model works extremely well at low energies poses tight challenges on theories that are meant to complete it. In this context, it is important to explore the peculiarities of the Standard Model that lead to its successful agreement with experiment. Such considerations gave rise to several extensions of the original Randall-Sundrum proposal, which finally brought up the custodial Randall-Sundrum model with bulk-gauge and -matter fields. In the first chapter we also review the evidence that causes the notion that the Standard Model will have to be replaced by another theory above a certain scale. This discussion will lead to the gauge hierarchy problem, which is finally examined, together with the puzzle of fermion hierarchies. Models with (warped) extra dimensions that can address these problems are introduced in Chapter 2 and at the beginning of Chapter 3.

The chapters 3-5 contain the main results of this thesis. Chapter 3, besides the introductory part at the very beginning, and Chapter 5 are based on my publications [1, 2, 3, 4]. Chapter 4 on propagators of massive gauge and fermion fields in five dimensions as well as Section 5.1.5 on the anomalous magnetic moment of the muon contain unpublished results.

A conclusion is presented in Chapter 6. Supplementary calculations and useful formulae can be found in the appendices.

This eprint version of the thesis contains minor modifications compared to the original version (correction of typing errors, *etc.*). The version submitted to the University of Mainz can be retrieved from the university library.

Chapter 1

Introduction: The Standard Model and Hierarchies in Nature

The first chapter is meant to introduce aspects of the Standard Model (SM) of particle physics and of effective field theories, with a focus on those topics which will be important for the following chapters. We will present the merits of the SM, which suggest that it is the right theory to describe nature up to (at least) the weak scale. Beyond that, we will illustrate its shortcomings which bring us to the conclusion that it is, however, not the final theory of nature and we will expound our expectations on the theory to complete it. In particular, we will discuss several puzzling hierarchies that we observe in particle physics. These represent a convincing motivation to study warped extensions of the SM, which will be the focus of this thesis.

1.1 Aspects of the SM and Effective Field Theories

As the SM has been extremely successful up to present collider energies of several hundred GeV, it is a good starting point for studying new ideas in particle physics. Its extensions should always have a SM-like theory as a low energy limit. Coming from an effective field theory approach, we will go into the main building blocks and tests of the model. When exploring warped setups, we will start from and refer to the structure of the SM, which represents the low energy tail of the KK decomposition of these setups. Since the phenomenological part of this thesis is mainly related to the Higgs and the flavor sector, as well as to precision tests, we will focus on these fields. During this introduction we will meet problems of the SM that provide a motivation to go beyond it. However, we will also see that the SM leads to a multitude of non-trivial well-tested predictions. Many of those will be jeopardized, when extending the minimal model of particle physics. For a successful model building it is thus important to be aware of the features that have lead to these predictions.

1.1.1 The SM of Particle Physics and Symmetries of Nature

The dream of having a consistent, anomaly free, and renormalizable theory that describes nature down to length scales of $\sim (1-10)$ TeV^{-1}, *beyond the weak scale*, has become true with the advent of the Standard Model of Particle Physics. These scales correspond to the energy frontier currently probed directly by mankind at large collider experiments. The success story of the SM started in the 1960s with the Glashow-Weinberg-Salam (GWS) theory of electroweak

unification [5, 6, 7] (Nobel Prize in Physics 1979). Other milestones were the inclusion of the theory of strong interactions, as a gauge theory of elementary particles carrying color charge, the discovery of asymptotic freedom by Gross, Politzer, and Wilcszek [8, 9, 10] (Nobel Prize in Physics 2004), and the prove of renormalizability of the SM by 't Hooft and Veltman [11] (Nobel Prize in Physics 1999). The SM incarnates the idea of combining special relativity and quantum mechanics into a quantum field theory that describes the world around us.[1] It has been tested at the quantum level in a plethora of experiments and so far resisted every attempt to refute its validity. Moreover, it lead to many successful predictions of phenomena and particles, before their experimental discovery, like the existence of neutral currents and of the massive $W^{\pm}$ and Z gauge bosons, including the corresponding mass ratio. The experimental observation of jets in the mid-1970s, in particular three-jet events at PETRA in 1979 [13], provided a striking confirmation of quantum chromodynamics (QCD), the theory of strong interactions. The experimental evidence for quarks, some years before, confirmed that the quark model, introduced by Gell-Mann and Zweig, is not only a mathematical model [14, 15], but is realized in nature. Beyond that, the prediction of the tau neutrino, the charm quark, and the third generation of quarks, before their experimental discovery (in particular the indirect determination of the approximate top mass), is to be assigned to the SM.

Before looking at the model in more detail, let us recapitulate a general guiding principle for constructing theories, that will finally lead us to the SM. The most fundamental properties of nature, and thus also of a theory that shall describe it, are probably symmetries. From Noether's theorem, we know that continuous symmetries lead to conservation laws. Without symmetries, the universe (if it would exist) would behave much more randomly and it would be very hard to derive meaningful predictions. The dynamics of a system in quantum field theory (QFT), which we will assume to be the right framework to describe particle physics, is given by its Lagrangian (including a quantization rule). Thus, one should write down the most general Lagrangian that corresponds to an experimentally given particle content and exhibits the symmetries of the system. Every combination of fields of the theory, whose absence can not be explained in terms of a symmetry, should appear. Certainly, a well established symmetry of nature is Poincaré invariance. The particles of a theory should correspond to irreducible representations of the Poincaré group. Beyond this space-time symmetry, internal *local* symmetries seem to be important, so-called (local) *gauge symmetries*.

The known matter fields of the universe (leptons and quarks) transform according to fundamental representations of a given gauge-symmetry group, if they are charged with respect to that group, and thus their appearance is related to these symmetries. Global invariance under such transformations corresponds to the freedom of redefining multiplets of matter fields with the same transformation parameter at every space-time point

$$\Psi \to e^{i\,\alpha^a T^a}\Psi\,. \tag{1.1}$$

Here, $\alpha^a \in \mathbb{R}$ and T^a are the generators of the gauge group, in generalization of $U(1)$ phase rotations, where $T^a = Q$ ($a = 1$) is the charge. For $SU(2)$, for example, the Pauli matrices

---

[1]Note that the SM does not incorporate a (quantum) theory of gravity, which is expected to become important at the Planck scale $M_{\mathrm{Pl}} = \sqrt{\hbar c/G_N} \approx 1.22 \cdot 10^{19}$ GeV/c^2 [12] at the latest. Here G_N is the gravitational constant, $\hbar$ is the reduced Planck constant and c is the speed of light in the vacuum. From now on we will work in natural units, setting $\hbar = c = 1$. For the discussion of the first chapter we will not consider gravitational interactions explicitly.

$T^a = \sigma^a/2$ ($a = 1, \ldots, 3$) can be used and $\Psi = (\Psi_1(x), \Psi_2(x))^T$, whereas the Gell-Mann matrices are generators of $SU(3)$, $T^a = \lambda^a/2$ ($a = 1, \ldots, 8$), see Appendix A.1. Throughout this thesis, a summation over repeated indices is understood. If the symmetry transformations (1.1) shall be local, *i.e.*, depending on space-time coordinates

$$\alpha^a \to \alpha^a(x), \tag{1.2}$$

one has to introduce corresponding *gauge fields* in order for the kinetic terms of the matter fields, containing derivatives, to be invariant. Without kinetic terms there would not be any physical propagating fields. Explicitly, these terms become invariant by replacing the ordinary derivative with the *covariant derivative*

$$\partial_\mu \to D_\mu = \partial_\mu - ig A_\mu^a T^a, \tag{1.3}$$

where A_μ^a are (gauge) vector fields, belonging to the generators T^a of the corresponding gauge group with coupling constant g. These fields have to transform according to the adjoint representation of the gauge group. In summary, the local symmetry transformations read

$$\Psi(x) \to V(x)\,\Psi(x), \quad V(x) = e^{i\,\alpha^a(x)T^a},$$
$$A_\mu^a(x)T^a \to V(x)\left(A_\mu^a(x)T^a + \frac{i}{g}\,\partial_\mu\right)V^\dagger(x). \tag{1.4}$$

Also from a geometrical perspective, the need for local gauge invariance of the kinetic terms can be understood, if one wants to introduce local gauge transformations for the matter fields. One requires a connection to define the derivative properly, which compares fields at different space-time point, where they transform differently. This gauge connection is provided by the gauge fields, together with their transformation properties, which are interpreted as physical, propagating degrees of freedom. These bosonic fields then act as force carriers. For more details see *e.g.* [16]. Local invariance under a certain gauge group induces and restricts the interactions of the fields (via gauge bosons) just how they are discovered in nature and prevents the theory from being possibly trivial. It is a defining criterion for a theory and, as we will see below, also essential from a formal point of view for constructing a consistent, sensible theory containing vector bosons. There is compelling experimental evidence (see Section 1.1.2) that the gauge group of nature contains the structure

$$G_{SM} = SU(3)_c \times SU(2)_L \times U(1)_Y. \tag{1.5}$$

The corresponding gauge bosons, induced by local gauge invariance, are the gluons, mediating the strong interactions, and the W^a and B bosons, responsible for the electroweak interactions, see below. Having identified this gauge invariance as an appropriate symmetry to describe interactions of matter fields, it should be imposed on the whole Lagrangian (in agreement with observation). Note however that a part of (1.5) will have to be hidden in a certain way, in order to obtain massive gauge bosons. This "encryption" of the symmetries also corresponds to a fundamental property of nature which has to be accounted for. The fact that we do not see the full gauge group in the form (1.5) at low energies, made it a demanding task to find the correct gauge theory. After the gauge group of the theory has been identified, the

matter content can be assigned to certain representations of the gauge group, according to experimental observations. These representations determine the interactions between matter and gauge fields, as explained above. For the known matter fields, the representations will be given in Table 1.1 below.

In addition to these symmetry constraints, remember that a Lagrangian should be hermitian in order to lead to a unitary scattering matrix (S-matrix) that conserves probabilities. It should preserve causality, which is achieved by including proper anti-particle operators in addition to particle operators and brings about the necessity of *field* operators [16]. Furthermore, to obtain a stable theory with a well-defined ground state, the spectrum of the corresponding Hamiltonian has to be bounded from below. With these conditions in mind, it seems sensible to write down the most general, translation-invariant, Lorentz scalar which contains spinor fields for the observed matter representations and is (locally) invariant with respect to the gauge group G_{SM} (1.5) - inducing the gauge fields - and call it the Standard Model. If one counts the number of terms that are allowed under these restrictions, one ends up with the rather large number of infinity, which would spoil the predictivity of the model. Luckily, it turns out that the situation is not as hopeless as it seems.

It is instructive to sort the terms in the Lagrangian according to the mass dimensions of the products of field operators that they contain. The naive mass dimension of a field operator can be read off from its standard kinetic term of its free theory (bilinear in the fields), by using the fact that a derivative has the mass dimension of a momentum ($D = 1$) and that the action has to be dimensionless in natural units. As in four space-time dimensions the Lagrangian needs to have mass dimension $D = 4$, terms that have a mass dimension smaller (bigger) than four have to appear with (inverse) powers of some yet unspecified mass scale[2] M

$$\mathcal{L} = \mathcal{L}_{\leq 4} + \frac{\mathcal{L}_5}{M} + \frac{\mathcal{L}_6}{M^2} + \cdots . \tag{1.6}$$

The subscripts in (1.6) denote the mass dimension of the corresponding sub-Lagrangians. Note that $\mathcal{L}_{\leq 4}$ contains all terms with mass dimensions equal to or less than four, including the possibly dimensionful coefficients. These are expected to scale like powers of M, if there is no second scale generated in the theory. The terms with $D < 4$ are generically problematic, see sections 1.1.6 and 1.2.1. Accordingly, all dimensionless coefficients present in the Lagrangian are expected to be of $\mathcal{O}(1)$, if there are no symmetries present, that would explain other values. For the moment, let us not assume that it is possible to construct the final theory of nature, valid up to arbitrary high energy scales, with just the particle content observed below the TeV scale. Let us rather assume that we see the low energy tail of a more complete theory. However, without direct hints for new particles, we would like to set up a theory, which is based on the observed particle content and symmetries, and is valid up to some fixed energy scale. This is assumed to lie above the scales at which we have already looked for new degrees of freedom. Considering the Lagrangian above as belonging to such a theory, this cutoff scale can now be identified with the scale M, see Appendix A.4. For example, M could be the mass of a new heavy particle, not present in our low energy theory. If we are interested in energies $E \ll M$, a description without this heavy particle as a propagating degree of freedom is perfectly fine.

---

[2]A more rigorous treatment of the idea of effective field theories (EFTs), used here, is given in Appendix A.4.

Crucially, the terms $\propto \mathcal{L}_i$, with $i > 4$, will be suppressed by powers of $E/M \ll 1$. As a consequence the most important part of the Lagrangian at low energies is given by $\mathcal{L}_{\leq 4}$, while the additional terms can be neglected to more or less good approximation (depending on the ratio E/M). Thus, one ends up with a finite number of terms, depending on the truncation of (1.6). The part with $D \leq 4$ is called the Standard Model of Particle Physics (with one ingredient related to the masses of the particles still missing, see below). Experiments can give a handle on the cutoff scale M by measuring effects of higher dimensional terms. As mentioned, all this holds, if we assume to observe the low energy part of a more fundamental theory with a scale M (the cutoff of our theory). The existence of a final ultraviolet (UV) completion guarantees the suppression of higher dimensional ($D > 4$) terms just by this new physics (NP) scale. This is the modern point of view of seeing the SM, see Section 1.1.6. Historically, the SM was not introduced as part of a more general Lagrangian, but rather as *the* Lagrangian of nature. The concept that singled out the terms with $D \leq 4$ will be introduced in Section 1.1.5. From the SM Lagrangian one obtains the corresponding SM-Feynman rules to compute S-matrix elements perturbatively (as a sum over all possible Feynman diagrams) via standard textbook techniques [16, 17].

From the previous discussion one expects $\mathcal{L}_{\leq 4}$ to be explored first in particle collisions. Having identified gauge invariance as a crucial concept, it is thus no wonder that the SM works so well (up to a certain energy). It just corresponds to the most important part of the most general gauge invariant Lagrangian that one can write down, given the observed particle content.[3] It does not mean that there is no NP, it rather means that the NP should be rather heavy. Nevertheless, the construction of the SM as a gauge theory with the appropriate (gauge) symmetries was a tremendous success. This is even more the case, given the fact that when the GWS model was constructed, not all gauge particles of the SM had been observed, yet. Their existence has been deduced from measuring fermion interactions. Along the lines discussed above, NP should already show up below being directly produced in terms of new particles, due to suppressed terms with $D > 4$. Measuring deviations from SM expectations can give a handle on the scale M, as mentioned before. It will turn out that in some sectors the SM works so well that the expected NP scale is much higher than currently accessible scales. Note that it is in principle not excluded that there exist unobserved particles which are very light, perhaps with masses much below our designated cutoff for the SM. These particles then have to posses very suppressed couplings to the known particles in order to have escaped detection. As an example, consider the so called dark photon, which appears as a force mediator in some models of Dark Matter. This could be rather light, *e.g.* $m_{\gamma'} \sim 1\,\text{GeV}$, and have couplings to the SM via kinetic mixings with a strongly suppressed coefficient $\epsilon \ll 1$, see *e.g.* [18].

Let us finally write down the SM Lagrangian

$$\mathcal{L}_{\text{SM}} \equiv \mathcal{L}_{\leq 4}. \tag{1.7}$$

It reads[4]

$$\mathcal{L}_{\text{SM}} = \mathcal{L}_{\text{ferm}} + \mathcal{L}_{\text{W,B,G}} + \mathcal{L}_{\text{Higgs}} + \mathcal{L}_{\text{Yukawa}} + \mathcal{L}_{\text{GF}} + \mathcal{L}_{\text{FP}}. \tag{1.8}$$

This is the Lagrangian that we will study in the next pages, and, for the time being, we will

---

[3]By gauge invariance we mean invariance with respect to the *local* symmetry transformations corresponding to (1.5), unless stated otherwise.

[4]For a review on QFT and the SM see *e.g.* [16, 17, 19, 20, 21].

not consider the possible higher dimensional terms. The first term in (1.8) contains kinetic terms for the matter fields (fermions) that we have observed in nature so far. The different fermion flavors present in the SM are grouped into three-component vectors (each component corresponding to a quark or lepton family) of up-type quark flavors $u \equiv (u, c, t)^T$, down-type quarks $d \equiv (d, s, b)^T$, charged leptons $e \equiv (e, \mu, \tau)^T$, and neutral leptons (neutrinos) $\nu \equiv (\nu_e, \nu_\mu, \nu_\tau)^T$. We end up with

$$\mathcal{L}_{\text{ferm}} = \bar{Q}_L i\slashed{D} Q_L + \bar{u}_R i\slashed{D} u_R + \bar{d}_R i\slashed{D} d_R + \bar{E}_L i\slashed{D} E_L + e_R i\slashed{D} e_R \,, \tag{1.9}$$

where $\bar{F} \equiv F^\dagger \gamma^0$, $F = Q, u, d, E, e$. The left-handed and right-handed components of the field operators belong to the two irreducible spin-1/2 representations of the Poincaré group in four dimensions (4D), respectively, and are projected out as $F_{L,R} = P_{L,R} F$, where $P_{L,R} = (1 \mp \gamma^5)/2$. The Dirac-gamma matrices are defined in Appendx A.1. In order for the kinetic terms of the matter fields to be gauge invariant, the spatial derivative ∂_μ has been replaced by the covariant derivative (in analogy to (1.3)) corresponding to the full SM gauge group (1.5)

$$\begin{aligned} \slashed{D} &:= \gamma^\mu D_\mu \\ D_\mu &= \partial_\mu - ig' Y B_\mu - ig\, T^i W^i_\mu - ig_s\, t^a G^a_\mu. \end{aligned} \tag{1.10}$$

This induces local interactions, *i.e.*, terms which contain more than two fields at the same space-time point, with the (spin-1) B, W^i, and G^a gauge fields, in agreement with observation. Here, Y, $T^i = \sigma^i/2$ ($i = 1, \ldots, 3$), and $t^a = \lambda^a/2$ ($a = 1, \ldots, 8$) correspond to the standard generators of $U(1)_Y$ (hypercharge), $SU(2)_L$ (weak isospin), and $SU(3)_c$ (color), as introduced before. The corresponding coupling constants are denoted by g', g, and g_s. Through quantum (loop) corrections, these couplings are running couplings, depending on the renormalization scale μ, see *e.g.* [16]. Their values at the Z-pole, $\mu = m_Z \approx 91.2\,\text{GeV}$, read [12]

$$g'(m_Z) \approx 0.36\,, \quad g(m_Z) \approx 0.65\,, \quad g_s(m_Z) \approx 1.22\,. \tag{1.11}$$

Note that the non-abelian $SU(3)_c$ gauge theory of QCD becomes strongly coupled at low energies $\mu \sim 1\,\text{GeV}$, explicitly $\alpha_s(\Lambda_{QCD}) \equiv g_s^2(\Lambda_{QCD})/(4\pi) \gtrsim \mathcal{O}(1)$, where $\Lambda_{QCD} \approx 200\,\text{MeV}$. This calls for non-perturbative methods. On the other hand, it becomes asymptotically free for high energies (which holds for less than 17 participating flavors) [8, 9, 10].

Experimentally, it turns out that the left-handed fermions form doublets under $SU(2)_L$

$$Q^i_L = \begin{pmatrix} u^i_L \\ d^i_L \end{pmatrix}\,, \quad E^i_L = \begin{pmatrix} \nu^i_L \\ e^i_L \end{pmatrix}\,, \tag{1.12}$$

while all quarks are triplets under $SU(3)_c$, which is not made explicit in (1.9). The representations of the SM fields with respect to the SM gauge group, including the hypercharge quantum numbers, *i.e.*, eigenvalues of the generator Y, are summarized in Table 1.1, which provides an overview of the particle content of the SM. Here, singlets (which do not transform under the corresponding gauge transformation) are denoted by **1**, doublets by **2**, *etc.* This field content, together with the corresponding representations/quantum numbers, guarantees that the SM is anomaly free, *i.e.*, that no gauge symmetries of the classical Lagrangian are broken at the quantum level.

spin	field	representation $(SU(3)_c, SU(2)_L)_{U(1)_Y}$
	Q_L^i	$(\mathbf{3}, \mathbf{2})_{1/6}$
	E_L^i	$(\mathbf{1}, \mathbf{2})_{-1/2}$
1/2	u_R^i	$(\mathbf{3}, \mathbf{1})_{2/3}$
	d_R^i	$(\mathbf{3}, \mathbf{1})_{-1/3}$
	e_R^i	$(\mathbf{1}, \mathbf{1})_{-1}$
	B_μ	$(\mathbf{1}, \mathbf{1})_0$
1	W_μ^i	$(\mathbf{1}, \mathbf{3})_0$
	G_μ^a	$(\mathbf{8}, \mathbf{1})_0$
0	Φ	$(\mathbf{1}, \mathbf{2})_{1/2}$

Table 1.1: Representations of the different fields in the SM. Right handed neutrinos have not been included, as they are not present in the original formulation of the SM. They are singlets under the SM gauge group, *i.e.*, transform as $(\mathbf{1}, \mathbf{1})_0$. The Higgs field Φ will be introduced further below.

As gauge invariance called for the existence of gauge fields, we should now look for further gauge invariant Lorentz scalars that can be constructed out of them. In addition to the interaction terms above, we end up with kinetic terms for the gauge fields, which allow them to propagate. They read

$$\mathcal{L}_{\mathrm{W,B,G}} = -\frac{1}{4} B_{\mu\nu} B^{\mu\nu} - \frac{1}{4} W_{\mu\nu}^i W_i^{\mu\nu} - \frac{1}{4} G_{\mu\nu}^a G_a^{\mu\nu} \tag{1.13}$$

and contain the field-strength tensors, defined as

$$\begin{aligned}
B_{\mu\nu} &= \partial_\mu B_\nu - \partial_\nu B_\mu \\
W_{\mu\nu}^i &= \partial_\mu W_\nu^i - \partial_\nu W_\mu^i + g\, \epsilon^{ijk}\, W_\mu^j W_\nu^k \\
G_{\mu\nu}^a &= \partial_\mu G_\nu^a - \partial_\nu G_\mu^a + g_s\, f^{abc}\, G_\mu^b G_\nu^c.
\end{aligned} \tag{1.14}$$

Here, ϵ^{ijk} and f^{abc} are the structure constants of $SU(2)$ and $SU(3)$, respectively, where

$$\left[T^i, T^j \right] = i\epsilon^{ijk} T^k \tag{1.15}$$

for the generators of $SU(2)$ and a similar relation holds for $SU(3)$. Before detailing the remaining parts of the Lagrangian, several comments are in order.

In its original formulation, the SM does not contain right handed neutrinos which correspond to the only possibility to account for massive neutrinos at the level of gauge invariant $D \leq 4$ terms. We know that neutrinos have non-zero masses from the observation of neutrino oscillations. Neutrino masses could be interpreted as the first evidence for physics beyond the SM (BSM). However, it is straightforward to extend the SM by adding right handed neutrinos (though without being able to explain the tininess of neutrino masses, see Section 1.1.6). Furthermore, the allowed term $\theta_{QCD}\, g_s^2/(64\pi^2)\epsilon^{\mu\nu\rho\sigma} G_{\mu\nu}^a G_{\rho\sigma}^a$ is not included in the SM, as experiments tell us that it seems not to be present. This term would violate the combined charge-conjugation and parity (CP) invariance, *i.e.*, the invariance with respect to the substitution of a particle by its anti-particle in combination with a reflection at the origin $\vec{x} \to -\vec{x}$,

in the sector of strong interactions (see *e.g.* [16]). Its unexplained absence or the extreme and unnatural smallness of its coefficient θ_{QCD} is called the *strong CP problem*. A possible solution is provided by the Peccei-Quinn theory, introducing a new particle, called the axion [22]. Note that analogous terms for the $U(1)$ and $SU(2)$ field strengths have no observable effects [16]. Most important, with just the fields introduced so far, corresponding to particles which been observed in nature, all fields of the SM would be massless, which is clearly in conflict with observation. The particles introduced so far thus still do not quite match those we observe in experiments. Given just these fields and no additional structure, it is simply not possible to write down gauge invariant mass terms for the (non-abelian) vector bosons and chiral fermions. However, no additional particles have been observed yet, so the mechanism that gives masses to the SM particles is still experimentally unobserved. We certainly do not want to abandon gauge invariance as a concept, as it was a key in constructing the SM with the correct interactions and results in non trivial relations between couplings, which are well tested. We will discuss some of these relations in Section 1.1.2. Moreover, note that breaking gauge invariance leads to big problems in the high energy behavior of the theory. This is already the case, if it is just broken in mass terms for the observed massive gauge bosons, while keeping the gauge connection for the fermion fields as well as internal gauge interactions as they are (motivated by phenomenology). Although gauge invariance in the massless gauge sector can be seen as a redundancy in the description of a spin-1 particle with two degrees of freedom by a four-component Lorentz vector, it guarantees that the SM is renormalizable and does not lose its validity at the TeV scale, see below. If we want to construct a decent theory for the TeV scale, gauge invariance should better not be broken in an uncontrolled way.

1.1.2   The Higgs Sector, Custodial Symmetry and Precision Tests

The most famous possibility to break the electroweak gauge symmetry in order to obtain massive SM particles while keeping the fundamental Lagrangian gauge invariant is the Higgs mechanism (which is a part of the SM) due to Brout, Englert, Higgs, Guralnik, Hagen and Kibble [23, 24, 25]. We will study the phenomenology of the corresponding sector in the context of RS models in detail in Section 5.3. The mechanism works as follows. A complex scalar doublet under $SU(2)_L$ (with hypercharge $Y = 1/2$)

$$\Phi(x) = \begin{pmatrix} \phi^+(x) \\ \phi^0(x) \end{pmatrix} , \qquad (1.16)$$

is included in the SM, with a potential, that results in a vacuum expectation value (VEV) for this doublet. Given the aforementioned appropriate charges for the Higgs field, the VEV

$$\langle\Phi\rangle = \frac{1}{\sqrt{2}} \begin{pmatrix} 0 \\ v \end{pmatrix} \qquad (1.17)$$

will break the electroweak part of the gauge symmetry *spontaneously* (*i.e.*, in the ground state of the theory, not at the fundamental Lagrangian level), according to the pattern

$$SU(2)_L \times U(1)_Y \longrightarrow U(1)_{EM} , \qquad (1.18)$$

which we observe in nature, and thus will generate masses for three electroweak gauge bosons. The photon, corresponding to the unbroken $U(1)_{EM}$ symmetry of quantum electrodynamics (QED) will remain massless, as the gluon does. The (gauge invariant) Higgs Lagrangian reads

$$\mathcal{L}_{\text{Higgs}} = (D_\mu \Phi)^\dagger (D^\mu \Phi) - V(\Phi), \qquad V(\Phi) = -\mu^2 \Phi^\dagger \Phi + \frac{\lambda}{2} \left(\Phi^\dagger \Phi \right)^2 . \tag{1.19}$$

Note the negative sign of the mass term ($\mu^2 > 0$) in the Higgs potential. This sign is responsible for the so-called mexican hat form of the potential, which allows for a nontrivial VEV $\langle |\Phi| \rangle > 0$. The Higgs quartic coupling $\lambda > 0$ has to be positive in order for the Higgs potential $V(\Phi)$ to be bounded from below and thus for the vacuum to be stable, see below. After electroweak symmetry breaking (EWSB), *i.e.*, after acquiring the VEV (1.17), we parametrize the Higgs doublet in terms of fluctuations around that VEV via the four real scalar fields φ^i, $i = 1, 2, 3$ and h as

$$\Phi(x) = \frac{1}{\sqrt{2}} \begin{pmatrix} -i\sqrt{2}\, \varphi^+(x) \\ v + h(x) + i\varphi^3(x) \end{pmatrix} . \tag{1.20}$$

Here, we have defined $\varphi^\pm = (\varphi^1 \mp i\varphi^2)/\sqrt{2}$. The field h corresponds to the famous Higgs particle. It is the last missing particle that is needed to complete the SM, after the discovery of the predicted $SU(2)_L$ partner of the tau, the tau neutrino, through the DONUT experiment at Fermilab in 2000 [26]. It corresponds to the residual physical scalar degree of freedom after EWSB and parametrizes massive fluctuations around v, whereas the unphysical Goldstone bosons $\varphi^\pm, \varphi^3$ correspond to flat directions in the potential. According to the Goldstone theorem, every spontaneously broken generator of a continuous symmetry results in a Goldstone boson. The breaking pattern (1.18) thus results in three Goldstone bosons. By a gauge transformation leading to the unitary gauge, they can be formally removed from the theory. Their degrees of freedom are absorbed by the electroweak gauge bosons, which now are massive and thus need a third polarization degree of freedom.

Let us have a look at how these masses are generated. After EWSB, (1.19) contains - besides interaction terms, kinetic terms, and the Higgs potential - the following quadratic terms in the fields

$$\mathcal{L}_{\text{Higgs}} \supset v^2 \frac{g^2 + g'^2}{8} Z_\mu Z^\mu + v^2 \frac{g^2}{4} W_\mu^+ W^{-\mu}, \tag{1.21}$$

where we have used the charges of the Higgs doublet given in Table 1.1 and the definition of the covariant derivative (1.10). Moreover, we have already performed a transformation to the mass basis, *i.e.*, the basis in which the gauge boson mass matrix is diagonal, via the orthogonal transformation

$$\begin{pmatrix} Z_\mu \\ A_\mu \end{pmatrix} = \begin{pmatrix} c_w & -s_w \\ s_w & c_w \end{pmatrix} \begin{pmatrix} W_\mu^3 \\ B_\mu \end{pmatrix} . \tag{1.22}$$

Here, the sine and cosine of the weak mixing angle, s_w and c_w, are given by

$$s_w \equiv \sin\theta_w = \frac{g'}{\sqrt{g^2 + g'^2}}, \qquad c_w \equiv \cos\theta_w = \frac{g}{\sqrt{g^2 + g'^2}}, \tag{1.23}$$

and

$$W_\mu^\pm = \frac{1}{\sqrt{2}} \left(W_\mu^1 \mp i W_\mu^2 \right) . \tag{1.24}$$

Thus, the physical $W^\pm$ and Z bosons get masses

$$m_W = v\,\frac{g}{2}\,, \qquad m_Z = v\,\frac{\sqrt{g^2 + g'^2}}{2}\,, \qquad (1.25)$$

while the photon A corresponds to a combination of symmetry generators which is left unbroken and remains massless. Furthermore the Higgs boson receives a mass $m_h = \sqrt{2}\mu = \sqrt{\lambda}v$. In the mass basis the covariant derivative (1.10) becomes

$$D_\mu = \partial_\mu - i\frac{g}{\cos\theta_w}\left(T^3 - \sin^2\theta_w Q\right)Z_\mu - ie\,QA_\mu - i\frac{g}{\sqrt{2}}\left(T^+ W_\mu^+ + T^- W_\mu^-\right) - ig_s t^a G_\mu^a\,, \quad (1.26)$$

where we have defined the generators

$$T^\pm = \left(T^1 \pm i\,T^2\right), \qquad (1.27)$$

as well as the $U(1)_{EM}$ generator of electromagnetism and the electric charge

$$Q = T^3 + Y\,, \quad e = g\sin\theta_w\,. \qquad (1.28)$$

Due to the gauge invariant mechanism of giving masses to the electroweak gauge bosons via the Higgs doublet, we arrive from (1.25) at the SM (tree-level) prediction

$$m_W = m_Z \cos\theta_w\,. \qquad (1.29)$$

Thus, at tree level, the properties of electroweak gauge bosons can be fully specified by the three parameters e, θ_w, and m_Z. Clearly, one can also trade one of these inputs for another quantity which provides the same information like *e.g.* the *Fermi coupling* $G_F \equiv g^2/(4\sqrt{2}m_W^2)$ (see Appendix A.4). From measuring the gauge-boson masses one can deduce $v = 246\,\text{GeV}$ as the scale of EWSB. The experimental results for these masses can be found in Appendix D.

The here described *GWS model* merged the electromagnetic and weak interactions together in the framework of a compact gauge theory. This was a big step towards having a more and more unified and simple picture of nature. It was developed some time before the direct experimental discovery of several of its ingredients. Due to the chosen gauge symmetry group (1.5), which is broken according to the pattern (1.18), it predicted the existence of neutral weak currents, in addition to the well known charged currents. These neutral currents have been discovered by the Gargamelle experiment some years later in 1973. The profound knowledge about the charged current interactions, like the maximally P violating structure and Cabibbo universality of the couplings, was very helpful in finding the correct theory. The apparent weakness of the weak force with respect to the electromagnetic force at low momentum transfer is not due to a small coupling constant (see (1.11)) but due to the suppression of the corresponding propagators by the large $W^\pm$- and Z-boson masses. This suppression is lifted above the electroweak scale $M_{\text{EW}} \sim 100$ GeV ($\sim m_W \sim m_Z$). This feature of electroweak unification has been tested successfully at HERA. In Figure 1.1 the measured $e^\pm p$ neutral-current and charged-current differential cross sections with respect to the virtuality Q^2 of the exchanged gauge boson are shown in blue and red, respectively. At low Q^2, the neutral-current cross section is dominated by photon exchange and the charged-current cross
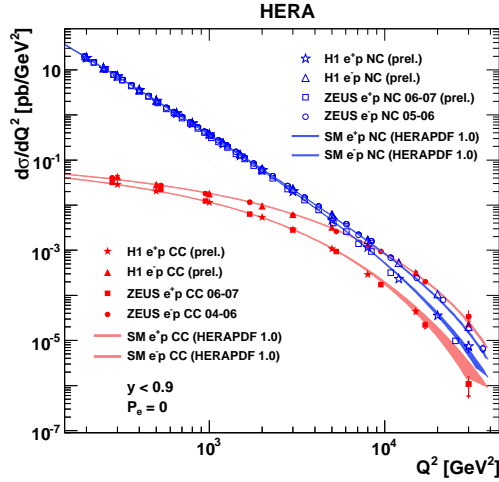
Figure 1.1: Neutral current (blue) and charged current (red) differential cross sections in $e^{\pm}p$ collisions with respect to the virtuality Q^2. Figure from [27] (with permission). Electroweak unification happens above $M_{\text{EW}} \sim 100$ GeV, see text for details.

section is strongly suppressed by the large $W^{\pm}$-boson mass. At high $Q^2 \sim m_W^2$, however, the exchange of massive gauge bosons becomes comparably important and the neutral and charged cross sections become similar, indicating electroweak unification.

The non-trivial relations of the GWS model discussed above, related to the special way of breaking electroweak symmetry spontaneously (without destroying the gauge invariance of the Lagrangian explicitly), diminish the number of parameters in the gauge sector and provide the possibility to test the given mechanism of symmetry breaking. For example, the SM prediction for the parameter

$$\varrho \equiv m_W^2/(m_Z^2 \cos^2 \theta_w)\,, \tag{1.30}$$

encoding the relation between gauge couplings and masses (*c.f.* (1.29)), is $\varrho_{SM} = 1$, at the tree level. Quantum corrections within the SM will alter this relation, as will NP contributions to the electroweak gauge boson masses. A measurement of the ϱ parameter can thus test the SM and constrain BSM physics, see Section 5.1.1. Note that the massive $W^{\pm}$ and Z bosons, predicted within the SM, have only been discovered experimentally in 1983 by the UA1 [28, 29] and UA2 [30, 31] collaborations at the CERN Super Proton Synchrotron, which had been upgraded to a two-beam collider in order to reach sufficient center of mass energies (Nobel Prize in Physics 1984 for Rubbia and van der Meer). Their masses were found to lie just in the region suggested by the relation (1.29), which provides a nontrivial experimental confirmation that some mechanism like described above is at work. The reference values compiled in Appendix D lead to $\varrho_{exp} \approx 1.01$, where the one per cent deviation could be due to loop corrections to the relation (1.29). The fact that a single value of the weak mixing angle accounts for all kinds of different observables of the electroweak theory (including interactions with different fermions), provides strong evidence for the existence of an underlying, spontaneously broken, gauge symmetry in nature [16].

The $SU(2)_L \times U(1)_Y$ gauge structure of the SM has been successfully tested at the Large Electron-Positron Collider (LEP) in trilinear gauge-boson couplings as well as in couplings to fermions in $e^+e^- \to W^+W^-$. Several Feynman graphs contributing to this process (neutrino
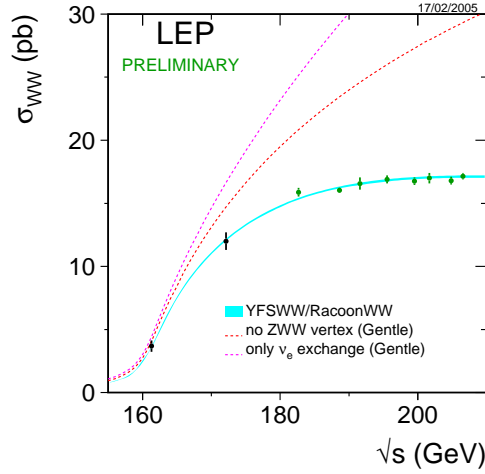
Figure 1.2: Cross section $\sigma(e^+e^- \to W^+W^-)$, measured at LEP2. The ZWW-vertex contribution, with exactly the relative strength as dictated by gauge invariance, is needed in order to preserve perturbative unitarity. Figure from [32] (with permission). See text for details.

exchange, Z-boson exchange, photon exchange) have to add up in a certain way, not to lead to a cross section that raises proportional to the squared center of mass energy s and violates (perturbative) unitarity at around $\sqrt{s} = 1\,\mathrm{TeV}$. In the SM, the necessary cancellation is guaranteed by Ward identities, following just from gauge invariance with respect to the SM gauge group. The resulting, well behaved, SM cross section agrees very well with experiment, see Figure 1.2. In fact, the only theories of massive vector bosons that do not have a violent high-energy behavior are those arising from a spontaneously broken gauge symmetry [33].

Custodial Symmetry and the $W^\pm$-Boson Mass

In summary, we can be quite certain that the $W^\pm$ and Z bosons arise from a spontaneously broken $SU(2) \times U(1)$ gauge symmetry with masses fulfilling the relation (1.29) to good accuracy. One can ask the question, if this already provides evidence for the existence of the SM Higgs mechanism, *i.e.*, if this relation is unique to the symmetry breaking by a scalar SM-Higgs doublet, or if other mechanisms are possible that feature the same breaking pattern including the relation (1.29). Being well tested, any model of NP should reproduce this mass relation to reasonable accuracy.

As a consequence, we will have a closer look on how this relation comes about and how much it depends on the mechanism that breaks $SU(2)_L \times U(1)_Y$. For that purpose, we construct the most general mass matrix for the electroweak gauge bosons, consistent with the breaking pattern $SU(2)_L \times U(1)_Y \to U(1)_{EM}$. In the basis corresponding to $(W^1_\mu, W^2_\mu, W^3_\mu, B_\mu)$, we make the ansatz

$$M^2 = \begin{pmatrix} m_W^2 & 0 & 0 & 0 \\ 0 & m_W^2 & 0 & 0 \\ 0 & 0 & m_3^2 & m^2 \\ 0 & 0 & m^2 & m_0^2 \end{pmatrix}. \tag{1.31}$$

Note that due to the $U(1)_{EM}$ gauge invariance, the coefficients of the quadratic terms $W^1_\mu W^{\mu\,1}$

and $W_\mu^2 W^{\mu\,2}$ must be identical $m_1^2 = m_2^2 \equiv m_W^2$. Electromagnetic gauge invariance together with hermiticity is also responsible for the zero entries in (1.31). The lower-right block represents the most general symmetric (squared) mass matrix for the corresponding two-component system. Its entries can be further specified by demanding one eigenvalue to be zero, corresponding to the massless photon, and a non-vanishing eigenvalue, denoted by m_Z^2. It turns out that, in order to arrive at the sought mass relation (1.29), one needs $m_3^2 = m_W^2$, see Appendix A.2. Thus, the mass matrix (1.31) has to fulfill

$$m_1^2 = m_2^2 = m_3^2 = m_W^2 \,. \tag{1.32}$$

This relation holds for the SM Higgs mechanism due to the fact that the Higgs boson is a scalar $SU(2)_L$ doublet. It is related to an accidental global $SU(2)_L \times SU(2)_R$ symmetry in the Higgs Lagrangian, broken by the Higgs VEV according to

$$SU(2)_L \times SU(2)_R \longrightarrow SU(2)_V \,, \tag{1.33}$$

which leaves its imprint in the gauge boson mass matrix, see Appendix A.2. The residual $SU(2)_V$ symmetry guarantees that the mass relation (1.32) is fulfilled. *Any* sector that breaks the SM gauge group according to (1.18) and exhibits this so-called *custodial symmetry* [34] thus has the potential to lead to a viable phenomenology in the gauge boson sector. For a more detailed discussion see Appendix A.2 and [16, 35]. In Section 3, a version of this symmetry will be used to protect the RS setup from large corrections to the T parameter, related to a breaking of the relation (1.29) (see the end of this section). Expressing this relation through a symmetry has the additional advantage that one can easily identify corrections to it, arising *e.g.* through symmetry breaking interactions at the quantum level. In the SM, the custodial symmetry is broken at the loop level through Yukawa interactions and interactions with the $U(1)_Y$ gauge boson and thus $\varrho_{SM} \neq 1$ beyond the tree level, as mentioned before. Analysing these interactions can give a handle on the size of the effect. On the other hand, measuring ϱ very accurately could also reveal (small) deviations from the SM prediction.

Another possibility to test the SM is to extract m_W *indirectly* from a measurement of e, θ_w and the Fermi coupling G_F, measured in muon decay. According to the SM relations (assuming no BSM physics in muon decay) one arrives at

$$(m_W^2)_{\text{indirect}} \equiv \frac{e^2}{4\sqrt{2}\sin^2\theta_w\,G_F}. \tag{1.34}$$

This extraction can be compared to the direct reconstruction of the $W^\pm$-boson mass. The results are shown in Figure 1.3 in the $m_W - m_t$ plane, where m_t is the mass of the top quark. The colored ellipses indicate the regions of 68%, 95%, and 99% confidence level (CL), following from the direct measurements at LEP2 [36] and the Tevatron [12]. The results obtained from (1.34) depend, due to loop effect, significantly on the Higgs mass and are shown by the green (gray) band for $m_h \in [60, 1000]\,\text{GeV}$. The central values and 1σ errors of the direct and indirect $W^\pm$-mass determinations are given by

$$m_W = (80.399 \pm 0.023)\,\text{GeV}\,, \qquad (m_W)_{\text{indirect}} = (80.348 \pm 0.015)\,\text{GeV}\,. \tag{1.35}$$
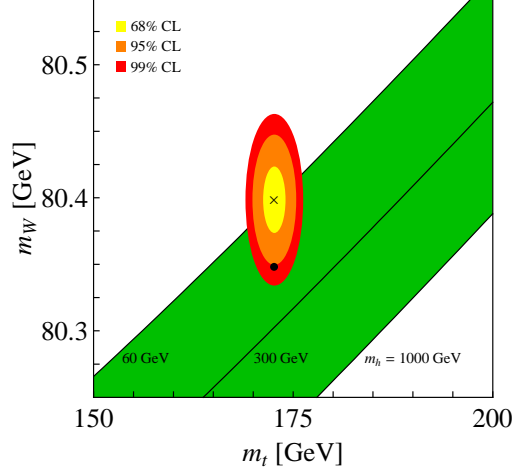
Figure 1.3: Regions in the m_t–m_W plane following from the direct and indirect deter-
mination of m_W. The colored ellipses correspond to 68%, 95%, and 99% probability,
and are obtained from the direct measurements of m_W and m_t at LEP2 and the Teva-
tron. The black dot shows the SM prediction based on G_F for our reference SM input,
whereas the green (gray) shaded band shows the SM expectation for values of the
Higgs-boson mass $m_h \in [60, 1000]$ GeV. See text for details.

The value of $(m_W)_{\text{indirect}}$ has been derived with the help of ZFITTER [37, 38] and we have used
the SM reference values for $\Delta\alpha_{\text{had}}^{(5)}(m_Z)$, $\alpha_s(m_Z)$, m_Z, and m_t, as well as $m_h = 150\,\text{GeV}$, as
given in Appendix D. The $2\,\sigma$ shift of around $50\,\text{MeV}$ between the two measurements, which
are expected to coincide within the SM, could be just a statistical fluctuation or already a
hint for NP, like *e.g.* for the RS model, as we will discuss in Section 5.1.1.

Fermion Masses and Theoretical Constraints on the Higgs-Boson Mass

Besides giving masses to gauge bosons, the Higgs mechanism can also provide gauge invariant
mass terms for the fermion fields via Yukawa couplings. The corresponding Lagrangian reads

$$\mathcal{L}_{\text{Yukawa}} = -\bar{Q}_L \Phi^c \, \boldsymbol{Y}_u u_R - \bar{Q}_L \Phi \, \boldsymbol{Y}_d \, d_R - \bar{E}_L \Phi \, \boldsymbol{Y}_e \, e_R + \text{h.c.}\,, \qquad (1.36)$$

where the Yukawa couplings $\boldsymbol{Y}_{u,d,e}$ are 3×3 matrices in flavor space. The left-handed fermion-
doublets and the Higgs doublet combine to $SU(2)$ singlets, which makes $\mathcal{L}_{\text{Yukawa}}$ gauge invari-
ant. After EWSB, (1.36) will contain mass terms for the charged SM fermions, see Sec-
tion 1.1.3. Note that in the SM it is possible to give masses to up- and down- type quarks
with a single Higgs doublet by defining $\Phi^c \equiv i\sigma_2\Phi^*$, whereas this is not the case for models of
supersymmetry (SUSY), which will be briefly reviewed later. Here, at least two $SU(2)$ doublet
scalars are needed. Let us stress again that the SM Lagrangian including $\mathcal{L}_{\text{Higgs}}$ and $\mathcal{L}_{\text{Yukawa}}$ is
still gauge invariant under the full gauge group (1.5). The gauge invariance of the full theory is
just encrypted, looking at the ground state. So it would be more correct to say that the sym-
metry is hidden, rather than broken. While symmetries are very interesting, spontaneously
broken symmetries are even more exciting, as they allow for a richer phenomenology, while still
possessing an underlying symmetry, as we have seen above. For additional details on the Higgs

mechanism see *e.g.* the literature cited at the beginning of this section and [39] as well the one on QFT and the SM given in the last footnote. The construction of such a mechanism was quite remarkable, since what we observe in nature are solutions following from a Lagrangian in the broken phase and not the Lagrangian itself. Since the SM Higgs mechanism of giving masses to gauge bosons and fermions seems to be quite promising, we should try to discover the Higgs boson and to test this sector of the SM directly. This is one of the main tasks of the LHC which started operation in 2008. However, already at LEP and at the Tevatron, searches for the Higgs boson have been performed, excluding several ranges for the mass of a SM Higgs, see below. Before introducing briefly the main production channels for Tevatron and the LHC, as well as the relevant decay channels, let us have a look at theoretical bounds on the Higgs-boson mass within the SM (see *e.g.* [39] and references therein). To this end, we start with constraints from *unitarity* of longitudinal $W^\pm$-boson scattering $W_L^+ W_L^- \to W_L^+ W_L^-$. As indicated before, it turns out that the presence of a Higgs sector, keeping the SM with *massive* gauge bosons gauge invariant, is essential for an appropriate high energy behavior of the theory. Without such (or a similar) sector, perturbative unitarity will also be violated in $W_L^+ W_L^- \to W_L^+ W_L^-$ around the TeV scale, due to a growth of the scattering amplitude with the center of mass energy $\sqrt{s}$. This process puts an upper bound on the mass of the physical scalar of the Higgs sector, which contributes to this process as a virtual particle, meaning that it has to complete the SM below a certain maximal scale [40]. Performing a partial wave analysis of the scattering amplitude and using the optical theorem, see Appendix A.3, one arrives at

$$m_h \lesssim 870\,\text{GeV}\,. \tag{1.37}$$

This limit becomes slightly stronger if additional scattering channels of massive bosons are included, decreasing to a value slightly above $700\,\text{GeV}$ [39] . Note that the tree-level derivation presented in Appendix A.3 relies on perturbativity of the theory. For large Higgs masses the Higgs self coupling λ becomes strong and higher order corrections could in principle restore unitarity for a Higgs mass slightly above the TeV scale, at the cost of ending up with a strongly coupled theory and loss of the predictive power of the SM.

Additional constraints on the Higgs mass can be obtained by studying the Higgs potential in (1.19) directly. The quartic coupling λ depends due to quantum corrections on the energy scale μ, see Appendix A.3. The requirement for λ not to exhibit a Landau pole nor to become negative below a scale μ_c leads to the constraint [39, 41]

$$\begin{aligned} \mu_c \gtrsim 10^{16}\,\text{GeV} \;\Rightarrow\; 130\,\text{GeV} \lesssim m_h \lesssim 180\,\text{GeV} \\ \mu_c \gtrsim 1\,\text{TeV} \;\Rightarrow\; 50\,\text{GeV} \lesssim m_h \lesssim 800\,\text{GeV}\,, \end{aligned} \tag{1.38}$$

where the idea of Grand Unification set the first cutoff scale above (see below). The corresponding leading order (LO) calculations are performed explicitly in Appendix A.3. The upper bound on the Higgs mass in (1.38), resulting from the requirement to avoid a Landau pole, is called *triviality bound*. If this pole would appear in the range of validity of the theory, one would have to set $\lambda \equiv 0$ in order to avoid this pole, rendering the Higgs sector non-interacting and thus trivial. The lower bound, coming from demanding $\lambda > 0$, is called *vacuum stability bound* since it has to be fulfilled in order for the Higgs potential to be bounded from below, as needed for the vacuum to be stable, see (1.19). For more details see Appendix A.3. Requiring the Higgs sector of the SM to be well behaved for the whole possible energy range of the
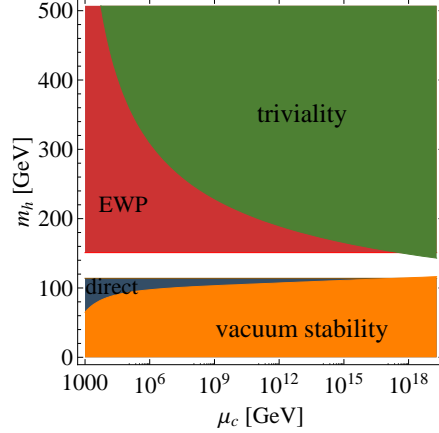
Figure 1.4:   Bounds on the Higgs-boson mass from triviality and vacuum stability, as well as from electroweak precision tests (EWP) and the direct searches at LEP (@ 95% CL). The colored regions are excluded. Recent bounds from Tevatron and the LHC are not shown for presentation purposes. See text for details.

theory, up to the Planck scale $\mu_c \sim M_{\mathrm{Pl}}$, cuts the allowed region for m_h to a small stripe, corresponding to a light Higgs boson. However, allowing for a low Landau pole at around a TeV, meaning that the SM only makes sensible predictions below that scale, allows for a heavy Higgs boson $m_h \sim 800\,\mathrm{GeV}$.

Again, this has to be taken with caution, since if the quartic coupling becomes large, higher order terms can alter the running and possibly avoid the emergence of a Landau pole. However, non-perturbative calculations on the lattice also lead to a bound of $m_h < 640$ GeV [42] in a pure scalar theory (assuming a SM cutoff at $2\pi\, m_h$), which shows a reasonable agreement with the perturbative estimations. Further note that the bounds from vacuum stability can be relaxed if the vacuum turns out to be metastable [43]. The emerging picture is presented in Figure 1.4 which shows the constraints from triviality and vacuum stability considerations, following from the calculations presented in Appendix A.3, together with those from electroweak precision measurements and the direct searches at LEP, see below. It is mandatory to emphasize that all the constraints derived above hold for the SM. Within BSM models, they can be altered. For example in RS models with a SM-type Higgs sector, studied in the main part of this thesis, it could be possible that unitarity can be preserved for higher values of m_h than $870\,\mathrm{GeV}$ due to an exchange of light Kaluza Klein gravitons [44]. Moreover, NP could alter the running of the Higgs quartic coupling and thus the corresponding triviality and vacuum stability bounds within BSM models can be different. Studying theoretical constraints on the Higgs mass within the RS setup (with bulk fields) in more detail, beyond a rough estimation of an upper bound of $m_h \lesssim 1$ TeV, would be interesting but is beyond the scope of this thesis. Nevertheless, in the light of the discussion of bounds in dependence on the cutoff of the theory, one should already mention that the cutoff of this model for processes involving couplings to the Higgs sector will be $\Lambda_{UV} \sim \mathcal{O}(\text{some TeV})$, see (3.31).

In summary, if we do *not* find a Higgs in the mass range of $130\,\mathrm{GeV} \lesssim m_h \lesssim 180\,\mathrm{GeV}$ (1.38) this means that the SM is probably not valid up to the scale of Grand Unification and that at least *new phenomena* are expected to appear well below that scale. Also if we find an Higgs in the mass range suggested by the SM, it is still important to test, whether the
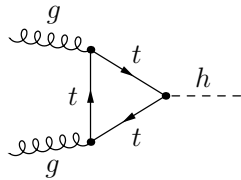
Figure 1.5: Leading-order contribution to Higgs-boson production via gluon fusion.

scalar sector really behaves exactly like the SM Higgs sector. For that purpose, one has to determine further properties of the Higgs boson, like *e.g.* its branching fractions, or look at the production cross section. One main purpose of this thesis is to study these observables in the context of RS models, to have an idea what to expect in this BSM scenario. We will find that *large corrections* with respect to the SM are possible even for high NP scales, see Section 5.3. These results help in discriminating between different models, should one see deviations from the SM expectations in the Higgs sector, and exhibit an (indirect) sensitivity to large scales within this sector. Furthermore they show that, although if one does not find a Higgs boson with some years of LHC data, this does not mean that there is no standard-type Higgs sector but merely could indicate that there is BSM physics that alters this sector such that the Higgs boson is much more difficult to discover.

Higgs-Boson Production and Decay in the SM

The couplings of the physical Higgs boson h to gauge bosons and fermions can easily be obtained from the covariant derivative (1.26) and the Yukawa couplings (1.36). We will work out the Higgs couplings in more detail in the context of RS models in Section 3.7. Nevertheless, we already want to give a brief overview of the main production cross sections and branching fractions in the SM at this point. Due to the particular mechanism of giving masses to the SM fields, the couplings of h to these fields within the SM are directly proportional to their *masses*. This means also that there are no flavor-changing tree-level couplings to the Higgs boson - a fact which, however, can change, if additional contributions to the fermion masses arise (see Section 3.7). In the SM, Higgs decays to heavy particles are generically enhanced. For the same reason, the direct production due to couplings to the light quark content of protons or due to electrons in the initial state are suppressed. The main production mechanisms at hadron colliders such as the Tevatron and the LHC is gluon fusion, which receives the main contribution from a heavy top-quark loop, see Figure 1.5. It can be described by the $D = 5$ operator $h/v \, G^a_{\mu\nu} G^{a\,\mu\nu}$ (see Section 5.3 and Appendix A.4), which interestingly remains valid for $m_h > m_t$, see *e.g.* [45]. Subleading production channels are associated $W^\pm$-boson production, $q\bar{q}' \to W^* \to Wh$, which is the only channel that could allow for a Higgs discovery at the Tevatron, as well as weak gauge-boson fusion, $qq^{(\prime)} \to qq^{(\prime)}V^*V^* \to qq^{(\prime)}h$ with $V = W, Z$, which is known to be quite useful for a potential Higgs discovery at the LHC. An overview of the relevant formulae to compute the corresponding cross sections and the Higgs branching fractions within the SM can be found in [39].

The SM results for the Higgs-boson production cross sections at the Tevatron and LHC for center-of-mass energies of $\sqrt{s} = 1.96 \, \text{TeV}$ and $\sqrt{s} = 10 \, \text{TeV}$ are shown in Figure 1.6. For the gluon-fusion channel, results from [46] are used, which combines the next-to-next-to-leading order (NNLO) corrections [47, 48, 49] in fixed order perturbation theory with a resummation
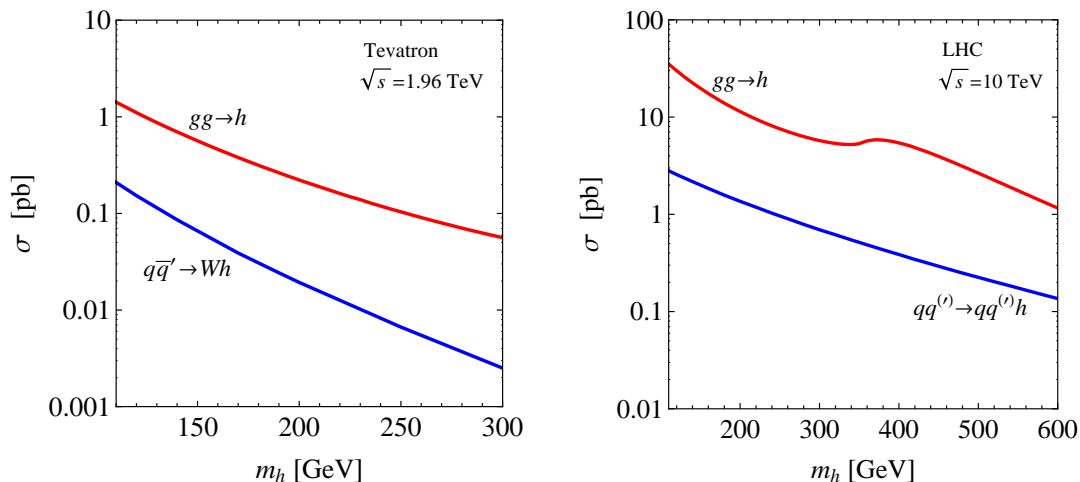
Figure 1.6:   Main Higgs-boson production cross sections at the Tevatron (left) and the LHC (right) for center-of-mass energies of $\sqrt{s} = 1.96\,\text{TeV}$ and $\sqrt{s} = 10\,\text{TeV}$, respectively. For the Tevatron the plot displays gluon-gluon fusion (red) and associated $W^{\pm}$-boson production (blue), while for the LHC gluon-gluon (red) and weak gauge-boson fusion (blue) are shown.

of both threshold logarithms from soft-gluon emission [50, 51, 52, 53, 54] and terms of the form $(N_c \pi \alpha_s)^n$ [55], where N_c is the number of colors. Moreover, the `MRST2006NNLO` parton distribution functions [56] and the associated normalization $\alpha_s(m_Z) = 0.1191$ for the strong coupling constant have been employed. The SM predictions for the subleading production channels have been obtained from [57]. The branching fractions of the Higgs boson within the SM are depicted in Figure 1.7. The plot confirms the expectation that couplings to heavy particles are most important (for $h \to gg$ corresponding to the top quark in the loop). The shown results have been calculated with the help of `HDECAY` [58].[5] We will compare these results to the predictions of the RS setup in Section 5.3.

The Higgs boson has been searched in various channels at the Tevatron and LEP. Currently the LHC is the main machine trying to discover the Higgs. A direct lower bound on m_h has been obtained from the LEP searches. It reads [59]

$$m_h > 114.4\,\text{GeV} \ @\,95\%\,\text{CL}\,. \tag{1.39}$$

Lately, Tevatron excluded a region [60]

$$m_h \notin [156, 177]\,\text{GeV} \ @\,95\%\,\text{CL}\,. \tag{1.40}$$

A very recent exclusion window has been given by the LHC. The ATLAS results, obtained from $\sim 2\text{fb}^{-1}$ of pp collisions at $\sqrt{s} = 7\,\text{TeV}$, are shown in Figure 1.8. In that plot, the ratio of the limit on the Higgs boson production cross section to the expected SM cross section is plotted in dependence on the Higgs-boson mass. Values below 1 indicate that a SM Higgs

---

[5]Expect for the parameters listed in Appendix D, the original input file of `HDECAY` version 3.51 has been used.
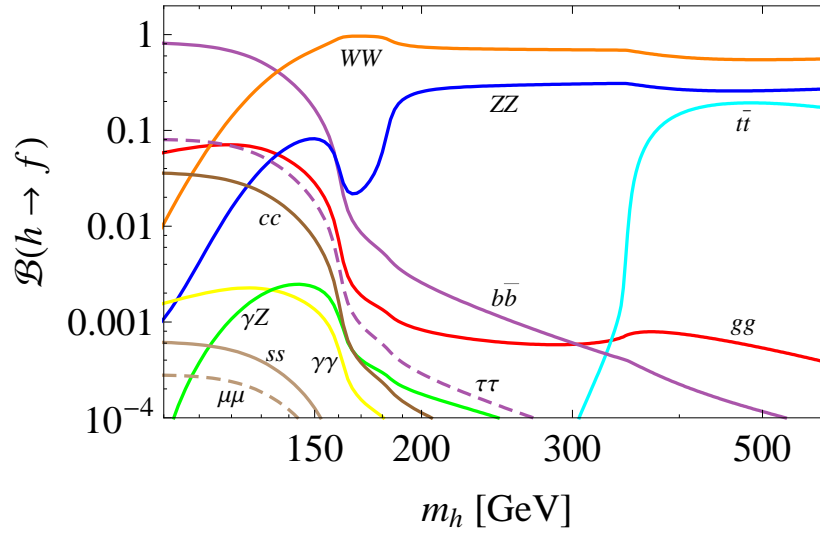
Figure 1.7: Branching fractions for $h \to f$ as functions of the Higgs-boson mass. Channels with fractions of less than 10^{-4} are not shown.

boson is excluded in the corresponding mass region at 95% CL. However, for all these limits it is important to recall that, if the production cross sections and/or branching fractions are changed with respect to the SM, the corresponding exclusion plots will also change. The ATLAS exclusion for the SM reads [61]

$$m_h \notin [149, 222] \cup [276, 470] \, \text{GeV} \, @ \, 95\% \, \text{CL} \, . \tag{1.41}$$

Beyond that, the plot shows a $2\,\sigma$ excess in the low mass region $m_h \in [120, 140]\,\text{GeV}$. However, the significance is not big enough to already speak of an evidence for the Higgs boson. More statistics will be needed to clarify the situation.

Electroweak Precision Tests

In addition to these direct limits, one can get a handle on the Higgs-boson mass indirectly from precision measurements. The Higgs boson (if it exists) will enter many processes as a virtual particle and thus potentially leaves an imprint in various observables, which thus depend on m_h (see *e.g.* Figure 1.3). The situation is summarized in Figure 1.9, which shows the $\Delta\chi^2$ of the SM-fit, obtained from high-Q^2 precision electroweak measurements, performed at LEP and by SLD, CDF, and DØ, as a function of the Higgs-boson mass [36, 62]. The best fit ($\Delta\chi^2 = 0$) and the corresponding 68%/,CL region are given by $m_h = 92^{+34}_{-26}\,\text{GeV}$, without taking into account the theoretical uncertainty. Moreover, alternative fits for a different value of $\Delta\alpha_{\text{had}}^{(5)}$ as well as for an inclusion of low-Q^2 data are shown. The maximal possible value of the Higgs-boson mass in the SM, suggested by electroweak precision measurements, reads

$$m_h < 161\,\text{GeV} \, @95\% \, \text{CL} \, , \tag{1.42}$$
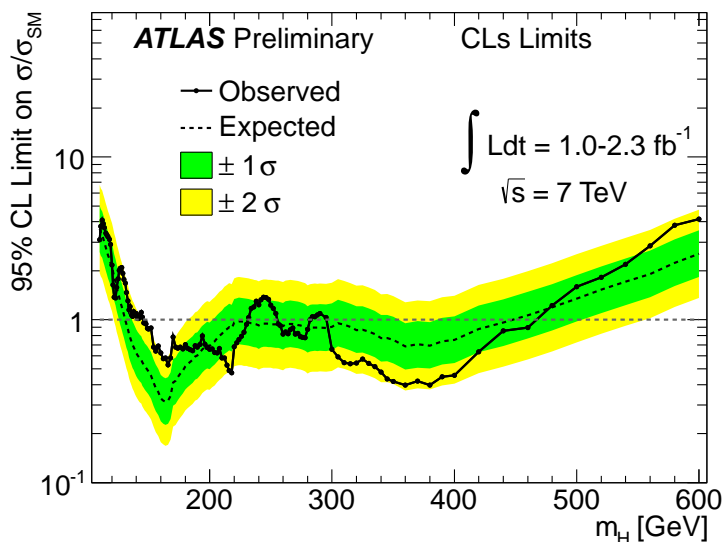
Figure 1.8:   Higgs search at the LHC. The solid line shows the combined upper limit on the SM Higgs boson production cross section divided the expected cross section in the SM as a function of m_h. The limit corresponds to 95% CL. The median expected limit in the absence of a signal is shown by the dotted line, while the green and yellow bands indicate the corresponding 68% and 95% regions. Figure from [61].

without taking into account direct exclusions. Thus, all considerations within the SM (theoretical as well as experimental) suggest that the Higgs boson is light, just around the LEP limit. Note that this picture will change in the minimal RS model, studied in chapters 3-5. Seen from another point of view, electroweak precision measurements together with the LEP exclusion hint to the fact that the SM could be valid up to very high energies, as reflected in Figure 1.4 by the fact that the experimentally allowed region matches with the closing throat of theoretical constraints at large cutoff. This perception is supported by the fact that the SM is a renormalizable theory.

Let us finally mention that there are several alternatives to the SM Higgs mechanism. The simplest extension is just a model of two Higgs doublets, one giving masses to the up type and one to the down type quarks, like used in models of SUSY. Furthermore, there are various ways of realizing a Higgs boson. It does not even have to correspond to an elementary particle, but could also be composite in the spirit of technicolor models, see Section 1.2.1 and Chapter 3. Another possibility to arrive at massive SM particles is to break the gauge invariance by boundary conditions in Higgsless models, see Chapter 3.

In order to get a feeling for the overall agreement of the SM with data at the mass scale of the weak gauge bosons, we will have a detailed look at the fit of the Z-pole (pseudo) observables, studied at LEP. For a detailed descriptions of these variables see [36]. These depend through quantum corrections on the masses of the top quark and the Higgs-boson which were not accessible directly at LEP with a center of mass energy of $\sqrt{s} \approx 91$ for LEP1. Including loop corrections, the SM input parameters relevant for the Z-pole observables are the electromagnetic and the strong coupling constants $\alpha(m_Z) \equiv e^2(m_Z)/(4\pi)$ and $\alpha_s(m_Z)$, evaluated at the scale m_Z, as well as the masses of the top-quark, the Z-boson and the
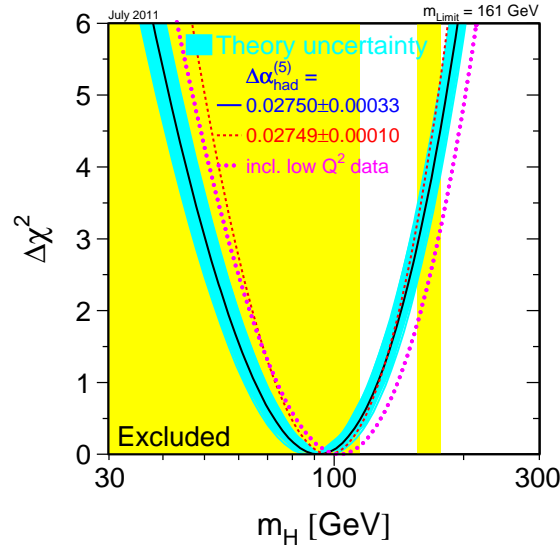
Figure 1.9: $\Delta\chi^2$ of the SM-fit, obtained from precision electroweak measurements, as a function of the Higgs-boson mass. The direct exclusion limits from LEP and the Tevatron are indicated by the yellow regions. Figure from [62] (with permission) . See text for details.

Higgs-boson. Note that the masses of all fermions, besides the top quark, are small compared to m_Z and their values are known to sufficient accuracy, such that their impact on Z-pole observables can be neglected. They are assumed to be fixed, which also holds for $G_F = 1.16637(1) \times 10^{-5}\,\mathrm{GeV}^{-2}$ which is known to excellent accuracy through muon decay. The values of the input parameters are now fitted to agree best with the measurements of the Z-pole observables together with the (five-flavor) hadronic vacuum polarization $\Delta\alpha_{\mathrm{had}}^{(5)}(m_Z)$. The resulting predictions for these observables are shown in Figure 1.10.

In total, the SM predictions agree well with the direct measurements of the corresponding observables. This means that the input parameters, introduced above, are able to describe the Z-pole consistently, which provides a test of the SM at the quantum level. The only discrepancy well above the level of $2\,\sigma$ is found in the forward-backward asymmetry for bottom quarks $A_{FB}^{0,b}$. While this could still be a statistical fluctuation, it might also be interpreted as a hint for BSM physics. We will study this possibility in Section 5.1.3. Note that, before its direct discovery at Tevatron, the electroweak precision fit at the Z-pole *predicted* the mass of the top quark to be approximately equal to $170\,\mathrm{GeV}$ (see [16]), in remarkable agreement with the direct measurement, see Appendix D. Moreover, from measuring the width of the Z-boson it was possible to exclude the existence of a fourth neutrino with standard-model couplings and a mass below $m_Z/2$. Comparing the measured invisible width with the SM prediction, depending on the number of light neutrinos N_ν, one concludes $N_\nu = 2.9840 \pm 0.0082$ [36], in agreement with the three leptonic doublets of the SM. This provides another remarkable confirmation of the consistency of the SM.

Another important test of the SM is provided by the electroweak precision observables S, T, and U, the Peskin-Takeuchi parameters. They parametrize (universal) deviations from the expected electroweak radiative corrections in the SM, entering through vacuum polarization

	Measurement	Fit	$\|O^{meas}-O^{fit}\|/\sigma^{meas}$
			0 1 2 3
$\Delta\alpha_{had}^{(5)}(m_Z)$	0.02750 ± 0.00033	0.02759	
m_Z [GeV]	91.1875 ± 0.0021	91.1874	
Γ_Z [GeV]	2.4952 ± 0.0023	2.4959	
σ_{had}^0 [nb]	41.540 ± 0.037	41.478	
R_l	20.767 ± 0.025	20.742	
$A_{fb}^{0,l}$	0.01714 ± 0.00095	0.01646	
$A_l(P_\tau)$	0.1465 ± 0.0032	0.1482	
R_b	0.21629 ± 0.00066	0.21579	
R_c	0.1721 ± 0.0030	0.1722	
$A_{fb}^{0,b}$	0.0992 ± 0.0016	0.1039	
$A_{fb}^{0,c}$	0.0707 ± 0.0035	0.0743	
A_b	0.923 ± 0.020	0.935	
A_c	0.670 ± 0.027	0.668	
A_l(SLD)	0.1513 ± 0.0021	0.1482	
$\sin^2\theta_{eff}^{lept}(Q_{fb})$	0.2324 ± 0.0012	0.2314	
m_W [GeV]	80.399 ± 0.023	80.378	
Γ_W [GeV]	2.085 ± 0.042	2.092	
m_t [GeV]	173.20 ± 0.90	173.27	

July 2011

0   1   2   3

Figure 1.10:   Comparison of a direct measurement of the Z-pole observables with the values obtained from the SM-fit. Figure from [62] (with permission). See text for details.

diagrams [16, 63, 64, 65, 66, 67, 68, 69]. Thus, at a SM reference point, they are normalized to zero. In terms of vacuum polarization amplitudes involving electroweak gauge bosons and their derivatives, evaluated at zero momentum, they read

$$S = \frac{16\pi s_w^2 c_w^2}{e^2}\left[\Pi'_{ZZ}(0) + \frac{s_w^2 - c_w^2}{s_w c_w}\Pi'_{ZA}(0) - \Pi'_{AA}(0)\right],$$

$$T = \frac{4\pi}{e^2 c_w^2 m_Z^2}\left[\Pi_{WW}(0) - c_w^2\,\Pi_{ZZ}(0) - 2\,s_w c_w\,\Pi_{ZA}(0) - s_w^2\,\Pi_{AA}(0)\right], \qquad (1.43)$$

$$U = \frac{16\pi s_w^2}{e^2}\left[\Pi'_{WW}(0) - c_w^2\,\Pi'_{ZZ}(0) - 2\,s_w c_w\,\Pi'_{ZA}(0) - s_w^2\,\Pi'_{AA}(0)\right].$$

The parameter T is sensitive to the difference between the corrections to the $W^\pm$- and Z-boson vacuum-polarization amplitudes and thus measures isospin violation. It is thus directly related to the ϱ parameter introduced before. The experimental central values and 68% CL bounds on the S and T parameters, corrected to the world average of the top-quark mass [70], as well as their correlation matrix are given by [36]

$$\begin{aligned} S &= 0.07 \pm 0.10\,, \\ T &= 0.16 \pm 0.10\,, \end{aligned} \qquad \rho = \begin{pmatrix} 1.00 & 0.85 \\ 0.85 & 1.00 \end{pmatrix}. \qquad (1.44)$$

In the global fit to the SLC and LEP measurements, the parameter U is set to zero. The subtraction point corresponds to the SM reference values as given in Appendix D. The experimental values in (1.44) are in rather good agreement with zero, indicating that there are no unexpectedly large electroweak corrections from BSM physics. The corresponding regions of 68%, 95%, and 99% probability in the S–T plane are shown in Figure 3.10 in Section 3.3, where we will discuss corrections to the electroweak precision parameters in the RS setup. Finally, an important test of the QED part of the SM deeply at the quantum level (≥ 4 loops) is provided by studies of the anomalous magnetic moment of the electron a_e. The experimental result agrees with the SM calculation at the level of 10^{-9} (one part per billion) [71, 72]!

$$
\begin{aligned}
a_e^{theo} &= 0.00115965218113(84), \\
a_e^{theo} &= 0.00115965218073(28).
\end{aligned}
\tag{1.45}
$$

This agreement between theory and experiment in one of the most precisely measured quantities in whole science is an impressing confirmation of QED.

1.1.3 Flavor and CP Violation

The Yukawa Lagrangian of the SM gives rise to a rich phenomenology in the flavor sector, *i.e.*, the sector that differentiates between different fermion flavors. For an introduction see *e.g.* [73, 74, 75]. After EWSB, the Lagrangian (1.36) leads to (non-diagonal) mass terms for the SM fermions which are proportional to the Higgs VEV v and entries of the Yukawa matrices

$$
\boldsymbol{m}_f = \frac{1}{\sqrt{2}} v \, \boldsymbol{Y}_f \,, \ f = u, d, e \,.
\tag{1.46}
$$

These are the only terms in the SM that distinguish between different fermion flavors of the same electromagnetic charge and break the $SU(3)_Q \times SU(3)_u \times SU(3)_d \times SU(3)_E \times SU(3)_e$ flavor symmetry that the SM would have otherwise. In order to end up in the physical basis of propagating mass eigenstates, we diagonalize these terms by bi-unitary transformations

$$
\boldsymbol{m}_u = \boldsymbol{U}_u \, \mathrm{diag} \, (m_u, m_c, m_t) \, \boldsymbol{W}_u^\dagger
\tag{1.47}
$$

and analogously for down-type quarks and charged leptons. The fermion mass eigenstates are thus obtained from the flavor eigenstates as $u_L^{\mathrm{mass}} = \boldsymbol{U}_u^\dagger u_L$, $u_R^{\mathrm{mass}} = \boldsymbol{W}_u^\dagger u_R$, *etc.* Experimental results for the quark and lepton masses can be found in [12]. Besides the Yukawa terms and those involving charged current interactions with the $W^\pm$-bosons, all remaining terms in the Lagrangian are invariant under this change of basis. Furthermore, as neutrinos are massless within the SM, it is always possible to go to a basis in which the charged current interactions in the lepton sector, as well as the mass matrix of the charged leptons are diagonal. The charged current interactions of quarks however become

$$
\mathcal{L}_{\mathrm{ferm}} \ni \frac{g}{\sqrt{2}} \gamma^\mu \, \bar{u}_L^{\mathrm{mass}} W_\mu^+ \boldsymbol{V}_{\mathrm{CKM}} \, d_L^{\mathrm{mass}} + \mathrm{h.c.},
\tag{1.48}
$$

where

$$
\boldsymbol{V}_{\mathrm{CKM}} \equiv \boldsymbol{U}_u^\dagger \boldsymbol{U}_d \,,
\tag{1.49}
$$

and the superscript of the quark fields signals that they are now in the mass basis. In the following, we will omit this superscript, unless it is necessary for clarity. Due to the misalignment of the up-type and down-type Yukawa matrices, encoded in the off-diagonal entries of the Cabibbo-Kobayashi-Maskawa (CKM) matrix

$$\boldsymbol{V}_{\mathrm{CKM}} \equiv \begin{pmatrix} V_{ud} & V_{us} & V_{ub} \\ V_{cd} & V_{cs} & V_{cb} \\ V_{td} & V_{ts} & V_{tb} \end{pmatrix}, \tag{1.50}$$

there are family-changing interactions at tree level in the charged current sector of the SM. However, due to the observed hierarchies in the CKM matrix, these are suppressed compared to interactions within the same family, see Section 1.2.2. Moreover, due to the unitarity of $\boldsymbol{U}_f$ and $\boldsymbol{W}_f$, there are *no flavor-changing neutral currents* (FCNCs) at tree level in the SM. This agrees nicely with the observed tininess of FCNCs in nature, which on the other hand leads to tight constraints on BSM physics, see Section 1.1.6. Due to this unitarity (leading to a unitary CKM matrix) FCNCs in the SM are also suppressed on the loop level. In fact, the sum over internal fermions in loop mediated FCNCs leads to combinations of CKM-matrix elements such as

$$V_{ud}V_{ub}^* + V_{cd}V_{cb}^* + V_{td}V_{tb}^* = 0, \tag{1.51}$$

which are zero due to the unitarity of $\boldsymbol{V}_{\mathrm{CKM}}$. Such relations, corresponding to the off-diagonal entries in $\boldsymbol{V}_{\mathrm{CKM}}\boldsymbol{V}_{\mathrm{CKM}}^\dagger = \boldsymbol{1}_{3\times3}$, can be interpreted as triangle equations in the complex plane, corresponding to so-called *unitarity triangles*. However, if the fermion masses are not degenerate, there are also terms, where each factor in (1.51) is multiplied by a corresponding (different) quark mass, spoiling the cancellation. If the masses are small compared to the electroweak scale (or the mass differences are small), the effect will be suppressed. Only the large top quark mass will lead to significant corrections, see *e.g.* [76]. This suppression of FCNCs within the SM is known under the name of Glashow-Iliopoulos-Maiani (GIM) mechanism [77]. Note that these authors used this mechanism to explain the smallness of the branching ratio of the decay $K^0 \to \pi^+\pi^-$. In this context, the prediction of the charm quark is usually assigned to them. Back in 1970, this quark had not been discovered yet. However, this fourth quark was needed in order to explain the smallness of the FCNC-Kaon-decay via the (2 generation) GIM mechanism, in addition to the need of an equal numbers of quarks and leptons for anomaly cancellation [78]. This shows how (precise) measurements in flavor physics can be sensitive to new physics. Since FCNCs are in general rather constrained by experiment, having a type of suppression as described above also in BSM models would be very useful. For up-type quark decays the GIM mechanism is generally extremely effective (since not broken by internal top quarks), leading to the tiny SM prediction for the branching fraction of a top quark decaying into a charm quark and a Z-boson [79, 80]

$$\mathcal{B}(t \to cZ) \simeq 1 \times 10^{-14}. \tag{1.52}$$

A suppression of phenomenological dangerous flavor changing processes for generic models can be achieved by assuming the only source of flavor violation, *i.e.*, breaking of the $SU(3)^5$ global flavor symmetry of the Lagrangian, to be the SM-Yukawa matrices. This assumption is called *minimal flavor violation* (MFV) [81, 82].

The CKM matrix, being a unitary 3×3 matrix, is described by nine parameters, out of which six are phases. However, by redefining the phases of the fermion fields, five of these six phases can be eliminated (corresponding to five independent phase differences between up- and down-type quark fields). So we end up with three mixing angles and one physical phase, which results in CP violation in weak interaction. It is the only source of CP violation in the SM. As a general unitary $n \times n$ matrix has $n(n + 1)/2$ phases, out of which $2n - 1$ can be eliminated, $n = 3$ is the minimum number of generations that allow for a CP-violating phase in the SM, however, see Section 3.2.3. As CP was known to be violated in Kaon decays, Kobayashi and Maskawa conjectured the existence of a third generation of quarks before their experimental discovery, which was another triumph of the SM [83]. In 2008 they received the Nobel Prize in Physics "for the discovery of the origin of the broken symmetry which predicts the existence of at least three families of quarks in nature". Another requirement for having a CP violating phase in the SM are Yukawa couplings with a non-vanishing imaginary part. More precisely, the necessary and sufficient condition for obtaining CP violation in the SM reads [84]

$$\text{Im}\{\det[Y_u Y_u^\dagger, Y_d Y_d^\dagger]\} \neq 0. \tag{1.53}$$

The fact that *complex* Yukawa couplings in the Lagrangian lead to CP violation can be understood intuitively as follows. For example, if we look at the down-type part of the Yukawa Lagrangian, and write down the hermitian conjugation explicitly, we end up with

$$\mathcal{L}_{\text{Yukawa}} \ni -(Y_d)_{ij} \, \bar{Q}_{Li} \Phi d_{Rj} - (Y_d)_{ij}^* \, \bar{d}_{Rj} \Phi^\dagger Q_{Li}, \tag{1.54}$$

where i and j are flavor indices. A CP transformation on this Lagrangian interchanges the operators $\bar{Q}_{Li} \Phi d_{Rj}$ and $\bar{d}_{Rj} \Phi^\dagger Q_{Li}$, but leaves their coefficients unchanged. Thus, only if the Yukawa matrices above are complex, it is in general not CP-invariant. CP violation has been experimentally well established in the neutral Kaon and B_d^0-meson systems, see *e.g.* [73].

Since CP violation is one of the Sakharov criteria [85] (together with C violation, baryon-number non-conservation and interactions out of thermal equilibrium) it is necessary for baryogenesis. While the SM could in principle fulfill the additional Sakharov criteria - baryon-number violation via unsuppressed non-perturbative (sphaleron) effects at high temperatures and a departure from thermal equilibrium during phase transitions in the expanding universe - the CP violation in the SM is orders of magnitude too small to account for the observed baryon asymmetry. Thus, CP violation *beyond the SM* seems to be necessary for baryogenisis to work. Furthermore, within the SM, the LEP bound $m_h > 114.4$ GeV seems to exclude the first order phase transition needed for a viable model of electroweak baryogenesis. For a review on the subject see *e.g.* [86]. We have seen that the number of physical parameters in the flavor sector turned out to be smaller than the number of parameters we started with. Some of them could be rotated to zero in a certain basis. Let us now recall a general strategy which is useful for determining the number of physical parameters due to the flavor sector of a theory. We will use this method in Section 3.2.3 to count the parameters of the RS setup.

Consider a theory with gauge invariant kinetic terms. In addition to the gauge symmetry, the theory in general also has a certain additional global symmetry group G with N_G generators. When adding a gauge invariant potential with N_{general} parameters (in a general basis) to the theory, the global symmetry might be broken down to a smaller symmetry H with N_H generators. Due to this breaking there is a freedom of rotating away *unphysical parameters*,

i.e., choosing a certain "direction", which leaves the theory invariant under the residual global symmetry, see *e.g.* [74]. Denoting the difference in the number of symmetry generators of G and H by $N_{\text{broken}} = N_G - N_H$, the number of physical parameters, affecting measurements, is given by

$$N_{\text{phys}} = N_{\text{general}} - N_{\text{broken}} , \qquad (1.55)$$

which holds separately for real and imaginary parameters. Let us apply this rule to the flavor sector of the SM. The kinetic terms of the quarks have the global symmetry

$$G = U(3)_Q \times U(3)_u \times U(3)_d, \qquad (1.56)$$

which corresponds to $N_G = (9, 18)$ real and imaginary generators. The Yukawa matrices $\boldsymbol{Y}_{u,d}$, being general 3×3 complex matrices, possess $N_{\text{general}} = N_Y = (18, 18)$ real moduli and CP-odd phases (in a general basis). They break down the global symmetry G down to

$$H = U(1)_B , \qquad (1.57)$$

see Section 1.1.4, which has $N_H = (0, 1)$ generators, resulting in $N_{\text{broken}} = (9, 17)$. The number of physical parameters, which cannot be rotated to zero, is thus given by

$$N_{\text{phys}} = (18, 18) - (9, 17) = (9, 1) . \qquad (1.58)$$

These parameters can be identified with the six quark masses and the three mixing angles and the CP violating phase of the CKM matrix.

A useful parametrization of the CKM matrix has been given to Wolfenstein. In terms of the four parameters $(\lambda, A, \bar{\rho}, \bar{\eta})$, it can be written as

$$\boldsymbol{V}_{\text{CKM}} = \begin{pmatrix} 1 - \frac{\lambda^2}{2} & \lambda & A\lambda^3(\bar{\rho} - i\bar{\eta}) \\ -\lambda & 1 - \frac{\lambda^2}{2} & A\lambda^2 \\ A\lambda^3(1 - \bar{\rho} - i\bar{\eta}) & -A\lambda^2 & 1 \end{pmatrix} + O(\lambda^4) , \qquad (1.59)$$

where $\lambda \approx 0.23 \ll 1$ plays the role of an expansion parameter and exhibits the diagonal-dominant, hierarchical, structure of the matrix. The Wolfenstein parameters are related to the entries of the CKM matrix as

$$\lambda = \frac{|V_{us}|}{\sqrt{|V_{ud}|^2 + |V_{us}|^2}}, \qquad A = \frac{1}{\lambda}\left|\frac{V_{cb}}{V_{us}}\right|, \qquad \bar{\rho} - i\bar{\eta} = -\frac{V_{ud}^* V_{ub}}{V_{cd}^* V_{cb}} . \qquad (1.60)$$

Their experimental values are given in Appendix D. A phase-convention invariant measure (independent of phase redefinitions of the fermion fields) of CP violation in $\boldsymbol{V}_{\text{CKM}}$ is given by the Jarlskog invariant J_{CKM} [84], which is defined via

$$\text{Im}\left[(V_{\text{CKM}})_{ij}(V_{\text{CKM}})_{kl}(V_{\text{CKM}}^*)_{il}(V_{\text{CKM}}^*)_{kj}\right] = J_{\text{CKM}} \sum_{m,n=1}^{3} \epsilon_{ikm}\epsilon_{jln} \quad (i, j, k, l = 1, 2, 3) , \qquad (1.61)$$

where ϵ_{ikm} is the Levi-Civita tensor. It corresponds to two times the area of any of the unitarity triangles. Note that J_{CKM} is not small due to a small CP violating phase but due to

small mixing angles in the CKM matrix The fact that it is not $\lesssim \mathcal{O}(1)$, but

$$J_{\mathrm{CKM}} \simeq \lambda^6 A^2 \bar{\eta} \sim 10^{-5} \tag{1.62}$$

quantifies the statement that CP violation is small within the SM. As mentioned before, flavor physics is sensitive (indirectly) to undiscovered particles. Beyond being known approximately from electroweak precision tests, the top-quark mass could also be determined from studies of B mesons, since the rates for rare FCNC processes such as $B \to X_s \gamma$ and those for B–$\bar{B}$-mixing are strongly sensitive on it. Moreover, many other properties of the top quark, like its flavor-changing couplings and CP-violating interactions, are known from Kaon and B-meson physics [87]. This approach of probing new physics *indirectly* is complementary to direct searches and often sensitive to much higher scales. It will be applied in many of the phenomenological studies in Chapter 5.

An important task in flavor physics is to overconstrain the flavor parameters (*e.g.* in terms of an unitarity triangle) by various measurements, in order to test the CKM mechanism. In particular, the fact that CP violation in the SM is induced by a single CP violating phase results in relations between different CP violating observables, which provide stringent tests for the model. Despite some tensions, the experimental situation provides evidence that the CKM mechanism is the dominant source of flavor violation as well as of CP violation in flavor-changing processes at low energies [73, 74, 88]. We will come back to CP violation and the corresponding observables as well as related tensions in Section 5.2.3. BSM physics generically introduces new sources of CP violation. In the latter section we will study in detail the impact of the RS proposal on certain CP violating observables.

1.1.4 Symmetries and Parameters of the SM Lagrangian

After having discussed aspects of the SM (and beyond), a final look at its complete Lagrangian, its symmetries and the parameters contained is instructive. So far we have discussed all ingredients of the SM Lagrangian (1.8), besides one sector which shall be shortly touched on before continuing. In order to eliminate unphysical degrees of freedom, related to the gauge redundancies in the description of the spin-1 gauge bosons by 4D Lorentz vectors, we have to introduce a gauge fixing Lagrangian $\mathcal{L}_{\mathrm{GF}}$. Otherwise the equivalence classes of physical undistinguishable fields will lead to singularities in the quantized theory. However, we do not want to destroy symmetries, but merely rewrite the theory in a way to avoid these singularities. Thus, in the course of fixing the gauge, we also end up with a Lagrangian of Faddeev-Popov ghost fields $\mathcal{L}_{\mathrm{FP}}$ (which are necessary to preserve unitarity). The rigorous way of quantizing a (non-abelian) gauge theory along the lines discussed above is called BRST quantization [89, 90]. The final Lagrangian is invariant under BRST transformations which generalize the concept of gauge transformations. We choose the (SM) gauge fixing

$$\begin{aligned} \mathcal{L}_{\mathrm{GF}} = &-\frac{1}{2\xi} \left(\partial^\mu A_\mu \right)^2 - \frac{1}{2\xi} \left(\partial^\mu Z_\mu - \xi m_Z \varphi_Z \right)^2 \\ &- \frac{1}{\xi} \left(\partial^\mu W_\mu^+ - \xi m_W \varphi_W^+ \right) \left(\partial^\mu W_\mu^- - \xi m_W \varphi_W^- \right) , \end{aligned} \tag{1.63}$$

which also has the convenient feature of eliminating mixed terms between gauge fields and Goldstone bosons in the Lagrangian. A later generalization of $\mathcal{L}_{\mathrm{GF}}$ to the RS model will be

straightforward. The parameter ξ interpolates between different so-called R_ξ (renormalizable) gauges and drops out in physical observables. The Faddeev-Popov Lagrangian is not needed for the calculations performed throughout this thesis. We refer the reader to the literature for more details [16]. Now we have collected all terms of the SM Lagrangian which are necessary to calculate scattering amplitudes and cross sections within the SM by means of standard techniques [16, 17].

The Lagrangian (1.8) exhibits several symmetries, of which two - BRST invariance and Poincaré invariance - have already been mentioned. Furthermore, the Lagrangian has *accidental* global symmetries. It is invariant under a global phase rotation of all quark fields $U(1)_B$ (see Section 1.1.3) which corresponds via Noether's theorem to the conservation of baryon number (B). As the SM Lagrangian does not include mass terms for the neutrino fields, it is furthermore invariant under separate phase rotations of the three lepton families $U(1)_e \times U(1)_\mu \times U(1)_\tau$, which corresponds to a conservation of the lepton-family number. If one includes Dirac mass terms for the neutrinos, this symmetry breaks down to the total lepton number (L). The conservation of lepton number can further be broken by including Majorana mass terms for the neutrinos, see Section 1.1.6. These symmetries are called accidental, since they do not have to be put in by hand, but rather follow from the particle content of the gauge theory and the restriction to $D \leq 4$ terms in the SM Lagrangian. This matches nicely with the experimental non-observation of the B-violating proton decay ($\tau_{p \to e^+ \pi^0} > 8.2 \times 10^{33}$ yr [91]).

The SM is not only in good agreement with experiment at the places, where it was designed to be, but also in many other accidental details. On the other hand, the non-observation of proton decay poses a problem for the *simplest Grand Unified Theories* (GUTs) [92], which allow for a unification of coupling constants but generically induce B violation (*e.g.* $p \to e^+ \pi^0$) at a too large rate [93]. At the quantum level however, L and B are broken inevitably already in the SM, due to the chiral anomaly. Non-perturbative sphaleron processes violate $B + L$ (but respect $B - L$). These processes are just important for very high temperatures $T > 100$ GeV, *e.g.* during the early universe. However, if a symmetry shall be fundamental, it seems that it has to be realized locally (*c.f.* general relativity). Further discrete symmetries that are for example present in electromagnetism, are violated in the SM. P is violated maximally in charged-current interactions which just couple *left-handed* fermions. It is furthermore violated in neutral-current interactions with the Z-boson. Moreover, the Yukawa Lagrangian (1.36) leads to a violation of CP, as discussed in Section 1.1.3. Due to the small (non-maximal) CP violation, also C is violated within the weak sector of the SM. However, CPT is a symmetry of the SM, as it is for every local and Lorentz invariant QFT. At the end it is our task to take a model, determine the parameters present in the Lagrangian and see if this Lagrangian consistently describes nature. Therefore we have to perform more independent measurements than there are independent parameters in the theory in order to overconstrain and thus test the model. If we find tensions, we should think about a modification of our Lagrangian, see Section 1.1.6.

The SM has 18 parameters, which can be chosen to be

- 3 gauge couplings: g, g', g_s

- 15 parameters in the Higgs/flavor sector:

    - m_h, v

- 6 quark masses: (m_u, m_c, m_t), (m_d, m_s, m_b)
- 3 lepton masses: (m_e, m_μ, m_τ)
- 3 mixing angles and one phase of $\boldsymbol{V}_{\mathrm{CKM}}$.

Note that we did not count $\theta_{QCD} = 0$ as a free parameter of the SM. Furthermore, allowing for neutrino masses increases the number of parameters, in dependence on the possible assumption of lepton number conservation (Dirac- vs. Majorana-mass terms). Note also that the choice of the parameters above is not unique. As discussed in Section 1.1.2, we can *e.g.* trade g and g' for the experimentally more common e and $\sin \theta_w$. In contrast to the gauge sector of the SM, which, due to gauge invariance has only a few parameters, there are many free parameters in the flavor sector. This suggests that we have not yet completely understood the fundamental characteristics of matter. Moreover, in contrast to $\mathcal{O}(1)$ gauge couplings, the flavor sector exhibits non understood hierarchies. We will come back to this point in Section 1.2.2.

1.1.5 Effective Field Theories, Renormalizability and the TeV Scale

We have so far introduced the SM as the leading $\mathcal{L}_{\leq 4}$ term in (1.6). Thus we assume, that it is the right theory at low energies - the theory we have studied in the last sections - but at the same time we allow for more than this theory, encoded in the terms with higher mass dimensions and suppressed by powers of the cutoff. That is the modern way of thinking about the SM.

Historically, its genesis was different. The SM was constructed on the purpose of providing an elegant and quite minimalistic gauge theory in order to describe electrodynamics as well as charged current interactions without limitations, which lead to the GWS theory, and later also included QCD. One of the paradigms was renormalizability. If a theory involves couplings with negative mass dimensions, it is not (power-counting) renormalizable (see *e.g.* [17]). Calculating Feynman diagrams containing closed loops of virtual particles often leads to divergent results, since one has to integrate over undetermined internal four-momenta. These results can be regularized by *e.g.* introducing a cutoff Λ in the (euclidean absolute) momentum integration. A theory is renormalizable, if all cutoff-dependent terms that appear can be canceled by introducing a finite number of counterterms in the Lagrangian. This corresponds to absorbing the terms which would diverge in the limit of removing the regularization ($\Lambda \to \infty$) into a redefinition of the (finite number of) fundamental parameters of the theory and is called renormalization. However, if a theory involves couplings with negative mass dimension, such a procedure is not possible. In the course of renormalization one would end up with an infinite number of counterterms of all possible mass dimensions, increasing with the order of the perturbative series. These can no longer be absorbed into redefinitions of a finite number of parameters of the theory. This means that the theory (foreseen as a theory valid up to arbitrary scales) would lose its predictivity as it is impossible to measure an infinite number of unknown couplings. As a consequence, it was argued that no terms in the Lagrangian should be allowed to have mass dimensions bigger than four, as otherwise their coefficients (coupling constants) would need to have a negative mass dimension. Renormalizability was the concept that singled out $\mathcal{L}_{\leq 4}$ out of (1.6) and is a useful method of constraining the possible form of a theory. Note that for a theory to be renormalizable it is also important that the counterterms are compatible with the defining symmetries of the model. In the early

days of the SM, theories that contained terms with mass dimensions bigger than four were considered unsatisfactory and unpredictive at the level of quantum corrections. The SM was defined as the most general, *renormalizable* (*i.e.* $D \leq 4$) theory, consistent with the symmetries of nature, which exactly corresponds to the term $\mathcal{L}_{\leq 4}$. Higher dimensional operators have not been included. Complemented by a concept of treating gravity, like asymptotic safe general relativity [94], the renormalizable SM including the Higgs mechanism could *in principle* be a UV complete theory of nature. This makes the SM very attractive and outstanding with respect to ideas like the (non renormalizable) Fermi theory of weak interactions, which is known to break down at scales of the order of m_W, see Appendix A.4. The fact that the electroweak gauge bosons get their masses through *spontaneous* symmetry breaking is essential for the renormalizability of the SM. It guarantees a gentle high energy behavior of processes involving massive gauge bosons (as we have seen before), which would otherwise violate the line of reasoning with naive mass dimensions above [11]. As a consequence, the SM can make *exact* predictions at a certain level of perturbation theory, with no unknown cutoff effects. Importantly, the SM is anomaly free which means that its gauge symmetries also hold at the quantum level.

However, although the SM is very successful up to energies of $\mathcal{O}(100\,\mathrm{GeV})$, this does not mean that it has to be at higher scales and indeed there is a bunch of evidence that the SM is not the final answer. For the time being, let us just mention the lack of a Dark Matter candidate and of unification of the coupling constants as well as the absence of a quantum theory of gravity. We will discuss more shortcomings of the SM in Section 1.1.6. Today, theories with higher dimensional operators are considered perfectly fine as *effective* field theories, valid up to a cutoff. If the expansion of the Lagrangian is stopped at a certain level of precision (*i.e.*, mass dimension), there is by definition just a finite number of parameters present in the theory which thus is automatically renormalizable (in the "modern" sense) and predictive up to suppressed terms. Indeed, also the RS proposal will turn out to be an EFT. With the model not being valid until arbitrary high energy scales, there is no reason not to include higher dimensional operators. In Appendix A.4 we will treat this concept, which we have already sketched at the beginning of this chapter. The content is assumed to be known in the following. It also demonstrates how our theory (1.6) with the particle content of the SM (*i.e.*, the SM including higher dimensional operators) could arise from a more complete, and possibly renormalizable, theory. This low energy EFT is the theory we see today and, being the most general one, should work with. The effects of its UV completion will be present in the coupling constants of the EFT - the *Wilson coefficients*. As suggested by the shortcomings of the SM, we should construct a theory that completes the SM at high energies. Considering the SM as an EFT, *i.e.*, allowing for higher dimensional operators and trying to determine their coefficients, is a first step on this way. The final theory, valid up to arbitrary high energies (if it exists and is a QFT), should however be renormalizable in the sense that it just contains operators with mass dimensions less or equal than four.

In Appendix A.4 we review an important virtue of the concept of EFTs. If a theory involves several widely separated scales, *e.g.* two scales $m \ll M$, loop calculations will generically feature large logarithms of these scales which can spoil the perturbative expansion. By integrating out physics at the larger scale, *i.e.*, by removing the corresponding dynamical degrees of freedom and constructing a theory just valid below the scale M, one can circumvent this problem and it is possible to *resum* the large logarithms. This is done with the help

of renormalization group (RG) equations, which evolve the Wilson coefficients between one scale and another. Effective theories provide the possibility to separate high energy physics (residing in the Wilson coefficients) from low energy physics (residing in the EFT matrix elements). We will use these techniques in sections 5.1.4 and 5.2.3. EFTs are often used for so-called model-independent studies (see Section 5.1.4). This corresponds just to writing down a general low-energy Lagrangian, including higher dimensional operators (respecting appropriate symmetries) and deriving predictions in terms of the undetermined coefficients of this Lagrangian. It avoids specifying a certain BSM model and resembles just the way in which we have introduced the SM in (1.6).

We have seen that the Higgs sector is important for the renormalizability of the SM. Let us stress that in the EFT picture of the SM, the Higgs boson remains relevant for the high energy behavior of the theory. It guarantees at least that the SM does not necessarily break down already at the TeV scale, due to uncontrolled high energy behavior such as unitarity violation in longitudinal $W^{\pm}$-boson scattering, but could have a much higher cutoff. One can see the Higgs sector as the UV completion of the SM without the Higgs, which provides the longitudinal components of the massive gauge bosons in a renormalizable way. This (or another) sector *has to* complete the SM at scales $\lesssim 1$ TeV, which is a convincing argument to build a collider just for that energy range. If there is no Higgs-boson significantly below a TeV, the SM breaks down at a TeV.

Moreover, the mass of such a Higgs boson should also be stabilized with respect to quantum corrections which might result in further interesting physics around the TeV scale, see Section 1.2.1. In the following, we will assume the existence of a Higgs-like scalar sector that provides masses for the electroweak gauge bosons and fermions, given all its successful properties, and the virtues due to the resulting gauge invariance. We assume that the possible new physics will complete the SM without making a (sub) TeV scale Higgs sector unnecessary for the proper behavior of the theory. It is mandatory trying to explore this important sector of particle physics. As mentioned, it is possible that BSM physics relies on a standard Higgs sector, but changes its properties quite dramatically. Thus, it is very important to study Higgs physics also in BSM scenarios, to be prepared for those changes.

1.1.6 Problems and Open Questions in the SM - the SM as an EFT

Up to now we have discussed many successful predictions of the SM and the gauge principle. It describes nature extremely well up to current collider energies. Despite all these agreements, there are compelling arguments suggesting that there is physics beyond the SM. Some of these we have already sketched before. First of all, the SM does not include a quantum theory of gravity, which is expected to become important at the Planck scale $M_{\rm Pl} \sim 10^{19}$ GeV, and thus seems not to be valid in the very early universe. However, if *e.g.* a scenario of fixed point gravity leads to a harmless high energy behavior of gravity, the SM, augmented with such a theory of gravity, could be in principle UV complete without the need of new particles (if the Higgs boson will be found in the appropriate mass range, see Section 1.1.2).

A striking argument for the existence of BSM physics is given by cosmology. There is evidence for the existence of non baryonic *Dark Matter* which cannot be explained within the SM and triggered a lot of model building, see *e.g.* [18]. Moreover, the running of the coupling constants implies that the SM gauge group could emerge from a single larger gauge group

which is broken down to G_{SM} below the scale of Grand Unification $M_{\mathrm{GUT}} \sim 10^{15}\,\mathrm{GeV}$. However, in the SM the coupling constants slightly miss each other at that scale. The mere fact that they come so close to each other suggests nevertheless the existence of such a GUT. In consequence, NP below M_{GUT} is needed for an appropriate renormalization group running for the couplings to match. In general, the many parameters in the SM (≥ 18), especially within the flavor sector, call for a more unified description. In addition to the already mentioned strong CP problem there is another even more severe problem with a parameter (of gravity) being unnaturally close to zero, which cannot be understood within the framework of a combined theory of general relativity and the SM. The so-called cosmological constant problem is caused by vacuum fluctuation corrections in quantum field theory, which drive the coefficient of the allowed renormalizable $D = 0$ operator in $\mathcal{L}_{\mathrm{SM}}$ to values of at least $\rho_\Lambda \equiv g_0 \sim m_t^4$, about 55 orders of magnitude above the experimental value, which is in the range of some meV^4.[6] Furthermore, as stated in Section 1.1.3, the SM is not able to account for the right amount of CP violation in order for baryogenesis to work. The isotropy, homogenity and flatness of the visible universe also calls for an explanation, like inflation, triggered by a BSM field - the inflaton. For a review see [95]. However, there are also ideas to generate inflation with the help of the SM Higgs boson [96], restricting its possible mass to $m_h \in [126, 194]\,\mathrm{GeV}$ [97]. Let us finish this first collection of theoretical and cosmological arguments with some fundamental questions, not answered within the SM.

What causes the representations of the fields to be like given in the SM?

Why are there three generations of fermions, just distinguishable by their masses?

Why is the gauge symmetry group given by G_{SM} and broken by a scalar $SU(2)_L$ doublet?

Why are the charges quantized in a certain way (see in this context [98])?

What causes the mass parameter $-\mu^2$ in the Higgs Potential in (1.19) to become negative?

There exist many more questions like that and even more fundamental ones, *e.g.* about space time. There is a class of theories that has the ambition to solve all these puzzles, see Section 2.1. However, these theories have little predictive power at low energies. The existence of non-zero neutrino masses can already be seen as BSM physics, but, as mentioned before, can easily be included into the SM, see also below. Two important issues related to hierarchies and not addressed in the SM will be discussed in more detail below in Section 1.2 - the large and radiatively unstable discrepancy between the electroweak and the Planck scale (the gauge hierarchy problem, which is not a problem *of* the SM) as well as the non-understood hierarchies within the fermion masses and mixings. Especially the first issue caused a big portion of the model building activity in the last decades. Both of them can be addressed in RS models, which provides a convincing motivation for studying the phenomenology of these models in detail. In addition, it is also possible to address further of the aforementioned puzzles in this setup, as we will comment on later.

In the sector of (precision) measurements there are several $\gtrsim 1\sigma$ effects which do not come unexpected when many observables are measured. However, worth mentioning are deviations in CP violating observables, like the discrepancy of nearly 4σ in the like-sign dimuon charge asymmetry in semileptonic b-hadron decays, A_{SL}^b [99] or the deviation of around 2σ in the combined CDF and DØ measurement in the $(\beta_s^{J/\psi\phi}, \Delta\Gamma_s)$–plane [100, 101], see Section 5.2.3.[7]

---

[6] Assuming contributions of Planck scale physics makes the problem even worse and amounts to a difference of about 120 orders of magnitude.

[7] Note that the brand new LHCb measurement does not seem to confirm this deviation [102].

Moreover, a deviation between theory and experiment of about 3σ has been observed in the branching fraction for $B^{\pm} \rightarrow \tau^{\pm}\nu$ decays [88]. A tension of about 2σ has been found between exclusive and inclusive determinations of V_{ub} [103] (see also [104]). In addition, the forward-backward asymmetry in top-quark pair-production $(A^t_{FB})^{p\bar{p}}$, measured at Tevatron [105, 106, 107], shows a deviation of similar size, see Section 5.1.4. Finally, there are the already stated discrepancy of nearly 3σ in $A^{0,b}_{FB}$ at the Z pole, see Section 5.1.3 and the (3-4) σ deviation in the anomalous magnetic moment of the muon a_{μ} [108], see Section 5.1.5. It is interesting that the largest effects seem to be present in observables involving the heavier fermion generations (a_{τ} is only poorly measured). A framework in which such a feature arises naturally, is the RS setup. We will discuss many of the aforementioned observables in these models and address the question if they can account for some of the measured deviations *quantitatively*, while still being in agreement with other important precision tests. Let us finally mention the recent anomaly in the invariant mass distribution of two-jet final states at the Tevatron, produced in association with a $W^{\pm}$-boson. The excess at (120-160)GeV, seen by CDF, resulted in many attempts to explain this bump in BSM scenarios, but it could also be explained by SM physics, due to the treatment of the single-top-quark background [109, 110].

Let us stress again that, despite these tensions and the theoretical arguments for NP given before, the SM still works extremely well up to at least the electroweak scale M_{EW}. In the light of the plethora of its successful predictions, the SM, with its peculiarities, should at least be seen as (part of) the low energy limit of the theory that will replace it. Such a theory most probably exists, given the sum of all the striking hints and shortcomings of the SM discussed before. Note that many arguments hint at BSM physics around the TeV scale, most notably the gauge hierarchy problem, but also for example the so called WIMP miracle, *i.e.*, the fact that a *weakly* interacting massive particle with a mass around the TeV scale just leads to the correct relic abundance to account for the Dark Matter in the universe, see *e.g.* [111].

When going beyond the SM, one has to give up some assumptions that lead to its construction. One of the easiest things to do is just to add further matter content. One can also change the (gauge-)symmetry group, add internal global symmetries, or add scalars, always taking care that at low energies the agreement with experiment is not spoiled. This is generally achieved by assuming the new particles to be heavy or having small couplings to the SM particles. There is a plethora of those models, like four-generation models, see-saw models featuring *e.g.* right handed neutrinos with large Majorana masses, Z' models, $SU(2)_L \times SU(2)_R$-symmetric models, GUTs, Peccei-Quinn models, "dark forces", two-Higgs-doublet models, and many more. Most of them try to solve the one or the other problem of the SM or aim on being theoretically more appealing. Some are just possibilities which are not excluded yet. When thinking about further options, it does not seem sensible to abandon the very successful gauge principle - its merits and the resulting problems in giving up this principle have already been examined before. It is possible to think about changes related to space-time symmetries. However, as special relativity is very well tested, we want to keep Poincaré invariance. One could anyhow try to extend the given Lie-algebra of symmetry generators, keeping those of the Poincaré group as well as internal generators, by involving new Lie-algebra generators related to space-time symmetry in a non-trivial way. Due to the *Theorem of Coleman and Mandula* [112] this is (under very general assumptions, like analyticity and non-triviality of the S-matrix as well as the presence of a mass gap) however not possible. Nevertheless, the theorem leaves a little "loophole" since it only talks about Lie-algebras

(with bosonic generators). Giving up this assumption, there is a single class of extensions of the trivial direct product of [space-time(=Poincaré)]⊗[internal symmetries] by employing so-called Lie-superalgebras (with fermionic symmetry generators which fulfill *anti*-commutation relations). Due to the theorem of Haag, Lopuszanski and Sohnius (HLS) [113] the most general (super)algebra of symmetry generators, that can combine states with different spin, is the so-called supersymmetry algebra, see Section 1.2.1. Another radical possibility would be to give up the concept of fundamental point-like constituents, see Section 2.1. This leads to UV finite results without the need of regularization, a very attractive feature for a UV completion of the SM. Other approaches just assume that some of the SM particles, like the Higgs boson, are composite states of elementary particles (see Section 1.2.1). Others extend the concept of particles by introducing so-called unparticles. These are states that arise as low energy degrees of freedom from a conformal sector weakly coupled to the SM [114]. They have non-integer scaling dimensions, leading to a spectral density depending like a fractional power on momentum. However, it was shown that theories like QCD can produce spectral densities for quarks and gluons that are virtually indistinguishable from those of unparticles [115]. We will stop the list here, however many more (more or less exotic) ideas like that are on the market.

From the phenomenology side, we have already explored several *constraints on the NP*. It is expected to have a highly non-generic flavor structure and new CP violating effects. In addition it ought to possess a Dark Matter candidate. Beyond that, it should address the gauge hierarchy problem as well as the fermion hierarchies, see Section 1.2. Let us mention that this (rough and not complete) list of requirements can be fulfilled in the RS framework, as we will see below. From now on we will consider the SM, including higher dimensional operators, as the low energy EFT of a more fundamental theory. At low energies, we consider the whole Lagrangian (1.6), truncated at a certain operator-dimension, which we now write more explicitly as

$$\mathcal{L}_{\text{eff}} = \mathcal{L}_{\text{SM}} + \sum_i \frac{C_i^{(5)}}{M} \mathcal{Q}_i^{(5)} + \sum_i \frac{C_i^{(6)}}{M^2} \mathcal{Q}_i^{(6)} + \cdots. \tag{1.64}$$

Here, $C_i^{(D)}$ are the (running) Wilson coefficients of the operators $\mathcal{Q}_i^{(D)}$ of mass dimension D. They contain the information about the high energy physics that has been "integrated out", as introduced in Appendix A.4. Let us have a first look at possible higher dimensional operators [116] and see how they give a handle on BSM physics. At the level of $D = 5$ there is just one possible gauge invariant term that can be constructed out of the SM fields. It reads

$$\mathcal{L}_{\text{eff}} \supset \frac{\lambda_{ij}}{\Lambda_L} (E_i \Phi)^T (E_j \Phi), \tag{1.65}$$

where the couplings λ_{ij} are assumed to be of $\mathcal{O}(1)$. This term leads (after EWSB) to a Majorana mass term for the left handed neutrinos with $m_\nu \sim v^2/\Lambda_L$. It breaks L by 2 units. Note that the scale of neutrino masses $m_\nu \approx 0.1\,\text{eV}$ indicates a fundamental scale $\Lambda_L \sim 10^{15}\,\text{GeV} \sim M_{\text{GUT}}$, around the GUT scale. Neutrino masses could be a first hint to a new energy scale in physics, below M_{Pl}. The SM as an EFT can thus account for these masses without introducing new fields at low energies. At the same time, assuming a large

cutoff scale around M_{GUT}, they are naturally tiny. This would have to be put in by hand for the case of pure Dirac mass terms with a right handed neutrino by assuming an unnaturally small $y_\nu \sim 10^{-12}$. Note that the $D = 5$ term (1.65) could arise from a UV completion of the SM via the see-saw mechanism, for a review see *e.g.* [117]. At the level of $D = 6$ operators, proton decay is induced by B and L violating terms like

$$\mathcal{L}_{\mathrm{eff}} \supset \frac{1}{\Lambda_B^2} \epsilon_{def} ((\bar{u}_R^d)^c d_R^e)((\bar{u}_R^f)^c e_R) \,, \tag{1.66}$$

where d, e, f are $SU(3)_c$ indices. These operators (which could be induced *e.g.* by a GUT) mediate processes like $p \to e^+ \pi^0$ which leads to the bound from Super-Kamiokande (see Section 1.1.4 above) of $\Lambda_B \gtrsim (10^{15} - 10^{16})\,\mathrm{GeV}$. The SM as an EFT with a large cutoff allows for interesting effects, *e.g.* the breaking of its global symmetries, and at the same time explains the tininess of these effects, which is needed to be not in conflict with observation. However, lowering the cutoff leads to problems, because then generically B- and L-violating operators will not be sufficiently suppressed to be in agreement with observation, given there is no symmetry which forbids them, see sections 2.2.1 and 3.1.5 in the context of BSM models.

For the time being, let us assume that the NP that will be possibly found well below the GUT scale does not induce the operators examined above. Still, measurements in flavor physics performed at low energies can constrain the scale or structure of BSM physics quite significantly. Remember that the flavor sector of the SM works impressively well. The facts that charged current interactions are universal (the CKM matrix is unitary) and that FCNCs are highly suppressed due to the GIM mechanism agrees with results from experiments. However, this flavor structure is special and NP models will generically not reproduce the same structure. To estimate the expected effects, consider $D = 6$ four-quark operators like

$$\mathcal{L}_{\mathrm{eff}} \supset \frac{q_1 \bar{q}_2 \, q_3 \bar{q}_4}{\Lambda_{\mathrm{flavor}}^2} \,, \tag{1.67}$$

where q_i can be arbitrary quarks, which however have to feature charges that sum up to zero. Measurements of meson mixing and CP violation can strongly constrain the scale $\Lambda_{\mathrm{flavor}}$ for generic $\mathcal{O}(1)$ dimensionless couplings and lead to the estimate (see *e.g.* [118])

$$\Lambda_{\mathrm{flavor}} \geq 10^4\,\mathrm{TeV} \,. \tag{1.68}$$

Thus, if there are no symmetries that account for a special flavor structure, from this estimate we expect new physics not to be lighter than $10^4\,\mathrm{TeV}$! However, as we will go into in Section 1.2.1, the gauge hierarchy problem indicates NP at a scale $\Lambda_{\mathrm{UV}} \sim 1\,\mathrm{TeV}$. This suggests that the NP cannot have a generic flavor structure which leads to assumptions like *e.g.* MFV (which however does not provide an *explanation* of this structure). This problem is called the *new physics flavor problem*. Note that a very strong constraint comes from the CP violating parameter ϵ_K in the Kaon system, see Section 5.2.3. We will come back to these issues later in the context of RS models.

1.2   Hierarchies as a Motivation for Physics Beyond the Standard Model

Many models given above address the one or the other unsolved problem, like *e.g.* the Peccei-Quinn theory solving the strong CP problem, but no testable theory known so far addresses all open questions. Some theories solve several problems at once, making them suitable candidates for completing the SM in a more unified way. In the following we focus on two important problems mentioned before, related to hierarchies, and briefly introduce models that are able to address at least one of these issues. The RS model can address both and will be introduced in detail in Chapter 3.

1.2.1   The Gauge Hierarchy Problem and Possible Solutions

The infamous gauge hierarchy problem has caused lots of attempts to construct models which are able to resolve it. This problem, in its modern formulation, arises, if we consider the SM as an EFT, UV completed by some NP below M_{Pl} (*e.g.* by a GUT). In the last section we have shown that there are many good reasons for such an assumption. The gauge hierarchy problem is caused by the enormous hierarchy of 17 orders of magnitude between the electroweak and the Planck scale, see the Figure on the left of this page. It is difficult to understand why the weak scale should be so much lower than the Planck scale, $M_{\mathrm{EW}} \ll M_{\mathrm{Pl}}$, or equivalently, why gravity is so much weaker than the electroweak force. After studying the details of the problem, we will introduce the most famous models that try to address it.

The Problem

E [GeV]

10^{19} — $M_{\mathbf{PL}}$

10^{15} — $M_{\mathbf{GUT}}$

? $M_{\mathbf{NP}}$

LHC

10^2 — m_h

From the arguments of Section 1.1.2 we expect the mass of the Higgs boson, setting the electroweak scale, to be very light compared to the Planck scale

$$m_h \sim 100\,\mathrm{GeV} \ll M_{\mathrm{Pl}}. \tag{1.69}$$

It is not difficult to account for such a mass on the tree level by choosing the Lagrangian parameters accordingly. However, the Higgs boson, being a fundamental scalar particle, has a priori no protection mechanism for its mass via symmetries. From an EFT point of view, one would naively expect the super-renormalizable (UV sensitive) $D = 2$ operator h^2 in $\mathcal{L}_{\mathrm{SM}}$ to have a coefficient of the order of the cutoff of the QFT, say

$$m_h^2 \sim M_{\mathrm{Pl}}^2. \tag{1.70}$$

It is now difficult to understand why the Higgs boson should be light, like indirect experiments and theory tell us. The only possibility to avoid this puzzle would be to introduce a mechanism which saves the Higgs mass from corrections above a certain scale.

That such large corrections to the mass are indeed created at the quantum level can be seen by studying the loop diagrams shown in Figure 1.11. The diagram on the left results in a quadratically divergent correction $\sim \Lambda_{\mathrm{UV}}^2$ (in cutoff regularization) to the Higgs-mass squared (see *e.g.* [119]) of

$$\Delta m_h^2 = \frac{|y_f|^2}{8\pi^2} \left[-\Lambda_{\mathrm{UV}}^2 + 6\, m_f^2 \ln \frac{\Lambda_{\mathrm{UV}}}{m_f} - 2\, m_f^2 \right] + \mathcal{O}(\Lambda_{\mathrm{UV}}^{-2}) , \qquad (1.71)$$

for every fermion with mass m_f and Yukawa coupling y_f running in the loop. For simplicity, we have assumed the fermion to be heavy, so that we can neglect the external Higgs momentum. The diagrams on the right, corresponding to scalar contributions (with mass m_S, trilinear coupling $v\lambda_S$, and quartic coupling λ_S) in the loop, also lead to quadratically divergent corrections of

$$\Delta m_h^2 = \frac{\lambda_s}{16\pi^2} \left[-\Lambda_{\mathrm{UV}}^2 + 2\, m_S^2 \ln \frac{\Lambda_{\mathrm{UV}}}{m_S} \right] - \frac{\lambda_s^2}{16\pi^2} v^2 \left[-1 + 2\ln \frac{\Lambda_{\mathrm{UV}}}{m_S} \right] + \mathcal{O}(\Lambda_{\mathrm{UV}}^{-2}) . \qquad (1.72)$$

Note that there are in addition contributions of the gauge bosons $\Delta m_h^2 \sim (3g^2 + g'^2) \Lambda_{\mathrm{UV}}^2$. [8] It is in principle possible to renormalize the theory (by adding counterterms to cancel the UV sensitive terms that would diverge in the limit $\Lambda_{\mathrm{UV}} \to \infty$) in such a way as to arrive at a Higgs mass around the electroweak scale, despite the quadratic UV sensitivity. However, assuming M_{Pl} as the scale of the corrections, this would need incredible fine-tuning of the parameters at the level of 1 in 10^{34}, and seems very unnatural.

Note that in order to arrive at this conclusion, one does not have to assign a significance to the quadratic divergences, which could be related to non understood high energy behavior of the theory. The crucial point is that all the heavy particles in the QFT, running in the loop, give a contribution to m_h^2 proportional to their mass squared and not coming with Λ_{UV}^2, see (1.71) and (1.72). In consequence one still has a physical correction to the Higgs mass, which is set by the heaviest particle running in the loop. In the following we assume the existence of heavy BSM physics, indicated by M_{NP} and M_{GUT} in the Figure on the left of the last page, for which we have collected very good arguments. Thus, if one believes for example in a GUT, one would expect the Higgs mass to reside at the scale

$$m_h^2 \sim M_{\mathrm{GUT}}^2 , \qquad (1.73)$$

and not around the mass scale of the electroweak gauge bosons. One would expect that in an effective Lagrangian like (1.64)

$$C_h^{(2)} = \mathcal{O}(1) , \quad \text{with } M^2 = M_{\mathrm{GUT}}^2, \qquad (1.74)$$

and not $C_h^{(2)} \ll 1$. Arriving at a Higgs mass around the electroweak scale would require a cancellation between the bare Lagrangian Higgs-mass parameter and the loop corrections to it, which are now both expected to be around $10^{30}\,\mathrm{GeV}^2$, at a level of 1 in 10^{26}. Let us stress that, seen in this way, the gauge hierarchy problem is not a problem of the SM but rather

---

[8]An alternative method to quickly obtain the quadratically divergent corrections to the scalar potential, without calculating Feynman diagrams, is to compute the Coleman-Weinberg potential [120], see also [35].
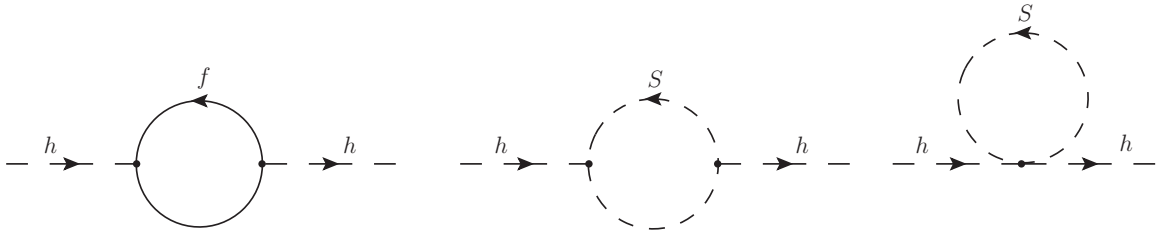
Figure 1.11: One-loop contribution to the Higgs-boson mass-squared from fermion loops (left) and scalar loops (middle, right).

a problem that comes about when extending the SM by new heavy particles - an issue that every extension of the SM has to face at a more or less severe level. Although not logically excluded, a desert without NP between the electroweak and the Planck scale seems not very likely, given all the arguments collected in Section 1.1.6. Also in such a scenario one still would have an unexplained large (though radiatively stable) discrepancy between two fundamental scales. In contrast to fundamental scalars, gauge bosons or chiral fermions do not have a problem in keeping a low mass. Without spontaneous symmetry breaking the chiral fermions of the SM as well as the gauge bosons would be massless. Before EWSB, they do not have mass terms, corresponding to relevant operators. Those operators are forbidden by the gauge symmetry. After EWSB, the (hidden) symmetry saves those particles from corrections to their masses above the scale of EWSB of $v \sim \mathcal{O}(100\,\mathrm{GeV})$. Thus it seems natural that the massive gauge bosons have masses just around that value. This argument can also be related to the fact that a massless spin-1 particle has two degrees of freedom and there is no continuous transformation to a massive boson with three degrees of freedom. In the Higgs mechanism, this additional longitudinal polarization is provided by a goldstone boson. However, without such a mechanism, massless gauge bosons will not receive a mass at the loop level. The same is true for massless (chiral) fermions, which only have one helicity. Note that corrections to the fermion masses are proportional to their own masses and only logarithmically divergent $\Delta m_f \sim m_f \ln(\Lambda_{\mathrm{UV}}/m_f)$. However, for the spin-0 Higgs boson, there is a priori no such argument, which leads to the expectation (1.70).

The gauge hierarchy problem hints strongly at NP at the TeV scale ($\Lambda_{\mathrm{UV}} \lesssim 4\pi M_{\mathrm{EW}} \sim 1\,\mathrm{TeV}$) that solves this issue. On the other hand, the good agreement of the SM with experiment in many details seems not to suggest new physics at such low scales. For example, electroweak precision tests rather indicate that generic new physics is not to be found below several times this scale ($\Lambda_{\mathrm{UV}} \gtrsim$ a few TeV), needless to mention constraints from Kaon mixing. As with a cutoff for the SM at such a scale, one ends up with a fine tuning of some per cent, a "little hierarchy problem" could remain after a possible solution to the large gauge hierarchy problem. As we will see later, much effort is made to address this issue in BSM models and to allow for lower NP scales. Excitingly the LHC just starts to approach the TeV scale and the gauge hierarchy problem lets us expect further discoveries, in addition to that of the sector of EWSB. The LHC will hopefully also reveal the sector that stabilizes the mass of the fundamental scalar Higgs boson (if present) against quantum fluctuations.
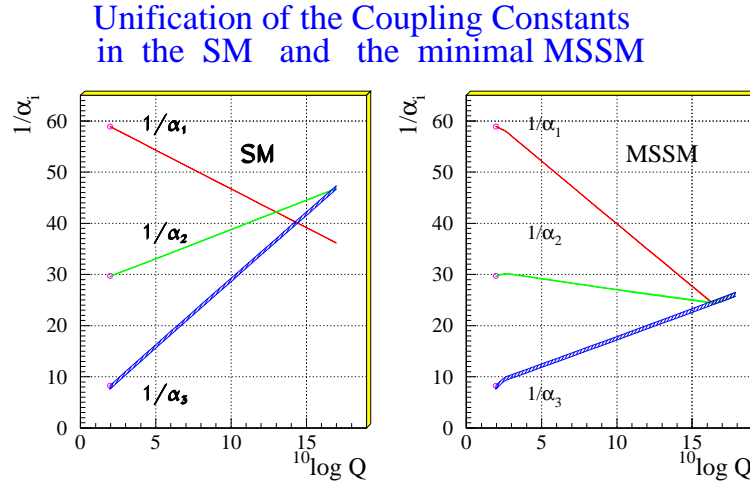
Figure 1.12: Renormalization group evolution of the gauge couplings in the SM as well as in the MSSM. Figure from [126], with permission from the author. See text for details.

Possible Solutions: From SUSY to Classicalization

The most popular ideas to address the gauge hierarchy problem are to invoke a new symmetry (to protect the Higgs mass), to introduce a new strongly coupled sector (with the scalar EWSB sector consisting of bound states of this new interaction) or to lower the cutoff of the theory (by extending space-time). Some models relate several of these classes to each other. Let us start with recalling the problematic contributions to the Higgs mass due to fermion and boson loops, see (1.71) and (1.72). Given the absence of a symmetry to protect the Higgs mass, these terms contribute to the gauge hierarchy problem. Consider the corrections of N_f fermions and those due to N_S scalar particles. If we now *assume* $y_f^2 = -\lambda_S$ and $N_S = 2N_f$ and add up both contributions (of particles with different spin-statistics) we arrive at [119]

$$\Delta m_h^2 = \frac{y_f^2 N_f}{4\pi^2} \left[(m_f^2 - m_S^2) \ln \frac{\Lambda_{\mathrm{UV}}}{m_S} + 3\, m_f^2 \ln \frac{m_S}{m_f} \right] + \mathcal{O}(\Lambda_{\mathrm{UV}}^{-2}). \qquad (1.75)$$

We see that the problematic quadratic divergences have vanished, seemingly ameliorating the gauge hierarchy problem. However the corrections to the Higgs mass are still proportional to the mass of the heaviest particle running in the loop. If in addition $m_f = m_S$ holds, the correction to the Higgs mass vanishes completely (note that all that is not possible within the SM). Thus, if there would be a symmetry that would lead to $y_f^2 = -\lambda_S$, $N_S = 2N_f$, and $m_f = m_S$, the gauge hierarchy problem would be solved (given a similar cancellation takes place for *all* contributions to the Higgs mass, including gauge boson corrections). Such a symmetry exists indeed and is just the so-called **supersymmetry**, introduced in Section 1.1.6, which allows to extend the spin-considerations of Section 1.2.1 to scalar particles. Interestingly, this new symmetry, relating bosonic to fermionic degrees of freedom, is the only possibility to generalize the direct product of [space-time]⊗[internal symmetries], along the lines of the HLS theorem as discussed in 1.1.6. For reviews on SUSY and a list of references see *e.g.*

[121, 122, 123, 124].

A SUSY Lagrangian is invariant (up to a total derivative) under SUSY transformations, mediated by fermionic sets of generators Q_α^i. These transform fermions into bosons (with the same internal quantum numbers) and vice versa. Here, α is a spinor index, and the N possible sets of generators are labeled by i. In the following we will consider $N = 1$ SUSY, corresponding to a single set of SUSY generators. Schematically, one has

$$Q_\alpha|\text{fermion}\rangle^\alpha = |\text{boson}\rangle, \quad Q_\alpha|\text{boson}\rangle = |\text{fermion}\rangle_\alpha. \tag{1.76}$$

The generators of the $N = 1$ super Poincaré algebra fulfill the relations

$$\begin{aligned}
[Q_\alpha, P^\rho] &= 0 \\
\{Q_\alpha, \bar{Q}_{\dot{\beta}}\} &= 2\,(\sigma^\rho)_{\alpha\dot{\beta}}\,P_\rho \\
[M^{\rho\sigma}, Q_\alpha] &= -i\,(\sigma^{\rho\sigma})_\alpha^{\ \beta}\,Q_\beta \\
\{Q_\alpha, Q_\beta\} &= \{\bar{Q}_{\dot{\alpha}}, \bar{Q}_{\dot{\beta}}\} = 0\,,
\end{aligned} \tag{1.77}$$

where Q_α and $\bar{Q}^{\dot{\alpha}} = (Q^\alpha)^\dagger$ are Weyl spinors, corresponding to the upper and lower components of a four-component Dirac spinor. The indices $\alpha, \dot{\alpha}$ can be raised and lowered with the totally antisymmetric tensor $\epsilon_{\alpha\beta}$ [123] and $\sigma^{\mu\nu} = i/2[\gamma^\mu, \gamma^\nu]$. The generators P^ρ and $M^{\rho\sigma}$ correspond to the four-momentum and the generalized angular momentum. The fields of a supersymmetric theory are grouped into irreducible representations of the SUSY algebra, so-called *supermultiplets*. If SUSY was an exact symmetry, as an immediate consequence the SUSY partners would have exactly the same mass as the corresponding SM fields. As such a scenario is clearly excluded by experiment, SUSY has to be broken. This is in general achieved by introducing super-renormalizable (soft) SUSY breaking terms. However, the mass scale of the SUSY partners of the SM particles M_{SUSY} should not be much larger than the TEV scale as otherwise the gauge hierarchy problem would be introduced again to a certain amount. In consequence, if SUSY solves the gauge hierarchy problem, we expect to find it at the LHC. In the following, we explore briefly some phenomenological consequences of the minimal supersymmetric extension of the SM (MSSM). This minimal extension features a fermionic partner for each SM gauge boson, as well as a bosonic partner for each SM (Weyl) fermion, such that in the end, as for every SUSY model, the number of fermionic and bosonic degrees of freedom is equal.

As mentioned before, SUSY models require the existence of more than one Higgs doublet. The MSSM features two Higgs doublets with 5 physical Higgs bosons (after EWSB) - two neutral CP even h, H, a CP odd one A, and two charged $H^\pm$. At the tree level the MSSM leads to the constraint

$$m_h < m_Z|\cos(2\beta)| \tag{1.78}$$

for the mass of the lightest neutral Higgs boson, where $\tan\beta = v_u/v_d$ and v_u, v_d are the VEVs belonging to the Higgs doublets giving masses to up and down type quarks, respectively. Although in the MSSM the LEP exclusion limit can be weakend (depending on $\tan\beta$) [119], this constraint would put the MSSM into some trouble. However, loop corrections can lift the limit to

$$m_h \lesssim 135\,\text{GeV}\,, \tag{1.79}$$

assuming that all sparticles that can contribute to m_h have masses below a TeV [119]. Note that the properties of the lightest Higgs boson of the MSSM are similar to the SM Higgs in the decoupling regime (where $m_A \sim \mathcal{O}(\text{TeV})$), however, outside this regime important differences can arise. For example, the couplings to bottom quarks can be strongly enhanced in the case of large $\tan\beta \gg 1$. There is still a puzzle in the Higgs sector of the MSSM, the so-called $\mu-$problem. This corresponds to the fact that it is difficult to understand why the magnitude of the SUSY preserving squared-mass in the Higgs potential should be in the region of $(100 - 1000)\,\text{GeV}$, which coincides with the scale of the (unrelated) soft breaking terms, as required by phenomenology, and not for example at the Planck scale. Some extensions of the minimal setup try to solve this problem by introducing the μ term as the VEV of a new field. Moreover, the number of parameters in the MSSM is significantly increased with respect to the SM, especially due to the SUSY breaking sector. In total, the MSSM possesses ~ 120 new parameters with respect to the SM.

Note that, beyond solving the gauge hierarchy problem, the MSSM solves several of the problems dealt with in Section 1.1.6. First of all, let us mention that the MSSM features a so-called R-parity in order to prevent the presence of B and L violating couplings in the Lagrangian, where $R = (-1)^{2s+3B+L}$ and s is the spin of the particle the operator acts on. This parity leads to the fact that SUSY partners of the SM particles can only be produced in pairs. In particular, the lightest supersymmetric partner (LSP) will be stable. In many cases, the LSP corresponds to the lightest of the so-called neutralinos, and is massive, weakly interacting and electrically neutral. This provides a good candidate for the *Dark Matter* of the universe within the MSSM. Moreover, the modification in the running of the gauge couplings due to the SUSY partners provides the possibility for them to meet each other to good accuracy around the scale M_{GUT}, allowing for a *grand unification* within the MSSM [125]. This fact is illustrated in Figure 1.12, where the evolution of the gauge couplings $\alpha_1 \equiv 5/3\, g'^2/(4\pi)\,, \alpha_2 \equiv g^2/(4\pi)\,, \alpha_3 \equiv g_s^2/(4\pi)$ is shown. Above the mass scale of the SUSY partners $M_{\text{SUSY}} \sim 1$ TeV, which has been fitted such that unification is possible, the running is modified with respect to the SM. The factor $5/3$ is needed for the correct normalization at the unification point. In addition, the MSSM, allows for *radiative electroweak symmetry breaking.* In the SM, the Higgs mechanism is only a description of EWSB but offers no explanation why it occurs. In contrast to the SM, where one has to put in the negative squared mass for the Higgs doublet by hand, the MSSM can generate the necessary conditions for a potential to result in electroweak symmetry breaking radiatively, at a certain scale, via renormalization group evolution. It is interesting that the MSSM solves all these puzzles, without being invented for that purpose. It was rather built as the most general extension of the Poincaré algebra, as explained before. Finally note that, if SUSY is introduced as a local symmetry, it naturally incorporates gravity (*supergravity*). For more details, *e.g.* on the SUSY breaking mechanism, related flavor issues or collider signatures see the literature cited before. If the SUSY-breaking mechanism is not flavor blind, SUSY models will generically have problems with flavor constraints, requiring an additional concept like MFV, see Section 1.1.6. For details on Higgs physics in SUSY see [119].

The next type of models that can address the gauge hierarchy problem are those that do not feature an elementary scalar and thus avoid the fine tuning problem. An example of this class of models is **technicolor** [127, 128]. Here, the scalar degrees of freedom responsible for the masses of the weak gauge bosons are realized as bound states of new massless fermions

(techni-fermions), that are charged under a new QCD-like $SU(N)$ gauge group as well as under the electroweak gauge group of the SM. The new strong interaction is asymptotically free at high energies, but assumed to be confining at M_{EW}. In analogy to QCD, chiral symmetry breaking is triggered and the resulting Goldstone bosons (techni-pions), corresponding just to bound states of the techni-fermions, provide the longitudinal degrees of freedom for the electroweak gauge bosons. In consequence, EWSB is realized dynamically. Importantly, it is possible to reproduce the relation (1.29) to leading order in technicolor models. Note however, that the simplest models are ruled out by electroweak precision tests, due to large corrections to the S parameter [64]. For a review, also about newer developments in the sector, see [129].

Similar ideas are used in **Little Higgs** theories [130, 131, 132, 133], where the Higgs boson itself is realized as a (pseudo-)Goldstone boson of a spontaneously broken global symmetry. This symmetry is also assumed to be broken explicitly (making the Higgs boson massive), but only by the interplay of at least two coupling constants. This *collective symmetry breaking* leads to a vanishing of the quadratic divergences in the Higgs mass at one loop. If one of these couplings does not contribute, the Higgs boson mass is zero due to the *shift symmetry* of the Goldstone boson. Little Higgs theories are weakly coupled effective field theories with a cutoff scale of the order of $\Lambda_{\mathrm{UV}} \sim 10$ TeV. They stabilize the hierarchy between this cutoff (which could be identified with a scale suggested by electroweak precision tests) and the electroweak scale M_{EW}. Above the cutoff, these theories have to be UV completed.

Such a completion could feature a breaking of the global symmetry by strong dynamics, resulting in a **composite Higgs** boson [134]. In this general class of theories the Higgs-boson mass is protected by the fact that at a certain scale it will not behave as an elementary particle anymore and a form factor will regularize the UV behavior. For interesting relations with the models studied in this thesis see [135, 136, 137].

Another recent approach that provides (amongst other interesting possible consequences) an idea how the gauge hierarchy problem could be solved, assumes the existence of **classi-calization** [138] at large energies. In this approach, the collision of two particles with a momentum transfer larger than the characteristic scale M_* of the (non-renormalizable) theory will cause the formation of an extended classical configuration of a classicalizer field, with radius r_*, in analogy to a black hole of gravity, UV completing the theory. As a consequence, the short distance behavior does not have to be specified to know the high energy behavior. The radius r^* grows with the energy localized in the system. If the Higgs scalar is sourced by energy-momentum of the SM particles, *e.g.* by an operator

$$\Phi^\dagger \Phi \, T^\mu_\mu \,, \tag{1.80}$$

where T^μ_μ corresponds to the trace of the energy-momentum tensor of the SM fields, it could just act as such a classicalizer [138]. It would develop a classical configuration above a scale M_*, which could solve the gauge hierarchy problem.

When trying to construct solutions to the gauge hierarchy problem, we have so far only talked about changing the SM along the lines discussed in 1.1.6. We have not explored another possibility yet, which would change quite drastically the picture of the universe we have so far. When looking at the world around us and feeling time passing by, we seem to know, that we are living in four space-time dimensions, an implicit assumption we have made before. When talking about Poincaré invariance, we were thinking about four-dimensional Minkowski
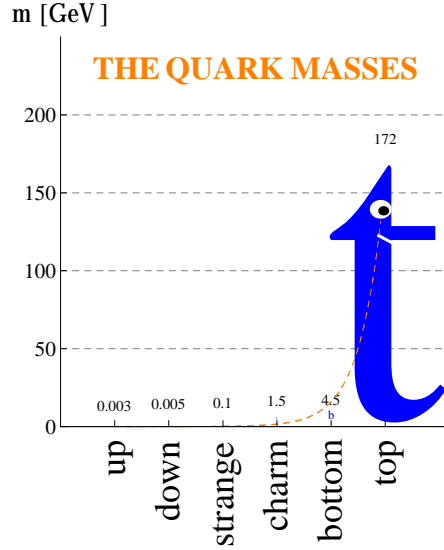
Figure 1.13:   Hierarchies in the quark masses.

space-time. However, already from high-school physics we know that our eyes or the human senses are not sufficient as measuring instruments. In the next chapters we will introduce models that involve *extra dimensions* and that are not in immediate conflict with observation. Some of these models, in particular RS models, offer an alternative possibility to solve the gauge hierarchy problem. Beyond that, they have further very interesting features.

1.2.2   Hierarchies in the Fermion Sector

In addition to the large hierarchy between the electroweak and the Planck scale, there are also non-understood hierarchies in the flavor sector of the SM. The masses and mixings of the SM fermions exhibit large ratios, which can be accounted for within the SM but which cannot be explained by the model. The tiny neutrino masses have already been discussed. However, there are also sizable hierarchies in between the quark masses as well as the charged lepton masses. Moreover, the mixing matrix in the quark sector also is strictly hierarchical, while the one of the lepton sector is not. Let us have a look at the hierarchies in the quark sector more quantitatively.

The quarks of the same charge in the SM are identical in all their properties besides their mass. Here, they exhibit very large ratios of roughly (see Appendix D) [9]

$$m_t/m_c/m_u \approx 100000/500/1 \,, \quad m_b/m_s/m_d \approx 1000/20/1 \,, \tag{1.81}$$

see Figure 1.13. Although the (running) quark masses depend on the energy scale, the hierarchies quoted before are to good accuracy stable with respect to scale variations [139]. The natural value for the scale of the quark masses would be $m \sim v/\sqrt{2}$, corresponding to an $\mathcal{O}(1)$ Yukawa coupling. This expectation is fulfilled only for the top quark. Although the

---

[9]As we are just interested in rough hierarchies, we do not have to worry about the issues in defining the quark masses.

hierarchies (1.81) can be put into the SM, it offers no *explanation* for the question why the masses of its fundamental constituents in the matter sector differ so much from each other.

Also the CKM matrix exhibits strong hierarchies, which are reflected in the expansion in the small Wolfenstein parameter $\lambda \approx 0.23$ (1.59). To LO in each entry

$$|\boldsymbol{V}_{\mathrm{CKM}}| \sim \begin{pmatrix} 1 & \lambda & \lambda^3 \\ \lambda & 1 & \lambda^2 \\ \lambda^3 & \lambda^2 & 1 \end{pmatrix} . \tag{1.82}$$

The fact that the diagonalizations of the up-type and down-type mass matrices lead, to first order, to the same rotation matrices $\boldsymbol{U}_u \approx \boldsymbol{U}_d$ can not be explained within the SM and calls for elucidation.

A model which can address both of these fermion hierarchies, has been presented by Froggatt and Nielsen [139]. Starting from anarchic Yukawa matrices, *i.e.*, matrices with random $\mathcal{O}(1)$ entries with arbitrary phases, the observed hierarchies are generated by assuming the left-handed and right-handed components of the quark fields to have different values for an almost conserved quantum number with respect to an abelian symmetry group $U(1)_F$. This model will be introduced in Section 3.2.3 and we will directly apply its results to the fermion sector of RS models, which, as we will show, feature a similar mechanism. Here, the Froggat-Nielsen mechanism arises automatically, if one puts fermions in the bulk, and no additional structure is needed. So, beyond solving the gauge hierarchy problem, the fermion hierarchies can also be addressed in these models, without the setup having been invented for that purpose.

Chapter 2

Extending Space-Time to Address Hierarchies

In this chapter we will give a survey of how the idea that nature could feature more than four space-time dimensions finally lead to an option to address the gauge hierarchy problem. After a short historical overview, we will review the Arkani-Hamed−Dimopoulos−Dvali model in some detail. This model can be seen as the forerunner of the RS model. Although the approach to address the large hierarchy between the electroweak and the Planck scale is different, it certainly influenced the following developments quite strongly.

2.1 Introduction: Extra Dimensions before ADD

The first serious appearance of the idea that space-time could feature more than four dimensions was due to *Kaluza* [140] and *Klein* [141] in the 1920s. They tried to unify gravity and electromagnetism, the only fundamental forces known at that time, by merging the photon vector field together with the 4D Minkowski metric into a 5×5 metric. However, their idea turned out to be not a correct description of nature, in particular after the discovery of the additional forces and the rise of the electroweak standard model. Moreover, already before, the attempt to quantize the theory lead to serious problems. The ideas of Kaluza and Klein were revived in the 1980s by the advent of *string theory* in its modern form (for a review and further references see *e.g.* [121, 142, 143, 144]). The roots of string theory go back to the 1960s, when Gabriele Veneziano [145] and others tried to use strings to describe the strong interaction. During the first superstring revolution (1984-1989) it was realized that string theory could serve as a fundamental description of nature if it is formulated in 9+1 space-time dimensions. The number of dimensions was set by the need for anomaly cancellation. In the framework of superstring theory, the fundamental ingredients of nature are not point-like particles but one dimensional strings of Planck-length size, characterized by their tension. This leads to a unification of the various different particles of the SM into one type of fundamental "particle", the string. How is it possible that the extra dimensions have not been discovered so far? For not being in conflict with observation these dimensions have to be hidden in some way. This is possible by compactifying them, *e.g.* on a higher dimensional torus (or on a more complicated manifold) with a natural length scale of the order of $M_{\rm Pl}$. One can imagine this additional geometry sitting at every space-time point of 4D Minkowski space-time, as illustrated in Figure 2.1
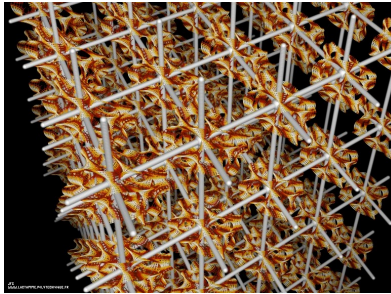
Figure 2.1: Illustration of a compactified higher-dimensional space-time. A Calabi-Yau manifold is attached to every point of the usual 4D space-time. Courtesy of J.-F. Colonna [146].

The second superstring revolution took place in the mid 1990s and was initiated by Edward Witten. He discovered that the different formulations of string theory known at that time (as well as 11D supergravity) are related to each other by dualities and could all be manifestations of the same theory, called M-theory. With the emergence of the concept of branes another option to hide the extra dimensions became available. Open strings, corresponding to SM particles in the low energy limit, have to end on their higher dimensional cousins, the branes. It could thus be possible that the particles we know are confined to live on a 4D sub-manifold of space-time, a 3-brane, see below. It seems to be possible to model the SM spectrum by an appropriate geometry of the extra dimensions. Beyond that, these theories have in principle the ambition to *explain* the presence of a certain gauge group and particle content present in nature and to address all other theoretical questions stated in 1.1.6. In particular they are UV finite due to the non vanishing extension of their fundamental constituents and contain a quantum theory of gravity. In this sense, they can be called theory of everything (TOE) (although it is in principle not possible to prove that a real TOE has been found). Despite their many promising features, string theories also have serious drawbacks. An important issue is that in the original spirit of residing at the Planck scale of $M_{\mathrm{Pl}} \sim 10^{19}\,\mathrm{GeV}$, string theories make (currently) no unique predictions for energies accessible in the near future. The expected excitations of the strings would have masses around M_{Pl}. The mechanism of compactifying the extra dimensions is not yet understood sufficiently. As mentioned before, the geometry of space-time is related to the low energy spectrum. However, it seems that the incredible number of 10^{500} different vacua are possible and thus, if there is no mechanism to chose a special vacuum, the geometry cannot be predicted and neither can the low energy spectrum. It is however possible to interpret a discovery of supersymmetry as a hint for string theory, since it can only be formulated in a supersymmetrized way. This still does not make the model really testable at current collider energies. Moreover, note that string theory is still at the level of quantum mechanics (no second quantization).

This pessimistic picture changed after it was realized that extra (spatial) dimensions could help in solving the gauge hierarchy problem in the late 1990s by Nima Arkani-Hamed, Savas Dimopoulos and Gia Dvali (ADD) [147]. To see how this works, let us recall that the gauge hierarchy problem is due to the fact that the Planck scale is so much bigger than the electroweak scale. An important point is that one deduces the gigantic size of the Planck scale from the enormous weakness of gravity (see footnote 1) $G_N = M_{\mathrm{Pl}}^{-2}$. In terms of the funda-

mental Planck mass $M_{\text{Pl}}^{(d)}$, the gravitational potential between two test masses m_1 and m_2 in d dimensions, has the form

$$V^d(r) \sim \frac{m_1 m_2}{[M_{\text{Pl}}^{(d)}]^{d-2}} \frac{1}{r^{d-3}} \,. \tag{2.1}$$

From measuring the gravitational force one deduces $d = 4$ and determines the Planck scale $M_{\text{Pl}} = M_{\text{Pl}}^{(4)} \sim 10^{19}\,\text{GeV}$. However, it is important to note that Newtons gravitational law has so far only be tested down to length scales of about $50\,\mu\text{m} \sim 250\,\text{eV}^{-1}$ [148].

2.2 From Large Extra Dimensions to Warped Extra Dimensions

The fact that Newton's law, (2.1) with $d = 4$, has by far not been tested up to the same energy scales as the other interactions of nature, not speaking of up to the Planck scale, lead ADD to the idea that the gravitational potential could be changed at small distances r, with however $r \gg M_{\text{EW}}^{-1}$. This allows for the existence of *large extra dimensions*, if only gravity is allowed to propagate into them [147]. How does this work in detail?

2.2.1 Large Extra Dimensions to Address the Gauge Hierarchy Problem

Imagine n extra dimensions, all of size $\sim R$ for simplicity, compactified on a corresponding manifold M_n with volume $\sim R^n$. For distances $r \ll R$, Gauss's law in d dimensions leads just to the gravitational potential (2.1) with $d = n + 4$

$$V^{4+n}(r) \sim \frac{m_1 m_2}{[M_{\text{Pl}}^{(4+n)}]^{n+2}} \frac{1}{r^{n+1}} \qquad (r \ll R)\,. \tag{2.2}$$

However, for distances $r \gg R$ the field lines of gravity will not resolve the extra dimensions, leading to the usual $1/r$ behavior we observe

$$V^{4+n}(r) \sim \frac{m_1 m_2}{[M_{\text{Pl}}^{(4+n)}]^{n+2}} \frac{1}{R^n} \frac{1}{r} \qquad (r \gg R)\,. \tag{2.3}$$

An interesting thing has happened here. If we do not assume the existence of extra dimensions, we would just identify the whole expression

$$M_{\text{Pl}}^{\text{eff}} \equiv [M_{\text{Pl}}^{(4+n)}]^{\frac{n+2}{2}} R^{\frac{n}{2}} \tag{2.4}$$

with the Planck scale (the cutoff of the SM) $M_{\text{Pl}} = M_{\text{Pl}}^{eff} \sim 10^{19}\,\text{GeV}$, without noticing the presence of additional dimensions. Thus, if only gravity is allowed to propagate into the extra dimensions they could be possibly as large as $50\,\mu\text{m}$, since below that scale the gravitational interaction has not been tested and above we would not notice the presence of the additional dimensions. The only consequence at large distances would be the fact that we would have determined the effective Planck scale (2.4) and not the fundamental one $M_{\text{Pl}}^{(4+n)}$. It is not digressive that (2.1) does not hold for the whole range from macroscopic distances down to

the Planck length $l_p \sim 10^{-35}$ m. We know many examples for theories in physics that are replaced by another one at a certain scale, see Appendix A.4. The law of gravity that we measure at macroscopic distances does not have to be the final answer. Furthermore, the fact that only gravity might propagate into the additional dimensions can be motivated by string theory. Here, the corresponding force mediators correspond to closed strings, allowed to propagate into the whole space-time, while the other particles would correspond to open strings, attached to D-branes [149]. Moreover, due to general relativity, gravity is directly related to space-time, whereas the other forces are not. In this picture, the weakness of gravity would be just a dynamically generated effective weakness, seen for large distances, due to the dilution of gravity propagating into extra dimensions. As the other fundamental interactions have been probed up to the electroweak scale, extra dimensions would have to be smaller than ~ 1 fm to have escaped detection, if the SM would be allowed to enter them. However this would still allow for additional dimensions much larger than the (4D) Planck scale. The SM could be localized on a sub-manifold of the whole space-time, with TeV^{-1} "thickness", for example due to topological defects. In order not to dilute the SM interactions, the thickness should not be bigger than the fundamental Planck scale.

Looking again at (2.4), we see how the gauge hierarchy problem could be addressed in such a setup of gravity propagating into large extra dimensions. The Planck scale would just appear to be huge due to the presence of additional dimensions that we do not resolve. We would just think that we measure the fundamental Planck scale, but in reality we would measure $M_{\mathrm{Pl}}^{\mathrm{eff}}$ (2.4), which is enhanced due to the volume of the extra dimensions, given that

$$R > \left(M_{\mathrm{Pl}}^{(4+n)} \right)^{-1}. \tag{2.5}$$

The *fundamental* Planck scale could well be of the order of

$$M_{\mathrm{Pl}}^{(4+n)} \sim M_{\mathrm{EW}}, \tag{2.6}$$

just as large that we would not have already noticed it, say around a TeV. Now this scale would set the cutoff for the model and for quantum corrections to the Higgs mass. Above this energy, a quantum theory of gravity like string theory could set in, cutting away potentially large radiative corrections at a TeV. The natural scale for the Higgs-boson mass would then be around this fundamental Planck scale and the fine-tuning problem as discussed in 1.2.1 would nearly completely vanish. The theory would have only one fundamental scale, the electroweak scale. When starting to probe the extra dimension, gravity would be of weak scale strength in $4+n$ dimensions and not suppressed by the huge effective Planck mass. From the requirement (2.6) one can derive the corresponding size of the extra dimensions R, in dependence on their number n. With the help of (2.4) we arrive at

$$R \sim \left[M_{\mathrm{Pl}}^{eff} \right]^{\frac{2}{n}} \left[M_{\mathrm{EW}} \right]^{-\frac{2}{n}-1} \sim 2 \cdot 10^{\frac{32}{n}-19} \mathrm{m} \times \left[\frac{\mathrm{TeV}}{M_{\mathrm{EW}}} \right]^{\frac{2}{n}+1}, \tag{2.7}$$

where we have used the relation $200\ \mathrm{MeV\,fm} \approx 1$.

For $\underline{n=1}$ we get $R \sim 10^{13}$ m, setting $M_{\mathrm{EW}} \sim 1\,\mathrm{TeV}$ for this discussion. This implies that if there is exactly one large extra dimension, it would have to be larger than the extension of

the solar system, which is around $7 \cdot 10^{12}$ m . Such a scenario is certainly excluded.

For $\underline{n=2}$ we end up with $R \sim 1$ mm, which is excluded by the experimental constraint $R \leq 44 \,\mu$m [148]. However, if we are willing to accept some amount of tuning, we can relax the requirement (2.6) and use the experimental result to set a lower limit on the fundamental Planck scale. We arrive at $M_{\mathrm{Pl}}^{(6)} > 7$ TeV which would again introduce a little hierarchy, but still would be a big improvement compared to the full gauge hierarchy problem. However, there are more stringent constraints for $n = 2$ from astrophysics, see below.

For $\underline{n \geq 3}$ we get $R \leq 10^{-8}$ m, which is not directly testable in the near future.

A weakness of the ADD model is that one could also see it as just rephrasing the gauge hierarchy problem. Instead of asking why $M_{\mathrm{EW}} \ll M_{\mathrm{Pl}}$ one can now ask the question why the extra dimensions should be so much bigger than their natural size of M_{EW}^{-1}

$$\frac{R}{(M_{\mathrm{EW}})^{-1}} \sim \left[\frac{M_{\mathrm{Pl}}}{M_{\mathrm{EW}}} \right]^{\frac{2}{n}} . \tag{2.8}$$

Nevertheless, the problem of the radiative instability of the large separation between two fundamental scales is not present anymore. A possibility to circumvent the necessity to justify the size of the extra dimensions is to take the limit $n \to \infty$. In this setup, the extra dimensions just have to be infinitesimally larger than the fundamental Planck scale $M_{\mathrm{Pl}}^{(4+n)} \sim M_{\mathrm{EW}}$ in order to generate an arbitrary high effective Planck scale (2.4). So, all input parameters could be of natural size $\sim \mathcal{O}(M_{\mathrm{EW}})$ and also the SM could propagate nearly into the whole higher-dimensional space-time, in the spirit of *universal extra dimensions*.

In conclusion, low energy strings *can* arise, if compactified extra dimensions are present, being much larger than their natural length of $1/M_{\mathrm{Pl}}$ or if there are many extra dimensions (or if the geometry is warped, see below). This "low-energy" (higher dimensional) setup will be UV completed by a 10 or 11 dimensional string theory at energies around M_{EW}. Such a UV completion should explain the emergence of (large) extra dimensions and their topology, which is not addressed within the ADD model. With a fundamental Planck scale of $\mathcal{O}(M_{\mathrm{EW}})$, gravity will already become strongly coupled at LHC energies and it could in principle be possible to create micro black holes at the LHC. However, these black holes are predicted to be very short-lived, evaporating quickly via Hawking radiation. Beyond that, potentially stable micro black holes would have already shown up in cosmic rays [150].

A generic problem of theories with such a low cutoff is that higher dimensional operators mediating for example proton decay or FCNCs are not sufficiently suppressed, see Section 1.1.6. A possible solution to this issue is to split the fermions by localizing them differently within the extra dimensions, suppressing these higher dimensional operators by small overlaps [151]. This scenario also provides the possibility to address hierarchies within the fermion masses geometrically, by means of different overlaps with the Higgs sector. Note furthermore that, within the ADD model, a potential Grand Unification of couplings would already have to happen at a much lower scale than M_{GUT}, see *e.g.* [152]. Moreover, the mechanism of generating tiny neutrino masses via the strongly suppressed $D = 5$ operator introduced in Section 1.1.6 does not work any longer (however, see [153]).

2.2.2   Constraints on Large/Flat Extra Dimensions

Before introducing models of warped extra dimensions, which can solve the gauge hierarchy problem without unnatural parameters and with only one additional dimension, let us have a short look on some of the tightest constraints on large extra dimensions, coming from astrophysics. Gravity propagating into compactified extra dimensions leads, from a 4D perspective (after integrating out the additional dimensions in the action) to the emergence of an infinite tower of massive KK excitations. These so-called KK gravitons, couple to matter suppressed by $1/M_{\text{Pl}}$. This can be seen in analogy to putting a particle into a box (corresponding to the compactified dimensions), which can be described by an infinite set of eigenfunctions, corresponding to different, quantized, energy levels. From the 4D perspective, the quantized components of the momentum in the compactified extra dimension correspond to a mass. For details on this method of performing a *KK decomposition* (in the context of warped extra dimensions) see Section 3.2.1. Note that in the following we only consider the spin-2 part $G_{\mu\nu}$, $\mu, \nu = 0, \ldots, 3$ of the higher dimensional metric tensor. The KK gravitons have masses $\sim 1/R$, explicitly

$$m_k \sim k/R \tag{2.9}$$

for one extra dimension ($d = 5$), where $k = 0, \ldots, \infty$ denotes the KK level and the *zero mode* ($k = 0$) corresponds to the standard massless (4D) graviton. Thus, with (2.7), we arrive at mass splittings of

$$\Delta m \sim \frac{1}{R} \sim 10^{19 - \frac{32}{n}} \text{m}^{-1} \sim 10^{12 - \frac{32}{n}} \text{ eV} , \tag{2.10}$$

This means that from a high energy point of view one could produce a nearly continuous spectrum of real massive KK gravitons, given the number of extra dimensions is not too large.

Before reviewing the constraints from astrophysics, let us estimate the production cross section for arbitrary spin-2 (KK) gravitons at high energy colliders. After noting that the possible number of graviton final states for an available energy of ΔE is $\left(\frac{\Delta E}{\Delta m}\right)^n \sim (\Delta E\, R)^n$, we arrive at

$$\sigma \sim \frac{1}{M_{\text{Pl}}^2}(\Delta E\, R)^n \sim \frac{\Delta E^n}{\left[M_{\text{Pl}}^{(4+n)}\right]^{n+2}} . \tag{2.11}$$

For energies available to the graviton of $\Delta E \lesssim M_{\text{EW}}$ and $M_{\text{Pl}}^{(4+n)} \sim M_{\text{EW}}$ one thus ends up with cross sections that could become as large as

$$\sigma \lesssim \frac{1}{\text{TeV}^2} . \tag{2.12}$$

Thus, graviton production can become important, if the available energies start to approach the weak scale region. This agrees with the statements of strongly coupled gravity at the electroweak scale made before. From the 4D point of view, the size of the cross section is due to the large multiplicity of possible graviton final states. Due to the small interaction cross section of a *single* graviton, they would be seen as missing energy at collider experiments. For example, at the LHC or the Tevatron one would have the characteristic signal of a single jet in association with missing energy, whereas at electron positron colliders like LEP one would

have for example a photon plus missing energy

$$pp \rightarrow j + E_{\text{miss}} \,,$$
$$e^+ e^- \rightarrow \gamma + E_{\text{miss}} \,.$$

(2.13)

For more details, see *e.g.* [154].

For $n = 2, 3$, the most stringent constraints however still come from astrophysics and are hard to challenge in current collider experiments. (KK) Gravitons can carry away energy in supernova collapses, thus leading to a faster cooling. From analyzing the data of the supernova SN1987A, one can set an upper limit on the rate of graviton emission. According to the standard theory of type-II supernovae, most of the gravitational binding energy released during the core collapse of a supernova, is carried away via neutrinos. Since the measured neutrino flux agreed well with the theory value for the corresponding energy, one can put tight constraints on the emission of other particles like axions or KK gravitons. The analysis of [155] considered "gravi-strahlung"

$$N + N \rightarrow N + N + G$$

(2.14)

within the ADD setup as the dominant graviton-emission process. Here, G stands for any (KK) graviton. The nucleon-nucleon interactions are modelled by one-pion exchange. Due to the low temperature of the core $(30 - 70\,\text{MeV})$, we expect strong limits only for $n \leq 4$. For higher n, the mass splittings (2.10) are approaching the available energy, which leads to a vanishing of the high multiplicity enhancement in graviton final states. The authors derive the following (conservative) lower bounds on the fundamental Planck scale

$$M_{\text{Pl}}^{(6)} \geq 50 \; TeV \,, \quad n = 2 \,,$$
$$M_{\text{Pl}}^{(7)} \geq 4 \; TeV \,, \quad n = 3 \,,$$
$$M_{\text{Pl}}^{(8)} \geq 1 \; TeV \,, \quad n = 4 \,.$$

(2.15)

For n $\geq$ 4 the LHC should be able to improve the limits significantly. The biggest uncertainty in the supernova analysis is due to the unknown temperature of the core. The authors are conservative and assume $T = 30$ MeV. With more realistic values tighter bounds would be possible. The supernova data clearly exclude the possibility to address the large hierarchy between the Planck scale and the electroweak scale within the ADD setup for 2 extra dimensions.

Now we move on to a model which completely avoids the appearance of different scales, without the necessity of introducing infinitely many extra dimensions. The RS model is able to solve the gauge hierarchy problem with only one additional spatial dimension with a large curvature and all fundamental parameters of the order of the Planck scale M_{Pl}. When exploring possibilities to extend the SM in Section 1.1.6, we were thinking about an extension of the Poincaré group, which was finally realized in SUSY models and extra dimensions. However, we were still assuming space-time to feature a Minkowsk metric in the vaccum. The RS model will even modify this assumption in a way, that is not in conflict with observation.

It is also able to address naturally the hierarchies in the fermion sector, by allowing the quarks and leptons to propagate into the warped extra dimension. Furthermore, it features an

automatic suppression mechanism for FCNCs and allows for gauge coupling unification as well as for the construction of a Dark Matter candidate, see below. It offers a rich phenomenology in the reach of the LHC, especially within the Higgs sector. In the next chapter, we will discuss the theoretical setup of the model and its further virtues and properties in detail.

The following chapters will be based on the publications [1, 2, 3, 4] (besides the first, introductory pages), which occurred in the context of preparing this thesis. Beyond that, they will also include updated analyses and several new aspects, in particular unpublished work on five-dimensional propagators in warped space, as well as on the anomalous magnetic moment of the muon, see Chapter 4 and Section 5.1.5.

Chapter 3

Warped Extra Dimensions: Theoretical Aspects

Hierarchies - Interactions - Custodial Extension - Summing KK Towers

In this chapter, we will first introduce the basic concepts of the original RS model, including the derivation of the RS metric as a solution to Einstein's equations. We will then review, how the model is able to solve the gauge hierarchy problem. After that introductory part, we will study in detail gauge fields as well as fermions in the bulk, coupled to a brane localized Higgs sector within the minimal RS setup. In contrast to the perturbative approach usually used in the literature, where the couplings to the Higgs sector are introduced as a small correction after having obtained the bulk solutions, we perform the KK decomposition directly in the mass basis. Electroweak symmetry breaking will be included exactly via boundary conditions (BCs), avoiding the truncation of the KK tower [156]. In this way we are able to derive simple analytic results for the profiles and masses of the fields as well as for the interactions, which allow for a clear understanding of important effects of the model. For example, we will see that the summation over the entire KK tower of intermediate gauge bosons leads to a characteristic dependence on the coordinates in the extra dimension, reflecting the full 5D structure, which is lost through truncation [157]. For fermions, the mixings between different generations are included in a completely general way. The hierarchies observed in the fermion masses and CKM mixing angles are explained by wave-function overlaps with the Higgs sector, starting from anarchic fundamental Yukawa matrices. Corresponding analytical expressions are given by demonstrating and exploring an analogy to the Froggatt-Nielsen mechanism. The special localization pattern of fermions, resulting from the RS setup, leads to the possibility to make generic predictions about the size of effects for the different quark generations. Although the main phenomenological part is devoted to Chapter 5, we will already discuss some aspects of electroweak precision tests as a motivation to extend the gauge group of the minimal model, in order to achieve a custodial protection. In this context we will also explore the possibility of having a heavy Higgs boson $m_h \lesssim 1$ TeV in the RS setup. The custodial extension to the gauge group $SU(2)_L \times SU(2)_R \times U(1)_X \times P_{LR}$ will then be discussed in detail. In particular, analytic formulae for the Peskin-Takeuchi parameters as well as $Zb\bar{b}$ couplings will be given that show explicitly which terms can be protected and which inevitably escape protection. Beyond that, simple and exact expressions for general interactions between gauge bosons and fermions as well as for the couplings to the Higgs boson will be presented and compared for
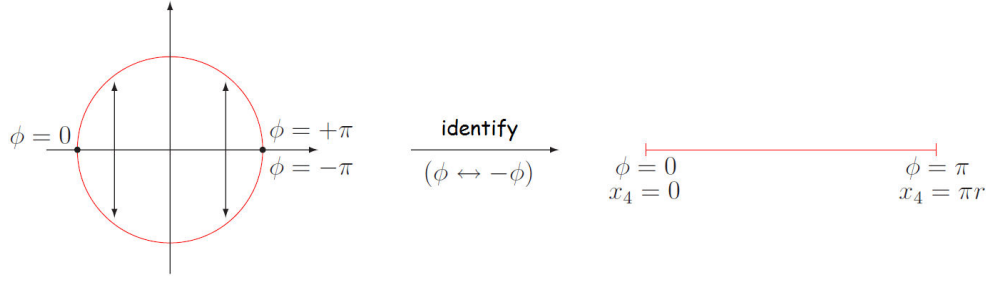
Figure 3.1: The Orbifold.

both models. These allow for a complete discussion of tree-level flavor-changing effects in the RS setup. Moreover, we will show how to perform sums over infinite towers of gauge-boson profiles in the minimal as well as in the custodial model.

3.1 Introduction and Solution to the Gauge Hierarchy Problem

3.1.1 The General Setup

The RS model [158] offers an elegant possibility to address the large hierarchy between the Planck scale and the electroweak scale by means of a non-trivial geometry in a five dimensional (5D) anti-de Sitter (AdS$_5$) space. The non-factorizable RS metric

$$ds^2 = e^{-2\sigma(\phi)}\eta_{\mu\nu}\, dx^\mu dx^\nu - r^2 d\phi^2 \,, \tag{3.1}$$

is constructed such that length scales within the usual 4D space-time of constant ϕ, labeled by coordinates x^μ ($\mu = 0 \dots 3$), are rescaled via an exponential *warp factor*, depending on the position $\phi \in [-\pi, \pi]$ in the extra dimension. In this thesis we will use the west coast convention for the Minkowski metric $\eta_{\mu\nu} = diag(1, -1, -1, -1)$. The exponential factor will turn out to be responsible for the solution to the gauge hierarchy problem and will be specified later. Importantly, the metric respects 4D Poincaré invariance. The fifth dimension is compactified on an orbifold S_1/Z_2, *i.e.*, a circle with radius r and with points identified, that are related to each other by a Z_2 (symmetry) transformation

$$(x^\mu, \phi) \leftrightarrow (x^\mu, -\phi)\,, \tag{3.2}$$

see figure 3.1. The radius is assumed to be not much larger than $\mathcal{O}(M_{\mathrm{Pl}})$, however, due to the warping, the model will have observable consequences down to the TeV scale. We assume the action to be invariant under Z_2 transformations Z. However, the fields do not have to be identical at points which are identified by the orbifold structure and can differ by a symmetry transformation which leaves the action invariant. Since $Z^2 = id$, Z has eigenvalues ± 1, corresponding to even and odd functions on the orbifold, respectively

$$\Phi(x^\mu, -\phi) = Z\Phi(x^\mu, \phi) = \pm\Phi(x^\mu, \phi)\,. \tag{3.3}$$

The Z_2 parity, gives rise to orbifold fixed points at $\phi = 0, \pi$, providing support for 3-branes, *i.e.*, sub-manifolds with three spatial and one time dimension, the so-called UV (or Planck) and IR (or TeV) branes. The reason for the names will become clear later. On these fixed points 4D field theories can be defined. The introduction of an orbifold also helps for phenomenological reasons, in particular for obtaining the correct low energy spectrum of the SM within the RS model (with the SM in the bulk), see below. Due to compactifying the extra dimension on an orbifold, one effectively ends up with an interval $\phi \in [0, \pi]$, bounded by the branes, which together with the Z_2 eigenvalues of the fields contain the whole information. The region in between the branes is called the "bulk". We impose Neumann or Dirichlet BCs for the fields at the branes, dictated by the low energy phenomenology, *i.e.*, the requirement to arrive at the SM spectrum in the low energy limit. Furthermore, the orbifold structure leads to periodic boundary conditions

$$\Phi(x^\mu, \phi) = \Phi(x^\mu, \phi + 2\pi) \,. \tag{3.4}$$

In the original RS proposal only gravity was allowed to propagate into the extra dimensions, which is sufficient to solve the gauge hierarchy problem. The SM was assumed to be confined to the IR brane. Thus we consider the (for the time being, classical) action of gravity propagating into the compactified fifth dimensions[1]

$$S = S_{\text{bulk}} + S_{\text{UV}} + S_{\text{IR}} \,,$$

$$S_{\text{bulk}} = \int d^4x \int_{-\pi}^{\pi} d\phi \sqrt{G} \left\{ -\Lambda - 2M^3 R \right\} ,$$

$$S_{\text{UV}} = \int d^4x \sqrt{-g^{UV}} \left\{ \mathcal{L}_{\text{UV}} - V_{\text{UV}} \right\} , \tag{3.5}$$

$$S_{\text{IR}} = \int d^4x \sqrt{-g^{IR}} \left\{ \mathcal{L}_{\text{IR}} - V_{\text{IR}} \right\} .$$

where $G_{MN}(x^\mu, \phi)$ is the 5D metric (not to be confused with the field strength tensor of the gluon), defined via (3.1) in the vacuum. Note that, due to the curved space-time, the square root of the determinant of the metric $\sqrt{G}$ has to be considered, which is not longer the identity and is needed to obtain an invariant integration measure. Latin (greek) indices $M, N = 0, \ldots, 3, \phi$ ($\mu, \nu = 0, \ldots, 3$) correspond to the 5D (4D) space-time. The 4D metric on the 3-branes is given by evaluating the 4D part of the bulk metric at the corresponding positions

$$g_{\mu\nu}^{UV}(x^\mu) \equiv G_{\mu\nu}(x^\mu, \phi = 0) \,, \quad g_{\mu\nu}^{IR}(x^\mu) \equiv G_{\mu\nu}(x^\mu, \phi = \pi) \,. \tag{3.6}$$

Above, $M \sim \bar{M}_{\text{Pl}}^{(5)}$ is the (reduced) fundamental scale of the theory and Λ is the 5D cosmological constant. In the most simple setup of an IR-brane SM and no UV localized fields we have $\mathcal{L}_{\text{IR}} = \mathcal{L}_{\text{SM}}$ from (1.8) and $\mathcal{L}_{\text{UV}} = 0$. However, due to the different metric, the fields in $\mathcal{L}_{\text{SM}}$ might have to be rescaled in order to obtain a canonical normalization and the numerical values of the input parameters might differ from their values in the "standard" SM (1.8) to match phenomenology. Non-vanishing "vacuum energies" $V_{\text{UV,IR}}$ on the branes, so-called brane tensions, are needed to allow for a non-trivial metric, responsible for the solution to the

---

[1]Note the difference in the signature of the metric with respect to [158], which results in a negative sign for the Ricci-scalar R.

gauge hierarchy problem.

3.1.2   Derivation of the Warp Factor

We now specify the form of the exponential warp factor $e^{-\sigma(\phi)}$. The metric (3.1) has to be a solution to Einstein's equations. In the form given, it corresponds to a general ansatz, respecting 4D Poincaré invariance. Since such an ansatz is not forbidden by any known principle, it is the most natural choice not to restrict it to the case of a vanishing warp factor. In the vacuum, Einstein's equations for the setup (3.5) read

$$
\begin{aligned}
\sqrt{G}\left(R_{MN} - \frac{1}{2}G_{MN}R\right) = \frac{1}{4M^3}[&\Lambda\sqrt{G}\,G_{MN} \\
&+ V_{\text{IR}}\sqrt{-g^{IR}}\,g_{\mu\nu}^{IR}\,\delta_M^\mu\delta_N^\nu\,\delta(\phi-\pi) \\
&+ V_{\text{UV}}\sqrt{-g^{UV}}\,g_{\mu\nu}^{UV}\,\delta_M^\mu\delta_N^\nu\,\delta(\phi)]\,.
\end{aligned}
\tag{3.7}
$$

Since the metric (3.1) is diagonal and just depends on ϕ, it is not intricate to calculate the corresponding Christoffel symbols. We obtain the Ricci-tensor

$$
\begin{aligned}
R_{\mu\nu} &= \frac{e^{-2\sigma(\phi)}}{r^2}\left(-\sigma''(\phi) + 4\left[\sigma'(\phi)\right]^2\right)\eta_{\mu\nu}\,, \\
R_{\phi\phi} &= 4\left(\sigma''(\phi) - \left[\sigma'(\phi)\right]^2\right)\,, \\
R_{\phi\nu} &= R_{\mu\phi} = 0\,,
\end{aligned}
\tag{3.8}
$$

as well as the Ricci-scalar

$$
R = \frac{4}{r^2}\left(-2\sigma''(\phi) + 5\left[\sigma'(\phi)\right]^2\right)\,.
\tag{3.9}
$$

Inserting these results into (3.7) we arrive at

$$
\begin{aligned}
6\left[\sigma'(\phi)\right]^2 &= -\Lambda\frac{r^2}{4M^3}\,, \\
3\sigma''(\phi) &= \frac{r}{4M^3}\left[V_{\text{IR}}\,\delta(\phi-\pi) + V_{\text{UV}}\,\delta(\phi)\right]\,.
\end{aligned}
\tag{3.10}
$$

From the first equation in (3.10) one deduces directly that a non-trivial solution $\sigma \neq$ const. is just possible for a non-vanishing 5D cosmological constant $\Lambda \neq 0$. The general solution which is consistent with the orbifold symmetry reads[2]

$$
\sigma(\phi) = \sqrt{\frac{-\Lambda}{24M^3}}\,r\,|\phi|\,.
\tag{3.11}
$$

This function, featuring periodic BCs $\sigma(\phi) = \sigma(\phi + 2\pi)$, has kinks at $\phi = 0, \pi$, see Figure 3.2, leading to δ-distributions in the second derivative. These contributions have to be compensated

---

[2]Note that we have not included an unobservable additive constant in the solution, which could be absorbed into a redefinition of the 4D coordinates x^μ, moreover the ambiguity in the sign does not change the physical setup, since it just corresponds to interchanging the branes.
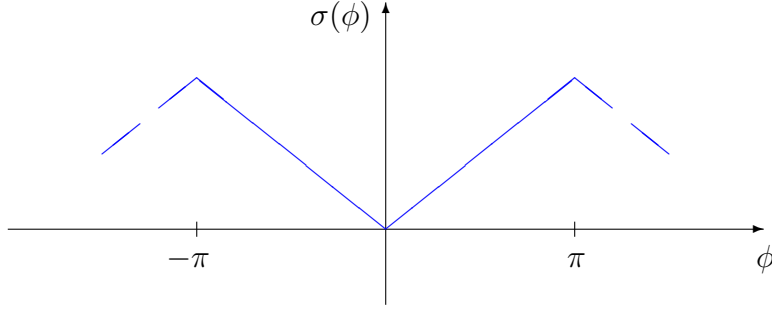
Figure 3.2: Periodic solution for the exponent of the warp factor (schematically).

by the brane vacuum energies, when inserting the solution into the second equation in (3.10), which requires

$$V_{\mathrm{UV}} = -V_{\mathrm{IR}} = 24M^3 k \,. \tag{3.12}$$

Here, we have defined the RS-curvature

$$k \equiv \sqrt{\frac{-\Lambda}{24M^3}} \,, \quad \Lambda = -24M^3 k^2 \,. \tag{3.13}$$

The brane tensions and the 5D cosmological constant are now linked in such a way, that the resulting 4D effective cosmological constant vanishes. This makes the 4D universe static and flat, consistent with the ansatz respecting 4D Poincaré invariance. In the RS model, the cosmological constant problem can be reformulated into the question why the brane tensions exactly cancel the 5D cosmological constant, a fact that has been put in by hand when choosing the ansatz. Remember that without the brane tensions, just the trivial solution $\sigma = $ const. would be consistent with a vanishing 4D cosmological constant, which would not allow for a solution to the gauge hierarchy problem. The explicit RS metric is now given by (3.1) with

$$\sigma(\phi) = kr\, |\phi| \,. \tag{3.14}$$

Due to the non-vanishing 5D cosmological constant, the extra dimension has a finite curvature within the vacuum. Therefore RS models are also called *warped extra dimensions*. The setup is shown in Figure 3.3. The factor $e^{-kr|\phi|}$, which describes the change of length scales when moving along the extra dimension is accordingly called *warp factor*. It is just the large curvature, which will allow for a solution to the gauge hierarchy problem. For the consistency of the solution, the 5D cosmological constant has to be negative, resulting in an AdS$_5$ space. Furthermore, note that the curvature has to be smaller than the fundamental Planck scale of the setup. At this point, the theory possesses three fundamental scales (M, k, r) which, for naturalness reasons, should all be of the same order. Indeed, this will turn out to be possible.

3.1.3   The Planck Scale

Let us now explore how the effective (4D) Planck scale M_{Pl}, that we observe, arises from the fundamental scale M of the RS model. Since we assume the extra dimension to be unresolvable
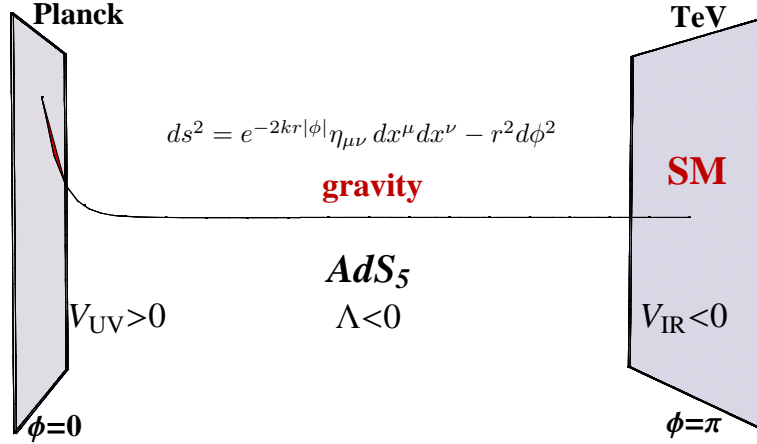
Figure 3.3:   The Randall-Sundrum setup corresponds to a five dimensional anti-de Sitter space with a non-factorizable metric, bounded by two four dimensional sub-manifolds, the Planck brane and the TeV brane. The vacuum energies are adjusted such that the effective four dimensional cosmological constant vanishes. See text for details.

directly by gravity experiments in the intermediate future, we will use an 4D EFT description. We extend the metric (3.1) by *massless* fluctuations around the vacuum solution, which will provide the right degrees of freedom to describe gravity at low energies [158]

$$ds^2 = e^{-2k\bar{b}(x)|\phi|} \left[\eta_{\mu\nu} + \bar{h}_{\mu\nu}(x) \right] dx^\mu dx^\nu - \bar{b}^2(x)d\phi^2 \,. \tag{3.15}$$

Here, $\bar{h}_{\mu\nu}(x)$ corresponds to the massless zero mode in the KK decomposition of the (spin-2) graviton and is the graviton of the 4D effective theory with a wave function $\psi(\phi) \sim e^{-2kr|\phi|}$ in the extra dimension, see also [159]. The effects of the massive KK excitations are suppressed at low energies by powers of the NP scale (see Appendix A.4) which will be above the TeV scale, see (3.32) below. Locally, (3.15) is identical to the vacuum solution (3.1), given that $\bar{h}_{\mu\nu}(x)$ and $\bar{b}$ are smooth functions. We did not include a term $A_\mu dx^\mu d\phi$, corresponding to vector fluctuations, since these off-diagonal fluctuations will be heavy and thus not part of the EFT [158]. $G_{\phi\phi}(x) \equiv b^2(x)$ corresponds to the *radion*, its zero mode $\bar{b}(x)$ determines the radius of the extra dimension. A priori, it is massless, since the radius, which we have fixed so far just at r, does not possess a potential in the first place. However, from the phenomenology side, this would not be acceptable, since a massless radion would lead to a measurable violation of the equivalence principle. It is essential that $\bar{b}(x)$ can be stabilized at a VEV of $\langle \bar{b} \rangle = r$ and obtain a mass of at least 10^{-4} eV [158]. This can be achieved due to the Goldberger-Wise mechanism [160] by introducing a new scalar field in the bulk. A radius which is in agreement with the solution to the gauge hierarchy problem can be reached without much fine tuning of parameters. In the following we assume that a mechanism a la Goldberger and Wise is at work and replace $\bar{b}$ by its VEV r.

   Inserting (3.15) into the action (3.5) one can, on the one hand, explicitly verify that the effective four dimensional cosmological constant vanishes $\Lambda_4 = 0$ and that the graviton zero mode has no effective potential. On the other hand, one deduces from the curvature term,

written in terms of the effective 4D metric

$$\bar{g}_{\mu\nu}(x) \equiv \eta_{\mu\nu} + \bar{h}_{\mu\nu}(x)\,, \tag{3.16}$$

how the reduced effective (4D) Planck scale $\bar{M}_{\mathrm{Pl}} \approx 2 \times 10^{18}\,\mathrm{GeV}$ emerges from the (reduced) fundamental scale M of the theory [158]. [3]

$$\bar{M}_{\mathrm{Pl}}^2 = \frac{M^3}{k}\left[1 - e^{-2kr\pi}\right]\,. \tag{3.17}$$

For $L \equiv kr\pi \gg 1$, which will be necessary to solve the gauge hierarchy problem, the second term becomes unimportant and we observe that $\bar{M}_{\mathrm{Pl}}$ only depends very weekly on the compactification radius r, in contrast to the ADD setup. Not wanting to produce large hierarchies between the input parameters of the theory, one sets

$$r^{-1} \lesssim k \sim M\,, \tag{3.18}$$

which leads to an effective Planck mass of the order of the fundamental scale of the RS model

$$\bar{M}_{\mathrm{Pl}} \sim M\,. \tag{3.19}$$

In consequence, this scale is expected to be $M \sim 10^{18}\,\mathrm{GeV}$ and not around the electroweak scale like in the ADD scenario. In the next section we discuss how the gauge hierarchy problem can be solved in such a completely natural setup. From (3.17) it follows that $\bar{M}_{\mathrm{Pl}}$ stays finite even in the limit $r \to \infty$! This setup has been worked out in [161].

3.1.4 Solution to the Gauge Hierarchy Problem

So far the RS model just contains fundamental scales which reside at M_{Pl}. Let us now see how, under this assumption, a Higgs-boson mass around the scale M_{EW} can arise and can be radiatively stable. Therefore, consider a fundamental Higgs scalar on the IR brane ($\phi = \pi$). The corresponding action reads

$$S_{\mathrm{IR}} \supset \int d^4x\, r \int_{-\pi}^{\pi} d\phi\, \mathcal{L}_{\mathrm{Higgs}}\,, \tag{3.20}$$

where, in analogy to (1.19)

$$\mathcal{L}_{\mathrm{Higgs}} = \delta(|\phi| - \pi)\frac{\sqrt{G}}{r^2}\left[G^{\mu\nu}(D_\mu\Phi)^\dagger(D_\nu\Phi) - V(\Phi)\right]\,, \qquad V(\Phi) = -\mu_5^2\Phi^\dagger\Phi + \frac{\lambda_5}{2}\left(\Phi^\dagger\Phi\right)^2\,. \tag{3.21}$$

Here, $\sqrt{G}$ denotes the square root of the determinant of the complete 5D metric. Note that $G_{\mu\nu}(x^\mu, \phi = \pi) \equiv \bar{g}_{\mu\nu}^{IR}(x^\mu)$. Moreover, we have already switched to a notation which suggests that in principle the fields of the theory are 5D bulk fields, making the IR localization of the Higgs sector explicit via the δ-distribution. The form of the Higgs doublet $\Phi(x)$ is identical

---

[3]Note that this relation can also be obtained by studying the interaction of the gravity zero mode with matter.

with the one given in (1.20) with however v replaced by v_5. Here, and above, the subscripts 5 denote that the input parameters are those of the fundamental (5D) theory with the metric (3.15) and before integrating out the extra dimension. Due to naturalness arguments, we assume $v_5 \lesssim M_{\text{Pl}}$. First we rewrite the Higgs potential in terms of the VEV $v_5 = \sqrt{2\mu_5^2/\lambda_5}$ as

$$V(\Phi) = \frac{\lambda_5}{2} \left(\Phi^\dagger \Phi - \frac{v_5^2}{2} \right)^2 , \tag{3.22}$$

where we have dropped a, for our discussion irrelevant, constant term. Evaluating (3.20) with the RS metric (3.15) and performing the integral over the extra dimension, we arrive at

$$S_{\text{IR}} \supset \int d^4x \sqrt{-\bar{g}}\, e^{-4kr\pi} \left\{ e^{2kr\pi} \bar{g}^{\mu\nu} (D_\mu \Phi)^\dagger (D_\nu \Phi) - \frac{\lambda_5}{2} \left(\Phi^\dagger \Phi - \frac{v_5^2}{2} \right)^2 \right\} . \tag{3.23}$$

In order to obtain a canonically normalized 4D Higgs doublet, we have to perform a wave-function renormalization $\Phi \to e^{kr\pi}\Phi$, which leads to the 4D action

$$S_{eff} \supset \int d^4x \sqrt{-\bar{g}} \left\{ \bar{g}^{\mu\nu} (D_\mu \Phi)^\dagger (D_\nu \Phi) - \frac{\lambda_5}{2} \left(\Phi^\dagger \Phi - e^{-2kr\pi} \frac{v_5^2}{2} \right)^2 \right\} . \tag{3.24}$$

Looking at the last term, we see that a remarkable thing has happened. The fundamental Higgs VEV v_5 gets rescaled by the (quadratic) warp factor $e^{-2kr\pi}$, such that the effective (4D) VEV, which sets the mass scale of the 4D theory, reads

$$v = e^{-kr\pi} v_5 . \tag{3.25}$$

Such a relation holds for *any* fundamental mass parameter m_5 present in the 5D theory. Measured on the IR brane, with the metric of the effective 4D theory $\bar{g}^{\mu\nu}$, it will correspond to a physical mass of $m = e^{-kr\pi} m_5$. Note that also μ_5 gets rescaled according to $\mu = e^{-kr\pi}\mu_5$, whereas dimensionless parameters will not receive such a rescaling $\lambda_5 = \lambda$. In consequence, starting from a fundamental Higgs VEV of $v_5 \lesssim k \lesssim M_{\text{Pl}}$, slightly below its natural Planck-scale value, one arrives at an effective 4D VEV of $v \sim M_{\text{EW}}$ by choosing

$$L \equiv kr\pi \approx 37 . \tag{3.26}$$

The same holds true for the Higgs mass, where $m_{h5} \lesssim k \lesssim M_{\text{Pl}}$ results in a (4D) mass for the Higgs boson of

$$m_h = e^{-L} m_{h5} \sim M_{\text{EW}} . \tag{3.27}$$

Note that the fundamental Higgs mass should be slightly below the Planck scale, because otherwise the Higgs boson would be heavier than the KK excitations of the model, see below. The question about the huge size of the hierarchy between M_{Pl} and M_{EW} which was reformulated into the question why $R \gg M_{\text{Pl}}^{-1}$ in the ADD setup has now been tamed to the question why the size of the extra dimension, in units of the inverse curvature, is moderately larger than one ($L > $ a few).

In summary, one can choose the radius of the extra dimension to be not far above the

inverse RS curvature $r/k^{-1} \sim \mathcal{O}(10)$, in order to generate the huge hierarchy between the Planck scale and the electroweak scale, due to the exponential warp factor

$$\epsilon \equiv e^{-L} \approx 10^{-16} \approx \frac{M_{\mathrm{EW}}}{M_{\mathrm{Pl}}}, \tag{3.28}$$

which arises naturally when solving Einstein's equations. The gauge hierarchy problem is thus solved in the AdS$_5$ background by gravitational red shifting, see Figure 3.4. The corresponding brane separation can be stabilized by a Goldberger-Wise mechanism, as discussed before. Thus all the dimensionful scales of the RS model are within 1-2 orders of magnitude

$$v_5 \sim M \sim 1/r \sim k \sim M_{\mathrm{Pl}}. \tag{3.29}$$

Note that many observables in warped extra dimensions are enhanced by the "volume factor" L. It is important that the Higgs mass (3.27) does not receive large corrections at the quantum level. For the following discussion, let us already generalize the RS setup, and allow also gauge bosons and fermions to propagate into the bulk. We will see that this does not spoil the solution to the gauge hierarchy problem.

The absence of large corrections to the Higgs-boson mass is automatically secured in the RS setup, since, from a 5D point of view as well as from a 4D point of view, this mass is just below the cutoff of the RS model. Note that the RS model *has* to be defined with a cutoff (also in the presence of gauge couplings only) since, being a QFT in more than four dimensions, it possesses gauge couplings with negative mass dimension, see (3.39). Thus, it is *not* expected to be the final theory of nature. It makes only sense as an EFT, see sections 1.1.6 and A.4, and needs a UV completion like string theory. The 5D cutoff of the RS model is given by a scale $\Lambda_5 \sim M_{\mathrm{Pl}}$. This translates into a cutoff for the 4D theory, depending on the position in the extra dimension, of

$$\Lambda_{\mathrm{UV}}(\phi) = e^{-kr|\phi|}\Lambda_5, \tag{3.30}$$

where we have used the generic suppression of fundamental mass scales by the warp factor, seen above. In loop diagrams containing general bulk fields, the 4D momentum flow in a propagator has to be cut off at a scale, defined by the position-dependent cutoff $\Lambda_{\mathrm{UV}}(\phi)$ evaluated at the adjacent vertices. In addition, energy-momentum conservation has to be considered. A sensible prescription to choose one of the two possible cutoff scales for a propagator in the bulk thus is to use $\phi = \max(\phi_1, \phi_2)$, where $\phi_{1,2}$ are the coordinates in the extra dimension, belonging to the adjacent vertices. For further details, including the renormalization of the Green's functions, see [162]. For the case of an IR-brane localized Higgs sector, these considerations lead to a cutoff for the leading corrections to the Higgs-boson mass of

$$\Lambda_{\mathrm{UV}}(\pi) = \epsilon\,\Lambda_5 = \mathcal{O}(\text{some TeV}) \tag{3.31}$$

in the 4D theory, solving the large gauge hierarchy problem (however still leaving a little hierarchy problem for the case of a light Higgs boson, see below). This holds independently of the localization of the other fields. Possible corrections of heavier particles will be effectively cut off at this scale. $\Lambda_{\mathrm{UV}}(\pi)$ is the scale around which gravity becomes strongly coupled for an 4D observer on the IR brane and at which the RS effective field theory is expected to be replaced by something else like string/M-theory. This theory would then have to answer the

question how the warped space comes about. In this context, it is interesting to know that higher dimensional spaces with warp factors arise naturally in flux compactifications of string theory [163, 164, 165, 166], see also [167, 168]. The effective mass scales on the UV and IR branes, resulting from fundamental scales of $\mathcal{O}(M_{\mathrm{Pl}})$, also explain their names - the Planck brane and the TeV brane. Since the masses of the fermions and gauge bosons are protected by symmetries, as discussed before, a large cutoff will not lead to large masses in these sectors. As we will explain below, the solution to the gauge hierarchy problem in RS, due to a higher-dimensional space-time with a non-trivial metric, is related to the technicolor/strong-coupling ideas of Section 1.2.1 via the AdS/CFT correspondence, with the Higgs-boson being composite.

3.1.5 The Standard Model Propagating into the Bulk

While in the original RS setup the whole SM was assumed to be localized on the TeV brane, we have seen that the solution to the gauge hierarchy problem will not be spoiled if gauge bosons [169, 170, 171, 172] and matter fields [172, 173] are allowed to propagate into the extra dimension, see Figure 3.4. In particular, this makes constraints from higher dimensional operators, like those mediating proton decay or FCNCs, less problematic. As the RS model is an EFT, there is no reason not to consider such operators. While the cutoff for an IR-brane localized Higgs sector $\Lambda_{\mathrm{UV}}(\pi)$ will be in the sought TeV range, operators of fields that propagate into the extra dimension will have a larger suppression factor Λ_{UV}, that depends on their localization. The more UV localized the fields are, the higher is the generic cutoff. This naturally results in different suppressions for different operators, *e.g.* for those leading to proton decay and those mediating meson mixing, a pattern which could well be realized in nature, see Section 1.1.6. Bulk fermions further offer the interesting possibility to address the observed hierarchies within the flavor sector via geometrical sequestering [151]. Starting from anarchical fundamental Yukawa couplings, as defined in Section 1.2.2, the large mass hierarchies of the SM fermions are generated naturally by localizing them differently in the fifth dimension, without the need to build in hierarchies in the input parameters by hand [173, 172, 174, 175]. These are generated due to exponentially enhanced differences in the fermion-Higgs couplings, due to the warp factor. In consequence, small mixing angles in the CKM matrix are generated automatically [175], since the scenario is in complete analogy to the Froggatt Nielsen mechanism, see Section 3.2.3. As a by-product, this way of generating fermion hierarchies implies an explicit suppression of dangerous FCNCs within the RS model for processes involving *light* quarks. The UV localization of these quarks results in small couplings to KK modes which mediate FCNCs already at the tree level [172]. This suppression is called RS-GIM mechanism [176, 177], in analogy to the GIM mechanism within the SM, which both share some features, see below. Importantly, bulk fermions mitigate significantly the RS corrections to the Peskin-Takeuchi S parameter, that arise through de-localized $W^{\pm}$ and Z bosons [172, 178, 179, 180]. The remaining sizable corrections to the T parameter will be studied in more detail below in Section 3.3. This RS setup, with the SM in the bulk, is the model that we will study in this thesis. We will call this setup, featuring the SM gauge group, the *minimal RS model*, in discrimination from the extension to the *custodial RS model*, which will be introduced later. The Higgs boson may only leave the region of the IR brane if one wants to give up the idea of solving the gauge hierarchy problem in RS or if one includes another mechanism to stabilize the weak scale, see Section 1.2.1.

With the SM (besides the Higgs sector) in the bulk, also the gauge bosons and fermions will develop KK excitations. These will turn out to be localized close to the TeV brane, see Figure 3.6 below. The mass scale for the lightest of these excitations (as well as for KK gravitons), will also be set by the warp factor and is called the "KK scale"

$$M_{\text{KK}} \equiv k\epsilon = k\,e^{-L} = \mathcal{O}(\text{TeV})\,, \tag{3.32}$$

see sections 3.2.1 and 3.2.2. The zero modes of the KK towers will correspond to the "SM-fields" we observe at low energies.[4] The KK excitations however, will correspond to BSM physics and their mass scale M_{KK} will set the NP scale.[5] For instance, the masses of the first KK photon and gluon will turn out to be approximately $2.45\,M_{\text{KK}}$. In contrast to the ADD model, the masses of the excitations are thus not given by the inverse compactification radius. This makes these modes in principle observable at colliders like the LHC, a big advantage compared to usual string theory, where the compactification radius as well as the mass of the string excitations are *both* expected to be around the Planck scale. The explicit form of the profiles and masses of the SM fields and their KK excitations in the RS setup will be given in the next sections. Note that the possibility to generate (KK) particle masses due to a compactified extra dimension without a Higgs sector also lead to the construction of Higgsless models of EWSB [181, 182, 183, 184, 185]. The breakdown of unitarity in longitudinal $W^{\pm}$ scattering in these models is raised by the exchange of KK towers of gauge bosons. Moreover, the presence of (4D) scalar degrees of freedom in higher dimensional gauge fields offers the possibility to achieve EWSB by supplying these components with a VEV [186, 187, 188, 189], see also [136]. The gauge symmetry then protects the mass of the Higgs component of the gauge field. This corresponds to an alternative option to extend the Poincaré group trivially by adding dimensions, in order to protect the Higgs sector The scalars and the (4D) gauge fields are then linked by the 5D Poincaré group (*c.f.* SUSY).

After having introduced the basic properties of KK modes within the RS setup, let us again study gravity. The weakness of gravity in the RS setup is reflected by the exponential localization of the graviton zero mode close to the UV brane (3.15), see Figure 3.4, which leads to dimensionful couplings, suppressed by the Planck scale $M_{\text{Pl}} \gtrsim M$. The KK excitations of the graviton will however be localized near the IR brane and thus their couplings will be enhanced by the warp factor, which, after solving the gauge hierarchy problem, will lead to a coupling, suppressed by the weak scale only [159]. As a consequence, from the 4D point of view of an observer sitting on the IR brane, gravity will become strong already at the weak scale. This reason for gravity becoming strong at the TeV scale - unsuppressed couplings of single IR localized KK gravitons with TeV masses - should be contrasted with the huge multiplicity of Planck-scale suppressed KK-graviton couplings in the ADD model. The fact that KK gravitons in the RS setup have masses above M_{KK} removes nearly completely the constraints from cosmology and astrophysics, see Section 2.2.2. Furthermore their stronger coupling makes them, in principle, directly observable as decaying spin-2 resonances at colliders like the LHC.

---

[4]Although they can receive non-vanishing masses via couplings to the Higgs sector, we will still call the lightest modes with masses $m_n \ll M_{\text{KK}}$ zero modes.

[5]Note that, after going to the mass basis, also the couplings of the zero mode sector will be changed with respect to the SM, due to mixings with the KK excitations.
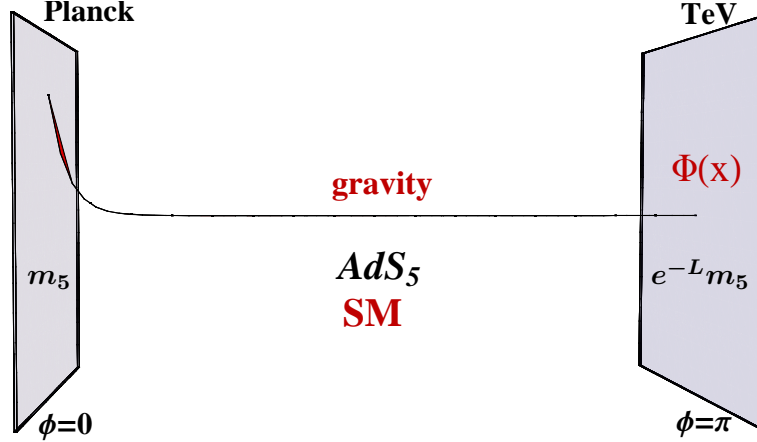
Figure 3.4: Setup of the minimal Randall-Sundrum model. The gauge hierarchy problem is solved since mass scales on the TeV brane, where the Higgs sector is localized, are suppressed by the warp factor. The warping is described by the profile of the massless graviton, depicted by the exponential line.

Let us finally have another look at the corrections to the Higgs-boson mass in the 4D theory. From naive dimensional analysis we conclude that the residual corrections in the RS model scale like

$$\delta m_h^2 \sim \frac{\Lambda_{\mathrm{UV}}^2(\pi)}{16\pi^2} \frac{\Lambda_{\mathrm{UV}}^2(\pi)}{M_{\mathrm{KK}}^2} \, . \tag{3.33}$$

These corrections grow like the fourth power of the UV cutoff, not like the second one as in 4D. Thus, the "little hierarchy problem" in RS is in general more severe than in standard 4D extensions of the SM. These considerations favor a heavy Higgs boson, not too far below the cutoff. Indeed, it will turn out that electroweak precision tests within the minimal RS model, studied at the tree level, also prefer a heavy Higgs boson $m_h \gtrsim 500$ GeV, see Section 3.3. However, since we have not seen strong hints for KK excitations below the TeV scale so far, the resulting UV cutoff of at least some TeV still results in a fine tuning at the per cent level for a heavy Higgs-boson and even worse for a light Higgs of $m_h \sim \mathcal{O}(100)$ GeV.

The discussion above can also be summarized from another point of view. By virtue of the AdS/CFT correspondence [190, 191, 192], a 5D gravitational theory in anti de-Sitter space is dual to a strongly coupled 4D conformal field theory (CFT). For the case of the RS setup, with the conformal symmetry being broken on the IR brane, implications of this correspondence have been studied *e.g.* in [168, 193, 194, 195]. A recent review can be found in [196].[6] Holography implies that 5D fields living near the IR brane correspond to composite objects in the CFT, whereas fields living near the UV brane correspond to elementary particles. In the RS setup, where the Higgs sector is localized on (or close to) the IR brane, the Higgs boson thus can be thought of as a composite object of the strongly coupled sector [198, 199], whose compositeness scale and mass is naturally of the order of the scale of the IR brane $\Lambda_{\mathrm{UV}}(\pi) \gtrsim M_{\mathrm{KK}}$. This may be different in models of gauge-Higgs unification, which we will not

---

[6]Note that by applying the AdS/CFT duality (approximative) to low energy QCD, one can still use warped 5D models as mathematical tools to calculate corresponding observables in a weakly coupled theory, even if nature would turn out to be four dimensional. For a review on these aspects, see [197].

study in this thesis. In this sense, a light Higgs boson with $m_h \ll M_{\text{KK}}$ would be unnatural in the RS models studied here. Along the same lines, the SM-fields propagating into the bulk correspond to elementary particles up to much higher scales. In this language, a bulk SM has the advantage that many observables can be calculated within the weakly coupled RS setup with less sensitivity on the details of the compositeness (*i.e.*, UV completion of the RS EFT).

3.2 The Minimal Randall-Sundrum Model: The SM in a Slice of AdS$_5$

After this general overview we will now study in detail the theory of the SM field content propagating into a warped extra dimension, in the presence of a brane-localized Higgs sector. First, we will discuss gauge fields in the bulk. After that, we will move on to bulk fermions and study the generation of the hierarchies in the fermion sector as discovered in nature. By constructing solutions to the bulk EOMs, subject to boundary conditions given by the couplings to the scalar sector, we obtain exact results for the masses and profiles of the SM fields and their KK excitations. This will pay off in the following discussion of interactions between fermions and gauge bosons as well as in studying interactions with the Higgs boson, where in all cases we will give simple analytic formulae for the couplings. Proceeding in this way we can then clearly distinguish between leading and subleading terms. At the end of this section, we will have a first look at the phenomenology of the RS model. Rather large corrections to electroweak precision observables will serve as a motivation to extend the gauge group of the minimal RS model. The following discussion is based on [1].

3.2.1 The Gauge Sector

In this section we study the SM gauge group in the warped RS background, incorporating the gauge fixing in a covariant R_ξ-gauge. We will focus on the electroweak sector as the generalization to the $SU(3)_c$ gauge group is straightforward. The starting point for the following discussion is the electroweak gauge sector of the SM, as given in Section 1.1.1.

Action of the 5D Theory

When generalizing the SM gauge sector to a five dimensional theory in a slice of AdS$_5$, we still want to keep the low energy sector of this theory similar to the SM version. Therefore we start from the SM action corresponding to the symmetry group $SU(2)_L \times U(1)_Y$ (1.13) (for the time being, without the gluon part), account for the additional dimension in the space-time integral and the non-trivial metric, and simply replace the gauge fields by five dimensional versions, *i.e.*, five-component vector fields

$$
\begin{aligned}
B_\mu &\to B_M \, , \\
W_\mu^a &\to W_M^a \, .
\end{aligned}
\tag{3.34}
$$

As we later want to study a 4D theory, we will decompose the 5D vectors above into representations of the *4D Lorentz group*, the vector B_μ and the scalar B_ϕ, which do not mix under 4D Lorentz transformations, and similar for the other gauge fields. In order to arrive at a low

energy spectrum that contains just SM-like fields and will be to leading order identical to the SM, we have to take care that the ϕ-components of the 5D gauge fields do not enter the low energy theory. We thus choose the scalar components to be odd under the Z_2 orbifold symmetry, and supply them with Dirichlet BCs, so that they will not possess light (or massless) modes, see below.[7] The vector components W_μ^a and B_μ however have to be even under Z_2 and obey Neuman BCs. We arrive at

$$S_{\text{gauge}} = \int d^4x \, r \int_{-\pi}^{\pi} d\phi \left(\mathcal{L}_{\text{B,W}} + \mathcal{L}_{\text{Higgs}} + \mathcal{L}_{\text{GF}} + \mathcal{L}_{\text{FP}} \right), \tag{3.35}$$

where the Lagrangian of the 5D gauge theory reads

$$\mathcal{L}_{\text{B,W}} = \frac{\sqrt{G}}{r} G^{KM} G^{LN} \left(-\frac{1}{4} B_{KL} B_{MN} - \frac{1}{4} W_{KL}^a W_{MN}^a \right). \tag{3.36}$$

The field-strength tensors are defined in analogy to the usual 4D definitions (1.14) by replacing four-component indices with five-component ones. The action (3.35) is invariant with respect to 5D gauge transformations, which are also in complete analogy to the 4D gauge transformations introduced in (1.4), see also [162]. Note that, due to the higher dimensional space-time, the gauge fields now have mass dimension $D = 3/2$.

In order to achieve EWSB, we couple these fields to a Higgs sector, which is localized on the IR brane. We know that this sector has to be localized close to the IR brane in order to solve the gauge hierarchy problem, so we assume it to be defined directly on the brane for simplicity. This enables us to obtain exact solutions by accounting for the Higgs couplings via BCs. The corresponding Lagrangian $\mathcal{L}_{\text{Higgs}}$ has already been given in (3.21), before evaluating the RS metric and performing the wave-function renormalization of the Higgs Field. After these operations and replacing fundamental parameters with 4D parameters according to (3.25) and below, we obtain

$$\mathcal{L}_{\text{Higgs}} = \frac{\delta(|\phi| - \pi)}{r} \left[(D_\mu \Phi)^\dagger (D^\mu \Phi) - V(\Phi) \right], \qquad V(\Phi) = -\mu^2 \Phi^\dagger \Phi + \frac{\lambda}{2} \left(\Phi^\dagger \Phi \right)^2. \tag{3.37}$$

After EWSB, the Higgs doublet can be decomposed in terms of the four real scalar fields φ^i, $i = 1, 2, 3$ and h, exactly like in (1.20). Note that, although the parameters in the RS model have the same names as the corresponding SM ones, the exact values might differ. For example the relation between the Higgs VEV and the $W^\pm$-boson or Z-boson (zero mode) mass will get corrections, suppressed by the NP scale M_{KK}, and thus the extracted Higgs VEV will differ from the SM value. While for $M_{\text{KK}} \gtrsim 3$ TeV, the correction is about $\lesssim 1\%$, for lower scales it can become important and exceeds 5% for $M_{\text{KK}} = 1$ TeV. Anyway, as the effect appears already at $\mathcal{O}(v^2/M_{\text{KK}}^2)$ one should include it [200], see below.

In order to diagonalize the 5D mass terms resulting from (3.37), we perform the usual redefinitions of the gauge fields

$$W_M^\pm = \frac{1}{\sqrt{2}} \left(W_M^1 \mp i W_M^2 \right),$$

---

[7]In the models of gauge-Higgs unification mentioned before, it is just such scalar components of gauge fields that are taken as candidates for a Higgs field.

$$Z_M = \frac{1}{\sqrt{g_5^2 + g_5'^2}} \left(g_5 W_M^3 - g_5' B_M \right) , \tag{3.38}$$

$$A_M = \frac{1}{\sqrt{g_5^2 + g_5'^2}} \left(g_5' W_M^3 + g_5 B_M \right) ,$$

where g_5 and g_5' are the 5D gauge couplings of $SU(2)_L$ and $U(1)_Y$, respectively. These have mass dimension $D[g_5^{(')}] = -1/2$ since interaction operators between two fermion fields and a gauge-boson field have mass dimension $D = 11/2$ in five dimensional space-time. Introducing 4D gauge couplings (see Section 3.2.4)

$$g = \frac{g_5}{\sqrt{2\pi r}} , \tag{3.39}$$

and similar for the other gauge couplings [169], we see that these field redefinitions are just like in the SM (1.22). Consequently, the definition of the weak mixing angle between the 5D fields,

$$\begin{aligned} \sin\theta_w &= \frac{g_5'}{\sqrt{g_5^2 + g_5'^2}} = \frac{g'}{\sqrt{g^2 + g'^2}} \\ \cos\theta_w &= \frac{g_5}{\sqrt{g_5^2 + g_5'^2}} = \frac{g}{\sqrt{g^2 + g'^2}} , \end{aligned} \tag{3.40}$$

agrees with the one of the SM (1.23). In analogy to (1.26), the 5D covariant derivative in this mass basis, including QCD for completeness, reads

$$D_M = \partial_M - i\frac{g_5}{\cos\theta_w} \left(T^3 - \sin^2\theta_w Q \right) Z_M - ie_5 Q A_M - i\frac{g_5}{\sqrt{2}} \left(T^+ W_M^+ + T^- W_M^- \right) - ig_{s,5} t^a G_M^a , \tag{3.41}$$

with Q defined as in (1.28). Evaluating the four-vector part of this expression, acting on the Higgs doublets in (3.37), we see that the bulk gauge fields $W^\pm$ and Z get "masses"

$$M_W = \frac{v g_5}{2} , \qquad M_Z = \frac{v\sqrt{g_5^2 + g_5'^2}}{2} , \tag{3.42}$$

while the photon remains massless ($M_A = 0$). This is again in complete analogy to the mechanism of EWSB in the SM with the symmetry breaking sector now localized at the boundary of an extra dimension. However, note that the mass parameters M_W and M_Z now have mass dimension $D = 1/2$.

The kinetic term for the Higgs field contains mixed terms of the gauge bosons and the scalar fields $\varphi^\pm$ and φ^3. They can be read off from

$$D_\mu \Phi = \frac{1}{\sqrt{2}} \begin{pmatrix} -i\sqrt{2} \left(\partial_\mu \varphi^+ + M_W W_\mu^+ \right) \\ \partial_\mu h + i \left(\partial_\mu \varphi^3 + M_Z Z_\mu \right) \end{pmatrix} + \text{terms bi-linear in fields} . \tag{3.43}$$

Moreover, the kinetic terms for the gauge fields in (3.36) comprise mixed terms consisting of the gauge boson vector fields and their scalar components $W_\phi^\pm$, Z_ϕ, and A_ϕ. We remove all of

these mixed terms with a suitable choice of the gauge-fixing Lagrangian (*cf.* (1.63))

$$
\begin{aligned}
\mathcal{L}_{\mathrm{GF}} = &-\frac{1}{2\xi}\left(\partial^\mu A_\mu - \xi\left[\frac{\partial_\phi\, e^{-2\sigma(\phi)}A_\phi}{r^2}\right]\right)^2 \\
&-\frac{1}{2\xi}\left(\partial^\mu Z_\mu - \xi\left[\frac{\delta(|\phi|-\pi)}{r}\,M_Z\,\varphi^3 + \frac{\partial_\phi\, e^{-2\sigma(\phi)}Z_\phi}{r^2}\right]\right)^2 \\
&-\frac{1}{\xi}\left(\partial^\mu W_\mu^+ - \xi\left[\frac{\delta(|\phi|-\pi)}{r}\,M_W\,\varphi^+ + \frac{\partial_\phi\, e^{-2\sigma(\phi)}W_\phi^+}{r^2}\right]\right) \\
&\times\left(\partial^\mu W_\mu^- - \xi\left[\frac{\delta(|\phi|-\pi)}{r}\,M_W\,\varphi^- + \frac{\partial_\phi\, e^{-2\sigma(\phi)}W_\phi^-}{r^2}\right]\right).
\end{aligned}
\tag{3.44}
$$

Note that each term above could be written with a different gauge-fixing parameter ξ_i, however, without loss of generality, we will choose them to be equal. Moreover, there is no problem in squaring the δ-distributions in the expression above. As we will see below, the derivatives of the scalar components of the gauge fields $W_\phi^\pm$ and Z_ϕ also contain δ-distributions, which exactly cancel the δ-distributions from the Higgs sector. In consequence, we do not have to introduce separate gauge-fixing Lagrangians in the bulk and on the IR brane as done in [201].

After integration by parts, the quadratic terms in the action finally become

$$
\begin{aligned}
S_{\mathrm{gauge},2} = \int d^4x\, r \int_{-\pi}^{\pi} d\phi\,\Bigg\{ &-\frac{1}{4}F_{\mu\nu}F^{\mu\nu} - \frac{1}{2\xi}\left(\partial^\mu A_\mu\right)^2 \\
&+\frac{e^{-2\sigma(\phi)}}{2r^2}\left[\partial_\mu A_\phi \partial^\mu A_\phi + \partial_\phi A_\mu \partial_\phi A^\mu\right] - \frac{\xi}{2}\left[\frac{\partial_\phi\, e^{-2\sigma(\phi)}A_\phi}{r^2}\right]^2 \\
&-\frac{1}{4}Z_{\mu\nu}Z^{\mu\nu} - \frac{1}{2\xi}\left(\partial^\mu Z_\mu\right)^2 + \frac{e^{-2\sigma(\phi)}}{2r^2}\left[\partial_\mu Z_\phi \partial^\mu Z_\phi + \partial_\phi Z_\mu \partial_\phi Z^\mu\right] \\
&-\frac{1}{2}W_{\mu\nu}^+ W^{-\mu\nu} - \frac{1}{\xi}\partial^\mu W_\mu^+\,\partial^\mu W_\mu^- + \frac{e^{-2\sigma(\phi)}}{r^2}\left[\partial_\mu W_\phi^+ \partial^\mu W_\phi^- + \partial_\phi W_\mu^+ \partial_\phi W^{-\mu}\right] \\
&+\frac{\delta(|\phi|-\pi)}{r}\left[\frac{1}{2}\partial_\mu h \partial^\mu h - \lambda v^2 h^2 + \partial_\mu \varphi^+ \partial^\mu \varphi^- + \frac{1}{2}\partial_\mu \varphi^3 \partial^\mu \varphi^3 + \frac{M_Z^2}{2}Z_\mu Z^\mu + M_W^2\,W_\mu^+ W^{-\mu}\right] \\
&-\frac{\xi}{2}\left[\frac{\delta(|\phi|-\pi)}{r}\,M_Z\,\varphi^3 + \frac{\partial_\phi\, e^{-2\sigma(\phi)}Z_\phi}{r^2}\right]^2 \\
&-\xi\left[\frac{\delta(|\phi|-\pi)}{r}\,M_W\,\varphi^+ + \frac{\partial_\phi\, e^{-2\sigma(\phi)}W_\phi^+}{r^2}\right]\left[\frac{\delta(|\phi|-\pi)}{r}\,M_W\,\varphi^- + \frac{\partial_\phi\, e^{-2\sigma(\phi)}W_\phi^-}{r^2}\right] + \mathcal{L}_{\mathrm{FP}}\Bigg\}.
\end{aligned}
\tag{3.45}
$$

The Faddeev-Popov ghost Lagrangian $\mathcal{L}_{\mathrm{FP}}$ will not be needed for the following derivations. Its form will however be discussed after the KK decomposition.

Before proceeding, we have to explain the precise definition of the δ-distributions above. For the consistency of the 5D gauge theory, it is important that we can integrate by parts in the action without encountering boundary terms. Otherwise the Lagrangian is not hermitian as required by unitarity, see Section 1.1.1. However, the presence of δ-distribution terms at
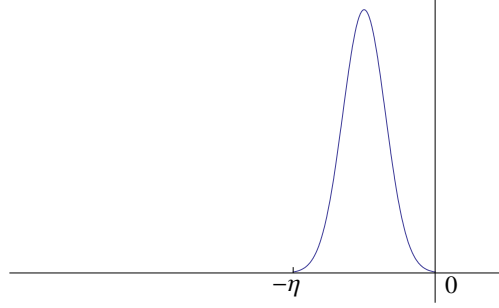
Figure 3.5: Regularized δ-distribution (schematically). See [2] and text for details.

the IR boundary gives rise to discontinuities of some of the fields at $|\phi| = \pi$, which seems to jeopardize this important feature. In order to avoid this problem, we will always regularize the δ-distributions by moving them infinitesimally into the bulk. When treating fermions, we will also have to furnish them with a finite width. We will thus view the δ-distribution as the limit $\eta \to 0$ of a sequence of regularized functions $\delta^\eta(x)$ with support on the interval $x \in [-\eta, 0]$, see Figure 3.5. This limit is understood in the weak sense such that

$$\lim_{\eta \to 0^+} \int_{-\infty}^{+\infty} dx\, \delta^\eta(x) f(x) = f(0)\,, \tag{3.46}$$

for all test functions $f(x)$, *i.e.*, smooth functions having compact support.

It turns out that for the gauge boson sector, we can take the limit of the width approaching zero from the beginning, nevertheless still keeping the δ-distribution infinitesimally away from the brane. The orbifold symmetry thus leads to the definition

$$\delta(|\phi| - \pi) \equiv \lim_{\eta \to 0^+} \frac{1}{2} \left[\delta(\phi - \pi + \eta) + \delta(\phi + \pi - \eta) \right]. \tag{3.47}$$

As a consequence, the discontinuities are moved into the bulk and we can assign standard BCs to the fields on the branes, being consistent with integration by parts (without boundary terms). All calculations are performed at small but finite η and in the end the (smooth) limit $\eta \to 0^+$ is taken, giving rise to well-defined jump conditions for Z_2-odd functions on the IR brane. We will use the notation $f(\pi^-) \equiv \lim_{\eta \to 0^+} f(\pi - \eta)$ to specify the value of a function which is discontinuous at $|\phi| = \pi$. For bulk fermions, however, it will turn out that we have to work with a finite width in the course of calculating the spectrum. The reason is, that in this sector, the δ-distributions multiply functions which feature discontinuities (in the limit $\eta \to 0$) within the support of the δ-distributions, see Section 3.2.2.

Kaluza-Klein Decomposition

We now perform a KK decomposition of the various 5D gauge fields. Not being able to probe directly the extra dimension, it is sensible to choose a 4D description by decomposing the fields into components, just depending on the non-compact 4D space-time, supplied with profile functions, depending on ϕ. Thus, after performing the integral over the fifth dimension, we will end up with an effective 4D theory containing infinite towers of (massive) 4D fields,

as discussed in Section 2.2.2. The zero mode sector has to correspond (to LO) to the SM, as the low-energy tail of the NP model.

In the spirit of performing a Fourier decomposition, we decompose the 4D-Lorentz vector (scalar) components of the 5D boson fields with respect to the complete set of (derivatives of) even functions on the orbifold $\chi_n^a(\phi)$, $a = A, Z, W$, which can be taken to obey the orthonormality conditions

$$\int_{-\pi}^{\pi} d\phi \, \chi_m^a(\phi) \, \chi_n^a(\phi) = \delta_{mn} \,. \tag{3.48}$$

The Fourier coefficients, still depending on x^μ, will then correspond to standard 4D gauge fields. We write

$$A_\mu(x, \phi) = \frac{1}{\sqrt{r}} \sum_n A_\mu^{(n)}(x) \, \chi_n^A(\phi) \,, \qquad\qquad A_\phi(x, \phi) = \frac{1}{\sqrt{r}} \sum_n a_n^A \, \varphi_A^{(n)}(x) \, \partial_\phi \chi_n^A(\phi) \,,$$

$$Z_\mu(x, \phi) = \frac{1}{\sqrt{r}} \sum_n Z_\mu^{(n)}(x) \, \chi_n^Z(\phi) \,, \qquad\qquad Z_\phi(x, \phi) = \frac{1}{\sqrt{r}} \sum_n a_n^Z \, \varphi_Z^{(n)}(x) \, \partial_\phi \chi_n^Z(\phi) \,,$$

$$W_\mu^\pm(x, \phi) = \frac{1}{\sqrt{r}} \sum_n W_\mu^{\pm(n)}(x) \, \chi_n^W(\phi) \,, \qquad W_\phi^\pm(x, \phi) = \frac{1}{\sqrt{r}} \sum_n a_n^W \, \varphi_W^{\pm(n)}(x) \, \partial_\phi \chi_n^W(\phi) \,,$$

$$\tag{3.49}$$

where the *Kaluza Klein modes* $A_\mu^{(n)}$ *etc.* are already the correct 4D mass eigenstates and thus no further transformation to the mass basis is necessary.

The 4D scalar fields can also be expanded in the basis of mass eigenstates as

$$\varphi^\pm(x) = \sum_n b_n^W \, \varphi_W^{\pm(n)}(x) \,, \qquad \varphi^3(x) = \sum_n b_n^Z \, \varphi_Z^{(n)}(x) \,. \tag{3.50}$$

The masses of the 4D vector fields will be denoted by $m_n^a \geq 0$ (with $a = A, Z, W$) and those of the scalar fields $\varphi_a^{(n)}$ are related to them by gauge invariance. Just as the scalar Goldstone bosons of the Higgs sector provide the longitudinal degrees of freedom for the massive gauge bosons (see Section 1.1.2), the scalar components of the 5D gauge fields provide the degrees of freedom for the 4D vector KK fields to become massive. After EWSB those fields will mix. The similar role that they play is reflected in the gauge fixing Lagrangian (3.44).

The EOMs which determine the form of the profiles χ_n^a can be obtained *e.g.* by inserting the decompositions (3.49) into the action and demanding that the 4D theory, after performing the integral over the unresolvable fifth dimension, looks like a standard 4D theory of (massive) gauge bosons (and scalar "Goldstone" bosons). We find [169, 170]

$$-\frac{1}{r^2} \, \partial_\phi \, e^{-2\sigma(\phi)} \, \partial_\phi \, \chi_n^a(\phi) = (m_n^a)^2 \, \chi_n^a(\phi) - \frac{\delta(|\phi| - \pi)}{r} \, M_a^2 \, \chi_n^a(\phi) \,. \tag{3.51}$$

As we work with a compact extra dimension with boundaries, we have to specify the BCs for our profiles. Integrating (3.51) over an infinitesimal interval across the orbifold fixed points

and keeping in mind that the functions χ_n^a have even Z_2 parity one arrives at

$$\partial_\phi \, \chi_n^a(0) = 0 \qquad\qquad\qquad \text{(UV brane)} \, ,$$
$$\partial_\phi \, \chi_n^a(\pi^-) = -\frac{r M_a^2}{2\epsilon^2} \, \chi_n^a(\pi) \qquad \text{(IR brane)} \, . \tag{3.52}$$

The IR BCs determine the mass eigenvalues m_n^a of the gauge-boson mass-eigenstates. Already the lightest modes of the $W^\pm$ and Z bosons receive finite masses $m_n^a \sim v$, due to the couplings to the Higgs sector, reflected by $M_a > 0$, $a = W, Z$. Note that Z_2-odd profiles, obeying canonical Dirichlet BCs, do not posses zero modes, *i.e.*, they have no solution with $m_n^a = 0$ (or $m_n^a \sim v$ after EWSB). Their lightest modes will develop masses of the order of $\mathcal{O}(M_{\mathrm{KK}})$. This holds in particular for the scalar components of the gauge fields, that have profiles proportional to the derivative of the vector components. However, they can still mix with light modes like the Goldstone bosons from the Higgs sector.

In the end the bilinear gauge-boson action takes the desired form

$$
\begin{aligned}
S_{\mathrm{gauge},2} = \sum_n \int d^4x \Bigg\{ &-\frac{1}{4} F_{\mu\nu}^{(n)} F^{\mu\nu(n)} - \frac{1}{2\xi} \left(\partial^\mu A_\mu^{(n)} \right)^2 + \frac{(m_n^A)^2}{2} \, A_\mu^{(n)} A^{\mu(n)} \\
&-\frac{1}{4} Z_{\mu\nu}^{(n)} Z^{\mu\nu(n)} - \frac{1}{2\xi} \left(\partial^\mu Z_\mu^{(n)} \right)^2 + \frac{(m_n^Z)^2}{2} \, Z_\mu^{(n)} Z^{\mu(n)} \\
&-\frac{1}{2} W_{\mu\nu}^{+(n)} W^{-\mu\nu(n)} - \frac{1}{\xi} \partial^\mu W_\mu^{+(n)} \partial^\mu W_\mu^{-(n)} + (m_n^W)^2 \, W_\mu^{+(n)} W^{-\mu(n)} \\
&+\frac{1}{2} \partial_\mu \varphi_A^{(n)} \partial^\mu \varphi_A^{(n)} - \frac{\xi (m_n^A)^2}{2} \, \varphi_A^{(n)} \varphi_A^{(n)} + \frac{1}{2} \partial_\mu \varphi_Z^{(n)} \partial^\mu \varphi_Z^{(n)} - \frac{\xi (m_n^Z)^2}{2} \, \varphi_Z^{(n)} \varphi_Z^{(n)} \\
&+ \partial_\mu \varphi_W^{+(n)} \partial^\mu \varphi_W^{-(n)} - \xi (m_n^W)^2 \, \varphi_W^{+(n)} \varphi_W^{-(n)} \Bigg\} \\
&+ \int d^4x \left(\frac{1}{2} \partial_\mu h \partial^\mu h - \lambda v^2 h^2 \right) + \sum_n \int d^4x \, \mathcal{L}_{\mathrm{FP}}^{(n)} \, ,
\end{aligned}
\tag{3.53}
$$

if and only if, in addition to the EOMs (3.51), the relations

$$a_n^a = -\frac{1}{m_n^a} \, , \qquad b_n^a = \frac{M_a}{\sqrt{r}} \, \frac{\chi_n^a(\pi^-)}{m_n^a} \tag{3.54}$$

hold. Looking at (3.53) we see that, as expected, we end up with an infinite number of copies of the 4D SM gauge sector, to be distinguished by the mass of the fields. We observe towers of massive gauge bosons with masses m_n^a, accompanied by towers of massive scalars with masses $\sqrt{\xi} \, m_n^a$, as well as the Higgs field h with mass $\sqrt{2\lambda} v$. The low energy tail of the gauge-boson spectrum, *i.e.*, the zero modes, can be interpreted as the SM gauge bosons we observe in nature. However, due to v^2/M_{KK}^2 suppressed mixing effects with the KK modes (already included in our KK decomposition), the massive gauge bosons will couple differently compared to the SM, see below. Measuring these deviations, as well as deviations due to the virtual exchange of KK excitations, provides a possibility to test the RS scenario, in addition to detecting directly the heavy KK modes with masses $m_1^a \sim M_{\mathrm{KK}}$.

Note that, after applying (3.54), the 4D gauge-fixing Lagrangian derived from (3.44) can be written as

$$r \int_{-\pi}^{\pi} d\phi \, \mathcal{L}_{\mathrm{GF}} = \sum_{n} \mathcal{L}_{\mathrm{GF}}^{(n)} \,, \tag{3.55}$$

where

$$
\begin{aligned}
\mathcal{L}_{\mathrm{GF}}^{(n)} = &-\frac{1}{2\xi} \left(\partial^{\mu} A_{\mu}^{(n)} - \xi m_n^A \varphi_A^{(n)} \right)^2 - \frac{1}{2\xi} \left(\partial^{\mu} Z_{\mu}^{(n)} - \xi m_n^Z \varphi_Z^{(n)} \right)^2 \\
&- \frac{1}{\xi} \left(\partial^{\mu} W_{\mu}^{+(n)} - \xi m_n^W \varphi_W^{+(n)} \right) \left(\partial^{\mu} W_{\mu}^{-(n)} - \xi m_n^W \varphi_W^{-(n)} \right).
\end{aligned}
\tag{3.56}
$$

For each KK mode these expressions resemble those of the SM. As a consequence, the Faddeev-Popov ghost Lagrangians $\mathcal{L}_{\mathrm{FP}}^{(n)}$ in (3.53) are completely analogous to the one of the SM. The only generalization being, that a ghost field is required for every KK mode.

Bulk Profiles

In this section we derive the explicit form of the gauge-boson profiles χ_n which are solutions to the EOMs (3.51). From now on, we omit the superscript a, denoting the gauge-boson type, unless it is needed for clarity. The corresponding expressions were first obtained in [169, 170] for the case of an unbroken gauge symmetry. As the EOMs in the bulk are the same, the structure of this solution remains valid also for a spontaneously broken symmetry. However, we have to take into account the modified BCs on the IR brane due to the couplings to the Higgs sector (3.52).

In the following it will turn out to be convenient to switch to the variable $t = \epsilon \, e^{\sigma}$ to describe the orbifold [173], which will take values between $t = \epsilon$ (UV brane) and $t = 1$ (IR brane), corresponding to the interval $\phi \in [0, \pi]$. The reflection at $\phi = 0$ will be defined via the Z_2 symmetry. Integrals over the orbifold can be obtained (for an Z_2 even integrand) using

$$\int_{-\pi}^{\pi} d\phi \to \frac{2\pi}{L} \int_{\epsilon}^{1} \frac{dt}{t} \,, \qquad \int_{-\pi}^{\pi} d\phi \, e^{\sigma(\phi)} \to \frac{2\pi}{L\epsilon} \int_{\epsilon}^{1} dt \,, \qquad etc. \tag{3.57}$$

After this transformation of coordinates, the EOMs (3.51) become [8]

$$t \, \partial_t \, t^{-1} \partial_t \, \chi_n(t) = -x_n^2 \, \chi_n(t) + \delta(t-1) \frac{M^2}{2k\epsilon^2} \, \chi_n(t) \,. \tag{3.58}$$

The parameters

$$x_n \equiv \frac{m_n}{M_{\mathrm{KK}}} \tag{3.59}$$

---

[8]Note that another useful formulation of the RS background is given by the conformally flat metric [202]

$$ds^2 = \left(\frac{R}{z} \right)^2 \left(\eta_{\mu\nu} \, dx^{\mu} dx^{\nu} - dz^2 \right),$$

restricted to the interval $z \in [R, R']$, where $z = \frac{t}{M_{\mathrm{KK}}}$. Here, $R = \frac{1}{k}$ and $R' = \frac{1}{M_{\mathrm{KK}}}$ denote the positions of the UV brane and the IR brane, respectively.

are the dimensionless versions of the masses of the gauge bosons and their KK excitations in the 4D theory. The ansatz

$$\chi_n(t) = N_n \sqrt{\frac{L}{\pi}} \, t \, c_n^+(t) \,, \tag{3.60}$$

finally leads to the Bessel equation

$$x_n^2 t^2 \, c_n^{+\,\prime\prime}(x_n t) + x_n t \, c_n^{+\,\prime}(x_n t) + (x_n^2 t^2 - 1) c_n^+(x_n t) = 0 \tag{3.61}$$

in the bulk ($t \neq \epsilon, 1$). This equation is solved by

$$c_n^+(t) = Y_0(x_n \epsilon) \, J_1(x_n t) - J_0(x_n \epsilon) \, Y_1(x_n t) \,, \tag{3.62}$$

where the coefficients have been determined by the UV BCs (3.52). We furthermore define

$$c_n^-(t) = \frac{1}{x_n t} \frac{d}{dt} \left[t \, c_n^+(t) \right] = Y_0(x_n \epsilon) \, J_0(x_n t) - J_0(x_n \epsilon) \, Y_0(x_n t) \,. \tag{3.63}$$

The normalization constants N_n are now fixed by the orthonormality condition (3.48) to obey

$$N_n^{-2} = \left[c_n^+(1) \right]^2 + \left[c_n^-(1) \right]^2 - \frac{2}{x_n} c_n^+(1) \, c_n^-(1) - \epsilon^2 \left[c_n^+(\epsilon) \right]^2 \,. \tag{3.64}$$

Since $c_n^-(\epsilon) = 0$, we easily see that (3.60) satisfies the BCs $\partial_t \chi_n(\epsilon) = 0$ on the UV brane.

The BCs (3.52) on the IR brane lead to the relation

$$x_n \, c_n^-(1) = -\frac{g^2 v^2}{4 M_{\mathrm{KK}}^2} \, L \, c_n^+(1) \,, \tag{3.65}$$

from which the mass eigenvalues x_n can be derived. Note that the condition (3.65) as stated above holds for the profiles of the $W^\pm$ bosons and their KK partners. For the case of the Z boson, the $SU(2)$-coupling g^2 has to be replaced by the combination $(g^2 + g'^2)$. In the absence of EWSB ($v = 0$), which corresponds to the case of the photon and the gluon which do not couple to the Higgs sector, the right hand side becomes zero. In this case the spectrum contains a massless zero mode ($m_0 = 0$) with a flat profile

$$\chi_{\gamma,g}(t) = \frac{1}{\sqrt{2\pi}} \,. \tag{3.66}$$

These massless modes are identified with the SM photon and gluon. The masses of their KK excitations will simply correspond to zeros of a combination of Bessel functions $c_n^-(1) = 0$, which, to good approximation corresponds to zeros of the Bessel function $J_0(x_n)$. This leads to $x_1 \approx 2.45$ and the heavier modes follow in spacings of about π. Due to the flat profile, the photon and the gluon zero modes will couple to bulk fermions exactly like in the SM, which will be important for the discussions of FCNCs in Section 3.2.4.

The results for the massive SM gauge bosons, which correspond to (light) modes with
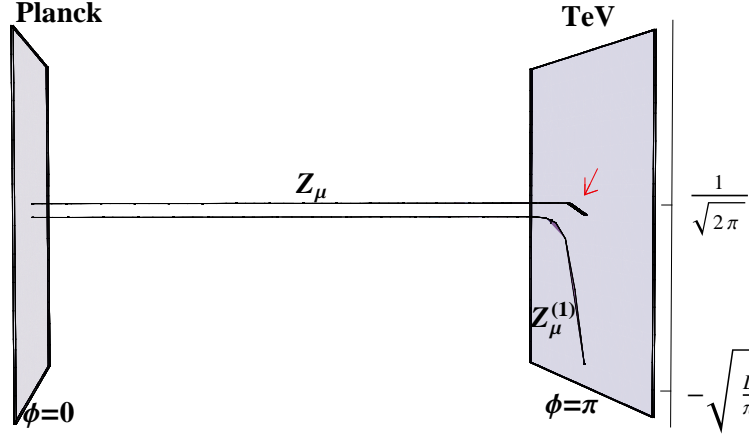
Figure 3.6: Zero mode and first KK excitation of the Z boson in a slice of AdS$_5$.

$m_0 \neq 0$, can be simplified, since $x_0 \ll 1$. Expanding (3.65) in powers of x_0 we arrive at

$$m_W^2 = \frac{g^2 v^2}{4} \left[1 - \frac{g^2 v^2}{8 M_{\mathrm{KK}}^2} \left(L - 1 + \frac{1 - \epsilon^2}{2L} \right) + \mathcal{O}\left(\frac{v^4}{M_{\mathrm{KK}}^4} \right) \right]. \tag{3.67}$$

An analogous relation with g^2 replaced by $(g^2 + g'^2)$ holds for the Z-boson mass. Comparing these results with the SM relations (1.25), one sees immediately that the tree-level ratio of the $W^\pm$-boson and Z-boson mass in RS models deviates from the SM prediction.[9] This is due to the mixings with the KK modes, *i.e.*, the contributions to the zero-mode masses from the compactification of the extra dimension. Moreover, the Higgs VEV, extracted from (3.67) will get corrections with respect to the SM value of $v_{\mathrm{SM}} = 246$ GeV. We will come back to both of these issues later in Section 5.1.1. It will also turn out to be useful to derive an approximate expression for the ground-state profile χ_0 for $x_0 \ll 1$. We obtain, in agreement with [202],

$$\chi_{W,Z}(t) = \frac{1}{\sqrt{2\pi}} \left[1 + \frac{m_{W,Z}^2}{4 M_{\mathrm{KK}}^2} \left(1 - \frac{1 - \epsilon^2}{L} + t^2 \left(1 - 2L - 2\ln t \right) \right) + \mathcal{O}\left(\frac{m_{W,Z}^4}{M_{\mathrm{KK}}^4} \right) \right]. \tag{3.68}$$

The deviations from the flat zero mode solution without EWSB (3.66) can be understood from a perturbative point of view as the mixings of the massive KK modes, being localized close to the IR brane, into the zero mode. This will lead to a dip in the zero mode profiles at this boundary, proportional to the mixing parameter $m_{W,Z}/M_{\mathrm{KK}}^2$, see Figure 3.6. The absolute value of the profiles of generic KK modes on the IR brane is to good approximation given by

$$|\chi_n(1)| \approx \sqrt{\frac{L}{\pi}}, \, n \geq 1. \tag{3.69}$$

The accuracy of this approximation increases with n.

---

[9]Note that, here and in the following, by Z boson ($W^\pm$ boson), we denote the *zero modes* of the Z boson ($W^\pm$ bosons).

3.2.2 Bulk Matter and Flavor Mixing

Now we move to the SM fermion content, propagating into the extra dimension. The warped background provides interesting possibilities for model building in this sector. After discussing the setup, we will perform the KK decomposition in the mass basis, incorporating flavor mixing in a completely general way. In this way we are again able to derive exact expressions from which the masses and mixings can be obtained. We will concentrate on the quark sector. The generalization to include the lepton sector, which will not be studied in this thesis, is straightforward.

In the subsequent section we will then show how hierarchies in the quark spectrum, as well as in the CKM mixing angles, arise naturally within the RS model. By performing an expansion in small parameters, we will work out explicit analytic expressions for the masses of the SM quarks (corresponding to the light "zero modes" in the RS model), as well as the CKM parameters, in terms of the input parameters of the RS model. To this end, we demonstrate and apply an analogy between the generation of flavor hierarchies in warped extra dimensions and in the Froggatt-Nielsen model.

Action of the 5D Theory

As we consider the SM field content, we start from (1.9), with the quantum numbers of the fermion fields still as given in Table 1.1, and generalize the corresponding action to 5D. However, in an odd number of space-time dimensions we have to face a subtlety when trying to define chiral fermions. To describe matter fields in five dimensions, we need a representation of the 5D-Clifford Algebra

$$\{\Gamma_M, \Gamma_N\} = 2\eta_{MN}. \tag{3.70}$$

An appropriate four dimensional representation in 5D is provided by taking the usual 4D representation, consisting of the Dirac matrices γ_μ (see Appendix A.1), and subjoining γ_5

$$\Gamma_M = (\gamma_\mu, i\gamma_5). \tag{3.71}$$

Note that the vector of Dirac matrices above is contracted with Lorentz vectors in curved space-time via the vielbein formalism, see *e.g.* [173].

In an even number of dimensions, the Dirac-spinor representation is reducible. For example, in 4D it can be decomposed into the well known (left-handed and right-handed) Weyl-spinor representations that do not mix under Lorentz transformations. The corresponding projections are just provided by the projectors $P_{L,R} \equiv (1 \mp \gamma^5)/2$, defined with the help of the chirality matrix γ^5, see Section 1.1.1. However, it turns out that in an odd number of dimensions, the Dirac-spinor representation is irreducible. Although we can formally still define projection operators in 5D out of γ^5, the spectrum will a priori have to consist of "vector-like" four-component Dirac fermions, *i.e.*, for every left handed fermion a right handed counterpart will appear with the same quantum numbers, and vice versa. Yet, as discussed before, nature is based on chiral matter fields. The left-handed fermions we observe are doublets under $SU(2)_L$, whereas the right-handed ones are singlets under this gauge group. At first sight, it seems impossible to generate such a setup in 5D. However, the obrifold will again furnish a way out and offer a possibility to arrive at chiral fermions in the low energy spectrum of the theory, after KK decomposition [173]. The Z_2 symmetry of the action results in opposite Z_2

parities for the left-handed and right-handed components of a Dirac fermion. This suggests to start with two sets of Dirac fermions in 5D, one containing doublets under $SU(2)_L$ and one containing the corresponding singlets, and assign the Z_2-parities/BCs properly, such that the doublets just have left-handed (4D) zero modes, while the singlets possess only right-hand zero modes. In consequence, the low energy spectrum will contain just the chiralities that we observe in Nature (in the limit $v \to 0$). At each level of KK excitations however, two full (vector-like) Dirac-fermions, a singlet and a doublet, will be present and thus twice the amount of degrees of freedom with respect to the zero mode level. Note that after EWSB, the doublets and singlets will mix, for example the right handed zero mode will receive a small doublet admixture from the KK excitations, leading to a (suppressed) "right handed" CKM matrix, see below.

So, let us consider N generations of 5D (SM-like) quarks in the bulk, denoting components of $SU(2)_L$ doublets by u, d and singlets by u^c, d^c. As we will discuss more complicated fermion contents in Section 3.4, we will give the action already in a notation which is appropriate for a richer fermion structure. The bilinear part of the 5D fermion action can be written as (cf. [173, 172])

$$
S_{\text{ferm},2} = \int d^4x\, r \int_{-\pi}^{\pi} d\phi \left\{ \sum_{q=U,u,D,d} \left(e^{-3\sigma(\phi)}\, \bar{\vec{q}}\, i\slashed{\partial}\, \vec{q} - e^{-4\sigma(\phi)}\, \text{sgn}(\phi)\, \bar{\vec{q}}\, \boldsymbol{M}_{\vec{q}}\, \vec{q} \right.\right.
$$
$$
\left. - \frac{1}{2r} \left[\bar{\vec{q}}_L\, e^{-2\sigma(\phi)}\, \overset{\leftrightarrow}{\partial}_\phi\, e^{-2\sigma(\phi)}\, \vec{q}_R + \text{h.c.} \right] \right)
$$
$$
\left. - \delta(|\phi| - \pi)\, e^{-3\sigma(\phi)} \frac{v}{\sqrt{2}r} \sum_{(Q,q)=(U,u),(D,d)} \left[\bar{\vec{Q}}_L\, \boldsymbol{Y}_{\vec{q}}^{(5D)C}\, \vec{q}_R + \bar{\vec{Q}}_R\, \boldsymbol{Y}_{\vec{q}}^{(5D)S}\, \vec{q}_L + \text{h.c.} \right] \right\},
$$
(3.72)

where $\overset{\leftrightarrow}{\partial}_\phi \equiv \overset{\rightarrow}{\partial}_\phi - \overset{\leftarrow}{\partial}_\phi$, and we have already evaluated explicitly the μ and ϕ components of the vielbein, entering the kinetic terms [173]. Moreover, note that the spin connection gives no contribution to (3.72). For the SM fermion content (Table 1.1), the vectors of fermions introduced here correspond merely to N-component vectors in flavor space (e.g. $u = (u, c, t)^T$ for the up-type quarks of the SM). We identify for the minimal RS model

$$
\vec{U} \equiv u, \ \vec{D} \equiv d, \quad \vec{u} \equiv u^c, \ \vec{d} \equiv d^c,
$$
(3.73)

and thus end up with the standard SM notation, as used in [1]. Note that for the extended model studied in Section 3.4, the fermion vectors will contain several types of quarks. In the spirit of writing down every term which is not forbidden by a symmetry, we include explicit gauge-invariant 5D Dirac mass terms for the vector-like quarks, with diagonal and real $N \times N$ bulk mass matrices

$$
\boldsymbol{M}_{\vec{U}} = \boldsymbol{M}_{\vec{D}} \equiv \boldsymbol{M}_Q
$$
(3.74)

for the $SU(2)_L$ doublets as well as $\boldsymbol{M}_{\vec{q}} \equiv \boldsymbol{M}_q$, $q = u, d$ for the singlets. Since the corresponding combination of field operators is always Z_2 odd, the mass matrices have to be multiplied by a Z_2 odd function in order to arrive at a Z_2 invariant action. Starting from generic hermitian

bulk mass matrices, it is easy to see that going to the *bulk mass basis* in which those matrices are real and diagonal does not spoil the canonical and diagonal form of the kinetic terms. Note however that the bulk masses can be positive as well as negative. In contrast to 4D theories, the sign of the Dirac mass term cannot be reversed by a field redefinition. In order to arrive at the correct low energy spectrum, as discussed before, the left-handed (right-handed) components of the $SU(2)_L$ doublet $Q \equiv (u, d)^T$ are taken to be even (odd) under the Z_2 orbifold symmetry, with appropriate canonical BCs. Likewise, the right-handed (left-handed) components of the singlets u^c and d^c are chosen even (odd), such that the zero modes of the even fields correspond to the SM particles. After EWSB on the IR brane, the quark fields are coupled by 5D $N \times N$ Yukawa matrices $\boldsymbol{Y}_{\vec{q}}^{(5D)C}$, connecting the Z_2 even components of the $SU(2)_L$ doublets with those of the singlets, as well as corresponding matrices $\boldsymbol{Y}_{\vec{q}}^{(5D)S}$, connecting Z_2-odd fields, where $q = u, d$. If not stated otherwise, those matrices correspond to the bulk mass basis of real and diagonal matrices $\boldsymbol{M}_{Q,q}$. Note that the second type of Yukawa couplings has not been taken into account in [1]. While such a setup is consistent and it is possible to generate the fermion masses without those couplings, it is not the most general or natural possibility, and we will include these couplings. Furthermore, if one considers the brane-localized Higgs-sector as the limit of a Higgs, propagating into the bulk, both types of Yukawa matrices have to be identical $\boldsymbol{Y}_{\vec{q}}^{(5D)C} = \boldsymbol{Y}_{\vec{q}}^{(5D)S} \equiv \boldsymbol{Y}_{\vec{q}}^{(5D)}$, which we will assume in the following. This is, again, due to the fact that in 5D the Dirac-spinor representation is irreducible. In a perturbative approach, the Yukawa terms containing Z_2 odd fields do not seem to contribute, as the corresponding profiles vanish on the IR brane. However, in the end this naive point of view will turn out to be wrong, as we will see below [203]. For the KK decomposition it will be convenient to define dimensionless 4D Yukawa matrices via

$$\boldsymbol{Y}_{\vec{q}}^{(5D)} \equiv \frac{2\boldsymbol{Y}_{\vec{q}}}{k}, \qquad q = u, d, \tag{3.75}$$

where again in the *minimal RS model* the vector notation is not necessary $\boldsymbol{Y}_{\vec{q}} \equiv \boldsymbol{Y}_q$. The chiral components of the spinor field are defined as usual as $\vec{q} = \vec{q}_L + \vec{q}_R$, *etc.* As discussed before, without the presence of the Yukawa interactions, each 5D fermion would induce a massless chiral fermion in the 4D theory, accompanied by a tower of massive, vector-like, KK excitations [173]. After EWSB, the Yukawa couplings replace the massless modes by light modes (compared to the KK scale), corresponding to the SM fermions.

Kaluza-Klein Decomposition

We want to arrive at a 4D theory of massive Dirac fermions $q^{(n)} = q_L^{(n)} + q_R^{(n)}$ with masses $m_n > 0$. To this end we perform a KK decomposition of the 5D fields in the mass basis and write

$$\vec{Q}_L(x, \phi) = \frac{e^{2\sigma(\phi)}}{\sqrt{r}} \sum_n \boldsymbol{C}_n^Q(\phi)\, \vec{a}_n^Q\, q_L^{(n)}(x), \qquad \vec{Q}_R(x, \phi) = \frac{e^{2\sigma(\phi)}}{\sqrt{r}} \sum_n \boldsymbol{S}_n^Q(\phi)\, \vec{a}_n^Q\, q_R^{(n)}(x),$$

$$\vec{q}_L(x, \phi) = \frac{e^{2\sigma(\phi)}}{\sqrt{r}} \sum_n \boldsymbol{S}_n^q(\phi)\, \vec{a}_n^q\, q_L^{(n)}(x), \qquad \vec{q}_R(x, \phi) = \frac{e^{2\sigma(\phi)}}{\sqrt{r}} \sum_n \boldsymbol{C}_n^q(\phi)\, \vec{a}_n^q\, q_R^{(n)}(x),$$

$$\tag{3.76}$$

where $Q = U, D$ and correspondingly $q = u, d$. For the SM fermion content studied in this section, we have with (3.73) $\vec{U} = u$ and $\vec{u} = u^c$ and similar for down type quarks. In that case, the spinor fields on the left hand side of the equations in (3.76), as well as the objects $\vec{a}_n^{Q,q}$, describing flavor mixing, are N component vectors in flavor space. The Z_2 even profiles $\boldsymbol{C}_n^{Q,q}$ and odd profiles $\boldsymbol{S}_n^{Q,q}$, however, are diagonal $N \times N$ matrices, where each entry corresponds to a different bulk mass parameter (in the bulk mass basis).[10] The 4D spinors $q^{(n)}$, on the right hand side of the equations in (3.76) are single spinor fields in the mass basis. The index n labels the mass eigenstates of masses m_n. For the case of up-type quarks these are $m_1 = m_u, m_2 = m_c, m_3 = m_t$, as well as the higher KK masses. Note that, due to gauge invariance, the components of the $SU(2)_L$ doublet Q have the same profiles

$$\boldsymbol{C}_n^U = \boldsymbol{C}_n^D \equiv \boldsymbol{C}_n^Q, \quad \boldsymbol{S}_n^U = \boldsymbol{S}_n^D \equiv \boldsymbol{S}_n^Q. \tag{3.77}$$

The associated vectors $\vec{a}_n^U$ and $\vec{a}_n^D$, nevertheless differ for the different components of Q.

Inserting the decompositions (3.76) into the action (3.72), one derives the equations of motion

$$\left(-\frac{1}{r}\partial_\phi - \boldsymbol{M}_{\vec{Q}}\,\mathrm{sgn}(\phi)\right)\boldsymbol{S}_n^Q(\phi)\,\vec{a}_n^Q = -m_n\,e^{\sigma(\phi)}\,\boldsymbol{C}_n^Q(\phi)\,\vec{a}_n^Q$$

$$+ \delta(|\phi| - \pi)\,e^{\sigma(\phi)}\,\frac{\sqrt{2}\,v}{kr}\,\boldsymbol{Y}_{\vec{q}}\,\boldsymbol{C}_n^q(\phi)\,\vec{a}_n^q\,,$$

$$\left(\frac{1}{r}\partial_\phi - \boldsymbol{M}_{\vec{q}}\,\mathrm{sgn}(\phi)\right)\boldsymbol{S}_n^q(\phi)\,\vec{a}_n^q = -m_n\,e^{\sigma(\phi)}\,\boldsymbol{C}_n^q(\phi)\,\vec{a}_n^q$$

$$+ \delta(|\phi| - \pi)\,e^{\sigma(\phi)}\,\frac{\sqrt{2}\,v}{kr}\,\boldsymbol{Y}_{\vec{q}}^\dagger\,\boldsymbol{C}_n^Q(\phi)\,\vec{a}_n^Q\,,$$

$$\left(\frac{1}{r}\partial_\phi - \boldsymbol{M}_{\vec{Q}}\,\mathrm{sgn}(\phi)\right)\boldsymbol{C}_n^Q(\phi)\,\vec{a}_n^Q = -m_n\,e^{\sigma(\phi)}\,\boldsymbol{S}_n^Q(\phi)\,\vec{a}_n^Q \tag{3.78}$$

$$+ \delta(|\phi| - \pi)\,e^{\sigma(\phi)}\,\frac{\sqrt{2}\,v}{kr}\,\boldsymbol{Y}_{\vec{q}}\,\boldsymbol{S}_n^q(\phi)\,\vec{a}_n^q\,,$$

$$\left(-\frac{1}{r}\partial_\phi - \boldsymbol{M}_{\vec{q}}\,\mathrm{sgn}(\phi)\right)\boldsymbol{C}_n^q(\phi)\,\vec{a}_n^q = -m_n\,e^{\sigma(\phi)}\,\boldsymbol{S}_n^q(\phi)\,\vec{a}_n^q$$

$$+ \delta(|\phi| - \pi)\,e^{\sigma(\phi)}\,\frac{\sqrt{2}\,v}{kr}\,\boldsymbol{Y}_{\vec{q}}^\dagger\,\boldsymbol{S}_n^Q(\phi)\,\vec{a}_n^Q\,,$$

where $(Q, q) = (U, u)\,, (D, d)$. In the bulk, *i.e.*, for $\phi \neq 0, \pm\pi$, these equations reduce to the relations first obtained in [173]. The corresponding general solutions can be written as linear combinations of Bessel functions, (see Section 3.2.2). The presence of the source terms on the IR brane, however, modifies the boundary behavior of the fields and causes both the Z_2-even and Z_2-odd profiles to become discontinuous on the IR brane with $\boldsymbol{C}_n^{Q,q}(\pm\pi) \neq \boldsymbol{C}_n^{Q,q}(\pm\pi^-)$

---

[10]Note that we have already exploited the fact that $\vec{Q}_{L,R}(x, \phi)\,(\vec{q}_{L,R}(x, \phi))$ can be expanded in terms of the same vector $\vec{a}_n^Q\,(\vec{a}_n^q)$. With this choice, the profiles $\boldsymbol{C}_n^Q(\phi)$ and $\boldsymbol{S}_n^Q(\phi)\,(\boldsymbol{C}_n^q(\phi)$ and $\boldsymbol{S}_n^q(\phi))$ will be normalized in the same way.

and $\boldsymbol{S}_n^{Q,q}(\pm\pi) = 0$ but $\boldsymbol{S}_n^{Q,q}(\pm\pi^-) \neq 0$ [204]. While the UV BCs remain canonical,

$$\boldsymbol{S}_n^{Q,q}(0) = 0\,, \tag{3.79}$$

finding the correct IR BCs requires a proper finite-width regularization of the δ-distributions appearing in (3.78). Such a regularization is needed since the δ-distributions appear together with functions that are discontinuous within their support. We will use the regularization as introduced in (3.46).

After switching to t coordinates, we study the EOMs (3.78) in an infinitesimal interval $t \in [1-\eta, 1]$, keeping in mind that at the end we will take the limit $\eta \to 0$. We regularize the δ-distributions and integrate these equations from $t \in [1-\eta, 1]$ to 1, taking into account that the odd fermion profiles vanish identically on the IR brane, *i.e.*, $\boldsymbol{S}_n^{Q,q}(1) = 0$ and dropping all terms $\propto \eta$. In this way we find (for finite n)

$$
\begin{aligned}
\boldsymbol{S}_n^Q(t)\,\vec{a}_n^Q &= \frac{v}{\sqrt{2}M_{\mathrm{KK}}}\,\boldsymbol{Y}_{\vec{q}}\int_t^1 dt'\left[\delta^\eta(t'-1)\,\boldsymbol{C}_n^q(t')\right]\vec{a}_n^q\,,\\[4pt]
\boldsymbol{S}_n^q(t)\,\vec{a}_n^q &= -\frac{v}{\sqrt{2}M_{\mathrm{KK}}}\,\boldsymbol{Y}_{\vec{q}}^\dagger\int_t^1 dt'\left[\delta^\eta(t'-1)\,\boldsymbol{C}_n^Q(t')\right]\vec{a}_n^Q\,,\\[4pt]
\boldsymbol{C}_n^Q(t)\,\vec{a}_n^Q &= \boldsymbol{C}_n^Q(1)\,\vec{a}_n^Q - \frac{v}{\sqrt{2}M_{\mathrm{KK}}}\,\boldsymbol{Y}_{\vec{q}}\int_t^1 dt'\left[\delta^\eta(t'-1)\,\boldsymbol{S}_n^q(t')\right]\vec{a}_n^q\,,\\[4pt]
\boldsymbol{C}_n^q(t)\,\vec{a}_n^q &= \boldsymbol{C}_n^q(1)\,\vec{a}_n^q + \frac{v}{\sqrt{2}M_{\mathrm{KK}}}\,\boldsymbol{Y}_{\vec{q}}^\dagger - \int_t^1 dt'\left[\delta^\eta(t'-1)\,\boldsymbol{S}_n^Q(t')\right]\vec{a}_n^Q\,,
\end{aligned}
\tag{3.80}
$$

indicating that the form of the profiles $\boldsymbol{C}_n^{Q,q}(t)$ and $\boldsymbol{S}_n^{Q,q}(t)$ becomes independent of the mass terms entering the EOMs.

In order to solve (3.80), we introduce the regularized Heaviside function

$$\bar{\theta}^\eta(x) \equiv 1 - \int_{-\infty}^x dy\,\delta^\eta(y)\,, \tag{3.81}$$

which obeys

$$\bar{\theta}^\eta(0) = 0\,, \qquad \bar{\theta}^\eta(-\eta) = 1\,, \qquad \partial_x\bar{\theta}^\eta(x) = -\delta^\eta(x)\,. \tag{3.82}$$

Using these properties it is easy to show that

$$\int_t^1 dt'\,\delta^\eta(t'-1)\left[\bar{\theta}^\eta(t'-1)\right]^n = \frac{1}{n+1}\left[\bar{\theta}^\eta(t-1)\right]^{n+1}\,. \tag{3.83}$$

This relation allows us to integrate hyperbolic functions of regularized θ-functions with regularized δ-distributions. For an arbitrary invertible matrix $\boldsymbol{A}$ we obtain

$$
\begin{aligned}
\int_t^1 dt'\,\delta^\eta(t'-1)\,\sinh\left(\bar{\theta}^\eta(t'-1)\boldsymbol{A}\right) &= \left[\cosh\left(\bar{\theta}^\eta(t-1)\boldsymbol{A}\right) - \boldsymbol{1}\right]\boldsymbol{A}^{-1}\,,\\[4pt]
\int_t^1 dt'\,\delta^\eta(t'-1)\,\cosh\left(\bar{\theta}^\eta(t'-1)\boldsymbol{A}\right) &= \sinh\left(\bar{\theta}^\eta(t-1)\boldsymbol{A}\right)\boldsymbol{A}^{-1}\,,
\end{aligned}
\tag{3.84}
$$

where the hyperbolic sine and cosine of a matrix are defined via their Taylor expansions. With the latter relations it is now easy to determine the solutions to (3.80). We find

$$
\boldsymbol{S}_n^Q(t)\,\vec{a}_n^Q = \boldsymbol{Y}_{\vec{q}}\left(\sqrt{\boldsymbol{Y}_{\vec{q}}^\dagger \boldsymbol{Y}_{\vec{q}}}\right)^{-1}\sinh\left(\frac{v}{\sqrt{2}M_{\mathrm{KK}}}\,\bar{\theta}^\eta(t-1)\,\sqrt{\boldsymbol{Y}_{\vec{q}}^\dagger \boldsymbol{Y}_{\vec{q}}}\right)\boldsymbol{C}_n^q(1)\,\vec{a}_n^q\,,
$$

$$
\boldsymbol{S}_n^q(t)\,\vec{a}_n^q = -\boldsymbol{Y}_{\vec{q}}^\dagger\left(\sqrt{\boldsymbol{Y}_{\vec{q}}\boldsymbol{Y}_{\vec{q}}^\dagger}\right)^{-1}\sinh\left(\frac{v}{\sqrt{2}M_{\mathrm{KK}}}\,\bar{\theta}^\eta(t-1)\,\sqrt{\boldsymbol{Y}_{\vec{q}}\boldsymbol{Y}_{\vec{q}}^\dagger}\right)\boldsymbol{C}_n^Q(1)\,\vec{a}_n^Q\,,
$$

$$
\boldsymbol{C}_n^Q(t)\,\vec{a}_n^Q = \cosh\left(\frac{v}{\sqrt{2}M_{\mathrm{KK}}}\,\bar{\theta}^\eta(t-1)\,\sqrt{\boldsymbol{Y}_{\vec{q}}\boldsymbol{Y}_{\vec{q}}^\dagger}\right)\boldsymbol{C}_n^Q(1)\,\vec{a}_n^Q\,,
$$

$$
\boldsymbol{C}_n^q(t)\,\vec{a}_n^q = \cosh\left(\frac{v}{\sqrt{2}M_{\mathrm{KK}}}\,\bar{\theta}^\eta(t-1)\,\sqrt{\boldsymbol{Y}_{\vec{q}}^\dagger \boldsymbol{Y}_{\vec{q}}}\right)\boldsymbol{C}_n^q(1)\,\vec{a}_n^q\,.
$$

(3.85)

Since no t-integration is left, we can now safely take the limit $\eta \to 0^+$ and use the second pair of equations to trade the brane values $\boldsymbol{C}_n^{Q,q}(1)$ in the first equations for the bulk values $\boldsymbol{C}_n^{Q,q}(1^-)$, obtained from the solutions to (3.78) by a limiting procedure. Introducing the rescaled Yukawa matrices[11]

$$
\tilde{\boldsymbol{Y}}_{\vec{q}} \equiv \boldsymbol{f}\left(\frac{v}{\sqrt{2}M_{\mathrm{KK}}}\,\sqrt{\boldsymbol{Y}_{\vec{q}}\boldsymbol{Y}_{\vec{q}}^\dagger}\right)\boldsymbol{Y}_{\vec{q}}\,,\qquad \boldsymbol{f}(\boldsymbol{A}) = \tanh(\boldsymbol{A})\,\boldsymbol{A}^{-1}\,,
$$

(3.86)

it is then easy to show that the resulting IR BCs are manifestly regularization independent[12] and can be written in ϕ coordinates as

$$
\boldsymbol{S}_n^Q(\pi^-)\,\vec{a}_n^Q = \frac{v}{\sqrt{2}M_{\mathrm{KK}}}\,\tilde{\boldsymbol{Y}}_{\vec{q}}\,\boldsymbol{C}_n^q(\pi^-)\,\vec{a}_n^q\,,
$$

$$
-\boldsymbol{S}_n^q(\pi^-)\,\vec{a}_n^q = \frac{v}{\sqrt{2}M_{\mathrm{KK}}}\,\tilde{\boldsymbol{Y}}_{\vec{q}}^\dagger\,\boldsymbol{C}_n^Q(\pi^-)\,\vec{a}_n^Q\,.
$$

(3.87)

They hence take precisely the same form as the BCs derived in [1], with the original Yukawa couplings replaced by the rescaled ones, as defined in (3.86). These coincide at LO in v^2/M_{KK}^2, i.e., $\tilde{\boldsymbol{Y}}_{\vec{q}} = \boldsymbol{Y}_{\vec{q}} + \mathcal{O}(v^2/M_{\mathrm{KK}}^2)$. In practice, the combinations of quark profiles and Yukawa matrices are chosen such that the masses of the zero mode fermions, as well as the CKM parameters, reproduce those determined by experiment. Thus, the rescaling of the Yukawa matrices, as described above, has no observable effect on the fermion spectrum and the mixings. However, as we will explain in detail in Section 3.7, the inclusion of the Yukawa couplings between Z_2-odd fermions alters the misalignment between the masses and Yukawa couplings. This leads to a change in the tree-level interactions of the Higgs-boson with fermions with respect to the results derived in [1].

Without the brane-localized Yukawa couplings, the profiles $\boldsymbol{C}_n^{Q,q}$ and $\boldsymbol{S}_n^{Q,q}$ form complete

---

[11]Generalizing this result to the case where Z_2-even and -odd fermion fields couple via different Yukawa matrices to the brane-localized Higgs sector requires to perform the replacements $\boldsymbol{Y}_{\vec{q}} \to \boldsymbol{Y}_{\vec{q}}^C$ and $\boldsymbol{Y}_{\vec{q}}^\dagger \to \boldsymbol{Y}_{\vec{q}}^{S\,\dagger}$. The same replacement rules also apply for (3.284) to (3.288).

[12]As a cross check, I have shown that different explicit regularization functions - rectangular, triangular, and bulk-Higgs motivated - all lead to the same result. However, these straightforward calculations will not be given here.

sets of even and odd functions on the orbifold, respectively, which can be chosen to obey separate orthonormality conditions with respect to the measure $d\phi \, e^\sigma$ [173]. However, the δ-distribution terms in the equations of motion are inconsistent with these orthonormality relations. We thus make the general ansatz

$$\int_{-\pi}^{\pi} d\phi \, e^{\sigma(\phi)} \, \boldsymbol{C}_m^{Q,q}(\phi) \, \boldsymbol{C}_n^{Q,q}(\phi) = \delta_{mn} \, \mathbf{1} + \boldsymbol{\Delta C}_{mn}^{Q,q} \, ,$$
$$\int_{-\pi}^{\pi} d\phi \, e^{\sigma(\phi)} \, \boldsymbol{S}_m^{Q,q}(\phi) \, \boldsymbol{S}_n^{Q,q}(\phi) = \delta_{mn} \, \mathbf{1} + \boldsymbol{\Delta S}_{mn}^{Q,q} \, . \tag{3.88}$$

We then find that the 4D action reduces to the desired canonical form

$$S_{\text{ferm},2} = \sum_{q=u,d} \sum_n \int d^4 x \left[\bar{q}^{(n)}(x) \, i \slashed{\partial} \, q^{(n)}(x) - m_n \, \bar{q}^{(n)}(x) \, q^{(n)}(x) \right] , \tag{3.89}$$

if and only if, in addition to the BCs, the relation

$$\vec{a}_m^{Q,q \, \dagger} \left(\delta_{mn} \mathbf{1} + \boldsymbol{\Delta C}_{mn}^{Q,q} \right) \vec{a}_n^{Q,q} + \vec{a}_m^{q,Q \, \dagger} \left(\delta_{mn} \mathbf{1} + \boldsymbol{\Delta S}_{mn}^{q,Q} \right) \vec{a}_n^{q,Q} = \delta_{mn} \tag{3.90}$$

is fulfilled. It is also straightforward to show that the equations of motion imply

$$m_m \, \boldsymbol{\Delta C}_{mn}^{Q,q} - m_n \, \boldsymbol{\Delta S}_{mn}^{Q,q} = \pm \frac{2}{r} \, \boldsymbol{C}_n^{Q,q}(\pi^-) \, \boldsymbol{S}_m^{Q,q}(\pi^-) \, . \tag{3.91}$$

Since an overall normalization can always be reshuffled between the profiles $\boldsymbol{C}_n^{Q,q}(\phi)$ and $\boldsymbol{S}_n^{Q,q}(\phi)$ and the eigenvectors $\vec{a}_n^{Q,q}$, we can choose the sum $\boldsymbol{\Delta C}_{nn}^{Q,q} + \boldsymbol{\Delta S}_{nn}^{Q,q}$ freely, without changing the physical result. The option $\boldsymbol{\Delta C}_{nn}^{Q,q} + \boldsymbol{\Delta S}_{nn}^{Q,q} = 0$ turns out to be particular convenient and thus will be applied hereafter. With this choice (3.90) splits up into

$$\vec{a}_n^{Q \, \dagger} \, \vec{a}_n^Q + \vec{a}_n^{q \, \dagger} \, \vec{a}_n^q = 1 \, , \tag{3.92}$$

and

$$\vec{a}_m^{Q,q \, \dagger} \, \boldsymbol{\Delta C}_{mn}^{Q,q} \, \vec{a}_n^{Q,q} + \vec{a}_m^{q,Q \, \dagger} \, \boldsymbol{\Delta S}_{mn}^{q,Q} \, \vec{a}_n^{q,Q} = 0 \, . \tag{3.93}$$

Thus, although the odd/even profiles of a certain KK-mode level n (with a definite chirality) alone do not fulfill standard orthonormalization conditions, taken together, in combination with the corresponding vectors $a_n^{Q,q}$, they are orthonormal in the sense of (3.90). The profiles alone do not obey such a relation due to the fact that (after EWSB) a certain 4D spinor receives contributions from doublets as well as singlets from the 5D theory. A part of the normalization is missing if one of these contributions is not present. This doublet-singlet mixing will become important when discussing FCNC couplings to the Z boson in Section 3.2.4 and thereafter.

Using the symmetry of the relations (3.88) in m and n, we finally obtain for $m \neq n$ the

explicit expressions

$$\Delta C_{mn}^{Q,q} = \pm \frac{2}{r} \frac{m_m \, \boldsymbol{C}_n^{Q,q}(\pi^-) \, \boldsymbol{S}_m^{Q,q}(\pi^-) - m_n \, \boldsymbol{C}_m^{Q,q}(\pi^-) \, \boldsymbol{S}_n^{Q,q}(\pi^-)}{m_m^2 - m_n^2} \,,$$

$$\Delta S_{mn}^{Q,q} = \mp \frac{2}{r} \frac{m_m \, \boldsymbol{C}_m^{Q,q}(\pi^-) \, \boldsymbol{S}_n^{Q,q}(\pi^-) - m_n \, \boldsymbol{C}_n^{Q,q}(\pi^-) \, \boldsymbol{S}_m^{Q,q}(\pi^-)}{m_m^2 - m_n^2} \,,$$

(3.94)

whereas for $m = n$ we get

$$\Delta \boldsymbol{C}_{nn}^{Q,q} = -\Delta \boldsymbol{S}_{nn}^{Q,q} = \pm \frac{1}{r m_n} \, \boldsymbol{C}_n^{Q,q}(\pi^-) \, \boldsymbol{S}_n^{Q,q}(\pi^-) \,.$$

(3.95)

Since they are proportional to $\boldsymbol{S}_n^{Q,q}(\pi^-)$ (which vanishes in the limit $v \to 0$), one would naively expect that the extra terms in the generalized orthonormality conditions (3.88) are small corrections of order v/M_{KK}. However, for the light SM fields, these terms are in fact of $\mathcal{O}(1)$.

Finally, we want to determine the mass eigenvalues m_n of the 4D Dirac fermions. They can be obtained by studying the system of $2N$ linear equations for the components of the vectors $\vec{a}_n^{Q,q}$, following from (3.87). It is straightforward to show that the mass eigenvalues m_n correspond to the solutions of the equation

$$\det \left(1 + \frac{v^2}{2 M_{\mathrm{KK}}^2} \, \tilde{\boldsymbol{Y}}_{\vec{q}} \, \boldsymbol{C}_n^q(\pi^-) \left[\boldsymbol{S}_n^q(\pi^-) \right]^{-1} \tilde{\boldsymbol{Y}}_{\vec{q}}^\dagger \, \boldsymbol{C}_n^Q(\pi^-) \left[\boldsymbol{S}_n^Q(\pi^-) \right]^{-1} \right) = 0 \,.$$

(3.96)

Once these are known, the eigenvectors $\vec{a}_n^{Q,q}$ can be derived from (3.87). Note that, while it is always possible to work with real and diagonal profile matrices $\boldsymbol{C}_n^{Q,q}(\phi)$ and $\boldsymbol{S}_n^{Q,q}(\phi)$, the vectors $\vec{a}_n^{Q,q}$ are, in general, complex-valued.

Bulk Profiles

In this section we derive the explicit form of the profiles $(C_n^{Q,q})_i$ and $(S_n^{Q,q})_i$, associated with bulk mass parameters M_{Q_i, q_i} (with $q = u, d$), in the presence of EWSB. The structure of the solutions is similar to the case of unbroken electroweak symmetry, as the EOMs within the bulk are the same for both cases. Combining the first and the third equation in (3.78), as well as the second and fourth one, we arrive again at Bessel equations. In terms of $t = \epsilon \, e^\sigma$, these have the general solutions [173, 172][13]

$$C_n^{Q,q}(t) = \mathcal{N}_n(c_{Q,q}) \sqrt{\frac{L \epsilon t}{\pi}} \, f_n^+(t, c_{Q,q}) \,,$$

$$S_n^{Q,q}(t) = \pm \mathcal{N}_n(c_{Q,q}) \, \mathrm{sgn}(\phi) \sqrt{\frac{L \epsilon t}{\pi}} \, f_n^-(t, c_{Q,q}) \,,$$

(3.97)

---

[13]Since, up to the BCs which in the end will determine the mass eigenvalues m_n and the flavor mixing vectors in (3.76), the problem decomposes into independent and similar equations for the different flavors, we will drop the index i in the following.

where $c_{Q,q} \equiv \pm M_{Q,q}/k$ are dimensionless parameters, derived from the bulk mass terms, and

$$f_n^{\pm}(t,c) = J_{-\frac{1}{2}-c}(x_n\epsilon)\, J_{\mp\frac{1}{2}+c}(x_n t) \pm J_{\frac{1}{2}+c}(x_n\epsilon)\, J_{\pm\frac{1}{2}-c}(x_n t)\,. \tag{3.98}$$

Remember that, as before, $x_n = m_n/M_{\mathrm{KK}}$. The orthonormality relations (3.88) lead to the normalization conditions

$$2\int_{\epsilon}^{1} dt\, t\, \left[f_n^{\pm}(t,c)\right]^2 = \frac{1}{\mathcal{N}_n^2(c)} \pm \frac{f_n^+(1,c)\, f_n^-(1,c)}{x_n}\,. \tag{3.99}$$

From these we derive

$$\mathcal{N}_n^{-2}(c) = \left[f_n^+(1,c)\right]^2 + \left[f_n^-(1,c)\right]^2 - \frac{2c}{x_n}\, f_n^+(1,c)\, f_n^-(1,c) - \epsilon^2 \left[f_n^+(\epsilon,c)\right]^2\,. \tag{3.100}$$

For the special cases where $c + 1/2$ is an integer, the profiles have to be obtained from the above expressions by a limiting procedure.

Since external fermions in low energy processes will always correspond to zero modes of the RS setup ($n = 1,2,3$), it will be useful to derive simple analytic expressions for the corresponding profiles. For those modes, it is a very good approximation to expand the above results in the limit $x_n \ll 1$, as even the top-quark is much lighter than the KK scale. In this way we find, dropping an phenomenological irrelevant term [1],

$$
\begin{aligned}
C_n^{Q,q}(\phi) &\approx \sqrt{\frac{L\epsilon}{\pi}}\, F(c_{Q,q})\, t^{c_{Q,q}},\\[2mm]
S_n^{Q,q}(\phi) &\approx \pm\mathrm{sgn}(\phi) \sqrt{\frac{L\epsilon}{\pi}}\, x_n F(c_{Q,q}) \frac{t^{1+c_{Q,q}} - \epsilon^{1+2c_{Q,q}}\, t^{-c_{Q,q}}}{1 + 2c_{Q,q}}\,.
\end{aligned}
\tag{3.101}
$$

Here, we have introduced the "zero-mode profile" [173, 172]

$$F(c) \equiv \mathrm{sgn}[\cos(\pi c)] \sqrt{\frac{1+2c}{1-\epsilon^{1+2c}}}\,, \tag{3.102}$$

which corresponds to the approximate value of the profile on the IR brane, divided by $\sqrt{L\epsilon/\pi}$. Note that the sign factor in (3.102) is chosen such that the signs in (3.101) agree with those derived from the exact profiles (3.97). The zeroth order in the expansion for the zero mode profiles performed above is often called (zeroth order) "zero-mode approximation" (ZMA). At this order, the even profile matrices do not depend on the level n and the odd profiles vanish. These results correspond to the starting point in the perturbative approach, in which one first solves for the fermion bulk profiles without the Yukawa couplings and then treats these couplings as a perturbation [173, 172, 174]. As we will see later in Section 3.2.4, it will sometimes be necessary to consider higher orders in the expansion to derive consistent non-trivial results in the ZMA. This can be done comfortably in our approach, as we just have to include the next order in the well-defined expansion of the exact profiles in powers of v^2/M_{KK}^2 (note that x_n, $n = 1,2,3$ scales like v/M_{KK}), and do not have to diagonalize (and truncate) infinite dimensional mass matrices.

The quantity $F(c)$ strongly depends on the value of c. One obtains to excellent approxi-

mation

$$F(c) \approx \begin{cases} -\sqrt{-1-2c}\ \epsilon^{-c-\frac{1}{2}}, & -3/2 < c < -1/2\,, \\[2mm] \sqrt{1+2c}\,, & -1/2 < c < 1/2\,. \end{cases} \tag{3.103}$$

This behavior signals that for $c < -1/2$ the zero-modes are localized close to the UV brane, while for $c > -1/2$ they have the biggest weight close to the IR brane. Thus, it turns out that rather than generating 4D masses, the bulk mass parameters control the localization of the 4D fermions in the extra dimension. The fact that for UV-localized fermions the zero-mode profile is exponentially small, while it is of $\mathcal{O}(1)$ for IR-localized fields can be used to generate large hierarchies in the fermion spectrum by means of different overlaps with the IR-brane Higgs sector via $\mathcal{O}(1)$ input parameters. This feature will be discussed in more detail in the following section.

3.2.3 Fermion Hierarchies: The Anarchic RS Model as a Predictive Model of Flavor

Due to the possibility of additional gauge invariant bulk mass terms, with hermitian mass matrices $\boldsymbol{M}_{Q,u,d}$, the minimal RS model has 27 new parameters in the flavor sector compared to the SM (for $N = 3$ generations). In the light of this significant number of new parameters, entering the model as exponents of the warp factor, see (3.102), one should address the question of the predictivity of the model. If one allows $e.g.$ for arbitrary values for the bulk mass parameters c_{Q_i, u_i, d_i} (addressing the fermion spectrum by hierarchical Yukawa matrices), a very broad range of effects is possible within the RS setup. This renders the model not very predictive at the first place. However, as mentioned before, a big virtue of the model is the possibility to address the hierarchies within the flavor sector, which cannot be understood within the SM. This approach will constrain the large parameter space and allow for more generic predictions. So we will understand the RS model in this way, $i.e.$, we do not build in hierarchies by hand but rather want to generate the SM flavor structure out of $\mathcal{O}(1)$ input parameters. To this end, we assume anarchical Yukawa matrices and generate the hierarchies via different values for the dimensionless bulk mass parameters. These input parameters are then constrained by the requirement to end up with the correct spectrum and CKM mixing angles. Due to the warping, as explained above, they can be of $\mathcal{O}(1)$, while still leading to hierarchies in the fermion spectrum. These naturalness considerations do not fix the input parameters completely, however, they significantly decrease the spread in the parameter space and thus also in the predictions of the model. While the precise values of the input parameters in the flavor sector will not be determined, their hierarchical structure will. This often allows for generic estimations for observables in the RS model, without an uncertainty in the prediction over many orders of magnitude (assuming M_{KK} to be fixed). Such an uncertainty would be generated when reshuffling too large contributions between the localization parameters and the Yukawa matrices, leaving the spectrum invariant. This is prevented by the anarchic approach (however, some amount of reshuffling is possible, see below).

To get an analytic handle on the relations between input parameters and the resulting spectrum and mixings, we will demonstrate and explore similarities between the RS setup of generating hierarchies by different fermion localizations in a slice of AdS$_5$ and the Froggatt-Nielsen mechanism. To this end, it is useful to perform an expansion to the first non-vanishing

order in v^2/M_{KK}^2 and to use the approximate formulae for the bulk profiles of the SM fermions, obtained in (3.101). For the purpose of discussing the fermion masses and mixings, we need these profiles evaluated at $t = 1$, where they couple to the Higgs sector. We arrive at the simple expressions

$$C_n^{Q,q}(1^-) \to \sqrt{\frac{L\epsilon}{\pi}}\, F(c_{Q,q})\,, \qquad S_n^{Q,q}(1^-) \to \pm\sqrt{\frac{L\epsilon}{\pi}}\, \frac{x_n}{F(c_{Q,q})}\,. \tag{3.104}$$

With their help, the BCs (3.87) can be recast to LO in v^2/M_{KK}^2 into the simple form

$$\frac{\sqrt{2}\, m_n}{v}\, \hat{a}_n^q = \boldsymbol{Y}_q^{\text{eff}}\, \hat{a}_n^{q^c}\,, \qquad \frac{\sqrt{2}\, m_n}{v}\, \hat{a}_n^{q^c} = (\boldsymbol{Y}_q^{\text{eff}})^\dagger\, \hat{a}_n^q\,. \tag{3.105}$$

Here

$$\left(Y_q^{\text{eff}}\right)_{ij} \equiv F(c_{Q_i})\, (Y_{\tilde{q}})_{ij}\, F(c_{q_j}) \tag{3.106}$$

are effective Yukawa matrices, and the rescaled flavor vectors $\hat{a}_n^q \equiv \sqrt{2}\, \vec{a}_n^Q$, $\hat{a}_n^{q^c} \equiv \sqrt{2}\, \vec{a}_n^q$ obey the normalization conditions

$$\hat{a}_n^{q\dagger}\, \hat{a}_n^q = \hat{a}_n^{q^c\dagger}\, \hat{a}_n^{q^c} = 1\,. \tag{3.107}$$

Moreover, we obtain from (3.105) the equalities

$$\left(m_n^2\, \boldsymbol{1} - \frac{v^2}{2}\, \boldsymbol{Y}_q^{\text{eff}}\, (\boldsymbol{Y}_q^{\text{eff}})^\dagger\right) \hat{a}_n^q = 0\,, \qquad \left(m_n^2\, \boldsymbol{1} - \frac{v^2}{2}\, (\boldsymbol{Y}_q^{\text{eff}})^\dagger\, \boldsymbol{Y}_q^{\text{eff}}\right) \hat{a}_n^{q^c} = 0\,, \tag{3.108}$$

and thus the mass eigenvalues can be obtained from the simple equation

$$\det\left(m_n^2\, \boldsymbol{1} - \frac{v^2}{2}\, \boldsymbol{Y}_q^{\text{eff}}\, (\boldsymbol{Y}_q^{\text{eff}})^\dagger\right) = 0\,. \tag{3.109}$$

These expressions hold to LO in v^2/M_{KK}^2. At this order, but not in general, the vectors $\vec{a}_n^{Q,q}$ that belong to different n are orthogonal on each other.

The eigenvectors $\hat{a}_n^q$ and $\hat{a}_n^{q^c}$ of the Yukawa matrices $\boldsymbol{Y}_q^{\text{eff}} \left(\boldsymbol{Y}_q^{\text{eff}}\right)^\dagger$ and $\left(\boldsymbol{Y}_q^{\text{eff}}\right)^\dagger \boldsymbol{Y}_q^{\text{eff}}$ (with $n = 1, 2, 3$ and $q = u, d$) form the columns of the unitary matrices $\boldsymbol{U}_q$ and $\boldsymbol{W}_q$ that appear in the singular-value decomposition

$$\boldsymbol{Y}_q^{\text{eff}} = \boldsymbol{U}_q\, \boldsymbol{\lambda}_q\, \boldsymbol{W}_q^\dagger\,, \tag{3.110}$$

respectively, where

$$\boldsymbol{\lambda}_u = \frac{\sqrt{2}}{v}\, \text{diag}(m_u, m_c, m_t)\,, \qquad \boldsymbol{\lambda}_d = \frac{\sqrt{2}}{v}\, \text{diag}(m_d, m_s, m_b)\,. \tag{3.111}$$

To LO in v^2/M_{KK}^2 the relations between the fundamental 5D fields and the SM mass eigenstates thus involve the matrices $\boldsymbol{U}_q$ and $\boldsymbol{W}_q$. In particular, the CKM matrix in the RS model is to LO given by

$$\boldsymbol{V}_{\text{CKM}} = \boldsymbol{U}_u^\dagger\, \boldsymbol{U}_d\,. \tag{3.112}$$

Before applying the Froggatt-Nielsen analysis to the RS setup we will count the number of physical parameters in the flavor sector.

Parameter Counting in the RS Model

Applying the method reviewed in Section 1.1.3, the number of physical parameters in the flavor sector of the RS model is derived as follows. To be completely general, we assume N quark generations and thus start with $N_Y = 2\,(N^2, N^2)$ real moduli and CP-odd phases for the 5D Yukawa matrices $\boldsymbol{Y}_{u,d}^{(\mathrm{5D})}$, as well as $N_c = 3\,(N(N+1)/2, N(N-1)/2)$ parameters for the hermitian bulk mass matrices $\boldsymbol{c}_{Q,u,d}$. Thus

$$N_{\mathrm{general}} = N_Y + N_c = (N(7N+3)/2, N(7N-3)/2)\,. \tag{3.113}$$

The Yukawa matrices break the global bulk flavor symmetry $G = U(N)_Q \times U(N)_u \times U(N)_d$ with $N_G = 3\,(N(N-1)/2, N(N+1)/2)$ parameters down to the subgroup $H = U(1)_B$ with $N_H = (0,1)$ parameters, resulting in

$$N_{\mathrm{broken}} = N_G - N_H = (3N(N-1)/2, 3N(N+1)/2 - 1)\,. \tag{3.114}$$

One thus arrives at

$$N_{\mathrm{phys}} = N_{\mathrm{general}} - N_{\mathrm{broken}} = (N(2N+3), (N-1)(2N-1)) \tag{3.115}$$

physical parameters. For $N = 3$ quark generations we end up with 27 moduli and ten phases [177]. In the ZMA we can identify the physical real parameters with the six quark masses, twelve mixing angles appearing in the mixing matrices $\boldsymbol{U}_{u,d}$ and $\boldsymbol{W}_{u,d}$, and the nine zero-mode profiles $\boldsymbol{F}_{Q,u,d}$. One of the ten phases can be identified with the phase of the CKM matrix. Moreover, nine new phases enter, in different combinations, the various matrices in (3.149) and (3.150), that describe the flavor-changing interactions of the RS model.

Interestingly, for $N = 2$ quark generations there still remain 14 moduli and three phases. Since, as we have seen in Section 1.1.3, the CKM matrix for two-generations can be made real by phase redefinitions, the phases can all be chosen to reside in the new mixing matrices. As a consequence, the RS model allows for CP-violating effects which do not involve all three fermion generations. Thus, CP violation in the RS model is much less suppressed than in the SM, see also Section 5.2.3. It would be interesting to work out the consequences of this fact for baryogenesis. Beyond that, note that the new CP-violating phases induce electric dipole moments for the electron and the neutron at the one-loop level. The stringent experimental bound on the neutron electric dipole moment leads to a lower bound on the masses of the KK excitations of $\sim 10\,\mathrm{TeV}$ [177]. There are several proposals to address this "CP problem" (and to allow for lighter KK excitations) [205, 206, 207], which postpone the contributions to the neutron electric dipole moment to the two-loop level by reducing the number of CP-odd phases. Neglecting the lepton sector (as well as gravity), the minimal RS model thus has, besides the "SM" parameters described in Section 1.1.4, as additional parameters the KK scale M_{KK}, the RS volume L, and the 27 new parameters in the flavor sector discussed above.

Warped-Space Froggatt-Nielsen Mechanism

We will now introduce the Froggatt-Nielsen mechanism and apply the corresponding analysis in the context of warped extra dimensions to show how fermion hierarchies arise naturally in these models. Starting from an anarchical Yukawa matrix, the Froggatt-Nielsen mechanism
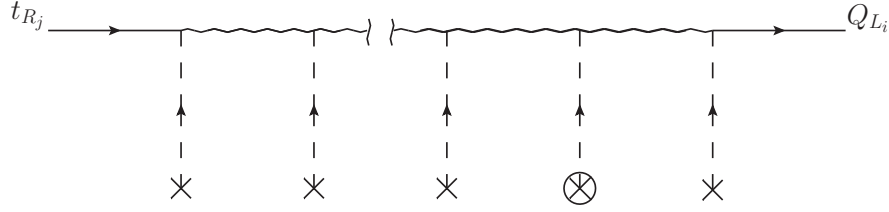
Figure 3.7: Contribution to the element $(m_u)_{ij}$ of the up-type quark mass matrix. Full lines correspond to SM quarks, whereas wavy lines represent ultra-heavy fermions. Insertions of the VEV $\langle \Phi_1 \rangle$ are depicted by crosses, while insertions of $\langle \Phi \rangle$ correspond to crossed circles.

generates the observed hierarchies in the quark sector by assuming the left-handed and right-handed components of the SM-quark fields to have different values for an almost conserved quantum number R, belonging to an abelian symmetry group $U(1)_F$. Quark-mass terms only arise via interactions with new ultra-heavy fermions and Higgs-scalars that have various different values of R, which is integrally quantized. Explicitly, the model introduces three Higgs fields Φ, Φ_1, Φ_2, where the VEV $\langle \Phi_2 \rangle > 0$ of the neutral ($R = 0$) Higgs scalar Φ_2 generates mass terms for the new fermions. The Higgs scalar Φ_1 is a gauge singlet, but has $R = 1$, and thus can mediate between fermions with a different R-charge. Its VEV $\langle \Phi_1 \rangle > 0$ breaks the $U(1)_F$ symmetry spontaneously and allows for mass terms of the light (SM) quarks via the mechanism depicted in Figure 3.7. Depending on the difference in R-quantum numbers between the left-handed and right-handed SM quark-fields, a certain number of insertions of transitions mediated by the the VEV $\langle \Phi_1 \rangle$ is needed to account for this difference via intermediate ultra-heavy fermions, in order to generate a mass term for the SM quarks. Moreover, an insertion of the VEV of the SM Higgs $\langle \Phi \rangle = v/\sqrt{2}$ is necessary to balance the different $SU(2)_L$ quantum numbers of left-handed and right-handed SM quarks. Every $\Delta |R| = 1$ transition together with the adjacent propagating ultra-heavy fermion leads to a suppression by the small symmetry breaking parameter

$$\epsilon \equiv \frac{y(\mu_q)}{y(\mu_0)} \frac{\langle \Phi_1 \rangle}{\langle \Phi_2 \rangle} \, . \tag{3.116}$$

The prefactor corresponds to the ratio of generic Φ_1-Yukawa couplings at the scale of the light fermions μ_q and the fundamental scale μ_0 of the model, where the Yukawa couplings are expected to be of $\mathcal{O}(1)$. Concentrating on the up-type sector, denoting the quantum numbers of the left-handed SM-doublets and right-handed SM-singlets by $R_{Q_i} = a_i$ and $R_{t_i} = b_i$, and assuming $a_i > 0$ and $b_i \leq 0$, the mass matrix arising from diagrams like the one in Figure 3.7 reads

$$(m_u)_{ij} = \frac{v}{\sqrt{2}} (G_u)_{ij} \, \epsilon^{a_i - b_j} \, . \tag{3.117}$$

Note that this matrix is order-of-magnitude factorizing. In the spirit of the model, all dimensionless couplings should be of $\mathcal{O}(1)$, which results in the complex coefficients $(G_u)_{ij}$ also being of $\mathcal{O}(1)$ times a factor due to evolving the Φ Yukawa couplings down to the scale $\langle \Phi \rangle$. One can now consistently evaluate the mass eigenvalues as well as the CKM matrix to LO in the small parameter ϵ. First, it can be shown that the product of the n largest eigenvalues of

m_u reads to LO [139]

$$\prod_{i=1}^{n} m_i = \left(\frac{v}{\sqrt{2}}\right)^n \det(\boldsymbol{G}_u^{(n)}) \, \epsilon^{\sum_{i=1}^{n}(a_i - b_i)} \,, \tag{3.118}$$

where $\boldsymbol{G}_u^{(n)}$ is obtained from $\boldsymbol{G}_u \equiv ((G_u)_{ij})$ by removing rows and columns with $i > n$ and $j > n$, respectively. Here, the quarks are ordered such that $a_i > a_{i-1}$ and $b_i < b_{i-1}$. In the case of degenerate values $a_i = a_{i-1}$ or $b_i = b_{i-1}$ the derivations are only order-of-magnitude wise correct. From (3.118) one obtains

$$m_n = \frac{v}{\sqrt{2}} \frac{\left|\det \boldsymbol{G}_u^{(n)}\right|}{\left|\det \boldsymbol{G}_u^{(n-1)}\right|} \epsilon^{a_n - b_n} \tag{3.119}$$

for the nth heaviest quark which leads to the hierarchical structure

$$\frac{m_i}{m_j} \sim \epsilon^{a_i - a_j - b_i + b_j} \,. \tag{3.120}$$

Due to the exponential dependence, this allows to reproduce the hierarchies (1.81) with a moderately small symmetry breaking parameter ϵ, meaning that $\langle \Phi_1 \rangle$ and $\langle \Phi_2 \rangle$ do not have to differ by orders of magnitude, and moderate different values for the various quantum numbers R_{Q_i} and R_{t_i}. In consequence, hierarchical and suppressed masses are a natural prediction of the model.

A nice feature of the Froggatt-Nielsen mechanism is that, given that the mass hierarchies are generated as described above with different quantum numbers for the various quark fields in the right-handed as well as in the left-handed sector, the CKM matrix is predicted to have a structure similar to (1.82). This can be seen from the form of the diagonalization matrices $\boldsymbol{U}_u$ and $\boldsymbol{U}_d$, obtained from the singular value decomposition of the matrix $\boldsymbol{m}_u$, see (1.47), and the corresponding equation for the down-type sector. To LO in ϵ and for the case of three generations, these matrices read [139]

$$\boldsymbol{U}_q = (u_q)_{ij} \, \epsilon^{|a_i - a_j|} \,, \quad q = u, d \,, \tag{3.121}$$

where

$$\boldsymbol{u}_q = \begin{pmatrix} 1 & \dfrac{(M_q)_{21}}{(M_q)_{11}} & \dfrac{(G_q)_{13}}{(G_q)_{33}} \\[2ex] -\dfrac{(M_q)_{21}^*}{(M_q)_{11}^*} & 1 & \dfrac{(G_q)_{23}}{(G_q)_{33}} \\[2ex] \dfrac{(M_q)_{31}^*}{(M_q)_{11}^*} & -\dfrac{(G_q)_{23}^*}{(G_q)_{33}^*} & 1 \end{pmatrix} \,. \tag{3.122}$$

Here, $(M_q)_{ij}$ denote the minors of $\boldsymbol{G}_q$, $i.e.$, the determinants of the matrices obtained by removing the ith row and the jth column of $\boldsymbol{G}_q$. Moreover, we have used the invariance of the singular-value decomposition with respect to phase rotations, to make the diagonal elements

Froggatt-Nielsen Mechanism	Warped Extra Dimensions
symmetry breaking parameter $\epsilon \sim \frac{\langle \Phi_1 \rangle}{\langle \Phi_2 \rangle}$	warp factor $\epsilon = e^{-L}$
quantum numbers (a_i, b_j)	localization parameters $(-c_{Q_i} - \frac{1}{2}, c_{q_j} + \frac{1}{2})$
combination of couplings $\boldsymbol{G}_q$	Yukawa matrix $\tilde{\boldsymbol{Y}}_{\vec{q}}$
ϵ^{a_i}	$F(c_{Q_i})$
ϵ^{b_j}	$F(c_{q_j})^{-1}$

Table 3.1: Analogy between parameters of the Froggatt-Nielsen mechanism and those of the RS model. The second row holds just for $-3/2 < c_{Q_i, q_j} < -1/2$, whereas the range of validity of the last two rows is not restricted.

$(U_q)_{ii}$ real. One obtains, as a prediction, the hierarchical structure of the CKM matrix

$$(V_{\text{CKM}})_{ik} = \sum_{j=1}^{3} \left(U_u^\dagger \right)_{ij} (U_d)_{jk} \sim \epsilon^{|a_i - a_k|} . \tag{3.123}$$

This is very similar to (1.82) (for appropriate values of a_i and ϵ), without having to put in the structure by hand. The diagonal dominant form of $\boldsymbol{V}_{\text{CKM}}$ is a robust prediction of the model. In the Froggatt-Nielsen model, both hierarchies, those within the masses as well as those of the CKM matrix, can be traced back to the same origin. Note, however that in this approach, the CP violating phase is not suppressed by any small parameter and thus it is difficult to explain why the measured CP violation is so small.

We will now apply the results presented here to the fermion sector of the Randall-Sundrum model. As we will see immediately, the RS model with fermions in the bulk automatically provides a complete analogy to the Froggatt-Nielsen mechanism, without the need to introduce a new $U(1)_F$-symmetry, new fermion representations, or additional Higgs fields. In that context, we will also determine the hierarchies for the RS analogon to the $U(1)_F$ charges, in dependence on the observed quark masses and CKM mixings Due to the form of the effective Yukawa matrices in (3.106), a *hierarchical* and order-of-magnitude *factorizing* mass matrix of exactly the same structure as in (3.117) is generated in the RS setup by assuming a hierarchical structure of the zero-mode profiles

$$|F(c_{A_1})| < |F(c_{A_2})| < |F(c_{A_3})| , \quad A = Q, u, d . \tag{3.124}$$

Importantly, in warped extra dimensions, such a hierarchy is induced naturally, since it only requires small differences in the bulk mass parameters c_{A_i}. Note that we assume the quarks to be ordered such that the relation (3.124) holds. In the case of degenerate profiles $|F(c_{A_i})| = |F(c_{A_{i+1}})|$, the following discussion is again only order-of-magnitude wise correct. The localization parameters c_{Q_i, q_i} of the minimal RS model play the role of the left-handed and right-handed $U(1)_F$ charges a_i, b_i of the Froggatt-Nielsen mechanism, however they are not integrally quantized. Explicitly, the product of functions $F(c_{Q_i}) F(c_{q_j})$ in (3.106) corresponds to the exponential factor $\epsilon^{a_i - b_j}$ of the symmetry breaking parameter $\epsilon \sim \langle \Phi_1 \rangle$ in (3.117). This correspondence can be split up as in Table 3.1, which gives an overview of the analogies of the models. Note that the direct relation between the localization parameters and the Froggatt-Nielsen charges, given in the second row, only holds for $-3/2 < c_{Q_i, q_j} < -1/2$. However, the general analogy, as well as the last three exact relations, hold independently of this restriction.

Thus, the hierarchies of fermion masses and mixings in a warped background result without further assumptions from the Froggatt-Nielsen mechanism. In the following we perform the corresponding analysis explicitly, starting from the relation (3.106). To LO, the products of up- and down-type quark masses in the RS model are given by, see (3.118),

$$m_u\, m_c\, m_t = \frac{v^3}{2\sqrt{2}}\,|\det{(\boldsymbol{Y}_u)}| \prod_{i=1,2,3} |F(c_{Q_i})\,F(c_{u_i})|\,,$$

$$m_d\, m_s\, m_b = \frac{v^3}{2\sqrt{2}}\,|\det{(\boldsymbol{Y}_d)}| \prod_{i=1,2,3} |F(c_{Q_i})\,F(c_{d_i})|\,.$$

(3.125)

Using $|F(c_{A_i})| < |F(c_{A_{i+1}})|$, one can evaluate all the mass eigenvalues to LO in hierarchies. We find, see (3.119),

$$m_u = \frac{v}{\sqrt{2}}\,\frac{|\det(\boldsymbol{Y}_u)|}{|(M_u)_{11}|}\,|F(c_{Q_1})F(c_{u_1})|\,, \qquad m_d = \frac{v}{\sqrt{2}}\,\frac{|\det(\boldsymbol{Y}_d)|}{|(M_d)_{11}|}\,|F(c_{Q_1})F(c_{d_1})|\,,$$

$$m_c = \frac{v}{\sqrt{2}}\,\frac{|(M_u)_{11}|}{|(Y_u)_{33}|}\,|F(c_{Q_2})F(c_{u_2})|\,, \qquad m_s = \frac{v}{\sqrt{2}}\,\frac{|(M_d)_{11}|}{|(Y_d)_{33}|}\,|F(c_{Q_2})F(c_{d_2})|\,, \qquad (3.126)$$

$$m_t = \frac{v}{\sqrt{2}}\,|(Y_u)_{33}|\,|F(c_{Q_3})F(c_{u_3})|\,, \qquad m_b = \frac{v}{\sqrt{2}}\,|(Y_d)_{33}|\,|F(c_{Q_3})F(c_{d_3})|\,,$$

where $(M_q)_{ij}$ denote the minors of $\boldsymbol{Y}_q$, as defined before.

The elements of the rotation matrices $\boldsymbol{U}_q$ and $\boldsymbol{W}_q$ are given, to LO in hierarchies, by

$$(U_q)_{ij} = (u_q)_{ij} \begin{cases} \dfrac{F(c_{Q_i})}{F(c_{Q_j})}\,, & i \le j\,, \\[2mm] \dfrac{F(c_{Q_j})}{F(c_{Q_i})}\,, & i > j\,, \end{cases} \qquad (W_q)_{ij} = (w_q)_{ij}\, e^{i\phi_j} \begin{cases} \dfrac{F(c_{q_i})}{F(c_{q_j})}\,, & i \le j\,, \\[2mm] \dfrac{F(c_{q_j})}{F(c_{q_i})}\,, & i > j\,, \end{cases} \qquad (3.127)$$

where the coefficient matrices $\boldsymbol{u}_q$ and $\boldsymbol{w}_q$ can be expressed through the elements $(Y_q)_{ij}$ of the original Yukawa matrices and their minors $(M_q)_{ij}$ and read

$$\boldsymbol{u}_q = \begin{pmatrix} 1 & \dfrac{(M_q)_{21}}{(M_q)_{11}} & \dfrac{(Y_q)_{13}}{(Y_q)_{33}} \\[3mm] -\dfrac{(M_q)^*_{21}}{(M_q)^*_{11}} & 1 & \dfrac{(Y_q)_{23}}{(Y_q)_{33}} \\[3mm] \dfrac{(M_q)^*_{31}}{(M_q)^*_{11}} & -\dfrac{(Y_q)^*_{23}}{(Y_q)^*_{33}} & 1 \end{pmatrix}, \qquad \boldsymbol{w}_q = \begin{pmatrix} 1 & \dfrac{(M_q)^*_{12}}{(M_q)^*_{11}} & \dfrac{(Y_q)^*_{31}}{(Y_q)^*_{33}} \\[3mm] -\dfrac{(M_q)_{12}}{(M_q)_{11}} & 1 & \dfrac{(Y_q)^*_{32}}{(Y_q)^*_{33}} \\[3mm] \dfrac{(M_q)_{13}}{(M_q)_{11}} & -\dfrac{(Y_q)_{32}}{(Y_q)_{33}} & 1 \end{pmatrix}. \qquad (3.128)$$

Invariance of the singular-value decomposition (3.110) under field redefinitions allows to make either the diagonal elements $(U_q)_{ii}$ or $(W_q)_{ii}$ real. In (3.127) we have used that freedom to choose $(U_q)_{ii}$ to be real, so that all phase factors $e^{i\phi_j}$ appear in the elements $(W_q)_{ij}$. They are given by

$$e^{i\phi_j} = \text{sgn}\big[F(c_{Q_j})\,F(c_{q_j})\big]\,e^{-i(\rho_j - \rho_{j+1})}\,, \qquad (3.129)$$

where

$$\rho_1 = \arg\left(\det(\boldsymbol{Y}_q)\right), \qquad \rho_2 = \arg\left((M_q)_{11}\right), \qquad \rho_3 = \arg\left((Y_q)_{33}\right), \tag{3.130}$$

and $\rho_4 = 0$. We observe that, to LO, the matrices $\boldsymbol{U}_q$ and thus also the CKM matrix do not depend on the right-handed profiles $F(c_{q_i})$. This has already been pointed out in [175].

It is now straightforward to derive the LO expressions for the Wolfenstein parameters of the CKM matrix λ, A, $\bar{\rho}$, and $\bar{\eta}$, defined in (1.60). From (3.112), (3.127), and (3.128), we obtain

$$\lambda = \frac{|F(c_{Q_1})|}{|F(c_{Q_2})|}\left|\frac{(M_d)_{21}}{(M_d)_{11}} - \frac{(M_u)_{21}}{(M_u)_{11}}\right|, \qquad A = \frac{|F(c_{Q_2})|^3}{|F(c_{Q_1})|^2\,|F(c_{Q_3})|}\left|\frac{\frac{(Y_d)_{23}}{(Y_d)_{33}} - \frac{(Y_u)_{23}}{(Y_u)_{33}}}{\left[\frac{(M_d)_{21}}{(M_d)_{11}} - \frac{(M_u)_{21}}{(M_u)_{11}}\right]^2}\right|,$$

$$\bar{\rho} - i\bar{\eta} = \frac{(Y_d)_{33}\,(M_u)_{31} - (Y_d)_{23}\,(M_u)_{21} + (Y_d)_{13}\,(M_u)_{11}}{(Y_d)_{33}\,(M_u)_{11}\left[\frac{(Y_d)_{23}}{(Y_d)_{33}} - \frac{(Y_u)_{23}}{(Y_u)_{33}}\right]\left[\frac{(M_d)_{21}}{(M_d)_{11}} - \frac{(M_u)_{21}}{(M_u)_{11}}\right]}\,. \tag{3.131}$$

Notice that, like in the case of the Froggatt-Nielsen mechanism, $\bar{\rho}$ and $\bar{\eta}$ are not suppressed by any small parameters [139]. They are to first order independent of the zero-mode profiles $F(c_{Q_i,q_i})$. The RS setup thus predicts that these parameters are of $\mathcal{O}(1)$, while the precise values remain unexplained.

Let us now try to determine the bulk mass parameters from the measurable quantities discussed here. The relations given in (3.126) and (3.131) do not allow to determine all zero-mode profiles solely in terms of the quark masses and Wolfenstein parameters (as well as $\mathcal{O}(1)$ Yukawa couplings). One profile remains as a free parameter. Choosing $F(c_{Q_2})$ to be that parameter and expressing the other profiles in terms of its value, we find for the left-handed quark profiles

$$|F(c_{Q_1})| = \frac{\lambda}{\left|\frac{(M_d)_{21}}{(M_d)_{11}} - \frac{(M_u)_{21}}{(M_u)_{11}}\right|}\,|F(c_{Q_2})|, \qquad |F(c_{Q_3})| = \frac{\left|\frac{(Y_d)_{23}}{(Y_d)_{33}} - \frac{(Y_u)_{23}}{(Y_u)_{33}}\right|}{A\lambda^2}\,|F(c_{Q_2})|. \tag{3.132}$$

For the right-handed profiles, we arrive at

$$|F(c_{u_1})| = \frac{\sqrt{2}m_u}{v}\,\frac{|(M_u)_{11}|\left|\frac{(M_d)_{21}}{(M_d)_{11}} - \frac{(M_u)_{21}}{(M_u)_{11}}\right|}{\lambda\,|\det(\boldsymbol{Y}_u)|}\,\frac{1}{|F(c_{Q_2})|},$$

$$|F(c_{u_2})| = \frac{\sqrt{2}m_c}{v}\,\frac{|(Y_u)_{33}|}{|(M_u)_{11}|}\,\frac{1}{|F(c_{Q_2})|}, \tag{3.133}$$

$$|F(c_{u_3})| = \frac{\sqrt{2}m_t}{v}\,\frac{A\lambda^2}{|(Y_u)_{33}|\left|\frac{(Y_d)_{23}}{(Y_d)_{33}} - \frac{(Y_u)_{23}}{(Y_u)_{33}}\right|}\,\frac{1}{|F(c_{Q_2})|},$$
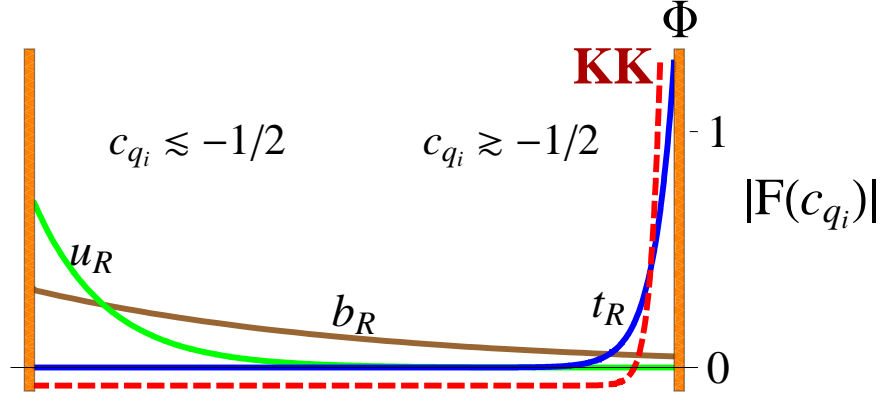
Figure 3.8:   Fermion localizations in the anarchic approach to flavor in warped extra dimensions. Hierarchies are generated from $\mathcal{O}(1)$ input parameters c_{q_i} due to the warped geometry. See [1] and text for details.

and

$$|F(c_{d_1})| = \frac{\sqrt{2}m_d}{v} \frac{|(M_d)_{11}| \left| \frac{(M_u)_{21}}{(M_u)_{11}} - \frac{(M_d)_{21}}{(M_d)_{11}} \right|}{\lambda \, |\det(\boldsymbol{Y}_d)|} \frac{1}{|F(c_{Q_2})|} \, ,$$

$$|F(c_{d_2})| = \frac{\sqrt{2}m_s}{v} \frac{|(Y_d)_{33}|}{|(M_d)_{11}|} \frac{1}{|F(c_{Q_2})|} \, , \qquad (3.134)$$

$$|F(c_{d_3})| = \frac{\sqrt{2}m_b}{v} \frac{A\lambda^2}{|(Y_d)_{33}| \left| \frac{(Y_u)_{23}}{(Y_u)_{33}} - \frac{(Y_d)_{23}}{(Y_d)_{33}} \right|} \frac{1}{|F(c_{Q_2})|} \, .$$

As expected, these relations call for a hierarchical structure among the quark profiles, which is naturally accommodated within warped extra dimensions. For the left-handed quark profiles we find

$$\frac{|F(c_{Q_1})|}{|F(c_{Q_2})|} \sim \lambda, \qquad \frac{|F(c_{Q_2})|}{|F(c_{Q_3})|} \sim \lambda^2, \qquad \frac{|F(c_{Q_1})|}{|F(c_{Q_3})|} \sim \lambda^3. \qquad (3.135)$$

The hierarchies of the right-handed profiles can then be fixed by the observed quark masses

$$\frac{|F(c_{u_1})|}{|F(c_{u_3})|} \sim \frac{m_u}{m_t} \frac{1}{\lambda^3}, \qquad \frac{|F(c_{u_2})|}{|F(c_{u_3})|} \sim \frac{m_c}{m_t} \frac{1}{\lambda^2},$$

$$\frac{|F(c_{d_1})|}{|F(c_{u_3})|} \sim \frac{m_d}{m_t} \frac{1}{\lambda^3}, \qquad \frac{|F(c_{d_2})|}{|F(c_{u_3})|} \sim \frac{m_s}{m_t} \frac{1}{\lambda^2}, \qquad \frac{|F(c_{d_3})|}{|F(c_{u_3})|} \sim \frac{m_b}{m_t}. \qquad (3.136)$$

These relations can be used to determine the hierarchical structure of the flavor mixing matrices $\boldsymbol{U}_q$ and $\boldsymbol{W}_q$ in (3.127). The rotation matrices in the left-handed quark sector have

the same structure as the CKM matrix. Their hierarchies are given by

$$\boldsymbol{U}_{u,d} \sim \boldsymbol{V}_{\text{CKM}} \sim \begin{pmatrix} 1 & \lambda & \lambda^3 \\ \lambda & 1 & \lambda^2 \\ \lambda^3 & \lambda^2 & 1 \end{pmatrix} \sim \begin{pmatrix} 1 & 0.23 & 0.01 \\ 0.23 & 1 & 0.05 \\ 0.01 & 0.05 & 1 \end{pmatrix}, \qquad (3.137)$$

whereas in the right-handed quark sector we obtain

$$\boldsymbol{W}_u \sim \begin{pmatrix} 1 & \frac{m_u}{m_c}\frac{1}{\lambda} & \frac{m_u}{m_t}\frac{1}{\lambda^3} \\ \frac{m_u}{m_c}\frac{1}{\lambda} & 1 & \frac{m_c}{m_t}\frac{1}{\lambda^2} \\ \frac{m_u}{m_t}\frac{1}{\lambda^3} & \frac{m_c}{m_t}\frac{1}{\lambda^2} & 1 \end{pmatrix} \sim \begin{pmatrix} 1 & 0.012 & 0.001 \\ 0.012 & 1 & 0.077 \\ 0.001 & 0.077 & 1 \end{pmatrix},$$

$$\boldsymbol{W}_d \sim \begin{pmatrix} 1 & \frac{m_d}{m_s}\frac{1}{\lambda} & \frac{m_d}{m_b}\frac{1}{\lambda^3} \\ \frac{m_d}{m_s}\frac{1}{\lambda} & 1 & \frac{m_s}{m_b}\frac{1}{\lambda^2} \\ \frac{m_d}{m_b}\frac{1}{\lambda^3} & \frac{m_s}{m_b}\frac{1}{\lambda^2} & 1 \end{pmatrix} \sim \begin{pmatrix} 1 & 0.26 & 0.12 \\ 0.26 & 1 & 0.44 \\ 0.12 & 0.44 & 1 \end{pmatrix}. \qquad (3.138)$$

The numerical values quoted here have been obtained by using the input parameters as compiled in Appendix D. Note that, while the fermion profiles are expected to be strongly hierarchical in the left-handed quark sector as well as in the right-handed up-type sector, this is not the case for the right-handed down-quark sector. Here, the hierarchies are much weaker

$$\frac{|F(c_{d_1})|}{|F(c_{d_2})|} \sim \frac{m_d}{m_s}\frac{1}{\lambda} \sim 0.3, \qquad \frac{|F(c_{d_2})|}{|F(c_{d_3})|} \sim \frac{m_s}{m_b}\frac{1}{\lambda^2} \sim 0.4. \qquad (3.139)$$

In this sector, and only there, it is thus a viable possibility to assume equal quark profiles $F(c_{d_i})$ by imposing a $U(3)$ flavor symmetry and to explain the required moderate splittings in terms of $\mathcal{O}(1)$ variations in the fundamental Yukawa couplings that break this symmetry. Although such a choice might seem to be *ad hoc*, it has the virtue of strongly suppressing dangerous tree-level FCNC contributions to $K\text{–}\bar{K}$ mixing [205].

To summarize the findings of this section, it is possible to address the hierarchies in the fermion sector, and to generate small masses out of $\mathcal{O}(1)$ fundamental parameters within warped extra dimensions. Those models thus provide also a solution to the second problem introduced in Section 1.2. At the same time, the anarchic approach to flavor narrows down many of the new parameters entering the RS setup, making the model more predictive. The relations (3.135) and (3.136) demonstrate how the (relative) localizations of the different quarks, expressed through profile functions $F(c)$, are given in terms of observable quantities. These new flavor quantities of the RS model can be fixed to first approximation by the observed quark masses and CKM parameters. The emerging picture is shown in Figure 3.8. The (right handed component of the) top quark, being the heaviest quark of the SM, should be localized closest to the IR brane, where the Higgs sector is localized. The light quarks, however, reside more closely to the UV brane. The fact that the top quark is localized next to the IR brane, where also KK modes live, results in potentially interesting effects in top physics. The same

holds true for the Higgs sector, being localized directly on the IR brane, see Chapter 5. Note that the localization of single profiles can only be fixed to certain regions, which depend on each other. Within these regions, the profiles can be shifted due to reparametrization invariances, leaving the quark masses and CKM elements unchanged, see below. The boundaries of these intervals are defined by naturalness, *i.e.*, we do not want to abandon the assumption of $\mathcal{O}(1)$ localization parameters, as well as of $\mathcal{O}(1)$ fundamental Yukawa couplings.

The regions in parameter space which are ocupied by 95% of our RS parameter points (see Chapter 5) are plotted in Figure 3.9. This plot confirms that indeed the quark spectrum and the mixing parameters constrain the localization of the quark fields and thus the generic RS predictions for observables. As expected, light quarks are predicted to have $c_{Q_i,q_i} < -1/2$, $i = 1, 2$, whereas the right-handed top quark and, to a lesser extend, the third generation doublet feature $c_{Q_3,u_3} > -1/2$. Importantly, the generic statement about the flavor structure, to expect the largest effects in the sector of third generation quarks, is quite robust. In particular, the relative localizations within the $SU(2)_L$ doublet as well as within the singlet sector are more or less fixed due to the observed hierarchies. However, also the absolute localizations are constrained, due to the requirement that *none* of the (correlated) parameters leaves its natural range. In that context note that the bulk masses should not significantly exceed the RS curvature $c_{Q_i,q_i} \lesssim 1$. To improve these order of magnitude estimations and to determine the precise values of the RS parameters, one has to perform significantly more measurements than within the SM. In the phenomenological studies presented in this thesis, we will scan over parameter sets, with the localization of the quarks determined just as described in this section. Starting from random anarchical Yukawa matrices we will find that, despite the remaining uncertainty in the localization of the fermion fields, generic predictions are possible in the RS setup without additional input, see sections 5.2.2, 5.1.4, and 5.3.

What concerns leptons, note that it is also possible to address the tiny neutrino masses in the RS setup, without a see-saw mechanism, by means of wave function overlaps [173, 208, 209], see also [210, 211, 212].

Reparametrization Invariance

As sketched before, the results for the quark masses and mixings in the ZMA are invariant under a set of reparametrization transformations, which change the input parameters of the theory. We will now give the explicit form of the corresponding transformations. The first type of reparametrization invariance (RPI-1) corresponds to a simultaneous rescaling of the profiles for the $SU(2)_L$ doublet and singlet fermions by opposite factors, while keeping the fundamental Yukawa couplings invariant

$$F(c_{Q_i}) \to e^{-\xi} F(c_{Q_i}), \qquad F(c_{q_i}) \to e^{+\xi} F(c_{q_i}), \qquad \boldsymbol{Y}_q \to \boldsymbol{Y}_q. \qquad \text{(RPI-1)} \qquad (3.140)$$

For UV localized quarks, with $c_i < -1/2$, these transformations correspond to good approximation to the shifts $c_{Q_i} \to c_{Q_i} - \xi/L$ and $c_{q_i} \to c_{q_i} + \xi/L$ of the bulk mass parameters.

A second type of reparametrization invariance (RPI-2) corresponds to a simultaneous rescaling of all fermion profiles by a common factor, while the fundamental Yukawa couplings are rescaled with an opposite factor (however still keeping them of $\mathcal{O}(1)$)

$$F(c_{Q_i}) \to \eta F(c_{Q_i}), \qquad F(c_{q_i}) \to \eta F(c_{q_i}), \qquad \boldsymbol{Y}_q \to \frac{1}{\eta^2} \boldsymbol{Y}_q. \qquad \text{(RPI-2)} \qquad (3.141)$$
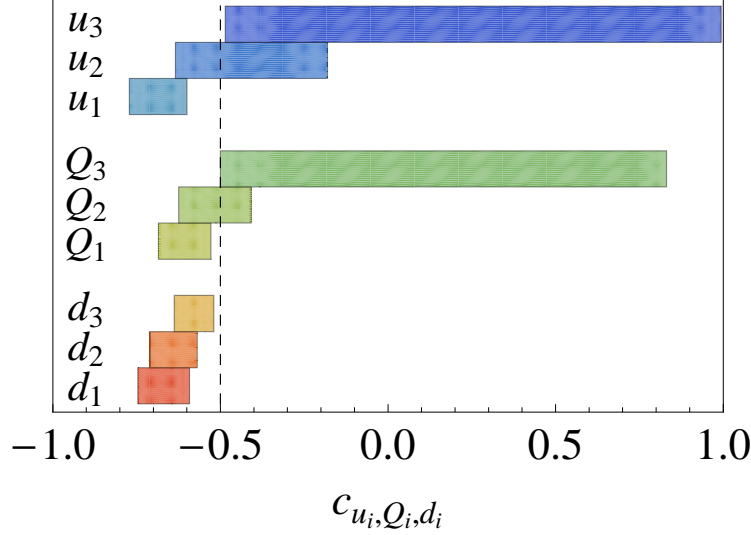
Figure 3.9: Localization parameters of quarks in the extra dimension. Values of $c_{Q_i,q_i} < -1/2$ lead to an UV localization, whereas IR-localization corresponds to $c_{Q_i,q_i} > -1/2$. The shown regions contain 95% of the points in the parameter space. See [1] and text for details.

For $c_i < -1/2$, the corresponding shifts of the bulk mass parameters are approximately universal and read $c_{Q_i} \to c_{Q_i} + L^{-1} \ln \eta$ and $c_{q_i} \to c_{q_i} + L^{-1} \ln \eta$. A stronger form of this relation is provided by allowing for different transformation parameters for up-type and down-type singlets $\eta_u \neq \eta_d$

$$F(c_{Q_i}) \to \eta\, F(c_{Q_i})\,, \qquad F(c_{q_i}) \to \eta_q\, F(c_{q_i})\,, \qquad \boldsymbol{Y}_q \to \frac{1}{\eta\eta_q}\, \boldsymbol{Y}_q\,. \qquad \text{(RPI-2$'$)} \qquad (3.142)$$

Of course the transformations (3.140) and (3.142) can be combined in arbitrary ways. While the masses and mixing angles in the ZMA are not affected by these transformations, the fermion bulk profiles do change. As a consequence also the result for the flavor-changing interactions (apart from the CKM matrix), that will be derived in the upcoming sections, will change under these reparametrizations. As discussed before, observables in the RS setup thus depend, besides on the NP scale M_{KK}, more or less strongly on additional new parameters, which are not completely fixed by the fermion hierarchies. However, these hierarchies tell us a lot about these parameters, and fix the relative sizes in the doublet as well as in the singlet sector to a good extent. The demand for fundamental $\mathcal{O}(1)$ Yukawa couplings constrains the deviations due to the second type of reparametrization invariance. The remaining freedom should then be constrained further by experiment, *e.g.* by Z-pole measurements, see Section 5.1.3.

3.2.4 Gauge-Boson Interactions with Fermions

With the results obtained so far, we are able to derive all Feynman rules for the minimal RS model in a straightforward way. In particular, we do not have to worry about the transformation to the mass basis anymore, which has already been implemented in our KK decomposition.

We start the discussion with the interactions between fermions and gauge bosons. The interactions involving the Higgs boson will be explored later in Section 3.7. The main results that will be presented here are exact to all orders in v^2/M_{KK}. However, also ZMA expressions will be given, which make the dependence on the model parameters more transparent. It will turn out that for the Z-boson interactions with SM fermions it is necessary to include the next-to-leading order (NLO) in the ZMA to derive a consistent result at $\mathcal{O}(v^2/M_{\mathrm{KK}}^2)$. This contribution had been neglected in the literature before [1].

Fermion Couplings to Massless Gauge Bosons and their KK Excitations

First we consider general fermion couplings to gauge bosons which do not receive masses from EWSB, *i.e.*, couplings to (KK) gluons and photons. Those have massless zero modes with a flat profile (3.66). The interaction terms follow, like in 4D, from local gauge invariance. They are analogous to the terms resulting from (1.9) but with an additional integration over the extra dimension and a non-trivial metric, as well as 5D instead of 4D fields. In particular, the 4D covariant derivative (1.10) is to be replaced by (3.41). Note that the ϕ-components of the gauge fields couple to fermion zero modes only at $\mathcal{O}(v^2/M_{\mathrm{KK}}^2)$. Moreover, they do not develop a zero mode themselves. Thus, we do not consider them here.

After KK decomposition, the 4D Lagrangian contains the interaction terms

$$
\mathcal{L}_{4D} \ni \sum_{n_1,n_2,n_3} \left\{ \left[\vec{a}_{n_2}^{U\dagger} \, \boldsymbol{I}_{n_1 n_2 n_3}^{C(Q)} \, \vec{a}_{n_3}^{U} + \vec{a}_{n_2}^{u\dagger} \, \boldsymbol{I}_{n_1 n_2 n_3}^{S(u)} \, \vec{a}_{n_3}^{u} \right] \bar{u}_{L}^{(n_2)} g_s \mathcal{G}^{(n_1)a} \, t^a \, u_{L}^{(n_3)} \right.
$$
$$
\left. + \left[\vec{a}_{n_2}^{u\dagger} \, \boldsymbol{I}_{n_1 n_2 n_3}^{C(u)} \, \vec{a}_{n_3}^{u} + \vec{a}_{n_2}^{U\dagger} \, \boldsymbol{I}_{n_1 n_2 n_3}^{S(Q)} \, \vec{a}_{n_3}^{U} \right] \bar{u}_{R}^{(n_2)} g_s \mathcal{G}^{(n_1)a} \, t^a \, u_{R}^{(n_3)} \right\},
$$
(3.143)

corresponding to couplings of gluons to up-type quarks. Analogous expressions hold for down-type quarks. Here, $g_s = g_{s,5}/\sqrt{2\pi r}$ is the 4D gauge coupling of QCD and we have defined the overlap integrals

$$
\boldsymbol{I}_{n_1 n_2 n_3}^{C(A)} = \int_{-\pi}^{\pi} d\phi \, \sqrt{2\pi} \, \chi_{n_1}(\phi) \, e^{\sigma(\phi)} \, \boldsymbol{C}_{n_2}^{A}(\phi) \, \boldsymbol{C}_{n_3}^{A}(\phi), \qquad A = Q, u, d. \tag{3.144}
$$

The overlaps $\boldsymbol{I}_{n_1 n_2 n_3}^{S(A)}$ are defined similarly in terms of integrals over $\boldsymbol{S}_n^{(A)}$ profiles. For fixed n_1, n_2, n_3 these integrals are $N \times N$ diagonal matrices in generation space. For the gluon zero mode, we obtain using (3.66) and (3.88)

$$
\boldsymbol{I}_{0 n_2 n_3}^{C(A)} = \delta_{n_2 n_3} \, \mathbf{1} + \Delta \boldsymbol{C}_{n_2 n_3}^{A}, \qquad \boldsymbol{I}_{0 n_2 n_3}^{S(A)} = \delta_{n_2 n_3} \, \mathbf{1} + \Delta \boldsymbol{S}_{n_2 n_3}^{A}. \tag{3.145}
$$

Thus, the relation (3.90) implies that the couplings of massless gauge boson modes are flavor diagonal and take the same form as in the SM, *i.e.*,

$$
\mathcal{L}_{4D} \ni \sum_{n} \bar{u}^{(n)} g_s \mathcal{G}^{(0)a} \, t^a \, u^{(n)}, \tag{3.146}
$$

where $u^{(n)} = u_L^{(n)} + u_R^{(n)}$. The couplings of KK gluons are however not flavor diagonal and must be worked out from (3.143). Due to the structure of the overlap integrals (3.144), the

effective couplings between heavy fermions and KK gluons, which are both localized close to the IR brane is not g_s but $\sqrt{L}\,g_s$ [169, 170]. The interactions between photons and fermions can be obtained from the relations above by the replacement $g_s t^a \to eQ_f$, where f can be any fermion species charged under electromagnetism.

Fermion Couplings to the **Z** Boson

The weak interactions of the minimal RS model can be worked out in a similar way. Nevertheless, some differences arise in this sector. In principle, the emerging overlap integrals have the same form as in (3.143). But, since the weak gauge bosons couple differently to $SU(2)_L$-doublet and -singlet fermions, the integrals appear in different combinations compared to (3.143). Moreover, already the zero modes of the weak gauge bosons, corresponding to the $W^\pm$ and Z bosons of the SM, are massive and thus have a non-trivial profile in the extra dimension. These facts result in modified weak gauge-boson couplings to fermions with respect to the SM. The RS corrections are non-diagonal in flavor space, leading to tree-level FCNCs due to interactions with the Z-boson. Interestingly, these corrections are parametrically enhanced by the "volume factor" L (measuring the radius of the extra dimension in units of the inverse curvature divided by π) with respect to the FCNC couplings of KK gauge bosons [213], see Section 3.5.

Technically, the emergence of tree-level FCNC-couplings to the Z-boson in the RS model has two reasons. First, the fermion profiles do not fulfill standard orthonormality relations but rather fulfill (3.88). As discussed above, this reflects the fact, that after EWSB the $SU(2)_L$ doublets and singlets mix. Thus, only the sum of the $SU(2)_L$ doublet and singlet contribution to a certain chirality leads to diagonal couplings due to the combined orthonormality relation (3.90), as is the case for the massless SM gauge bosons. If one term is coming with another prefactor, like in the Z-boson couplings, being different for singlets and doublets, an off-diagonal contribution to the interaction will remain, due to fermion mixing. Second, due to the non-trivial dependence of the Z-boson profile on ϕ, the interaction integrals can not collapse to the (combined) orthonormality relation (3.90), which would lead to diagonal couplings, even if singlets and doublets would couple similarly. This source of tree FCNCs would remain even without the presence of doublet-singlet mixing, *i.e.*, when the odd profiles of the zero modes vanish and the even profiles obey standard orthonormality relations with $\Delta\boldsymbol{C}_{mn}^A \to \delta_{mn}\boldsymbol{1}$. From a perturbative point of view, this can be understood through the fact that before going from the flavor basis to the fermion mass basis, the Z-couplings are flavor (and KK mode) diagonal but non universal due to the different overlaps. This will induce off-diagonal entries in the interaction matrix, after going to the fermion-mass basis. In the same way, one can understand the tree-level FCNCs due to fermion mixing, since here the $SU(2)_L$ doublets and singlets, that are contributing to the same chirality (due to the presence of vector-like KK excitations), couple differently [175, 214, 215], see also [216]. This source of tree-level FCNCs would remain even for couplings to *massless* gauge bosons that couple differently to $SU(2)_L$ doublets and singlets. Before, this effect has usually been neglected in the literature since it is proportional to the masses of the light SM fermions. However, we will show that it is parametrical as well as numerical as important as the other source of FCNCs. In [1], we have given for the first time exact expressions for the corresponding contributions and presented compact analytical results, valid at first non-trivial order in the ZMA.

Including RS corrections to $\mathcal{O}(m_Z^2/M_{\text{KK}}^2)$, the couplings of the Z-boson to SM-fermions

and their KK excitations can be written as

$$
\mathcal{L}_{\text{4D}} \ni \frac{g}{\cos\theta_w} \left[1 + \frac{m_Z^2}{4M_{\text{KK}}^2} \left(1 - \frac{1}{L} \right) \right] Z_\mu
$$
$$
\times \sum_{f,m,n} \left[(g_L^f)_{mn}\, \bar{f}_{L,m}\gamma^\mu f_{L,n} + (g_R^f)_{mn}\, \bar{f}_{R,m}\gamma^\mu f_{R,n} \right],
$$

(3.147)

where g and $\cos\theta_w$ are the 4D weak $SU(2)_L$ gauge coupling and the cosine of the weak mixing angle as defined in (3.39) and (3.40). The prefactor in brackets in the first line above corresponds to a universal correction due to the constant terms in the bulk profile (3.68). The left- and right-handed couplings $\boldsymbol{g}_{L,R}^f$ are infinite-dimensional matrices in the space of fermion modes, depending on the fermion type $f = u, d, \nu, e$.[14] They can be parametrized as

$$
\boldsymbol{g}_L^f = \left(T_3^f - \sin^2\theta_w\, Q_f \right) \left[\mathbf{1} - \frac{m_Z^2}{2M_{\text{KK}}^2} \left(L\,\boldsymbol{\Delta}_F - \boldsymbol{\Delta}'_F \right) \right] - T_3^f \left[\boldsymbol{\delta}_F - \frac{m_Z^2}{2M_{\text{KK}}^2} \left(L\,\boldsymbol{\varepsilon}_F - \boldsymbol{\varepsilon}'_F \right) \right],
$$
$$
\boldsymbol{g}_R^f = -\sin^2\theta_w\, Q_f \left[\mathbf{1} - \frac{m_Z^2}{2M_{\text{KK}}^2} \left(L\,\boldsymbol{\Delta}_f - \boldsymbol{\Delta}'_f \right) \right] + T_3^f \left[\boldsymbol{\delta}_f - \frac{m_Z^2}{2M_{\text{KK}}^2} \left(L\,\boldsymbol{\varepsilon}_f - \boldsymbol{\varepsilon}'_f \right) \right],
$$

(3.148)

where T_3^f and Q_f denote the weak isospin and the electric charge (in units of e) of the fermion f. A subscript F on the matrices $\boldsymbol{\Delta}$, $\boldsymbol{\Delta}'$, $\boldsymbol{\delta}$, $\boldsymbol{\varepsilon}$, and $\boldsymbol{\varepsilon}'$, refers to a fermion of an $SU(2)_L$ doublet ($F = U, D$ in the quark sector, and $F = \nu, E$ in the lepton sector), while a subscript f refers to a singlet ($f = u, d$ or $f = \nu_R, e$). The matrices $\boldsymbol{\Delta}^{(\prime)}$ and $\boldsymbol{\varepsilon}^{(\prime)}$ arise due to the t-dependent terms in the gauge-boson profile (3.68) and mediate FCNCs. The elements of the former read

$$
(\Delta_F)_{mn} = \frac{2\pi}{L\epsilon} \int_\epsilon^1 dt\, t^2 \left[\vec{a}_m^{F\dagger}\, \boldsymbol{C}_m^F(\phi)\, \boldsymbol{C}_n^F(\phi)\, \vec{a}_n^F + \vec{a}_m^{f\dagger}\, \boldsymbol{S}_m^f(\phi)\, \boldsymbol{S}_n^f(\phi)\, \vec{a}_n^f \right],
$$
$$
(\Delta_f)_{mn} = \frac{2\pi}{L\epsilon} \int_\epsilon^1 dt\, t^2 \left[\vec{a}_m^{f\dagger}\, \boldsymbol{C}_m^f(\phi)\, \boldsymbol{C}_n^f(\phi)\, \vec{a}_n^f + \vec{a}_m^{F\dagger}\, \boldsymbol{S}_m^F(\phi)\, \boldsymbol{S}_n^F(\phi)\, \vec{a}_n^F \right],
$$
$$
(\Delta'_F)_{mn} = \frac{2\pi}{L\epsilon} \int_\epsilon^1 dt\, t^2 \left(\frac{1}{2} - \ln t \right) \left[\vec{a}_m^{F\dagger}\, \boldsymbol{C}_m^F(\phi)\, \boldsymbol{C}_n^F(\phi)\, \vec{a}_n^F + \vec{a}_m^{f\dagger}\, \boldsymbol{S}_m^f(\phi)\, \boldsymbol{S}_n^f(\phi)\, \vec{a}_n^f \right],
$$
$$
(\Delta'_f)_{mn} = \frac{2\pi}{L\epsilon} \int_\epsilon^1 dt\, t^2 \left(\frac{1}{2} - \ln t \right) \left[\vec{a}_m^{f\dagger}\, \boldsymbol{C}_m^f(\phi)\, \boldsymbol{C}_n^f(\phi)\, \vec{a}_n^f + \vec{a}_m^{F\dagger}\, \boldsymbol{S}_m^F(\phi)\, \boldsymbol{S}_n^F(\phi)\, \vec{a}_n^F \right].
$$

(3.149)

Keep in mind that for the profiles of $SU(2)_L$ doublet fermions no distinction is to be made between $F = U$ and $F = D$ (3.77), as well as between $F = \nu$ and $F = E$. For the minimal RS model, the matrices $\boldsymbol{\varepsilon}^{(\prime)}$ are identical to those given above, just with the even profiles $\boldsymbol{C}_n^{F,f}$ omitted. Finally, there are also the contributions from the fact that the fermion profiles are not orthonormal on each other, i.e., from doublet-singlet mixing. They are parametrized by the matrices $\boldsymbol{\delta}$, defined as

$$
(\delta_F)_{mn} = \vec{a}_m^{f\dagger} \left(\delta_{mn} + \Delta\boldsymbol{S}_{mn}^f \right) \vec{a}_n^f, \qquad (\delta_f)_{mn} = \vec{a}_m^{F\dagger} \left(\delta_{mn} + \Delta\boldsymbol{S}_{mn}^F \right) \vec{a}_n^F.
$$

(3.150)

---

[14]The discussion of the Z couplings in this section refers to quarks as well as leptons. In the rest of this thesis we will, however, focus on the quark sector.

We will now have a closer look on the couplings of the Z-boson to the light (SM) fermions, which will be particular relevant for the following discussions. These are described by the upper-left 3×3 blocks of the matrices $\boldsymbol{g}^f_{L,R}$. First, note that the weight factor t^2, present in the overlap integrals (3.149), emphasizes the region close the IR brane, where $t = \mathcal{O}(1)$. However, the SM fermions are, with the exception of the heavy top quark and, to a lesser extend, the left-handed component of the bottom quark, all localized near the UV brane (see Figure 3.8 and the related discussion). However, in that region the weight factor is exponentially suppressed $t^2 \to \mathcal{O}(\epsilon^2)$. This leads to a strong suppression of FCNCs containing light quarks, which is known as the RS-GIM mechanism [176, 177, 217]. This is a very important feature of RS models, as without such a mechanism, bounds from flavor physics would immediately drive the KK scale way beyond the reach of the LHC, see the discussion of the *new physics flavor problem* in Section 1.1.6. Like the GIM mechanism of the SM, RS-GIM is broken by the large top-quark mass, see Section 1.1.3, which leads to an IR localization of the corresponding singlet profile as well as (less strongly) of the corresponding doublet profile. However, its dynamical origin is different from the GIM mechanism of the SM.

It will be very useful to have approximate analytical expressions for the exact overlap integrals at hand, from which the size of their effects as well as the dependence on the input parameters of the model will become more transparent. To this end, we employ the zeroth order in the ZMA to the fermion profiles entering the overlap integrals of (3.149). This is justified, since in (3.147) the profiles already feature a coefficient scaling like v^2/M^2_{KK} and higher orders are neglected anyway. We perform the replacements

$$\boldsymbol{C}^{Q,u}_n(\phi)\, \vec{a}^{U,u}_n \to \sqrt{\frac{L\epsilon}{2\pi}}\, \mathrm{diag}(F(c_{Q_i,u_i})\, t^{c_{Q_i,u_i}})\, \hat{a}^{u,u^c}_n \,, \qquad \boldsymbol{S}^{Q,u}_n(\phi)\, \vec{a}^{U,u}_n \to 0 \,, \qquad (3.151)$$

and similar for down-type quarks, meaning that the even profiles reduce to the zero mode profiles obtained without EWSB [173], while the odd profiles are suppressed by an extra power of $x_n = m_n/M_{\mathrm{KK}}$ and thus vanish to the order considered. Analogous expressions hold for the down-quark sector.

With these replacements we find [211, 218, 219]

$$\begin{aligned}
\boldsymbol{\Delta}_F &\to \boldsymbol{U}^\dagger_f\, \mathrm{diag}\left[\frac{F^2(c_{F_i})}{3 + 2c_{F_i}}\right] \boldsymbol{U}_f \,, \\[2mm]
\boldsymbol{\Delta}_f &\to \boldsymbol{W}^\dagger_f\, \mathrm{diag}\left[\frac{F^2(c_{f_i})}{3 + 2c_{f_i}}\right] \boldsymbol{W}_f \,, \\[2mm]
\boldsymbol{\Delta}'_F &\to \boldsymbol{U}^\dagger_f\, \mathrm{diag}\left[\frac{5 + 2c_{F_i}}{2(3 + 2c_{F_i})^2}\, F^2(c_{F_i})\right] \boldsymbol{U}_f \,, \\[2mm]
\boldsymbol{\Delta}'_f &\to \boldsymbol{W}^\dagger_f\, \mathrm{diag}\left[\frac{5 + 2c_{f_i}}{2(3 + 2c_{f_i})^2}\, F^2(c_{f_i})\right] \boldsymbol{W}_f \,.
\end{aligned} \qquad (3.152)$$

All these objects are 3×3 matrices in generation space, and the diagonal matrices contain the elements in the corresponding brackets on the diagonal. Note that, with the c_{F_i,f_i} parameters being close to $-1/2$, we have $\boldsymbol{\Delta}_A \approx \boldsymbol{\Delta}'_A$ for $A = F, f$ to good approximation. The matrices $\boldsymbol{\varepsilon}^{(\prime)}_A$ vanish at zeroth order in the ZMA - they are suppressed by an additional factor of v^2/M^2_{KK}. The same is true for the matrices $\boldsymbol{\delta}_A$, since they can also be written as integrals containing

only $\boldsymbol{S}_n^{(A)}$ profiles. However, we have to be careful, since these contributions come with an unsuppressed $\mathcal{O}(1)$ coefficient in (3.148). Thus we have to include the NLO in the ZMA which yields

$$\boldsymbol{S}_n^{Q,u}(\phi)\,\vec{a}_n^{U,u} \to \pm\mathrm{sgn}(\phi)\,\sqrt{\frac{L\epsilon}{2\pi}}\,x_n \,\mathrm{diag}\left(F(c_{Q_i,u_i})\,\frac{t^{1+c_{Q_i,u_i}} - \epsilon^{1+2c_{Q_i,u_i}}\,t^{-c_{Q_i,u_i}}}{1+2c_{Q_i,u_i}}\right)\hat{a}_n^{u,u^c}\,, \quad (3.153)$$

from which we derive

$$\begin{aligned}
\boldsymbol{\delta}_F &\to \boldsymbol{x}_f\,\boldsymbol{W}_f^\dagger\,\mathrm{diag}\left[\frac{1}{1-2c_{f_i}}\left(\frac{1}{F^2(c_{f_i})}-1+\frac{F^2(c_{f_i})}{3+2c_{f_i}}\right)\right]\boldsymbol{W}_f\,\boldsymbol{x}_f\,, \\
\boldsymbol{\delta}_f &\to \boldsymbol{x}_f\,\boldsymbol{U}_f^\dagger\,\mathrm{diag}\left[\frac{1}{1-2c_{F_i}}\left(\frac{1}{F^2(c_{F_i})}-1+\frac{F^2(c_{F_i})}{3+2c_{F_i}}\right)\right]\boldsymbol{U}_f\,\boldsymbol{x}_f\,.
\end{aligned} \quad (3.154)$$

Here, the diagonal matrix $\boldsymbol{x}_f = \mathrm{diag}(m_{f_1}, m_{f_2}, m_{f_3})/M_{\mathrm{KK}}$ contains the masses of the SM fermions. The important expressions (3.154) have not been presented before [1]. Approximate results for the admixture of singlet contributions in the wave functions of predominantly $SU(2)_L$ doublet SM fermions due to mixing with their KK excitations have been given in [214, 215, 220, 221]. However, this effect has not been discussed systematically in the context of flavor-changing processes. By making use of the scaling relations obtained via the Froggatt-Nielsen analysis in Section 3.2.3 we arrive at

$$\begin{aligned}
(\Delta_F)_{ij} &\sim (\Delta_F')_{ij} \sim F(c_{F_i})\,F(c_{F_j})\,, \\
(\Delta_f)_{ij} &\sim (\Delta_f')_{ij} \sim F(c_{f_i})\,F(c_{f_j})\,, \\
(\delta_F)_{ij} &\sim \frac{m_{f_i}m_{f_j}}{M_{\mathrm{KK}}^2}\,\frac{1}{F(c_{f_i})\,F(c_{f_j})} \sim \frac{v^2\,Y_f^2}{M_{\mathrm{KK}}^2}\,F(c_{F_i})\,F(c_{F_j})\,, \\
(\delta_f)_{ij} &\sim \frac{m_{f_i}m_{f_j}}{M_{\mathrm{KK}}^2}\,\frac{1}{F(c_{F_i})\,F(c_{F_j})} \sim \frac{v^2\,Y_f^2}{M_{\mathrm{KK}}^2}\,F(c_{f_i})\,F(c_{f_j})\,,
\end{aligned} \quad (3.155)$$

valid to LO in hierarchies. Here, Y_f represents an (combination of) element(s) of the Yukawa matrix $\boldsymbol{Y}_f$. The relations (3.155) make the RS-GIM suppression factors due to the fermion zero-mode profiles explicit. Moreover, one observes explicitly that the contributions of the (usually neglected) $\boldsymbol{\delta}_A$ matrices in (3.148), are of the same order as the effects proportional to the $\boldsymbol{\Delta}_A^{(\prime)}$ matrices. The chiral suppression is lifted by the inverse powers of the corresponding fermion zero-mode profiles. Explicit expressions for the mixing matrices, in which the relevant combinations of Yukawa matrices are included, can be found in [1].

Let us finally mention how the flavor-changing couplings discussed here transform under the reparametrizations of Section 3.2.3, which leave the quark spectrum and CKM parameters (in the ZMA) invariant. From (3.140), we obtain for a RPI-1 transformation

$$\begin{aligned}
\boldsymbol{\Delta}_F &\to e^{-2\xi}\,\boldsymbol{\Delta}_F\,, & \boldsymbol{\Delta}_f &\to e^{+2\xi}\,\boldsymbol{\Delta}_f\,, \\
\boldsymbol{\delta}_F &\to e^{-2\xi}\,\boldsymbol{\delta}_F\,, & \boldsymbol{\delta}_f &\to e^{+2\xi}\,\boldsymbol{\delta}_f\,.
\end{aligned} \quad (3.156)$$

which redistributes effects between the left- and right-handed sectors. For a RPI-2$'$ transfor-

mation, we obtain from (3.142)

$$\boldsymbol{\Delta}_F \to \eta^2 \, \boldsymbol{\Delta}_F \,, \qquad \boldsymbol{\Delta}_f \to \eta_q^2 \, \boldsymbol{\Delta}_f \,,$$
$$\boldsymbol{\delta}_F \to \frac{1}{\eta_q^2} \, \boldsymbol{\delta}_F \,, \qquad \boldsymbol{\delta}_f \to \frac{1}{\eta^2} \, \boldsymbol{\delta}_f \,. \tag{3.157}$$

This corresponds to a reshuffling of contributions between the two sources of flavor violations, one arising from the non-trivial gauge-boson profiles ($\boldsymbol{\Delta}_A$) and one from fermion mixing ($\boldsymbol{\delta}_A$).

Fermion Couplings to $W^\pm$ Bosons

Similar to the way of deriving the interactions between fermions and the Z boson, we can obtain expressions for the couplings of the charged $W^\pm$ bosons to fermions. In this sector, of course, flavor-changing effects at the tree-level are already unsuppressed within the SM. Focusing on the quark sector and working up to $\mathcal{O}(m_W^2/M_{\text{KK}}^2)$, we obtain

$$\mathcal{L}_{4\text{D}} \ni \frac{g}{\sqrt{2}} W_\mu^+ \sum_{n_1, n_2} \left[\left(\tilde{V}_L\right)_{n_1 n_2} \bar{u}_{L,n1} \gamma^\mu d_{L,n_2} + \left(\tilde{V}_R\right)_{n_1 n_2} \bar{u}_{R,n1} \gamma^\mu d_{R,n_2} \right] + \text{h.c.} \,, \tag{3.158}$$

where

$$\left(\tilde{V}_L\right)_{n_1 n_2} = \vec{a}_{n_1}^{U\dagger} \, \boldsymbol{I}_{0 n_1 n_2}^{C(Q)} \, \vec{a}_{n_2}^D \,, \qquad \left(\tilde{V}_R\right)_{n_1 n_2} = \vec{a}_{n_1}^{U\dagger} \, \boldsymbol{I}_{0 n_1 n_2}^{S(Q)} \, \vec{a}_{n_2}^D \tag{3.159}$$

and the corresponding overlap integrals have been defined in (3.144).

The couplings to the SM fermions are again encoded in the upper-left 3×3 blocks of these matrices. In the leading order of the ZMA we obtain

$$\tilde{\boldsymbol{V}}_L \to \boldsymbol{U}_u^\dagger \boldsymbol{U}_d = \boldsymbol{V}_{\text{CKM}} \,, \qquad \tilde{\boldsymbol{V}}_R \to 0 \,, \tag{3.160}$$

where the tilde symbol indicates that the charged-current interaction-matrices differ from the quantities which would be experimentally identified with the CKM matrix (for the left handed interactions) as well as the corresponding object in the right handed sector (which arises due to doublet-singlet mixing). Here, the definition corresponds to the single $W u_L^i d_L^j$ and $W u_R^i d_R^j$ vertices, whereas a more physical definition includes the exchange of the whole tower of $W^\pm$-boson KK modes. We will give such a definition, based on four-fermion interactions, after having discussed the necessary formalism to sum up KK towers in Section 3.5. At $\mathcal{O}(v^2/M_{\text{KK}}^2)$, corrections to the two matrices in (3.159) arise. These lead to a non-unitarity of the matrix $\tilde{\boldsymbol{V}}_L$ describing $W u_L^i d_L^j$ interactions and to right-handed charged currents. The matrix $\tilde{\boldsymbol{V}}_R$ can be estimated by using the first non-trivial order in the ZMA for the S_n^A profiles, as given in (3.153). We obtain

$$\tilde{\boldsymbol{V}}_R \to \boldsymbol{x}_u \boldsymbol{U}_u^\dagger \, \text{diag}\left[\frac{1}{1 - 2c_{Q_i}} \left(\frac{1}{F^2(c_{Q_i})} - 1 + \frac{F^2(c_{Q_i})}{3 + 2c_{Q_i}} \right) \right] \boldsymbol{U}_d \, \boldsymbol{x}_d \,. \tag{3.161}$$

The scaling relations from the Froggatt-Nielsen analysis of Section 3.2.3 imply

$$\left(\tilde{V}_R\right)_{ij} \sim \frac{v^2}{M_{\text{KK}}^2} \, F(c_{u_i}) \, F(c_{d_j}) \sim \frac{m_{u_i} m_{d_j}}{M_{\text{KK}}^2} \, \frac{1}{F(c_{Q_i}) F(c_{Q_j})} \,. \tag{3.162}$$

The non-unitarity of the matrix $\tilde{\boldsymbol{V}}_L$ is determined by the deviations of the Z_2-even fermion profiles and the corresponding flavor vectors $\vec{a}_n^{Q,q}$ from their ZMA expressions, *i.e.*, fermion mixing, as well as by the t-dependent terms in the gauge-boson profile (3.68). These effects are easiest to study with the help of the exact results for the fermion profiles and eigenvectors derived in Section 3.2.2, see [1]. However, we will focus on the definition of the CKM matrix via the exchange of the whole KK tower, see Section 3.6. After that discussion, we will also explore the fermion couplings to the Higgs boson, directly in the context of both RS variants studied in this thesis, see Section 3.7.

3.3 The T Parameter and $Zb\bar{b}$ Observables as a Motivation to Extend the Gauge Group

After having examined the interactions of the SM fields propagating in a warped extra dimension in detail in the last sections, we will have a first look at the phenomenological consequences of this setup, which can be derived with the help of these results. For the time being, we will concentrate on the electroweak precision parameters S, T and U due to Peskin and Takeuchi, and corrections to $Zb\bar{b}$ couplings. It will turn out that the RS setup presented so far generically produces sizable contributions to these quantities. This will provide a motivation for the following part in this theory chapter - the introduction of the custodial Randall-Sundrum model, which can help improving the electroweak fit with respect to the minimal model. However, we will also advocate another option of allowing for low NP scales $M_{\text{KK}} \sim (2-3)$ TeV, within the minimal RS model (at the tree level).

The S, T, and U parameters have been introduced in Section 1.1.2, see (1.43). They measure deviations from the electroweak radiative corrections of the SM, due to NP contributions in universal electroweak corrections. Thus, they are defined as zero for a SM reference point. In the following, we will derive these parameters in the minimal RS model. Here, they already get contributions on the born level, due to the tree-level corrections to the $W^{\pm}$- and Z-boson masses, as well as corrections to the trivial flat profiles. Thus we will not consider loop corrections to the electroweak parameters, although a complete one-loop calculation, extending the work of [222, 223, 224] would be desirable. However, this is beyond the scope of this thesis. To calculate the RS contributions to the electroweak precision parameters, we use an effective Lagrangian approach [202]. First note that, due to the RS-GIM mechanism, non universal corrections to the $W^{\pm}$- and Z-boson interactions are strongly suppressed for the first two generations of SM fermions. In such a case, the corrections are adequately parametrized by the S, T and U parameters. Neglecting non-universal corrections, we first rescale the gauge fields in order to bring the interactions with zero-mode fermions to their SM form, working at lowest order in the ZMA. Using (3.67) and (3.68) we can then read off (from the kinetic terms and mass terms of the electroweak gauge bosons) the contributions to the correlators in the RS model

$$\Pi_{WW}(0) = -\frac{g^4 v^4}{32 M_{\text{KK}}^2} \left(L - \frac{1}{2L} \right), \quad \Pi_{ZZ}(0) = -\frac{(g^2 + g'^2)^2 \, v^4}{32 M_{\text{KK}}^2} \left(L - \frac{1}{2L} \right),$$

$$\Pi'_{WW}(0) = \frac{g^2 v^2}{8 M_{\text{KK}}^2} \left(1 - \frac{1}{L} \right), \qquad \Pi'_{ZZ}(0) = \frac{(g^2 + g'^2) \, v^2}{8 M_{\text{KK}}^2} \left(1 - \frac{1}{L} \right). \tag{3.163}$$
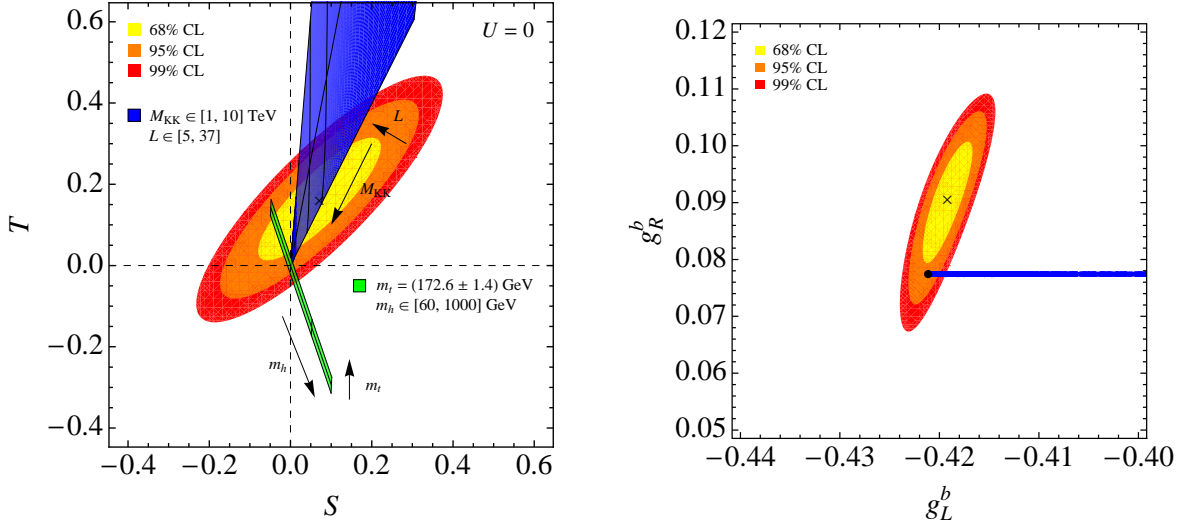
Figure 3.10: Left: Regions of 68%, 95%, and 99% probability in the S–T plane. The green (light-shaded) shaded stripe shows the SM predictions for $m_t = (172.6 \pm 1.4)\,\text{GeV}$ and $m_h \in [60, 1000]\,\text{GeV}$. The blue (dark-shaded) area indicates the RS corrections for $M_{\text{KK}} \in [1, 10]\,\text{TeV}$ and $L \in [5, 37]$. Right: Same regions of probability in the g_L^b–g_R^b plane. The horizontal stripe consists of a large number of points in the RS parameter space, while the black dot corresponds to the SM prediction. See [1] and text for details.

Gauge invariance ensures that $\Pi_{AA}(0) = 0$ to all orders in perturbation theory. Further, working at tree-level results in $\Pi_{ZA}(0) = \Pi'_{ZA}(0) = 0$.

Inserting the results (3.163) into the definitions of the Peskin-Takeuchi parameters (1.43), we find, in agreement with [219, 225], the positive corrections

$$S = \frac{2\pi v^2}{M_{\text{KK}}^2}\left(1 - \frac{1}{L}\right), \qquad T = \frac{\pi v^2}{2\cos^2\theta_w\, M_{\text{KK}}^2}\left(L - \frac{1}{2L}\right), \tag{3.164}$$

while U vanishes. As mentioned in Section 3.1.5, allowing the fermion fields to propagate into the bulk significantly diminishes the corrections to S, with respect to a scenario with bulk gauge fields and brane fermions, for which $S, T \sim -L\pi v^2/M_{\text{KK}}^2$ are both large and negative [202]. The expressions above show the expected behavior of decreasing with an increasing mass scale M_{KK} of the NP. Explicit values for the experimental 68% CL bounds on the S and T parameters and their correlation matrix are given in (1.44). The corresponding regions of 68%, 95%, and 99% probability in the S–T plane are depicted in the left panel of Figure 3.10. The SM predictions for different values of m_h and m_t are shown by the green (light-shaded) stripe, whereas the blue (dark-shaded) area represents the RS corrections for different values of the NP scale M_{KK} and the volume factor L, which we will keep variable for this discussion. From requiring the RS corrections to satisfy the experimental bounds from S and T leads, for the SM reference point of Appendix D and $L = 37$, to the constraint on the KK scale

$$M_{\text{KK}} > 4.0\,\text{TeV} \quad (99\%\,\text{CL}). \tag{3.165}$$

Recalling that the lightest KK excitations have masses around $2.45 M_{\mathrm{KK}}$, we arrive at masses of the first KK-gauge bosons of at least about $10\,\mathrm{TeV}$. This large scale is driven by the sizable corrections to T, which is enhanced by the volume factor L, and makes the KK excitations impossible to be discovered directly at the LHC. Moreover, such a high scale increases the fine-tuning problem discussed in Section 3.1.5 since it leads to a higher cutoff for the minimal RS model (recall that $\Lambda_{\mathrm{UV}}(\pi) > M_{\mathrm{KK}}$). This sizable "little hierarchy problem" calls for a cure. Interestingly, it is possible to show that the rather tight constraint form T is present in any 5D warped model with the SM gauge group in the bulk, which solves the gauge hierarchy problem by a moderately large volume factor [219]. There are at least *five possibilities* to mitigate the strong constraint from the T parameter in models with a warped extra dimension.

Looking at the left panel of Figure 3.10 it seems to be possible to compensate the large positive corrections (3.164) to T in the minimal RS model by negative corrections due to a *heavy Higgs boson* [226, 227, 228, 229, 230]. Explicitly, the leading logarithmic corrections to S and T, due to a Higgs-boson mass different from the reference value of $m_h^{\mathrm{ref}} = 150\,\mathrm{GeV}$, read [64]

$$\Delta S = \frac{1}{6\pi} \ln \frac{m_h}{m_h^{\mathrm{ref}}}\,, \qquad \Delta T = -\frac{3}{8\pi \cos^2 \theta_w} \ln \frac{m_h}{m_h^{\mathrm{ref}}}\,, \qquad (3.166)$$

whereas U remains unchanged. From these relations one concludes that taking for example $m_h = 1\,\mathrm{TeV}$, can significantly relax the bounds from the T parameter by providing a negative contribution of $\Delta T \approx -0.30$. Note that a large Higgs-boson mass also induces a positive shift in the parameter S. However, since $\Delta T/\Delta S \approx -3$ the combined effect will still lead to a less stringent bound on M_{KK}. Taking $m_h = 1\,\mathrm{TeV}$ we arrive at

$$M_{\mathrm{KK}} > 2.6\,\mathrm{TeV} \quad (99\%\ \mathrm{CL})\,. \qquad (3.167)$$

Remember that the bound on the Higgs-boson mass from unitarity of longitudinal $W^{\pm}$-boson scattering, see (1.37), can be relaxed in RS models [44]. Thus we consider $m_h \lesssim 1\,\mathrm{TeV}$ as a rough upper bound for our analysis. As we additionally argued that in warped models, with the Higgs sector residing on the IR-brane, we naturally *do expect* the mass of the Higgs boson to be of the order of the KK scale and not the electroweak scale, the option to see electroweak precision tests as a hint for a heavy Higgs boson, rather than a high KK scale of the minimal RS model, should not be directly discarded. Moreover, a smaller value of the top-quark mass can relax the bound further as it provides a negative contribution to T without changing S. The total error on the top-quark mass of $\Delta m_t = 1.4\,\mathrm{GeV}$ translates into a possible shift of $\Delta T \approx \pm 0.02$. A heavy Higgs boson in combination with a slightly lighter top quark might thus allow for first KK gauge-bosons as light as $6\,\mathrm{TeV}$, without changing the setup of the minimal RS model.

As the corrections to T are enhanced by the RS volume L, a second, obvious, way to diminish them would be to assume a *smaller RS volume*. This removes the possibility of addressing the complete hierarchy between the Planck scale and the electroweak scale within the RS model. However, as this model is an EFT, it is anyway well possible that it will be replaced by a UV completion well *below* the Planck scale $\Lambda_{\mathrm{UV}}(0) \ll M_{\mathrm{Pl}}$. In the spirit of "little Higgs" models, stabilizing the Higgs mass only up to scales of the order of $(10\text{--}100)\,\mathrm{TeV}$ [132, 133], see Section 1.2.1, the "little RS" model could be replaced by a more fundamental theory already at such a low scale. As many observables in the RS model are enhanced by L,

such a possibility seems viable to improve the agreement between the model and experiment also in other sectors. However, note that the situation is not that simple. As has been shown in [157], a small volume factor leads to stronger constraints from the CP-violating quantity ϵ_K, due to a softening of the RS-GIM mechanism. Moreover, the true solution to the gauge hierarchy problem is only postponed to larger energies. We will not consider this possibility in the main phenomenological part of this thesis. However, choosing for example a volume-truncated background with $L = \ln(10^3) \approx 7$ to address the hierarchy between the electroweak scale and 10^3 TeV, the RS bound from electroweak precision is weakened to the "little RS" bound of

$$M_{\mathrm{KK}} > 1.5\,\mathrm{TeV} \quad (99\%\ \mathrm{CL})\,. \tag{3.168}$$

The lightest KK modes in such a scenario would have masses of approximately $2.65\,M_{\mathrm{KK}}$. As a result, T only constrains the masses of the lowest-lying KK gauge-boson excitation to be heavier than around 4 TeV. This bound relaxes further for a larger Higgs-boson mass. For example, using $m_h = 500$ GeV instead of the reference value of $m_h = 150$ GeV would allow for light KK gauge bosons of around 3 TeV.

A third possibility to lower the KK scale while still achieving good agreement with electroweak precision data would be to introduce *large brane-localized kinetic terms* for the electroweak gauge bosons, allowing for masses of the first KK gauge-boson modes of the order of 5 TeV [225, 231, 232]. The appearance of such terms in orbifold theories is expected on general grounds since they are needed as counterterms to cancel divergences arising at the loop level [233, 234]. However, in our analysis, we do not want to follow this direction as a possibility to weaken constraints from electroweak precision measurement. The bare contributions to these terms correspond to unknown UV physics above the cutoff. We simply assume these contributions to be small in order to retain the predictivity of the model. Moreover we ignore possible loop contributions to brane-localized kinetic terms since we concentrate on the leading contributions to the precision observables. Note that, even if these assumptions would be relaxed, a heavier Higgs boson in RS would still help in lowering the limit on the KK scale, so that this scenario will still be viable in the presence of brane-localized kinetic terms, see also [225].

A fourth option is given by promoting the *Higgs to a bulk field* by removing it slightly from the IR brane. This will lead to a smaller overlap of the Higgs boson with KK modes and in consequence to a slightly reduced contribution to T. If one assumes in addition a small *deformation of the geometry* from the AdS_5 metric (3.1) near the IR brane, the constraint on the lightest KK gauge-boson masses due to electroweak precision tests can be lowered to about 2 TeV [235, 236, 237, 238]. However, in the following we will stick to the original RS solution and do not consider additional structure that could lead to such a deformation of the geometry.

Before coming to the fifth possibility to evade large corrections to the T parameter, which will be studied detailed in the next sections, let us mention another sector of electroweak precision, where sizable RS corrections are expected. The left-handed bottom quark, residing in the same $SU(2)_L$ doublet as the top quark, will have a rather large overlap with the IR brane (see Figure 3.9). Therefore, sizable deviations in couplings of this quark to massive gauge bosons are generated, since those have the largest deviation from a flat profile close to the IR brane, too. Precise measurements of different bottom-quark pseudo observables at the Z-pole have been performed at LEP. These lead to quite stringent constraints on the left-handed

and right-handed couplings of bottom quarks to the Z-boson, g_L^b and g_R^b. The corresponding expressions in the minimal RS model have been given in (3.148), where $g_c^b \equiv (g_c^d)_{33}$, $c = L, R$. Note that the universal prefactor in (3.147) cancels out in the observables considered. A thorough analysis of the $Zb\bar{b}$ couplings in RS models will be performed in Section 5.1.3, where we will also specify the observables, mentioned before. The results in the g_L^b–g_R^b plane for the minimal RS model are shown in the right panel of Figure 3.10. The horizontal stripe corresponds to a scan over the RS parameter space, guaranteeing that the quark masses as well as the CKM mixing angles and phase are reproduced within the $1\,\sigma$ range, see Chapter 5. The SM prediction for our reference point is depicted by the black dot. One can see that large positive corrections to g_L^b arise, leading potentially out of the $3\,\sigma$ range.[15] Moreover, the anomaly in $A_{FB}^{0,b}$ can not be resolved directly by RS corrections, see Section 5.1.3. One might interpret this measurement as a *determination* of the RS input parameters, constraining their values. Note that *e.g.* for $M_{\rm KK} \sim 1.5$ TeV it is always possible to find flavor parameters in the anarchic RS setup, such that the constraints from $Z \to b\bar{b}$ are fulfilled, see the analysis of Section 5.1.3. For example for the RS reference point, given in [1], we arrive at a constraint on the KK scale of $M_{\rm KK} > 1.6\,{\rm TeV}$ (@ 99% CL). Thus, after an adjustment of the flavor parameters, the constraint from $Z \to b\bar{b}$ is in general weaker than the one from the Peskin-Takeuchi parameters. However, in the light of the generically large corrections to g_L^b, it would be interesting to find a mechanism to evade these large RS contributions.

A setup that can avoid large corrections to the T parameter as well as to the left-handed $Zb\bar{b}$ coupling is provided by the *custodial Randall-Sundrum model*. As we have seen in Section 1.1.2 and Appendix A.2, the custodial symmetry of the Higgs sector is responsible for a protection of the ρ parameter (and thus also of the T parameter) in the SM. If we want to have a protection for the T parameter in a slice of AdS$_5$, it seems to be a good idea to explore the possibility of a similar protection mechanism. First of all, as we are using a SM Higgs sector one can ask the question, why the standard protection of the T parameter does no longer work in the minimal RS model. This can be understood again from the dual 4D perspective. To have a protection for the T parameter, we would like to have a custodial symmetry for the CFT of which the minimal Higgs is a light composite. However, a *global symmetry group* on the CFT side (with a weakly gauged subgroup) corresponds to a *gauge symmetry* in the bulk of the AdS$_5$ space-time [193]. In consequence, we need to gauge the complete $SU(2)_L \times SU(2)_R$ symmetry responsible for a custodial protection [218], see Section 1.1.2. The absence of a $SU(2)_R$ gauge symmetry in the minimal RS model is the reason for its large generic contributions to the T parameter at the tree-level. Explicitly, the mixing with the heavy KK modes, that get their masses from compactification, destroys the sought relation for the $W^{\pm}$ and Z-boson *zero modes* in the minimal RS model, in the absence of the gauged custodial symmetry. In addition to providing such a symmetry, the custodial RS model features a protection for $Zb_L\bar{b}_L$ couplings, given an appropriate embedding of the left handed bottom quark (i.e., the bottom quark which has a left-handed zero mode in the perturbative approach) and invariance under the interchange of both $SU(2)$ groups [239]. This requires an extended fermion sector with respect to the minimal RS model. We will elaborate on this protection in sections 3.4.3 and 5.1.3. To summarize this discussion, the gauge group, which leads to a custodial protection of the T parameter in warped extra dimensions, and which is also appropriate for a protection of the $Zb_L\bar{b}_L$ vertex,

---

[15]Note that the tiny corrections in g_R^b are always negative.

reads

$$SU(3)_c \times SU(2)_L \times SU(2)_R \times U(1)_X \times P_{LR} \,, \tag{3.169}$$

where P_{LR} interchanges the two $SU(2)$ groups. The RS variant employing this gauge group is called the custodial Randall-Sundrum model (with P_{LR} symmetry). Note, however, that this symmetry group has to experience a first breaking above the electroweak scale, as we do not see additional gauge bosons at low energies. Thus, we will break the extended hypercharge gauge group $SU(2)_R \times U(1)_X$ down to $U(1)_Y$ on the UV brane via BCs, so as to arrive at the SM gauge group (1.5) in the low energy theory. In the end, it will turn out that the extended symmetry results in a vanishing of the *leading* RS contribution to the T parameter, which is enhanced by the RS volume L, see (5.10) below. Thus, the T parameter will become tiny which leads to a lower bound on the KK scale, due to the S parameter which remains unchanged, of

$$M_{\mathrm{KK}} > 2.4 \,\mathrm{TeV} \quad (99\% \,\mathrm{CL}) \,. \tag{3.170}$$

This translates into a lower bound on the first KK gauge-boson masses of about $6 \,\mathrm{TeV}$. This bound is marginally better that the one (3.167) of the minimal RS setup without custodial symmetry, but with a heavy Higgs boson. In this context, note that in the case of the RS scenario with extended electroweak sector, the existence of a heavy Higgs boson would be rather problematic with respect to the global electroweak fit. The remaining corrections to T are generically too small to compensate for the negative shift ΔT due to a large Higgs mass.

So far we have only talked about tree-level corrections to the electroweak parameters. Another virtue of the gauged custodial symmetry is that it makes one-loop corrections to the T parameter finite and thus calculable within the RS setup [218]. These can, depending on the realization of the model and the region in parameter space, improve or worsen the agreement with experiment. On the other hand, without a custodial gauge symmetry, uncontrolled loop effects might also raise the lower bounds (3.167) and (3.168) to substantially higher values. We will study the custodial protection of the T parameter as well as the $Zb_L\bar{b}_L$ couplings in the custodial model in detail in the upcoming sections, where we also will comment more specifically on the loop corrections mentioned before. Nevertheless, in the light of the heavy Higgs option, we still do not discard the minimal RS model and will study the phenomenology of both variants in Chapter 5.

3.4 The Custodial Randall-Sundrum Model

In this section we will perform a thorough analysis of the structure of the RS proposal featuring custodial protection, due to an extended gauge group in the bulk. We will again avoid to expand the theory in powers of v^2/M_{KK}^2 from the very beginning and to truncate the KK tower after one (or a few) modes, as done in the literature on the custodial RS model. The approach of performing the KK decomposition directly in the mass basis is particularly suited for understanding clearly and analytically important features of the custodial model, like the level of protection of the left-handed $Zb\bar{b}$ couplings. Calculating analytically all terms of order v^2/M_{KK}^2, we will identify (ir)reducible sources of custodial symmetry breaking in different sectors, which remain somewhat hidden if a perturbative approach is used. Our exact approach allows to include the mixing of fermions between different generations in a completely general way. This makes the dependence on the exact realization of the matter

sector transparent and it becomes straightforward to study the model-dependence of the gauge- and Higgs-boson interactions with the SM fermions. A thorough treatment of the perturbative approach featuring truncation after the first mode can be found in [240].

We start with discussing the KK decomposition of the bulk gauge fields of the custodial gauge group, in the presence of a brane-localized Higgs sector, working in a covariant R_ξ gauge. Here we will also study the custodial protection of the T parameter. After that we will examine the extended fermion sector of the custodial RS model. The particular fermion representations that we choose allow for a protection of the $Zb_L\bar{b}_L$ couplings [239]. It will turn out to be possible to write the KK decomposition in a form which allows to apply directly the general formalism developed in Section 3.2.2. Then we will study the structure of gauge-boson interactions with SM fermions in detail. A crucial part is the analysis of the custodial protection mechanism. We will give analytic formulae that show, on the one hand, the requirements for achieving a custodial protection of the left-handed Z-boson couplings and that expose, on the other, the terms that necessarily escape protection. We will distinguish between the protection from gauge-boson corrections and from those arising from fermion mixing. Moreover, we will show explicitly that no protection mechanism is present in the charged-current sector, confirming existing model-independent results. The interactions of the Higgs boson with matter will be studied further below, together for both, the minimal RS variant and the custodial RS model. The exact dependence of the interactions on the realization of the fermion sector will be worked out. The following is based on [2].

3.4.1　The Gauge Sector in the Custodial RS Model

In this section we will perform the KK decomposition of the extended gauge sector of the custodial RS model in the mass basis. We will derive exact solutions for the profiles and masses of the bulk fields, including the effects of an IR brane-localized Higgs sector. The formulae derived here will build the basis for studying interactions of the model and in particular for analyzing the custodial protection mechanism.

Action of the 5D Theory

We consider the RS model with custodial protection as proposed in [218] and introduced above, with the bulk gauge symmetry $SU(2)_L \times SU(2)_R \times U(1)_X \times P_{LR}$. On the IR brane, the symmetry-breaking pattern $SU(2)_L \times SU(2)_R \to SU(2)_V$ provides a custodial symmetry, which protects the T parameter, whereas the breaking $SU(2)_R \times U(1)_X \to U(1)_Y$ on the UV brane generates the SM gauge group, which we observe at low energies. The further breaking down to $U(1)_{\mathrm{EM}}$ is due to an interplay of UV and IR BCs and will become clear later. The 5D action of the gauge sector takes the form

$$S_{\mathrm{gauge}} = \int d^4x\, r \int_{-\pi}^{\pi} d\phi \left(\mathcal{L}_{\mathrm{L,R,X}} + \mathcal{L}_{\mathrm{Higgs}} + \mathcal{L}_{\mathrm{GF}} \right), \qquad (3.171)$$

with the gauge-kinetic terms

$$\mathcal{L}_{\mathrm{L,R,X}} = \frac{\sqrt{G}}{r}\, G^{KM} G^{LN} \left(-\frac{1}{4}\, L^a_{KL} L^a_{MN} - \frac{1}{4}\, R^a_{KL} R^a_{MN} - \frac{1}{4}\, X_{KL} X_{MN} \right), \qquad (3.172)$$

where the assignment of the fields to the gauge groups should be self-explanatory. We choose the four-vector components of the gauge fields to be even under the Z_2 parity, while the scalar fifth components are odd, in order to arrive at a low-energy spectrum that is consistent with observation. As it is not needed for our analysis, we ignore the Faddeev-Popov Lagrangian.

The Higgs Lagrangian

$$\mathcal{L}_{\text{Higgs}} = \frac{\delta(|\phi| - \pi)}{r} \left(\frac{1}{2} \operatorname{Tr} |(D_\mu \Phi)|^2 - V(\Phi) \right) \tag{3.173}$$

is localized on the IR brane. A prescription of how to deal with $\delta(|\phi| - \pi)$ has already been presented before in (3.47). The Higgs is extended to a bi-doublet under $SU(2)_L \times SU(2)_R$, and is responsible for breaking $SU(2)_L \times SU(2)_R$ to the diagonal subgroup $SU(2)_V$ on the IR brane. It transforms as $(\mathbf{2}, \mathbf{2})_0$ and explicitly reads (see (A.14) and [224]),

$$\Phi(x) = \frac{1}{\sqrt{2}} \begin{pmatrix} v + h(x) - i\varphi^3(x) & -i\sqrt{2}\,\varphi^+(x) \\ -i\sqrt{2}\,\varphi^-(x) & v + h(x) + i\varphi^3(x) \end{pmatrix}, \tag{3.174}$$

with real scalar fields φ^i and h, $\varphi^\pm = (\varphi^1 \mp i\varphi^2)/\sqrt{2}$. The VEV of the Higgs fields is again only to first approximation given by the SM value, $v \approx 246\,\text{GeV}$, and will receive corrections at $\mathcal{O}(v^2/M_{\text{KK}}^2)$, see Section 5. In the notation above, $SU(2)_L$ transformations act from the left on the bi-doublet, while the $SU(2)_R$ transformations act from the right. The covariant derivative acting on the Higgs sector reads

$$D_\mu \Phi = \partial_\mu \Phi - i g_{L5} L_\mu^a T_L^a \, \Phi + i g_{R5} \, \Phi \, R_\mu^a T_R^a \,, \tag{3.175}$$

with $T_{L,R}^a = \sigma^a/2$. An explicit calculation leads to

$$D_\mu \Phi = \frac{1}{\sqrt{2}} \begin{pmatrix} \partial_\mu (h - i\varphi^3) - i\frac{v}{2} \left(g_{L5} L_\mu^3 - g_{R5} R_\mu^3 \right) & -\partial_\mu i\sqrt{2}\varphi^+ - i\frac{v}{2} \left(g_{L5} L_\mu^+ - g_{R5} R_\mu^+ \right) \\ -\partial_\mu i\sqrt{2}\varphi^- - i\frac{v}{2} \left(g_{L5} L_\mu^- - g_{R5} R_\mu^- \right) & \partial_\mu (h + i\varphi^3) + i\frac{v}{2} \left(g_{L5} L_\mu^3 - g_{R5} R_\mu^3 \right) \end{pmatrix} \tag{3.176}$$
$$+ \text{ terms bi-linear in fields} \,,$$

where we have introduced

$$L_\mu^\pm = \frac{1}{\sqrt{2}} \left(L_\mu^1 \mp i L_\mu^2 \right), \qquad R_\mu^\pm = \frac{1}{\sqrt{2}} \left(R_\mu^1 \mp i R_\mu^2 \right), \tag{3.177}$$

in analogy to the charged $W^\pm$ bosons of the SM. The structure of (3.176) motivates us to define the new fields

$$\begin{pmatrix} \tilde{A}_M \\ V_M \end{pmatrix} = \frac{1}{\sqrt{g_L^2 + g_R^2}} \begin{pmatrix} g_L & -g_R \\ g_R & g_L \end{pmatrix} \begin{pmatrix} L_M \\ R_M \end{pmatrix}, \tag{3.178}$$

which result in a diagonal mass matrix. The 4D gauge couplings are related to 5D couplings as introduced in (3.39). The rotations above are in analogy to the usual definitions of the Z boson and photon fields, like in the SM, which are themselves postponed to (3.184). Note that

the P_{LR} symmetry forces $g_L = g_R$. However, for the time being, we will keep both couplings separately, in order to be able to identify the dependence of observables on the presence of the extra symmetry. Finally, the mass term adopts the form

$$\mathcal{L}_{\text{Higgs}} \supset \frac{\delta(|\phi| - \pi)}{r} \frac{(g_{L5}^2 + g_{R5}^2)\, v^2}{8} \tilde{A}_\mu^a \tilde{A}^{\mu\, a} \equiv \frac{\delta(|\phi| - \pi)}{r} \frac{1}{2} M_{\tilde{A}}^2 \tilde{A}_\mu^a \tilde{A}^{\mu\, a}, \qquad (3.179)$$

and reveals the breaking pattern (c.f. (A.18))

$$SU(2)_L \times SU(2)_R \xrightarrow{\text{IR}} SU(2)_V, \qquad (3.180)$$

induced by the Higgs VEV $\langle \Phi \rangle = v/\sqrt{2}\, \mathbf{1}$. Appropriate BCs break the extended electroweak gauge group down to the SM gauge group on the UV boundary

$$SU(2)_R \times U(1)_X \xrightarrow{\text{UV}} U(1)_Y. \qquad (3.181)$$

Explicitly, this is achieved by introducing the new fields

$$\begin{pmatrix} Z'_M \\ B_M^Y \end{pmatrix} = \frac{1}{\sqrt{g_R^2 + g_X^2}} \begin{pmatrix} g_R & -g_X \\ g_X & g_R \end{pmatrix} \begin{pmatrix} R_M^3 \\ X_M \end{pmatrix}, \qquad (3.182)$$

and giving Dirichlet BCs to Z'_μ and $R_\mu^{1,2}$ on the UV brane, which prevent the emergence of corresponding zero modes. The $U(1)_Y$ hypercharge coupling is related to the $SU(2)_R \times U(1)_X$ couplings by

$$g_Y = \frac{g_R\, g_X}{\sqrt{g_R^2 + g_X^2}} \qquad (3.183)$$

and the SM-like neutral electroweak gauge bosons are defined in the standard way through

$$\begin{pmatrix} Z_M \\ A_M \end{pmatrix} = \frac{1}{\sqrt{g_L^2 + g_Y^2}} \begin{pmatrix} g_L & -g_Y \\ g_Y & g_L \end{pmatrix} \begin{pmatrix} L_M^3 \\ B_M^Y \end{pmatrix}. \qquad (3.184)$$

It follows that the definitions of the sine and cosine of the weak-mixing angle,

$$\sin \theta_w = \frac{g_Y}{\sqrt{g_L^2 + g_Y^2}}, \qquad \cos \theta_w = \frac{g_L}{\sqrt{g_L^2 + g_Y^2}}, \qquad (3.185)$$

agree again formally with those in the SM, see (3.40) and (1.23). Note that the fields V_M^3 and X_M can be rotated to the photon field A_M and a state Z_M^H via

$$\begin{pmatrix} Z_M^H \\ A_M \end{pmatrix} = \frac{1}{g_{LRX}^2} \begin{pmatrix} g_L\, g_R & -g_X \sqrt{g_L^2 + g_R^2} \\ g_X \sqrt{g_L^2 + g_R^2} & g_L\, g_R \end{pmatrix} \begin{pmatrix} V_M^3 \\ X_M \end{pmatrix}, \qquad (3.186)$$

where

$$g_{LRX}^2 = \sqrt{g_L^2\, g_R^2 + g_L^2\, g_X^2 + g_R^2\, g_X^2}. \qquad (3.187)$$

Moreover, we write $\tilde{Z}_M \equiv \tilde{A}_M^3$, as we will see that it is a linear combination of Z_M and Z'_M, which is orthogonal to Z_M^H.

$\partial_\phi L_\mu^\pm(x,0) = 0$	$L_5^\pm(x,0) = 0$	$\partial_\phi \tilde{A}_\mu^\pm(x,\pi^-) = -\frac{r}{2\epsilon^2}M_{\tilde{A}}^2 \tilde{A}_\mu^\pm(x,\pi)$	$\tilde{A}_5^\pm(x,\pi) = 0$
$R_\mu^\pm(x,0) = 0$	$R_5^\pm(x,0) = 0$	$\partial_\phi V_\mu^\pm(x,\pi) = 0$	$V_5^\pm(x,\pi) = 0$
$\partial_\phi Z_\mu(x,0) = 0$	$Z_5(x,0) = 0$	$\partial_\phi \tilde{Z}_\mu(x,\pi^-) = -\frac{r}{2\epsilon^2}M_{\tilde{A}}^2 \tilde{Z}_\mu(x,\pi)$	$\tilde{Z}_5(x,\pi) = 0$
$Z'_\mu(x,0) = 0$	$Z'_5(x,0) = 0$	$\partial_\phi Z_\mu^H(x,\pi) = 0$	$Z_5^H(x,\pi) = 0$
$\partial_\phi A_\mu(x,0) = 0$	$A_5(x,0) = 0$	$\partial_\phi A_\mu(x,\pi) = 0$	$A_5(x,\pi) = 0$

Table 3.2: UV (left) and IR (right) BCs.

In Table 3.2 we collect the BCs that we choose for the fields in order to obtain the correct SM spectrum. They are given in terms of fields with individual BCs on the corresponding branes. In the following we will refer to these sets of fields as the UV and the IR basis, respectively. The situation is summarized in Figure 3.11, where we also recall the symmetry-breaking patterns on the different branes. The BCs can easily be transformed to another basis at the expense of obtaining expressions that mix different fields. The photon A_μ has individual and source-free Neumann BCs on both branes, and therefore its zero mode remains massless. Note that there is just one mass parameter $M_{\tilde{A}}$ entering the IR BCs, in contrast to the two parameters M_Z and M_W appearing in the minimal model. In the custodial model, the different masses for the lightest electroweak gauge bosons are accomplished through the mixed UV BCs of the gauge fields in the IR basis (see (3.188) below). The fact that there is just one fundamental mass parameter is crucial for the custodial protection of the T parameter. We will elaborate on this later in this section.

The action of the theory contains again mixed terms between gauge fields and scalars, which can be removed by an appropriate gauge-fixing Lagrangian. As the Higgs sector is localized on the IR brane, it is natural to work in the IR basis for that purpose. For this reason, we define the 5D theory in the IR basis. The concrete form of the gauge fixing will be given below in (3.196).

Before discussing the KK decomposition, we summarize the relations between the UV (right) and the IR basis (left). They read

$$\begin{pmatrix} \tilde{Z}_M \\ Z_M^H \end{pmatrix} = \begin{pmatrix} \cos\theta_Z & -\sin\theta_Z \\ \sin\theta_Z & \cos\theta_Z \end{pmatrix} \begin{pmatrix} Z_M \\ Z_M' \end{pmatrix} \equiv \boldsymbol{R}_Z \begin{pmatrix} Z_M \\ Z_M' \end{pmatrix},$$

$$\begin{pmatrix} \tilde{A}_M^\pm \\ V_M^\pm \end{pmatrix} = \begin{pmatrix} \cos\theta_W & -\sin\theta_W \\ \sin\theta_W & \cos\theta_W \end{pmatrix} \begin{pmatrix} L_M^\pm \\ R_M^\pm \end{pmatrix} \equiv \boldsymbol{R}_W \begin{pmatrix} L_M^\pm \\ R_M^\pm \end{pmatrix},$$

(3.188)

where

$$\sin\theta_Z = \frac{g_R^2}{\sqrt{(g_L^2 + g_R^2)(g_R^2 + g_X^2)}}, \qquad \cos\theta_Z = \frac{g_{LRX}^2}{\sqrt{(g_L^2 + g_R^2)(g_R^2 + g_X^2)}},$$

$$\sin\theta_W = \frac{g_R}{\sqrt{g_L^2 + g_R^2}}, \qquad \cos\theta_W = \frac{g_L}{\sqrt{g_L^2 + g_R^2}}, \qquad (3.189)$$

and g_{LRX}^2 has been defined in (3.187). In order to shorten the notation we will hereafter employ the abbreviations $s_a \equiv \sin\theta_a$ and $c_a \equiv \cos\theta_a$ for $a = w, Z, W$.
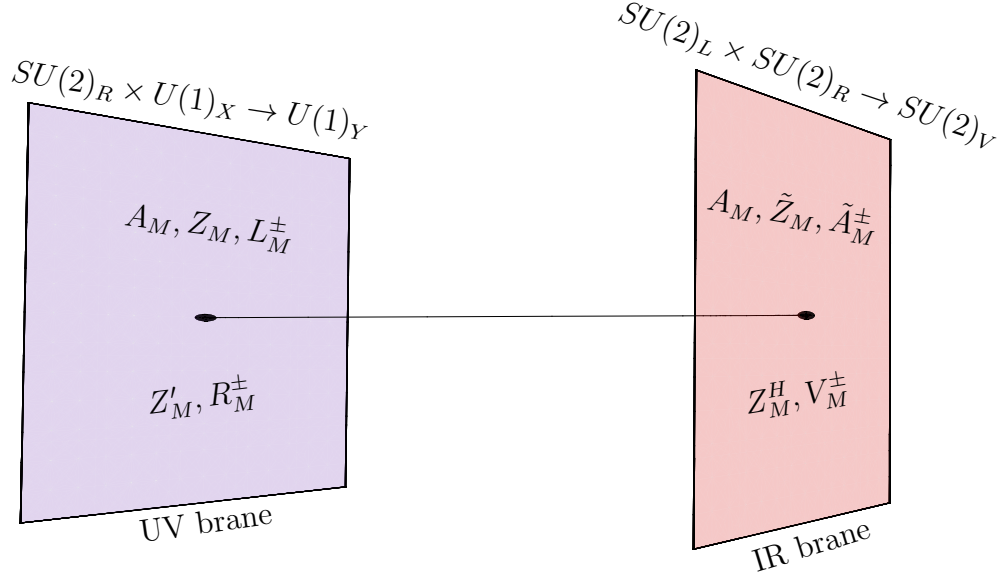
Figure 3.11:   UV and IR basis, *i.e.*, gauge fields with individual BCs on the corresponding branes. The fields in the first (second) row on the UV brane do (do not) possess a zero mode. The symmetry-breaking pattern on the UV and IR brane is also indicated. See [2] and text for details.

Kaluza-Klein Decomposition

We now perform the KK decomposition of the fields of the 5D theory, which we formulated in the IR basis. However, it is convenient to work with profiles that obey definite Neumann (+) or Dirichlet (−) BCs on the UV brane. Therefore we include a rotation to the UV basis, *i.e.*, the basis in which the UV BCs decouple, in our decomposition. Furthermore, as different UV fields get mixed by the IR BCs, these fields should be expressed through the same 4D basis. We consequently introduce the vectors $\vec{Z}_M = (\tilde{Z}_M, Z_M^H)^T$ and $\vec{W}_M^\pm = (\tilde{A}_M^\pm, V_M^\pm)^T$ and write

$$A_\mu(x,\phi) = \frac{1}{\sqrt{r}} \sum_n \chi_n^{(+)}(\phi)\, A_\mu^{(n)}(x)\,, \qquad A_\phi(x,\phi) = \frac{1}{\sqrt{r}} \sum_n \partial_\phi \chi_n^{(+)}(\phi)\, a_n^A\, \varphi_A^{(n)}(x)\,,$$

$$\vec{Z}_\mu(x,\phi) = \frac{\boldsymbol{R}_Z}{\sqrt{r}} \sum_n \boldsymbol{\chi}_n^+(\phi)\, \vec{A}_n^Z\, Z_\mu^{(n)}(x)\,, \qquad \vec{Z}_\phi(x,\phi) = \frac{\boldsymbol{R}_Z}{\sqrt{r}} \sum_n \partial_\phi \boldsymbol{\chi}_n^+(\phi)\, \vec{A}_n^Z a_n^Z\, \varphi_Z^{(n)}(x)\,,$$

$$\vec{W}_\mu^\pm(x,\phi) = \frac{\boldsymbol{R}_W}{\sqrt{r}} \sum_n \boldsymbol{\chi}_n^+(\phi)\, \vec{A}_n^W\, W_\mu^{\pm(n)}(x)\,, \quad \vec{W}_\phi^\pm(x,\phi) = \frac{\boldsymbol{R}_W}{\sqrt{r}} \sum_n \partial_\phi \boldsymbol{\chi}_n^+(\phi)\, \vec{A}_n^W a_n^W\, \varphi_W^{\pm(n)}(x)\,,$$

$$(3.190)$$

where the sums run over $n = 0, \ldots, \infty$. Note that $A_\mu^{(n)}(x)$ *etc.* are 4D mass eigenstates and the lightest modes are identified with the SM gauge bosons, which we observe at low energies.

The matrices $\boldsymbol{R}_{Z,W}$ have been defined in (3.188) and we have introduced the diagonal profile matrices

$$\boldsymbol{\chi}_n^+(\phi) = \begin{pmatrix} \chi_n^{(+)}(\phi) & 0 \\ 0 & \chi_n^{(-)}(\phi) \end{pmatrix}, \tag{3.191}$$

as well as two-component vectors $\vec{A}_n^a$, with $a = Z, W$, representing the mixings between the different gauge fields and their KK excitations. These vectors are normalized according to

$$(\vec{A}_n^a)^T \vec{A}_n^a = 1. \tag{3.192}$$

Notice that the matrices $\boldsymbol{\chi}_n^+(\phi)$ should in principle also carry a superscript a, indicating the field to which they belongs, but we will not show it, as the correct index should be always clear from the context. The superscripts $(+)$ and $(-)$ label the type of BC we impose on the profiles on the UV brane, *i.e.*, they indicate untwisted and twisted even functions[16] on the orbifold. Remember from Table 3.2 that both types of profiles satisfy Neumann BCs on the IR boundary, which we do not indicate explicitly by a superscript $(+)$ to avoid unnecessary clutter of notation. Let us also introduce the shorthand notations

$$\vec{\chi}_n^Z(\phi) = \begin{pmatrix} \chi_n^Z(\phi) \\ \chi_n^{Z'}(\phi) \end{pmatrix} = \boldsymbol{\chi}_n^+(\phi)\,\vec{A}_n^Z, \qquad \vec{\chi}_n^W(\phi) = \begin{pmatrix} \chi_n^L(\phi) \\ \chi_n^R(\phi) \end{pmatrix} = \boldsymbol{\chi}_n^+(\phi)\,\vec{A}_n^W, \tag{3.193}$$

for the profiles of the UV fields. In analogy to the fermion profiles of the minimal model (3.88), the profiles $\boldsymbol{\chi}_n^+(\phi)$ do not obey exact orthonormality conditions. This fact is related to the decomposition of different fields into the same 4D states (*i.e.*, mixing). The complete vectors $\vec{\chi}_n^a(\phi)$ with $a = Z, W$ are however orthonormal on each other,

$$\int_{-\pi}^{\pi} d\phi \, \vec{\chi}_m^{a\,T}(\phi)\,\vec{\chi}_n^a(\phi) = \delta_{mn}. \tag{3.194}$$

Note also that the photon obeys the standard orthonormality condition (3.48), as before. As in (3.50), we also expand the 4D Goldstone bosons in the basis of mass eigenstates $\varphi_Z^{(n)}(x)$ and $\varphi_W^{\pm(n)}(x)$ by writing

$$\vec{\varphi}^3(x) = \sum_n \vec{b}_n^Z \, \varphi_Z^{(n)}(x), \qquad \vec{\varphi}^\pm(x) = \sum_n \vec{b}_n^W \, \varphi_W^{\pm(n)}(x). \tag{3.195}$$

---

[16]We use the term twisted even functions for profiles with even Z_2-parity, which obey Dirichlet BC on the UV brane and are thus not smooth at this orbifold fix point. These fields are sometimes called odd, as they look like an odd function (at the UV brane) if one just considers half of the orbifold. Untwisted even functions correspond to ordinary profiles with Neumann UV BCs.

Employing the notation introduced in this section, the gauge-fixing Lagrangian takes the form

$$
\begin{aligned}
\mathcal{L}_{\mathrm{GF}} = {} & -\frac{1}{2\xi} \left(\partial^\mu A_\mu - \xi \left[\frac{\partial_\phi\, e^{-2\sigma(\phi)}}{r^2}\, A_\phi \right] \right)^2 \\
& -\frac{1}{2\xi} \left(\partial^\mu \vec{Z}_\mu - \xi \left[\frac{\delta(|\phi| - \pi)}{r} M_{\tilde{A}}\, \vec{\varphi}^3 + \frac{\partial_\phi\, e^{-2\sigma(\phi)}}{r^2}\, \vec{Z}_\phi \right] \right)^2 \\
& -\frac{1}{\xi} \left(\partial^\mu \vec{W}_\mu^+ - \xi \left[\frac{\delta(|\phi| - \pi)}{r} M_{\tilde{A}}\, \vec{\varphi}^+ + \frac{\partial_\phi\, e^{-2\sigma(\phi)}}{r^2}\, \vec{W}_\phi^+ \right] \right)^T \\
& \times \left(\partial^\mu \vec{W}_\mu^- - \xi \left[\frac{\delta(|\phi| - \pi)}{r} M_{\tilde{A}}\, \vec{\varphi}^- + \frac{\partial_\phi\, e^{-2\sigma(\phi)}}{r^2}\, \vec{W}_\phi^- \right] \right).
\end{aligned}
\tag{3.196}
$$

Inserting the decompositions (3.190) into the action and defining the projectors $\boldsymbol{P}_{(+)} = \mathrm{diag}(1,0)$ and $\boldsymbol{P}_{(-)} = \mathrm{diag}(0,1)$, we derive the EOMs [1, 169, 170]

$$
-\frac{1}{r^2}\, \partial_\phi\, e^{-2\sigma(\phi)}\, \partial_\phi \boldsymbol{R}_a\, \boldsymbol{\chi}_n^+(\phi) \vec{A}_n^a = (m_n^a)^2\, \boldsymbol{R}_a\, \boldsymbol{\chi}_n^+(\phi) \vec{A}_n^a - \frac{\delta(|\phi| - \pi)}{r} M_a^2\, \boldsymbol{P}_{(+)} \boldsymbol{R}_a\, \boldsymbol{\chi}_n^+(\phi) \vec{A}_n^a,
\tag{3.197}
$$

where $a = Z, W, A$ with $M_Z = M_W = M_{\tilde{A}}$ and $M_A = 0$, as well as $\boldsymbol{R}_A = \mathbf{1}$ and $\vec{A}_n^A = (1,0)^T$. In order to avoid boundary terms due to integration by parts, we move the δ-distribution by an infinitesimal amount into the bulk, as explained before (3.47). We will again indicate values obtained by a limiting procedure by a superscript in the argument, e.g. by writing $\boldsymbol{\chi}_n^+(\pi^-)$. The appropriate IR BCs for the profiles can be obtained by integrating the EOMs (3.197) over an infinitesimal interval around $|\phi| = \pi$. At the 5D level the BCs have already been presented in Table 3.2. However, note that the discontinuities of the scalar components, whose profiles are proportional to the ϕ-derivative of the vector profiles, have not been given yet. We arrive at

$$
\frac{m_n^a}{M_{\mathrm{KK}}}\, \boldsymbol{R}_a\, \boldsymbol{\chi}_n^-(\pi^-) \vec{A}_n^a = -X^2 L \boldsymbol{P}_{(+)} \boldsymbol{R}_a\, \boldsymbol{\chi}_n^+(\pi) \vec{A}_n^a,
\tag{3.198}
$$

where

$$
\boldsymbol{\chi}_n^-(\phi) \equiv \frac{1}{m_n^a r}\, e^{-\sigma(\phi)} \partial_\phi\, \boldsymbol{\chi}_n^+(\phi), \qquad X^2 \equiv \frac{(g_L^2 + g_R^2)\, v^2}{4 M_{\mathrm{KK}}^2}.
\tag{3.199}
$$

For the photon the right-hand side in (3.198) is equal to zero. After applying the EOMs and the orthonormality condition (3.194), we observe that the 4D action takes the desired canonical form, given that

$$
a_n^a = -\frac{1}{m_n^a}, \qquad \vec{b}_n^a = \frac{M_a}{\sqrt{r}\, m_n^a} \boldsymbol{P}_{(+)} \boldsymbol{R}_a\, \boldsymbol{\chi}_n^+(\pi^-) \vec{A}_n^a.
\tag{3.200}
$$

Thus, we finally end up again with a low energy theory that corresponds to the SM gauge fields, with quadratic terms in analogy to (3.53). However, due to the extended gauge group we started with, the theory now contains a custodial protection mechanism for electroweak precision observables, as discussed before. Due to the need to reproduce the SM at low energies, this protection cannot be perfect. It will be broken by the BCs that we chose in order to match to the particle content that we observe in nature. The spectrum of the theory

is determined by the IR BCs (3.198). The dimensionless eigenvalues $x_n^a \equiv m_n^a/M_{\mathrm{KK}}$ are thus solutions of

$$\det\left[x_n^a\,\boldsymbol{\chi}_n^-(\pi^-) + LX^2\boldsymbol{D}_a\boldsymbol{\chi}_n^+(\pi)\right] = 0\,, \tag{3.201}$$

with

$$\boldsymbol{D}_a = \boldsymbol{R}_a^{-1}\boldsymbol{P}_{(+)}\boldsymbol{R}_a = \begin{pmatrix} c_a^2 & -s_a c_a \\ -s_a c_a & s_a^2 \end{pmatrix}. \tag{3.202}$$

Once the eigenvalues are known, the eigenvectors $\vec{A}_n^a$ are determined from (3.198).

Bulk Profiles

We now derive expressions for the profiles $\chi_n^{(\pm)}(\phi)$. In order to obtain the EOMs for the UV-basis profiles, we multiply (3.197) by $\boldsymbol{R}_a^T$ from the left. We write the solutions as

$$\chi_n^{(+)}(t) = N_n^{(+)}\sqrt{\frac{L}{\pi}}\,t\,c_n^{(+)+}(t)\,, \qquad \chi_n^{(-)}(t) = N_n^{(-)}\sqrt{\frac{L}{\pi}}\,t\,c_n^{(-)+}(t)\,, \tag{3.203}$$

where

$$\begin{aligned}
c_n^{(+)+}(t) &= Y_0(x_n\epsilon)J_1(x_nt) - J_0(x_n\epsilon)\,Y_1(x_nt)\,, \\[4pt]
c_n^{(-)+}(t) &= Y_1(x_n\epsilon)J_1(x_nt) - J_1(x_n\epsilon)\,Y_1(x_nt)\,, \\[4pt]
c_n^{(+)-}(t) &= \frac{1}{x_nt}\frac{d}{dt}\Big(t\,c_n^{(+)+}(t)\Big) = Y_0(x_n\epsilon)\,J_0(x_nt) - J_0(x_n\epsilon)\,Y_0(x_nt)\,, \\[4pt]
c_n^{(-)-}(t) &= \frac{1}{x_nt}\frac{d}{dt}\Big(t\,c_n^{(-)+}(t)\Big) = Y_1(x_n\epsilon)\,J_0(x_nt) - J_1(x_n\epsilon)\,Y_0(x_nt)\,.
\end{aligned} \tag{3.204}$$

The normalized masses x_n are determined by the IR BCs as explained above. From the latter expressions, it is obvious that the profiles fulfill the sought UV BCs, since $c_n^{(+)-}(\epsilon) = c_n^{(-)+}(\epsilon) = 0$. The normalization constants $N_n^{(\pm)}$ are determined from the orthonormality condition (3.194). With respect to the minimal model (3.64), they contain additional terms due to the different UV BCs. We obtain

$$\begin{aligned}
\left(N_n^{(\pm)}\right)^{-2} &= \left[c_n^{(\pm)+}(1)\right]^2 + \left[c_n^{(\pm)-}(1)\right]^2 - \frac{2}{x_n}\left(c_n^{(\pm)+}(1)\,c_n^{(\pm)-}(1) - \epsilon\,c_n^{(\pm)+}(\epsilon)\,c_n^{(\pm)-}(\epsilon)\right) \\
&\quad - \epsilon^2\left(\left[c_n^{(\pm)+}(\epsilon)\right]^2 + \left[c_n^{(\pm)-}(\epsilon)\right]^2\right).
\end{aligned} \tag{3.205}$$

Note that, depending on the type of the UV BCs, some of the terms in (3.205) vanish identically.

Again, it will be useful to have simple analytical expressions for the masses and profiles of the lightest gauge-boson modes. Expanding (3.201) in powers of v^2/M_{KK}^2 and inserting the definitions of the mixing angles (3.189), which connect the UV and IR bases, we arrive at analytic expressions for the masses of the $W^\pm$ and Z bosons. They read

$$m_W^2 = \frac{g_L^2v^2}{4}\left[1 - \frac{g_L^2v^2}{8M_{\mathrm{KK}}^2}\left(L - 1 + \frac{1}{2L}\right) - \frac{g_R^2v^2}{8M_{\mathrm{KK}}^2}L + \mathcal{O}\left(\frac{v^4}{M_{\mathrm{KK}}^4}\right)\right],$$

$$m_Z^2 = \frac{(g_L^2 + g_Y^2)\, v^2}{4} \left[1 - \frac{(g_L^2 + g_Y^2)\, v^2}{8 M_{\mathrm{KK}}^2} \left(L - 1 + \frac{1}{2L} \right) - \frac{(g_R^2 - g_Y^2)\, v^2}{8 M_{\mathrm{KK}}^2}\, L + \mathcal{O}\left(\frac{v^4}{M_{\mathrm{KK}}^4} \right) \right],$$
(3.206)

where the last terms inside the square brackets are new compared to the minimal model, respectively, *c.f.* (3.67). Interestingly, the latter terms in (3.206) will be responsible for the custodial protection of the Peskin-Takeuchi parameter T, which is sensitive to the difference between the corrections to the $W^{\pm}$-boson and Z-boson vacuum-polarization functions. The RS corrections lead again to a shift in the Higgs VEV compared to the SM value, see Section 5.1.1.

The zero-mode profiles, expanded in v^2/M_{KK}^2, read

$$\chi_0^{(+)}(t) = \frac{1}{\sqrt{2\pi}} \left[1 + \frac{x_a^2}{4} \left(1 - \frac{1}{L} + t^2 \left(1 - 2L - 2\ln t \right) \right) + \mathcal{O}\left(x_a^4 \right) \right],$$

$$\chi_0^{(-)}(t) = \sqrt{\frac{L}{2\pi}}\, t^2 \left[-2 + \frac{x_a^2}{4} \left(t^2 - \frac{2}{3} \right) + \mathcal{O}\left(x_a^4 \right) \right],$$
(3.207)

for $a = W, Z$. Here $x_a^2 \equiv (m_0^a)^2 / M_{\mathrm{KK}}^2$ denotes the corresponding zero-mode solution, given in (3.206). The profiles $\chi_0^{(+)}(t)$, featuring Neumann IR BCs are identical to those appearing in the minimal model, while the profiles $\chi_0^{(-)}(t)$, satisfying Dirichlet IR BCs, are new and scale like $\sqrt{L}$, which reflects the localization of KK modes close to the IR boundary. Notice that (3.207) contains, besides the t-independent terms, also t-dependent contributions that will in general lead to non-universal vertex corrections. While these corrections do modify the interactions of the SM fermions with the $W^{\pm}$ and Z bosons, they turn out to be negligibly small for light fermions localized near the UV brane. This is the case for the first two generations of SM fermions, and it helps to avoid excessive contributions to FCNCs, as discussed before.

Finally, we can also expand the mixing vectors $\vec{A}_0^a$. Including corrections up to v^2/M_{KK}^2, we find

$$\vec{A}_0^a = \begin{pmatrix} 1 \\ -s_a c_a \dfrac{X^2}{4}\, \sqrt{L} \end{pmatrix},$$
(3.208)

where the second component parametrizes the admixture of $\chi_0^{(-)}(t)$ in the zero mode. As we will see below in Section 3.4.3, the results (3.207) and (3.208) play a crucial role in the custodial protection mechanism of the $Z b_L \bar{b}_L$ vertex and its flavor-changing counterparts.

3.4.2   Bulk Matter in the Custodial RS Model

We will now present our explicit realization of the quark sector in the custodial RS model. Then we will turn to the KK decomposition and derive the bulk profiles for the corresponding fields. As we want to have a custodial protection of the $Z b_L \bar{b}_L$ vertex, we impose the aforementioned discrete P_{LR} symmetry [239] on (part of) the Lagrangian and take the left-handed bottom quark to reside in a $SU(2)_L \times SU(2)_R$ bi-doublet, with isospin quantum numbers $T_L^3 = -T_R^3 = -1/2$. This will turn out to lead to the sought protection, see Section 3.4.3, and fixes the quantum numbers of the other quark-fields uniquely, implying the following multiplet structure

for the fields with even Z_2 parity:

$$Q_L \equiv \begin{pmatrix} u_L^{(+)}{}_{\frac{2}{3}} & \lambda_L^{(-)}{}_{\frac{5}{3}} \\ d_L^{(+)}{}_{-\frac{1}{3}} & u_L'^{(-)}{}_{\frac{2}{3}} \end{pmatrix}_{\frac{2}{3}}, \qquad u_R^c \equiv \left(u_R^{c\,(+)}{}_{\frac{2}{3}} \right)_{\frac{2}{3}},$$

$$\mathcal{T}_R \equiv \mathcal{T}_{1R} \oplus \mathcal{T}_{2R} \equiv \begin{pmatrix} \Lambda_R'^{(-)}{}_{\frac{5}{3}} \\ U_R'^{(-)}{}_{\frac{2}{3}} \\ D_R'^{(-)}{}_{-\frac{1}{3}} \end{pmatrix}_{\frac{2}{3}} \oplus \left(D_R^{(+)}{}_{-\frac{1}{3}} \; U_R^{(-)}{}_{\frac{2}{3}} \; \Lambda_R^{(-)}{}_{\frac{5}{3}} \right)_{\frac{2}{3}}.$$

(3.209)

Here, the superscripts $(+)$ and $(-)$ of the chiral fields specify the type of BC on the UV boundary, and as before we have not explicitly shown the BCs on the IR brane, which are understood to be of Neumann type in all cases.

The choice of the parities/BCs is motivated by the constraint to arrive at a low-energy spectrum of the theory that is consistent with observations. Fields that feature a Dirichlet boundary condition will not develop a zero mode. The inner (outer) subscripts correspond to the $U(1)_{\text{EM}}$ $(U(1)_X)$ charges, which are connected through the relations $Q = T_L^3 + Y$ and $Y = -T_R^3 + Q_X$. For completeness and future reference, we summarize the quantum numbers of the quark fields in Table 3.3. The right-handed down-type quarks have to be embedded in a $SU(2)_R$ triplet in order to arrive at an $U(1)_X$-invariant Yukawa coupling. Note that we have chosen the same $SU(2)_L \times SU(2)_R$ representations for all three generations, which is necessary, if one wants to incorporate consistently quark mixing in the fully anarchic approach to flavor in warped extra dimensions. The chosen representations play a crucial role in the suppression of flavor-changing left-handed Z-boson couplings [241]. Altogether they feature 15 different quark fields in the up-type and nine in the down-type sector (for the case of three generations). Due to the BCs, there will be three light modes in each sector to be identified with the SM quarks. These are accompanied by KK towers, which consist of groups of 15 and nine modes of similar masses in each *KK level* in the up- and down-type quark sector, respectively. Moreover one also faces a KK tower of exotic fermion fields of electric charge 5/3, which exhibits nine excitations with small mass splitting in each level and no light modes with $m_n \ll M_{\text{KK}}$. In addition to (3.209), there is a second set of multiplets, belonging to the components of opposite chirality. The corresponding states have opposite BCs. In particular, they all obey Dirichlet BCs on the IR brane. Thus one ends up with the same particle content as in the minimal RS model at low energies. Remember that the $SU(2)_L$ transformations act vertically, while the $SU(2)_R$ transformations act horizontally on the multiplets.

Fermionic Action and Yukawa Couplings

The structure of the 5D action of the quark fields has already been given in (3.72). It is straightforward to generalize this action to the custodial model [240]. The only non-trivial part is due to the Yukawa couplings, where the possible gauge-invariant terms take the form

$$S_{\text{Yukawa}} = - \int d^4x \, r \int_{-\pi}^{\pi} d\phi \, \delta(|\phi| - \pi) \, \frac{e^{-3\sigma(\phi)}}{r} \left[\left\{ \left(\bar{Q}_L \right)_{a\alpha} \boldsymbol{Y}_u^{(5D)C} u_R^c + \left(\bar{Q}_R \right)_{a\alpha} \boldsymbol{Y}_u^{(5D)S} u_L^c \right\} \Phi_{a\alpha}$$

	Q	Q_X	Y	T^3_L	T^3_R
$u_L^{(+)}$	$2/3$	$2/3$	$1/6$	$1/2$	$1/2$
$d_L^{(+)}$	$-1/3$	$2/3$	$1/6$	$-1/2$	$1/2$
$\lambda_L^{(-)}$	$5/3$	$2/3$	$7/6$	$1/2$	$-1/2$
$u_L^{\prime(-)}$	$2/3$	$2/3$	$7/6$	$-1/2$	$-1/2$

	Q	Q_X	Y	T^3_L	T^3_R
$u_R^{c\,(+)}$	$2/3$	$2/3$	$2/3$	0	0
$\Lambda_R^{\prime(-)}$	$5/3$	$2/3$	$2/3$	1	0
$U_R^{\prime(-)}$	$2/3$	$2/3$	$2/3$	0	0
$D_R^{\prime(-)}$	$-1/3$	$2/3$	$2/3$	-1	0

	Q	Q_X	Y	T^3_L	T^3_R
$D_R^{(+)}$	$-1/3$	$2/3$	$-1/3$	0	1
$U_R^{(-)}$	$2/3$	$2/3$	$2/3$	0	0
$\Lambda_R^{(-)}$	$5/3$	$2/3$	$5/3$	0	-1

Table 3.3:   Charge assignments for the different quark fields in the custodial RS model.

$$
+ \frac{1}{\sqrt{2}} \left\{ \left[\left(\bar{Q}_L \right)_{a\alpha} \boldsymbol{Y}_d^{(5D)C} \left(\mathcal{T}_{1R} \right)^c + \left(\bar{Q}_R \right)_{a\alpha} \boldsymbol{Y}_d^{(5D)S} \left(\mathcal{T}_{1L} \right)^c \right] \left(\sigma^c \right)_{ab} \Phi_{b\alpha} \right.
$$

$$
\left. + \left[\left(\bar{Q}_L \right)_{a\alpha} \boldsymbol{Y}_d^{(5D)C} \left(\mathcal{T}_{2R} \right)^\gamma + \left(\bar{Q}_R \right)_{a\alpha} \boldsymbol{Y}_d^{(5D)S} \left(\mathcal{T}_{2L} \right)^\gamma \right] \left(\sigma^\gamma \right)_{\alpha\beta} \Phi_{a\beta} \right\} + \text{h.c.} \right]. \qquad (3.210)
$$

Here, Φ is the Higgs bi-doublet introduced in (3.174), $\sigma^{c,\gamma}$ are the Pauli matrices, and repeated indices are understood to be summed over. The Latin (Greek) letters from the beginning of the alphabet refer to $SU(2)_L$ ($SU(2)_R$) indices. Moreover, for the case of 3 generations, all components of the quark multiplets are three-vectors in flavor space. Note that the components of the triplets in the expression above refer to the representations

$$
\mathcal{T}_{1R} = \begin{pmatrix} \frac{1}{\sqrt{2}} \left(D_R^{\prime(-)}{}_{-\frac{1}{3}} + \Lambda_R^{\prime(-)}{}_{\frac{5}{3}} \right) \\ \frac{i}{\sqrt{2}} \left(D_R^{\prime(-)}{}_{-\frac{1}{3}} - \Lambda_R^{\prime(-)}{}_{\frac{5}{3}} \right) \\ U_R^{\prime(-)}{}_{\frac{2}{3}} \end{pmatrix}, \qquad
\mathcal{T}_{2R} = \begin{pmatrix} \frac{1}{\sqrt{2}} \left(D_R^{(+)}{}_{-\frac{1}{3}} + \Lambda_R^{(-)}{}_{\frac{5}{3}} \right) \\ \frac{i}{\sqrt{2}} \left(-D_R^{(+)}{}_{-\frac{1}{3}} + \Lambda_R^{(-)}{}_{\frac{5}{3}} \right) \\ U_R^{(-)}{}_{\frac{2}{3}} \end{pmatrix}^T, \qquad (3.211)
$$

which ensures that one ends up in the desired mass basis. After electroweak symmetry breaking, the Yukawa couplings (3.210) give rise to mass terms which mix different 5D fields with the same $U(1)_{\text{EM}}$ charge. Similar as for the case of the gauge bosons in the custodial model, as well as of the fermions in the minimal model, the fields that mix will be decomposed into the same 4D fields. It is sensible to collect them into the vectors

$$
\vec{U} \equiv \begin{pmatrix} u \\ u' \end{pmatrix}, \quad \vec{u} \equiv \begin{pmatrix} u^c \\ U' \\ U \end{pmatrix}, \quad \vec{D} \equiv d, \quad \vec{d} \equiv \begin{pmatrix} D \\ D' \end{pmatrix}, \quad \vec{\Lambda} \equiv \lambda, \quad \vec{\lambda} \equiv \begin{pmatrix} \Lambda' \\ \Lambda \end{pmatrix}, \qquad (3.212)
$$

which leads to a formal one-to-one correspondence between the analysis of fermions in the minimal model and the one presented here. The resulting action will have exactly the same form as in the minimal model (3.72), with the only differences of the extension of the sums to

account for the charge-5/3 λ-quarks

$$S_{\text{ferm},2} = (3.72) \quad \text{with} \quad \sum_{q=U,u,D,d} \rightarrow \sum_{q=U,u,D,d,\Lambda,\lambda}, \quad \sum_{(Q,q)=(U,u),(D,d)} \rightarrow \sum_{(Q,q)=(U,u),(D,d),(\Lambda,\lambda)} \quad (3.213)$$

and the higher dimension of the fermion structure, given by (3.212) and to be compared with (3.73). The Yukawa matrices appearing in the action for the custodial model are higher-dimensional with respect to those of the minimal model and read

$$Y_{\vec{u}}^{(5D)} \equiv \begin{pmatrix} Y_u^{(5D)} & \frac{1}{\sqrt{2}} Y_d^{(5D)} & \frac{1}{\sqrt{2}} Y_d^{(5D)} \\ Y_u^{(5D)} & -\frac{1}{\sqrt{2}} Y_d^{(5D)} & -\frac{1}{\sqrt{2}} Y_d^{(5D)} \end{pmatrix}, \qquad Y_{\vec{d}}^{(5D)} \equiv Y_{\vec{\lambda}}^{(5D)} \equiv \begin{pmatrix} Y_d^{(5D)} & Y_d^{(5D)} \end{pmatrix}. \quad (3.214)$$

Here, we have already chosen the same Yukawa matrices for the couplings of both chirality structures (LR and RL), setting $Y_{\vec{q}}^{(5D)C} = Y_{\vec{q}}^{(5D)S} \equiv Y_{\vec{q}}^{(5D)}$. Like for the minimal model, this should be regarded as the limit of a set-up with a bulk Higgs, approaching the IR brane. The generalization to the case of different Yukawa matrices is straightforward. The relation between 5D and 4D Yukawa matrices is still given by (3.75). In the case of three generations, each entry of (3.214) is a 3×3 matrix. The generalized bulk mass matrices $M_{\vec{q}}$ take the form

$$M_{\vec{U}} \equiv \begin{pmatrix} M_Q & 0 \\ 0 & M_Q \end{pmatrix}, \qquad M_{\vec{D}} \equiv M_Q, \qquad M_{\vec{\Lambda}} \equiv M_Q,$$

$$(3.215)$$

$$M_{\vec{u}} \equiv \begin{pmatrix} M_{u^c} & 0 & 0 \\ 0 & M_{\mathcal{T}_1} & 0 \\ 0 & 0 & M_{\mathcal{T}_2} \end{pmatrix}, \quad M_{\vec{d}} \equiv \begin{pmatrix} M_{\mathcal{T}_2} & 0 \\ 0 & M_{\mathcal{T}_1} \end{pmatrix}, \quad M_{\vec{\lambda}} \equiv \begin{pmatrix} M_{\mathcal{T}_1} & 0 \\ 0 & M_{\mathcal{T}_2} \end{pmatrix},$$

where M_A are the 3×3 bulk mass matrices of the corresponding multiplets $A = Q, u^c, \mathcal{T}_1, \mathcal{T}_2$. We turn now to the KK decomposition of the matter sector introduced in this Section.

Kaluza-Klein Decomposition

Due to the effort of formulating the fermion sector in the minimal RS model in a completely general way, the KK decomposition performed there can be applied to the extended matter sector of the custodial model straightforwardly. The main formulae are identical to the ones presented in Section 3.2.2. However, the contained flavor structure is now given by (3.212), (3.214), and (3.215), as well as (3.216) and (3.217) below, which replace the expressions of Section 3.2.2 for the custodial model. Explicitly,

- the KK decomposition is given by (3.76), with $(Q, q) = (U, u), (D, d), (\Lambda, \lambda)$.

- the EOMs are given by (3.78), where $(Q, q) = (U, u), (D, d), (\Lambda, \lambda)$.

- the BCs are given by (3.87).

- the orthonormality relations are given by (3.88), together with (3.90)-(3.95).

- the determinant, determining the masses of the 4D states, is given by (3.96).

- all fermion fields, Yukawa matrices, bulk-mass matrices, profiles, and flavor vectors are to be replaced by (3.212), (3.214),(3.215), (3.216), and (3.217), respectively.

The profiles in the custodial model are given by

$$
\begin{aligned}
\boldsymbol{C}_n^U &\equiv \mathrm{diag}\big(\boldsymbol{C}_n^{Q(+)}, \boldsymbol{C}_n^{Q(-)}\big), & \boldsymbol{C}_n^u &\equiv \mathrm{diag}\big(\boldsymbol{C}_n^{u^c(+)}, \boldsymbol{C}_n^{\mathcal{T}_1(-)}, \boldsymbol{C}_n^{\mathcal{T}_2(-)}\big), \\
\boldsymbol{S}_n^U &\equiv \mathrm{diag}\big(\boldsymbol{S}_n^{Q(+)}, \boldsymbol{S}_n^{Q(-)}\big), & \boldsymbol{S}_n^u &\equiv \mathrm{diag}\big(\boldsymbol{S}_n^{u^c(+)}, \boldsymbol{S}_n^{\mathcal{T}_1(-)}, \boldsymbol{S}_n^{\mathcal{T}_2(-)}\big), \\[6pt]
\boldsymbol{C}_n^D &\equiv \boldsymbol{C}_n^{Q(+)}, & \boldsymbol{C}_n^d &\equiv \mathrm{diag}\big(\boldsymbol{C}_n^{\mathcal{T}_2(+)}, \boldsymbol{C}_n^{\mathcal{T}_1(-)}\big), \\
\boldsymbol{S}_n^D &\equiv \boldsymbol{S}_n^{Q(+)}, & \boldsymbol{S}_n^d &\equiv \mathrm{diag}\big(\boldsymbol{S}_n^{\mathcal{T}_2(+)}, \boldsymbol{S}_n^{\mathcal{T}_1(-)}\big), \\[6pt]
\boldsymbol{C}_n^\Lambda &\equiv \boldsymbol{C}_n^{Q(-)}, & \boldsymbol{C}_n^\lambda &\equiv \mathrm{diag}\big(\boldsymbol{C}_n^{\mathcal{T}_1(-)}, \boldsymbol{C}_n^{\mathcal{T}_2(-)}\big), \\
\boldsymbol{S}_n^\Lambda &\equiv \boldsymbol{S}_n^{Q(-)}, & \boldsymbol{S}_n^\lambda &\equiv \mathrm{diag}\big(\boldsymbol{S}_n^{\mathcal{T}_1(-)}, \boldsymbol{S}_n^{\mathcal{T}_2(-)}\big),
\end{aligned}
\tag{3.216}
$$

while the flavor vectors read

$$
\vec{a}_n^U \equiv \begin{pmatrix} a_n^u \\ a_n^{u'} \end{pmatrix}, \quad
\vec{a}_n^u \equiv \begin{pmatrix} a_n^{u^c} \\ a_n^{U'} \\ a_n^U \end{pmatrix}, \quad
\vec{a}_n^D \equiv a_n^d, \quad
\vec{a}_n^d \equiv \begin{pmatrix} a_n^D \\ a_n^{D'} \end{pmatrix}, \quad
\vec{a}_n^\Lambda \equiv a_n^\lambda, \quad
\vec{a}_n^\lambda \equiv \begin{pmatrix} a_n^{\Lambda'} \\ a_n^\Lambda \end{pmatrix}. \tag{3.217}
$$

The 3×3 matrices $\boldsymbol{C}_n^{A(\pm)}(\phi)$ $(\boldsymbol{S}_n^{A(\pm)}(\phi))$ with $A = Q, u^c, \mathcal{T}_1, \mathcal{T}_2$ correspond to even (odd) profiles on the orbifold, and the superscript $(\pm)$ indicates the type of BC on the UV brane. With some abuse of notation, the superscripts of the odd profiles refer to the UV BCs of the associated even profiles. The quarks present already in the minimal RS model hence all carry a $(+)$ superscript. Labels for the IR BCs are again omitted to simplify the notation. The flavor structure is encoded in the three-component vectors a_n^A with $A = u, u', u^c, U', U, d, D', D, \lambda, \Lambda', \Lambda$, which are then combined into the larger flavor vectors defined above. As stated below (3.76), the spinors on the right hand side of the KK decomposition $q_L^{(n)}(x)$ and $q_R^{(n)}(x)$ are still 4D spinors in the mass basis, and the index n labels the different mass eigenstates with masses m_n, i.e., $m_1 = m_u$, $m_2 = m_c$, $m_3 = m_t$, etc. in the case of up-type quarks.

Bulk Profiles

The form of the solutions $\big(C_n^{A(+)}(\phi)\big)_i$ and $\big(S_n^{A(+)}(\phi)\big)_i$ associated with bulk mass parameters M_{A_i}, has already been given in (3.97). The functions $\big(C_n^{A(-)}(\phi)\big)_i$ and $\big(S_n^{A(-)}(\phi)\big)_i$ can be derived in a similar fashion by requiring a Dirichlet BC for the even mode, $\big(C_n^{A(-)}(0)\big)_i = 0$, to account for the additional twist of the non-SM-like fermions on the UV boundary. In consequence, the treatment is analogous to that of the odd modes of the SM-like fermions, for which $\big(S_n^{A(+)}(0)\big)_i = 0$. In the following we will drop the label A and the index i since they

should be clear from the context. In t-notation, one finds in the bulk (*i.e.*, for $t \in]\epsilon, 1[$)

$$C_n^{(\pm)}(\phi) = \mathcal{N}_n^{(\pm)}(c) \sqrt{\frac{L\epsilon t}{\pi}} f_n^{(\pm)+}(t, c),$$

$$S_n^{(\pm)}(\phi) = \pm \mathcal{N}_n^{(\pm)}(c) \, \text{sgn}(\phi) \sqrt{\frac{L\epsilon t}{\pi}} f_n^{(\pm)-}(t, c),$$

(3.218)

where the overall "+" sign entering the Z_2-odd profiles holds if $c = c_Q \equiv +M_Q/k$ refers to the bi-doublet, while the "−" sign applies in the case of $c = c_A \equiv -M_A/k$, where $A = u^c, \mathcal{T}_1, \mathcal{T}_2$. The functions $f_n^{(\pm)\pm}(t, c)$ are given by

$$f_n^{(+)\pm}(t, c) = J_{-\frac{1}{2}-c}(x_n\epsilon) J_{\mp\frac{1}{2}+c}(x_n t) \pm J_{+\frac{1}{2}+c}(x_n\epsilon) J_{\pm\frac{1}{2}-c}(x_n t),$$

$$f_n^{(-)\pm}(t, c) = J_{+\frac{1}{2}-c}(x_n\epsilon) J_{\mp\frac{1}{2}+c}(x_n t) \mp J_{-\frac{1}{2}+c}(x_n\epsilon) J_{\pm\frac{1}{2}-c}(x_n t).$$

(3.219)

They satisfy the relations

$$f_n^{(+)+}(t, c) = f_n^{(-)-}(t, -c), \qquad f_n^{(+)-}(t, c) = -f_n^{(-)+}(t, -c).$$

(3.220)

The orthonormality conditions (3.88) imply

$$2 \int_\epsilon^1 dt \, t \left[f_n^{(a)\pm}(t, c) \right]^2 = \frac{1}{\left[\mathcal{N}_n^{(a)}(c) \right]^2} \pm \frac{f_n^{(a)+}(1, c) \, f_n^{(a)-}(1, c)}{x_n},$$

(3.221)

where $a = \pm$, from which we derive

$$\left[\mathcal{N}_n^{(a)}(c) \right]^{-2} = \left[f_n^{(a)+}(1, c) \right]^2 + \left[f_n^{(a)-}(1, c) \right]^2$$

$$- \frac{2c}{x_n} f_n^{(a)+}(1, c) \, f_n^{(a)-}(1, c) - \epsilon^2 \left(\left[f_n^{(a)+}(\epsilon, c) \right]^2 + \left[f_n^{(a)-}(\epsilon, c) \right]^2 \right).$$

(3.222)

This extends the result (3.100) of Section 3.2.2 to the case of Z_2-odd profiles with a non-zero value on the UV boundary. For the special case where $c + 1/2$ is an integer, the profiles must be again obtained from the above relations by a limiting procedure.

For the SM fermions, it is again a very good approximation to perform an expansion in $x_n \ll 1$. Using the results (3.101), in combination with (3.220), we obtain

$$C_n^{(+)}(\phi) \approx \sqrt{\frac{L\epsilon}{\pi}} F(c) \, t^c, \qquad S_n^{(+)}(\phi) \approx \pm\text{sgn}(\phi) \sqrt{\frac{L\epsilon}{\pi}} x_n F(c) \frac{t^{1+c} - \epsilon^{1+2c} t^{-c}}{1 + 2c},$$

$$C_n^{(-)}(\phi) \approx -\sqrt{\frac{L\epsilon}{\pi}} x_n F(-c) \frac{t^{1-c} - \epsilon^{1-2c} t^c}{1 - 2c}, \qquad S_n^{(-)}(\phi) \approx \pm\text{sgn}(\phi) \sqrt{\frac{L\epsilon}{\pi}} F(-c) \, t^{-c},$$

(3.223)

with the zero-mode profile $F(c)$ as defined in (3.102). Remember that this profile is exponentially small for UV-localized fermions, while it is of $\mathcal{O}(1)$ for IR-localized fields. Moreover, note that the profiles $C_n^{(+)}(\phi)$ and $S_n^{(-)}(\phi)$ are of $\mathcal{O}(1)$, while $C_n^{(-)}(\phi)$ and $S_n^{(+)}(\phi)$ are of $\mathcal{O}(v/M_{\text{KK}})$. As we will explain in detail in the next section, this feature will be important for the (partially)

shielding of the $Zb_L\bar{b}_L$ and $Zd_L^i\bar{d}_L^j$ vertices from corrections due to mixing of zero-mode quarks with their KK excitations.

3.4.3   Gauge-Boson Interactions with Fermions

In this section we examine explicitly, how a protection of the left-handed down-type couplings of the Z boson can be achieved. A protection from both gauge-boson as well as fermion corrections is possible by choosing an appropriate embedding of the fermions into the enlarged gauge group in the bulk. Later we will also derive the four-fermion charged-current interactions and show that a custodial protection is not at work in this case. First, let us give the covariant derivative of the custodial RS model in the UV basis. It reads

$$
\begin{aligned}
D_\mu = \partial_\mu - i\,\frac{g_{L5}}{\sqrt{2}}\left(L_\mu^+ T_L^+ + L_\mu^- T_L^-\right) + i\,\frac{g_{R5}}{\sqrt{2}}\left(R_\mu^+ T_R^+ + R_\mu^- T_R^-\right) \\
- i\,g_{Z5}\,Q_Z Z_\mu - i\,g_{Z'5}\,Q_{Z'} Z_\mu' - i\,e_5 Q A_\mu\,.
\end{aligned}
\tag{3.224}
$$

The fundamental Z-boson couplings to fermionic currents are given by

$$
\begin{aligned}
g_Z = \sqrt{g_L^2 + g_Y^2}\,, &\qquad g_{Z'} = \sqrt{g_R^2 + g_X^2}\,, \\
Q_Z = T_L^3 - \frac{g_Y^2}{g_Z^2}Q\,, &\qquad Q_{Z'} = -T_R^3 - \frac{g_X^2}{g_{Z'}^2}Y\,,
\end{aligned}
\tag{3.225}
$$

where we have replaced 5D couplings by 4D couplings as in (3.39). At this point we have to specify the form of the $SU(2)_{L,R}$ generators when acting on different fermion representations. Acting on fermion bi-doublets, the generators $T_{L,R}^i$ with $i = 1, 2, 3$ are given by the Pauli matrices in the standard convention times a factor of $1/2$, as defined below (1.10). As usual, we define $T_{L,R}^\pm = T_{L,R}^1 \pm i\,T_{L,R}^2$. If, on the other hand, the generators act on $SU(2)_{L,R}$ triplets, they read explicitly

$$
T_{L,R}^+ = \begin{pmatrix} 0 & \sqrt{2} & 0 \\ 0 & 0 & \sqrt{2} \\ 0 & 0 & 0 \end{pmatrix}, \qquad
T_{L,R}^- = \begin{pmatrix} 0 & 0 & 0 \\ \sqrt{2} & 0 & 0 \\ 0 & \sqrt{2} & 0 \end{pmatrix}, \qquad
T_{L,R}^3 = \begin{pmatrix} 1 & 0 & 0 \\ 0 & 0 & 0 \\ 0 & 0 & -1 \end{pmatrix}.
\tag{3.226}
$$

Note that the current-operators in interaction terms involve a trace with respect to the fundamental gauge indices, and that again the T_R^i act to the left. When they are not needed, we will often drop the subscripts L, R in the following. For the calculation of the corrections to the quark-mixing matrices (which will be performed in Section 3.6) it will turn out to be useful to introduce the vector of couplings

$$
\vec{g}_Z = \begin{pmatrix} g_Z Q_Z \\ g_{Z'} Q_{Z'} \end{pmatrix},
\tag{3.227}
$$

as well as the charged-current vectors

$$
\vec{J}_{W_Q}^{\mu\pm} = \frac{1}{\sqrt{2}}\left(g_L\,\mathrm{Tr}\left[\bar{Q}\,\gamma^\mu\,T^\pm\,Q\right], g_R\,\mathrm{Tr}\left[\bar{Q}\,\gamma^\mu\,Q\,T^\pm\right]\right),
$$

$$\vec{J}_{W\tau}^{\mu\pm} = \frac{1}{\sqrt{2}} \left(g_L \bar{\mathcal{T}}_1 \gamma^\mu T^\pm \mathcal{T}_1 \,,\; g_R \, \mathrm{Tr}\left[\bar{\mathcal{T}}_2 \gamma^\mu \mathcal{T}_2 T^\pm \right] \right), \tag{3.228}$$

which will multiply $\left(L_\mu^\pm \,, R_\mu^\pm \right)^T$ from the left.

Before going into the interactions of fermions with massive gauge bosons, note that in the custodial model the interactions with gauge bosons that have massless zero modes (which can be worked out from (3.224)) are in complete analogy to the corresponding expressions presented in Section 3.2.4. The fermion structure present in the latter section is to be trivially replaced with the objects of the custodial model, presented in Section 3.4.2. In addition to the interactions with up- and down-type quarks, there will also be photon as well as gluon interactions with the charge-5/3 λ-quarks.

Custodial Protection: Gauge-Boson Contributions

Using (3.207) and (3.208), we find that the coupling of the Z boson to a current of q-quarks is proportional to

$$\left(\vec{g}_Z^q \right)^T \vec{\chi}_0^Z(\phi) = \frac{g_Z Q_Z^q}{\sqrt{2\pi}} \left\{ 1 + \frac{m_Z^2}{4 M_{\mathrm{KK}}^2} \left[-2 L \, t^2 \, \omega_Z^q + 1 - \frac{1}{L} + 2 t^2 \left(\frac{1}{2} - \ln t \right) \right] \right\} + \mathcal{O}\left(\frac{m_Z^4}{M_{\mathrm{KK}}^4} \right), \tag{3.229}$$

with

$$\omega_Z^q = 1 - \frac{s_Z}{c_Z} \frac{g_{Z'} Q_{Z'}^q}{g_Z Q_Z^q} . \tag{3.230}$$

This is an important result, as it allows us to understand the custodial protection of the $Z b_L \bar{b}_L$ vertex. Note that the first term in the square bracket in (3.229), which is enhanced by the volume factor L, gets modified by the prefactor ω_Z^q, *i.e.*, a combination of the fundamental charges and couplings. While $\omega_Z^q = 1$ for all quarks in the minimal RS model, it is possible to arrange for

$$\omega_Z^{b_L} = 0 \quad \Longleftrightarrow \quad g_Z Q_Z^{b_L} = \frac{s_Z}{c_Z} g_{Z'} Q_{Z'}^{b_L}, \tag{3.231}$$

by virtue of the extension of the gauge group in the bulk. It is interesting to observe that the interplay of neutral gauge bosons can only protect leading term in L, while no such mechanism is available for the subleading terms in L. Those arise from the fact that the profiles $\chi_0^{(\pm)}(t)$ obey different BCs, which represents an irreducible source of P_{LR} symmetry breaking. Numerically, the corrections to the $Z b_L \bar{b}_L$ vertex arising from the gauge sector are thus suppressed by a factor of $L \approx 37$ in the $SU(2)_L \times SU(2)_R \times P_{LR}$ custodial model relative to the minimal RS model.

Formula (3.230) can be recast into the form

$$\omega_Z^q = \frac{c_w^2}{2 g_L^2} \frac{(g_L^2 + g_R^2)(T_L^{3\,q} + T_R^{3\,q}) + (g_L^2 - g_R^2)(T_L^{3\,q} - T_R^{3\,q})}{T_L^{3\,q} - s_w^2 Q_q} , \tag{3.232}$$

which allows to read off that the choices

$$T_L^{3\,q} = T_R^{3\,q} = 0 \qquad (P_C \text{ symmetry}), \tag{3.233}$$

and

$$g_L = g_R \,, \qquad T_L^{3\,q} = -T_R^{3\,q} \qquad (P_{LR} \text{ symmetry}) \,, \tag{3.234}$$

are suitable to protect the Z-boson vertices from receiving L-enhanced corrections. Since the representation (3.209) features $T_L^{3\,d_L} = -T_{R}^{3\,d_L} = -1/2$ and $T_L^{3\,u_R} = T_R^{3\,u_R} = 0$, it is then immediately clear that the $Z d_L^i \bar{d}_L^j$ and $Z u_R^i \bar{u}_R^j$ vertices are protected to leading order in L by the P_{LR} and P_C symmetries, respectively. On the other hand, the $Z d_R^i \bar{d}_R^j$ and $Z u_L^i \bar{u}_L^j$ vertices do receive L-enhanced corrections, since the corresponding quantum numbers are $T_L^{3\,d_R} = 0$, $T_R^{3\,d_R} = 1$ and $T_L^{3\,u_L} = T_R^{3\,u_L} = 1/2$. We also add that devising the quark sector as in (3.209) implies $\omega_Z^{b_R} > 0$, so that the shift in the right-handed Z-boson coupling to bottom quarks arising from the gauge-boson sector is predicted to be strictly negative. This suggests that the well-known tension in the global fit to the $Z \to b\bar{b}$ pseudo observables cannot be softened in the model under considerations. We will come back to this point in Section 5.1.3.

Fermion Couplings to the Z Boson

We will now identify all phenomenologically relevant RS contributions to weak neutral gauge interactions of quark currents at relative order v^2/M_{KK}^2 in the custodial model. The Z-boson couplings to left- and right-handed quarks can be read off from the Lagrangian

$$\mathcal{L}_{\text{4D}} \ni \frac{g_L}{c_w} \left[1 + \frac{m_Z^2}{4M_{\text{KK}}^2} \left(1 - \frac{1}{L} \right) \right] Z_\mu \times \sum_{q,m,n} \left[\left(g_L^q \right)_{mn} (\bar{q}_L^m \gamma_\mu q_L^n) + \left(g_R^q \right)_{mn} (\bar{q}_R^m \gamma_\mu q_R^n) \right] , \tag{3.235}$$

where the prefactor accounts for a universal correction due to the t-independent terms in (3.229), identical to (3.147). The left- and right-handed couplings $\boldsymbol{g}_{L,R}^q$ are infinite-dimensional matrices in the space of quark modes, and can be parametrized as

$$\boldsymbol{g}_L^q = \left(T_L^{3\,q_L} - s_w^2 Q_q \right) \left[\mathbf{1} - \frac{m_Z^2}{2M_{\text{KK}}^2} \left(\omega_Z^{q_L} L \, \boldsymbol{\Delta}_Q - \boldsymbol{\Delta}_Q' \right) \right] - \boldsymbol{\delta}_Q + \frac{m_Z^2}{2M_{\text{KK}}^2} \left(\frac{c_w^2}{g_L^2} L \, \boldsymbol{\varepsilon}_Q - \boldsymbol{\varepsilon}_Q' \right) ,$$
$$\boldsymbol{g}_R^q = -s_w^2 Q_q \left[\mathbf{1} - \frac{m_Z^2}{2M_{\text{KK}}^2} \left(\omega_Z^{q_R} L \, \boldsymbol{\Delta}_q - \boldsymbol{\Delta}_q' \right) \right] + \boldsymbol{\delta}_q - \frac{m_Z^2}{2M_{\text{KK}}^2} \left(\frac{c_w^2}{g_L^2} L \, \boldsymbol{\varepsilon}_q - \boldsymbol{\varepsilon}_q' \right) . \tag{3.236}$$

The labels of the charges appearing in these expressions (as well as above) indicate that the quantum numbers of the corresponding zero modes are to be employed. In $\boldsymbol{g}_L^q$ they read $T_L^{3\,u_L}(= T_L^{3\,u}) = T_R^{3\,u_L}(= T_R^{3\,u}) = T_R^{3\,d_L}(= T_R^{3\,d}) = 1/2$ and $T_L^{3\,d_L}(= T_L^{3\,d}) = -1/2$, whereas for $\boldsymbol{g}_R^q$ one has $T_L^{3\,u_R}(= T_L^{3\,u^c}) = T_R^{3\,u_R}(= T_R^{3\,u^c}) = T_L^{3\,d_R}(= T_L^{3\,D}) = 0$ and $T_R^{3\,d_R}(= T_R^{3\,D}) = 1$. The quoted numerical values correspond to the choice (3.209). We do not consider the sector of λ and $\Lambda^{(\prime)}$ quarks at this point, as these fields do not possess zero modes. The L-enhanced term proportional to ω_Z^q vanishes for the assignments (3.233) and (3.234), making the custodial protection explicit. Following (3.148), we have split the corrections to the Z-boson couplings into leading contributions in the ZMA, denoted by $\boldsymbol{\Delta}_{Q,q}^{(\prime)}$, and subleading ones, parametrized by $\boldsymbol{\varepsilon}_{Q,q}^{(\prime)}$. The elements of the leading-order matrices $\boldsymbol{\Delta}_{Q,q}^{(\prime)}$ are defined as

$$\left(\Delta_Q \right)_{mn} = \frac{2\pi}{L\epsilon} \int_\epsilon^1 dt\, t^2 \left[\vec{a}_m^{Q\dagger} \boldsymbol{C}_m^Q(t)\, \boldsymbol{C}_n^Q(t)\, \vec{a}_n^Q + \vec{a}_m^{q\dagger} \boldsymbol{S}_m^q(t)\, \boldsymbol{S}_n^q(t)\, \vec{a}_n^q \right],$$

$$(\Delta_q)_{mn} = \frac{2\pi}{L\epsilon} \int_\epsilon^1 dt\, t^2 \left[\vec{a}_m^{q\dagger}\, \boldsymbol{C}_m^q(t)\, \boldsymbol{C}_n^q(t)\, \vec{a}_n^q + \vec{a}_m^{Q\dagger}\, \boldsymbol{S}_m^Q(t)\, \boldsymbol{S}_n^Q(t)\, \vec{a}_n^Q \right],$$

$$(\Delta_Q')_{mn} = \frac{2\pi}{L\epsilon} \int_\epsilon^1 dt\, t^2 \left(\frac{1}{2} - \ln t \right) \left[\vec{a}_m^{Q\dagger}\, \boldsymbol{C}_m^Q(t)\, \boldsymbol{C}_n^Q(t)\, \vec{a}_n^Q + \vec{a}_m^{q\dagger}\, \boldsymbol{S}_m^q(t)\, \boldsymbol{S}_n^q(t)\, \vec{a}_n^q \right],$$

$$(\Delta_q')_{mn} = \frac{2\pi}{L\epsilon} \int_\epsilon^1 dt\, t^2 \left(\frac{1}{2} - \ln t \right) \left[\vec{a}_m^{q\dagger}\, \boldsymbol{C}_m^q(t)\, \boldsymbol{C}_n^q(t)\, \vec{a}_n^q + \vec{a}_m^{Q\dagger}\, \boldsymbol{S}_m^Q(t)\, \boldsymbol{S}_n^Q(t)\, \vec{a}_n^Q \right], \qquad (3.237)$$

while the elements of the matrices $\boldsymbol{\varepsilon}_{Q,q}^{(\prime)}$ take the form

$$(\varepsilon_Q)_{mn} = \frac{2\pi}{L\epsilon} \int_\epsilon^1 dt\, t^2 \Big[\vec{a}_m^{Q\dagger}\, \boldsymbol{C}_m^Q(t) \left\{ g_L^2 \left(T_L^{3\,q_L}\boldsymbol{1} - \boldsymbol{T}_L^{3\,Q} \right) + g_R^2 \left(T_R^{3\,q_L}\boldsymbol{1} - \boldsymbol{T}_R^{3\,Q} \right) \right\} \boldsymbol{C}_n^Q(t)\, \vec{a}_n^Q$$
$$+ \vec{a}_m^{q\dagger}\, \boldsymbol{S}_m^q(t) \left\{ g_L^2 \left(T_L^{3\,q_L}\boldsymbol{1} - \boldsymbol{T}_L^{3\,q} \right) + g_R^2 \left(T_R^{3\,q_L}\boldsymbol{1} - \boldsymbol{T}_R^{3\,q} \right) \right\} \boldsymbol{S}_n^q(t)\, \vec{a}_n^q \Big],$$

$$(\varepsilon_q)_{mn} = \frac{2\pi}{L\epsilon} \int_\epsilon^1 dt\, t^2 \Big[\vec{a}_m^{q\dagger}\, \boldsymbol{C}_m^q(t) \left\{ g_L^2\, \boldsymbol{T}_L^{3\,q} - g_R^2 \left(T_R^{3\,q_R}\boldsymbol{1} - \boldsymbol{T}_R^{3\,q} \right) \right\} \boldsymbol{C}_n^q(t)\, \vec{a}_n^q$$
$$+ \vec{a}_m^{Q\dagger}\, \boldsymbol{S}_m^Q(t) \left\{ g_L^2\, \boldsymbol{T}_L^{3\,Q} - g_R^2 \left(T_R^{3\,q_R}\boldsymbol{1} - \boldsymbol{T}_R^{3\,Q} \right) \right\} \boldsymbol{S}_n^Q(t)\, \vec{a}_n^Q \Big], \qquad (3.238)$$

$$(\varepsilon_Q')_{mn} = \frac{2\pi}{L\epsilon} \int_\epsilon^1 dt\, t^2 \left(\frac{1}{2} - \ln t \right) \Big[\vec{a}_m^{Q\dagger}\, \boldsymbol{C}_m^Q(t) \left(T_L^{3\,q_L}\boldsymbol{1} - \boldsymbol{T}_L^{3\,Q} \right) \boldsymbol{C}_n^Q(t)\, \vec{a}_n^Q$$
$$+ \vec{a}_m^{q\dagger}\, \boldsymbol{S}_m^q(t) \left(T_L^{3\,q_L}\boldsymbol{1} - \boldsymbol{T}_L^{3\,q} \right) \boldsymbol{S}_n^q(t)\, \vec{a}_n^q \Big],$$

$$(\varepsilon_q')_{mn} = \frac{2\pi}{L\epsilon} \int_\epsilon^1 dt\, t^2 \left(\frac{1}{2} - \ln t \right) \left[\vec{a}_m^{q\dagger}\, \boldsymbol{C}_m^q(t)\, \boldsymbol{T}_L^{3\,q}\, \boldsymbol{C}_n^q(t)\, \vec{a}_n^q + \vec{a}_m^{Q\dagger}\, \boldsymbol{S}_m^Q(t)\, \boldsymbol{T}_L^{3\,Q}\, \boldsymbol{S}_n^Q(t)\, \vec{a}_n^Q \right].$$

Finally, the elements of the matrices $\boldsymbol{\delta}_{Q,q}$, which arise because of the non-orthonormality of the quark profiles and describe mixings between the different multiplets, read

$$(\delta_Q)_{mn} = \frac{2\pi}{L\epsilon} \int_\epsilon^1 dt \left[\vec{a}_m^{Q\dagger}\, \boldsymbol{C}_m^Q(t) \left(T_L^{3\,q_L}\boldsymbol{1} - \boldsymbol{T}_L^{3\,Q} \right) \boldsymbol{C}_n^Q(t)\, \vec{a}_n^Q$$
$$+ \vec{a}_m^{q\dagger}\, \boldsymbol{S}_m^q(t) \left(T_L^{3\,q_L}\boldsymbol{1} - \boldsymbol{T}_L^{3\,q} \right) \boldsymbol{S}_n^q(t)\, \vec{a}_n^q \right],$$

$$(\delta_q)_{mn} = \frac{2\pi}{L\epsilon} \int_\epsilon^1 dt \left[\vec{a}_m^{q\dagger}\, \boldsymbol{C}_m^q(t)\, \boldsymbol{T}_L^{3\,q}\, \boldsymbol{C}_n^q(t)\, \vec{a}_n^q + \vec{a}_m^{Q\dagger}\, \boldsymbol{S}_m^Q(t)\, \boldsymbol{T}_L^{3\,Q}\, \boldsymbol{S}_n^Q(t)\, \vec{a}_n^Q \right]. \qquad (3.239)$$

In the expressions above we have used the charge matrices $\boldsymbol{T}_{L,R}^{3\,Q,q}$, defined as

$$\boldsymbol{T}_{L,R}^{3\,U} = \begin{pmatrix} T_{L,R}^{3\,u} & 0 \\ 0 & T_{L,R}^{3\,u'} \end{pmatrix}, \qquad \boldsymbol{T}_{L,R}^{3\,u} = \begin{pmatrix} T_{L,R}^{3\,u^c} & 0 & 0 \\ 0 & T_{L,R}^{3\,U'} & 0 \\ 0 & 0 & T_{L,R}^{3\,U} \end{pmatrix},$$

$$\boldsymbol{T}_{L,R}^{3\,D} = T_{L,R}^{3\,d}, \qquad \boldsymbol{T}_{L,R}^{3\,d} = \begin{pmatrix} T_{L,R}^{3\,D} & 0 \\ 0 & T_{L,R}^{3\,D'} \end{pmatrix}. \qquad (3.240)$$

One can easily check that for our choice (3.209), the quantities $\varepsilon_{Q,q}^{(\prime)}$ are indeed suppressed by v^2/M_{KK}^2 with respect to the matrices $\boldsymbol{\Delta}_{Q,q}^{(\prime)}$. Note that with this embedding, the matrices $\boldsymbol{T}_{L,R}^{3\,u}$ vanish identically.

Custodial Protection: Fermionic Contributions

Finally, we want to have a look at the custodial protection of the $Zb_L\bar{b}_L$ vertex from effects arising from quark mixing, parametrized by the matrices $\boldsymbol{\delta}_{Q,q}$. These objects scale in general as v^2/M_{KK}^2, but as they appear with an $\mathcal{O}(1)$ coefficient in (3.236) they contribute at the same order as the matrices $\boldsymbol{\Delta}_{Q,q}^{(\prime)}$. In the case of the left-handed down-type quark-sector, one has

$$
\begin{aligned}
(\delta_D)_{mn} &= \frac{2\pi}{L\epsilon} \int_\epsilon^1 dt \left[a_m^{D\dagger} \, \boldsymbol{S}_m^{\mathcal{T}_2(+)}(t) \left(T_L^{3d_L} - T_L^{3D} \right) \boldsymbol{S}_n^{\mathcal{T}_2(+)}(t) \, a_n^D \right. \\
&\qquad\qquad \left. + a_m^{D'\dagger} \, \boldsymbol{S}_m^{\mathcal{T}_1(-)}(t) \left(T_L^{3\,d_L} - T_L^{3\,D'} \right) \boldsymbol{S}_n^{\mathcal{T}_1(-)}(t) \, a_n^{D'} \right] \\
&= -\frac{1}{2} \frac{2\pi}{L\epsilon} \int_\epsilon^1 dt \left[a_m^{D\dagger} \, \boldsymbol{S}_m^{\mathcal{T}_2(+)}(t) \, \boldsymbol{S}_n^{\mathcal{T}_2(+)}(t) \, a_n^D - a_m^{D'\dagger} \, \boldsymbol{S}_m^{\mathcal{T}_1(-)}(t) \, \boldsymbol{S}_n^{\mathcal{T}_1(-)}(t) \, a_n^{D'} \right],
\end{aligned}
\tag{3.241}
$$

where in the second step we have inserted the quantum numbers corresponding to our choice (3.209) of multiplets.

The relative sign between the two terms in the second line of (3.241) suggests that also for the corrections due to quark mixing, a custodial protection mechanism could be at work. To see analytically if this is indeed the case, let us derive the ZMA expression for $\boldsymbol{\delta}_D$. Using the approximate expressions (3.223), the system of equations (3.87) can be brought into the form

$$
\frac{\sqrt{2}\,m_n}{v} \hat{a}_n^d = \boldsymbol{Y}_d^{\mathrm{eff}} \, \hat{a}_n^D, \qquad \frac{\sqrt{2}\,m_n}{v} \hat{a}_n^D = \left(\boldsymbol{Y}_d^{\mathrm{eff}}\right)^\dagger \hat{a}_n^d,
\tag{3.242}
$$

and

$$
\hat{a}_n^{D'} = x_n \operatorname{diag}\left(F^{-1}(c_{\mathcal{T}_{2i}}) \, F^{-1}(-c_{\mathcal{T}_{1i}}) \right) \hat{a}_n^D,
\tag{3.243}
$$

where we have defined the effective Yukawa couplings

$$
(\boldsymbol{Y}_d^{\mathrm{eff}})_{ij} \equiv F(c_{Q_i}) \, (Y_d)_{ij} \, F(c_{\mathcal{T}_{2j}}),
\tag{3.244}
$$

in analogy to (3.106). Moreover, the rescaled vectors $\hat{a}_n^A \equiv \sqrt{2}\, a_n^A$ with $A = d, D, D'$, obey the normalization conditions

$$
\hat{a}_n^{D\dagger} \hat{a}_n^D = 1, \qquad \hat{a}_n^{d\dagger} \hat{a}_n^d + \hat{a}_n^{D'\dagger} \hat{a}_n^{D'} = 1.
\tag{3.245}
$$

We obtain from (3.242) the LO equalities

$$
\left(m_n^2 \mathbf{1} - \frac{v^2}{2} \boldsymbol{Y}_d^{\mathrm{eff}} \left(\boldsymbol{Y}_d^{\mathrm{eff}}\right)^\dagger \right) \hat{a}_n^d = 0, \qquad \left(m_n^2 \mathbf{1} - \frac{v^2}{2} \left(\boldsymbol{Y}_d^{\mathrm{eff}}\right)^\dagger \boldsymbol{Y}_d^{\mathrm{eff}} \right) \hat{a}_n^D = 0,
\tag{3.246}
$$

and the mass eigenvalues are the solutions to the equation

$$\det\left(m_n^2\,\mathbf{1} - \frac{v^2}{2}\,\boldsymbol{Y}_d^{\mathrm{eff}}\left(\boldsymbol{Y}_d^{\mathrm{eff}}\right)^\dagger\right) = 0\,. \tag{3.247}$$

This exactly resembles (3.109) and implies that to LO in v/M_{KK} the values m_n are unaffected by the presence of the D' quarks embedded in the multiplet $\mathcal{T}_1$. In the ZMA, but not in general, the vectors $\hat{a}_n^d$ and $\hat{a}_n^D$ belonging to different n are orthogonal on each other.

In complete analogy to the discussion below (3.109), the eigenvectors $\hat{a}_n^d$ and $\hat{a}_n^D$ of the matrices $\boldsymbol{Y}_d^{\mathrm{eff}}\left(\boldsymbol{Y}_d^{\mathrm{eff}}\right)^\dagger$ and $\left(\boldsymbol{Y}_d^{\mathrm{eff}}\right)^\dagger\boldsymbol{Y}_d^{\mathrm{eff}}$, with $n = 1, 2, 3$, form the columns of the unitary matrices $\boldsymbol{U}_d$ and $\boldsymbol{W}_d$ appearing in the singular-value decomposition

$$\boldsymbol{Y}_d^{\mathrm{eff}} = \boldsymbol{U}_d\,\boldsymbol{\lambda}_d\,\boldsymbol{W}_d^\dagger\,, \tag{3.248}$$

with $\boldsymbol{\lambda}_d$ as given in (3.111). Similar relations hold in the up-type quark sector and will be given explicitly in Section 3.7. In the ZMA, the definition of the CKM matrix is identical to the one of the minimal RS model, given in (3.112). As the quark profiles, in combination with the Yukawa matrices, are fixed such that the physical quark masses and CKM parameters are reproduced (and the formulae above are identical to those of the minimal model), the profiles of the SM-like quarks will be to LO identical to those of the minimal RS model.

With these results at hand, it is a matter of simple algebra to find the expression for $\boldsymbol{\delta}_D$ in the ZMA. Working to first order in v^2/M_{KK}^2, and using (3.223) and (3.243) we arrive at

$$\boldsymbol{\delta}_D = -\frac{1}{2}\,\boldsymbol{x}_d\,\boldsymbol{W}_d^\dagger\,\mathrm{diag}\left[\frac{1}{1 - 2c_{\mathcal{T}_{2i}}}\left(\frac{1}{F^2(c_{\mathcal{T}_{2i}})}\left[1 - \frac{1 - 2c_{\mathcal{T}_{2i}}}{F^2(-c_{\mathcal{T}_{1i}})}\right] - 1 + \frac{F^2(c_{\mathcal{T}_{2i}})}{3 + 2c_{\mathcal{T}_{2i}}}\right)\right]\boldsymbol{W}_d\,\boldsymbol{x}_d\,, \tag{3.249}$$

where $\boldsymbol{x}_d \equiv \mathrm{diag}(m_d, m_s, m_b)/M_{\mathrm{KK}}$. Compared to the ZMA result in the minimal RS model (3.154), this relation contains an additional term involving the zero-mode profile $F(-c_{\mathcal{T}_{1i}})$. It stems from the admixture of the $\mathcal{T}_1$ multiplet in the zero mode, which is parametrized by the value of $\hat{a}_n^{D'}$. Notice that although this admixture is suppressed by v/M_{KK}, the fact that the profile $\boldsymbol{S}_n^{\mathcal{T}_1(-)}(t)$ is enhanced with respect to $\boldsymbol{S}_n^{\mathcal{T}_2(+)}(t)$ by the reciprocal factor promotes the second term in the last line of (3.241) to a leading contribution.

Note that the relations (3.242) and (3.243) are valid to leading order in v/M_{KK}. Beyond that order the first relation in (3.242) receives corrections from the profiles $\boldsymbol{C}_n^{\mathcal{T}_1(-)}(1^-)$ which scale like $x_n/F(-c_{\mathcal{T}_{1i}})$ as can be seen from (3.223). Thus in order to avoid exponentially enhanced terms of the form $v/M_{\mathrm{KK}}\,\epsilon^{1 - 2c_{\mathcal{T}_{1i}}}$ in the mass eigenvalues m_n, which, barring accidental cancellations, would make it impossible to reproduce the observed zero-mode down-type quark masses, one has to require that all the bulk mass parameters belonging to the multiplet $\mathcal{T}_1$ obey the relation $c_{\mathcal{T}_{1i}} < 1/2$. In this case the profiles $\boldsymbol{C}_n^{\mathcal{T}_1(-)}(t)$ are IR localized and one has to an excellent accuracy

$$\boldsymbol{\delta}_D = -\frac{1}{2}\,\boldsymbol{x}_d\,\boldsymbol{W}_d^\dagger\,\mathrm{diag}\left[\frac{1}{1 - 2c_{\mathcal{T}_{2i}}}\left(\frac{1}{F^2(c_{\mathcal{T}_{2i}})}\left[1 - \frac{1 - 2c_{\mathcal{T}_{2i}}}{1 - 2c_{\mathcal{T}_{1i}}}\right] - 1 + \frac{F^2(c_{\mathcal{T}_{2i}})}{3 + 2c_{\mathcal{T}_{2i}}}\right)\right]\boldsymbol{W}_d\,\boldsymbol{x}_d\,. \tag{3.250}$$

This result implies that the leading term in $\boldsymbol{\delta}_D$, *i.e.*, the contribution that is inversely propor-

tional to $F^2(c_{\mathcal{T}_{2i}}) \ll 1$, is absent if the bulk-mass parameters $c_{\mathcal{T}_{1i}}$ satisfy

$$c_{\mathcal{T}_{1i}} = c_{\mathcal{T}_{2i}} \,. \tag{3.251}$$

Thus, due to quark mixing, the conditions (3.233) and (3.234) alone are not sufficient to entirely shield the $Zb_L\bar{b}_L$ vertex from the leading corrections. However, since already for not too different values of $c_{\mathcal{T}_{2i}} \approx -1/2$ and $c_{\mathcal{T}_{1i}} \lesssim 0$ the first term in brackets in (3.250) is smaller in magnitude than 1, a partial protection is in place for a large range of bulk parameters. In consequence, effects due to quark mixing entering the left-handed down-type Z-boson couplings are generically suppressed in the custodial RS model relative to the minimal scenario as long as the corresponding Z_2-odd quark fields are not too far localized in the UV. The subleading terms in $\boldsymbol{\delta}_D$ are independent of $c_{\mathcal{T}_{1i}}$ and therefore not protected even if $c_{\mathcal{T}_{1i}} = c_{\mathcal{T}_{2i}}$.

Notice that (3.251) can be enforced by requiring the action to be invariant under the exchange of the D' and D quark fields,

$$P_{LR}(D') = D \,, \qquad \text{(extended P_{LR} symmetry)} \tag{3.252}$$

which extends the P_{LR} symmetry to the part of the quark sector that mixes with the left-handed down-type zero modes. This extended symmetry will necessarily be broken by the different BCs of D' and D, which embody irreducible sources of symmetry breaking and lead to non-vanishing sub-leading terms in (3.250). The symmetry (3.252) can also be broken softly by choosing bulk masses for D' that differ from those of D, which is a phenomenological viable option as long as $c_{\mathcal{T}_{1i}} < 1/2$, because it does not affect the SM down-type quark masses in an appreciable way. The protection mechanism discussed here has also been studied in [242] employing a perturbative approach. Our analysis based on the exact solution of the EOMs (3.78) including the BCs (3.87) goes beyond the latter work in the sense that it makes the dependence of $\boldsymbol{\delta}_D$ on the bulk masses $\boldsymbol{M}_{\mathcal{T}_{1,2}}$ explicit. It therefore allows for a clear understanding of the custodial protection mechanism in two respects. First, it makes transparent what the requirements are that need to be satisfied to achieve a protection and, second, which the terms in $\boldsymbol{\delta}_D$ are that inevitably escape protection. Compared to the perturbative approach, the exact solution thus has the salient advantage that the protection of the $Zd_L^i \bar{d}_L^j$ vertices from effects due to quark mixing can be clearly deciphered.

3.5 Summing over Kaluza-Klein Excitations

When calculating Feynman diagrams involving tree-level exchange of a SM gauge boson, accompanied by corresponding KK excitations, one encounters a combination of propagator and vertex functions, which in the low-energy limit, $i.e.$, for small momentum transfer q^2, can be expanded as

$$\sum_n \frac{\vec{\chi}_n^a(t)\,\vec{\chi}_n^{a\,T}(t')}{(m_n^a)^2 - q^2} = \sum_{N=1}^{\infty} \left(q^2\right)^{N-1} \sum_n \frac{\vec{\chi}_n^a(t)\,\vec{\chi}_n^{a\,T}(t')}{(m_n^a)^{2N}}$$
$$\equiv \sum_{N=1}^{\infty} \frac{1}{q^2} \left(\frac{q^2}{M_{\text{KK}}^2}\right)^N \boldsymbol{\Sigma}_a^{(N)}(t,t') \,. \tag{3.253}$$

The gauge-boson profiles $\vec{\chi}_n^a$ will be integrated with further profiles at each end of the propagator. As stated above, the formula holds for gauge bosons in the *custodial RS variant* with a massive zero mode, for which we will discuss these sums in the following. However, the special case of the minimal RS model will be easy to obtain at the end, where we will also study towers featuring a massless zero mode.

The infinite sums over profiles weighted by inverse powers of $(m_n^a)^2$ can be calculated in closed form by generalizing a method developed in [243]. The key to perform these sums is to make use of the fact that the bulk profiles $\vec{\chi}_n$ form a complete set of orthonormal, even functions on the orbifold, subject to the BCs given in (3.198) and in Table 3.2. The corresponding completeness relations read

$$\sum_n \vec{\chi}_n^a(\phi)\,\vec{\chi}_n^a(\phi') = \frac{1}{2}\left[\delta(\phi-\phi') + \delta(\phi+\phi')\right]\mathbf{1}\,, \quad \sum_n \frac{1}{t}\,\vec{\chi}_n^a(t)\,\vec{\chi}_n^{a\,T}(t') = \frac{L}{2\pi}\,\delta(t-t')\,\mathbf{1}\,. \quad (3.254)$$

Integrating the EOMs (3.197) twice and accounting for the BCs on both the UV and the IR brane leads to

$$\frac{\vec{\chi}_n^a(t)}{(x_n^a)^2} = \vec{\mathcal{I}}_n^a(t) - \left(t^2 - \epsilon^2\right)\boldsymbol{X}_a\,\vec{\mathcal{I}}_n^a(1) + \left[\mathbf{1} - \left(t^2 - \epsilon^2\right)\boldsymbol{X}_a\right]\boldsymbol{P}_{(+)}\frac{\vec{\chi}_n^a(\epsilon)}{\left(x_n^a\right)^2}\,, \quad (3.255)$$

where we have defined

$$\vec{\mathcal{I}}_n^a(t) \equiv \int_\epsilon^t dt'\,t' \int_{t'}^{1^-}\frac{dt''}{t''}\,\vec{\chi}_n^a(t'')\,, \qquad \boldsymbol{X}_a \equiv \tilde{X}^2\,\boldsymbol{D}_a \equiv \frac{LX^2}{2 + LX^2\left(1-\epsilon^2\right)}\,\boldsymbol{D}_a\,. \quad (3.256)$$

Using the completeness relation (3.254), it is then easy to prove that

$$\sum_n \vec{\mathcal{I}}_n^a(t)\,\vec{\chi}_n^{a\,T}(\phi') = \frac{L}{4\pi}\left(t_<^2 - \epsilon^2\right)\mathbf{1}\,, \quad (3.257)$$

where $t_< \equiv \min(t,t')$. With the help of these results we finally arrive at the result

$$\begin{aligned}
\boldsymbol{\Sigma}_a^{(1)}(t,t') = \frac{L}{4\pi}&\left[\left(t_<^2 - \epsilon^2\right)\mathbf{1} + \left(t^2 - \epsilon^2\right)\left(t'^2 - \epsilon^2\right)\boldsymbol{X}_a\right]\\
&+ \left[\mathbf{1} - \left(t^2 - \epsilon^2\right)\boldsymbol{X}_a\right]\boldsymbol{P}_{(+)}\boldsymbol{\Sigma}_a^{(1)}(\epsilon,\epsilon)\,\boldsymbol{P}_{(+)}\left[\mathbf{1} - \left(t'^2 - \epsilon^2\right)\boldsymbol{X}_a\right]^T\,,
\end{aligned} \quad (3.258)$$

for the leading sum, which is exact to all orders in v^2/M_{KK}^2.

Using the orthonormality relation (3.194), the remaining sum over gauge profiles evaluated on the UV brane can be written as

$$\begin{aligned}
\boldsymbol{P}_{(+)}\boldsymbol{\Sigma}_a^{(1)}(\epsilon,\epsilon)\,\boldsymbol{P}_{(+)} = \frac{L}{2\pi x_a^2}\left(\vec{\chi}_0^a(\epsilon)\right)_1&\left[\int_\epsilon^1 \frac{dt}{t}\left[\left(1 - c_a^2\tilde{X}^2\left(t^2 - \epsilon^2\right)\right)\left(\vec{\chi}_0^a(t)\right)_1\right.\right.\\
&\left.\left.+ s_a c_a\tilde{X}^2\left(t^2 - \epsilon^2\right)\left(\vec{\chi}_0^a(t)\right)_2\right]\right]^{-1}\boldsymbol{P}_{(+)}\,,
\end{aligned} \quad (3.259)$$

where $\left(\vec{\chi}_0^a(t)\right)_i$ denotes the ith component of the corresponding zero-mode vector. This formula

can easily be expanded in powers of v^2/M_{KK}^2 by employing (3.207) and (3.208), leading to

$$\boldsymbol{P}_{(+)}\,\boldsymbol{\Sigma}_a^{(1)}(\epsilon,\epsilon)\,\boldsymbol{P}_{(+)} = \left(\frac{1}{2\pi x_a^2} + \frac{1}{4\pi}\left[1 - \frac{1}{2L} - \epsilon^2\left(L - \frac{1}{2L}\right)\right] + \mathcal{O}(x_a^2)\right)\boldsymbol{P}_{(+)}\,. \qquad (3.260)$$

In the end, we obtain

$$\boldsymbol{\Sigma}_a^{(1)}(t,t') = \frac{L}{4\pi}\left[t_<^2\,\boldsymbol{1} - \boldsymbol{P}_a\,t^2 - \boldsymbol{P}_a^T\,t'^2\right] + \left[\frac{1}{2\pi x_a^2} + \frac{1}{4\pi}\left(1 - \frac{1}{2L}\right)\right]\boldsymbol{P}_{(+)} + \mathcal{O}(x_a^2)\,, \quad (3.261)$$

where we have employed that $X^2 = x_a^2/c_a^2 + O(x_a^4)$ and defined

$$\boldsymbol{P}_a = \begin{pmatrix} 1 & 0 \\ -\frac{s_a}{c_a} & 0 \end{pmatrix}\,. \qquad (3.262)$$

Notice that we have dropped phenomenological irrelevant terms of $\mathcal{O}(\epsilon) \sim 10^{-16}$, which we will also do in the following.

It is also useful to have an analytic expression for the zero-mode contribution to (3.253) alone

$$\boldsymbol{\Pi}_a(t,t') \equiv \frac{\vec{\chi}_0^a(t)\,\vec{\chi}_0^{a\,T}(t')}{x_a^2}\,. \qquad (3.263)$$

With the help of (3.207) and (3.208), we obtain

$$\boldsymbol{\Pi}_a(t,t') = -\frac{L}{4\pi}\left[\boldsymbol{P}_a\,t^2 + \boldsymbol{P}_a^T\,t'^2\right]$$
$$+ \left[\frac{1}{2\pi x_a^2} + \frac{1}{4\pi}\left(1 - \frac{1}{L} + t^2\left(\frac{1}{2} - \ln t\right) + t'^2\left(\frac{1}{2} - \ln t'\right)\right)\right]\boldsymbol{P}_{(+)} + \mathcal{O}(x_a^2)\,. \qquad (3.264)$$

Comparing (3.261) to (3.264), we infer that all the L-enhanced terms in $\boldsymbol{\Sigma}_a^{(1)}(t,t')$, besides the non-factorizable term proportional to $t_<^2$, arise from the zero-mode contribution $\boldsymbol{\Pi}_a(t,t')$. Factorizable contributions due to the $W^\pm$- and Z-boson zero-modes are thus enhanced by the logarithm of the inverse warp factor with respect to the contributions from the tower of KK excitations [1]. The term $t_<^2$ reflects the full 5D structure of the RS model, which is lost when considering only a few low-lying KK modes [157].

To obtain the corresponding results for the weak gauge bosons of the *minimal RS model*, one just needs to replace the two component profile vectors to start with in (3.253) by the simple profiles χ_n^a of the minimal model, see (3.49), and to use the appropriate relations of the minimal model. However, it is easy to see that the corresponding sum is already contained in the upper left element of $\boldsymbol{\Sigma}_a^{(1)}$ (3.261)

$$\Sigma_a^{(1)\,\text{min}} = \left(\boldsymbol{\Sigma}_a^{(1)}\right)_{11}\,. \qquad (3.265)$$

For the case of the photon and gluon, which possess massless zero modes, the ground state

with $x_{\gamma,g} = 0$ must be subtracted from the sum. We find

$$\sideset{}{'}\sum_{n} \frac{\chi_n(t)\,\chi_n(t')}{x_n^2} = \frac{1}{4\pi}\left[L\,t_<^2 - t^2\left(\frac{1}{2} - \ln t\right) - t'^2\left(\frac{1}{2} - \ln t'\right) + \frac{1}{2L}\right], \tag{3.266}$$

where the prime on the sum indicates that n runs from 1 to ∞, *i.e.*, the zero mode contribution is missing. Notice that the terms proportional to t^2 and t'^2 in the "massive" sum (3.261) are enhanced by a factor L, whereas this is not the case for the "massless" sum (3.266). This fact has important consequences for the phenomenology of flavor-violating processes (see [213]). It implies that in the RS model the NP contributions to $\Delta F = 2$ processes, such as K–$\bar{K}$ or B–$\bar{B}$ mixing, are dominated by the tree-level exchange of KK gluons, while those to $\Delta F = 1$ processes, such as rare meson decays, arise predominantly from the FCNC couplings of the Z-boson zero-mode.

It is possible to extend the procedure presented above in an iterative way to sums with $N > 1$ in (3.253). For example, for $N = 2$ we get

$$\begin{aligned}
\Sigma_a^{(2)\,\mathrm{min}}(t,t') = {}& \frac{1}{2\pi x_a^4} + \frac{1}{4\pi x_a^2}\left(1 - \frac{1}{L}\right) - \frac{1}{32\pi}\left(L - 5 + \frac{29}{4L} - \frac{3}{L^2}\right) \\
& - \left[\frac{1}{4\pi x_a^2} + \frac{1}{8\pi}\left(1 - \frac{1}{2L}\right)\right]\left[t^2\left(L - \frac{1}{2} + \ln t\right) + t'^2\left(L - \frac{1}{2} + \ln t'\right)\right] \\
& + \frac{L}{32\pi}\left[t_>^4 + 4t^2 t'^2\left(L - \frac{1}{2} + \ln t_<\right)\right] + \mathcal{O}\left(x_a^2\right),
\end{aligned} \tag{3.267}$$

while for the massless case we arrive at

$$\begin{aligned}
\sideset{}{'}\sum_{n} \frac{\chi_n(t)\,\chi_n(t')}{x_n^4} = {}& \frac{1}{32\pi}\left(\frac{5}{8L} - \frac{1}{L^2}\right) \\
& - \frac{1}{32\pi}\left[t^4\left(L - \frac{5}{4} + \ln t\right) + \frac{2t^2}{L}\left(L - \frac{1}{2} + \ln t\right)\right] \\
& - \frac{1}{32\pi}\left[t'^4\left(L - \frac{5}{4} + \ln t'\right) + \frac{2t'^2}{L}\left(L - \frac{1}{2} + \ln t'\right)\right] \\
& + \frac{1}{32\pi}\left[L\,t_>^4 + 4t^2 t'^2\left[L\ln t_< - \left(L - \frac{1}{2}\right)\left(\ln tt' - \frac{1}{2}\right) - \ln t\ln t'\right]\right].
\end{aligned} \tag{3.268}$$

The analytic results presented here are phenomenologically quite important, since they allow for a clear understanding of the structure of $\Delta F = 1$ and $\Delta F = 2$ FCNC interactions, mediated by towers of KK modes.

3.6 Four-Fermion Charged-Current Interactions

With the help of the low energy expansion derived in the last section, we are able to integrate out the complete towers of the $W^{\pm}$-bosons and their KK excitations and to derive the induced effective four-fermion interactions, for the minimal as well as for the custodial model, see
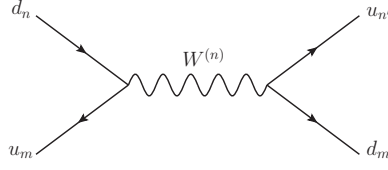
Figure 3.12:   Four-fermion interactions due to the exchange of the $W^\pm$-bosons and their KK excitations.

Figure 3.12. The effective Hamiltonian reads

$$
\mathcal{H}_{\text{eff}}^{(W)} = 2\sqrt{2}\, G_F \Big\{ \big[\, \bar{u}_{m_L} \gamma_\mu (\mathbf{V}_L)_{mn} d_{n_L} + \bar{u}_{m_R} \gamma_\mu (\mathbf{V}_R)_{mn} d_{n_R} \big]
$$
$$
\otimes\, \big[\, \bar{d}_{m'_L} \gamma^\mu (\mathbf{V}_L^\dagger)_{m'n'} u_{n'_L} + \bar{d}_{m'_R} \gamma^\mu (\mathbf{V}_R^\dagger)_{m'n'} u_{n'_R} \big](+\text{h.c.}) \Big\}, \tag{3.269}
$$

where $m, n, m', n' \in \{1, 2, 3\}$ and a summation over the flavor indices is understood. The tensor symbol merely indicates that the full analytic result contains terms that can not be separated into independent matrix products. This is due to the sum over $W^\pm$-boson profiles (3.261), which contains a term $\propto t_<^2$ that prevents a factorization into separate vertex factors.

The elements of the mixing matrices $\mathbf{V}_{L,R}$ are computed with the help of this expression, as well as the currents (3.228) and the respective simpler expressions for the minimal model. Including corrections up to $\mathcal{O}(v^2/M_{\text{KK}}^2)$, we obtain

$$
(\mathbf{V}_L)_{mn} \otimes (\mathbf{V}_L^\dagger)_{m'n'} = \left(\Delta_{mn}^{+Q} + \sqrt{2}\, \varepsilon_{mn}^{+q} \right) \left(\Delta_{n'm'}^{+Q} + \sqrt{2}\, \varepsilon_{n'm'}^{+q} \right)^*
$$
$$
- \frac{m_W^2}{2M_{\text{KK}}^2} L \left[\left(\bar{\Delta}_{mn}^{+Q} + \sqrt{2}\, \bar{\varepsilon}_{mn}^{+q} \right) \left(\Delta_{n'm'}^{+Q} + \sqrt{2}\, \varepsilon_{n'm'}^{+q} \right)^* \right.
$$
$$
+ \left(\Delta_{mn}^{+Q} + \sqrt{2}\, \varepsilon_{mn}^{+q} \right) \left(\bar{\Delta}_{n'm'}^{+Q} + \sqrt{2}\, \bar{\varepsilon}_{n'm'}^{+q} \right)^*
$$
$$
\left. - \left(\Delta_{mn}^{UD} + \sqrt{2}\, \varepsilon_{mn}^{ud} \right) \otimes \left(\Delta_{m'n'}^{DU} + \sqrt{2}\, \varepsilon_{m'n'}^{du} \right) \right], \tag{3.270}
$$

where the other combinations are obtained by the replacements

$$
\mathbf{V}_L \to \mathbf{V}_R: \quad \Delta \leftrightarrow \varepsilon, \tag{3.271}
$$

and, for the *custodial model*,

$$
\Delta_{mn}^{+Q,q} = \frac{2\pi}{L\epsilon} \int_\epsilon^1 dt\, \vec{a}_m^{U,u\dagger}\, \boldsymbol{C}_m^{U,u}(t)\, \boldsymbol{\Omega}^{Q,q}\, \boldsymbol{C}_n^{D,d}(t)\, \vec{a}_n^{D,d},
$$

$$
\bar{\Delta}_{mn}^{+Q,q} = \frac{2\pi}{L\epsilon} \int_\epsilon^1 dt\, t^2\, \vec{a}_m^{U,u\dagger}\, \boldsymbol{C}_m^{U,u}(t)\, \bar{\boldsymbol{\Omega}}^{Q,q}\, \boldsymbol{C}_n^{D,d}(t)\, \vec{a}_n^{D,d},
$$

$$
\Delta_{mn}^{UD} \otimes \Delta_{m'n'}^{du} = \left(\frac{2\pi}{L\epsilon} \right)^2 \int_\epsilon^1 dt \int_\epsilon^1 dt'\, t_<^2 \left(\vec{a}_m^{U\dagger}\, \boldsymbol{C}_m^U(t)\, \tilde{\boldsymbol{\Omega}}^Q\, \boldsymbol{C}_n^D(t)\, \vec{a}_n^D \right) \otimes \left(\vec{a}_{m'}^{d\dagger}\, \boldsymbol{C}_{m'}^d(t')\, \tilde{\boldsymbol{\Omega}}^{q\dagger}\, \boldsymbol{C}_{n'}^u(t')\, \vec{a}_{n'}^u \right),
$$

$$
\text{etc.} \tag{3.272}
$$

Note that in the last integrals $(a + b) \otimes (c + d) \equiv ac + bd$ and the corresponding expressions with $\Delta \to \epsilon$ are obtained by the replacements $\boldsymbol{C}_n^A \to \boldsymbol{S}_n^A$, $A = U, D, u, d$ at the appropriate places. Moreover

$$
\boldsymbol{\Omega}^Q = \begin{pmatrix} 1 \\ 0 \end{pmatrix}, \quad \boldsymbol{\Omega}^q = \begin{pmatrix} 0 & 0 \\ 0 & 1 \\ 0 & 0 \end{pmatrix}, \quad \bar{\boldsymbol{\Omega}}^Q = \begin{pmatrix} 1 \\ -\dfrac{g_R^2}{g_L^2} \, 1 \end{pmatrix}, \quad \bar{\boldsymbol{\Omega}}^q = \begin{pmatrix} 0 & 0 \\ 0 & 1 \\ -\dfrac{g_R^2}{g_L^2} \, 1 & 0 \end{pmatrix},
$$

$$
\tilde{\boldsymbol{\Omega}}^Q = \begin{pmatrix} 1 \\ \dfrac{g_R}{g_L} \, 1 \end{pmatrix}, \quad \tilde{\boldsymbol{\Omega}}^q = \begin{pmatrix} 0 & 0 \\ 0 & 1 \\ \dfrac{g_R}{g_L} \, 1 & 0 \end{pmatrix}.
$$

$$(3.273)$$

Notice that in [2], the simplifying assumption of an interaction with leptons featuring SM-couplings at one vertex was made, whereas here we have included deviations from the SM at both vertices.

For the semileptonic case we assume all the left- and right-handed 5D lepton fields to have the same bulk mass parameters and to be localized sufficiently close to the UV brane so as not to violate the constraints imposed by the electroweak precision tests. Then, the interactions of the lepton zero modes with the $W^{\pm}$ boson and its KK excitations are flavor universal and the deviations from the SM are numerically insignificant. In that case, the right hand side of the tensor structure in (3.269) reduces to a SM leptonic current $\sum_l (\bar{l}_L \gamma^\mu \nu_{lL})$ and the remaining (factorizing) quark transition is described by the left- and right-handed "CKM-matrices"

$$
\begin{aligned}
\boldsymbol{V}_L &= \boldsymbol{\Delta}^{+Q} + \sqrt{2}\,\boldsymbol{\varepsilon}^{+q} - \frac{m_W^2}{2M_{\text{KK}}^2} L \left(\bar{\boldsymbol{\Delta}}^{+Q} + \sqrt{2}\,\bar{\boldsymbol{\varepsilon}}^{+q} \right), \\
\boldsymbol{V}_R &= \sqrt{2}\,\boldsymbol{\Delta}^{+q} + \boldsymbol{\varepsilon}^{+Q} - \frac{m_W^2}{2M_{\text{KK}}^2} L \left(\sqrt{2}\,\bar{\boldsymbol{\Delta}}^{+q} + \bar{\boldsymbol{\varepsilon}}^{+Q} \right).
\end{aligned}
$$

$$(3.274)$$

The definition of the CKM matrix as $\boldsymbol{V}_L$ accounts for the fact that in four-fermion interactions one automatically measures the effect of the entire towers of $W^{\pm}$ bosons and their KK excitations. Thus the experimentally determined CKM-matrix elements rather correspond to those of the matrix $\boldsymbol{V}_L$, and not $\tilde{\boldsymbol{V}}_L$ (3.159) (if the RS setup is realized). This differs from the definition of the CKM matrix employed in [1, 242], which is based on the $W u_L^i d_L^j$ and $W u_R^i d_R^j$ vertices.

Note that above we have absorbed a universal factor $(1 + m_W^2/(2M_{\text{KK}}^2)(1 - 1/(2L)))$ into the Fermi constant G_F in (3.269), due to the normalization to muon decay, from which G_F is extracted, see Section 5.1.1. This factor is independent of the (possibly extended) gauge group. Proceeding in this way renders the individual factors in the combination $G_F \boldsymbol{V}_{L,R}$ physically observable.

From the formulae (3.270) it is evident that no custodial protection mechanism is at work in the charged-current sector. This is due to the embedding of the up-type quarks in (3.209) and has already been pointed out in [239]. The leading contribution to $(V_L)_{mn}$ stems from Δ_{mn}^{+Q}, which is unitary to very good approximation. Corrections of order v^2/M_{KK}^2 arise from

the non-universality of KK gauge boson couplings encoded in $\bar{\Delta}_{mn}^{+Q}$ as well as the admixture from U' and D' quarks described by ϵ_{mn}^{+q}. Contributions arising from the admixture of U, D, and u' quarks are of order v^4/M_{KK}^4 and will be neglected in the following. The full expression for $\boldsymbol{V}_L$, obtained by employing the ZMA, is given by

$$
\begin{aligned}
\boldsymbol{V}_L = \boldsymbol{U}_u^\dagger \Bigg[\boldsymbol{1} &- \frac{m_W^2}{2M_{\mathrm{KK}}^2}\, L\, \mathrm{diag}\bigg(\frac{F^2(c_{Q_i})}{3+2c_{Q_i}} \bigg) \\
&+ \frac{v^2}{2M_{\mathrm{KK}}^2}\, \mathrm{diag}\big(F(c_{Q_i})\big)\, \boldsymbol{Y}_d\, \mathrm{diag}\big(F^{-2}(-c_{\mathcal{T}_{1i}})\big)\, \boldsymbol{Y}_d^\dagger\, \mathrm{diag}\big(F(c_{Q_i})\big) \Bigg] \boldsymbol{U}_d\,,
\end{aligned}
\tag{3.275}
$$

which is obviously not unitary. Note that this matrix agrees with the matrix $\tilde{\boldsymbol{V}}_L$, defined in (3.159) only to leading order

$$
\boldsymbol{V}_L = \tilde{\boldsymbol{V}}_L + \mathcal{O}(v^2/M_{\mathrm{KK}}^2)\,. \tag{3.276}
$$

As far as $(V_R)_{mn}$ is concerned, the dominant contribution is given by ϵ_{mn}^{+Q}, which is suppressed both by v^2/M_{KK}^2 and a chiral factor $m_m^u m_n^d/v^2$. The chiral suppression present in each of the terms contributing to $\boldsymbol{V}_R$ reflects the mere fact that they all originate from quark mixing. As a result, right-handed charged-current interactions are small in RS models.

In the *minimal RS model* the expressions above will be modified. First, the $\boldsymbol{\varepsilon}$ matrices in (3.270) will not be present (however the replacement rules below still apply). This means also that in $\boldsymbol{V}_L$ ($\boldsymbol{V}_R$) in (3.274) the $\boldsymbol{\varepsilon}^{+q}$ and $\bar{\boldsymbol{\varepsilon}}^{+q}$ ($\boldsymbol{\Delta}^{+q}$ and $\bar{\boldsymbol{\Delta}}^{+q}$) contributions are not present. Moreover, the profiles appearing under the integrals (3.272) are now given by those of the minimal model (3.77). The same holds true for the flavor-mixing vectors $\vec{a}_n^A$, which are now three-component vectors. Finally, the $\boldsymbol{\Omega}$ matrices are replaced by the identity $\boldsymbol{\Omega}, \bar{\boldsymbol{\Omega}}, \tilde{\boldsymbol{\Omega}} \to \boldsymbol{1}_{3\times3}$. As a consequence, the third term in the ZMA expression (3.275) is not present in the minimal RS model. However, identifying the whole expression (3.275) with the experimentally determined CKM matrix, such a deviation will not be observable in measuring single CKM matrix elements. In Appendix B.5 we will give ZMA expressions for the charged current four-fermion interactions, after having identified factorizable contributions with measured CKM matrix elements. We will study the impact of the mentioned unitarity violation briefly in Section 5.2.1.

The four-fermion interactions resulting from the exchange of the remaining SM gauge boson and their KK partners can be worked out similarly from the formulae of Section 3.5. For the minimal RS variant they can be found in [213].

3.7 Fermion Couplings to the Higgs Boson

In the SM, the couplings of matter and gauge fields to the Higgs boson are directly proportional to their masses, due to the mechanism of EWSB, see Section 1.1.2. Thus they are flavor diagonal in the mass basis. However, within RS models, this is not true anymore [244]. As the fields receive masses from couplings to the Higgs sector, as well as from compactification, a misalignment between the masses and the Yukawa couplings is present, leading for example to FCNCs at tree level. As they will be important for the following analyses, we will now discuss the Higgs-couplings in RS models in detail.

Working in unitary gauge, we first identify the relevant terms in the 4D Yukawa Lagrangian, describing the couplings of the Higgs boson to quarks. They read

$$\mathcal{L}_{4\mathrm{D}} \ni - \sum_{q,m,n} (g_h^q)_{mn}\, h\, \bar{q}_L^m\, q_R^n + \mathrm{h.c.}\,, \tag{3.277}$$

where the couplings $(g_h^q)_{mn}$ are given by

$$(g_h^q)_{mn} = \frac{\sqrt{2}\,\pi}{L} \int_{-\pi}^{\pi} d\phi\, \delta(|\phi| - \pi)\, e^{\sigma(\phi)} \Big[\vec{a}_m^{Q\dagger}\, \boldsymbol{C}_m^Q(\phi) \boldsymbol{Y}_{\bar{q}}\, \boldsymbol{C}_n^q(\phi)\, \vec{a}_n^q + \vec{a}_m^{q\,\dagger}\, \boldsymbol{S}_m^q(\phi) \boldsymbol{Y}_{\bar{q}}^\dagger\, \boldsymbol{S}_n^Q(\phi)\, \vec{a}_n^Q \Big]. \tag{3.278}$$

Note that this equation, as well as the following derivations, hold for both the custodial as well as for the minimal RS variants. By making use of the EOMs one can eliminate the term bi-linear in the Z_2-even profiles from (3.278) and express the tree-level Higgs FCNCs solely in terms of overlap integrals involving Z_2-odd fields.

Defining the misalignment $(\Delta g_h^q)_{mn}$ between the SM masses and the Yukawa couplings via

$$(g_h^q)_{mn} \equiv \delta_{mn}\, \frac{m_m^q}{v} - (\Delta g_h^q)_{mn}\,, \tag{3.279}$$

it is easy to show that

$$(\Delta g_h^q)_{mn} = \frac{m_m^q}{v}\, (\Phi_q)_{mn} + (\Phi_Q)_{mn}\, \frac{m_n^q}{v} + (\Delta \tilde{g}_h^q)_{mn}\,, \tag{3.280}$$

where in t-notation

$$(\Phi_q)_{mn} = \frac{2\pi}{L\epsilon} \int_\epsilon^1 dt\, \vec{a}_m^{Q\dagger}\, \boldsymbol{S}_m^Q(t)\, \boldsymbol{S}_n^Q(t)\, \vec{a}_n^Q\,, \qquad (\Phi_Q)_{mn} = \frac{2\pi}{L\epsilon} \int_\epsilon^1 dt\, \vec{a}_m^{q\dagger}\, \boldsymbol{S}_m^q(t)\, \boldsymbol{S}_n^q(t)\, \vec{a}_n^q\,, \tag{3.281}$$

and

$$(\Delta \tilde{g}_h^q)_{mn} = -\sqrt{2}\, \frac{2\pi}{L\epsilon} \int_\epsilon^1 dt\, \delta(t-1)\, \vec{a}_m^{q\,\dagger}\, \boldsymbol{S}_m^q(t)\, \boldsymbol{Y}_{\bar{q}}^\dagger \boldsymbol{S}_n^Q(t)\, \vec{a}_n^Q\,. \tag{3.282}$$

The latter contribution is induced only by operators of the form $(Y_q^{(5\mathrm{D})})_{ij} \big(\bar{Q}_R^i\big)_{a\alpha} q_L^{cj}\, \Phi_{a\alpha}$, containing Z_2-odd fields evaluated at the boundary of the extra dimension. In order to evaluate $(\Delta \tilde{g}_h^q)_{mn}$ one has to regularize the δ-distribution appearing in (3.282) as explained in Section 3.2.2. Employing

$$\int_t^1 dt'\, \delta^\eta(t'-1) \left[\sinh\big(\bar{\theta}^\eta(t'-1)\boldsymbol{A}\big)\right]^2 = \frac{1}{2} \left[\sinh\big(\bar{\theta}^\eta(t-1)\, 2\boldsymbol{A}\big)\big(2\boldsymbol{A}\big)^{-1} - \bar{\theta}^\eta(t-1)\, \boldsymbol{1}\right], \tag{3.283}$$

we obtain the following regularization independent result

$$(\Delta \tilde{g}_h^q)_{mn} = \frac{1}{\sqrt{2}} \frac{2\pi}{L\epsilon} \frac{v^2}{3M_{\mathrm{KK}}^2}\, \vec{a}_m^{Q\dagger}\, \boldsymbol{C}_m^Q(1^-)\, \boldsymbol{Y}_{\bar{q}} \boldsymbol{Y}_{\bar{q}}^\dagger\, \boldsymbol{g}\left(\frac{v}{\sqrt{2}M_{\mathrm{KK}}} \sqrt{\boldsymbol{Y}_{\bar{q}} \boldsymbol{Y}_{\bar{q}}^\dagger}\right) \boldsymbol{Y}_{\bar{q}} \boldsymbol{C}_n^q(1^-)\, \vec{a}_n^q\,, \tag{3.284}$$

with

$$\boldsymbol{g}(\boldsymbol{A}) = \frac{3}{2} \left[\sinh\big(2\boldsymbol{A}\big)\big(2\boldsymbol{A}\big)^{-1} - \boldsymbol{1}\right] \big(\cosh\big(\boldsymbol{A}\big)\boldsymbol{A}\big)^{-2}\,. \tag{3.285}$$

It is also straightforward to express (3.284) in terms of the rescaled Yukawa matrices introduced in (3.86). Using

$$\frac{v}{\sqrt{2}M_{\mathrm{KK}}}\sqrt{\boldsymbol{Y}_{\vec{q}}\boldsymbol{Y}_{\vec{q}}^{\dagger}} = \tanh^{-1}\left(\frac{v}{\sqrt{2}M_{\mathrm{KK}}}\sqrt{\tilde{\boldsymbol{Y}}_{\vec{q}}\tilde{\boldsymbol{Y}}_{\vec{q}}^{\dagger}}\right),\tag{3.286}$$

we obtain

$$(\Delta\tilde{g}_h^q)_{mn} = \frac{1}{\sqrt{2}}\frac{2\pi}{L\epsilon}\frac{v^2}{3M_{\mathrm{KK}}^2}\,\vec{a}_m^{Q\,\dagger}\,\boldsymbol{C}_m^Q(1^-)\,\tilde{\boldsymbol{Y}}_{\vec{q}}\,\bar{\boldsymbol{Y}}_{\vec{q}}^{\dagger}\tilde{\boldsymbol{Y}}_{\vec{q}}\,\boldsymbol{C}_n^q(1^-)\,\vec{a}_n^q\,,\tag{3.287}$$

where

$$\bar{\boldsymbol{Y}}_{\vec{q}}^{\dagger} \equiv \tilde{\boldsymbol{Y}}_{\vec{q}}^{\dagger}\,\boldsymbol{h}\left(\frac{v}{\sqrt{2}M_{\mathrm{KK}}}\sqrt{\tilde{\boldsymbol{Y}}_{\vec{q}}\tilde{\boldsymbol{Y}}_{\vec{q}}^{\dagger}}\right),\quad \boldsymbol{h}(\boldsymbol{A}) = \frac{3}{2}\left[\boldsymbol{A}^{-2} + \tanh^{-1}\left(\boldsymbol{A}\right)\boldsymbol{A}^{-1}\left(1 - \boldsymbol{A}^{-2}\right)\right].\tag{3.288}$$

The relevant matrix-valued functions can be computed by diagonalizing the hermitian products $\tilde{\boldsymbol{Y}}_{\vec{q}}\tilde{\boldsymbol{Y}}_{\vec{q}}^{\dagger}$ and $\tilde{\boldsymbol{Y}}_{\vec{q}}^{\dagger}\tilde{\boldsymbol{Y}}_{\vec{q}}$ with the help of unitary matrices $\boldsymbol{\mathcal{U}}_{\vec{q}}$ and $\boldsymbol{\mathcal{V}}_{\vec{q}}$,

$$\tilde{\boldsymbol{Y}}_{\vec{q}}\tilde{\boldsymbol{Y}}_{\vec{q}}^{\dagger} = \boldsymbol{\mathcal{U}}_{\vec{q}}\,\tilde{\boldsymbol{y}}_{\vec{q}}\tilde{\boldsymbol{y}}_{\vec{q}}^{T}\,\boldsymbol{\mathcal{U}}_{\vec{q}}^{\dagger},\qquad \tilde{\boldsymbol{Y}}_{\vec{q}}^{\dagger}\tilde{\boldsymbol{Y}}_{\vec{q}} = \boldsymbol{\mathcal{V}}_{\vec{q}}\,\tilde{\boldsymbol{y}}_{\vec{q}}^{T}\tilde{\boldsymbol{y}}_{\vec{q}}\,\boldsymbol{\mathcal{V}}_{\vec{q}}^{\dagger}.\tag{3.289}$$

Here $\tilde{\boldsymbol{y}}_{\vec{q}}$ is, depending on the value of the index $\vec{q}$, a non-square matrix of dimension 3×6 or 6×9 (in the custodial model) containing the non-negative eigenvalues of $\sqrt{\tilde{\boldsymbol{Y}}_{\vec{q}}\tilde{\boldsymbol{Y}}_{\vec{q}}^{\dagger}}$ on its diagonal. It follows that

$$\tilde{\boldsymbol{Y}}_{\vec{q}}\bar{\boldsymbol{Y}}_{\vec{q}}^{\dagger}\tilde{\boldsymbol{Y}}_{\vec{q}} = \boldsymbol{\mathcal{U}}_{\vec{q}}\,\tilde{\boldsymbol{y}}_{\vec{q}}\,\tilde{\boldsymbol{y}}_{\vec{q}}^{T}\,\boldsymbol{h}\left(\frac{v}{\sqrt{2}M_{\mathrm{KK}}}\sqrt{\tilde{\boldsymbol{y}}_{\vec{q}}\tilde{\boldsymbol{y}}_{\vec{q}}^{T}}\right)\tilde{\boldsymbol{y}}_{\vec{q}}\boldsymbol{\mathcal{V}}_{\vec{q}}^{\dagger}.\tag{3.290}$$

Note finally that the Yukawa matrices introduced in (3.86) and (3.288) satisfy $\tilde{\boldsymbol{Y}}_{\vec{q}} = \boldsymbol{Y}_{\vec{q}} + \mathcal{O}(v^2/M_{\mathrm{KK}}^2)$ and $\bar{\boldsymbol{Y}}_{\vec{q}}^{\dagger} = \boldsymbol{Y}_{\vec{q}}^{\dagger} + \mathcal{O}(v^2/M_{\mathrm{KK}}^2)$. In consequence, as long as one is interested in the ZMA results for $(\Delta\tilde{g}_h^q)_{mn}$ only, one can replace $\tilde{\boldsymbol{Y}}_{\vec{q}}\bar{\boldsymbol{Y}}_{\vec{q}}^{\dagger}\tilde{\boldsymbol{Y}}_{\vec{q}}$ by the combination $\boldsymbol{Y}_{\vec{q}}\boldsymbol{Y}_{\vec{q}}^{\dagger}\boldsymbol{Y}_{\vec{q}}$ of original Yukawa matrices.

It will be useful to derive ZMA results for the elements $(\Delta g_h^q)_{mn}$. For this purpose, we still need the $\mathcal{O}(v^2/M_{\mathrm{KK}}^2)$ expressions for the rescaled eigenvectors $\hat{a}_n^A$ with $A = u, u', u^c, U', U$ in the custodial RS model. First note that the relations (3.242), (3.244), and (3.246) to (3.248) also hold in the up-type quark sector after the replacements $d \to u$, $D \to u^c$, $c_{\mathcal{T}_{2i}} \to c_{u_i^c}$ with $\boldsymbol{\lambda}_u = \sqrt{2}/v\,\mathrm{diag}\,(m_u, m_c, m_t)$. The remaining $\hat{a}_n^A$ are found to satisfy

$$\hat{a}_n^{u'} = x_n\,\mathrm{diag}\left(F^{-1}(-c_{Q_i})\,F^{-1}(c_{Q_i})\right)\hat{a}_n^u\,,$$

$$\hat{a}_n^{U'} = \mathrm{diag}\left(F(-c_{\mathcal{T}_{2i}})\,F^{-1}(-c_{\mathcal{T}_{1i}})\right)\hat{a}_n^U\,,\tag{3.291}$$

$$\hat{a}_n^{U} = \frac{x_n}{\sqrt{2}}\,\mathrm{diag}\left(F^{-1}(-c_{\mathcal{T}_{2i}})\right)\boldsymbol{Y}_d^{\dagger}\left[\boldsymbol{Y}_u^{\dagger}\right]^{-1}\mathrm{diag}\left(F^{-1}(c_{u_i^c})\right)\hat{a}_n^{u^c}\,.$$

It is also easy to show that the eigenvectors satisfy the sum rules

$$\hat{a}_n^{u^c\,\dagger}\hat{a}_n^{u^c} + \hat{a}_n^{u'\,\dagger}\hat{a}_n^{u'} = 1\,,\qquad \hat{a}_n^{u\,\dagger}\hat{a}_n^{u} + \hat{a}_n^{U\,\dagger}\hat{a}_n^{U} + \hat{a}_n^{U'\,\dagger}\hat{a}_n^{U'} = 1\,.\tag{3.292}$$

With these relations at hand, it is straightforward to derive analytic expressions for the $\mathcal{O}(v^2/M_{\mathrm{KK}}^2)$ corrections to $\boldsymbol{\Phi}_q$, $\boldsymbol{\Phi}_Q$, and $\boldsymbol{\Delta\tilde{g}}_h^q$. Studying first the *custodial model,* we find in the case of down-type quarks,

$$\boldsymbol{\Phi}_d = \boldsymbol{x}_d\,\boldsymbol{U}_d^\dagger\,\mathrm{diag}\left[\frac{1}{1-2c_{Q_i}}\left(\frac{1}{F^2(c_{Q_i})}-1+\frac{F^2(c_{Q_i})}{3+2c_{Q_i}}\right)\right]\boldsymbol{U}_d\,\boldsymbol{x}_d\,,$$

$$\boldsymbol{\Phi}_D = \boldsymbol{x}_d\,\boldsymbol{W}_d^\dagger\,\mathrm{diag}\left[\frac{1}{1-2c_{\mathcal{T}_{2i}}}\left(\frac{1}{F^2(c_{\mathcal{T}_{2i}})}\left[1+\frac{1-2c_{\mathcal{T}_{2i}}}{F^2(-c_{\mathcal{T}_{1i}})}\right]-1+\frac{F^2(c_{\mathcal{T}_{2i}})}{3+2c_{\mathcal{T}_{2i}}}\right)\right]\boldsymbol{W}_d\,\boldsymbol{x}_d\,, \quad (3.293)$$

$$\boldsymbol{\Delta\tilde{g}}_h^d = \frac{\sqrt{2}\,v^2}{3M_{\mathrm{KK}}^2}\,\boldsymbol{U}_d^\dagger\,\mathrm{diag}\left[F(c_{Q_i})\right]\boldsymbol{Y}_d\boldsymbol{Y}_d^\dagger\boldsymbol{Y}_d\,\mathrm{diag}\left[F(c_{\mathcal{T}_{2i}})\right]\boldsymbol{W}_d\,,$$

while for up-type quarks we obtain

$$\boldsymbol{\Phi}_u = \boldsymbol{x}_u\,\boldsymbol{U}_u^\dagger\,\mathrm{diag}\left[\frac{1}{1-2c_{Q_i}}\left(\frac{1}{F^2(c_{Q_i})}\left[1+\frac{1-2c_{Q_i}}{F^2(-c_{Q_i})}\right]-1+\frac{F^2(c_{Q_i})}{3+2c_{Q_i}}\right)\right]\boldsymbol{U}_u\,\boldsymbol{x}_u\,,$$

$$\boldsymbol{\Phi}_U = \boldsymbol{x}_u\,\boldsymbol{W}_u^\dagger\left\{\mathrm{diag}\left[\frac{1}{1-2c_{u_i^c}}\left(\frac{1}{F^2(c_{u_i^c})}-1+\frac{F^2(c_{u_i^c})}{3+2c_{u_i^c}}\right)\right]+\frac{1}{2}\,\mathrm{diag}\left(F^{-1}(c_{u_i^c})\right)\boldsymbol{Y}_u^{-1}\,\boldsymbol{Y}_d\right.$$

$$\left.\times\,\mathrm{diag}\left(\frac{1}{F^2(-c_{\mathcal{T}_{2i}})}+\frac{1}{F^2(-c_{\mathcal{T}_{1i}})}\right)\boldsymbol{Y}_d^\dagger\left[\boldsymbol{Y}_u^\dagger\right]^{-1}\mathrm{diag}\left(F^{-1}(c_{u_i^c})\right)\right\}\boldsymbol{W}_u\,\boldsymbol{x}_u\,,$$

$$\boldsymbol{\Delta\tilde{g}}_h^u = \frac{\sqrt{2}\,v^2}{3M_{\mathrm{KK}}^2}\,\boldsymbol{U}_u^\dagger\,\mathrm{diag}\left[F(c_{Q_i})\right]\boldsymbol{Y}_u\boldsymbol{Y}_u^\dagger\boldsymbol{Y}_u\,\mathrm{diag}\left[F(c_{u_i^c})\right]\boldsymbol{W}_u\,,$$

$$(3.294)$$

with $\boldsymbol{x}_u \equiv \mathrm{diag}(m_u, m_c, m_t)/M_{\mathrm{KK}}$. Remember that $\boldsymbol{U}_u$ ($\boldsymbol{W}_u$) are the left- (right-)handed rotation matrices diagonalizing the effective up-type Yukawa coupling.

At this point some comments are in order. First, notice that the ZMA expressions in the *minimal model* can be obtained from the expressions above by dropping all terms involving the zero-mode profiles $F(-c_{\mathcal{T}_{1i}})$, $F(-c_{\mathcal{T}_{2i}})$, and $F(-c_{Q_i})$ and performing the replacements $c_{\mathcal{T}_{2i}} \to c_{d_i}$, $c_{u_i^c} \to c_{u_i}$. Note that $\boldsymbol{\Phi}_d$ is the same in both models. The corrections $\boldsymbol{\Delta\tilde{g}}_h^{d,u}$ have to be divided by a factor of 2 in the minimal model. The new terms in (3.293) and (3.294) arise from the admixture of the $\boldsymbol{S}_n^{\mathcal{T}_1(-)}(t)$, $\boldsymbol{S}_n^{\mathcal{T}_2(-)}(t)$, and $\boldsymbol{S}_n^{Q(-)}(t)$ profiles in the corresponding zero-mode wave functions. In each case, the suppression by v/M_{KK} due to the admixture is offset by the $\mathcal{O}(M_{\mathrm{KK}}/v)$ enhancement of the Z_2-odd $(-)$ profile relative to its $(+)$ counterpart. For $c_{Q_i} < 1/2$, the leading contribution in $\boldsymbol{\Phi}_u$ is numerically enhanced by a factor of 2 with respect to the minimal model. If the $Zd_L^i\bar{d}_L^j$ vertices are protected from fermion mixing by (3.251) and $c_{\mathcal{T}_{1i}} < 1/2$, then the same is true for $\boldsymbol{\Phi}_D$. Depending on the structure of the Yukawa matrices and bulk masses, a similar enhancement is possible in $\boldsymbol{\Phi}_U$. Notice that the extra suppression by factors of m_n^q/v in $\boldsymbol{\Phi}_{d,D,u,U}$ imply that for light quark flavors the Higgs-boson FCNCs arising from the latter terms are parametrically suppressed relative to those mediated by the exchange of a Z boson. This makes the chirally unsuppressed contributions $\boldsymbol{\Delta\tilde{g}}_h^{d,u}$, that arise from the Z_2-odd Yukawa couplings, the dominant sources of flavor violation in the Higgs sector. This has been pointed out in [203]. As far as the $\mathcal{O}(v^2/M_{\mathrm{KK}}^2)$ corrections to $\boldsymbol{\Delta\tilde{g}}_h^{d,u}$, as given in (3.293) and (3.294) are concerned, we find perfect agreement with the

results presented in the latter article for the case of a brane-localized Higgs sector. The results presented here generalize these findings to our exact treatment of KK profiles and thus to all orders in $v/M_{\rm KK}$, for both the minimal as well as the custodial RS model. Notice also that the factor of 1/3 arising in the ZMA expressions for $\boldsymbol{\Delta\tilde{g}}_h^{d,u}$ follows immediately if one applies (3.83) to a composite operator containing two Z_2-odd fermion fields.

A model-independent analysis of the flavor misalignment of the SM fermion masses and the Yukawa couplings has been presented in [245]. There it has been shown that, in models where the Higgs is a bound state of a new strongly-interacting theory, at the level of dimension six, chirally unsuppressed contributions to flavor-changing Higgs-boson vertices generically will arise from composite operators like $\bar{q}_L^i H q_R^j (H^\dagger H)$. If present, the latter terms will dominate over the chirally suppressed contributions originating from operators of the form $\bar{q}_L^i \slashed{D} q_L^j (H^\dagger H)$, because the couplings y_{q*} of the composite Higgs to the other strong interacting states can be as large as $y_{q*}^2/(16\pi^2) \gg m_q/v$. Notice that in our concrete model, considering all relevant dimension-six operators in lowest-order of the mass insertion approximation, leads to the ZMA results (3.293) and (3.294) quantifying the misalignment between the Yukawa couplings and the zero-mode masses (see [203] for a illuminating discussion). We emphasize that in our exact solution (3.279), (3.280), (3.281), and (3.287), all new-physics effects induced by the mass insertions are resummed to all orders in $v^2/M_{\rm KK}^2$ at tree level. Note that in the case of $\Delta F = 2$ processes, the importance of Higgs FCNCs turns out to be limited. The most pronounced effects occur in the case of the CP-violating parameter ϵ_K, but are still typically smaller than the corrections due to KK gluon exchange [246]. In Chapter 5 we will apply the results derived here to analyze $\Delta F = 1$ Higgs-couplings as well as the impact of the RS model on Higgs-boson production and decay at hadron colliders.

Chapter 4

5D Propagators

We have seen that particles in the presence of a compactified extra dimension can be described by towers of KK modes. Often it turns out to be easier to avoid the presence of these KK excitations as virtual particles in amplitudes and to work directly with the 5D fields. This evades the necessity of performing infinite sums over profiles (that just appeared due to the decomposition), weighted by 4D propagators, which can easily become impractical. In this section we will derive propagators of 5D gauge bosons, including their scalar components, and of fermions. While such propagators have been studied in the literature [162, 247, 248, 249, 250], we will include effects of EWSB, mediated by a boundary Higgs-scalar, as well as present for the first time analytic solutions that include the full flavor structure of the SM. The flavor mixing will be included in a completely general way. Our results will make calculations of loop-mediated flavor-changing processes in RS models, which in the KK picture involve multiple sums over fermion profiles, more feasible. The following formulae hold for the minimal RS variant, however, the generalization to the custodial model is straightforward.

4.1   Massive Gauge Bosons

The quadratic part of the gauge-boson action, which is the starting point to derive the corresponding 5D propagators, has already been given in 3.45, employing the gauge fixing (3.44). It is possible to retain this gauge-fixing Lagrangian in the 5D approach due to relations between the scalar fields, as discussed below (3.44). This will lead to a propagator that mixes the scalar components of the gauge fields with the brane-localized Goldstone bosons. However, for the following applications of the 5D propagators it will be sufficient and more convenient to follow [201] and to use the gauge fixing

$$
\begin{aligned}
\mathcal{L}_{\text{GF2}} = {} & -\frac{1}{2\xi}\left(\partial^\mu A_\mu - \xi\left[\frac{\partial_\phi\, e^{-2\sigma(\phi)}A_\phi}{r^2}\right]\right)^2 - \frac{1}{2\xi}\left(\partial^\mu Z_\mu - \xi\left[\frac{\partial_\phi\, e^{-2\sigma(\phi)}Z_\phi}{r^2}\right]\right)^2 \\
& - \frac{1}{\xi}\left(\partial^\mu W_\mu^+ - \xi\left[\frac{\partial_\phi\, e^{-2\sigma(\phi)}W_\phi^+}{r^2}\right]\right)\left(\partial^\mu W_\mu^- - \xi\left[\frac{\partial_\phi\, e^{-2\sigma(\phi)}W_\phi^-}{r^2}\right]\right) \\
& + \delta(|\phi|-\pi)\left[-\frac{1}{2\xi}\left(\partial^\mu Z_\mu - \frac{\xi}{r}M_Z\,\varphi^3\right)^2 - \frac{1}{\xi}\left(\partial^\mu W_\mu^+ - \frac{\xi}{r}M_W\,\varphi^+\right)\left(\partial^\mu W_\mu^- - \frac{\xi}{r}M_W\,\varphi^-\right)\right].
\end{aligned}
$$
(4.1)

This still eliminates mixed terms containing vector bosons and scalar fields. The quadratic terms in the resulting action, denoted by $\tilde{S}_{\text{gauge},2}$, follow from (3.45) by a proper replacement of the gauge fixing

$$\tilde{S}_{\text{gauge},2} = \int d^4x \, r \int_{-\pi}^{\pi} d\phi \left(\mathcal{L}_{\text{gauge},2} - \mathcal{L}_{\text{GF}} + \mathcal{L}_{\text{GF2}} \right). \tag{4.2}$$

When deriving the propagators corresponding to the fields present in the action (4.2), we have to be careful to take into account the non-trivial determinant of the RS metric in the right way in order to arrive at the correct covariant expressions in curved space-time.

4.1.1   Derivation of the Green's Functions

We start with the propagator for the vector components of the massive Z bosons, *i.e.*, the two point Green's function $D_{\mu\nu}(x_1, x_2, \phi_1, \phi_2) \equiv \langle Z_\mu(x_1, \phi_1) Z_\nu(x_2, \phi_2) \rangle$. Afterwards, we will turn to the scalar component. The propagators for the other gauge bosons can be derived in a similar way.

We perform a Fourier transformation to momentum space for the non-compactified 4D space-time but work in position space for the compactified direction. In this way we can easily impose the correct BCs at the orbifold fixed points and account for geometric overlaps with KK-decomposed fields at vertices. The sought position/momentum-space propagator, $\tilde{D}_{\nu\rho}(p, \phi, \phi')$, corresponding to a four-momentum transfer p^μ, is given by the solution to the differential equation

$$\left[-p^2 \eta^{\mu\nu} + (1 - \frac{1}{\xi}) p^\mu p^\nu - \partial_\phi \frac{e^{-2\sigma(\phi)}}{r^2} \partial_\phi \eta^{\mu\nu} \right.$$
$$\left. + \delta(|\phi| - \pi) \left(-\frac{1}{\xi} p^\mu p^\nu + \frac{M_Z^2}{r} \eta^{\mu\nu} \right) \right] \tilde{D}_{\nu\rho}(p, \phi, \phi') = \frac{i}{2r} \delta^\mu_\rho \, \delta(\phi - \phi'). \tag{4.3}$$

Note that the factor of $1/2$ on the right hand side above is necessary for the correct normalization on the orbifold. The ansatz [162]

$$\tilde{D}_{\mu\nu}(p, \phi, \phi') = -iG_p(\phi, \phi') \left(\eta_{\mu\nu} - \frac{p_\mu p_\nu}{p^2} \right) - iG'_p(\phi, \phi') \frac{p_\mu p_\nu}{p^2} \tag{4.4}$$

leads to

$$\delta^\mu_\rho \left(p^2 + \partial_\phi \frac{e^{-2\sigma(\phi)}}{r^2} \partial_\phi - \frac{M_Z^2}{r} \delta(|\phi| - \pi) \right) G_p(\phi, \phi')$$
$$- \frac{p^\mu p_\rho}{p^2} \left[\left(p^2 + \partial_\phi \frac{e^{-2\sigma(\phi)}}{r^2} \partial_\phi - \frac{M_Z^2}{r} \delta(|\phi| - \pi) \right) G_p(\phi, \phi') \right. \tag{4.5}$$
$$\left. - \left(\frac{p^2}{\xi} + \partial_\phi \frac{e^{-2\sigma(\phi)}}{r^2} \partial_\phi - \left(\frac{M_Z^2}{r} - \frac{p^2}{\xi} \right) \delta(|\phi| - \pi) \right) G'_p(\phi, \phi') \right] = \frac{1}{2r} \delta^\mu_\rho \, \delta(\phi - \phi').$$

It follows that $G'_p = \tilde{G}_{\frac{p}{\sqrt{\xi}}}$, where $\tilde{G}_p$ has exactly the same form as G_p in the bulk, but different

BCs on the IR brane.

The shape of the solution is now determined by

$$\left(p^2 + \partial_\phi \frac{e^{-2\sigma(\phi)}}{r^2} \partial_\phi - \frac{M_Z^2}{r} \delta(|\phi| - \pi) \right) G_p(\phi, \phi') = \frac{1}{2r} \delta(\phi - \phi'). \tag{4.6}$$

Switching to t coordinates, we arrive at

$$G_p(t, t') = N t_< t_> \left(A\, J_1(p/M_{\text{KK}}\, t_<) + B\, Y_1(p/M_{\text{KK}}\, t_<) \right) \\ \times \left(C\, J_1(p/M_{\text{KK}}\, t_>) + D\, Y_1(p/M_{\text{KK}}\, t_>) \right), \tag{4.7}$$

where, as before $t_< = \min(t, t')$ and $t_> = \max(t, t')$, and $p \equiv \sqrt{p^2}$. The correct normalization is obtained by matching the result to the δ-distribution on the right-hand side of (4.6). Integrating this equation over ϕ in an infinitesimal interval around $\phi = \phi'$ leads to

$$N = \frac{L}{4r(AD - BC)M_{\text{KK}}^2}. \tag{4.8}$$

The remaining coefficients are dictated by the BCs, which can also be determined from (4.6) and read (remember that the vector components are chosen to be even under the Z_2 parity)

$$\partial_{\phi_<} G_p \big|_{\phi_< = 0} = 0, \\ \partial_{\phi_>} G_p \big|_{\phi_> = \pi^-} = -\frac{rM_Z^2}{2\epsilon^2} G_p \big|_{\phi_> = \pi}. \tag{4.9}$$

This leads to

$$A = Y_0\left(p\epsilon/M_{\text{KK}} \right), \quad B = -J_0\left(p\epsilon/M_{\text{KK}} \right), \\ C = Y_0\left(p/M_{\text{KK}} \right) + \frac{M_Z^2}{2p\,\epsilon} Y_1\left(p/M_{\text{KK}} \right), \quad D = -J_0\left(p/M_{\text{KK}} \right) - \frac{M_Z^2}{2p\,\epsilon} J_1\left(p/M_{\text{KK}} \right). \tag{4.10}$$

For $\tilde{G}_p$ the same BCs hold with the replacement $M_Z^2 \to M_Z^2 - rp^2$ which translates into the same replacement in the coefficients C and D.

We now turn to the derivation of the propagator for the scalar components of the 5D gauge fields. From the action (4.2) we deduce

$$\left(p^2 + \frac{\xi}{r^2} \partial_\phi^2 e^{-2\sigma(\phi)} \right) \tilde{D}_{\phi\phi}(p, \phi, \phi') = i\frac{r}{2} e^{2\sigma(\phi)} \delta(\phi - \phi'). \tag{4.11}$$

Defining $\tilde{D}_{\phi\phi}(p, \phi, \phi') \equiv \frac{i}{\xi} \tilde{D}'_{5\frac{p}{\sqrt{\xi}}}(\phi, \phi')$ leads to

$$\left(p^2 + \frac{1}{r^2} \partial_\phi^2 e^{-2\sigma(\phi)} \right) \tilde{D}'_{5p}(\phi, \phi') = \frac{r}{2} e^{2\sigma(\phi)} \delta(\phi - \phi'). \tag{4.12}$$

The fully normalized solution can finally be written as

$$\tilde{D}'_{5p}(t,t') = \frac{L^2 k\, t_<^2 t_>^2}{4\pi(AD - BC)M_{\mathrm{KK}}^4} \left(A\, J_0(p/M_{\mathrm{KK}}\, t_<) + B\, Y_0(p/M_{\mathrm{KK}}\, t_<)\right)$$
$$\times \left(C\, J_0(p/M_{\mathrm{KK}}\, t_>) + D\, Y_0(p/M_{\mathrm{KK}}\, t_>)\right), \tag{4.13}$$

where the coefficients are derived from the (Dirichlet) BCs and read

$$A = Y_0\left(p\epsilon/M_{\mathrm{KK}}\right), \quad B = -J_0\left(p\epsilon/M_{\mathrm{KK}}\right),$$
$$C = Y_0\left(p/M_{\mathrm{KK}}\right), \quad D = -J_0\left(p/M_{\mathrm{KK}}\right). \tag{4.14}$$

4.1.2   Limits of the Propagators

In the following we discuss several limits in the momentum of the 5D propagators. For this purpose, we switch to the euclidean momentum, *i.e.*, we substitute $p^0 = ip_E^0$ and evaluate scalar products in euclidean space. The solutions (4.7) and (4.13) become

$$G_p(t,t') = \frac{k\, t_< t_>}{2(BC - AD)M_{\mathrm{KK}}^2} \left(A\, I_1(p_E/M_{\mathrm{KK}}\, t_<) + B\, K_1(p_E/M_{\mathrm{KK}}\, t_<)\right)$$
$$\times \left(C\, I_1(p_E/M_{\mathrm{KK}}\, t_>) + D\, K_1(p_E/M_{\mathrm{KK}}\, t_>)\right), \tag{4.15}$$

$$A = K_0\left(p_E\, \epsilon/M_{\mathrm{KK}}\right), \quad B = I_0\left(p_E\, \epsilon/M_{\mathrm{KK}}\right),$$
$$C = K_0\left(p_E/M_{\mathrm{KK}}\right) - \frac{M_Z^2}{2p_E\epsilon}K_1\left(p_E/M_{\mathrm{KK}}\right), \quad D = I_0\left(p_E/M_{\mathrm{KK}}\right) + \frac{M_Z^2}{2p_E\epsilon}I_1\left(p_E/M_{\mathrm{KK}}\right), \tag{4.16}$$

where $p_E \equiv \sqrt{p_E^2}$ and $M_Z^2 \to M_Z^2 - rp^2$ for $\tilde{G}_p$, as well as

$$\tilde{D}'_{5p}(t,t') = \frac{L^2 k\, t_<^2 t_>^2}{2\pi^2(BC - AD)M_{\mathrm{KK}}^4} \left(A\, I_0(p_E/M_{\mathrm{KK}}\, t_<) + B\, K_0(p_E/M_{\mathrm{KK}}\, t_<)\right)$$
$$\times \left(C\, I_0(p_E/M_{\mathrm{KK}}\, t_>) + D\, K_0(p_E/M_{\mathrm{KK}}\, t_>)\right), \tag{4.17}$$

$$A = K_0\left(p_E\, \epsilon/M_{\mathrm{KK}}\right), \quad B = -I_0\left(p_E\, \epsilon/M_{\mathrm{KK}}\right),$$
$$C = K_0\left(p_E/M_{\mathrm{KK}}\right), \quad D = -I_0\left(p_E/M_{\mathrm{KK}}\right). \tag{4.18}$$

Small Momenta

<u>Vectors:</u> The limit of $p_E \ll M_{\mathrm{KK}}$ is particularly interesting, since in that case the 5D gauge-boson propagator

$$\langle Z_\mu(x,\phi)Z_\nu(x',\phi')\rangle = \frac{1}{r}\sum_n \chi_n^Z(\phi)\,\chi_n^Z(\phi')\langle Z_\mu^{(n)}(x)Z_\nu^{(n)}(x')\rangle \tag{4.19}$$

is related to the KK sums derived in Section 3.5. The successive expansion of the expression $(-r\, G_p(\phi,\phi'))$ in p_E corresponds to the series of KK sums on the right hand side of (3.253).

In particular, the lowest order KK sum (3.265) will be given by the first term in the expansion

$$\sum_n \frac{\chi_n^Z(t)\,\chi_n^Z(t')}{m_n^2} = \Sigma_Z^{(1)\,\mathrm{min}} = \lim_{p_E \to 0} (-rG_p)\,. \tag{4.20}$$

We arrive at

$$G_p(t_<, t_>) \xrightarrow[p_E \ll M_{\mathrm{KK}}]{} -\frac{1}{M_Z^2} + \frac{L(t_>^2 - 1)}{4\pi r M_{\mathrm{KK}}^2}\,. \tag{4.21}$$

We emphasize that this is the *exact* result for the corresponding KK sum, *i.e.*, no higher order terms are missing, *c.f.* (3.261). For the massless case ($M_Z \to 0$) we get [162]

$$G_p(t_<, t_>) \xrightarrow[p_E \ll M_{\mathrm{KK}}]{} -\frac{1}{2\pi r p_E^2}, \tag{4.22}$$

and the next term in the p_E^2/M_{KK}^2 expansion reads

$$-\frac{1}{8\pi r M_{\mathrm{KK}}^2 L} + \frac{(t_<^2 + t_>^2 - 2t_<^2 \ln t_< - 2t_>^2 \ln t_> - 2L\, t_<^2)}{8\pi r M_{\mathrm{KK}}^2}\,. \tag{4.23}$$

This coincides with the KK sum (3.266). Note that, again, we neglect terms of $\mathcal{O}(\epsilon)$.

<u>Scalars:</u> The scalar propagator behaves like

$$\tilde{D}'_{5p}(t_<, t_>) \xrightarrow[p_E \ll M_{\mathrm{KK}}]{} \frac{L^2 t_<^2 t_>^2 \ln t_> \,(L + \ln t_<)}{2\pi r\, \pi^2 M_{\mathrm{KK}}^4}\,. \tag{4.24}$$

Large Momenta

<u>Vectors:</u> We first consider the limit $p_E \gg M_{\mathrm{KK}}$, but $p_E t_</M_{\mathrm{KK}} \ll 1$ and $p_E t_>/M_{\mathrm{KK}} \ll 1$, which means that the momenta are below the position-dependent cutoff, see (3.30). We arrive at

$$G_p(t_<, t_>) \to -\frac{L}{2\pi r p_E^2 \,(\ln(2k/p_E) - \gamma_e)}\,. \tag{4.25}$$

Note that the regions of momenta that fulfill the hierarchies quoted above get smaller and finally vanish, the closer the propagator is evaluated to the TeV brane. Therefore the expression is just applicable for large momenta near the Planck brane. On the TeV brane, the large-momentum limit $p_E \gg M_{\mathrm{KK}}$ (but still $p_E < k$) leads to

$$G_p(1, 1) \to -\frac{L}{2\pi r\, p_E\, M_{\mathrm{KK}}}\,. \tag{4.26}$$

The propagator changes to a $1/p_E$ behavior and thus cannot be trusted for $p_E \gg M_{\mathrm{KK}}$ on the TeV brane. Here, the theory has to be cut off in the TeV region, as discussed before. Finally, for $p_E \gg M_{\mathrm{KK}}$ and $p_E t_</M_{\mathrm{KK}} > 1$, $p_E t_>/M_{\mathrm{KK}} > 1$, the propagator becomes

$$G_p(t_<, t_>) \to -e^{-p_E \frac{(t_> - t_<)}{M_{\mathrm{KK}}}} \frac{L\sqrt{t_> t_<}}{4\pi\, r p_E\, M_{\mathrm{KK}}}, \tag{4.27}$$

and vanishes if $t_<$ and $t_>$ are well separated from each other.

Scalars: In the following we consider the scalar propagator in the limit of large momenta. For $p_E \gg M_{\mathrm{KK}}$, but $p_E\, t_</M_{\mathrm{KK}} \ll 1$ and $p_E\, t_>/M_{\mathrm{KK}} \ll 1$, the Green's function becomes

$$\tilde{D}'_{5p}(t_<,t_>) \to -\frac{L^3 t_>^2 t_<^2 (L + \ln(t_<))\left(\ln\left(\frac{p_E\, t_>}{2M_{\mathrm{KK}}}\right) + \gamma_e\right)}{2\pi r\, \pi^2 M_{\mathrm{KK}}^4\left(\ln\left(\frac{p_E}{2k}\right) + \gamma_e\right)} . \tag{4.28}$$

On the TeV brane it vanishes due to the BC, while for $p_E \gg M_{\mathrm{KK}}$ and $p_E\, t_</M_{\mathrm{KK}} > 1$, $p_E\, t_>/M_{\mathrm{KK}} > 1$ we arrive at

$$\tilde{D}'_{5p}(t_<,t_>) \to -e^{-p_E \frac{t_> - t_<}{M_{\mathrm{KK}}}}\frac{L^3\, t_>^{3/2} t_<^{3/2}}{4\pi r\pi^2 p_E\, M_{\mathrm{KK}}^3} . \tag{4.29}$$

The results derived here will be applied in Section 5.1.5 to calculate the anomalous magnetic moment of the muon in the RS setup.

4.2   Massive Fermions

We consider the 5D action for quarks as given in (3.72). The generalization to the lepton sector as well as to the custodial model is straightforward. First we introduce our notation. We merge the $SU(2)_L$ doublets Q and singlets q^c into 2-component vectors

$$\Omega_q \equiv \begin{pmatrix} Q \\ q^c \end{pmatrix}, \quad \bar{\Omega}_q \equiv \begin{pmatrix} \bar{Q} & \bar{q}^c \end{pmatrix}, \tag{4.30}$$

and introduce the projection operators

$$P^Q\, \Omega_q = \begin{pmatrix} Q \\ 0 \end{pmatrix}, \qquad P^q\, \Omega_q = \begin{pmatrix} 0 \\ q^c \end{pmatrix}, \tag{4.31}$$

acting on states in the doublet/singlet (representation) space. In matrix notation, corresponding to the basis introduced above, they read

$$P^Q = \begin{pmatrix} 1 & 0 \\ 0 & 0 \end{pmatrix}, \quad P^q = \begin{pmatrix} 0 & 0 \\ 0 & 1 \end{pmatrix}. \tag{4.32}$$

Furthermore we introduce the off-diagonal operators

$$P^{Qq} = \begin{pmatrix} 0 & 1 \\ 0 & 0 \end{pmatrix}, \quad P^{qQ} = \begin{pmatrix} 0 & 0 \\ 1 & 0 \end{pmatrix}, \tag{4.33}$$

which pick out the singlet and doublet component of Ω_q, respectively, and raise/lower it to the other position in the vector. The bilinear terms in the action (3.72) can now be written as

$$
\begin{aligned}
S_{\text{ferm},2} = \sum_{q^c=u^c,d^c} \int d^4x\, r \int_{-\pi}^{\pi} d\phi \bigg\{ & e^{-3\sigma(\phi)} \bar{\Omega}_q\, i\slashed{\partial}\, \Omega_q - \frac{e^{-2\sigma(\phi)}}{r} \bar{\Omega}_q\, \partial_\phi\, e^{-2\sigma(\phi)} \gamma^5\, \Omega_q \\
& - e^{-4\sigma(\phi)}\, \text{sgn}(\phi)\bar{\Omega}_q \left(P^Q \boldsymbol{M}_Q + P^q \boldsymbol{M}_{q^c} \right) \Omega_q \\
& - \delta^\eta(|\phi| - \pi)\, e^{-3\sigma(\phi)} \frac{\sqrt{2}\pi v}{L} \Big[\bar{\Omega}_u \left(\boldsymbol{Y}_u^C P^{Qq} + \boldsymbol{Y}_u^{S\dagger} P^{qQ} \right) P_R\, \Omega_u \\
& + \bar{\Omega}_d \left(\boldsymbol{Y}_d^C P^{Qq} + \boldsymbol{Y}_d^{S\dagger} P^{qQ} \right) P_R\, \Omega_d + \text{h.c.} \Big] \bigg\},
\end{aligned}
\tag{4.34}
$$

where $\Omega_{u,d} \equiv (u, u^c)^T$, $(d, d^c)^T$ and $\boldsymbol{M}_{q^c} \equiv \boldsymbol{M}_q$, defined before. The 4D Yukawa matrices $\boldsymbol{Y}_q^{C,S}$ describe the couplings of the Higgs doublet to Z_2-even and -odd fermions, respectively, normalized according to (3.75). Note that we will understand $Q \equiv (Q, 0)^T$ and $q \equiv (0, q)^T$ as two-component vectors in the following derivations.

4.2.1 Derivation of the Green's Functions

Before calculating the 5D propagator $\boldsymbol{G}_q(p, \phi, \phi') \equiv \langle \Omega_q(p, \phi)\bar{\Omega}_q(-p, \phi') \rangle$ with $q = u, d$ explicitly, let us have a look at the matrix structure of this object. As the following derivations will be similar for up-type and down-type quarks, we will drop the subscript q of the propagator from now on. First, $\boldsymbol{G}$ is a 2×2 matrix in representation space with projections $\boldsymbol{G}^{Qq} \equiv P^Q \boldsymbol{G} P^q = \langle Q\bar{q} \rangle$, etc. Second, it is a 2×2 matrix in Dirac space with $\boldsymbol{G}_{LR}^{Qq} \equiv P_L \boldsymbol{G}^{Qq} P_L = \langle Q_L \bar{q}_R \rangle$, etc. Furthermore, it is also a 3×3 matrix in flavor space. It is determined from

$$
\begin{aligned}
\bigg[& e^{\sigma(\phi)}\slashed{p} - \frac{e^{2\sigma(\phi)}}{r} \partial_\phi\, e^{-2\sigma(\phi)} \gamma^5 - \text{sgn}(\phi) \left(P^Q \boldsymbol{M}_Q + P^q \boldsymbol{M}_q \right) \\
& - \delta^\eta(|\phi| - \pi)\, e^{\sigma(\phi)} \frac{\sqrt{2}\pi v}{L} \Big(\left(\boldsymbol{Y}_q^C P^{Qq} + \boldsymbol{Y}_q^{S\dagger} P^{qQ} \right) P_R \\
& + \left(\boldsymbol{Y}_q^{C\dagger} P^{qQ} + \boldsymbol{Y}_q^S P^{Qq} \right) P_L \Big) \bigg] \boldsymbol{G}(\phi, \phi') = i \frac{e^{4\sigma(\phi)}}{2r} \delta(\phi - \phi') \boldsymbol{1},
\end{aligned}
\tag{4.35}
$$

where we have suppressed the dependence of $\boldsymbol{G}(\phi, \phi')$ on the four-momentum transfer and the index q now corresponds to up type singlets. Applying all possible combinations of projection operators introduced above from the left and the right on eq. (4.35), we arrive at four blocks of differential equations. Each of them contains four coupled equations for certain components of the propagator, while the four blocks are decoupled from each other. Note that the matrix equation above mixes different components in representation space, due to the Yukawa couplings. For example, $P^Q P^{Qq} \boldsymbol{G} P^Q = P^{Qq} \boldsymbol{G} P^Q$ belongs to the non-vanishing entry of $\boldsymbol{G}^{qQ}$, mediating off-diagonal transitions in representation space. However, it features

the corresponding entry in the upper-left corner. After employing the ansatz

$$\boldsymbol{G}^{QQ}_{LL}(t,t') \equiv iP^Q P_L \slashed{p}\, \boldsymbol{G}^{QQ}_{++}(t,t')\,, \qquad \boldsymbol{G}^{QQ}_{RL}(t,t') \equiv iP^Q P_R \boldsymbol{G}^{QQ}_{-+}(t,t')\,,$$
$$\boldsymbol{G}^{qQ}_{LL}(t,t') \equiv iP^{qQ} P_L \slashed{p}\, \boldsymbol{G}^{qQ}_{-+}(t,t')\,, \qquad \boldsymbol{G}^{qQ}_{RL}(t,t') \equiv iP^{qQ} P_R \boldsymbol{G}^{qQ}_{++}(t,t')\,,$$

(4.36)

the first block of equations becomes

$$\frac{t}{M_{\mathrm{KK}}}\boldsymbol{G}^{QQ}_{-+}(t,t') + (t\partial_t - 2 - \boldsymbol{c}_Q)\boldsymbol{G}^{QQ}_{++}(t,t') = \delta^\eta(t-1)\frac{v}{\sqrt{2}M_{\mathrm{KK}}}\boldsymbol{Y}^S_q \boldsymbol{G}^{qQ}_{-+}(t,t')\,,$$

$$\frac{tp^2}{M_{\mathrm{KK}}}\boldsymbol{G}^{QQ}_{++}(t,t') - (t\partial_t - 2 + \boldsymbol{c}_Q)\boldsymbol{G}^{QQ}_{-+}(t,t') = \delta^\eta(t-1)\frac{v}{\sqrt{2}M_{\mathrm{KK}}}\boldsymbol{Y}^C_q \boldsymbol{G}^{qQ}_{++}(t,t') + \frac{t^4}{\epsilon^4}\delta(t-t')t'\,,$$

$$\frac{t}{M_{\mathrm{KK}}}\boldsymbol{G}^{qQ}_{++}(t,t') + (t\partial_t - 2 + \boldsymbol{c}_q)\boldsymbol{G}^{qQ}_{-+}(t,t') = \delta^\eta(t-1)\frac{v}{\sqrt{2}M_{\mathrm{KK}}}\boldsymbol{Y}^{C\dagger}_q \boldsymbol{G}^{QQ}_{++}(t,t')\,,$$

$$\frac{tp^2}{M_{\mathrm{KK}}}\boldsymbol{G}^{qQ}_{-+}(t,t') - (t\partial_t - 2 - \boldsymbol{c}_q)\boldsymbol{G}^{qQ}_{++}(t,t') = \delta^\eta(t-1)\frac{v}{\sqrt{2}M_{\mathrm{KK}}}\boldsymbol{Y}^{S\dagger}_q \boldsymbol{G}^{QQ}_{-+}(t,t')\,,$$

(4.37)

where we have performed a transformation to the coordinate t. Remember the definition of the regularized δ-distribution (3.46) and that $\boldsymbol{c}_{Q,q} \equiv \pm \boldsymbol{M}_{Q,q}/k$. The first propagator in (4.36) mediates diagonal transitions in both representation space, as well as in chirality, the second is diagonal in representation space but off-diagonal in chirality, the third vice versa, and the fourth propagator is off-diagonal with respect to both spaces. The subscripts $+(-)$ denote even (odd) functions in t, t' with respect to the Z_2 parity on the orbifold. The corresponding propagator functions are still 3×3 matrices in flavor space, while the further matrix structure has been pulled out in terms of chirality projectors and the matrices defined in (4.32) and (4.33). The other three blocks of equations can be obtained from (4.37) by the replacements

$$Z_2 : + \leftrightarrow -\,, \quad (t\partial_t - 2) \to -(t\partial_t - 2)\,, \quad \boldsymbol{Y}^C_q \leftrightarrow \boldsymbol{Y}^S_q\,, \tag{4.38}$$

$$Z_2 : + \leftrightarrow -\,, \quad Q \leftrightarrow q\,, \quad \boldsymbol{c}_Q \leftrightarrow -\boldsymbol{c}_q\,, \quad \boldsymbol{Y}^C_q \leftrightarrow \boldsymbol{Y}^{S\dagger}_q\,, \tag{4.39}$$

$$Q \leftrightarrow q\,, \quad (t\partial_t - 2) \to -(t\partial_t - 2)\,, \quad \boldsymbol{c}_Q \leftrightarrow -\boldsymbol{c}_q\,, \quad \boldsymbol{Y}^{C,S}_q \to \boldsymbol{Y}^{C,S\dagger}_q\,, \tag{4.40}$$

where the first replacements (first two replacements in (4.39)) correspond to the indices of the ansatz, respectively, given by

$$\boldsymbol{G}^{QQ}_{RR}(t,t') \equiv iP^Q P_R \slashed{p}\, \boldsymbol{G}^{QQ}_{--}(t,t')\,, \qquad \boldsymbol{G}^{QQ}_{LR}(t,t') \equiv iP^Q P_L \boldsymbol{G}^{QQ}_{+-}(t,t')\,,$$
$$\boldsymbol{G}^{qQ}_{RR}(t,t') \equiv iP^{qQ} P_R \slashed{p}\, \boldsymbol{G}^{qQ}_{+-}(t,t')\,, \qquad \boldsymbol{G}^{qQ}_{LR}(t,t') \equiv iP^{qQ} P_L \boldsymbol{G}^{qQ}_{--}(t,t')\,,$$

(4.41)

$$\boldsymbol{G}^{qq}_{LL}(t,t') \equiv iP^q P_L \slashed{p}\, \boldsymbol{G}^{qq}_{--}(t,t')\,, \qquad \boldsymbol{G}^{qq}_{RL}(t,t') \equiv iP^q P_R \boldsymbol{G}^{qq}_{+-}(t,t')\,,$$
$$\boldsymbol{G}^{Qq}_{LL}(t,t') \equiv iP^{Qq} P_L \slashed{p}\, \boldsymbol{G}^{Qq}_{+-}(t,t')\,, \qquad \boldsymbol{G}^{Qq}_{RL}(t,t') \equiv iP^{Qq} P_R \boldsymbol{G}^{Qq}_{--}(t,t')\,,$$

(4.42)

$$\boldsymbol{G}^{qq}_{RR}(t,t') \equiv iP^q P_R \slashed{p}\, \boldsymbol{G}^{qq}_{++}(t,t')\,, \qquad \boldsymbol{G}^{qq}_{LR}(t,t') \equiv iP^q P_L \boldsymbol{G}^{qq}_{-+}(t,t')\,,$$
$$\boldsymbol{G}^{Qq}_{RR}(t,t') \equiv iP^{Qq} P_R \slashed{p}\, \boldsymbol{G}^{Qq}_{-+}(t,t')\,, \qquad \boldsymbol{G}^{Qq}_{LR}(t,t') \equiv iP^{Qq} P_L \boldsymbol{G}^{Qq}_{++}(t,t')\,.$$

(4.43)

In the following we will show explicitly how to solve the first block. The other components

of the propagator can be obtained with the help of the replacements (4.38)-(4.40), taking into account the correct boundary conditions. First note that the presence of the δ-distributions gives rise to discontinuities of some components of the propagator (or its derivative) at the boundaries (in the limit $\eta \to 0$) and at $t = t'$. For example $\boldsymbol{G}_{RL}^{QQ}(t, t')$ will jump at $t = t'$, whereas $\boldsymbol{G}_{LL}^{QQ}(t, t')$ will be continuous at that point while its derivative $\partial_t \boldsymbol{G}_{LL}^{QQ}(t, t')$ will jump. The behavior at the boundaries is similar to that of the KK modes in the decomposed theory and has already been discussed in Section 3.2.2. It is straightforwardly generalized to the 5D propagators. Combining the first two equations of block (4.37) decouples the system and leads to a second order differential equation in t for $\boldsymbol{G}_{++}^{QQ}(t, t')$, valid for $t \in (\epsilon, 1)$, $t \neq t'$, which reads

$$\left(t^2 \partial_t^2 - 4t\partial_t + t^2 \frac{p^2}{M_{\mathrm{KK}}^2} - \boldsymbol{c}_Q^2 + \boldsymbol{c}_Q + 6 \right) \boldsymbol{G}_{++}^{QQ} = 0. \tag{4.44}$$

The solution to this equation is given by

$$\boldsymbol{G}_{++}^{QQ}(t, t') = t^{5/2} \left(\mathrm{dg} \left(J_{c_{Q_i} - \frac{1}{2}}(p/M_{\mathrm{KK}} \, t) \right) \boldsymbol{a}_{++}^{QQ \, \gtrless}(t') + \mathrm{dg} \left(J_{-c_{Q_i} + \frac{1}{2}}(p/M_{\mathrm{KK}} \, t) \right) \boldsymbol{b}_{++}^{QQ \, \gtrless}(t') \right) \, (t \gtrless t'). \tag{4.45}$$

Note that, here and in the following $\mathrm{dg} \equiv \mathrm{diag}$. For the case of $c_{Q_i} = 1/2 + z$, $z \in \mathbb{Z}$, the solution has to be obtained from (4.45) by a limiting procedure. The propagator (4.45) depends on t' through the 3×3 coefficient matrices $\boldsymbol{a}_{++}^{QQ \, \gtrless}(t')$ and $\boldsymbol{b}_{++}^{QQ \, \gtrless}(t')$. These are to be determined from the BCs at the branes and the jump conditions at $t = t'$, which introduce the dependence on the second coordinate. They will be discussed in detail below. Similarly, we can derive second order equations for the other components present in (4.37), which leads to

$$\boldsymbol{G}_{-+}^{QQ}(t, t') = t^{5/2} \left(\mathrm{dg} \left(J_{-c_{Q_i} - \frac{1}{2}}(p/M_{\mathrm{KK}} \, t) \right) \boldsymbol{a}_{-+}^{QQ \, \gtrless}(t') + \mathrm{dg} \left(J_{c_{Q_i} + \frac{1}{2}}(p/M_{\mathrm{KK}} \, t) \right) \boldsymbol{b}_{-+}^{QQ \, \gtrless}(t') \right), \, (t \gtrless t')$$

$$\boldsymbol{G}_{-+}^{qQ}(t, t') = t^{5/2} \left(\mathrm{dg} \left(J_{-c_{q_i} - \frac{1}{2}}(p/M_{\mathrm{KK}} \, t) \right) \boldsymbol{a}_{-+}^{qQ}(t') + \mathrm{dg} \left(J_{c_{q_i} + \frac{1}{2}}(p/M_{\mathrm{KK}} \, t) \right) \boldsymbol{b}_{-+}^{qQ}(t') \right),$$

$$\boldsymbol{G}_{++}^{qQ}(t, t') = t^{5/2} \left(\mathrm{dg} \left(J_{c_{q_i} - \frac{1}{2}}(p/M_{\mathrm{KK}} \, t) \right) \boldsymbol{a}_{++}^{qQ}(t') + \mathrm{dg} \left(J_{-c_{q_i} + \frac{1}{2}}(p/M_{\mathrm{KK}} \, t) \right) \boldsymbol{b}_{++}^{qQ}(t') \right). \tag{4.46}$$

Up to now, we have only determined the general form of the solutions following from the second order differential equations in t. These feature 12 coefficient functions which still have to be derived. In the following we will again work in the limit $\boldsymbol{Y}_q^S = \boldsymbol{Y}_q^C \equiv \boldsymbol{Y}_q$. On the UV brane, we impose standard Dirichlet BCs for the propagators that are Z_2 odd in t

$$\boldsymbol{G}_{-+}^{QQ}(\epsilon, t') = 0, \quad \boldsymbol{G}_{-+}^{qQ}(\epsilon, t') = 0. \tag{4.47}$$

The IR BCs follow from a regularization of the delta distributions at $t = 1$, in analogy to the

derivation within the KK decomposed theory presented before, and read

$$-\boldsymbol{G}^{qQ}_{-+}(1^-,t') = \frac{v}{\sqrt{2}M_{\mathrm{KK}}}\tilde{\boldsymbol{Y}}^{\dagger}_q\boldsymbol{G}^{QQ}_{++}(1^-,t')\,,$$

$$\boldsymbol{G}^{QQ}_{-+}(1^-,t') = \frac{v}{\sqrt{2}M_{\mathrm{KK}}}\tilde{\boldsymbol{Y}}^{\dagger}_q\boldsymbol{G}^{qQ}_{++}(1^-,t')\,, \tag{4.48}$$

with $\tilde{\boldsymbol{Y}}_q$ as defined in (3.86). By integrating the second equation in (4.37) over an infinitesimal interval around $t = t'$, we obtain in addition the jump condition

$$\lim_{\eta\to0}\left[\boldsymbol{G}^{QQ}_{-+}(t,t')\right]^{t=t'+\eta}_{t=t'-\eta} = -\frac{t'^4}{\epsilon^4}\mathbf{1}\,. \tag{4.49}$$

Furthermore, from the second order equation for $\boldsymbol{G}^{QQ}_{++}$ we obtain

$$\lim_{\eta\to0}\left[\partial_t\boldsymbol{G}^{QQ}_{++}(t,t')\right]^{t=t'+\eta}_{t=t'-\eta} = \frac{t'^4}{\epsilon^4 M_{\mathrm{KK}}}\mathbf{1}\,, \tag{4.50}$$

as well as from continuity of $\boldsymbol{G}^{QQ}_{++}$ at $t = t'$

$$\lim_{\eta\to0}\left[\boldsymbol{G}^{QQ}_{++}(t,t')\right]^{t=t'+\eta}_{t=t'-\eta} = 0\,. \tag{4.51}$$

So far we have collected 7 conditions for the 12 unknowns functions of t' which is not sufficient for determining the solutions uniquely. Imposing just the BCs above is not enough, we have to extract additional information from the system (4.37). This is indeed possible. In the course of deriving the decoupled equations, we lost the information about the relative normalization of the components of the propagator with respect to each other. This can be implemented by evaluating (4.37) at $t = \epsilon$, taking into account (4.47), which leads to

$$(t\partial_t - 2 - \boldsymbol{c}_Q)\boldsymbol{G}^{QQ}_{++}(t,t')\Big|_{t=\epsilon} = 0\,,$$

$$(t\partial_t - 2 + \boldsymbol{c}_Q)\boldsymbol{G}^{QQ}_{-+}(t,t')\Big|_{t=\epsilon} = \frac{\epsilon\,p^2}{M_{\mathrm{KK}}}\boldsymbol{G}^{QQ}_{++}(\epsilon,t')\,,$$

$$(t\partial_t - 2 + \boldsymbol{c}_q)\boldsymbol{G}^{qQ}_{-+}(t,t')\Big|_{t=\epsilon} = -\frac{\epsilon}{M_{\mathrm{KK}}}\boldsymbol{G}^{qQ}_{++}(\epsilon,t')\,, \tag{4.52}$$

$$(t\partial_t - 2 - \boldsymbol{c}_q)\boldsymbol{G}^{qQ}_{++}(t,t')\Big|_{t=\epsilon} = 0\,.$$

The last missing piece of information is provided by evaluating the second equation in (4.37) at $t = t'\pm\eta$

$$\lim_{\eta\to0}\left[(t\partial_t - 2 + \boldsymbol{c}_Q)\boldsymbol{G}^{QQ}_{-+}(t,t')\right]^{t=t'+\eta}_{t=t'-\eta} = \lim_{\eta\to0}\left[\frac{tp^2}{M_{\mathrm{KK}}}\boldsymbol{G}^{QQ}_{++}(t,t')\right]^{t=t'+\eta}_{t=t'-\eta}\,. \tag{4.53}$$

It is now possible to determine the coefficient functions by solving the equations (4.47)-(4.53)

for them. We obtain

$$
\begin{aligned}
\boldsymbol{a}_{++}^{QQ<}(t') &= \mathrm{dg}\left(\frac{J_{-c_{Q_i}-\frac{1}{2}}(p/M_{\mathrm{KK}}\,\epsilon)}{J_{c_{Q_i}+\frac{1}{2}}(p/M_{\mathrm{KK}}\,\epsilon)}\right)\boldsymbol{b}_{++}^{QQ<}(t')\,, \\
\boldsymbol{a}_{++}^{QQ>}(t') &= \boldsymbol{a}_{++}^{QQ<}(t') - \frac{\pi}{2M_{\mathrm{KK}}\,\epsilon^4}\,t'^{5/2}\,\mathrm{dg}\left(J_{-c_{Q_i}+\frac{1}{2}}(p/M_{\mathrm{KK}}\,t')\sec(c_{Q_i}\pi)\right)\,, \\
\boldsymbol{b}_{++}^{QQ>}(t') &= \boldsymbol{b}_{++}^{QQ<}(t') + \frac{\pi}{2M_{\mathrm{KK}}\,\epsilon^4}\,t'^{5/2}\,\mathrm{dg}\left(J_{c_{Q_i}-\frac{1}{2}}(p/M_{\mathrm{KK}}\,t')\sec(c_{Q_i}\pi)\right)\,, \\
\boldsymbol{a}_{-+}^{QQ<}(t') &= -p\,\boldsymbol{b}_{++}^{QQ<}(t')\,, \quad \boldsymbol{b}_{-+}^{QQ<}(t') = p\,\boldsymbol{a}_{++}^{QQ<}(t')\,, \\
\boldsymbol{a}_{-+}^{QQ>}(t') &= -p\,\boldsymbol{b}_{++}^{QQ>}(t')\,, \quad \boldsymbol{b}_{-+}^{QQ>}(t') = p\,\boldsymbol{a}_{++}^{QQ>}(t')\,, \\
\boldsymbol{a}_{++}^{qQ}(t') &= \mathrm{dg}\left(\frac{J_{-c_{q_i}-\frac{1}{2}}(p/M_{\mathrm{KK}}\,\epsilon)}{J_{c_{q_i}+\frac{1}{2}}(p/M_{\mathrm{KK}}\,\epsilon)}\right)\boldsymbol{b}_{++}^{qQ}(t')\,, \\
\boldsymbol{a}_{-+}^{qQ}(t') &= p^{-1}\boldsymbol{b}_{++}^{qQ}(t')\,, \quad \boldsymbol{b}_{-+}^{qQ}(t') = -p^{-1}\boldsymbol{a}_{++}^{qQ}(t')
\end{aligned}
\tag{4.54}
$$

where $\boldsymbol{b}_{++}^{QQ<}(t')$ and $\boldsymbol{b}_{++}^{qQ}(t')$ can be determined from the IR BCs (4.48). Finally, we arrive at

$$
\begin{aligned}
\boldsymbol{b}_{++}^{QQ<}(t') = {}& \frac{1}{M_{\mathrm{KK}}}\frac{\pi}{2\epsilon^4}t'^{5/2} \\
& \left(\mathrm{dg}\left(\frac{1}{J_{c_{Q_i}+\frac{1}{2}}(p/M_{\mathrm{KK}}\,\epsilon)}\left(J_{-c_{Q_i}-\frac{1}{2}}(p/M_{\mathrm{KK}}\,\epsilon)J_{c_{Q_i}+\frac{1}{2}}(p/M_{\mathrm{KK}}) - J_{c_{Q_i}+\frac{1}{2}}(p/M_{\mathrm{KK}}\,\epsilon)J_{-c_{Q_i}-\frac{1}{2}}(p/M_{\mathrm{KK}})\right)\right)\right. \\
& \left. - \frac{v^2}{2M_{\mathrm{KK}}^2}\tilde{\boldsymbol{Y}}_q\,\mathrm{dg}\left(\frac{J_{-c_{q_i}-\frac{1}{2}}(p/M_{\mathrm{KK}}\,\epsilon)J_{c_{q_i}-\frac{1}{2}}(p/M_{\mathrm{KK}}) + J_{c_{q_i}+\frac{1}{2}}(p/M_{\mathrm{KK}}\,\epsilon)J_{-c_{q_i}+\frac{1}{2}}(p/M_{\mathrm{KK}})}{J_{-c_{q_i}-\frac{1}{2}}(p/M_{\mathrm{KK}}\,\epsilon)J_{c_{q_i}+\frac{1}{2}}(p/M_{\mathrm{KK}}) - J_{c_{q_i}+\frac{1}{2}}(p/M_{\mathrm{KK}}\,\epsilon)J_{-c_{q_i}-\frac{1}{2}}(p/M_{\mathrm{KK}})}\right)\tilde{\boldsymbol{Y}}_q^\dagger \right. \\
& \left. \mathrm{dg}\left(\frac{1}{J_{c_{Q_i}+\frac{1}{2}}(p/M_{\mathrm{KK}}\,\epsilon)}\left(J_{-c_{Q_i}-\frac{1}{2}}(p/M_{\mathrm{KK}}\,\epsilon)J_{c_{Q_i}-\frac{1}{2}}(p/M_{\mathrm{KK}}) + J_{c_{Q_i}+\frac{1}{2}}(p/M_{\mathrm{KK}}\,\epsilon)J_{-c_{Q_i}+\frac{1}{2}}(p/M_{\mathrm{KK}})\right)\right)\right)^{-1} \\
& \left(\frac{v^2}{2M_{\mathrm{KK}}^2}\tilde{\boldsymbol{Y}}_q\,\mathrm{dg}\left(\frac{J_{-c_{q_i}-\frac{1}{2}}(p/M_{\mathrm{KK}}\,\epsilon)J_{c_{q_i}-\frac{1}{2}}(p/M_{\mathrm{KK}}) + J_{c_{q_i}+\frac{1}{2}}(p/M_{\mathrm{KK}}\,\epsilon)J_{-c_{q_i}+\frac{1}{2}}(p/M_{\mathrm{KK}})}{J_{-c_{q_i}-\frac{1}{2}}(p/M_{\mathrm{KK}}\,\epsilon)J_{c_{q_i}+\frac{1}{2}}(p/M_{\mathrm{KK}}) - J_{c_{q_i}+\frac{1}{2}}(p/M_{\mathrm{KK}}\,\epsilon)J_{-c_{q_i}-\frac{1}{2}}(p/M_{\mathrm{KK}})}\right)\tilde{\boldsymbol{Y}}_q^\dagger\right. \\
& \left. \mathrm{dg}\left(J_{c_{Q_i}-\frac{1}{2}}(p/M_{\mathrm{KK}}\,t')J_{-c_{Q_i}+\frac{1}{2}}(p/M_{\mathrm{KK}}) - J_{-c_{Q_i}+\frac{1}{2}}(p/M_{\mathrm{KK}}\,t')J_{c_{Q_i}-\frac{1}{2}}(p/M_{\mathrm{KK}})\right)\right. \\
& \left. + \mathrm{dg}\left(J_{c_{Q_i}-\frac{1}{2}}(p/M_{\mathrm{KK}}\,t')J_{-c_{Q_i}-\frac{1}{2}}(p/M_{\mathrm{KK}}) + J_{-c_{Q_i}+\frac{1}{2}}(p/M_{\mathrm{KK}}\,t')J_{c_{Q_i}+\frac{1}{2}}(p/M_{\mathrm{KK}})\right)\right)\mathrm{dg}\left(\sec(c_{Q_i}\pi)\right)\,,
\end{aligned}
\tag{4.55}
$$

$$\boldsymbol{b}_{++}^{qQ}(t') = \frac{p}{M_{\rm KK}} \frac{v}{\sqrt{2}M_{\rm KK}} \frac{\pi}{2\epsilon^4} t'^{5/2}$$

$$\mathrm{dg}\left(J_{c_{q_i}+\frac{1}{2}}(pM_{\rm KK}\,\epsilon)\left(J_{-c_{q_i}-\frac{1}{2}}(pM_{\rm KK}\,\epsilon)J_{c_{q_i}+\frac{1}{2}}(pM_{\rm KK}) - J_{c_{q_i}+\frac{1}{2}}(pM_{\rm KK}\,\epsilon)J_{-c_{q_i}-\frac{1}{2}}(pM_{\rm KK})\right)^{-1}\right)\tilde{\boldsymbol{Y}}_q^\dagger$$

$$\left\{\left(\left(\mathrm{dg}\left(\frac{J_{-c_{Q_i}-\frac{1}{2}}(p/M_{\rm KK}\,\epsilon)J_{c_{Q_i}+\frac{1}{2}}(p/M_{\rm KK}) - J_{c_{Q_i}+\frac{1}{2}}(p/M_{\rm KK}\,\epsilon)J_{-c_{Q_i}-\frac{1}{2}}(p/M_{\rm KK})}{J_{-c_{Q_i}-\frac{1}{2}}(p/M_{\rm KK}\,\epsilon)J_{c_{Q_i}-\frac{1}{2}}(p/M_{\rm KK}) + J_{c_{Q_i}+\frac{1}{2}}(p/M_{\rm KK}\,\epsilon)J_{-c_{Q_i}+\frac{1}{2}}(p/M_{\rm KK})}\right)\right.\right.$$

$$\left.\left.- \frac{v^2}{2M_{\rm KK}^2}\tilde{\boldsymbol{Y}}_q\,\mathrm{dg}\left(\frac{J_{-c_{q_i}-\frac{1}{2}}(p/M_{\rm KK}\,\epsilon)J_{c_{q_i}-\frac{1}{2}}(p/M_{\rm KK}) + J_{c_{q_i}+\frac{1}{2}}(p/M_{\rm KK}\,\epsilon)J_{-c_{q_i}+\frac{1}{2}}(p/M_{\rm KK})}{J_{-c_{q_i}-\frac{1}{2}}(p/M_{\rm KK}\,\epsilon)J_{c_{q_i}+\frac{1}{2}}(p/M_{\rm KK}) - J_{c_{q_i}+\frac{1}{2}}(p/M_{\rm KK}\,\epsilon)J_{-c_{q_i}-\frac{1}{2}}(p/M_{\rm KK})}\right)\tilde{\boldsymbol{Y}}_q^\dagger\right)^{-1}\right.$$

$$\left(\frac{v^2}{2M_{\rm KK}^2}\tilde{\boldsymbol{Y}}_q\,\mathrm{dg}\left(\frac{J_{-c_{q_i}-\frac{1}{2}}(p/M_{\rm KK}\,\epsilon)J_{c_{q_i}-\frac{1}{2}}(p/M_{\rm KK}) + J_{c_{q_i}+\frac{1}{2}}(p/M_{\rm KK}\,\epsilon)J_{-c_{q_i}+\frac{1}{2}}(p/M_{\rm KK})}{J_{-c_{q_i}-\frac{1}{2}}(p/M_{\rm KK}\,\epsilon)J_{c_{q_i}+\frac{1}{2}}(p/M_{\rm KK}) - J_{c_{q_i}+\frac{1}{2}}(p/M_{\rm KK}\,\epsilon)J_{-c_{q_i}-\frac{1}{2}}(p/M_{\rm KK})}\right)\tilde{\boldsymbol{Y}}_q^\dagger\right.$$

$$\mathrm{dg}\left(J_{c_{Q_i}-\frac{1}{2}}(p/M_{\rm KK}\,t')J_{-c_{Q_i}+\frac{1}{2}}(p/M_{\rm KK}) - J_{-c_{Q_i}+\frac{1}{2}}(p/M_{\rm KK}\,t')J_{c_{Q_i}-\frac{1}{2}}(p/M_{\rm KK})\right)$$

$$\left.+ \mathrm{dg}\left(J_{c_{Q_i}-\frac{1}{2}}(p/M_{\rm KK}\,t')J_{-c_{Q_i}-\frac{1}{2}}(p/M_{\rm KK}) + J_{-c_{Q_i}+\frac{1}{2}}(p/M_{\rm KK}\,t')J_{c_{Q_i}+\frac{1}{2}}(p/M_{\rm KK})\right)\right)$$

$$\left.+ \mathrm{dg}\left(J_{c_{Q_i}-\frac{1}{2}}(p/M_{\rm KK}\,t')J_{-c_{Q_i}+\frac{1}{2}}(p/M_{\rm KK}) - J_{-c_{Q_i}+\frac{1}{2}}(p/M_{\rm KK}\,t')J_{c_{Q_i}-\frac{1}{2}}(p/M_{\rm KK})\right)\right\}\mathrm{dg}\left(\sec(c_{Q_i}\pi)\right).$$

$$(4.56)$$

In the case of a vanishing Higgs VEV, the coefficient $\boldsymbol{b}_{++}^{qQ}(t')$ is zero. This makes the propagators mediating singlet-doublet transitions vanish, which could be expected from (4.34). In this limit, the other coefficient becomes

$$\boldsymbol{b}_{++}^{QQ<}(t') \xrightarrow[v\to 0]{} \frac{1}{M_{\rm KK}} \frac{\pi}{2\epsilon^4} t'^{5/2}\,\mathrm{dg}(\sec(c_{Q_i}\pi))$$

$$\mathrm{dg}\left(J_{c_{Q_i}+\frac{1}{2}}(p/M_{\rm KK}\,\epsilon)\frac{J_{c_{Q_i}-\frac{1}{2}}(p/M_{\rm KK}\,t')J_{-c_{Q_i}-\frac{1}{2}}(p/M_{\rm KK}) + J_{-c_{Q_i}+\frac{1}{2}}(p/M_{\rm KK}\,t')J_{c_{Q_i}+\frac{1}{2}}(p/M_{\rm KK})}{J_{-c_{Q_i}-\frac{1}{2}}(p/M_{\rm KK}\,\epsilon)J_{c_{Q_i}+\frac{1}{2}}(p/M_{\rm KK}) - J_{c_{Q_i}+\frac{1}{2}}(p/M_{\rm KK}\,\epsilon)J_{-c_{Q_i}-\frac{1}{2}}(p/M_{\rm KK})}\right).$$

$$(4.57)$$

4.2.2   Limit of Small Momentum Transfer

Let us finally give the expressions for the Green's functions in the limit of a negligible momentum transfer. For $p \to 0$ the propagators reduce to

$$\boldsymbol{G}_{LL}^{QQ}(t,t') \to 0\,, \quad \boldsymbol{G}_{RL}^{QQ}(t,t') \to -iP^Q P_R \frac{t^2 t'^2}{2\,\epsilon^4}\,\mathrm{dg}\left((t'/t)^{c_{Q_i}}\right)\theta(t-t')\,,$$

$$\boldsymbol{G}_{LL}^{qQ}(t,t') \to 0\,, \quad \boldsymbol{G}_{RL}^{qQ}(t,t') \to -iP^{qQ} P_R \frac{M_{\rm KK}}{\sqrt{2}v} \frac{t^2 t'^2}{\epsilon^4}\,\mathrm{dg}\left(t^{c_{q_i}}\right)\tilde{\boldsymbol{Y}}^{-1}\mathrm{dg}\left(t'^{c_{Q_i}}\right)\,.$$

$$(4.58)$$

The zeroes reflect the fact that the chirality-diagonal propagators are induced only by a non-vanishing momentum-flow.

Chapter 5

Warped Extra Dimensions: Phenomenology

After studying in detail the setup, the interactions, as well as KK sums in both the minimal as well as the custodial RS model, we will now apply these results to analyze the phenomenology of these models. First, we will give an overview of the status of RS models, in particular concerning the compatibility of a low KK scale with experimental constraints. In Section 3.3, we have already explored electroweak precision observables and discussed possibilities to end up with KK scales in the range of a few TeV, which can *e.g.* be achieved by employing a custodial symmetry. We have also argued that the RS-GIM mechanism will suppress the majority of flavor-changing transitions in the quark sector below their experimental limits. Thus, at first sight the (custodial) RS model seems to offer a reasonable chance to be directly discovered at the LHC, when running at $\sqrt{s} = 14\,\text{TeV}$.

In the last decade, various studies of the flavor structure of RS models have been performed. Properties of the (generalized) CKM matrix, neutral-meson mixing, and CP violation were studied in [175]. Z-mediated FCNCs in the Kaon system were examined in [211] and effects of KK gauge bosons on CP asymmetries in rare hadronic B-meson decays, induced by $b \to s$ transitions, were explored in [252]. A first analysis of $\Delta F = 2$ and $\Delta F = 1$ processes in the RS framework was presented in [176, 177], where the second paper treats a variety of possible effects and analyzes several rare decay processes. The branching ratios for the flavor-changing top-quark decays $t \to cZ(\gamma, g)$ were discussed in [244]. Model-independent approaches for analyzing NP contributions to $\Delta F = 2$ and $\Delta F = 1$ operators were developed in [217, 253]. The first complete examination of all operators relevant to K–$\bar{K}$ mixing was presented in [220]. A comprehensive analysis of $B_{d,s}$–$\bar{B}_{d,s}$ mixing has been performed in [241]. Moreover, rare leptonic K- and B-meson decays [254, 255] as well as the radiative $B \to X_s\gamma$ decay [256] have been studied quite recently. A comprehensive analysis of $\Delta F = 1$ and $\Delta F = 2$ processes, taking into account the exchange of the whole towers of KK excitations has been presented in [213]. Higgs- [203, 245] and radion-mediated [257, 258] FCNCs have been investigated, too. It has been recognized that the only observables where a considerable fine-tuning of parameters seems to be unavoidable are the neutron electric dipole moment [176, 177] and CP-violating effects in the neutral Kaon system [220, 253, 259, 260]. For generic parameters, these turn out to be too large unless the scale of the first KK-gauge bosons is raised to $\mathcal{O}(10)\,\text{TeV}$, beyond the reach of the LHC. Due to these problems, several modifications of the quark flavor sector of warped models have been proposed. Many of them try to implement the idea of MFV into the RS setup by means of a bulk flavor symmetry [205, 206, 261, 262], see also [263].

Others explore the possibility of textures of the 5D Yukawa matrices [221] or use a bulk-Higgs [256, 260] to weaken the constraints. The idea of spontaneous CP violation in the context of RS models has been used to address the problem of too large electric dipole moments [207].

Recently, a model of "flavor triviality" has been proposed [264], where the solution to the puzzle of fermion hierarchies is given up (see also [265, 266]). This model assumes that both the bulk and the IR brane are invariant under the (gauged) SM flavor symmetries. The Yukawa hierarchy is assumed to be generated by some unknown physics on the UV brane. The model belongs to the MFV class and can have a KK scale as low as 2 TeV, while being in agreement with flavor as well as electroweak precision constraints. Beyond that, it offers an interesting phenomenology [267]. However, we do not want to give up the anarchic approach to flavor and thus assume other alternatives of flavor protection to be at work.

What concerns the lepton sector, flavor violation also leads to generically quite stringent bounds on the masses of the first KK gauge bosons in the range of $\gtrsim 5$ TeV [250, 268]. These bounds, however, depend quite strongly on the concrete model parameters. They can be lowered by an appropriate choice of the lepton representations under the custodial gauge group [269] or by flavor symmetries [270, 271, 272, 273].

After this general survey of the status of RS models with respect to (precision) measurements, let us review to what extend the setup can answer some of the additional open questions in the SM, besides solving the flavor puzzle and the gauge hierarchy problem. First of all, it has been shown that warped extra dimensions offer the possibility of high-scale gauge-coupling unification [274, 275, 276]. Moreover, viable dark matter scenarios arise naturally in some variants of RS setups, typically involving (sterile) neutrinos, GUTs, fields with special boundary conditions, or discrete symmetries like KK parity [209, 277, 278, 279, 280, 281, 282]. Brane fluctuations, so-called branons, could furnish WIMP dark matter, see *e.g.* [283]. In addition, the strong CP problem can be addressed in the context of RS models via spontaneous CP violation [207]. Note finally that there are interesting possibilities to generate cosmic inflation in (warped) extra dimensions [284, 285, 286].

Subsequent to this overview we will analyze in detail various observables, which are expected to show interesting signatures of the RS setup. The first part of this chapter is devoted to precision tests. We start by discussing modifications of SM input parameters due to warped extra dimensions. We will go into a tension between different determinations of the $W^{\pm}$-boson mass and elaborate on RS modifications concerning the Higgs VEV. Next, we will continue our examination of the Peskin-Takeuchi parameters. A careful analysis of the bottom-quark pseudo observables at the Z-pole follows, where we will study in detail the parameter dependence and the level of custodial protection for the RS corrections. A possibility to improve the agreement of the forward-backward asymmetry in bottom-quark pair production at the Z-pole with experiment will be examined. Randall-Sundrum models have been used to address the enhancement in the $t\bar{t}$ forward-backward asymmetry, measured at Tevatron, with respect to the theoretical prediction. We will investigate if it is possible to account for this anomaly in an anarchic approach to flavor. After that, we apply the formalism derived in Chapter 4 to examine RS corrections to the anomalous magnetic moment of the muon. Then we will turn to flavor physics and CP violation. First we will study numerically the unitarity violating corrections to the matrix which would be identified with the CKM matrix of the SM. After an analysis of rare top-quark decays, the phenomenological survey will be continued with a discussion of B_s^0–$\bar{B}_s^0$ mixing. A calculation of the absorptive part of the mixing amplitude in

the presence of new physics is presented and the impact of the Randall-Sundrum setup on several CP-violating observables is investigated. Finally, we will perform a detailed survey on Higgs Physics in warped extra dimensions. We will analyze the Higgs-boson production cross sections at Tevatron and at the LHC, as well as the most important branching fractions. For the first time, a complete one-loop calculation for the (custodial) RS model is presented, incorporating the effects stemming from the extended electroweak gauge-boson and fermion sectors. Although deviations are generically expected for an IR-brane localized Higgs sector, the RS modifications will actually exceed the expectations. This observation could have an significant impact on the LHC physics program.

In order to present predictions for different observables in the RS setup we need to specify a large number of model parameters. These are, besides the NP scale M_{KK} and the logarithm of the inverse warp factor L, the bulk mass parameters of the 5D fermion fields as well as the 5D Yukawa matrices. As explained in Section 3.2.3, their choice is restricted by the fact that the known values of the quark masses and CKM matrix elements should be reproduced within errors, but this information still leaves some freedom.

In parts of our following analysis, we will perform a scan over the parameter space of the RS model. For this purpose, we generate 10000 randomly chosen parameter sets using uniform initial distributions for the input parameters. The parameter ranges are $M_{\text{KK}} \in [1, 10]\,\text{TeV}$ for the KK scale and $|(Y_{u,d})_{ij}| \in [0.1, 3]$ for the Yukawa couplings. Moreover, we require that the Wolfenstein parameters $\bar{\rho}$ and $\bar{\eta}$ agree with experiment within 1σ. The bulk-mass parameters are then determined using the warped-space Froggatt-Nielsen formulae given in Section 3.2.3, such that all points reproduce the quark masses and CKM parameters with a global χ^2/dof of better than $11.5/10$ (corresponding to 68% CL), subject to the constraints $|c_{Q_i,q_i}| < 1$ and $c_{u_3} \in \,]-1/2, 1]$. This large set of points provides a reasonable range of predictions that can be obtained for a given observable.[1] Only for a subset of the 10000 scatter points the predictions for the $Zb\bar{b}$ couplings in the minimal RS model are consistent with experiment at 99% CL. We will consider these constraints by discarding points that are in conflict with them. We use $M_{\text{KK}} = 1.5\,\text{TeV}$ as a default KK scale for the minimal RS model, corresponding to masses of about $3.7\,\text{TeV}$ for the first KK excitations of the gauge bosons. We sometimes use twice that value, $M_{\text{KK}} = 3\,\text{TeV}$, as a second reference point. For the custodial model, being less constraint by electroweak precision measurements, we will use the scales $M_{\text{KK}} = 1\,\text{TeV}$ and $M_{\text{KK}} = 2\,\text{TeV}$. Unless noted otherwise, we set $L = \ln(10^{16})$ for the logarithm of the inverse warp factor. It will be instructive to have default sets of input parameters, which are consistent with all experimental constraints concerning the quark masses and CKM parameters. Such sets will be given in Appendix C.

The following is based on [1, 2, 3, 4]. Note that the numerical analysis of [1] has been redone with the same parameter sets as used for the analysis of the custodial model. Moreover, the Yukawa couplings involving Z_2-odd fields, that have been neglected in the latter article, are included. The same holds true for the $\mathcal{O}(v^2/M_{\text{KK}}^2)$ shift in the Higgs VEV.

---

[1]For more details concerning the algorithm that generates the parameter points of the RS model, the interested reader is referred to [213].
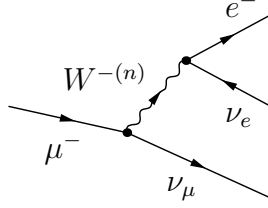
Figure 5.1: Tree-level contributions to $\mu^- \to e^- \nu_\mu \bar{\nu}_e$ arising from the exchange of a W^- boson and its KK partners. See [1] and text for details.

5.1 Precision Tests

5.1.1 Modifications of SM Parameters

Let us first have a look on how values of SM-input parameters will change if the RS setup is realized. Recall that the zero modes of the photon and gluon in RS models, interpreted as the SM photon and gluon, have flat profiles in the extra dimension. Thus their tree-level couplings to the zero mode fermions are universal and flavor diagonal, just like in the SM, see (3.146). As a consequence, the low energy extraction of the fine structure constant α, defined in the Thompson limit, as well as the strong coupling α_s are to excellent approximation unaffected by the presence of the extra dimension. Moreover, the definition of the weak mixing angle θ_w in RS, in terms of (4D) weak gauge couplings, agrees with the one of the SM, see (3.40), which results in the relation

$$g^2 = \frac{4\pi\alpha}{s_w^2} \, . \tag{5.1}$$

Defined in this way, θ_w can be extracted from measuring the left-right polarization asymmetries of light fermions at the Z-pole. Due to the RS-GIM mechanism, the corrections to the Z couplings are given to very good approximation by the universal prefactor in (3.147) and (3.235), which cancels in the asymmetry

$$
\begin{aligned}
A_f &= \frac{\Gamma(Z \to f_L \bar{f}_R) - \Gamma(Z \to f_R \bar{f}_L)}{\Gamma(Z \to f_L \bar{f}_R) + \Gamma(Z \to f_R \bar{f}_L)} = \frac{(g_L^f)^2 - (g_R^f)^2}{(g_L^f)^2 + (g_R^f)^2} \\
&\approx \frac{(1/2 - |Q_f|s_w^2)^2 - (Q_f s_w^2)^2}{(1/2 - |Q_f|s_w^2)^2 + (Q_f s_w^2)^2} \, .
\end{aligned}
\tag{5.2}
$$

From measuring A_f one can thus directly determine the weak mixing angle, which will have the same value in the SM and in RS models. Note that this discussion holds for the minimal as well as for the custodial RS model (where $g \to g_L$).

We now turn to phenomenological consequences of the RS corrections to the $W^\pm$ mass. They have already played a role in determining the T parameter. However, will give here a more detailed analysis, including a survey about different possibilities to determine the $W^\pm$-boson mass and RS predictions in this context.

The mass of the $W^\pm$-bosons can be measured in several ways, see Section 1.1.2. First, it can be obtained directly from $W^\pm$-decays. Just from this single experiment it is not possible to differentiate between the SM and the RS model, since the RS corrections to the $W^\pm$ mass,

as given in (3.67) and (3.206), can be absorbed into a redefinition of the Higgs VEV in (1.25), which will then differ from the SM value of $v_{SM} = 246\,\text{GeV}$ [200]. From (3.67) one deduces that within the minimal RS model one should use the VEV

$$v_{\text{RS}} = v_{\text{SM}} \left(1 + \frac{v_{\text{SM}}^2}{2M_{\text{KK}}^2} \frac{g^2}{8} \left(L - 1 + \frac{1}{2L} \right) + \mathcal{O}\left(\frac{v_{\text{SM}}^4}{M_{\text{KK}}^4} \right) \right). \tag{5.3}$$

Here, we have neglected small loop corrections, which are subleading compared to the L-enhanced RS corrections (for low KK scales). For the custodial model we derive from (3.206) the VEV shift

$$v_{\text{RS}_{\text{C}}} = v_{\text{SM}} \left(1 + \left(\frac{v_{\text{SM}}^2}{2M_{\text{KK}}^2} \left(\frac{g_L^2}{8} \left(L - 1 + \frac{1}{2L} \right) + \frac{g_R^2}{8} L \right) \right) + \mathcal{O}\left(\frac{v_{\text{SM}}^4}{M_{\text{KK}}^4} \right) \right). \tag{5.4}$$

For the case of $g_L = g_R$ the effect is thus approximately twice as big as in the minimal RS model and can become quite significant for low KK scales. We will always employ v_{RS} ($v_{\text{RS}_{\text{C}}}$) for the minimal (custodial) RS model, but drop the subscript, as it will be clear from the context. Note that in some cases, the VEV shift will correspond to a higher order correction in v^2/M_{KK}^2 that will not be considered, however *e.g.* in Higgs couplings of the $W^{\pm}$- and Z-bosons or of SM quarks it will be a LO correction and needs to be taken into account.

The correction to the $W^{\pm}$-boson mass can become observable if several quantities are measured. As explained in 1.1.2, one can also determine the $W^{\pm}$ mass indirectly by measuring the electromagnetic coupling, the weak mixing angle and the Fermi constant, making use of the SM relation (1.34). The former quantities are expected to feature negligible RS corrections, as discussed above. The Fermi constant G_F, obtained from muon decay however, will receive sizable corrections in the RS setup. At tree level, this decay receives contributions from the whole towers of the $W^{\pm}$ bosons and their KK excitations, as depicted in Figure 5.1. The corresponding KK sum over intermediate states is given in (3.261) and below for the minimal model. As muon decay involves only light leptons we can ignore the terms proportional to t^2 and t'^2 due to the RS-GIM mechanism. Thus only the constant term in (3.261) contributes. We arrive at the RS prediction

$$\frac{G_F}{\sqrt{2}} = \frac{g^2}{8m_W^2} \left[1 + \frac{m_W^2}{2M_{\text{KK}}^2} \left(1 - \frac{1}{2L} \right) + \mathcal{O}\left(\frac{m_W^4}{M_{\text{KK}}^4} \right) \right], \tag{5.5}$$

valid both for the minimal as well as for the custodial RS model. Here, the RS-correction term receives a contribution $(1 - 1/L)$ from the modification of the $W^{\pm}$-boson ground state as well as a subleading term $1/(2L)$ from the tower of KK excitations.

Thus when applying the SM relation (1.34) to determine the $W^{\pm}$-boson mass, we will actually not measure its real mass, but rather

$$(m_W)_{\text{indirect}}^{RS} = m_W \left[1 - \frac{m_W^2}{4M_{\text{KK}}^2} \left(1 - \frac{1}{2L} \right) + \mathcal{O}\left(\frac{m_W^4}{M_{\text{KK}}^4} \right) \right]. \tag{5.6}$$

In Figure 5.2 we show again the comparison between the indirect constraint and the direct measurements of m_W and m_t in the SM (see Section 1.1.2), this time overlaid with the RS prediction for m_W, following from (5.6) for $M_{\text{KK}} \in [1, 10]\,\text{TeV}$ and depicted by the blue (dark
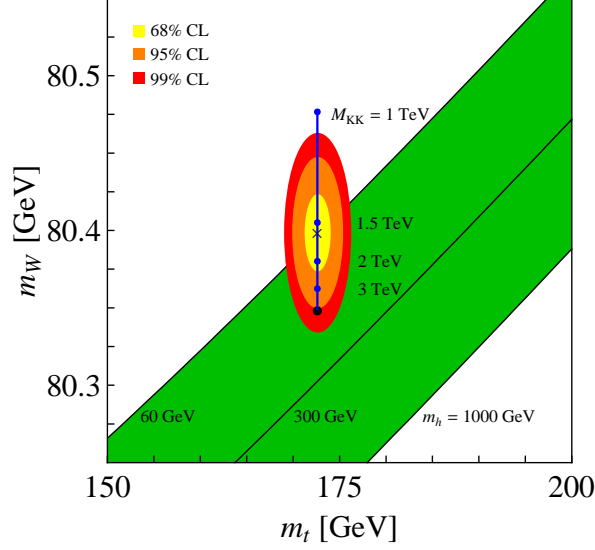
Figure 5.2:   Regions of 68%, 95%, and 99% probability in the m_t–m_W plane due to the direct measurements of m_W and m_t at LEP2 and the Tevatron. The black dot shows the SM prediction based on G_F for our reference input values, whereas the green (medium gray) shaded band corresponds to the SM expectation for varying values of the Higgs-boson mass of $m_h \in [60, 1000]$ GeV. The blue (dark gray) line and the corresponding points represent the RS prediction for $M_{KK} \in [1, 10]$ TeV, valid for both RS variants studied in this thesis. See [1] and text for details.

gray) line and points. The SM limit ($M_{KK} \to \infty$) is shown by the black dot, where we assume the SM reference point from Appendix D with $m_h = 150$ GeV. Recall that the ellipses show the regions of 68%, 95%, and 99% probability, following from the direct measurements at LEP2 and the Tevatron. The SM prediction based on (1.34), for Higgs-boson masses in the range of $m_h \in [60, 1000]$ GeV, is depicted by the shaded band. As noted in Section 1.1.2, the direct and indirect $W^\pm$-boson mass determinations, assuming the SM to be valid, deviate by about 2σ (1.35). However, such a shift of about 50 MeV can be explained in the RS model. Here, we do not expect the two determinations, using SM formulae, to match, see (5.6). Using this relation to determine the real $W^\pm$ mass from the indirect measurement we see from the blue (dark gray) line, that a perfect match can be achieved for KK scales slightly above $M_{KK} = 1.5$ TeV. Note that also for a heavy Higgs boson, agreement between m_W and $(m_W)_{\text{indirect}}$ can be reached at the 99% CL level for KK scales above 1 TeV. Taking for example $m_h = 400$ GeV ($m_h = 1000$ GeV) would indicate KK scales of 1.5 TeV (1 TeV).

Due to the RS corrections to the $W^\pm$- and Z-boson masses, the SM relation between the weak mixing angle and the masses of the weak gauge bosons, encoded in the ϱ parameter (1.30), will deviate from its SM value $\varrho_{SM} = 1$ (at the tree level). If the $W^\pm$-boson mass is measured directly, we derive from (3.67) the result

$$\varrho = \left[1 + s_w^2 \frac{m_Z^2}{2M_{KK}^2} \left(L - 1 + \frac{1}{2L} \right) + \mathcal{O}\left(\frac{m_Z^4}{M_{KK}^4} \right) \right]. \tag{5.7}$$

Note that the correction term features a contribution enhanced by a factor of L. This L-

enhanced term vanishes, if the extended gauge group of the custodial RS model is present. It is canceled by the additional corrections appearing in the contributions to the mass formulae (3.206).

Alternatively, if m_W is determined indirectly, we arrive via (5.6) at the RS prediction

$$\varrho = 1 + \frac{m_Z^2}{2M_{\text{KK}}^2} \left(Ls_w^2 - 1 + \frac{1}{2L} \right) + \mathcal{O} \left(\frac{m_Z^4}{M_{\text{KK}}^4} \right). \tag{5.8}$$

Remember that the T parameter, measuring differences in the corrections to the $W^\pm$ and Z vacuum polarization amplitudes, which contain differences in the corresponding mass corrections, is (trivially) related to the ϱ parameter. As we have already analyzed RS corrections to the T parameter numerically in Section 3.3 (which will be continued below), we will stop our discussion of the ϱ parameter here.

5.1.2 S, T and U Parameters

We will now compute the S, T, and U parameters in the custodial RS model for completeness and compare the findings to the minimal model. The set of oblique corrections, defined in (1.43), can be calculated as described in Section 3.3, where we have already performed the corresponding calculation for the minimal RS model. The non-zero tree-level correlators $\Pi_{aa}(0)$ with $a = W, Z$ are calculated from the corrections to the zero-mode masses (3.206) and profiles (3.207), where the latter also give rise to non-zero derivatives $\Pi'_{aa}(0)$ of the correlators at zero momentum. We find to LO

$$
\begin{aligned}
\Pi_{WW}(0) &= -\frac{g_L^2 v^4}{32 M_{\text{KK}}^2} \left[g_L^2 \left(L - \frac{1}{2L} \right) + g_R^2 L \right], \\
\Pi'_{WW}(0) &= \frac{g_L^2 v^2}{8 M_{\text{KK}}^2} \left(1 - \frac{1}{L} \right), \\
\Pi_{ZZ}(0) &= -\frac{\left(g_L^2 + g_Y^2 \right) v^4}{32 M_{\text{KK}}^2} \left[\left(g_L^2 + g_Y^2 \right) \left(L - \frac{1}{2L} \right) + \left(g_R^2 - g_Y^2 \right) L \right], \\
\Pi'_{ZZ}(0) &= \frac{\left(g_L^2 + g_Y^2 \right) v^2}{8 M_{\text{KK}}^2} \left(1 - \frac{1}{L} \right).
\end{aligned}
\tag{5.9}
$$

Inserting these expressions into (1.43) yields the tree-level prediction

$$S = \frac{2\pi v^2}{M_{\text{KK}}^2} \left(1 - \frac{1}{L} \right), \qquad T = -\frac{\pi v^2}{4\, c_w^2 M_{\text{KK}}^2} \frac{1}{L}, \qquad U = 0, \tag{5.10}$$

in agreement with [218, 219]. In contrast to the results in the minimal model, given in (3.164), there is no L-enhanced term in the T parameter. Like in the ϱ parameter, it has been canceled by the additional corrections appearing in the mass formulae (3.206), which introduce extra terms in the correlators $\Pi_{WW}(0)$ and $\Pi_{ZZ}(0)$, reflecting the underlying (gauged) custodial symmetry. The S and U parameters however remain unaffected.

The contributions to the S and T parameters in the custodial RS model are shown in the right panel of Figure 5.3. The experimental regions of 68%, 95%, and 99% probability in the
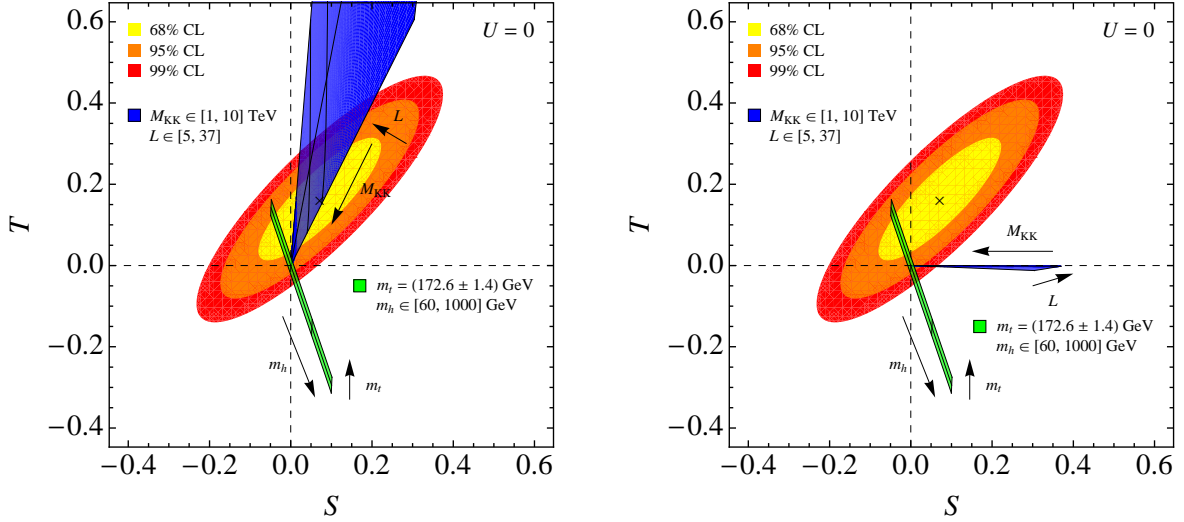
Figure 5.3:   Right: Corrections in the S–T plane due to the custodial RS model for $M_{\rm KK} \in [1, 10]\,{\rm TeV}$ and $L \in [5, 37]$, depicted by the blue (dark-shaded) shaded area. The experimental regions of 68%, 95%, and 99% probability are shown by the colored ellipses. The green (light-shaded) stripe shows the SM predictions for $m_t = (172.6 \pm 1.4)\,{\rm GeV}$ and $m_h \in [60, 1000]\,{\rm GeV}$. Left: corresponding plot in the minimal RS proposal for comparison. See [1] and text for details.

S–T plane are again depicted by the colored ellipses, while the SM predictions for different values of m_h and m_t are shown by the green (light-shaded) stripe. The blue (dark-shaded) area represents the corrections of the custodial RS model for different values of the KK scale and the volume factor L. The corresponding contributions in the minimal RS model, already given in Section 3.3 are shown in the left panel for comparison. Requiring the corrections of the custodial model to satisfy the experimental bounds from S and T leads, for the SM reference point of Appendix D and $L = 37$, to the constraint of $M_{\rm KK} > 2.4\,{\rm TeV}$ @ 95% CL which we quoted in (3.170). This is now driven by the S parameter, see Figure 5.3, and is slightly lower than the corresponding constraint in the minimal RS model with a heavy Higgs boson $m_h \lesssim 1$ TeV, given in (3.167).

Quantum corrections to the T parameter have been studied in [218], in the context of the gauged custodial symmetry without an additional protection for $Zb_L\bar{b}_L$ couplings. It has been shown that, due to this symmetry, the loop contributions to T are UV-finite. The dominant one-loop corrections, coming from fermions in the loop, are found to be positive and allow to lower the KK scale for a sufficiently light Higgs boson. For the model including quark bi-doublets under $SU(2)_L \times SU(2)_R$ to protect the $Zb_L\bar{b}_L$ coupling, the one-loop corrections to T have been studied in [222, 223]. It has been observed that contributions due to KK excitations that couple to the Higgs via the top Yukawa coupling generically induce a negative shift in the T parameter. It is clear from Figure 5.3 that a total negative correction to T, together with a positive value of S would be rather problematic. However, the authors state that positive corrections to T are possible in some regions of parameter space. The one-loop corrections to the S parameter in the custodial RS model arising from (4D) Higgs loops have

been calculated in [224] and found to be logarithmically UV divergent. This could result in a large and positive S parameter, which is clearly rather problematic in points of the consistency of the global fit of the oblique electroweak precision observables. A more detailed analysis of RS loop corrections to the Peskin-Takeuchi parameters would certainly be interesting.

5.1.3 Bottom-Quark Pseudo Observables

We now turn to a more detailed analysis of the bottom quark pseudo observables, which we already have started in Section 3.3 to motivate the custodial extension of the RS model. In order to arrive at simple analytic expressions for $g_L^b \equiv (g_L^d)_{33}$ and $g_R^b \equiv (g_R^d)_{33}$, we employ the ZMA to our closed and exact formulae of Section 3.4.3. This offers the possibility to clearly interpret the RS corrections in terms of model parameters. In the numerical studies, we will however use the exact expressions. First, we need formulae for the leading contributions to the overlap integrals $\left(\Delta_{D,d}^{(\prime)}\right)_{33}$. For the minimal model they have been given in (3.152). For the custodial RS variant, the corresponding expressions turn out to be identical to those of the minimal model (with $c_{f_i} \to c_{\mathcal{T}_{2i}}$ and $c_{F_i} \to c_{Q_i}$). Remember that, while $\varepsilon_{D,d}^{(\prime)}$ vanish at leading order in the ZMA and can be neglected, the matrices $\boldsymbol{\delta}_{D,d}$ have to be considered as they enter (3.148) and (3.236) with an unsuppressed coefficient. The ZMA expressions for $\boldsymbol{\delta}_D$ have been given in (3.154) and (3.250), and the last missing ingredient $\boldsymbol{\delta}_d$ takes the form as given in (3.154) for both RS variants.

After a Taylor expansion of the mixing matrices $\boldsymbol{U}_d$ and $\boldsymbol{W}_d$ in powers of the Cabibbo angle λ, as done in Section 3.2.3,[2] we finally arrive at

$$
g_L^b = \left(-\frac{1}{2} + \frac{s_w^2}{3}\right) \left[1 - \frac{m_Z^2}{2M_{\text{KK}}^2} \frac{F^2(c_{b_L})}{3 + 2c_{b_L}} \left(\omega_Z^{b_L} L - \frac{5 + 2c_{b_L}}{2(3 + 2c_{b_L})}\right)\right]
$$
$$
+ \frac{m_b^2}{2M_{\text{KK}}^2} \left\{\frac{1}{1 - 2c_{b_R}} \left(\frac{1}{F^2(c_{b_R})} \left[1 - \omega_Z^c \frac{1 - 2c_{b_R}}{1 - 2c_{b'_R}}\right] - 1 + \frac{F^2(c_{b_R})}{3 + 2c_{b_R}}\right)\right.
$$
$$
\left. + \sum_{i=1}^{2} \frac{|(Y_d)_{3i}|^2}{|(Y_d)_{33}|^2} \frac{1}{1 - 2c_{\mathcal{T}_{2i}}} \frac{1}{F^2(c_{b_R})} \left[1 - \omega_Z^c \frac{1 - 2c_{\mathcal{T}_{2i}}}{1 - 2c_{\mathcal{T}_{1i}}}\right]\right\}, \tag{5.11}
$$

$$
g_R^b = \frac{s_w^2}{3} \left[1 - \frac{m_Z^2}{2M_{\text{KK}}^2} \frac{F^2(c_{b_R})}{3 + 2c_{b_R}} \left(\omega_Z^{b_R} L - \frac{5 + 2c_{b_R}}{2(3 + 2c_{b_R})}\right)\right]
$$
$$
- \frac{m_b^2}{2M_{\text{KK}}^2} \left\{\frac{1}{1 - 2c_{b_L}} \left(\frac{1}{F^2(c_{b_L})} - 1 + \frac{F^2(c_{b_L})}{3 + 2c_{b_L}}\right) + \sum_{i=1}^{2} \frac{|(Y_d)_{i3}|^2}{|(Y_d)_{33}|^2} \frac{1}{1 - 2c_{Q_i}} \frac{1}{F^2(c_{b_L})}\right\},
$$

where in the *custodial RS model* $c_{b_L} \equiv c_{Q_3}$, $c_{b_R} \equiv c_{\mathcal{T}_{23}}$, $c_{b'_R} \equiv c_{\mathcal{T}_{13}}$, and $\omega_Z^c = 1$. Furthermore, $m_b \equiv m_b(M_{\text{KK}})$ denotes the bottom-quark $\overline{\text{MS}}$ mass evaluated at the KK scale and we have demanded $c_{b'_R}, c_{\mathcal{T}_{1i}} < 1/2$. Notice that we kept $c_{\mathcal{T}_{1i}} \neq c_{\mathcal{T}_{2i}}$, thereby allowing the P_{LR} symmetry to be broken by the triplet bulk masses. We also retained the parameters $\omega_Z^{b_L}$ and $\omega_Z^{b_R}$. In the

---

[2] Note that these LO formulae still hold for the custodial model.

custodial model one has

$$\omega_Z^{b_L} = 0 \,, \ \omega_Z^{b_R} = \frac{3c_w^2}{s_w^2} \approx 10.0 \,, \tag{5.12}$$

where in order to arrive at the numerical values, we have employed $s_w^2 \approx 0.23$, corresponding to the value of the weak mixing angle at the Z-pole.[3]

In the *minimal RS model*, (5.11) holds with

$$\omega_Z^c = 0, \ \ \omega_Z^{b_L} = \omega_Z^{b_R} = 1 \,, \ c_{b_R} \equiv c_{d_3} \,, \ c_{\mathcal{T}_{2i}} \to c_{di}. \tag{5.13}$$

In that case, the non-universal corrections always reduce the couplings with respect to their SM values in magnitude. With the freedom of reparametrization invariance, see (3.140) and (3.142), one can redistribute contributions between the left-handed and right-handed couplings, without changing the zero-mode quark masses and CKM parameters. However, the value of $F(c_{b_L})$ cannot be made too small due to the need of reproducing the large top-quark mass with $\mathcal{O}(1)$ Yukawa couplings.

In the custodial model, we observe that the non-universal corrections to the $Zb\bar{b}$ couplings reduce both g_L^b and g_R^b if the extended P_{LR} symmetry (3.252) is at work. If one allows the P_{LR} symmetry to be broken by $c_{\mathcal{T}_{1i}} \neq c_{\mathcal{T}_{2i}}$, then the shift in g_L^b can also be positive as a result of fermion mixing. As we will see, this always worsens the quality of the $Z \to b\bar{b}$ fit. Due to the custodial protection $\omega_Z^{b_L} = 0$, the constraints arising from the bottom-quark pseudo observables are naively much less stringent in the custodial model with respect to the minimal model, where the shift δg_L^b is large and positive while δg_R^b is small and negative. In order to gauge the improvement and to fully understand the parameter dependence, in particular on the bulk mass parameters $c_{\mathcal{T}_{1i}}$, one has to perform a detailed numerical analysis. This exercise is the subject of the next pages.

Consider the ratio of the width of the Z-boson decay into bottom quarks and the total hadronic width, R_b^0, the bottom-quark left-right asymmetry, A_b, and the forward-backward asymmetry for bottom quarks, $A_{\mathrm{FB}}^{0,b}$. The dependences of these quantities on the left- and right-handed bottom-quark couplings are given by [287]

$$R_b^0 = \left[1 + \frac{4 \sum_{q=u,d} [(g_L^q)^2 + (g_R^q)^2]}{\eta_{\mathrm{QCD}} \, \eta_{\mathrm{QED}} \left[(1 - 6z_b)(g_L^b - g_R^b)^2 + (g_L^b + g_R^b)^2 \right]} \right]^{-1} ,$$

$$A_b = \frac{2\sqrt{1 - 4z_b} \, \dfrac{g_L^b + g_R^b}{g_L^b - g_R^b}}{1 - 4z_b + (1 + 2z_b)\left(\dfrac{g_L^b + g_R^b}{g_L^b - g_R^b} \right)^2} \,, \qquad A_{\mathrm{FB}}^{0,b} = \frac{3}{4} \, A_e \, A_b \,. \tag{5.14}$$

Radiative QCD and QED corrections are encoded by the factors $\eta_{\mathrm{QCD}} = 0.9954$ and $\eta_{\mathrm{QED}} = 0.9997$, while the parameter $z_b \equiv m_b^2(m_Z)/m_Z^2 = 0.997 \cdot 10^{-3}$ describes the effects of the

---

[3]The electromagnetic coupling and the weak mixing angle are running parameters in the low-energy effective theory obtained after integrating out the RS contributions at the scale M_{KK}. We included the associated large logarithms effectively by replacing $s_w^2(M_{\mathrm{KK}})$ by $s_w^2(m_Z)$ in the couplings $g_{L,R}^b$. However, the value of the bottom-quark mass entering the matching is frozen at the high scale and does not evolve in the effective theory.

non-zero bottom-quark mass. Since to an excellent approximation one can neglect the RS contributions to the left- and right-handed couplings of the light quarks, $g_{L,R}^q$, and to the asymmetry parameter of the electron, A_e, we will fix these quantities to their SM values $(g_L^u)_{\text{SM}} = 0.34674$, $(g_R^u)_{\text{SM}} = -0.15470$, $(g_L^d)_{\text{SM}} = -0.42434$, $(g_R^d)_{\text{SM}} = 0.077345$ [36], and $(A_e)_{\text{SM}} = 0.1462$ [38]. The quoted numbers correspond to the SM input parameters given in Appendix D.

Evaluating the relations (5.14) using $(g_L^b)_{\text{SM}} = -0.42114$ and $(g_R^b)_{\text{SM}} = 0.077420$ [36], we obtain for the central values of the bottom-quark pseudo observables

$$\left(R_b^0\right)_{\text{SM}} = 0.21578\,, \qquad \left(A_b\right)_{\text{SM}} = 0.935\,, \qquad \left(A_{\text{FB}}^{0,b}\right)_{\text{SM}} = 0.1025\,. \tag{5.15}$$

One should compare these numbers with the experimental results [36]

$$\begin{aligned}
\left(R_b^0\right)_{\text{exp}} &= 0.21629 \pm 0.00066\,, \\
\left(A_b\right)_{\text{exp}} &= 0.923 \pm 0.020\,, \\
\left(A_{\text{FB}}^{0,b}\right)_{\text{exp}} &= 0.0992 \pm 0.0016\,,
\end{aligned} \qquad
\rho = \begin{pmatrix} 1.00 & -0.08 & -0.10 \\ -0.08 & 1.00 & 0.06 \\ -0.10 & 0.06 & 1.00 \end{pmatrix}, \tag{5.16}$$

where ρ is the correlation matrix. While the R_b^0 and A_b measurements agree within $+0.8\sigma$ and -0.6σ with their SM predictions for $m_h = 150\,\text{GeV}$, the $A_{\text{FB}}^{0,b}$ measurement quoted in (5.16) is almost -2.1σ away from its SM expectation.[4] Shifts of order $+20\%$ and -0.5% in the right- and left-handed bottom-quark couplings relative to the SM could explain the observed discrepancy. Such a pronounced correction in g_R^b would affect A_b and $A_{\text{FB}}^{0,b}$, which both depend linearly on the ratio g_R^b/g_L^b, in a significant way, while it would not spoil the good agreement in $R_b^0 \propto (g_L^b)^2 + (g_R^b)^2$.

Our predictions for the anomalous couplings $\delta g_{L,R}^b \equiv g_{L,R}^b - \left(g_{L,R}^b\right)_{\text{SM}}$, following from (5.11), are shown in Figure 5.4 as functions of the bulk mass parameters $c_{b_{L,R}}$. These are the most important parameters as they enter (5.11) through their zero-mode profiles $F(c_{b_{L,R}})$. Similar plots have been presented in [222]. Correlations between these bulk masses will be taken into account further below. The shown curves correspond to $c_{Q_i} = c_{\mathcal{T}_{1i}} = c_{\mathcal{T}_{2i}}(= c_{d_i}) = -1/2$ and $|(Y_d)_{3i}| = |(Y_d)_{i3}| = |(Y_d)_{33}| = 1$ with $i = 1, 2$. First we identify the large and always positive corrections δg_L^b in the minimal RS model (red dashed line, c.f. Figure 3.10) for $c_{b_L} > -1/2$, which is the generic range in order to reproduce the large third-generation masses, see Figure 3.9. In contrast, the prediction for δg_L^b in the RS model with extended P_{LR} symmetry (blue solid line) is, owing to (3.231), essentially independent of c_{b_L}.[5] It is thus generically within the experimental 99% CL bound (light gray band), which gives a strong motivation to protect the $Zb_L\bar{b}_L$ vertex through the mechanism of [239]. Notice that in the case of the minimal RS model, δg_L^b can be suppressed by pushing the right-handed top quark very close to the IR brane. This feature is illustrated by the ticks on the upper border of the frame in the left panel. The given values of $c_{t_R} \equiv c_{u_3^{(c)}}$ have been obtained by solving $m_t = v/\sqrt{2}\,|(Y_u)_{33}|\,|F(c_{b_L})F(c_{t_R})|$ for the bulk mass parameter c_{t_R}, see (3.126), evaluating the top-quark $\overline{\text{MS}}$ mass at $M_{\text{KK}} = 1\,\text{TeV}$ and setting $|(Y_u)_{33}| = 3$. For smaller (larger) values of $|(Y_u)_{33}|$ the ticks are shifted to the right (left).

---

[4]For $m_h = 115\,\text{GeV}$ the discrepancy in $A_{\text{FB}}^{0,b}$ would amount to around -2.5σ.

[5]In order not to induce unacceptably large corrections to δg_R^b due to fermion mixing, one has to require $c_{b_L} \gtrsim -0.55$.
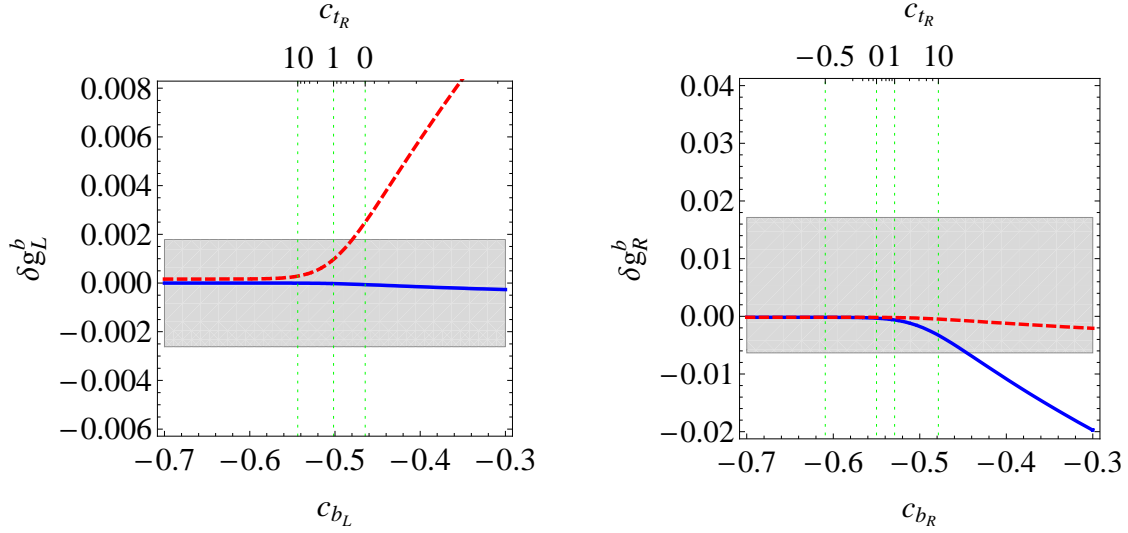
Figure 5.4:   Anomalous couplings δg_L^b (left) and δg_R^b (right) in the RS setup as functions of c_{b_L} and c_{b_R}. The blue solid (red dashed) lines correspond to the predictions obtained in the RS model with extended P_{LR} symmetry (minimal RS model). Bulk mass parameters not explicitly shown are set to $-1/2$, and all elements of the down-type Yukawa matrix entering the prediction are taken to be equal to 1 in magnitude. The light gray bands indicate the experimentally allowed 99% CL ranges. See [2] and text for details.

In the case of δg_R^b we observe instead, that as a result of (5.12), the corrections to the anomalous coupling are always larger in the RS model with extended P_{LR} symmetry (blue solid line) than in the minimal formulation (red dashed line).[6] It is however important to remark that even in the former case the $Zb_R\bar{b}_R$ coupling is predicted to be SM-like, since shifts in δg_R^b outside the experimental 99% CL range (light gray band) would require the bulk mass parameter of the right-handed top quark to be significantly larger than 1. Such a choice appears unnatural, since $c_{t_R} > 1$ implies that the corresponding bulk mass exceeds the curvature scale, in which case the right-handed top quark should be rather treated as a brane-localized field and not considered as a bulk fermion. The latter feature can be inferred from the ticks on the upper border of the frame in the right panel. They have been obtained by combining the equality $m_b = v/\sqrt{2} \, |(Y_d)_{33}| \, |F(c_{b_L}) F(c_{b_R})|$ with the one for m_t given earlier, solving again for c_{t_R}. The Yukawa parameters have been fixed to $|(Y_d)_{33}| = 1$ and $|(Y_u)_{33}| = 3$. For smaller (larger) values of $|(Y_d)_{33}|$ the ticks move to the right (left). Rescaling $|(Y_u)_{33}|$ has the opposite effect. This observation brings us to the conclusion that, irrespectively of the RS bulk gauge group, naturalness in combination with the requirement to reproduce the observed top- and bottom-quark masses excludes large corrections to δg_R^b in models of warped extra dimensions in which the left-handed bottom and top quark reside in the same multiplet.

The predictions in the g_L^b–g_R^b plane for a scan over 10000 randomly generated points in the RS parameter space, as described at the beginning of this chapter, are shown in Figure 5.5. The results, derived by applying the exact formulae for the $Zb\bar{b}$ couplings, will confirm our

---

[6]Notice that in order to reproduce the large top-quark mass with Yukawa couplings of $\mathcal{O}(1)$ one has to require $c_{t_R} > -1/2$, corresponding to $c_{b_R} \gtrsim -0.6$.
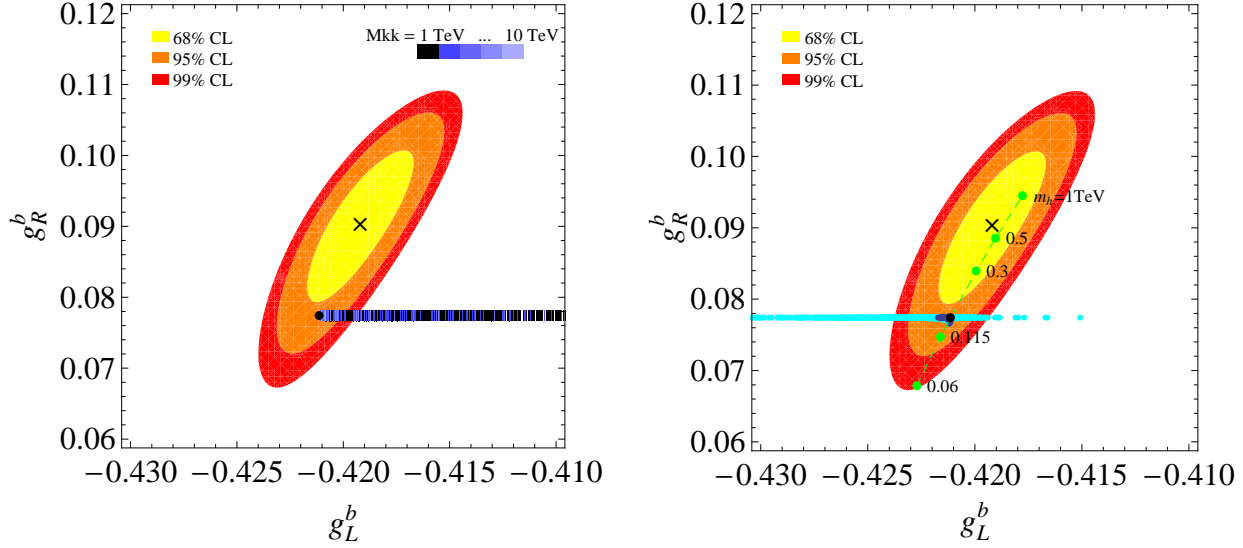
Figure 5.5:   Regions of 68%, 95%, and 99% probability in the g_L^b–g_R^b plane. The horizontal stripes consist of a large number of points in parameter space for the minimal RS model (left) and the custodial model (right). The blue (cyan) points in the right panel represent the result for $c_{b'_R} = c_{b_R}$ ($c_{b'_R} \neq c_{b_R}$). The black dot is the SM expectation for the reference point, and the green dashed line indicates the SM predictions for $m_h \in [0.06, 1]\,\mathrm{TeV}$. See [1, 2] and text for details.

findings from above and allow to study the potential size of P_{LR} breaking corrections in the custodial RS setup. The regions of 68%, 95%, and 99% CL, obtained from a global fit to the $Z \to b\bar{b}$ pseudo observables (5.16), are indicated by the colored ellipses. The RS predictions for the minimal (custodial) RS model are superimposed on the left (right) panel. For the latter, the predictions with (without) extended P_{LR} symmetry are depicted as blue (cyan) scatter points. As discussed before, it is evident that the prediction for g_L^b in the minimal model is always larger than the SM reference value indicated by the black dot, while g_R^b is essentially unaffected. The corresponding negative shift is tiny. In turn, the values $g_{L,R}^b$ are necessarily shifted further away from the best fit $g_L^b = -0.41918$ and $g_R^b = 0.090677$ (black cross). For the custodial model featuring the extended P_{LR} symmetry, the prediction is more or less SM-like. The potential size of P_{LR} symmetry-breaking corrections is shown by the cyan points in the right panel. They have been obtained by allowing the bulk mass parameters $c_{\mathcal{T}_{1i}}$, with $i = 1, 2, 3$, to take any value in the range $[-1, 0]$.[7] While in the case of the extended symmetry, the small RS contributions always drive g_L^b to smaller values with respect to the SM reference point, in the latter case moderate positive and large negative corrections in g_L^b are possible, leading further away from the best fit values. In both cases g_R^b remains essentially unaffected, confirming the discussion in the context of Figure 5.4.[8] In conclusion, in the custodial RS model, as well as in the model featuring a SM gauge group, the corrections (5.11) alone cannot account for the positive shift in g_R^b needed to explain the anomaly in $A_{\mathrm{FB}}^{0,b}$.

---

[7]Note that here we still keep $g_L = g_R$, as we will do for the remainder of this thesis.

[8]Also in the custodial model the corrections to g_R^b are always negative but tiny and hence hardly visible in the figure.
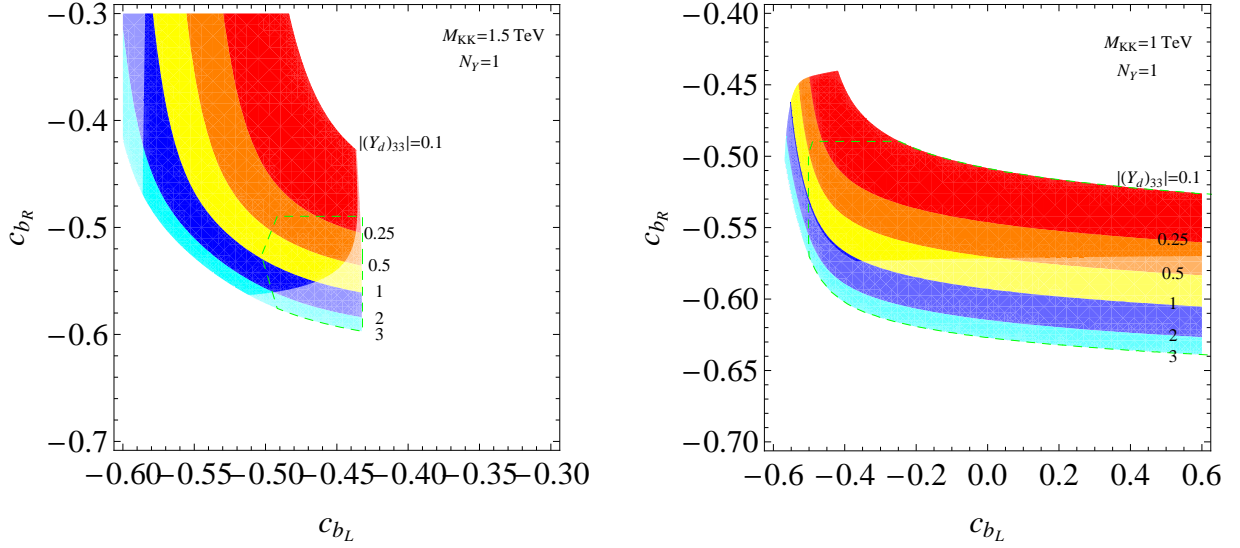
Figure 5.6:   Region of 99% probability in the c_{b_L}–c_{b_R} plane for the minimal RS model for $M_{KK} = 1.5\,\text{TeV}$ (left) and the custodial extension (right) for $M_{KK} = 1\,\text{TeV}$. We set $c_{Q_i} = c_{\mathcal{T}_{1i}} = c_{\mathcal{T}_{2i}}(= c_{d_i}) = -1/2$ for $i, j = 1, 2$ and $N_Y \equiv |(Y_d)_{ij}|/|(Y_d)_{33}| = 1$. The colored contours indicate the value of $|(Y_d)_{33}|$ necessary to reproduce the bottom-quark mass. For the minimal RS model the results with (without) the m_b^2/M_{KK}^2 terms are indicated by bright (faint) colors. For the custodial model the whole colored region corresponds to the RS results with $c_{b'_R} = c_{b_R}$, while only the parameter space indicated by bright colors is accessible for $c_{b'_R} = 0$. The green dashed, fin-shaped regions contains 99% of the parameter points that lead to consistent values of the quark masses and mixings. See [1, 2] and text for details.

This should be contrasted with the analysis of [288], which finds sizable corrections in δg_R^b. However, this is due to chosen bulk mass parameters $c_{b_{L,R}}$ and c_{t_R} that lead to bottom- and top-quark masses of $m_b \approx 40\,\text{GeV}$ and $m_t \approx 75\,\text{GeV}$, which are in conflict with observation. Let us finally mention that, if the left-handed bottom and top quarks arise as an admixture of the zero-mode fields of two $SU(2)_L$ doublets, then the bottom- and top-quark masses are determined by two independent sets of bulk mass parameters, so that it is possible to account simultaneously for the quark masses and mixings as well as for the $A_{FB}^{0,b}$ anomaly [289].

The apparent large positive corrections to g_L^b in the minimal RS variant imply that the R_b^0, A_b, and $A_{FB}^{0,b}$ measurements impose stringent constraints on the parameter space of this RS scenario. As discussed before, the distribution of points depends strongly on the bulk mass parameters c_{b_L} and c_{b_R}, while the exact values of the elements of the down-type Yukawa matrices, as well as the bulk masses of the first two generations and the KK scale have only a minor impact on the overall picture. The last fact is illustrated by the blue coloring of the RS predictions in the left panel of Figure 5.5. Also for low KK scales, indicated in black, the RS predictions enter the 2σ range. This explains the rather low bound on the KK scale quoted in Section 3.3.

In summary, the allowed values of $c_{b_{L,R}}$ in the minimal model are strongly constrained by the $Z \to b\bar{b}$ pseudo observables, whereas the other parameters are only weakly bounded. The

former feature is illustrated in the left panel of Figure 5.6, which shows the regions of 99% probability in the c_{b_L}–c_{b_R} plane for the minimal RS model for $M_{KK} = 1.5 \, \text{TeV}$. The colored contours indicate the magnitude $|(Y_d)_{33}|$ necessary to achieve the correct value of the bottom-quark mass. This requirement correlates c_{b_L} and c_{b_R}. We find that under the restriction $0.1 < |(Y_d)_{33}| < 3$ the allowed $c_{b_{L,R}}$ parameters all lie in the intervals $c_{b_L} \in [-0.59, -0.44]$ and $c_{b_R} > -0.56$ for $M_{KK} = 1.5 \, \text{TeV}$. For $M_{KK} = 3 \, \text{TeV}$ the corresponding ranges read $c_{b_L} \in [-0.61, -0.16]$ and $c_{b_R} > -0.59$. Note that the RS results with (without) the m_b^2/M_{KK}^2 terms in (5.11) are indicated by bright (faint) colors. These terms result from the matrix elements $(\delta_D)_{33}$ and $(\delta_d)_{33}$ in (3.236), arising due to fermion mixing, They have usually been neglected in the literature. Comparing the allowed regions makes clear that neglecting these contributions is in general not justified.

Increasing the magnitude $|(Y_d)_{33}|$ decreases the available parameter space. This can be understood from the fact that for a larger Yukawa coupling the profiles have to be localized closer to the UV brane in order to reproduce the correct bottom-quark mass. *Naively* one might expect that this feature diminishes the RS corrections. However, the corrections due to fermion mixing increase in that case, as it is reflected by the dependence on the *inverse* zero-mode profile $F^{-1}(c_{b_{L,R}})$. Notice also that the terms in (5.11) proportional to m_Z^2/M_{KK}^2 depend linearly on L, whereas the terms proportional to m_b^2/M_{KK}^2 are independent of the RS volume factor. In consequence these latter terms cannot be removed by truncating the volume of the RS background and are typically dominant for moderate and small values of L. The requirement of obtaining consistent values for all the quark masses and CKM parameters restricts the parameter space further. This constraint is indicated by the green dashed regions in Figure 5.6, which contains 99% of the allowed parameter points.

The impact of a possible breaking of the P_{LR} symmetry of the custodial setup by the bulk-mass parameters $c_{\mathcal{T}_{1i}}$ is shown in the right panel of Figure 5.6. The plot is analogous to the one shown in the left panel with however $M_{KK} = 1 \, \text{TeV}$ and the m_b^2/M_{KK}^2 terms included for the whole colored region. This region corresponds to the case of the extended P_{LR} symmetry. Allowing for $c_{b'_R} \neq c_{b_R}$ potentially cuts away a sizable part of parameter space. This is demonstrated by the bright colored region, which shows the allowed range for the choice $c_{b'_R} = 0$. The P_{LR}-breaking correction to g_{b_L} in (5.11) arising from $c_{b'_R} \neq c_{b_R}$ scales like $-v^2/M_{KK}^2 \, |(Y_d)_{33}|^2 \, F^2(c_{b_L})$. This explains, why values $|(Y_d)_{33}| \gtrsim 1$ are not compatible with the $Z \to b\bar{b}$ data in the case of $c_{b'_R} = 0$.

In the light of the insufficient corrections to g_R^b to explain the $A_{FB}^{0,b}$ anomaly with the help of RS contributions alone, note finally that a perfect fit can however be achieved by allowing for a heavy Higgs boson. The corrections

$$\Delta g_L^b = 1.77 \cdot 10^{-3} \ln \frac{m_h}{m_h^{\text{ref}}}, \qquad \Delta g_R^b = 0.92 \cdot 10^{-2} \ln \frac{m_h}{m_h^{\text{ref}}} \tag{5.17}$$

in $g_{L,R}^b$ due to a Higgs-boson mass different from the reference value $m_h^{\text{ref}} = 150 \, \text{GeV}$ are both positive for $m_h > m_h^{\text{ref}}$. The relations (5.17) parametrize the leading logarithmic Higgs-mass dependences of $g_{L,R}^b$. They have been derived with the help of `ZFITTER`.[9] The shifts in the $Zb\bar{b}$ couplings for $m_h \in [0.06, 1] \, \text{TeV}$ are indicated by the green dashed line in the right panel of

---

[9]The default flags of `ZFITTER` version 6.42 are used, except for setting `ALEM=2` to take into account the externally supplied value of $\Delta\alpha_{\text{had}}^{(5)}(m_Z)$.

Figure 5.5. One observes that a Higgs-boson mass in the ballpark of $m_h = 0.5\,\text{TeV}$ would bring the predictions of $g^b_{L,R}$ so close to the best fit values that already the small corrections in the custodial RS model with extended P_{LR} symmetry are sufficient to reach the minimum of the χ^2 distribution. Warped models with the Higgs field localized in the IR might thus indirectly allow for an explanation of the $A^{0,b}_{\text{FB}}$ anomaly, since, as we have argued in Section 3.1.5, the Higgs boson is naturally expected to be heavy in these set-ups. However, remember that in RS models with custodial protection of the T parameter a large Higgs-boson mass is not unproblematic and can potentially spoil the global electroweak fit.

5.1.4 Top-Quark Forward-Backward Asymmetry

As explained in Section 3.2.3, the top quark plays a special role in RS models with flavor anarchy. Being mostly composite (from the holographic point of view) it interacts significantly with the KK excitations. As a consequence, non-negligible effects of the RS setup are expected in top-quark observables.

The CDF and DØ experiments at the Tevatron have collected thousands of $t\bar{t}$ events, allowing to measure the top-quark mass, m_t, and its total inclusive cross section, $\sigma_{t\bar{t}}$, with an accuracy of below 1% [290] and 10% [291, 292], respectively. However, for the search of BSM physics, kinematic distributions and charge asymmetries in $t\bar{t}$ production are more interesting. These observables are particularly sensitive to non-standard dynamics. Studies in that direction have been performed at the Tevatron [293, 294, 295], and a result for the $t\bar{t}$ invariant mass spectrum, $d\sigma_{t\bar{t}}/dM_{t\bar{t}}$, obtained from CDF data has been presented [296, 297].

Interestingly, also the $t\bar{t}$ forward-backward asymmetry, A^t_{FB}, has been measured [105, 106, 298, 299, 300, 301] and persistently found to be larger than expected. In the laboratory $(p\bar{p})$ frame, the most recent CDF result, obtained from semileptonic $t\bar{t}$ events, reads

$$\left(A^t_{\text{FB}}\right)^{p\bar{p}}_{\text{exp}} = (15.0 \pm 5.0_{\text{stat.}} \pm 2.4_{\text{syst.}})\,\% \,. \tag{5.18}$$

In the SM the asymmetry A^t_{FB} vanishes at LO in QCD. This suppression makes it a well suited observable for the potential discovery of NP. At NLO or $\mathcal{O}(\alpha^3_s)$ it receives non-vanishing contributions. These arise from the interference of one-loop QCD box diagrams with tree-level gluon exchange and the interference of initial- and final-state radiation. Including NLO QCD and electroweak corrections [302, 303], the SM prediction in the $p\bar{p}$ frame for the inclusive asymmetry is [304]

$$\left(A^t_{\text{FB}}\right)^{p\bar{p}}_{\text{SM}} = (5.1 \pm 0.6)\,\% \,. \tag{5.19}$$

The total error includes the uncertainties due to different choices of the parton distribution functions (PDFs) and the factorization and renormalization scales, as well as due to a variation of m_t within its experimental error. General arguments suggest that the prediction (5.19) is robust with respect to higher-order QCD corrections [305]. This is supported by explicit calculations of $(A^t_{\text{FB}})_{\text{SM}}$, which include the resummation of logarithmically enhanced threshold effects at NLO [306] and NNLO [307] and which are in substantial agreement with the latter number, making it a firm SM prediction.

The CDF result (5.18) deviates from this prediction by nearly $2\,\sigma$. A recent combination of this measurement with a new result obtained in the di-lepton channel [107] slightly increases the discrepancy [308]. In addition, the very recent DØ measurement [309] finds a similar

deviation from the SM prediction.[10] An effect of high statistical significance ($3.4\,\sigma$) has been observed in the distribution of the asymmetry at high invariant masses $M_{t\bar{t}} > 0.45\,\mathrm{TeV}$ [106]. The sharp growth of the excess with $M_{t\bar{t}}$ suggests the exchange of a new heavy particle in the production of top quarks.

The persistently large values of the observed asymmetry over the last years have triggered a lot of activity in the theory community [267, 310, 311, 312, 313, 314, 315, 316, 317, 318, 319, 320, 321, 322, 323, 324, 325].[11] An apparent option is to generate A_{FB}^{t} already at LO by tree-level exchange of new heavy particles with axial-vector couplings to fermions. However, a viable model must simultaneously avoid generating too large corrections to $\sigma_{t\bar{t}}$ or $d\sigma_{t\bar{t}}/dM_{t\bar{t}}$, which are both in good agreement with the SM prediction. This makes it non-trivial to explain the large experimental value. A first class of models features new physics in the t channel or u channel with large flavor-violating couplings due to vector-boson exchange, namely Z' [312, 318, 319, 320, 321, 322], or W' bosons [313, 320, 321], or due to the exchange of color singlet, triplet or sextet scalars [315, 316, 317, 318, 319, 321, 324]. In this context, note that it is not always clear, how the necessary flavor-changing couplings can be generated without *ad hoc* assumptions. A second class of models involves tree-level exchange of new vector states in the s-channel, which have to exhibit sizable axial-vector couplings to both the light quarks, g_{A}^{q}, and the top quark, g_{A}^{t} [267, 310, 311, 314, 318, 319, 321, 323, 324, 325]. Suitable candidates are color octets, which maximize the interference with QCD.[12] The new states need to have axial-vector couplings to the first and the third generation of quarks with opposite sign [327], implying $g_{A}^{q} g_{A}^{t} < 0$, in order to achieve a positive shift in A_{FB}^{t}. Examples of theories that turn out to lead to a positive shift in the charge asymmetry are flavor non-universal chiral color models [314, 323], and warped extra dimension [267, 310, 325], which both contain heavy partners of the SM gluon. Indeed the RS model seems to be a prototype for models that address such an anomaly. However, a thorough analysis is necessary to answer the question if the RS setup can really naturally account for the enhancement in the asymmetry.

In the following we will show that, in the wide class of BSM scenarios that rely on the virtual exchange of vector bosons in the s channel, the NLO corrections to A_{FB}^{t} can exceed the LO corrections if the axial-vector couplings to light quarks are suppressed.[13] This applies in particular to NP models that explain the hierarchical structures observed in the masses and mixing of the SM fermions geometrically, see Section 3.2.3. Since this sequestering of flavor allows for an effective suppression of FCNCs, it is likely to be an integral part of any setup that addresses the problems of the SM via a low NP scale in the reach of the LHC. Although our discussion will be inspired by warped extra dimensions, as a prototype of the models described above, the use of EFT methods will make the considerations rather model-independent.

We will work out in detail the relevant LO *and NLO* corrections to A_{FB}^{t} in the RS setup. To this end, the heavy KK modes of the model are integrated out explicitly. At Born level, contributions due to the exchange of KK gluons and photons, the Z boson and its KK partners, as well as the Higgs boson are included. Beyond LO, we consider the interference of tree-level

---

[10]Beyond that, in an approach based only on the rapidity of the final state lepton, the asymmetry $A_{FB}^{l} = (15.2\pm4.0)\,\%$ is obtained, to be compared with the theory prediction by `MC@NLO` of $(2.1\pm0.1)\,\%$, which amounts to a $\gtrsim 3\sigma$ deviation.

[11]For an overview including additional references, see [326].

[12]For a thorough analysis of direct and indirect constraints on massive spin-one color octets see [328].

[13]Note that the importance of NLO corrections has been briefly mentioned in [329] in the context of the charge asymmetry in the exclusive channel $p\bar{p} \to t\bar{t}X$.

KK-gluon exchange with one-loop QCD box diagrams and corresponding bremsstrahlungs corrections. We will then answer the question about the potential of the RS setup to explain the observed $A_{\rm FB}^t$ anomaly. As we stick to the EFT approach, our final results will be applicable to a wide class of scenarios with non-standard dynamics above the electroweak scale.

Top-Antitop Production

At the Tevatron, $t\bar{t}$ pairs are produced in proton-antiproton collisions, $p\bar{p} \to t\bar{t}X$. In the SM, this hadronic process receives partonic tree-level contributions from quark-antiquark annihilation and gluon fusion.

$$
\begin{aligned}
q(p_1) + \bar{q}(p_2) &\to t(p_3) + \bar{t}(p_4)\,, \\
g(p_1) + g(p_2) &\to t(p_3) + \bar{t}(p_4)\,.
\end{aligned}
\tag{5.20}
$$

Here, $p_{1,2}$ denote the four-momenta of the initial state partons, which can be expressed as fractions $x_{1,2}$ of the four-momenta $P_{1,2}$ of the colliding hadrons, $p_{1,2} = x_{1,2}P_{1,2}$. The hadronic center-of-mass (CM) energy squared is given by $s = (P_1 + P_2)^2$. The partonic cross section is a function of the kinematic invariants

$$
\hat{s} = (p_1+p_2)^2\,,\quad t_1 = (p_1-p_3)^2 - m_t^2 = -\frac{\hat{s}}{2}(1-\beta\cos\theta)\,,\quad u_1 = (p_2-p_3)^2 - m_t^2 = -\frac{\hat{s}}{2}(1+\beta\cos\theta)\,,
\tag{5.21}
$$

which for $m_t \to 0$ reduce to the Mandelstam variables. In the following we will be interested in the differential cross section, with respect to the angle θ between $\vec{p}_1$ and $\vec{p}_3$ in the partonic CM frame, and with respect to the invariant mass $M_{t\bar{t}} = \sqrt{(p_3 + p_4)^2}$ of the $t\bar{t}$ pair. Thus, we have expressed t_1 and u_1 in terms of θ and the top-quark velocity $\beta = \sqrt{1-\rho}$, $\rho = 4m_t^2/\hat{s}$. Momentum conservation at Born level implies that $\hat{s} + t_1 + u_1 = 0$.

We write the hadronic differential cross section as

$$
\frac{d\sigma^{p\bar{p}\to t\bar{t}X}}{d\cos\theta} = \frac{\alpha_s}{m_t^2} \sum_{i,j} \int_{4m_t^2}^{s} \frac{d\hat{s}}{s} \, f\!f_{ij}\big(\hat{s}/s, \mu_f\big) \, K_{ij}\left(\frac{4m_t^2}{\hat{s}}, \cos\theta, \mu_f\right)\,,
\tag{5.22}
$$

where μ_f denotes the factorization scale. The corresponding parton luminosity functions are given by

$$
f\!f_{ij}(y, \mu_f) = \int_y^1 \frac{dx}{x} \, f_{i/p}(x, \mu_f) \, f_{j/\bar{p}}(y/x, \mu_f)\,,
\tag{5.23}
$$

and, for $ij = q\bar{q}, \bar{q}q$, are understood to be summed over all light species of quarks. Finally, the functions $f_{i/p}(x, \mu_f)$ $(f_{i/\bar{p}}(x, \mu_f))$ are the universal (non-perturbative) PDFs, which describe the probability of finding the parton i in the proton (antiproton) with longitudinal momentum fraction x. The hard-scattering kernels $K_{ij}(\rho, \cos\theta, \mu_f)$ are related to the partonic cross sections and have a perturbative expansion in α_s

$$
K_{ij}(\rho, \cos\theta, \mu_f) = \sum_{n=0}^{\infty} \left(\frac{\alpha_s}{4\pi}\right)^n K_{ij}^{(n)}(\rho, \cos\theta, \mu_f)\,.
\tag{5.24}
$$

At LO in α_s only the kernels with $ij = q\bar{q}, \bar{q}q, gg$ are non-zero within the SM. For the ampli-

tudes corresponding to s-channel gluon exchange we obtain

$$
K_{q\bar{q}}^{(0)} = \alpha_s \frac{\pi\beta\rho}{8} \frac{C_F}{N_c} \left(\frac{t_1^2 + u_1^2}{\hat{s}^2} + \frac{2m_t^2}{\hat{s}} \right),
$$

$$
K_{gg}^{(0)} = \alpha_s \frac{\pi\beta\rho}{8(N_c^2 - 1)} \left(C_F \frac{\hat{s}^2}{t_1 u_1} - N_c \right) \left[\frac{t_1^2 + u_1^2}{\hat{s}^2} + \frac{4m_t^2}{\hat{s}} - \frac{4m_t^4}{t_1 u_1} \right].
$$

(5.25)

Note that the coefficient $K_{\bar{q}q}^{(0)}$ is obtained from $K_{q\bar{q}}^{(0)}$ by replacing $\cos\theta$ with $-\cos\theta$. The color factors of $SU(3)_c$ are given by $N_c = 3$ and $C_F = 4/3$.

The forward-backward asymmetry in top-pair production is defined as

$$
A_{\mathrm{FB}}^t \equiv \frac{\displaystyle\int_0^1 d\cos\theta \, \frac{d\sigma^{p\bar{p}\to t\bar{t}X}}{d\cos\theta} - \int_{-1}^0 d\cos\theta \, \frac{d\sigma^{p\bar{p}\to t\bar{t}X}}{d\cos\theta}}{\displaystyle\int_0^1 d\cos\theta \, \frac{d\sigma^{p\bar{p}\to t\bar{t}X}}{d\cos\theta} + \int_{-1}^0 d\cos\theta \, \frac{d\sigma^{p\bar{p}\to t\bar{t}X}}{d\cos\theta}}.
$$

(5.26)

Our notation is such that in a process labeled by the superscript $p\bar{p} \to t\bar{t}X$ ($p\bar{p} \to \bar{t}tX$) the angle θ corresponds to the scattering angle of the top (antitop) quark in the partonic CM frame. Since QCD is symmetric under charge conjugation, which implies that

$$
\left. \frac{d\sigma^{p\bar{p}\to t\bar{t}X}}{d\cos\theta} \right|_{\cos\theta=c} = \left. \frac{d\sigma^{p\bar{p}\to\bar{t}tX}}{d\cos\theta} \right|_{\cos\theta=-c},
$$

(5.27)

for any fixed value of c, the forward-backward asymmetry can also be understood as a charge asymmetry

$$
A_{\mathrm{FB}}^t = A_c^t \equiv \frac{\displaystyle\int_0^1 d\cos\theta \, \frac{d\sigma_a}{d\cos\theta}}{\displaystyle\int_0^1 d\cos\theta \, \frac{d\sigma_s}{d\cos\theta}} = \frac{\sigma_a}{\sigma_s},
$$

(5.28)

where the charge-asymmetric (a) and -symmetric (s) averaged differential cross sections are defined as [306]

$$
\frac{d\sigma_{a,s}}{d\cos\theta} \equiv \frac{1}{2} \left[\frac{d\sigma^{p\bar{p}\to t\bar{t}X}}{d\cos\theta} \mp \frac{d\sigma^{p\bar{p}\to\bar{t}tX}}{d\cos\theta} \right].
$$

(5.29)

This notation, with $d\sigma^{p\bar{p}\to t\bar{t}X}/d\cos\theta$ given in (5.22), will turn out to be convenient for the following discussion. The total hadronic cross section is now given by

$$
\sigma_{t\bar{t}} = \int_{-1}^1 d\cos\theta \, \frac{d\sigma_s}{d\cos\theta}.
$$

(5.30)

We write the asymmetric contribution to the cross section as

$$
\sigma_a = \frac{\alpha_s}{m_t^2} \sum_{i,j} \int_{4m_t^2}^s \frac{d\hat{s}}{s} \, ff_{ij}\left(\hat{s}/s, \mu_f \right) A_{ij}\left(\frac{4m_t^2}{\hat{s}} \right),
$$

(5.31)

and similar for the case of the symmetric contribution σ_s, where the hard-scattering charge-asymmetric coefficient $A_{ij}(4m_t^2/\hat{s})$ is to be replaced by its symmetric counterpart $S_{ij}(4m_t^2/\hat{s})$. Note that the perturbative expansions of the symmetric and asymmetric kernels are defined in analogy to (5.24).

In the SM, the LO coefficients of the symmetric contribution to the cross section read

$$
\begin{aligned}
S_{q\bar{q}}^{(0)} &= \alpha_s \frac{\pi\beta\rho}{27} \left(2 + \rho\right), \\
S_{gg}^{(0)} &= \alpha_s \frac{\pi\beta\rho}{192} \left[\frac{1}{\beta} \ln\left(\frac{1+\beta}{1-\beta}\right) \left(16 + 16\rho + \rho^2\right) - 28 - 31\rho\right],
\end{aligned}
\tag{5.32}
$$

while the asymmetric contributions $A_{q\bar{q}}^{(0)}$ and $A_{gg}^{(0)}$ both vanish.

Below, we will discuss in detail how at NLO a non-zero coefficient $A_{q\bar{q}}^{(1)}$ is generated in the SM. This will lead to a charge asymmetric cross section which is suppressed by $\alpha_s/(4\pi)$ with respect to the symmetric one.

Cross Section and Asymmetry in Warped Models

For the following discussion, recall from Section 3.2.3 the RS mechanism of generating fermion hierarchies geometrically, via wave-function overlaps. An important consequence, following from the structure of the overlap integrals is, that the effective coupling strength of KK gluons to heavy quarks is enhanced relatively to the SM couplings by a factor $\sqrt{L}$, see Section 3.2.4. Since left- and right-handed fermions are localized differently in the bulk[14], the KK-gluon couplings to quarks are in general not purely vector-like, but receive non-vanishing axial-vector components. These couplings lead to a charge asymmetric cross section σ_a already at LO due to quark-antiquark annihilation $q\bar{q} \to t\bar{t}$ mediated by tree-level exchange of KK gluons in the s channel.

Further tree-level contributions to A_{FB}^t arise in RS models due to the fact that KK gluons and photons, the Z boson and its KK excitations, as well as the Higgs boson feature flavor non-diagonal couplings, which have been discussed in Chapter 3. These couplings lead to flavor-changing $u\bar{u} \to t\bar{t}$ transitions, affecting the t channel. In principle, also $d\bar{d} \to t\bar{t}$ transitions receive corrections due to the t-channel exchange of the $W^{\pm}$ bosons and their KK excitations. However, it turns out that these effects are negligibly small for realistic input parameters and can be ignored in the following. In contrast to processes with quarks in the initial state, the gluon-fusion channel $gg \to t\bar{t}$ does not receive a correction at the Born level. Due to the orthonormality of gauge-boson profiles, the coupling of two massless gluons to a KK gluon is zero. The Feynman diagrams that need to be considered at the tree-level are shown in Figure 5.7.

Calculation of LO effects   As we expect the NP scale (here $M_{\text{NP}} = M_{\text{KK}}$) to be at least of the order of several times the electroweak scale $M_{\text{KK}} >> M_{\text{EW}}$ and also well above the energies directly probable at Tevatron, virtual effects appearing in RS models can be described

---

[14]Remember that although the bulk-masses are associated to the representations under the gauge group and not to the chiralities, a $SU(2)_L$-doublet zero-mode will be mostly left-handed, *etc.*, so that for zero-modes the both can be identified to first approximation.

by an effective low-energy theory consisting out of dimension-six operators, see Appendix A.4. In the case at hand, the appropriate effective Lagrangian which accounts for the effects of intermediate vector and scalar states reads

$$
\mathcal{L}_{\text{eff}} = \sum_{q,u} \sum_{A,B=L,R} \left[C_{q\bar{q},AB}^{(V,8)} Q_{q\bar{q},AB}^{(V,8)} + C_{t\bar{u},AB}^{(V,8)} Q_{t\bar{u},AB}^{(V,8)} + C_{t\bar{u},AB}^{(V,1)} Q_{t\bar{u},AB}^{(V,1)} + C_{t\bar{u},AB}^{(S,1)} Q_{t\bar{u},AB}^{(S,1)} \right], \quad (5.33)
$$

where

$$
\begin{aligned}
Q_{q\bar{q},AB}^{(V,8)} &= (\bar{q}\gamma_\mu T^a P_A q)(\bar{t}\gamma^\mu T^a P_B t)\,, \\
Q_{t\bar{u},AB}^{(V,8)} &= (\bar{u}\gamma_\mu T^a P_A t)(\bar{t}\gamma^\mu T^a P_B u)\,, \\
Q_{t\bar{u},AB}^{(V,1)} &= (\bar{u}\gamma_\mu P_A t)(\bar{t}\gamma^\mu P_B u)\,, \\
Q_{t\bar{u},AB}^{(S,1)} &= (\bar{u} P_A t)(\bar{t} P_B u)\,.
\end{aligned}
\qquad (5.34)
$$

The sum over q (u) involves all light (up-type) quark flavors and the superscripts V and S (8 and 1) label vector and scalar (color-octet and -singlet) contributions, respectively. The $SU(3)_c$ generators T^a are normalized such that $\text{Tr}\left(T^a T^b\right) = T_F\,\delta_{ab}$ with $T_F = 1/2$.

   With the help of the effective Lagrangian (5.33) we can now easily calculate the interference between the tree-level matrix element describing s-channel gluon exchange in the SM and the s- and t-channel new-physics contributions arising from the diagrams displayed in Figure 5.7. We arrive at the hard-scattering kernels

$$
\begin{aligned}
K_{q\bar{q},\text{RS}}^{(0)} &= \frac{\beta\rho}{32}\frac{C_F}{N_c}\left[\frac{t_1^2}{\hat{s}}C_{q\bar{q},\perp}^{(V,8)} + \frac{u_1^2}{\hat{s}}C_{q\bar{q},\parallel}^{(V,8)} + m_t^2\left(C_{q\bar{q},\parallel}^{(V,8)} + C_{q\bar{q},\perp}^{(V,8)}\right)\right], \\
K_{t\bar{u},\text{RS}}^{(0)} &= \frac{\beta\rho}{32}\frac{C_F}{N_c}\left[\left(\frac{u_1^2}{\hat{s}} + m_t^2\right)\left(\frac{1}{N_c}C_{t\bar{u},\parallel}^{(V,8)} - 2C_{t\bar{u},\parallel}^{(V,1)}\right) + \left(\frac{t_1^2}{\hat{s}} + m_t^2\right)C_{t\bar{u},\perp}^{(S,1)}\right],
\end{aligned}
\qquad (5.35)
$$

where we have defined appropriate combinations of Wilson coefficients,

$$
C_{ij,\parallel}^{(P,a)} = \text{Re}\left[C_{ij,LL}^{(P,a)} + C_{ij,RR}^{(P,a)}\right], \qquad C_{ij,\perp}^{(P,a)} = \text{Re}\left[C_{ij,LR}^{(P,a)} + C_{ij,RL}^{(P,a)}\right]. \qquad (5.36)
$$

Just like in the SM, the coefficient $K_{\bar{q}q,\text{RS}}^{(0)}$ $\left(K_{\bar{t}u,\text{RS}}^{(0)}\right)$ is obtained from $K_{q\bar{q},\text{RS}}^{(0)}$ $\left(K_{t\bar{u},\text{RS}}^{(0)}\right)$ by replacing $\cos\theta$ with $-\cos\theta$.

   The LO corrections to the symmetric and asymmetric parts of the cross section, as defined in (5.31), are now obtained by integrating over $\cos\theta$. We find in the partonic CM system

$$
\begin{aligned}
S_{u\bar{u},\text{RS}}^{(0)} &= \frac{\beta\rho}{216}\left(2+\rho\right)\hat{s}\left[C_{u\bar{u},\parallel}^{(V,8)} + C_{u\bar{u},\perp}^{(V,8)} + \frac{1}{3}C_{t\bar{u},\parallel}^{(V,8)} - 2C_{t\bar{u},\parallel}^{(V,1)}\right] + f_S(z)\,\tilde{C}_{t\bar{u}}^S\,, \\
S_{d\bar{d},\text{RS}}^{(0)} &= \frac{\beta\rho}{216}\left(2+\rho\right)\hat{s}\left[C_{d\bar{d},\parallel}^{(V,8)} + C_{d\bar{d},\perp}^{(V,8)}\right],
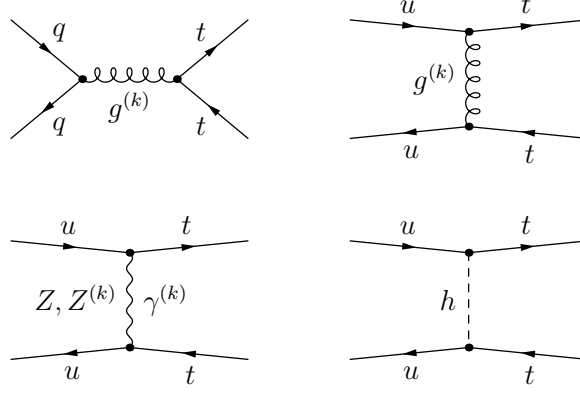\end{aligned}
\qquad (5.37)
$$

Figure 5.7: Upper row: Tree-level contributions to $q\bar{q} \to t\bar{t}$ (left) and $u\bar{u} \to t\bar{t}$ (right) transitions, mediated by s- and t-channel exchange of KK gluons. Lower row: Tree-level contributions to the $u\bar{u} \to t\bar{t}$ transition arising from t-channel exchange of the Z boson and its KK partners, of KK photons, as well as of the Higgs boson. The s-channel (t-channel) amplitudes involve all light up- and down-type (up-type) quarks. See [3] and text for details.

as well as

$$A_{u\bar{u},\text{RS}}^{(0)} = \frac{\beta^2 \rho}{144}\,\hat{s}\,\left[C_{u\bar{u},\|}^{(V,8)} - C_{u\bar{u},\perp}^{(V,8)} + \frac{1}{3}C_{t\bar{u},\|}^{(V,8)} - 2C_{t\bar{u},\|}^{(V,1)}\right] + f_A(z)\,\tilde{C}_{t\bar{u}}^S\,,$$

$$A_{d\bar{d},\text{RS}}^{(0)} = \frac{\beta^2 \rho}{144}\,\hat{s}\,\left[C_{d\bar{d},\|}^{(V,8)} - C_{d\bar{d},\perp}^{(V,8)}\right]\,. \tag{5.38}$$

Obviously, there is no flavor-changing t-channel contribution to the coefficients involving down-type quarks. For the following considerations it is important to note that the coefficients $C_{q\bar{q},\|}^{(V,8)}$ and $C_{q\bar{q},\perp}^{(V,8)}$ enter (5.37) in the combination $C_{q\bar{q}}^V \equiv \left(C_{q\bar{q},\|}^{(V,8)} + C_{q\bar{q},\perp}^{(V,8)}\right)$, while in (5.38) they always appear in the form $C_{q\bar{q}}^A \equiv \left(C_{q\bar{q},\|}^{(V,8)} - C_{q\bar{q},\perp}^{(V,8)}\right)$. This reflects the fact that the symmetric (asymmetric) LO cross section σ_s (σ_a) measures the product $g_V^q g_V^t$ ($g_A^q g_A^t$) of the vector (axial-vector) parts of the couplings of the KK gluons to light quarks and top quarks. As we want to include a potentially light Higgs boson with $m_h \ll M_{\text{KK}}$ into our analysis, we have kept the full Higgs-boson mass dependence arising from the t-channel propagator. This dependence is described by the phase-space factors $f_{S,A}(z)$ with $z \equiv m_h^2/m_t^2$, which are given explicitly in Appendix B.1. The new coefficient $\tilde{C}_{t\bar{u}}^S$ is the dimensionless counterpart of $C_{t\bar{u},\perp}^{(S,1)}$.[15]

So far, the expressions (5.37) and (5.38) contain in a model-independent way possible new-physics contributions to $\sigma_{s,a}$ that arise from the operators given in (5.34). Thus they are

---

[15]Note that we do not have to introduce form factors for the t-channel contribution arising from Z-boson zero-mode exchange, since these corrections are of $\mathcal{O}(v^4/M_{\text{KK}}^4)$, which we will neglect in the following. The t-channel exchange requires a flavor changing transition at *both* vertices, which at $\mathcal{O}(v^2/M_{\text{KK}}^2)$ is only mediated by the non-factorizable $t_<$ contribution in the KK sum. However, this is only induced by the KK excitations, see (3.261) and the discussion below.

appropriate for general models that feature tree-level exchange of color-octet vectors in the s and t channels, as well as t-channel corrections due to both new color-singlet, vector, and scalar states, making them useful beyond the context of RS models. However, we now want to apply the results to models with a warped extra dimension.

The Wilson coefficients appearing in $S_{ij,\mathrm{RS}}^{(0)}$ and $A_{ij,\mathrm{RS}}^{(0)}$ can be worked out with the help of the formulae derived in Section 3.5. In the minimal RS formulation we find[16]

$$C_{q\bar{q},\|}^{(V,8)} = -\frac{2\pi\alpha_s}{M_{\mathrm{KK}}^2}\left\{\frac{1}{L} - \sum_{a=Q,q}\left[(\Delta_a')_{11} + (\Delta_a')_{33} - 2L\,(\widetilde{\Delta}_a)_{11}\otimes(\widetilde{\Delta}_a)_{33}\right]\right\},$$

$$C_{q\bar{q},\perp}^{(V,8)} = -\frac{2\pi\alpha_s}{M_{\mathrm{KK}}^2}\left\{\frac{1}{L} - \sum_{a=Q,q}\left[(\Delta_a')_{11} + (\Delta_a')_{33}\right] + 2L\left[(\widetilde{\Delta}_Q)_{11}\otimes(\widetilde{\Delta}_q)_{33} + (\widetilde{\Delta}_q)_{11}\otimes(\widetilde{\Delta}_Q)_{33}\right]\right\},$$

$$C_{t\bar{u},\|}^{(V,8)} = -\frac{4\pi\alpha_s}{M_{\mathrm{KK}}^2}\,L\sum_{a=U,u}\left[(\widetilde{\Delta}_a)_{13}\otimes(\widetilde{\Delta}_a)_{31}\right], \qquad (5.39)$$

$$C_{t\bar{u},\|}^{(V,1)} = -\frac{4\pi\alpha_e}{M_{\mathrm{KK}}^2}\,\frac{L}{s_w^2 c_w^2}\left[\left(T_3^u - s_w^2 Q_u\right)^2(\widetilde{\Delta}_U)_{13}\otimes(\widetilde{\Delta}_U)_{31} + \left(s_w^2 Q_u\right)^2(\widetilde{\Delta}_u)_{13}\otimes(\widetilde{\Delta}_u)_{31}\right]$$
$$- \frac{4\pi\alpha_e}{M_{\mathrm{KK}}^2}\,L\,Q_u^2\sum_{a=U,u}\left[(\widetilde{\Delta}_a)_{13}\otimes(\widetilde{\Delta}_a)_{31}\right],$$

for $q = u, d$ and $Q = U, D$. Because the coefficient $C_{t\bar{u},\perp}^{(S,1)}$ is of $\mathcal{O}(v^4/M_{\mathrm{KK}}^4)$, we do not present its explicit form. Similar expressions with the index 1 replaced by 2 hold if the initial-state quarks belong to the second generation. The effective couplings $(\Delta_{Q,q}^{(l)})_{ij}$, encoding the overlap between KK gauge bosons and $SU(2)_L$ doublet and singlet quarks of generations i and j, can be found in (3.149). The non-factorizable products $(\widetilde{\Delta}_Q)_{ij}\otimes(\widetilde{\Delta}_q)_{kl}$, *etc.*, arising from the $t_<$ contribution in the KK sums of Section 3.5 are given in Appendix B.2 for completeness. The Wilson coefficients (5.39) are understood to be evaluated at the scale M_{KK}. The inclusion of RG effects (see Appendix A.4) from the evolution down to the top-quark mass scale has only a subleading impact on the results. Details on this evolution can be found in Appendix B.3. While the expressions for $C_{q\bar{q},\|}^{(V,8)}$, $C_{q\bar{q},\perp}^{(V,8)}$, and $C_{t\bar{u},\|}^{(V,8)}$ are exact, in the coefficient $C_{t\bar{u},\|}^{(V,1)}$ containing the exchange of towers with a massive zero mode, we have only kept the leading terms in v^2/M_{KK}^2. The complete expression for $C_{t\bar{u},\|}^{(V,1)}$, including the subleading $\mathcal{O}(v^4/M_{\mathrm{KK}}^4)$ effects from the corrections due to the mixing of fermion zero modes with their KK excitations, can be obtained from the exact formulae given in Chapter 3.

The expressions (5.39) can be easily generalized to the custodial RS model based on the $SU(2)_L \times SU(2)_R \times U(1)_X \times P_{LR}$ bulk gauge group with the help of the expressions presented in sections 3.4 and 3.5. One finds that the left-handed part of the Z-boson contribution to $C_{t\bar{u},\|}^{(V,1)}$ is enhanced by a factor of around 3. The right-handed contribution, however, is protected by the custodial symmetry and thus smaller by a factor of roughly $1/L \approx 1/37$. Importantly, the KK-gluon contributions $C_{q\bar{q},\|}^{(V,8)}$, $C_{q\bar{q},\perp}^{(V,8)}$, and $C_{t\bar{u},\|}^{(V,8)}$, remain unchanged at LO in $\mathcal{O}(v^2/M_{\mathrm{KK}}^2)$. As these corrections will turn out to be the most significant ones, this implies that the predictions for the $t\bar{t}$ observables are rather model-independent.

---

[16]See [213] for the effective $D = 6$ Hamiltonian of the minimal RS model.

Explicit analytic expressions for the Wilson coefficients (5.39) in the ZMA are given in Appendix B.2. Considering just the α_s contributions, and suppressing relative $\mathcal{O}(1)$ factors and numerically subleading terms, one finds from the expressions given in (B.3) the scaling relations

$$S_{u\bar{u},\mathrm{RS}}^{(0)} \sim \frac{4\pi\alpha_s}{M_{\mathrm{KK}}^2} \sum_{A=L,R} F^2(c_{t_A}),$$

$$A_{u\bar{u},\mathrm{RS}}^{(0)} \sim -\frac{4\pi\alpha_s}{M_{\mathrm{KK}}^2} L \left\{ \prod_{q=t,u} \left[F^2(c_{q_R}) - F^2(c_{q_L}) \right] + \frac{1}{3} \sum_{A=L,R} F^2(c_{t_A}) F^2(c_{u_A}) \right\},$$

(5.40)

for the (up-quark) coefficient functions introduced in (5.37) and (5.38). Here, $c_{t_L} \equiv c_{Q_3}$, $c_{t_R} \equiv c_{u_3}$, $c_{u_L} \equiv c_{Q_1}$, and $c_{u_R} \equiv c_{u_1}$.

Given that the bulk-mass parameters of the top and up quarks satisfy $c_{t_A} > -1/2$ and $c_{u_A} < -1/2$, as required to reproduce their masses in an anarchic approach to flavor (see Section 3.2.3, Figure 3.9), the zero-mode profile-factors can be approximated by

$$F^2(c_{t_A}) \approx 1 + 2c_{t_A}, \qquad F^2(c_{u_A}) \approx (-1 - 2c_{u_A}) e^{L(2c_{u_A}+1)},$$

(5.41)

where $A = L, R$. Note that the difference of bulk mass parameters for light quarks $(c_{u_L} - c_{u_R})$ is typically small and positive, while $(c_{t_L} - c_{t_R})$ can be of $\mathcal{O}(1)$ and is usually negative. Applying the approximations given above and expanding in powers of $(c_{u_L} - c_{u_R})$, we finally find

$$S_{u\bar{u},\mathrm{RS}}^{(0)} \sim \frac{4\pi\alpha_s}{M_{\mathrm{KK}}^2} 2 \left(1 + c_{t_L} + c_{t_R} \right),$$

$$A_{u\bar{u},\mathrm{RS}}^{(0)} \sim \frac{4\pi\alpha_s}{M_{\mathrm{KK}}^2} 2 L \, e^{L(1+c_{u_L}+c_{u_R})} \left(1 + c_{u_L} + c_{u_R} \right)$$

$$\times \left\{ \left(2 + \frac{1}{3} \right) L \left(c_{t_L} - c_{t_R} \right) \left(c_{u_L} - c_{u_R} \right) + \frac{1}{3} \left(1 + c_{t_L} + c_{t_R} \right) \right\}.$$

(5.42)

The symmetric function $S_{u\bar{u},\mathrm{RS}}^{(0)}$ is entirely induced by s-channel KK-gluon exchange, whereas the contributions to the asymmetric coefficient $A_{u\bar{u},\mathrm{RS}}^{(0)}$ arise from s channel as well as t channel exchange, corresponding to the term(s) with coefficient 2 and 1/3 in the curly bracket, respectively.

From the relations (5.42) one can read off a couple of interesting consequences. First, the symmetric contribution $S_{u\bar{u},\mathrm{RS}}^{(0)}$, entering the RS prediction for σ_s in (5.31), is in this approximation independent of the localization of the up-quark fields and strictly positive (as long as $c_{t_A} > -1/2$). This leads to an enhancement of the inclusive $t\bar{t}$ production cross section, which gets the more pronounced the closer the right- and left-handed top-quark profiles are localized towards the IR brane.

On the other hand, the asymmetric function $A_{u\bar{u},\mathrm{RS}}^{(0)}$ is exponentially suppressed for UV-localized up quarks, i.e., $c_{u_A} < -1/2$. For typical values of the bulk-mass parameters of $c_{t_L} = -0.34$, $c_{t_R} = 0.57$, $c_{u_L} = -0.63$, and $c_{u_R} = -0.68$ [213], one finds numerically that the first term in the curly bracket of (5.42), which is suppressed by the small difference $(c_{u_L} - c_{u_R})$ of bulk mass parameters, but enhanced by the volume factor L, is larger in magnitude than the

second one by about a factor of 10. As a consequence, to first order the charge asymmetry can be described by only keeping the effects from s-channel KK-gluon exchange. Since generically $(1 + c_{u_L} + c_{u_R})(c_{u_L} - c_{u_R}) < 0$, we find that a positive LO contribution to $A_{u\bar{u},\mathrm{RS}}^{(0)}$ needs $(c_{t_L} - c_{t_R})$ to be negative. This can be achieved in a natural way by localizing the right-handed top quark sufficiently far in the IR. Employing the formulae derived in Section 3.2.3, we obtain, to leading powers in hierarchies, the condition

$$c_{t_R} \gtrsim \frac{m_t}{\sqrt{2}\, v\, |Y_t|} - \frac{1}{2}. \tag{5.43}$$

The top-quark mass is understood to be normalized at the KK scale and $Y_t \equiv (Y_u)_{33}$. Numerically, we find that for $m_t(1\,\mathrm{TeV}) = 144\,\mathrm{GeV}$ and $|Y_t| = 1$, values of c_{t_R} bigger than 0 lead to $A_{u\bar{u},\mathrm{RS}}^{(0)} > 0$ and in consequence to a positive shift in σ_a.

However, the exponential suppression of $A_{u\bar{u},\mathrm{RS}}^{(0)}$ due to the UV-localization of up quarks, as well as the small difference in the bulk-masses for their chiral components (leading to very suppressed axial-vector couplings) render the tree-level contribution to the charge asymmetry in the RS framework tiny.[17] As we will explicitly verify in our numerical analysis, the inclusion of electroweak corrections due to Born-level exchange of the Z boson and its KK excitations, KK excitations of the photon, and of the Higgs boson, do not change this conclusion.

Calculation of NLO effects We have seen that in models with small axial-vector couplings to light quarks and no significant FCNC effects in the t channel, the charge-asymmetric cross section σ_a is suppressed at LO. In the following we want to study if this suppression can be evaded by going to NLO, after paying the price of an additional factor of $\alpha_s/(4\pi)$. Therefore, we first recall how the charge asymmetry arises in the SM (in QCD). Since QCD has only vector couplings, the lowest-order processes $q\bar{q} \to t\bar{t}$ and $gg \to t\bar{t}$, appearing at $\mathcal{O}(\alpha_s^2)$, do not contribute to A_{FB}^t. Starting at $\mathcal{O}(\alpha_s^3)$, quark-antiquark annihilation $q\bar{q} \to t\bar{t}(g)$, as well as flavor excitation $qg \to qt\bar{t}$ receive charge-asymmetric contributions [302, 303]. Gluon fusion $gg \to t\bar{t}(g)$, remains charge-symmetric to all orders in perturbation theory.

Using charge conjugation invariance of QCD, one can show that, as far as the virtual corrections to $q\bar{q} \to t\bar{t}$ are concerned, only the interference between the lowest-order and the QCD box graphs generates an asymmetry at NLO. For the real bremsstrahlungs contributions, along the same lines only the interference between amplitudes that are odd under the exchange of t and $\bar{t}$ contribute to the asymmetric cross section. Since the axial-vector current is even under this exchange, the NLO contribution to the asymmetry is completely due to vector-current contributions.

This implies that at NLO the charge-asymmetric cross section is proportional to the $d_{abc}^2 = \left(2\mathrm{Tr}\left(\{T^a, T^b\}T^c\right)\right)^2$ terms that result from the interference of both the one-loop box and the $t\bar{t}g$ final state diagrams with the tree-level quark-antiquark annihilation diagram [302, 303]. The relevant Feynman diagrams are obtained from the ones shown in Figure 5.8 by replacing the operator insertions by s-channel gluon exchange. The QCD expression for σ_a can be derived from generalizing the result from the electromagnetic process $e^+e^- \to \mu^+\mu^-$ [331, 332] by an appropriate replacement of the QED coupling and the electromagnetic charges. Explicit expressions for the asymmetric contributions to the $t\bar{t}$ production cross section in QCD are

---

[17]See also the statements made in [330] concerning the mostly vector-like couplings of light quarks.
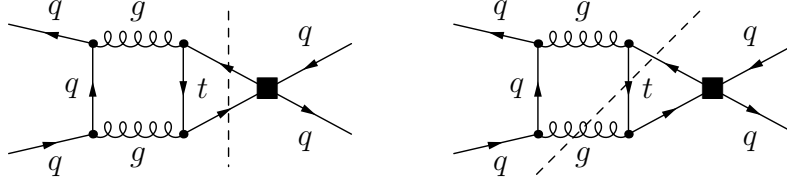
Figure 5.8:   Representative diagrams contributing to A_{FB}^t at NLO. The black square indicates the insertion of an effective operator. The two-particle (three-particle) cut, represented by a dashed line, corresponds to the interference of $q\bar{q} \to t\bar{t}$ ($q\bar{q} \to t\bar{t}g$) with $Q_{q\bar{q},AB}^{(V,8)}$. The SM contribution can be obtained by replacing the operator insertion by s-channel gluon exchange. See [3] and text for details

presented in [303]. Because contributions from flavor excitation are negligibly small at the Tevatron, they will not be taken into account in the following.

From the considerations above we learn that, beyond LO, vector couplings alone are sufficient to generate non-vanishing values of A_{FB}^t. In the case of the EFT (5.33) this means that cut diagrams like the ones shown in Figure 5.8, can give a sizable contribution to the charge asymmetry, if the symmetric combination $C_{q\bar{q}}^V = \left(C_{q\bar{q},\parallel}^{(V,8)} + C_{q\bar{q},\perp}^{(V,8)} \right)$ of Wilson coefficients is large enough. Interestingly, this combination is not suppressed by quark localizations in the RS setup but can become sizable due to the large overlap of the third-generation up-type quark wave functions with those of the KK gluons. From (5.37), (5.38), and (5.42) it is not difficult to show that for the RS model the NLO corrections to σ_a should dominate over the LO corrections, if the condition

$$\frac{\alpha_s}{4\pi}\left(1 + c_{t_L} + c_{t_R}\right) \gtrsim L\, e^{L(1 + c_{u_L} + c_{u_R})} \tag{5.44}$$

is satisfied.[18] Employing the values $c_{t_L} = -0.34$, $c_{u_L} = -0.63$, and $c_{u_R} = -0.68$, the condition (5.44) tells us that for $c_{t_R} = 0.57$ the NLO contributions exceed the LO corrections by a factor of ~ 25. This first look suggests that it might be possible to lift the LO suppression of the asymmetry and reach contributions to A_{FB}^t at the per cent level at NLO with typical and completely natural choices of parameters.

Unlike in QCD, the RS model features further diagrams that generate a charge-asymmetric cross section at NLO, besides those shown in Figure 5.8. Self-energy, vertex, and counterterm diagrams will also contribute to the asymmetry. However, just as the Born-level contribution, these corrections are all exponentially suppressed by the UV localization of the light-quark fields (and the small axial-vector coupling of the light quarks for what concerns the contributions from the operators $Q_{q\bar{q},AB}^{(V,8)}$). Compared to the tree-level corrections, these contributions are thus suppressed by an additional factor of $\alpha_s/(4\pi)$, so that they can be safely ignored. Moreover, we will not consider corrections due to box diagrams involving the virtual exchange of KK gluons.

Encouraged by these considerations we perform a calculation of A_{FB}^t in the RS model beyond LO. The Feynman graphs that we consider are those displayed in Figure 5.8. The

---

[18]This relation only corresponds to a crude approximation, valid up to $\mathcal{O}(1)$ factors.

most important contributions stem from the interference of $q\bar{q} \to t\bar{t}$ and $q\bar{q} \to t\bar{t}g$ with $Q^{(V,8)}_{q\bar{q},AB}$. After integrating over $\cos\theta$, we obtain in the partonic CM frame ($q\bar{q} = u\bar{u}, d\bar{d}$) the asymmetric function[19]

$$A^{(1)}_{q\bar{q},\mathrm{RS}} = \frac{\hat{s}}{16\pi\alpha_s} C^V_{q\bar{q}} A^{(1)}_{q\bar{q}} \,. \tag{5.45}$$

Here, $A^{(1)}_{q\bar{q}}$ is the NLO asymmetric SM coefficient, normalized according to (5.24), which can be parametrized by the function

$$A^{(1)}_{q\bar{q}} = \frac{\alpha_s \, d^2_{abc}}{16 N^2_c} \, 5.994 \, \beta\rho \left[1 + 17.948\,\beta - 20.391\,\beta^2 + 6.291\,\beta^3 + 0.253\,\ln\left(1 - \beta\right)\right], \tag{5.46}$$

which is accurate to the permille level. Here, $N_c = 3$ and $d^2_{abc} = \left(N^2_c - 1\right)\left(N^2_c - 4\right)/N_c = 40/3$. The function (5.46) has been obtained by integrating the expressions for the charge-asymmetric contributions to the differential $t\bar{t}$ production cross section given in [303] over the relevant phase space. For more details see [3]. To judge the quantitative impact of the RS contribution (5.45) we will now perform a numerical analysis.

Numerical Analysis and Discussion

For the numerical analysis we have to take into account that the Wilson coefficients appearing in the effective Lagrangian (5.33) are not only constrained by the measurements of the forward-backward asymmetry A^t_{FB}, but also by the total cross section $\sigma_{t\bar{t}}$, and the $t\bar{t}$ invariant mass spectrum $d\sigma_{t\bar{t}}/dM_{t\bar{t}}$. The Tevatron results ($\sqrt{s} = 1.96\,\mathrm{TeV}$) for these quantities read [291, 296, 297]

$$(\sigma_{t\bar{t}})_{\mathrm{exp}} = (7.50 \pm 0.31_{\mathrm{stat.}} \pm 0.34_{\mathrm{syst.}} \pm 0.15_{\mathrm{lumi.}})\,\mathrm{pb}\,,$$

$$\left(\frac{d\sigma_{t\bar{t}}}{dM_{t\bar{t}}}\right)^{M_{t\bar{t}} \in [800,1400]\,\mathrm{GeV}}_{\mathrm{exp}} = (0.068 \pm 0.032_{\mathrm{stat.}} \pm 0.015_{\mathrm{syst.}} \pm 0.004_{\mathrm{lumi.}})\,\frac{\mathrm{fb}}{\mathrm{GeV}}\,, \tag{5.47}$$

where the quoted individual errors are of statistical and systematic origin, and due to the luminosity uncertainty, respectively. In the case of the $t\bar{t}$ invariant mass spectrum, we consider only the last bin of the CDF measurement, *i.e.*, $M_{t\bar{t}} \in [800, 1400]\,\mathrm{GeV}$, as this is most sensitive to the presence of new degrees of freedom with masses in the TeV range.

These results are to be compared to the predictions obtained in the SM, supplemented by the dimension-six Lagrangian (5.33). In the following we will ignore tiny contributions due to the (anti)strange-, (anti)charm-, and (anti)bottom-quark content of the proton (antiproton). By convoluting the kernels (5.37) with the parton luminosities $f\!f_{ij}(\hat{s}/s, \mu_f)$, by means of the charge-symmetric analogon of formula (5.31), one finds in terms of the dimensionless

---

[19]Note that the quark luminosities $f\!f_{ij}(\hat{s}/s, \mu_f)$ fall off strongly with $\hat{s}$, behaving roughly like $1/\hat{s}^2$. This compensates the factor of $\sqrt{s}$ in (5.45) so that the integrated asymmetric cross section in (5.31) is saturated well before the upper integration limit s is reached [3].

c_{t_L}	c_{t_R}	$\tilde{C}^V_{u\bar{u}}/\alpha_s$	$\tilde{C}^A_{u\bar{u}}/\alpha_s$	$\tilde{C}^V_{d\bar{d}}/\alpha_s$	$\tilde{C}^A_{d\bar{d}}/\alpha_s$	$\tilde{C}^V_{t\bar{u}}/\alpha_s$	$\tilde{C}^S_{t\bar{u}}$
-0.41	0.09	4.50	$0.71 \cdot 10^{-2}$	0.68	$-1.40 \cdot 10^{-3}$	$-1.35 \cdot 10^{-4}$	$8.2 \cdot 10^{-7}$
-0.47	0.48	4.95	$0.22 \cdot 10^{-2}$	0.27	$-0.03 \cdot 10^{-3}$	$-0.70 \cdot 10^{-4}$	$4.1 \cdot 10^{-7}$
-0.49	0.90	5.31	$1.79 \cdot 10^{-2}$	0.08	$-0.64 \cdot 10^{-3}$	$-2.45 \cdot 10^{-4}$	$122 \cdot 10^{-7}$

Table 5.1: Results for the Wilson coefficients corresponding to three different parameter points of the RS setup with $SU(2)_L \times U(1)_Y$ bulk gauge symmetry and brane-localized Higgs sector. The coefficients in the first five columns (last column) scale as $(1\,\text{TeV}/M_{\text{KK}})^2$ $((1\,\text{TeV}/M_{\text{KK}})^4)$.

coefficients $\tilde{C}^V_{q\bar{q}} \equiv 1\,\text{TeV}^2\, C^V_{q\bar{q}}$ and $\tilde{C}^V_{t\bar{u}} \equiv 1\,\text{TeV}^2 \left(1/3\, C^{(V,8)}_{t\bar{u},\parallel} - 2 C^{(V,1)}_{t\bar{u},\parallel}\right)$ the RS results [3]

$$(\sigma_{t\bar{t}})_{\text{RS}} = \left[1 + 0.053\left(\tilde{C}^V_{u\bar{u}} + \tilde{C}^V_{t\bar{u}}\right) - 0.612\,\tilde{C}^S_{t\bar{u}} + 0.008\,\tilde{C}^V_{d\bar{d}}\right]\left(6.73^{+0.52}_{-0.80}\right)\text{pb}\,,$$

$$\left(\frac{d\sigma_{t\bar{t}}}{dM_{t\bar{t}}}\right)^{M_{t\bar{t}} \in [800,1400]\,GeV}_{\text{RS}} = \left[1 + 0.33\left(\tilde{C}^V_{u\bar{u}} + \tilde{C}^V_{t\bar{u}}\right) - 0.81\,\tilde{C}^S_{t\bar{u}} + 0.02\,\tilde{C}^V_{d\bar{d}}\right]\left(0.061^{+0.012}_{-0.006}\right)\frac{\text{fb}}{\text{GeV}}\,.$$
(5.48)

The numerical factors multiplying $\tilde{C}^S_{t\bar{u}}$ correspond to a Higgs mass of $m_h = 115\,\text{GeV}$, which we take as the reference value for the present analysis. The Wilson coefficients are understood to be evaluated at m_t. The RG evolution from M_{KK} down to m_t is performed with the formulae given in Appendix B.3. The result (5.48) corresponds to the `MSTW2008LO` PDFs [333] with renormalization and factorization scales fixed to the reference point $\mu_r = \mu_f = m_t = 173.1$ GeV. The strong coupling constant reads $\alpha_s(m_Z) = 0.139$, which evolves to $\alpha_s(m_t) = 0.126$ using one-loop RG running.

We now present our NLO prediction for the $t\bar{t}$ forward-backward asymmetry. Inserting (5.38),(5.45),(5.46) into (5.31) and (5.28), performing the convolution with the `MSTW2008LO` PDFs with the unphysical scales fixed to m_t and transforming to the $p\bar{p}$ frame one obtains [3]

$$(A^t_{\text{FB}})^{p\bar{p}}_{\text{RS}} = \left[\frac{1 + 0.22\left(\tilde{C}^A_{u\bar{u}} + \tilde{C}^V_{t\bar{u}}\right) + 0.72\tilde{C}^S_{t\bar{u}} + 0.03\tilde{C}^A_{d\bar{d}} + 0.034\tilde{C}^V_{u\bar{u}} + 0.005\tilde{C}^V_{d\bar{d}}}{1 + 0.053\left(\tilde{C}^V_{u\bar{u}} + \tilde{C}^V_{t\bar{u}}\right) - 0.612\tilde{C}^S_{t\bar{u}} + 0.008\tilde{C}^V_{d\bar{d}}}\right]\left(5.6^{+0.8}_{-1.0}\right)\%\,,$$
(5.49)

Here, the NLO result for σ_s has been used for the normalization of the asymmetric cross section, which has been calculated with the help of `MCFM` [334]. All coefficient functions should be evaluated at the scale m_t. The SM prediction for the asymmetry has been obtained by integrating the formulae given in [303] over the relevant phase space, weighted with `MSTW2008LO` PDFs with the unphysical scales fixed to m_t. It is in good agreement with (5.19) as well as with the results of [306, 307].

In the central value of (5.49), we have decided not to include electroweak corrections to the asymmetric cross section. These have been studied in [304, 335] and found to enhance the $t\bar{t}$ forward-backward asymmetry by around 9% to 4%, depending on whether only mixed electroweak-QCD contributions or also purely electroweak corrections are included. In order to account for the additional uncertainty in neglecting these effects we have added in quadrature an error of 5% to the combined scale and PDF uncertainties.

To get a feeling for the importance of the different contributions that enter the RS predic-
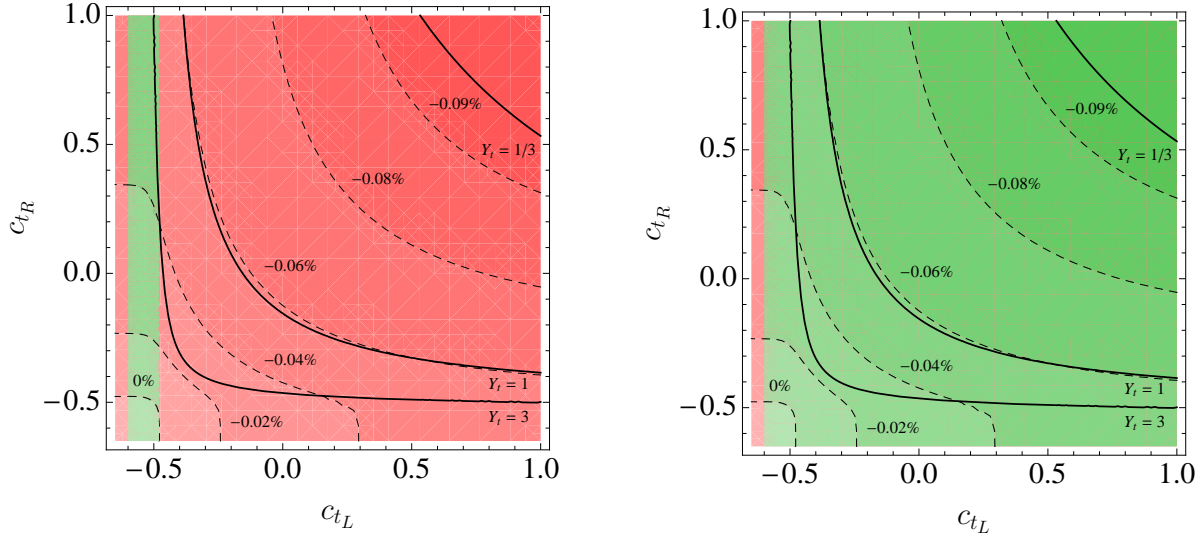
Figure 5.9: Absolute corrections to $(A_{\mathrm{FB}}^t)_{\mathrm{RS}}^{p\bar{p}}$ in the c_{t_L}–c_{t_R} plane for a KK scale of 1 TeV. The solid lines indicate the value of Y_t necessary to reproduce the mass of the top quark. In the left (right) panel the parameter region which satisfies the constraints from the $Z \to b\bar{b}$ pseudo observables for the minimal RS setup (custodial RS setup with extended P_{LR}-symmetry) is displayed in green. See [3] and text for details.

tions (5.48) and (5.49) for the $t\bar{t}$ observables, we give in Table 5.1 numerical results for the relevant Wilson coefficients at the KK scale. The quoted numbers correspond to $M_{\mathrm{KK}} = 1$ TeV and can be easily translated to other scales via the given scaling relations. We present result for three different typical sets of parameters that reproduce the observed quark masses as well as the angles and the CP-violating phase in the quark mixing matrix within errors (68% CL). Out of these parameters we show in the table just the values of the left- and right-handed top-quark bulk mass parameters c_{t_L} and c_{t_R} in order to keep the presentation simple. The complete parameter points, including numerical values for the remaining bulk mass parameters and for the Yukawa matrices, are spelled out in Appendix C. It is important to emphasize that the magnitudes of the shown results are generic predictions in the allowed parameter space and do not reflect a specific choice or tuning of model parameters.

The coefficients in the table exhibit significant hierarchies, which are given approximately by $|\tilde{C}_{q\bar{q}}^A|/|\tilde{C}_{q\bar{q}}^V| = \mathcal{O}(10^{-3})$, $|\tilde{C}_{t\bar{u}}^V|/|\tilde{C}_{u\bar{u}}^V| = \mathcal{O}(10^{-5})$, and $|\tilde{C}_{t\bar{u}}^S|/|\tilde{C}_{u\bar{u}}^V| = \mathcal{O}(10^{-6})$. The contributions due to flavor changing interactions in the t-channel, encoded in $\tilde{C}_{t\bar{u}}^V$ and $\tilde{C}_{t\bar{u}}^S$, are strongly suppressed in the RS model. This is due to the fact that the light up quark is involved, for which the RS-GIM mechanism is very effective. In the minimal RS setup, the ratio of neutral electroweak gauge boson (Higgs-boson) to KK-gluon effects in the t-channel is roughly 1/3 (on average 1/50). In custodial extensions one finds approximately the same suppressions. These factors imply that the predictions for the $t\bar{t}$ observables considered here are to very good approximation model-independent, as they do not depend sensitively on the exact realizations of neither the electroweak gauge, nor the fermionic, nor the Higgs sector. The numerical dominant corrections arise from s-channel KK-gluon exchange. Here, the contributions from up quarks $\tilde{C}_{u\bar{u}}^V$ and $\tilde{C}_{u\bar{u}}^A$ are a factor of a few larger in magnitude than their counterparts

involving down quarks. This feature is amplified by the suppression of the down-quark luminosities $f\!\!f_{d\bar{d}}$ relative to their counterparts for up-quarks entering our predictions, rendering the contributions of the former negligible, not exceeding the per cent level. In the rest of this section we will thus restrict our attention to the coefficients $\tilde{C}_{u\bar{u}}^{V,A}$ that furnish by far the largest contributions to the $t\bar{t}$ observables in RS models.

From the first three columns of Table 5.1, we observe that $\tilde{C}_{u\bar{u}}^{V}$ grows with $(c_{t_L} + c_{t_R})$, *i.e.*, with increasing localization of the top-quark in the IR. This behavior has been expected from (5.42) and (5.43). A similar (expected) trend in terms of c_{t_R} can be seen in $\tilde{C}_{u\bar{u}}^{A}$, however being less pronounced. Our main conclusion from the last Section of strongly suppressed axial-vector couplings, $|\tilde{C}_{u\bar{u}}^{A}|/|\tilde{C}_{u\bar{u}}^{V}| \ll 1$ is also confirmed by the numerical analysis. Inserting the corresponding values into the numerator of (5.49), we observe that also our third expectation holds true. Indeed, in RS models the NLO corrections to the asymmetric cross section, arising from $\tilde{C}_{u\bar{u}}^{V}$, are significantly bigger than the LO contributions, stemming from $\tilde{C}_{u\bar{u}}^{A}$. Numerically, it turns out that the vector-current contributions are, despite their loop suppression, typically larger by about a factor of 100 compared to the corrections due to the axial-vector current. In the light of the experimentally observed enhancement of the asymmetry with respect to the SM prediction, this strong enhancement looks promising at first sight.

However, a closer look at (5.49) shows that in the ratio of the asymmetric and symmetric cross sections the effects of $\tilde{C}_{u\bar{u}}^{V}$ tend to cancel. Because both $\sigma_a^{p\bar{p}}$ and σ_s are enhanced for $\tilde{C}_{u\bar{u}}^{V} > 0$, but the dependence of $\sigma_a^{p\bar{p}}$ on $\tilde{C}_{u\bar{u}}^{V}$ is weaker than the one of σ_s, the found positive values of $\tilde{C}_{u\bar{u}}^{V}$ will effectively lead to a *reduction* and not to an enhancement of the $t\bar{t}$ forward-backward asymmetry. Here, $\sigma_a^{p\bar{p}}$ denotes the asymmetric contribution to the cross section in the $p\bar{p}$ frame. Due to the fact that $\tilde{C}_{u\bar{u}}^{V} > 0$ is a robust prediction of the RS framework, following from the IR localization of the top quark, we conclude that the RS corrections to A_{FB}^{t} are necessarily negative.

Due to the aforementioned cancellation, however, the impact of the RS setup on the $t\bar{t}$ forward-backward asymmetry is very small. This is confirmed by the numerical results presented in Figure 5.9. Here, we show our predictions for the absolute RS corrections to the forward-backward asymmetry in the $p\bar{p}$ frame as a function of c_{t_L} and c_{t_R}. We have employed $M_{\mathrm{KK}} = 1\,\mathrm{TeV}$ and the typical bulk-mass parameters of $c_{u_L} = c_{d_L} = -0.63$, $c_{u_R} = -0.68$, $c_{d_R} = -0.66$, $c_{c_L} = c_{s_L} = -0.56$, $c_{c_R} = -0.53$, $c_{s_R} = -0.63$. Moreover, we have set all minors of $Y_{u,d}$ equal, however $Y_t = (Y_u)_{33}$ is allowed to vary in order to reproduce the correct top-quark mass. Note that only the dominant KK-gluon corrections to $\tilde{C}_{u\bar{u}}^{V,A}$ have been considered. In the left (right) panel the parameter region which satisfies the 99% CL constraints from the $Z \to b\bar{b}$ pseudo observables for the minimal RS setup (custodial RS setup with extended P_{LR}-symmetry) is displayed in green. These constraints have been discussed in detail in Section 5.1.3. Both panels exhibit that in the whole c_{t_L}–c_{t_R} plane the RS corrections to $(A_{\mathrm{FB}}^{t})_{\mathrm{RS}}^{p\bar{p}}$ interfere destructively with the SM contributions. On the other hand, even for the optimistic value of $M_{\mathrm{KK}} = 1\,\mathrm{TeV}$, the maximal possible effect after imposing the $Z \to b\bar{b}$ constraints amounts to -0.10% (-0.05%) for the extended (minimal) RS model. While the $Z \to b\bar{b}$ constraint is very restrictive in the minimal model, cutting the allowed parameter space to a thin stripe of $c_{t_L} \in [-0.60, -0.49]$, it does not affect the extended scenario significantly. Note that the inclusion of the NLO RS contributions to the asymmetric cross section is important to arrive at a consistent result. They contribute at the same order to (5.49) as the RS tree-level corrections to the symmetric cross section. Including all RS corrections, we obtain
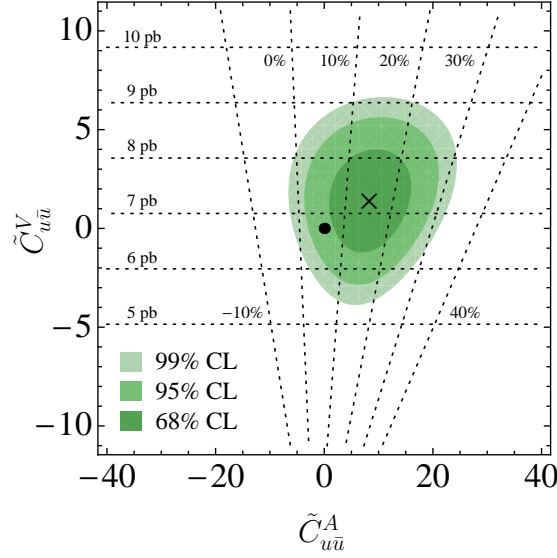
Figure 5.10: Results of a combined fit to $\sigma_{t\bar{t}}$, the last bin of $d\sigma_{t\bar{t}}/dM_{t\bar{t}}$, and the value of $(A_{\mathrm{FB}}^t)^{p\bar{p}}$ allowing for NP in s-channel exchange. The green contours indicate the experimentally allowed regions of 68%, 95%, and 99% probability in the $\tilde{C}_{u\bar{u}}^A$–$\tilde{C}_{u\bar{u}}^V$ plane. The horizontal (almost vertical) dashed lines correspond to the values of the total $t\bar{t}$ cross section (forward-backward asymmetry in the $p\bar{p}$ frame). Further details can be found in the text. Figure from [3].

for the three parameter points considered before the absolute shifts of -0.04%, -0.05%, and -0.05% with respect to the SM value. In conclusion, despite the strong IR localization of top quarks, the RS impact on A_{FB}^t is deemed to be far too small to be able to explain the observed discrepancy between experiment and the SM expectation.

The results presented here should be contrasted with the analysis performed in [310], which finds positive corrections to the $t\bar{t}$ forward-backward asymmetry of up to 5.6% (7%) arising from KK gluons (Z'-boson exchange) at LO. These large corrections are generated by localizing the left- and right-handed components of the light-quark fields at different ends of the extra dimension by choosing $c_{u_L} = c_{d_L} \in [-0.4, 0.4]$ (IR-localized) and $c_{u_R} = c_{d_R} = -0.8$ (UV-localized), which leads to large axial-vector couplings and thus sizable corrections to $\tilde{C}_{q\bar{q}}^A$.[20] However, in an anarchic approach to flavor such a choice is in conflict with observation, as it fails to reproduce the hierarchies of light-quark masses and mixings. Also the more recent analyses of [267] ([325]) abandon the anarchic approach to flavor completely (to some extend).

Our studies have shown that the sensitivity of $A_{\mathrm{FB}}^t = \sigma_a/\sigma_s$ to vector currents is not very pronounced. Our arguments do not only apply to the RS setup but to the broader class of models with new heavy vector states that have suppressed axial-vector couplings to light quarks. In such new-physics scenarios large contributions to the $t\bar{t}$ forward-backward asymmetry are essentially impossible to achieve, once the experimental information on $\sigma_{t\bar{t}}$ and the high-energy tail of the $t\bar{t}$ invariant mass spectrum $d\sigma_{t\bar{t}}/dM_{t\bar{t}}$ is taken into account. This

---

[20]Notice that the convention for the bulk-mass parameters used in [310] differs from ours by an overall sign.

feature is illustrated in Figure 5.10, which shows the results of a fit to the $t\bar{t}$ data (5.18) and (5.47), in the presence of NP in the s channel. The green contours display the experimentally allowed regions of 68%, 95%, and 99% probability in the $\tilde{C}_{u\bar{u}}^{A}$–$\tilde{C}_{u\bar{u}}^{V}$ plane. They makes evident, that in order to achieve a significant improvement in the quality of the fit, large corrections to the axial-vector coefficient $\tilde{C}_{u\bar{u}}^{A}$ are needed. Vector contributions $\tilde{C}_{u\bar{u}}^{V}$ alone are not sufficient to get from the SM point (black dot) at $(0,0)$ to the best-fit value (black cross) at $(8.3, 1.4)$. If we require the $t\bar{t}$ predictions to be within the combined 95% (99%) CL region, the maximal possible values for $(A_{\mathrm{FB}}^{t})^{p\bar{p}}$ from vector contributions alone are 5.8% (6.0%). A possibly large correction to the $t\bar{t}$ forward-backward asymmetry inevitably has to arise from tree-level effects involving either axial-vector currents in the s channel with flavor-specific couplings of opposite sign to light quarks and top quarks or large flavor-changing currents in the t channel. Both of these options are not easy to realize in explicit BSM models, without *ad hoc* assumptions about the structure of the light-quark sector. In consequence, there seems to be a tension between generating large effects in A_{FB}^{t} and achieving a natural solution to the flavor problem.

We have seen that it is not very likely to find hints for warped extra dimensions in measuring the $t\bar{t}$ forward-backward asymmetry. Also the current experimental and theoretical errors on the total and the differential cross sections $\sigma_{t\bar{t}}$ and $d\sigma_{t\bar{t}}/dM_{t\bar{t}}$ are still too large to see a possible impact of the RS setup (see (5.47) and (5.48)). However, in the much cleaner environment of a possible International Linear Collider (ILC), avoiding the complications of colored particles in the initial state, corresponding observables allow to probe very high KK scales. For example a sensitivity to KK masses of (10-30) TeV is possible by a measurement of $\sigma_{t\bar{t}}$ to better than 1% or of the top-quark left-right asymmetry to the same accuracy [336]. Another promising sector where we expect sizable deviations from SM expectations and sensitivities to large KK scales, without having to wait for a new linear collider is Higgs physics, as we will demonstrate in Section 5.3.

5.1.5   The Anomalous Magnetic Moment of the Muon

In the following, we will apply some of the results derived in Chapter 4 to study the anomalous magnetic moment of the muon in the background of a warped extra dimension. In particular, we will show that the corresponding one-loop diagram leads to a finite result. As the muon is a light fermion, we may assume it to be localized on the Planck brane to good approximation. Thus, we will neglect possible contributions from KK fermions in the following. It will turn out that, due to the special structure of the emerging sum, the calculation is also possible in the decomposed theory. We will present this derivation further below. Although the RS EFT is defined with a cutoff, showing the convergence is useful, as this means that it will be possible to sum up the complete tower in closed form.

The magnetic moment $\boldsymbol{\mu}_f$ of a fermion of mass m_f and electromagnetic charge e is proportional to its spin $\boldsymbol{S}$ via

$$\boldsymbol{\mu}_f = g_f \; \frac{e}{2m_f} \boldsymbol{S}. \tag{5.50}$$

The constant g_f is called the *Landé g-factor*. In terms of the form factors $F_1(q^2)$ and $F_2(q^2)$ it is given as

$$g_f = 2\left[F_1(0) + F_2(0)\right]. \tag{5.51}$$

These form factors are defined as coefficients of the possible Lorentz structures in the vertex
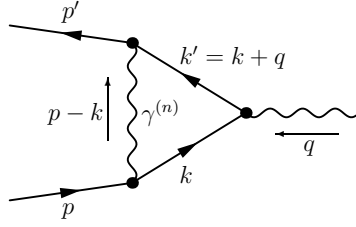
Figure 5.11: NLO contribution to the magnetic moment of a fermion. A straight line corresponds to a fermion while a wiggly line represents a photon. In the RS model, heavy KK excitations of the photon propagate in the loop. See text for details.

function

$$\Gamma^\mu(p', p) = \gamma^\mu F_1(q^2) + \frac{i\sigma^{\mu\nu} q_\nu}{2m_f} F_2(q^2), \tag{5.52}$$

where p (p') is the momentum of the incoming (outgoing) fermion and $q = p' - p$ is the momentum of the external photon, see *e.g.* [16]. Note that $F_1(0) = 1$ to all orders in perturbation theory and $F_2(0) = 0$ to leading order. At the one-loop order, QED predicts a deviation from the Dirac value for an elementary fermion $g_f = 2$, which is determined by the vertex-correction diagram depicted in Figure 5.11 (with $\gamma^{(n)} \to \gamma$). In the case of the electron, this contribution was first calculated by Schwinger [251] who determined the *anomalous magnetic moment* to be

$$a_e \equiv \frac{g_e - 2}{2} = \frac{\alpha}{2\pi}. \tag{5.53}$$

In the RS model, corrections to a_f arise at the one-loop level due to the exchange of a photon that propagates into the extra dimension, as indicated by $\gamma^{(n)}$ in Figure 5.11. In the following, we will show analytically that these corrections are finite, working with the five dimensional mixed momentum/position-space propagators derived in Chapter 4. To this end, we look at the region where the loop-momentum becomes large compared to the KK scale, as this region is critical for the convergence of the result.

5D Calculation

As we study the case of a UV-brane localized fermion, we use the photon propagator for $p \gg M_{\mathrm{KK}}$, given in (4.27), at $t = t' = \epsilon$.

Writing the vertex function as $\Gamma^\mu = \gamma^\mu + \delta\Gamma^\mu$, we obtain at $\mathcal{O}(\alpha)$

$$\bar{u}(p')\delta\Gamma^\mu u(p) = 2ie^2 \frac{iL\epsilon}{2M_{\mathrm{KK}}} \int \frac{d^4k}{(2\pi)^4} \frac{\bar{u}(p') \left[\not{k}\gamma^\mu \not{k}' + m_\mu^2 \gamma^\mu - 2m_\mu(k + k')^\mu \right] u(p)}{\sqrt{(k-p)^2 + i\epsilon} \, (k'^2 - m_\mu^2 + i\epsilon)(k^2 - m_\mu^2 + i\epsilon)}. \tag{5.54}$$

Here, $u(p)$ and $\bar{u}(p')$ are Dirac spinors, belonging to the in- and out-going muon, respectively (see Figure 5.11), and the $i\epsilon$ prescription shifts the poles of the expression above infinitesimally away from the real axis. Note that we have already performed the trivial integral over the extra dimension. While the numerator algebra is in analogy to the SM calculation [16], after

Feynman parametrization, the denominator becomes

$$\int_0^1 dxdydz\,\delta(x+y+z-1)z^{-1/2}\frac{3}{4D^{5/2}}\,, \tag{5.55}$$

with

$$D = l^2 - \Delta + i\epsilon\,. \tag{5.56}$$

Here, as in the SM calculation,

$$\Delta = -xyq^2 + (1-z)^2 m_\mu^2\,, \quad l \equiv k + yq - zp\,. \tag{5.57}$$

Note that (5.54) is just correct for $(k-p)_E \gg M_{\mathrm{KK}}$, which is the region we are interested in. In consequence, after Wick rotation, we evaluate the integral

$$\int_{M_{\mathrm{KK}}}^\infty dl_E \frac{l_E^3}{(l_E^2 + \Delta)^{5/2}} = \frac{2\Delta + 3M_{\mathrm{KK}}^2}{3(\Delta + M_{\mathrm{KK}}^2)^{3/2}}\,. \tag{5.58}$$

The remaining Feynman-parameter integral can easily be solved after performing an expansion in m_μ/M_{KK}. We finally arrive at the UV contribution to the form factor

$$F_2^{\mathrm{RS_{UV}}}(0) = \frac{\alpha}{2\pi}\, L\epsilon\left(-\frac{8}{35}\frac{m_\mu^2}{M_{\mathrm{KK}}^2} + \mathcal{O}\left(\frac{m_\mu^4}{M_{\mathrm{KK}}^4}\right)\right)\,, \tag{5.59}$$

which shows the finiteness of the RS corrections.

4D Calculation

In the following we calculate the RS corrections to the anomalous magnetic moment of the muon in the KK decomposed theory. To this end, we have to compute the contributions to $F_2(0)$ stemming from the infinite sum over vertex-correction diagrams in Figure 5.11, with massive KK photons running in the loop. After performing the loop integral, we arrive at

$$F_2(0) = \frac{\alpha}{2\pi}\left(1 + 2\sum_{n=1}^\infty \int_0^1 dz \int_0^{1-z} dy\, \frac{m_\mu^2\, z(1-z)}{m_\mu^2(1-z)^2 + m_n^2 z}\, I_n\right)\,, \tag{5.60}$$

where m_n $(n > 0)$ is the mass of the nth KK excitation of the photon. The interactions of the fermions with the photons in the extra dimension are described by

$$I_n = 2\pi \chi_n^\gamma(0)\chi_n^\gamma(0)\,, \tag{5.61}$$

where $\chi_n^\gamma(\phi)$ is the profile of the nth KK photon. Expanding (5.60) in the small ratio m_μ/m_n and performing the Feynman parameter integrals, we get

$$F_2(0) = \frac{\alpha}{2\pi}\left(1 + \frac{2m_\mu^2}{3}\sum_{n=1}^\infty \frac{I_n}{m_n^2}\left(1 + \mathcal{O}\left(\frac{m_\mu^2}{m_n^2}\right)\right)\right)\,. \tag{5.62}$$

We are lucky because we can actually perform the infinite sum over boson profiles, weighted by inverse powers of KK masses, appearing in (5.62). Neglecting subleading terms in ϵ it reads (see (3.266))

$$\sum_{n=1}^{\infty} \frac{I_n}{m_n^2} = \frac{1}{2M_{\mathrm{KK}}^2} \frac{1}{2L} + \mathcal{O}\left(\frac{v^2}{M_{\mathrm{KK}}^4}\right), \tag{5.63}$$

which finally leads to

$$F_2(0) = \frac{\alpha}{2\pi}\left(1 + \frac{m_\mu^2}{3M_{\mathrm{KK}}^2}\frac{1}{2L}\right) + \mathcal{O}\left(\frac{m_\mu^2 v^2}{M_{\mathrm{KK}}^4}\right). \tag{5.64}$$

The RS correction to the anomalous magnetic moment of the muon a_μ scales like $\alpha/(2\pi)\, m_\mu^2/(LM_{\mathrm{KK}}^2)$. It is orders of magnitude to small to explain the observed discrepancy in a_μ, mentioned in Section 1.1.6. While the derivations presented here were mainly for illustration purposes, there are more complicated situations, where the approach of using 5D propagators will make calculations more feasible, see Chapter 6.

5.2 Flavor Physics

5.2.1 The CKM Matrix

Remember that our definition of the CKM matrix $\boldsymbol{V}_L$ via effective four-fermion interactions includes the exchange of the whole tower of $W^\pm$ bosons and their KK excitations. As discussed in Section 3.6, this matrix is not unitary (which would also hold true for the mixing matrix $\tilde{\boldsymbol{V}}_L$ defined via the $Wu_L^i d_L^j$ vertex).

As a measure of unitarity violation, one can consider the deviation of the sum of the squares of the elements in the first row of $\boldsymbol{V}_L$ from unity [213],

$$\Delta_1^{\mathrm{non}} = 1 - (|V_{ud}|^2 + |V_{us}|^2 + |V_{ub}|^2) = \left(\boldsymbol{1} - \boldsymbol{V}_L\boldsymbol{V}_L^\dagger\right)_{11}. \tag{5.65}$$

After expanding the mixing matrices $\boldsymbol{U}_{u,d}$ in powers of the Cabibbo angle λ, using the warped-space Froggatt-Nielsen formulae given in Section 3.2.3, and normalizing the result to the typical value of the bulk mass parameter $c_{Q_1} \approx -0.63$, we obtain

$$\Delta_1^{\mathrm{non}} \approx 2 \cdot 10^{-6} \left(\frac{F(c_{Q_1})}{F(-0.63)}\right)^2 \left(\frac{M_{\mathrm{KK}}}{\mathrm{TeV}}\right)^{-2}$$
$$\times \left[\left|\mathrm{diag}\left(\sqrt{\frac{2}{3+2c_{Q_i}}}\right)\vec{u}\right|^2 - \frac{1}{4}\left|\mathrm{diag}\left(\sqrt{\frac{2}{1-2c_{\mathcal{T}_{1i}}}}\right)\boldsymbol{Y}_d^T\vec{u}\right|^2\right], \tag{5.66}$$

where the vector $\vec{u}$ is given by minors of $\boldsymbol{Y}_u$

$$\vec{u} = \left(1, -(M_u)_{21}/(M_u)_{11}, (M_u)_{31}/(M_u)_{11}\right). \tag{5.67}$$

The first contribution in the square brackets in (5.66) stems from the exchange of the whole tower of $W^\pm$ bosons and is also present in the *minimal RS model*. It provides a strictly positive

contribution to Δ_1^{non}, which is typically well below the current experimental uncertainty of $6.5 \cdot 10^{-4}$ [213]. However, the effects due to the admixture of U' and D' quarks add to (5.66) with opposite sign and can in principle lead to negative values of Δ_1^{non}. This is not possible in the minimal RS variant. A detailed discussion of the breakdown of the unitarity of the quark mixing matrix in the minimal RS model has been presented in [213]. A similar analysis for the custodial setup has been performed in [242]. However, in that paper the CKM matrix is defined via the $W u_L^i d_L^j$ vertex and not via the effective four-fermion interactions as discussed above. This prevents us from an easy comparison of the results in [242] with ours. The non-unitarity of the CKM matrix has also been touched on previously in [175, 207]. Yet, a thorough discussion of all relevant effects has not been given in these articles. Note that, while the misalignment between the mass and flavor eigenbases in the sector of quark zero modes is small - as reflected by the Froggatt-Nielsen like mechanism of generating fermion hierarchies in the RS setup - this is not the case for the higher KK levels.

The mixings between the states of the first level of KK excitations are encoded in the flavor vectors $\vec{a}_{4-9}^{(U,D)}$ and $\vec{a}_{4-9}^{(u,d)}$ for the minimal RS variant (and the respective expressions for the custodial model). Naively, one would expect the mixings between KK fermions to be suppressed by the Higgs VEV over the KK scale. On the contrary, one finds very large effects, especially for down type quarks, due to the near degeneracy of the corresponding bulk masses. The mass splittings of the undisturbed KK states, before EWSB, are typical of the order of $100\,\mathrm{GeV}$. Since this is not large compared to v, the Yukawa couplings generically induce $\mathcal{O}(1)$ mixings among the KK excitations of the same KK level (see [1]). These mixings give rise to unsuppressed flavor changing transitions through KK modes within loop diagrams. Numerical values for the neutral-current as well as charged-current mixing-matrices for a default parameter point can be found in [1]. In that article we also presented a numerical analysis of the left- and right-handed CKM matrices, defined via the $W u^i d^j$ vertex.

5.2.2 Rare Decays

As they are suppressed within the SM, FCNCs offer a promising possibility to discover BSM physics. Due to the large mass of the top quark, that leads to its IR localization, one naturally expects sizable effects of RS models in processes involving flavor-changing top-quark couplings. Since FCNCs in the up-type quark sector are less constrained by K- and B-meson physics than those in the down-type quark sector, the presence of such anomalous couplings of non-negligible size is not ruled out experimentally. In consequence, radiative and rare $\Delta F = 1$ processes involving the top quark offer a high potential to test the RS setup. In the following we study the rare decays $t \to cZ$ and $t \to ch$.

Rare Decay $t \to cZ$

From (3.147) we can derive the branching ratio for the decay $t \to cZ$, which is given to excellent approximation by

$$\mathcal{B}(t \to cZ) = \frac{2 \left(1 - r_Z^2\right)^2 \left(1 + 2r_Z^2\right)}{\left(1 - r_W^2\right)^2 \left(1 + 2r_W^2\right)}$$

$$\times \left\{ |(g_L^u)_{23}|^2 + |(g_R^u)_{23}|^2 - \frac{12 r_c r_Z^2}{(1 - r_Z^2)(1 + 2r_Z^2)} \, \mathrm{Re}\big[(g_L^u)_{23}^* \, (g_R^u)_{23} \big] \right\}$$

$$\approx 1.842 \left[|(g_L^u)_{23}|^2 + |(g_R^u)_{23}|^2 \right] - 0.048 \, \mathrm{Re}\big[(g_L^u)_{23}^* \, (g_R^u)_{23} \big] \,, \tag{5.68}$$

where $r_i \equiv m_i^{\mathrm{pole}}/m_t^{\mathrm{pole}}$. For simplicity we keep only terms up to first order in v^2/M_{KK}^2 and the charm-quark mass ratio $r_c \approx 8.7 \cdot 10^{-3}$. As given above, this formula holds for both RS variants studied in this thesis.

The flavor-changing couplings in the *custodial model* are given by

$$(g_L^u)_{23} = -\frac{m_Z^2}{2 M_{\mathrm{KK}}^2} \left(\frac{1}{2} - \frac{2}{3} s_w^2 \right) \left[\omega_Z^{u_L} L \, (\Delta_U)_{23} - (\Delta_U')_{23} \right] - (\delta_U)_{23} \,,$$
$$(g_R^u)_{23} = \frac{m_Z^2}{2 M_{\mathrm{KK}}^2} \frac{2}{3} s_w^2 \left[\omega_Z^{u_R} L \, (\Delta_u)_{23} - (\Delta_u')_{23} \right] + (\delta_u)_{23} \,. \tag{5.69}$$

The ZMA expressions for the matrices $\boldsymbol{\Delta}_U$, $\boldsymbol{\Delta}_U'$, and $\boldsymbol{\Delta}_u'$ are obtained from (3.152) by the replacements $c_{F_i} \to c_{Q_i}$, $c_{f_i} \to c_{u_i^c}$. In the same approximation one has $\boldsymbol{\delta}_U = 1/2 \, \boldsymbol{\Phi}_U$ with $\boldsymbol{\Phi}_U$ introduced in (3.294) and

$$\boldsymbol{\delta}_u = \frac{1}{2} \, \boldsymbol{x}_u \, \boldsymbol{U}_u^\dagger \, \mathrm{diag} \left[\frac{1}{1 - 2c_{Q_i}} \left(\frac{1}{F^2(c_{Q_i})} \left[1 - \frac{1 - 2c_{Q_i}}{F^2(-c_{Q_i})} \right] - 1 + \frac{F^2(c_{Q_i})}{3 + 2c_{Q_i}} \right) \right] \boldsymbol{U}_u \, \boldsymbol{x}_u \,. \tag{5.70}$$

In the *minimal model*, (5.69) holds true with $\omega_Z^{u_L} = \omega_Z^{u_R} = 1$ and an additional factor of $1/2$ in front of $(\delta_{U,u})_{23}$. The corresponding ZMA expressions are given in (3.152) and (3.154). Notice that, compared to the ZMA result in the minimal RS model, the mixing matrix $\boldsymbol{\delta}_u$ above contains an additional term involving the zero-mode profile $F(-c_{Q_i})$.

Inserting the quantum numbers of the representation (3.209) into (3.232), we see that the leading contribution to $(g_L^u)_{23}$ in the custodial model is enhanced by a factor

$$\omega_Z^{u_L} = \frac{2 c_w^2}{1 - \frac{4}{3} s_w^2} \approx 2.2 \,. \tag{5.71}$$

In contrast to the minimal model, the right-handed coupling does not receive an L-enhanced contribution, because

$$\omega_Z^{u_R} = 0 \,. \tag{5.72}$$

Moreover, the contribution that is inversely proportional to $F^2(c_{Q_i})$ in $\boldsymbol{\delta}_u$ is highly suppressed, if $c_{Q_i} < 1/2$, since $F^2(-c_{Q_i}) \approx 1 - 2c_{Q_i}$ in such a case. The leading corrections to the $Z u_R^i \bar{u}_R^j$ vertices due to quark mixing are therefore protected by the custodial symmetry. While these features remove a possible source of large effects associated with the composite nature of the right-handed top quark, they also imply that the chirality of the Ztc interactions in the model under consideration is predicted to be left-handed. Of course, other choices of the quantum numbers of the right-handed up-type quarks than those in Table 3.3 are possible, so that the RS framework does not lead to a firm prediction of the chirality of Ztc interactions. In the minimal RS formulation a slight preference for left-handed couplings is given due to the prefactors in (5.69), however, there is also a large part of the parameter space in which
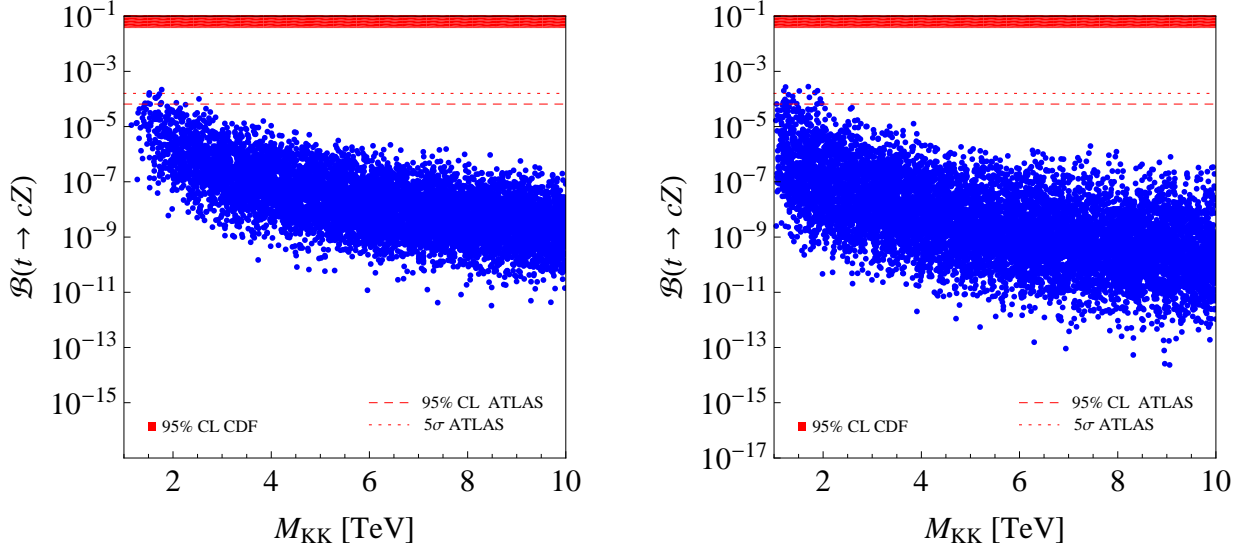
Figure 5.12:   Branching ratio of the rare decay $t \to cZ$ as a function of M_{KK} in the minimal RS model (left) and in the variant with extended custodial protection $c_{\mathcal{T}_{1i}} = c_{\mathcal{T}_{2i}}$ (right). Points that do not satisfy the constraints form the $Z \to b\bar{b}$ pseudo observables are rejected. The red band is excluded at 95% CL by the CDF search for $t \to u(c)Z$. The red dotted and dashed lines indicate the expected discovery and exclusion sensitivities of ATLAS for $100\,\mathrm{fb}^{-1}$ integrated luminosity. See [1, 2] and text for details.

the chirality of Ztc interactions is predominantly right handed. For more details, also on correlations with $B \to X_s l^+ l^-$ decays, see [1].

The predictions for $\mathcal{B}(t \to cZ)$ in the minimal as well as in the custodial RS model with extended P_{LR} symmetry, as a function of M_{KK}, are shown in the left and right panel of Figure 5.12, respectively. The experimental upper bound on FCNC $t \to u(c)Z$ from the CDF experiment amounts to $\mathcal{B}(t \to u(c)Z) < 3.7\%$ at 95% CL [337] and is shown as a band. At the LHC, one can search for rare FCNC top-quark transitions in top-quark production and decays. The ATLAS [338] and CMS [339] collaborations have examined this possibility in simulation studies. The minimal branching ratio $\mathcal{B}(t \to cZ)$ allowing for a 5σ signal discovery with $100\,\mathrm{fb}^{-1}$ integrated luminosity is expected to be $1.6 \cdot 10^{-4}$ at ATLAS. In the absence of a signal, the expected upper bound at 95% CL is $6.5 \cdot 10^{-5}$. These values are visualized by the red dotted and dashed lines in the plots. Our numerical studies show that in the custodial setup, for low KK mass scales in the ballpark of 2 TeV,[21] the branching ratio $\mathcal{B}(t \to cZ)$ can come close to the region which can be probed at the LHC.[22] Such a low KK scale is a realistic possibility in RS models with custodial protection. In the minimal RS model the possible branching ratios are smaller. To a large extend this is due to the rejection of points which fail to satisfy the constraints form the $Z \to b\bar{b}$ pseudo observables. The custodial protection of the $Zb_L\bar{b}_L$ vertex thus leads indirectly to improved prospects of a detection of the decay

---

[21]Corresponding to masses of the lightest KK gauge bosons of around 5 TeV.

[22]As a result of $|F(c_{Q_1})|/|F(c_{Q_2})| \sim \lambda$ the branching ratio of $t \to uZ$ is typically suppressed by two orders of magnitude compared to $t \to cZ$, rendering the former mode unobservable at the LHC. Similar statements apply to the branching ratio of $t \to uh$.
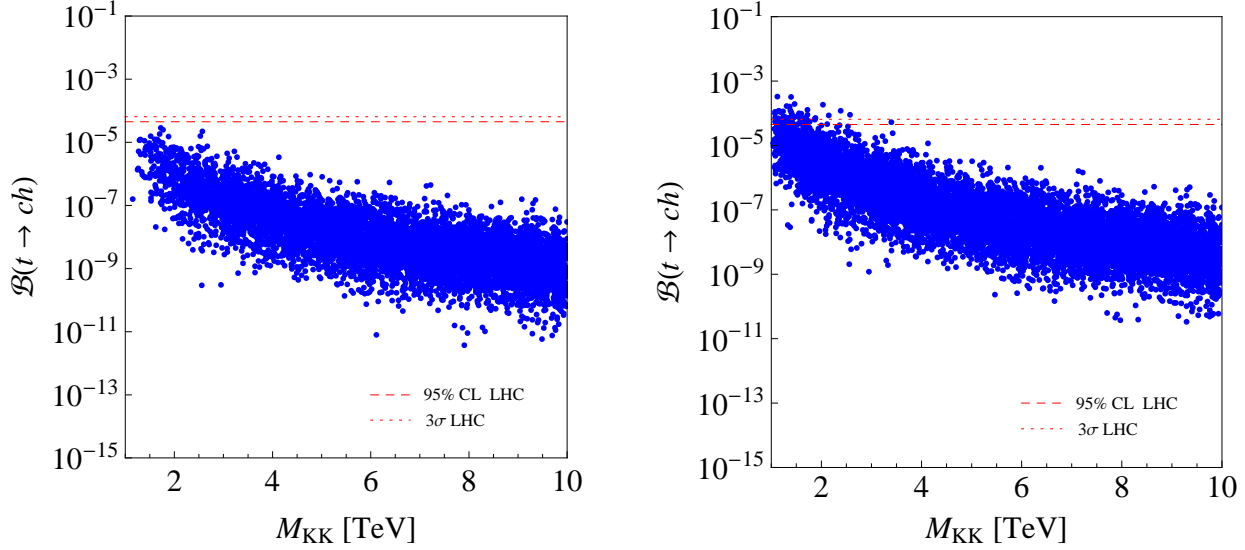
Figure 5.13:   Branching ratio of the rare decay $t \to ch$ as a function of M_{KK} in the minimal RS model (left) and the RS model with extended custodial protection (right). The red dotted and dashed lines indicate the expected discovery and exclusion sensitivities of the LHC for $100\,\mathrm{fb}^{-1}$ integrated luminosity. See [2] and text for details.

$t \to cZ$ at the LHC. Note that there is a strong correlation between the left-handed Ztc and $Zb\bar{b}$ couplings due to the fact that the left-handed top quark resides in the same $SU(2)_L$ doublet as the corresponding bottom quark. On the other hand, the range of predictions in the custodial model also reaches lower values compared to the minimal model. This is due to the custodial protection of the right-handed couplings. These are anti-correlated with the left-handed ones due to the mass relations (3.119). Points that show a pronounced right-handed contribution in the minimal model feature a strongly suppressed Ztc coupling in the custodial model.

Rare Decay $t \to ch$

The general form of the interactions of fermions with the Higgs boson has been given in (3.277). These couplings allow for the flavor-changing decay $t \to ch$ (if kinematically accessible) with a branching ratio

$$\mathcal{B}(t \to ch) = \frac{2\left(1 - r_h^2\right)^2 r_W^2}{\left(1 - r_W^2\right)^2 \left(1 + 2r_W^2\right) g^2} \left\{ |(g_h^u)_{23}|^2 + |(g_h^u)_{32}|^2 + \frac{4r_c}{1 - r_h^2} \mathrm{Re}\left[\,(g_h^u)_{23}\,(g_h^u)_{32}\,\right] \right\}, (5.73)$$

where as before $r_i \equiv m_i^{\mathrm{pole}}/m_t^{\mathrm{pole}}$, and g is the $SU(2)_L$ gauge coupling. Again, we have included terms up to first order in the charm-quark mass. In our numerical analysis we will use $r_h = 0.87$, corresponding to a Higgs-boson mass of $m_h = 150\,\mathrm{GeV}$.

The predictions for $\mathcal{B}(t \to ch)$ in the minimal RS model (custodial RS model with extended P_{LR} symmetry) as a function of M_{KK} are shown in the left (right) panel of Figure 5.13. The LHC is expected to provide a 3σ evidence for $\mathcal{B}(t \to ch)$ larger than $6.5 \cdot 10^{-5}$ or set an upper bound of $4.5 \cdot 10^{-5}$ with 95% CL if the decay is not observed [340]. These limits are indicated

by the red dotted and dashed lines in the plot. We see that for low KK mass scales, the predicted values for the branching ratio in the custodial scenario can even exceed the LHC reach, so that a detection of a possible RS signal with $t \to ch$ could become reality. Let us add that without the inclusion of the Yukawa couplings involving Z_2-odd fermion profiles, the obtained branching fractions would be typically smaller by almost two orders of magnitude, see [1]. In the minimal RS model the prospects for an observation of $t \to ch$ turn out to be less favorable, since the constraints from $Z \to b\bar{b}$ typically eliminate those points in parameter space that would show pronounced effects.

5.2.3 CP Violation in B_s^0-Meson Decays

We have seen in Section 3.2.3 that the RS setup features nine new phases with respect to the SM, providing new sources of CP violation. In this section, we will study CP violating observables in the framework of warped extra dimensions. We will focus on B_s^0-mesons, since due to the hierarchy of CKM matrix elements, CP violation in B_s^0 mixing should be tiny within the SM (and models of MFV). This offers a nice prerequisite to find signs for NP like warped extra dimensions. Moreover, B_s^0 mesons are promising since they are the only mesons that are expected to mix but do not contain first-generation quarks. This lets us expect potentially more significant NP corrections. Beyond that, some anomalies have been reported in the B_s^0-meson sector, recently (see Section 1.1.6 and the remainder of this section). We will analyze corrections to the width difference $\Delta\Gamma_s$, to the semileptonic CP asymmetry A_{SL}^s, as well as to the CP asymmetry $S_{\psi\phi}$. We will perform a thorough calculation of the decay amplitude Γ_{12}^s in the framework of an EFT, based on operator product expansion. As a by-product, we identify a SM contribution missing in the literature. However, although it is of the same size as terms that have been considered, it belongs to a class of numerically suppressed terms and its omission has no significant impact on the numerical predictions. Due to the EFT approach, our results can be used for many new physics models.

Theory of B-Meson Mixing and CP Violation

We start with a breif review of the theory of CP violation in B_q^0-meson ($q = d, s$) decays. For a comprehensive introduction see *e.g.* [73, 74, 75, 118]. One can distinguish between three types of CP violation in meson decays:

(a) CP violation in mixing

(b) CP violation in decay

(c) CP violation in the interference of decays with and without mixing.

Before discussing the origin of these different classes, we have to introduce the theoretical framework to describe B_q^0–$\bar{B}_q^0$ mixing.

For times t that are much larger than the strong interaction scale, the time evolution of the neutral B_q^0–$\bar{B}_q^0$ system can be described by a time-dependent Schrödinger equation [341, 342, 343]. Writing an arbitrary neutral B-meson state at time t as a superposition of the strong interaction eigenstates B_q^0 and $\bar{B}_q^0$

$$|B_q^{0\,\text{phys}}(t)\rangle = b(t)|B_q^0\rangle + \bar{b}(t)|\bar{B}_q^0\rangle, \tag{5.74}$$

its time evolution is given by

$$i\frac{d}{dt}\begin{pmatrix} b(t) \\ \bar{b}(t) \end{pmatrix} = \boldsymbol{H}^q \begin{pmatrix} b(t) \\ \bar{b}(t) \end{pmatrix}. \tag{5.75}$$

The effective 2×2 Hamiltonian

$$\boldsymbol{H}^q = \left(\boldsymbol{M}^q - \frac{i}{2}\boldsymbol{\Gamma}^q \right) \tag{5.76}$$

governs the oscillation and decay of B-mesons and therefore contains an anti-hermitian part proportional to the decay matrix $\boldsymbol{\Gamma}^q$. This matrix and the mass matrix $\boldsymbol{M}^q$ are hermitian and obtained in QFT as the absorptive and dispersive part of the amplitude governing $(B_q^0, \bar{B}_q^0) \leftrightarrow (B_q^0, \bar{B}_q^0)$ transitions, respectively. For example, M_{12}^q corresponds to the dispersive part of the $B_q^0 \to \bar{B}_q^0$ transition. CPT invariance guarantees that $M_{11}^q = M_{22}^q$ and $\Gamma_{11}^q = \Gamma_{22}^q$ and hermiticity leads to $M_{21}^q = M_{12}^{q*}$ and $\Gamma_{21}^q = \Gamma_{12}^{q*}$. The eigenstates of $\boldsymbol{H}^q$ correspond to

$$|B_q^L\rangle = p|B_q^0\rangle + q|\bar{B}_q^0\rangle, \quad |B_q^H\rangle = p|B_q^0\rangle - q|\bar{B}_q^0\rangle, \tag{5.77}$$

with eigenvalues

$$\mu_{L,H}^q = M_{L,H}^q + i\Gamma_{L,H}^q, \tag{5.78}$$

where $|p|^2 + |q|^2 = 1$. Here, $M_{L,H}^q$ and $\Gamma_{L,H}^q$ denote the masses and decay widths of the light and heavy mass eigenstates $B_q^{L,H}$, respectively. We define the mass difference as well as the width difference between these states as

$$\Delta m_{B_q} \equiv M_H^q - M_L^q, \quad \Delta\Gamma_q \equiv \Gamma_L^q - \Gamma_H^q. \tag{5.79}$$

Solving the eigenvalue equation leads to

$$\Delta\Gamma_q = -\frac{4\,\mathrm{Re}(M_{12}^q\Gamma_{12}^{q*})}{\Delta m_{B_q}}, \quad (\Delta m_{B_q})^2 - \frac{1}{4}(\Delta\Gamma_q)^2 = (4|M_{12}^q|^2 - |\Gamma_{12}^q|^2),$$
$$\frac{q}{p} = -\frac{2M_{12}^{q*} - i\Gamma_{12}^{q*}}{\Delta m_{B_q} + \frac{i}{2}\Delta\Gamma_q}. \tag{5.80}$$

It is experimentally known that for B-mesons $\Delta m_{B_q} \gg \Delta\Gamma_q$ and in consequence also $|M_{12}^q| \gg |\Gamma_{12}^q|$ [73, 344]. It follows that to zeroth order in $|\Gamma_{12}^q|/|M_{12}^q|$, which is a very good approximation,

$$\Delta m_{B_q} = 2|M_{12}^q|. \tag{5.81}$$

This results in [345, 346]

$$\Delta\Gamma_q = -\frac{2\,\mathrm{Re}(M_{12}^q\Gamma_{12}^{q*})}{|M_{12}^q|} = 2\,|\Gamma_{12}^q|\,\cos\phi_q, \tag{5.82}$$

where we have defined the relative phase ϕ_q between the mixing and the decay amplitude according to the convention

$$\frac{M_{12}^q}{\Gamma_{12}^q} = -\frac{|M_{12}^q|}{|\Gamma_{12}^q|}\, e^{i\phi_q}, \qquad \phi_q = \arg(-M_{12}^q \Gamma_{12}^{q*})\,. \tag{5.83}$$

Note that, including corrections to first order in $|\Gamma_{12}^q|/|M_{12}^q|$

$$\frac{q}{p} = -\frac{|M_{12}^{q*}|}{|M_{12}^q|}\left[1 - \frac{1}{2}\mathrm{Im}\left(\frac{\Gamma_{12}^q}{M_{12}^q}\right)\right]\,. \tag{5.84}$$

Moreover, we define the decay amplitudes of B-mesons, decaying into a final state f via a decay Hamiltonian $\mathcal{H}_d$, as

$$A_f = \langle f|\mathcal{H}_d|B\rangle\,, \quad \bar{A}_f = \langle f|\mathcal{H}_d|\bar{B}\rangle\,, \tag{5.85}$$

where CP relates A_f and $\bar{A}_f$.[23] Now we can identify conditions for the different types of CP violation mentioned above to be present (see *e.g.* [73]).

1. **CP violation in mixing**: $|q/p| \neq 1$
   This type of CP violation is induced, if the mass eigenstates of the mesons differ from the CP eigenstates. It requires a relative phase between the dispersive and the absorptive part of the $B_q^0 \to \bar{B}_q^0$ transition, *i.e.*, $\phi_q \neq 0, \pi$. CP violation in mixing can be observed through a non-vanishing *semileptonic CP asymmetry*

$$A_{\mathrm{SL}}^q = \frac{\Gamma(\bar{B}_q^{0\,\mathrm{phys}}(t) \to l^+\nu_l X) - \Gamma(B_q^{0\,\mathrm{phys}}(t) \to l^-\bar{\nu}_l X)}{\Gamma(\bar{B}_q^{0\,\mathrm{phys}}(t) \to l^+\nu_l X) + \Gamma(B_q^{0\,\mathrm{phys}}(t) \to l^-\bar{\nu}_l X)}\,, \tag{5.86}$$

   where

$$A_{\mathrm{SL}}^q = \frac{1 - |q/p|^4}{1 + |q/p|^4} = \mathrm{Im}(\Gamma_{12}^q/M_{12}^q)\,. \tag{5.87}$$

   Note that, here and in the following, we denote with $B_q^{0\,\mathrm{phys}}(t)$ ($\bar{B}_q^{0\,\mathrm{phys}}(t)$) a time evolved, initially pure B_q^0-meson ($\bar{B}_q^0$-meson).

2. **CP violation in decay**: $|\bar{A}_{\bar{f}}/A_f| \neq 1$
   CP violation in the decay of a meson requires at least two terms in the decay amplitude to have different weak phases, *i.e.*, phases due to complex parameters in the Lagrangian, and different strong phases, *i.e.*, phases due to intermediate on-shell states. For example this type of CP violation is the only source of the *CP asymmetry in charged B-meson decays*, given by

$$a_{f^\pm} = \frac{\Gamma(B^+ \to f^+) - \Gamma(B^- \to f^-)}{\Gamma(B^+ \to f^+) + \Gamma(B^- \to f^-)}\,. \tag{5.88}$$

---

[23]Note that we will not always use an index to denote the decaying meson type, which however should be clear from the context.

This asymmetry can be calculated from the decay amplitudes as

$$\frac{1 - |\bar{A}_{f-}/A_{f+}|^2}{1 + |\bar{A}_{f-}/A_{f+}|^2}. \tag{5.89}$$

3. **CP violation in the interference of decays with and without mixing**: $\text{Im}(\lambda_f) \neq 0$
This type of CP violation is an effect of the interference between an amplitude for a meson to first mix and then decay and a direct decay amplitude into the same final state. It is induced by a non-vanishing value for the imaginary part of the quantity

$$\lambda_f = \frac{q}{p}\frac{\bar{A}_f}{A_f}. \tag{5.90}$$

It enters the *time dependent CP asymmetry* in the decay into a CP eigenstate $f = \bar{f} = f_{\text{CP}}$

$$\mathcal{A}^q_{f_{\text{CP}}}(t) = \frac{\Gamma(\bar{B}_q^{0\,\text{phys}}(t) \to f_{\text{CP}}) - \Gamma(B_q^{0\,\text{phys}}(t) \to f_{\text{CP}})}{\Gamma(\bar{B}_q^{0\,\text{phys}}(t) \to f_{\text{CP}}) + \Gamma(B_q^{0\,\text{phys}}(t) \to f_{\text{CP}})}, \tag{5.91}$$

which is given by [73]

$$\mathcal{A}^q_f(t) = S_f \sin(\Delta m_{B_q} t) - C_f \cos(\Delta m_{B_q} t),$$
$$S_f = \frac{2\text{Im}\lambda_f}{1 + |\lambda_f|^2}, \qquad C_f = \frac{1 - |\lambda_f|^2}{1 + |\lambda_f|^2}. \tag{5.92}$$

In the case that CP violation from mixing as well as from the direct decay are negligible, one has $|\lambda_{f_{\text{CP}}}| = 1$ and thus $C_{f_{\text{CP}}} = 0$. In consequence $\text{Im}(\lambda_{f_{CP}}) \neq 0$ is the only contributing effect.

Note that all the three types of CP violation have been experimentally observed in Kaon physics, namely by measuring non-zero values for the quantities $\text{Re}(\epsilon_K)$, $\text{Re}(\epsilon'_K)$, and $\text{Im}(\epsilon_K)$, respectively (see *e.g.* [73]).

B_s^0-Meson Observables in the SM and Beyond

Many of the quantities introduced above have been measured in the B_s^0-system, which allows to confront theoretical predictions with experiment.

For example, CDF and DØ presented combined results in the $(\beta_s^{J/\psi\phi}, \Delta\Gamma_s)$–plane [100] which differ from the SM prediction by about 2σ.[24] Here, $\beta_s^{J/\psi\phi} \in [-\pi/2, \pi/2]$ is the CP-violating phase in the interference of mixing and decay (see below), obtained from the time-dependent angular analysis of flavor-tagged $B_s^0 \to J/\psi\phi$ decays. In the SM it is given by [347, 348]

$$\beta_s^{J/\psi\phi} = -\arg\left(-\frac{\lambda_t^{bs}}{\lambda_c^{bs}}\right) = 0.020 \pm 0.005, \tag{5.93}$$

---

[24]However, the latest individual CDF results disagree by 1σ only [101].

with $\lambda_q^{bs} = V_{qb}V_{qs}^*$. The SM value for the width difference reads [349]

$$\Delta\Gamma_s^{\mathrm{SM}} = (0.087 \pm 0.021)\,\mathrm{ps}^{-1}\,. \tag{5.94}$$

The SM prediction for the semileptonic CP asymmetry $(A_{\mathrm{SL}}^s)_{\mathrm{SM}} = (1.9 \pm 0.3)\cdot 10^{-5}$ [349], which is often denoted by a_{sl}^s or a_{fs}^s in the literature, agrees with the direct measurement $(A_{\mathrm{SL}}^s)_{\mathrm{exp}} = -0.0017 \pm 0.0092$ [350] within the (large) error. However, recent measurements of the like-sign dimuon charge asymmetry A_{SL}^b [99], which measures a combination of A_{SL}^s and its counterpart A_{SL}^d of the B_d^0-meson sector [351], imply a deviation in A_{SL}^s of almost 2σ.

In the presence of NP contributions to M_{12}^s and Γ_{12}^s, the observables in B_s^0-physics will receive modifications. We follow [352] and extend the SM expressions according to

$$\begin{aligned}
M_{12}^s &= M_{12}^{s\,\mathrm{SM}} + M_{12}^{s\,\mathrm{NP}} = M_{12}^{s\,\mathrm{SM}} R_M\, e^{i\phi_M}\,, \\
\Gamma_{12}^s &= \Gamma_{12}^{s\,\mathrm{SM}} + \Gamma_{12}^{s\,\mathrm{NP}} = \Gamma_{12}^{s\,\mathrm{SM}} R_\Gamma\, e^{i\phi_\Gamma}\,.
\end{aligned} \tag{5.95}$$

Applying these relations to (5.82) we arrive at the width difference in the presence of NP [353, 354]

$$\Delta\Gamma_s = 2\,|\Gamma_{12}^{s\,\mathrm{SM}}|\,R_\Gamma\,\cos(\phi_s^{\mathrm{SM}} + \phi_M - \phi_\Gamma)\,, \tag{5.96}$$

whereas the semileptonic CP asymmetry (5.87) becomes

$$A_{\mathrm{SL}}^s = \frac{|\Gamma_{12}^{s\,\mathrm{SM}}|}{|M_{12}^{s\,\mathrm{SM}}|}\,\frac{R_\Gamma}{R_M}\,\sin(\phi_s^{\mathrm{SM}} + \phi_M - \phi_\Gamma)\,. \tag{5.97}$$

In order to obtain predictions for these observables in RS models, a calculation of the corresponding corrections $R_{M,\Gamma}$ and $\Phi_{M,\Gamma}$ is necessary. Within the SM, the leading contribution to the dispersive part of the B_s^0–$\bar{B}_s^0$ mixing amplitude appears at the one-loop level. If NP involves FCNCs at the tree level, these give rise to sizable corrections to M_{12}^s and thus also to the mass difference Δm_{B_s}, see (5.81). In the context of RS scenarios, the corrections to M_{12}^s have been calculated in [213, 241] (see also [176, 177] for a first estimate).

Moreover, the presence of tree-level FCNCs and right-handed charged-current interactions gives rise to new decay diagrams. However, NP corrections to the absorptive part of the amplitude are generically suppressed by m_W^2/M_{NP}^2 with respect to the SM contribution, where M_{NP} is the NP mass scale. Yet, as a concrete calculation of such corrections in RS models has not been presented before, we will provide it in the following, for the sake of obtaining a more quantitative prediction. We will give the results both for the minimal as well as the custodial RS variant. Beyond that, since we use an EFT approach, our results will be applicable to a more general class of NP models. Recently, model-independent estimates on A_{SL}^s in the presence of heavy gluons have been presented in [355], taking into account modifications in Γ_{12}^s. NP contributions from electroweak (EW) penguin operators as well as right-handed charged currents have not been considered. However, in RS models the former can compete with or even dominate contributions from QCD penguins. Moreover, part of the latter tend to give the dominant contribution to $\Gamma_{12}^{s\,\mathrm{RS}}$ for the most natural choice of input parameters.

Calculation of Γ_{12}^s in the Presence of New Physics

Within the SM, Γ_{12}^s has been calculated to NLO in QCD [347, 356, 357, 358, 359, 360, 361]. It is given by the hadronic matrix element of the transition operator, which converts $\bar{B}_s^0$ into B_s^0

$$\Gamma_{12}^s = \frac{1}{2m_{B_s}} \langle B_s^0 | \mathcal{T} | \bar{B}_s^0 \rangle \,,$$

$$\mathcal{T} = \text{Disc} \int d^4x \, \frac{i}{2} \, T \left[\mathcal{H}_{\text{eff}}^{\Delta B=1}(x) \mathcal{H}_{\text{eff}}^{\Delta B=1}(0) \right] \,.$$

(5.98)

Taking the discontinuity in the expression above projects out those intermediate states, that are on-shell. A systematic evaluation of the matrix element in powers of $1/m_b$ is possible in the framework of the heavy-quark expansion (HQE), assuming local quark-hadron duality (for a review and references see [362]). At zeroth order, the momentum of the B-meson in its rest frame is equal to the momentum of the bottom quark, while the strange-quark momentum is set to zero. Long-lived intermediate states (with respect to hadronic scales) would normally jeopardize a short-distance treatment of the transition amplitude. For B_q^0-mesons, however, the bottom quark mass corresponds to an additional short-distance scale, leading to a large energy transfer into the intermediate states. Thus, at typical hadronic distances $x > 1/m_b$, the transition of $\bar{B}_s^0$ into B_s^0 is again a local process [356] and the matrix element can be expanded in terms of local $\Delta B = 2$ operators.

We derive the leading contribution to Γ_{12}^s in the presence of NP. The most important corrections to the SM result are given by the interference of SM and NP insertions. QCD corrections are implemented by evolving the Wilson coefficients of the $\Delta B = 1$ operators from the matching scale down to m_b. The leading SM contributions can be written as matrix elements of the $\Delta B = 2$ operators

$$\mathcal{Q}_1 = (\bar{s}_i b_i)_{V-A} (\bar{s}_j b_j)_{V-A} \,,$$

$$\mathcal{Q}_2 = (\bar{s}_i b_i)_{S+P} (\bar{s}_j b_j)_{S+P} \,,$$

(5.99)

where i and j denote color indices (that are summed over). The notation $V \pm A$ denotes the Dirac structure $\gamma^\mu (1 \pm \gamma^5)$ in between the spinors, whereas $S \pm P$ corresponds to $(1 \pm \gamma^5)$. Right-handed charged currents, which occur in RS models, bring about the necessity of further $\Delta B = 2$ operators,

$$\mathcal{Q}_3 = (\bar{s}_i b_j)_{S+P} (\bar{s}_j b_i)_{S+P} \,,$$

$$\mathcal{Q}_4 = (\bar{s}_i b_i)_{S-P} (\bar{s}_j b_j)_{S+P} \,,$$

$$\mathcal{Q}_5 = (\bar{s}_i b_j)_{S-P} (\bar{s}_j b_i)_{S+P} \,,$$

(5.100)

due to the interference of SM with NP insertions. The appropriate $\Delta B = 1$ Hamiltonian, allowing for new right-handed charged currents as well as FCNCs, is given by

$$\mathcal{H}_{\text{eff}}^{\Delta B=1} = \frac{G_F}{\sqrt{2}} \lambda_c^{bs} \left[\sum_{i=1,2} \left(C_i Q_i + C_i^{LL} Q_i + C_i^{LR} Q_i^{LR} + C_i^{RL} Q_i^{RL} \right) + \sum_{i=3}^{10} C_i Q_i \right]$$

$$+ \sum_{i=3}^{10} \left(C_i^{\text{NP}} Q_i + \tilde{C}_i^{\text{NP}} \tilde{Q}_i \right) \,.$$

(5.101)

The operators

$$Q_1 = (\bar{s}_i c_j)_{V-A}(\bar{c}_j b_i)_{V-A}\,,$$
$$Q_2 = (\bar{s}_i c_i)_{V-A}(\bar{c}_j b_j)_{V-A}\,,$$
$$Q_1^{LR} = (\bar{s}_i c_j)_{V-A}(\bar{c}_j b_i)_{V+A}\,,$$
$$Q_2^{LR} = (\bar{s}_i c_i)_{V-A}(\bar{c}_j b_j)_{V+A}\,,$$

(5.102)

arise from (KK) $W^{\pm}$-boson exchange ($Q_{1,2}$), as well as from right handed charged currents ($Q_{1,2}^{LR}$) which correspond to a new structure - compared to the SM - see Section 3.6. The operators Q_i^{RL} are chirality flipped with respect to Q_i^{LR}. We do not include operators of the type RR as their coefficients scale like v^4/M_{KK}^4 in the models at hand. Due to the hierarchies in the CKM matrix and the RS-GIM mechanism, it is sufficient to restrict ourselves on c quarks as intermediate states, when calculating RS corrections involving the charged current-sector. For the SM contribution however, we will include all combinations uc, cu, and uu in our analysis, in addition to the operators given above. Concerning the NP corrections LL, LR, RL, we factor out the CKM factor λ_c^{bs} only for convenience.

As explained in Section 3.6, the experimentally determined values for V_{cb} and V_{cs} from semileptonic B and D decays should be identified with the exchange of all $SU(2)_L$ gauge bosons. In turn, the NP coefficients $C_{1,2}^{LL}$ arise only due to the non-factorizable corrections in (3.270), which can not be absorbed into λ_c^{bs}. In addition to the operators discussed so far, there are also QCD penguin operators

$$Q_3 = (\bar{s}_i b_i)_{V-A}\sum_q (\bar{q}_j q_j)_{V-A}\,,$$
$$Q_4 = (\bar{s}_i b_j)_{V-A}\sum_q (\bar{q}_j q_i)_{V-A}\,,$$
$$Q_5 = (\bar{s}_i b_i)_{V-A}\sum_q (\bar{q}_j q_j)_{V+A}\,,$$
$$Q_6 = (\bar{s}_i b_j)_{V-A}\sum_q (\bar{q}_j q_i)_{V+A}\,,$$

(5.103)

and EW penguin operators

$$Q_7 = \frac{3}{2}(\bar{s}_i b_i)_{V-A}\sum_q Q_q\,(\bar{q}_j q_j)_{V+A}\,,$$
$$Q_8 = \frac{3}{2}(\bar{s}_i b_j)_{V-A}\sum_q Q_q\,(\bar{q}_j q_i)_{V+A}\,,$$
$$Q_9 = \frac{3}{2}(\bar{s}_i b_i)_{V-A}\sum_q Q_q\,(\bar{q}_j q_j)_{V-A}\,,$$
$$Q_{10} = \frac{3}{2}(\bar{s}_i b_j)_{V-A}\sum_q Q_q\,(\bar{q}_j q_i)_{V-A}\,,$$

(5.104)

with $q = u, c, d, s$.

Here, no CKM factors are involved and all light quarks have to be kept as intermediate states, when considering neutral-current insertions only. Finally, there exist also chirality-flipped operators with respect to (5.103) and (5.104), denoted by $\widetilde{Q}_{3..10}$. Note that the possi-

bility of a flavor change on both vertices for NP penguins, as well as the dependence of the Wilson coefficients on the quark flavor q, can be safely neglected due to an additional RS-GIM suppression. For the same reason the chirality flipped penguins $\widetilde{C}^{\text{RS}}_{3..10}$ can be neglected compared to $C^{\text{RS}}_{3..10}$ for bs transitions [213].

Despite of the α/α_s-suppression, the EW penguin operators in the minimal RS model can dominate over the gluon penguins [176, 177, 213]. This is due to the enhancement of the leading correction to the left-handed Z-coupling by the RS-volume L, see Section 3.5. Note that this is not the case in the custodial RS variant featuring a protection for the $Zb_L\bar{b}_L$ vertex. The RS Wilson coefficients for the penguin operators can be obtained from Section 3.5 and have been worked out in [213]. We give them in Appendix B.4 for completeness. There further is the possibility of flavor-changing Higgs couplings which, however, can be neglected compared to the contributions of flavor-changing heavy gauge bosons in RS models.

In double-penguin insertions, we include all light quarks with masses set to zero, besides for m_c. Double penguins also allow for leptons within the cut-diagram. However, as the related SM coefficient is suppressed by α/α_s, it is not possible to obtain large effects from $\bar{s}b \to \bar{\tau}\tau$ transitions, which are less constrained by experiment [363]. Note that this conclusion can be evaded, if this transition is mediated at tree level by light NP particles in the range of $\sim 100\,\text{GeV}$. In that case, the double NP insertion can become comparable to the SM diagrams [364]. Possible candidates are scalar leptoquarks [352, 365]. Given the loose bounds imposed by existing tree- and loop-level mediated $B^0_{d,s}$-meson decays, it has been shown recently [366], that the presence of a single $(\bar{s}b)(\bar{\tau}\tau)$ operator can lead model-independently to an enhancement of Γ^s_{12} of maximally 40% compared to the SM value.

Neglecting intermediate leptons, we find to LO in the HQE

$$\Gamma^s_{12} = -\frac{m_b^2}{12\pi(2M_{B_s})}\,G_F^2(\lambda_c^{bs})^2\,\sqrt{1-4z}$$

$$\left\{ \left[(1-z)(\Sigma_1 + \Sigma_1^{LL}) + \frac{1}{2}(1-4z)(\Sigma_2 + \Sigma_2^{LL}) + 3z\,(\Sigma_3 + K_3^{'LL}) \right.\right.$$

$$-\frac{3}{2}\sqrt{z}\,(\Sigma_1^{LR} + \Sigma_2^{LR} + K_3^{'LR} + K_4^{'LR})$$

$$+\frac{1}{\sqrt{1-4z}}\Big((3\bar{K}_1'' + K_{s1}'' + \frac{3}{2}\bar{K}_2'' + \frac{1}{2}K_{s2}'') + \frac{\lambda_u^{bs}}{\lambda_c^{bs}}(1-z)^2\big((2+z)K_1 + (1-z)K_2\big)$$

$$+\left.\frac{1}{2}\frac{(\lambda_u^{bs})^2}{(\lambda_c^{bs})^2}(2K_1 + K_2)\Big)\right]\langle\mathcal{Q}_1\rangle$$

$$+\left[(1+2z)(\Sigma_1 + \Sigma_1^{LL} - \Sigma_2 - \Sigma_2^{LL}) - 3\sqrt{z}\,(2\Sigma_1^{LR} + \Sigma_2^{LR} - K_4^{'LR}) \right.$$

$$+\frac{1}{\sqrt{1-4z}}\Big((3\bar{K}_1'' + K_{s1}'' - 3\bar{K}_2'' - K_{s2}'')$$

$$+\left. 2\,\frac{\lambda_u^{bs}}{\lambda_c^{bs}}(1-z)^2(1+2z)(K_1 - K_2) + \frac{(\lambda_u^{bs})^2}{(\lambda_c^{bs})^2}(K_1 - K_2)\Big)\right]\langle\mathcal{Q}_2\rangle$$

$$\left. -3\sqrt{z}\,(\Sigma_1^{LR} + 2\Sigma_2^{LR} + K_3^{'LR})\,\langle\mathcal{Q}_3\rangle + 3\sqrt{z}\,(\Sigma_1^{RL} - K_3^{'RL})\,\langle\mathcal{Q}_4\rangle + 3\sqrt{z}\,(\Sigma_2^{RL} - K_4^{'RL})\,\langle\mathcal{Q}_5\rangle \right\}$$

$$-\frac{m_b^2}{12\pi(2M_{B_s})}\sqrt{2}\,G_F\lambda_c^{bs}\,\sqrt{1-4z}$$

$$\left\{\left[(1-z)\,\Sigma_1^{\mathrm{NP}}+\frac{1}{2}(1-4z)\,\Sigma_2^{\mathrm{NP}}+3z\,\Sigma_3^{\mathrm{NP}}\right.\right.$$

$$\left.+\frac{1}{\sqrt{1-4z}}(3\bar{K}_1^{''\mathrm{NP}}+K_{s1}^{''\mathrm{NP}}+\frac{3}{2}\bar{K}_2^{''\mathrm{NP}}+\frac{1}{2}K_{s2}^{''\mathrm{NP}})\right]\langle\mathcal{Q}_1\rangle$$

$$+\left[(1+2z)(\Sigma_1^{\mathrm{NP}}-\Sigma_2^{\mathrm{NP}})\right.$$

$$\left.\left.+\frac{1}{\sqrt{1-4z}}(3\bar{K}_1^{''\mathrm{NP}}+K_{s1}^{''\mathrm{NP}}-3\bar{K}_2^{''\mathrm{NP}}-K_{s2}^{''\mathrm{NP}})\right]\langle\mathcal{Q}_2\rangle\,+\,\mathcal{O}\left(\frac{1}{m_b}\right)\right\},\qquad(5.105)$$

where $z=m_c^2/m_b^2$ and $\langle\mathcal{Q}\rangle\equiv\langle B_s^0|\,\mathcal{Q}\,|\bar{B}_s^0\rangle$. In order to get a compact result, we have defined the linear combinations ($A,B\in\{L,R\}$)

$$\begin{aligned}
\Sigma_i &= K_i+K_i'+K_i''\,,\\
\Sigma_i^{AB} &= K_i^{AB}+K_i'^{AB}\,,\quad i=1,2,\\
\Sigma_3 &= K_3'+K_3''\,,\\
\Sigma_i^{\mathrm{NP}} &= K_i'^{\mathrm{NP}}+K_i''^{\mathrm{NP}}\quad i=1,2,3\,,
\end{aligned}\qquad(5.106)$$

where the coefficients on the right-hand side of (5.106) are again linear combinations of Wilson coefficients. In agreement with [356] we get ($C_{i+j}\equiv C_i+C_j$)

$$\begin{aligned}
K_1 &= N_c C_1^2+2\,C_1 C_2\,,\quad K_2=\,C_2^2\,,\\
K_1' &= 2\,(N_c C_1 C_{3+9}+C_1 C_{4+10}+C_2 C_{3+9})\,,\\
K_2' &= 2\,C_2 C_{4+10}\,,\\
K_3' &= 2\,(N_c C_1 C_{5+7}+C_1 C_{6+8}+C_2 C_{5+7}+C_2 C_{6+8})\,,\\
K_1'' &= N_c C_{3+9}^2+2\,C_{3+9}C_{4+10}+N_c C_{5+7}^2+2\,C_{5+7}C_{6+8}\,,\\
K_2'' &= C_{4+10}^2+C_{6+8}^2\,,\\
K_3'' &= 2(N_c C_{3+9}C_{5+7}+C_{3+9}C_{6+8}+C_{4+10}C_{5+7}+C_{4+10}C_{6+8})\,.
\end{aligned}\qquad(5.107)$$

The combinations K_i are due to insertions of charged-current operators and are responsible for the dominant contribution in the SM. The coefficients K_i' and K_i'' correspond to the interference of charged-current operators with penguin operators and penguin-penguin insertions, respectively. As we consider light quarks ($q=u,d,s$) in the limit $m_q=0$, there is a cancellation in the EW penguin sector due to the electric charges. The coefficients $\bar{K}_i''$ therefore resemble the K_i'', with $C_{7..10}$ set to zero. For strange quarks as intermediate states, there is a second possibility for the penguin insertion. In the limit $m_s=0$, there are additional

contributions from

$$
\begin{aligned}
K''_{s1} &= (2 + N_c)(C_4 - C_{10}/2)^2 + 2\,(N_c + 1)(C_3 - C_9/2)(C_4 - C_{10}/2) + 2\,(C_3 - C_9/2)^2\,, \\
K''_{s2} &= 2\,(C_3 - C_9/2)(C_4 - C_{10}/2) + (C_3 - C_9/2)^2\,.
\end{aligned}
\tag{5.108}
$$

Note that these terms have not been taken into account in [356]. On the other hand, as all double-penguin insertions are numerically suppressed, this omission has no significant effect.

Next we come to the interference of SM diagrams with NP penguins, which is collected in

$$
\begin{aligned}
K'^{\mathrm{NP}}_1 &= 2\,(N_c C_1 C^{\mathrm{NP}}_{3+9} + C_1 C^{\mathrm{NP}}_{4+10} + C_2 C^{\mathrm{NP}}_{3+9})\,, \\
K'^{\mathrm{NP}}_2 &= 2\,C_2 C^{\mathrm{NP}}_{4+10}\,, \\
K'^{\mathrm{NP}}_3 &= 2\,(N_c C_1 C^{\mathrm{NP}}_{5+7} + C_1 C^{\mathrm{NP}}_{6+8} + C_2 C^{\mathrm{NP}}_{5+7} + C_2 C^{\mathrm{NP}}_{6+8})\,, \\
K''^{\mathrm{NP}}_{s1} &= 2\,\big((N_c + 2)C_4(C^{\mathrm{NP}}_4 - C^{\mathrm{NP}}_{10}/2) + (N_c + 1)C_4(C^{\mathrm{NP}}_3 - C^{\mathrm{NP}}_9/2) \\
&\qquad + (N_c + 1)C_3(C^{\mathrm{NP}}_4 - C^{\mathrm{NP}}_{10}/2) + 2C_3(C^{\mathrm{NP}}_3 - C^{\mathrm{NP}}_9/2)\big)\,, \\
K''^{\mathrm{NP}}_{s2} &= 2\,\big(C_3(C^{\mathrm{NP}}_3 - C^{\mathrm{NP}}_9/2) + C_3(C^{\mathrm{NP}}_4 - C^{\mathrm{NP}}_{10}/2) + C_4(C^{\mathrm{NP}}_3 - C^{\mathrm{NP}}_9/2)\big)
\end{aligned}
\tag{5.109}
$$

and

$$
\begin{aligned}
K''^{\mathrm{NP}}_1 &= 2\,(N_c C_3 C^{\mathrm{NP}}_{3+9} + C_3 C^{\mathrm{NP}}_{4+10} + C_4 C^{\mathrm{NP}}_{3+9} + N_c C_5 C^{\mathrm{NP}}_{5+7} + C_5 C^{\mathrm{NP}}_{6+8} + C_6 C^{\mathrm{NP}}_{5+7})\,, \\
K''^{\mathrm{NP}}_2 &= 2\,(C_4 C^{\mathrm{NP}}_{4+10} + C_6 C^{\mathrm{NP}}_{6+8})\,, \\
K''^{\mathrm{NP}}_3 &= 2\,(N_c C_3 C^{\mathrm{NP}}_{5+7} + C_3 C^{\mathrm{NP}}_{6+8} + C_4 C^{\mathrm{NP}}_{5+7} + C_4 C^{\mathrm{NP}}_{6+8} \\
&\qquad + N_c C_5 C^{\mathrm{NP}}_{3+9} + C_5 C^{\mathrm{NP}}_{4+10} + C_6 C^{\mathrm{NP}}_{3+9} + C_6 C^{\mathrm{NP}}_{4+10})\,.
\end{aligned}
\tag{5.110}
$$

Here, we have neglected the tiny contributions from the interference of SM EW penguins with NP graphs. In addition, there are contributions from the interference of NP charged currents with SM penguins

$$
\begin{aligned}
K'^{LL}_1 &= 2\,(N_c C_3 C^{LL}_1 + C_3 C^{LL}_2 + C_4 C^{LL}_1)\,, \\
K'^{LL}_2 &= 2\,C_4 C^{LL}_2\,, \\
K'^{LL}_3 &= 2\,(N_c C_5 C^{LL}_1 + C_5 C^{LL}_2 + C_6 C^{LL}_1 + C_6 C^{LL}_2)\,, \\
K'^{LR}_1 &= 2\,(N_c C_3 C^{LR}_1 + C_3 C^{LR}_2 + C_4 C^{LR}_1)\,, \\
K'^{LR}_2 &= 2\,C_4 C^{LR}_2\,, \\
K'^{LR}_3 &= 2\,(N_c C_5 C^{LR}_1 + C_5 C^{LR}_2 + C_6 C^{LR}_1)\,, \\
K'^{LR}_4 &= 2\,C_6 C^{LR}_2\,.
\end{aligned}
\tag{5.111}
$$

The corrections to the purely charged-current interactions are given by

$$
\begin{aligned}
K_1^{LL} &= 2\left(N_c C_1 C_1^{LL} + C_1 C_2^{LL} + C_2 C_1^{LL}\right), \\
K_2^{LL} &= 2\,C_2 C_2^{LL}, \\
K_1^{LR} &= 2\left(N_c C_1 C_1^{LR} + C_1 C_2^{LR} + C_2 C_1^{LR}\right), \\
K_2^{LR} &= 2\,C_2 C_2^{LR}.
\end{aligned}
\tag{5.112}
$$

The coefficients $K_i^{(')RL}$ resemble $K_i^{(')LR}$, with C_i^{LR} replaced by C_i^{RL}. In oder to arrive at the form (5.105) we have used several chiral Fierz identities [367]. A nice method to obtain them in an easy way is presented in [368]. All NP coefficients should by calculated at the NP mass scale and then evolved down to m_b. Explicit expressions for the Wilson coefficients of the minimal as well as the custodial RS model are given in the appendices B.4 and B.5.

The dispersive part of the mixing amplitude has been calculated for RS models in the literature [213, 241]. The required effective Hamiltonian reads

$$
\mathcal{H}_{\mathrm{eff}}^{\Delta B=2} = \sum_{i=1}^{5} C_i \mathcal{Q}_i + \sum_{i=1}^{3} \widetilde{C}_i \widetilde{\mathcal{Q}}_i.
\tag{5.113}
$$

Note that there are no tree-level contributions to $C_{2,3}$ and $\widetilde{C}_{2,3}$ in the RS model. The RS correction to

$$
2\,m_{B_s} M_{12}^s = \langle B_s^0 | \mathcal{H}_{\mathrm{eff}}^{\Delta B=2} | \bar{B}_s^0 \rangle
\tag{5.114}
$$

is given by [213, 241]

$$
M_{12}^{s\,\mathrm{RS}} = \frac{4}{3}\, m_{B_s} f_{B_s}^2 \left[\left(C_1^{\mathrm{RS}}(\bar{m}_b) + \widetilde{C}_1^{\mathrm{RS}}(\bar{m}_b) \right) B_1 + \frac{3}{4}\, R(\bar{m}_b)\, C_4^{\mathrm{RS}}(\bar{m}_b) B_4 + \frac{1}{4}\, R(\bar{m}_b)\, C_5^{\mathrm{RS}}(\bar{m}_b) B_5 \right].
\tag{5.115}
$$

The bag parameters $B_{1,4,5}$, related to hadronic matrix elements evaluated on the lattice, are listed in (5.120). The $\Delta B = 2$ Wilson coefficients can be found in Appendix B.6. Compared to $C_1^{\mathrm{RS}}(\bar{m}_b)$, the coefficient $C_4^{\mathrm{RS}}(\bar{m}_b)$ is suppressed by about two orders of magnitude due to a stronger RS-GIM mechanism. The coefficients $\widetilde{C}_1^{\mathrm{RS}}(\bar{m}_b)$ and $C_5^{\mathrm{RS}}(\bar{m}_b)$ are even further suppressed. The SM mixing amplitude can be obtained from [76, 347, 369] and reads

$$
M_{12}^{s\,\mathrm{SM}} = \frac{G_F^2}{12\,\pi^2}\, (\lambda_t^{bs})^2 m_W^2 m_{B_s} \eta_B f_{B_s}^2 B_1 S_0(x_t).
\tag{5.116}
$$

Here $\eta_B = 0.837$ includes NLO QCD corrections in naive dimensional reduction (NDR). $S_0(x_t)$ is the Inami-Lim function and $x_t = \bar{m}_t(\bar{m}_t)^2/m_W^2$ with $\bar{m}_t(\bar{m}_t) = (163.8 \pm 2.0)\,\mathrm{GeV}$. We use $m_{B_s} = 5.366(1)\,\mathrm{GeV}$ [12] and $f_{B_s} = (238.8 \pm 9.5)\,\mathrm{MeV}$ [370] for the B_s^0 meson mass and decay constant, respectively. If not stated otherwise, all other experimental input for this section is taken from [12].

Numerical Analysis for RS Models and Discussion

We now present our numerical predictions for the RS setup, based on the anarchic parameter sets described at the beginning of this Chapter. In Table 5.2, we give the contributions of

Model/Coef.	$|\tilde{K}_2'|$	$|\tilde{K}_2''|$	$|K_2^{(LL)}|$	$|K_2^{LR}|$	$|K_2^{RL}|$	$\times$
SM	0.543	0.016	12.656	-	-	10^{-1}
mean (min RS)	0.16	0.03	0.01	4.40	0.04	10^{-3}
stand. dev.	0.17	0.03	0.05	7.41	0.06	10^{-3}
mean (cust)	0.94	0.06	0.23	2.22	0.03	10^{-3}
stand. dev.	1.39	0.09	1.38	4.98	0.05	10^{-3}

Table 5.2: Selected SM-penguin and charged-current coefficients contributing to Γ_{12}^s compared to the mean absolute values of the corresponding RS coefficients for $M_{\text{KK}} = 2\,\text{TeV}$ and $\mu = \bar{m}_b$. See text for details.

selected individual ingredients of Γ_{12}^s (5.105). The SM coefficients are taken from [371]. As they are not supplemented with a CKM factor in (5.101), we rescale the RS penguin coefficients - for instance $\tilde{K}_2'^{\text{RS}} \equiv \sqrt{2}\,(G_F \lambda_c^{bs})^{-1} K_2'^{\text{RS}}$ (SM: $\tilde{K}_2' = K_2'$) - to allow for an easier comparison. The mean absolute values of our RS predictions should be compared to the corresponding SM results, where the numbers have to be multiplied by the order of magnitude given in the last column. The maximum values exceed the given numbers by at least one order of magnitude, as suggested by the large standard deviations. We have set the NP scale to $M_{\text{KK}} = 2\,\text{TeV}$ and have discarded all points, which are in conflict with the $Z \to b\bar{b}$ pseudo observables. For the purpose of this analysis, we reject all points lying outside the 95% confidence region in the $g_L^b - g_R^b$ plane. For the minimal RS model this sets a quite stringent upper limit on c_{b_L}, see Section 5.1.3. Within the custodial RS variant with a protection for the $Zb_L\bar{b}_L$-vertex, the respective bound vanishes.

Neglecting experimental constraints, there is no difference between the minimal and the custodial RS variant at LO in v^2/M_{KK}^2 in the charged current sector (see Appendix B.5). For the natural assumption of $c_{Q_2} < -1/2$, see Figure 3.9, the biggest correction stems from the operator Q_2^{LR}. This is easy to understand if we apply the Froggatt-Nielsen analysis of Section 3.2.3 to (B.12) and (B.15). Setting all Yukawa factors to one and performing an expansion in the Wolfenstein parameter λ, we find as a crude approximation

$$C_2^{LL} \propto \frac{m_W^2}{2M_{\text{KK}}^2}\,L\,F(c_{Q_2})^2 F(c_{Q_3})^2\,, \tag{5.117}$$

$$C_2^{LR} \propto \frac{v^2}{2M_{\text{KK}}^2}\,\frac{F(c_{Q_3})}{F(c_{Q_2})}\,F(c_{u_2})F(c_{d_3}) \propto \frac{m_c m_b}{M_{\text{KK}}^2}\,\frac{1}{F(c_{Q_2})^2}\,,$$

$$C_2^{RL} \propto \frac{v^2}{M_{\text{KK}}^2}\,F(c_{u_2})F(c_{d_2}) \propto \frac{2\,m_c m_s}{M_{\text{KK}}^2}\,\frac{1}{F(c_{Q_2})^2}\,.$$

Note that the importance of C_2^{LR} grows with increasing *UV-localization* of the $(c_L, s_L)^T$ doublet, which explains its rather large size. This effect is caused by fermion mixing. Technically, the chiral suppression in small masses is lifted by the inverse zero-mode profiles (which are strongly suppressed) entering C_2^{LR}. The same holds true for C_2^{RL}, which is however smaller by a factor of m_s/m_b. The coefficients C_1^{AB} with $A, B \in \{L, R\}$ are zero at the matching scale, but generated through operator mixing in the evolution down to $\mu = \bar{m}_b$. At $\mu = \bar{m}_b$, the values of $|K_1^{AB}|$ amount to about a third of the corresponding values of $|K_2^{AB}|$. In the RS

model the contributions from the coefficients C_i^{LL} and C_i^{RL} can be safely neglected, just as those of the chirality flipped penguins.

The coefficients $K_i'^{\text{RS}}$ and $K_i''^{\text{RS}}$ grow with an increasing IR localization value of c_{b_L} and $c_{s_L} \equiv c_{Q_2}$. The reason is, that the RS corrections due to penguin operators are dominated by overlap integrals of left-handed fermions with intermediate KK-gauge bosons and mixing effects of the latter with the Z-boson. The corresponding RS expressions are given in (B.8). As KK modes are peaked towards the IR brane, overlap integrals with UV localized fermions are exponentially suppressed and the RS-GIM mechanism is at work. As mentioned before, the leading correction due to Z exchange is enhanced by a factor L within the minimal RS variant. Nevertheless, because of the stringent bounds from $Zb\bar{b}$, the total penguin contributions remain smaller than in the custodial model. In both RS setups, it is sufficient to consider only the contributions stemming from the coefficients $K_i'^{\text{NP}}$ in the neutral-current sector. The impact of double penguin contributions amounts typically to about 1% of the leading correction due to charged currents.

In order to arrive at a global picture, we have to evaluate the whole expressions (5.105) and (5.115). In terms of

$$R(\mu) \equiv \left(\frac{M_{B_s}}{\bar{m}_b(\mu) + \bar{m}_s(\mu)} \right)^2, \tag{5.118}$$

the matrix elements are given by

$$\begin{aligned}
\langle \mathcal{Q}_1 \rangle &= \frac{8}{3} M_{B_s}^2 f_{B_s}^2 B_1(\mu), \\
\langle \mathcal{Q}_2 \rangle &= -\frac{5}{3} M_{B_s}^2 f_{B_s}^2 R(\mu) B_2(\mu), \\
\langle \mathcal{Q}_3 \rangle &= \frac{1}{3} M_{B_s}^2 f_{B_s}^2 R(\mu) B_3(\mu), \\
\langle \mathcal{Q}_4 \rangle &= 2 M_{B_s}^2 f_{B_s}^2 R(\mu) B_4(\mu), \\
\langle \mathcal{Q}_5 \rangle &= \frac{2}{3} M_{B_s}^2 f_{B_s}^2 R(\mu) B_5(\mu).
\end{aligned} \tag{5.119}$$

The bag parameters B_i are obtained from the lattice. We take the values of [372] in the NDR-$\overline{\text{MS}}$ scheme of [357]. They read

$$\begin{aligned}
B_1 &= 0.87(2) \left({}^{+5}_{-4} \right), \quad B_2 = 0.84(2)(4), \quad B_3 = 0.91(3)(8), \\
B_4 &= 1.16(2) \left({}^{+5}_{-7} \right), \quad B_5 = 1.75(3) \left({}^{+21}_{-6} \right),
\end{aligned} \tag{5.120}$$

where the first (second) number in brackets corresponds to the statistical (systematic) error. In order to resum large logarithms we employ $\bar{z} = \bar{m}_c^2(\bar{m}_b)/\bar{m}_b^2(\bar{m}_b) = 0.048(4)$ [347] in our numerical analysis. We use $\bar{m}_b(\bar{m}_b) = (4.22 \pm 0.08)\,\text{GeV}$ and $\bar{m}_s(\bar{m}_b) = (0.085 \pm 0.017)\,\text{GeV}$ for the quark masses in the $\overline{\text{MS}}$ scheme.

The left panel of Figure 5.14 shows the RS corrections to the magnitude and CP-violating phase of the $\bar{B}_s^0$–B_s^0 decay width, R_Γ and ϕ_Γ, for the 10000 parameter sets, generated as described before. For the analysis of this section we do not vary the KK scale but rather chose $M_{\text{KK}} = 2\,\text{TeV}$. The blue (dark gray) points correspond to the minimal RS model, where only points that are in agreement with the $Z \to b\bar{b}$ pseudo observables are shown. The orange
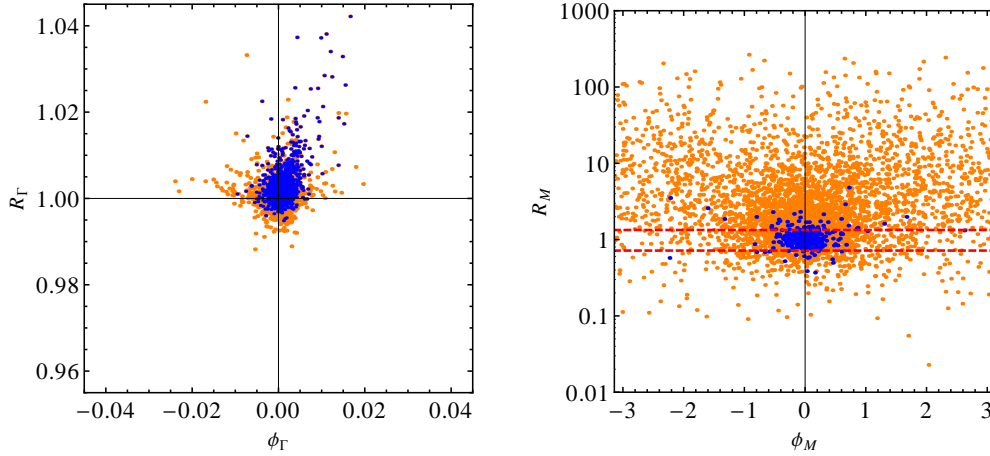
Figure 5.14: RS corrections to the magnitude and CP-violating phase of the $\bar{B}_s^0$–B_s^0 decay amplitude, R_Γ and ϕ_Γ (left), as well as of the dispersive part of the mixing amplitude, R_M and ϕ_M (right). Blue (dark gray) points correspond to the minimal, orange (light gray) to the custodial RS model. The dashed lines indicate the 95% confidence region from the measurement of Δm_{B_s}. See [4] and text for details.

(light gray) points correspond to the custodial extension, where the latter constraint effectively vanishes. As we are just interested in the approximate size of RS corrections, we work with the LO SM expressions. However, for precise predictions for a certain parameter point, one should include the full NLO corrections to Γ_{12}^s and M_{12}^s. As expected, the RS corrections to $|\Gamma_{12}^s|$ are rather small, typically not exceeding $\pm 4\%$. The right panel displays the corrections to the magnitude and phase of the dispersive part of the mixing amplitude, R_M and ϕ_M. For this analysis, important constraints arise from the measurement of the $\bar{B}_s^0$–B_s^0 oscillation frequency. The corresponding result for the mass difference reads [373]

$$\Delta m_{B_s}^{\mathrm{exp}} = (17.77 \pm 0.10\,(\mathrm{stat}) \pm 0.07\,(\mathrm{syst}))\,\mathrm{ps}^{-1}\,, \tag{5.121}$$

and is in good agreement with the SM prediction of $(17.3 \pm 2.6)\,\mathrm{ps}^{-1}$ [349]. As a consequence, we exclude all points with $R_M \notin [0.718, 1.336]$, which corresponds to the 95% CL region of (5.121). This is indicated by the dashed lines. Note that for a sufficient amount of scatter points, the phase correction ϕ_M can take any value in $[-\pi, \pi]$ within the custodial RS model. Comparing the results for the new phase ϕ_Γ to those for ϕ_M, we see that the former can be neglected to very good approximation, what we will do from now on.

Another important constraint for our analysis comes from the CP-violating observable $\epsilon_K = \epsilon_K^{\mathrm{SM}} + \epsilon_K^{\mathrm{RS}}$ [157, 213, 220, 241]. Explicitly, we demand $|\epsilon_K| \in [1.2, 3.2] \cdot 10^{-3}$ [213], where

$$\epsilon_K = \frac{\kappa_\epsilon\, e^{i\varphi_\epsilon}}{\sqrt{2}\,(\Delta m_K)_{\mathrm{exp}}} \mathrm{Im}(M_{12}^{K\,\mathrm{SM}} + M_{12}^{K\,\mathrm{RS}})\,, \tag{5.122}$$

with $\varphi_\epsilon = (43.51 \pm 0.05)°$ [12] and $\kappa_\epsilon = 0.92 \pm 0.02$ [374]. The neutral Kaon mixing amplitude
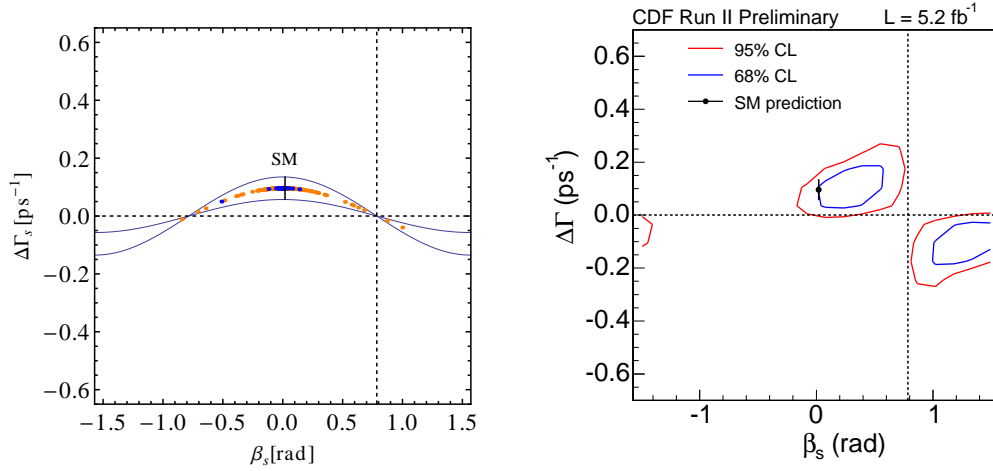
Figure 5.15: Left: Corrections in the $\Delta\Gamma_s^{\mathrm{SM}}/\beta_s$-plane for the minimal (blue/dark gray) and custodial (orange/light gray) RS model. Bounds from $Zb\bar{b}$, Δm_{B_s}, and ϵ_K are satisfied. See [4] and text for details. Right: Experimental constraints from flavor-tagged $B_s^0 \to J/\psi\phi$ decays. Figure from [101].

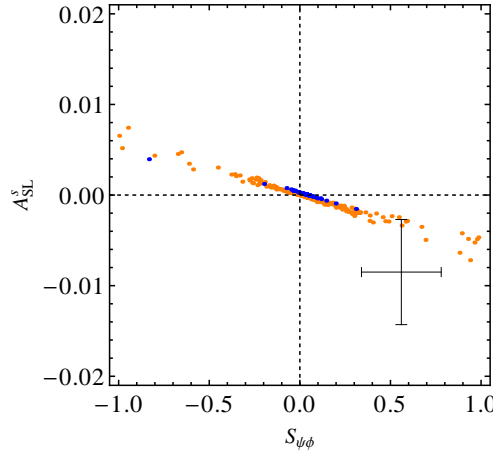Figure 5.16: Corrections in the $A_{\mathrm{SL}}^s/S_{\psi\phi}$-plane for the minimal (blue/dark gray) and custodial (orange/light gray) RS model. Bounds from $Zb\bar{b}$, Δm_{B_s}, and ϵ_K are satisfied. See [4] and text for details.

is defined in analogy to (5.114). The input data needed for the calculation can be found in Appendix B of [213]. As it turns out, without some tuning, the prediction for ϵ_K is generically too large. Note that the dangerous contributions from the operators $Q_{4,5}^{sd}$ [220], which can become comparable to those of Q_1^{sd} due to $R_K = (M_K/(\bar{m}_d + \bar{m}_s))^2 \approx 20$ for $\mu = 2\,\mathrm{GeV}$ and a more pronounced RG running, could be suppressed by imposing a $U(3)$ flavor symmetry in the right-handed down-quark sector [205], as mentioned in Section 3.2.3. Although this symmetry

will inevitably be broken by the Yukawa couplings, the possibility to choose all down-type bulk masses equally allows to forbid tree-level down-type FCNCs in the ZMA. This can be seen from (B.16), since $(\boldsymbol{W}_d^\dagger)_{mj}(\boldsymbol{W}_d)_{jn} = 0$ for $m \neq n$ due to the unitarity of $\boldsymbol{W}_d$. Non-vanishing contributions from the exchange of KK gauge bosons arise only at $\mathcal{O}(v^4/M_{\mathrm{KK}}^4)$ from the mixing of the right-handed fermion zero modes with their KK excitations. For $M_{\mathrm{KK}} = 2\,\mathrm{TeV}$, it would thus be possible to reduce $C_{4,5}^{sd}$ by a factor of about 100, by imposing such a symmetry. The same suppression factor also applies to the B-meson sector. For the coefficient C_1^{RS} however, such a protection is not possible. In our analysis, we do not impose an additional flavor symmetry on the bulk masses, but rather use the bound from ϵ_K as an additional constraint on our scatter points and discard those that are in conflict with it.

Setting the tiny SM phases to zero, the width difference (5.96) can be written as

$$\Delta\Gamma_s = \Delta\Gamma_s^{\mathrm{SM}}\, R_\Gamma\, \cos 2\beta_s\,, \tag{5.123}$$

where $2\beta_s \approx -\phi_M$ [100]. Thus, in the absence of large corrections to the magnitude of Γ_{12}^s, NP contributions always lead to a negative shift in $\Delta\Gamma_s$ [353]. Note that the preliminary CDF analysis [101] uses the older SM prediction $\Delta\Gamma_s^{\mathrm{SM}} = (0.096 \pm 0.039)\mathrm{ps}^{-1}$ [347], which we will also take as central value for our calculation. Taking the more recent value will not change our conclusions. In the left panel of Figure 5.15 we plot our predictions for $\Delta\Gamma_s$ against β_s in the RS model. A comparison to the CDF results in the right panel leads to the conclusion that both the minimal (blue/dark gray) as well as the custodial RS model (orange/light gray) can enter the 68% confidence region and come close to the best fit value. They stay below the desired value for $\Delta\Gamma_s$, as there are no sizable positive corrections to $|\Gamma_{12}^s|$.

Neglecting the tiny SM phases and the NP phase corrections related to decay, the semileptonic CP asymmetry A_{SL}^s is proportional to $S_{\psi\phi}$ [348]. The latter quantity is given by the amplitude of the time-dependent asymmetry in $B_s^0 \to J/\psi\phi$ decays, $\mathcal{A}_{\mathrm{CP}}^s(t) = S_{\psi\phi}\sin(\Delta m_{B_s}t)$, see (5.91). Setting just the NP phase in decay to zero, one obtains the well known expression $S_{\psi\phi} = \sin(2\beta_s^{J/\psi\phi} - \phi_M)$ [375]. Thus one has to good approximation

$$A_{\mathrm{SL}}^s \approx -\frac{|\Gamma_{12}^{s\,\mathrm{SM}}|}{|M_{12}^{s\,\mathrm{SM}}|}\frac{R_\Gamma}{R_M}\,S_{\psi\phi}\,. \tag{5.124}$$

The results for A_{SL} and $S_{\psi\phi}$ in the RS model are shown in Figure 5.16. They confirm the approximately linear dependence (5.124) between the plotted quantities. The experimentally favored regions $S_{\psi\phi} = 0.56 \pm 0.22$ [376] and $A_{\mathrm{SL}}^s = -0.0085 \pm 0.0058$ [350] are marked by the black cross. The latter has been obtained by a combination of the direct measurement with the results derived from A_{SL}^b together with the average $A_{\mathrm{SL}}^d = -0.0047 \pm 0.0046$ from B-factories. It is evident from the plot that the best fit value of $S_{\psi\phi}$ can be reproduced (however, some amount of tuning will be necessary in the minimal RS variant), which has already been noted in [213, 241]. Furthermore, the RS setup allows to enter the 1σ range of the measured value of A_{SL}^s. The same conclusion has been drawn in [355] recently, using a different approach. The authors did not use any concrete sets of input parameters, but rather scanned the predictions for FCNC vertices in a range constrained by bounds from $\Delta\Gamma_s$ and Δm_{B_s}. Note that due to $S_{\psi\phi} \approx \sin 2\beta_s$, the corrections in the $\Delta\Gamma_s^{\mathrm{SM}}/\beta_s$-plane and the $A_{\mathrm{SL}}^s/S_{\psi\phi}$-plane are correlated. An improvement with respect to experiment in the former leads to an improvement in the latter.
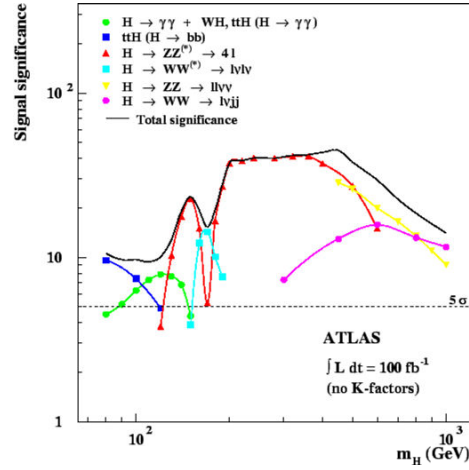
Figure 5.17: Expected statistical significance for a discovery of the SM Higgs boson at ATLAS as a function of the Higgs-boson mass for an integrated luminosity of $100\,\text{fb}^{-1}$. Plot from [377] (with permission).

In conclusion, in particular the custodial RS model allows for a better agreement of the theoretical values for A_{SL}^s, $S_{\psi\phi}$, and $\Delta\Gamma_s$ with experiment. However the concrete predictions for these observables still depend sensitively on the RS parameters (and not only on the scale M_{KK}). Essentially this is due to the fact that the range for the new phase Φ_M is not very limited by the constraints that are imposed on the parameters.

5.3   Higgs Physics

As we have seen in Chapter 1, a Higgs boson with a mass not exceeding the TeV scale is an important ingredient of the SM and also of many of its extensions. However, such a boson has not been observed experimentally yet.

The SM Higgs boson is expected to be found with a statistical significance of $\gtrsim 10\,\sigma$ over the full mass range with $100\,\text{fb}^{-1}$ integrated luminosity, see Figure 5.17. Imagine that we do not discover this particle at the LHC in the first years of running. Does this already mean that we have to abandon the corresponding mechanism of EWSB? The answer to this question is certainly no. BSM physics could feature a standard Higgs mechanism that however could be much harder to detect than the one of the SM, even for a Higgs-boson mass easily accessible at the LHC. It is thus important to study Higgs physics in various models to be prepared for different possible scenarios. In warped extra dimensions, large effects are expected due to the localization of this sector on the IR brane, where also the KK modes as well as heavy SM quarks are peaked. In the following we will study Higgs-boson production and decay within the custodial RS model. Although Higgs physics has been looked at in related models [200, 203, 245, 249, 378, 379, 380, 381, 382, 383], there has not been a complete analysis of the subject in the context of the models studied in this thesis, taking into account all important effects induced by the KK excitations at the one-loop order. This will be provided in the following.

5.3.1 Higgs-Boson Production

We will start with the leading (SM) production mechanism for the Higgs boson at hadron colliders, which is gluon-gluon fusion. In the SM, this mechanism, which receives its dominant contribution from a top-quark triangle loop, has been introduced in Section 1.1.2. Within the RS framework, one has to take into account in addition the KK tower of the top quark as well as of all the other quark flavors, since all these modes contribute to the $gg \to h$ amplitude at $\mathcal{O}(v^2/M_{\mathrm{KK}}^2)$. The relevant Feynman diagrams are shown on the very left in the top row of Figure 5.18 and on the left-hand side of Figure 5.19.

In order to calculate the $gg \to h$ production cross section in the RS model, we rescale the SM prediction according to

$$\sigma(gg \to h)_{\mathrm{RS}} = |\kappa_g|^2 \, \sigma(gg \to h)_{\mathrm{SM}} , \tag{5.125}$$

where

$$\kappa_g = \frac{\sum_{i=t,b} \kappa_i A_q^h(\tau_i) + \sum_{j=u,d,\lambda} \nu_j}{\sum_{i=t,b} A_q^h(\tau_i)} , \tag{5.126}$$

and $\tau_i \equiv 4m_i^2/m_h^2$. The first term in the numerator corresponds to top- and bottom-quark zero modes running in the loop, with Higgs couplings (normalized to the SM) given by [384]

$$\kappa_t = \mathrm{Re}[(g_h^u)_{33}]/\left(\frac{m_t}{v_{\mathrm{SM}}}\right) , \quad \kappa_b = \mathrm{Re}[(g_h^d)_{33}]/\left(\frac{m_b}{v_{\mathrm{SM}}}\right). \tag{5.127}$$

These couplings differ from those of the SM, $\kappa_{t,b} \neq 1$, due to contributions to the fermion masses from compactification, see Section 3.7, and due to $v_{\mathrm{RS_C}} \neq v_{\mathrm{SM}}$. The form factor $A_q^h(\tau_i)$, needed for a correct weight of the different contributions in (5.126), approaches 1 for $\tau_i \to \infty$ and vanishes proportional to τ_i for $\tau_i \to 0$. Its analytic form is given in Appendix B.8.

Due to power suppression, the only phenomenologically relevant correction in $\sigma(gg \to h)_{\mathrm{SM}}$ from lighter fermions stems from the bottom quark. We include the interference term of the bottom- and the top-quark amplitude approximately, by multiplying the cross section $\sigma(gg \to h)_{\mathrm{SM}}$ by $\left(1 + 2 \, \mathrm{Re} A_q^h(\tau_b)\right)$. Numerically, this approximate treatment decreases the SM cross section by about 9%, 2%, and below 1% for $m_h = 100\,\mathrm{GeV}, 300\,\mathrm{GeV}$, and $600\,\mathrm{GeV}$, which is in good agreement with the NLO calculation including the exact mass dependence [385].

In Figure 5.20 we show the ratios (5.127) as functions of M_{KK} for a set of 150 random parameter points. These correspond to the custodial model with extended P_{LR} symmetry (3.252), which we will always employ in the following analysis. They reproduce the quark masses as well as the CKM parameters at 68% CL. The same sample of model parameter points will be used in the remainder of this section. We observe that both the $ht\bar{t}$ and the $hb\bar{b}$ coupling are reduced in the custodial RS scenario with respect to the SM, resulting in $\kappa_{t,b} \leq 1$. The same conclusion has been drawn in [203] for the minimal RS model. Numerically, we find that for $M_{\mathrm{KK}} = 2\,\mathrm{TeV}$ ($M_{\mathrm{KK}} = 3\,\mathrm{TeV}$) the average corrections amount to around -25% and -15% (-10% and -5%) in the top- and bottom-quark sectors, respectively. Since the RS corrections to the Higgs couplings scale as v^2/M_{KK}^2, the average value of the ratios $\kappa_{t,b}$ can be parametrized by $1 - a_{t,b} v^2/M_{\mathrm{KK}}^2$. The resulting coefficients $a_{t,b}$ are given in Table 5.3. The quoted values of $a_{t,b}$ have been obtained from the best fits to the shown sample of scatter points. Note that the RS predictions depend most strongly on the KK scale, while the additional
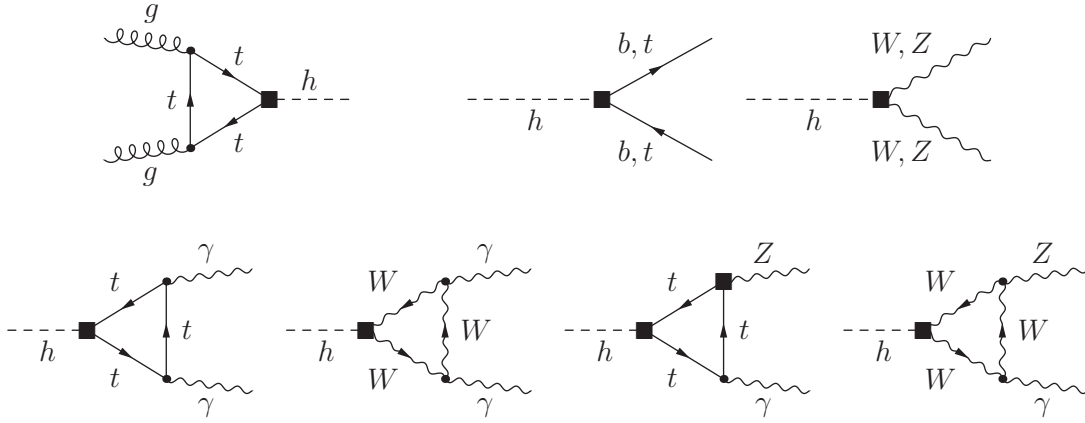
Figure 5.18:   Examples of zero mode contributions to the production and the decay of the Higgs boson at leading order of perturbation theory. Vertices indicated by a black square can receive sizable shifts in the RS model relative to the SM couplings. See [2] and text for details.

dependence on the explicit parameter points is less important. Moreover, as expected from the arguments of Section 3.2.3, the correction to the top-quark coupling is more pronounced than this to the bottom-quark coupling.

It is not difficult to understand the suppression of the Yukawa couplings of the third-generation quarks, $\kappa_{t,b} \leq 1$, analytically by analyzing the structure of (3.280). First, one has $m_3^q/v \left((\Phi_q)_{33} + (\Phi_Q)_{33} \right) \geq 0$ since the diagonal elements of the matrices $\boldsymbol{\Phi}_{q,Q}$ introduced in (3.281) are absolute squares. Second, the third term in (3.280) can be written in the ZMA as

$$(\Delta \tilde{g}_h^u)_{33} = \frac{4 m_t^2}{3 v M_{\text{KK}}^2} \sum_{j=1}^{3} m_j^u \left(\boldsymbol{U}_u^\dagger \, \text{diag} \left[F^{-2}(c_{Q_i}) \right] \boldsymbol{U}_u \right)_{j3} \left(\boldsymbol{W}_u^\dagger \, \text{diag} \left[F^{-2}(c_{u_i^c}) \right] \boldsymbol{W}_u \right)_{3j} \quad (5.128)$$

and a similar formula applies to the case of $(\Delta \tilde{g}_h^d)_{33}$. Because the diagonal elements of the matrices $\boldsymbol{U}_u^\dagger \, \text{diag} \left[F^{-2}(c_{Q_i}) \right] \boldsymbol{U}_u$ and $\boldsymbol{W}_u^\dagger \, \text{diag} \left[F^{-2}(c_{u_i^c}) \right] \boldsymbol{W}_u$ are absolute squares, the term with $j = 3$ is positive semi-definite. The terms with $j = 1, 2$, on the other hand, can have an arbitrary complex phase. Yet, due to the strong chiral suppression, $m_c/m_t \approx 1/275$ and $m_u/m_t \approx 10^{-5}$, these terms cannot drive the real part of $\Delta(\tilde{g}_h^u)_{33}$ negative. The same holds true for $(\Delta \tilde{g}_h^d)_{33}$, although the chiral suppression is weaker in this case, $m_s/m_b \approx 1/50$ and $m_d/m_b \approx 1/800$. Recalling that $(\Delta g_h^q)_{33} = m_3^q/v \left((\Phi_q)_{33} + (\Phi_Q)_{33} \right) + (\Delta \tilde{g}_h^q)_{33} \geq 0$ enters (3.279) with a minus sign, we conclude that the $ht\bar{t}$ and $hb\bar{b}$ couplings are predicted to be suppressed relative to their SM values in both the minimal and the extended RS models. This result seems to be independent of the particular realization of the setup and to hold for a large class of RS setups. The same conclusion has been drawn in the context of models where the Higgs-boson arises as a pseudo Nambu-Goldstone boson [249, 386].

The second term in the numerator of (5.126) represents the contribution arising from the virtual exchange of KK quarks. Here, all quark flavors have to be taken into account, since a possible UV localization of a zero mode does not apply for the KK excitations. The
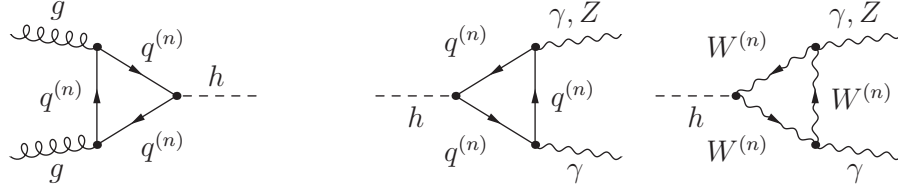
Figure 5.19: Examples of one-loop diagrams involving KK excitations that contribute to the production and the decay of the Higgs boson at leading order of perturbation theory. See [2] and text for details.

corresponding Feynman diagram is shown on the very left in Figure 5.19. In the up-type quark sector the associated coefficient takes the form

$$
\begin{aligned}
\nu_u &= v_{\text{SM}} \sum_{n=4}^{\infty} \frac{\text{Re}\left[(g_h^u)_{nn}\right]}{m_n^u} A_q^h(\tau_n^u) \\
&= \frac{2\pi}{\epsilon L} \frac{v_{\text{SM}}}{v_{\text{RS}_\text{C}}} \sum_{n=4}^{\infty} \frac{\text{Re}\left[\vec{a}_n^{U\dagger} \boldsymbol{C}_n^U(\pi^-) \left(1 - \frac{v_{\text{RS}_\text{C}}^2}{3 M_{\text{KK}}^2} \tilde{\boldsymbol{Y}}_{\vec{u}} \bar{\boldsymbol{Y}}_{\vec{u}}^\dagger\right) \boldsymbol{S}_n^U(\pi^-) \vec{a}_n^U\right]}{x_n^u} A_q^h(\tau_n^u) .
\end{aligned}
\tag{5.129}
$$

Similar relations hold in the sector of down-type and λ quarks. Note that the VEV shift $v_{\text{SM}}/v_{\text{RS}_\text{C}} \neq 1$ does not contribute to ν_u at $\mathcal{O}(v^2/M_{\text{KK}}^2)$. Since the mass of the first KK up-type quark is already much larger than the mass of the Higgs-boson, $m_4^u/M_{\text{KK}} = \mathcal{O}(\text{a few}) \gg m_h/M_{\text{KK}}$, it is an excellent approximation to replace the function $A_q^h(\tau_n^u)$ by its asymptotic value of 1 obtained for $\tau_n^u \equiv 4\left(m_n^u\right)^2/m_h^2 \to \infty$.

Before presenting our numerical results for these contributions, some comments about the infinite sum in (5.129) are in order. First of all, since the RS model is an EFT defined with a cutoff $\Lambda_{\text{UV}}(\pi) \ll M_{Pl}$, the KK modes above a certain level will not be part of the EFT anymore. Thus the potentially divergent sum is effectively cut off after a certain KK level. However, as we will see below, there are in addition cancellations within the sum in (5.129) that cause the terms to decrease quadratically with the mass of the KK fermions in the loop, which renders the sum convergent. At the same time it becomes IR dominated, *i.e.*, the lowest lying modes become most important, whereas the difference between truncating the sum at a finite level n_{max} and *extrapolating* till infinity scales like $1/n_{\text{max}}$. This corresponds to a subleading effect if at least a few modes are present below the cutoff. Importantly, this line of reasoning with a cutoff prevents UV physics above this RS cutoff to modify the behavior of the KK sum. For the following analysis we will assume the fundamental parameters of the RS model to be such that $\Lambda_{\text{UV}}(\pi)$, which cuts off the KK sums, is above the mass scale of $\mathcal{O}(4)$ complete KK levels.

In the SM, the top-quark contribution to the $gg \to h$ amplitude is proportional to y_t/m_t in the decoupling limit. As mentioned in Section 1.1.2, it can be described by the effective operator $h/v\, G_{\mu\nu}^a G^{a\,\mu\nu}$. Naively, also the contributions of the KK levels in (5.129) scale like $1/m_n$, which would lead to a divergent sum. However, due to low-energy theorems appropriate to external Higgs bosons with vanishing momentum [386, 387, 388, 389], which apply to any
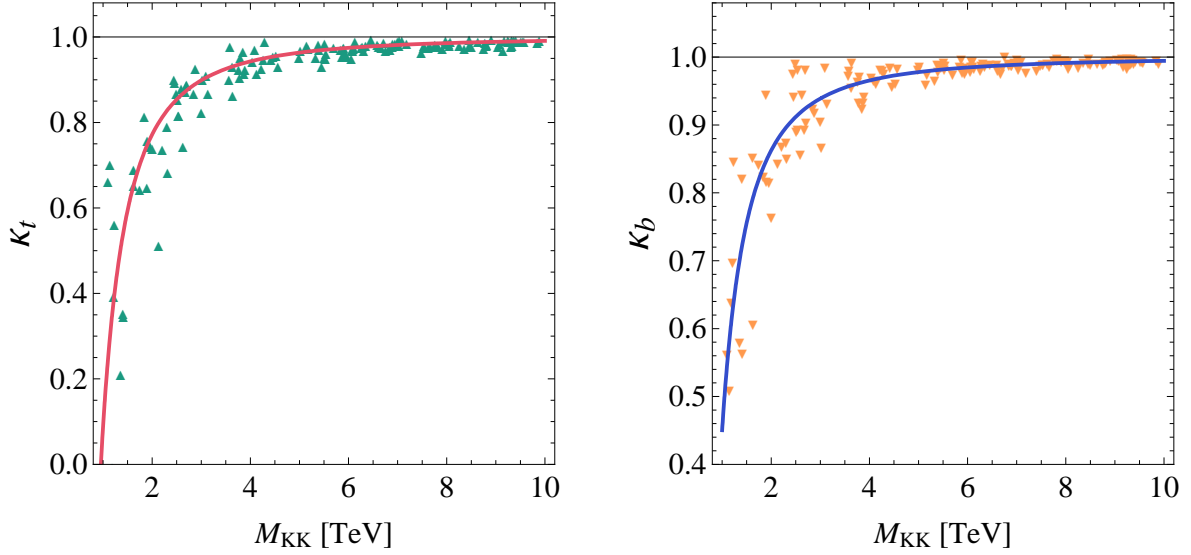
Figure 5.20:   Predictions for the ratios of the $ht\bar{t}$ (left) and $hb\bar{b}$ (right) coupling in the custodial RS model relative to the SM value. The solid lines show fits to the samples of parameter points. See [2] and text for details.

quantum field theory, the Wilson coefficient of the $D = 5$ operator above (encoding the whole KK-towers) is related to the QCD β-function. In the context of the RS framework this implies that the sum in (5.129) must be convergent, because the running of α_s can be shown to be logarithmic in warped extra-dimension models [162, 275, 390, 391, 392, 393, 394, 395]. While the finiteness of the effective hgg coupling is thus guaranteed on general grounds, an explicit calculation of the complete sum (5.129) in the KK decomposed 4D theory for the full flavor structure turns out to be non-trivial. This is due to the fact that the Higgs VEV induces $\mathcal{O}(1)$ mixings between the various modes of a single KK level, see Section 5.2.1. For example, in the up-type quark sector there are five types of fields, namely u, u', u^c, U', and U. Each of them exists in three different flavors, so that there are altogether 15 KK modes of similar mass in each level. Since the mixing effects among the states of the same KK level are large, they cannot be treated perturbatively, and one has to resort to numerical methods or 5D propagators (see Section 4) as long as one is interested in the case of three families. However, in the toy example of a single generation, it turns out to be possible to derive an expression for (5.129) in the KK decomposed theory, revealing analytically the dependence on the fermion localization.

   In order to calculate the KK sum numerically, one first has to find the solutions to the eigenvalue equation (3.96). In the case of the up-type quark sector, this requires determining the roots of a 6×6 determinant, which in practice turns out to be intricate, because one needs to find suitable starting points to search for the roots which feature tiny splittings. We obtain these starting values by diagonalizing a truncated mass matrix obtained in the perturbative approach [156, 175, 214]. In Figure 5.21 we display the results of our numerical calculations for one parameter point with $M_{\mathrm{KK}} = 2\,\mathrm{TeV}$. The dots correspond to the individual terms in the sum (5.129) for up- and down-type quarks, while the filled boxes indicate the values obtained by summing up the contributions of one KK level. Results for the exotic λ-type quarks are
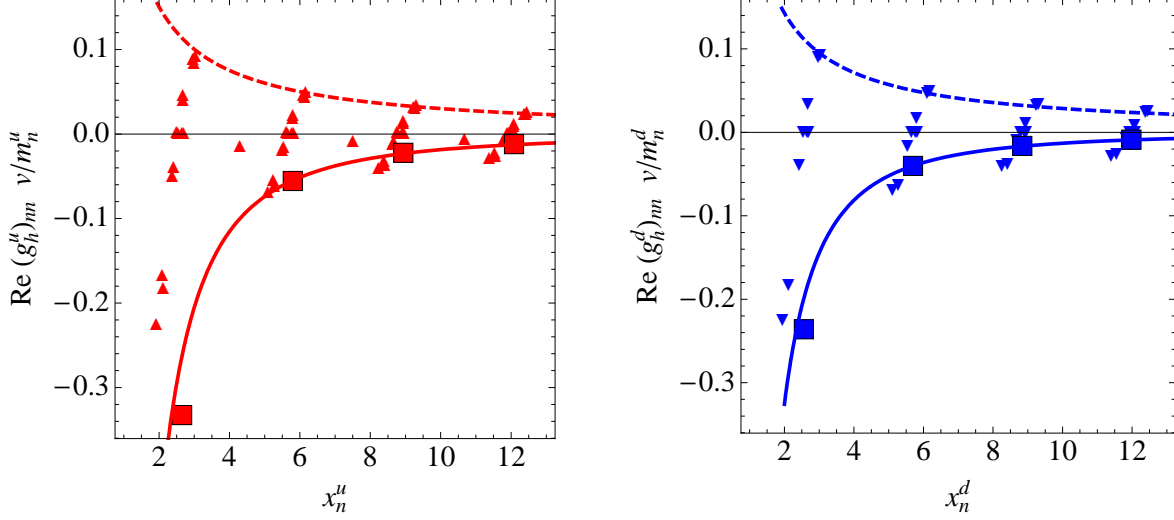
Figure 5.21: Numerical results for the coefficients $\nu_{u,d}$ corresponding to a specific parameter point with $M_{\rm KK} = 2\,{\rm TeV}$. The red (blue) dots in the left (right) panel display the first 60 (36) terms in the KK sum for up- (down-type) quarks, while the red (blue) filled boxes indicate the sums over complete KK levels. See [2] and text for details.

not shown, since they resemble those found in the down-type quark sector. By inspection of the two panels one immediately notices two important features of the KK contributions. First, even though the contribution of an individual mode can be positive and negative, the sum over an entire KK level is strictly negative. Second, the importance of higher-level KK sums decreases quadratically, ensuring that (5.129) converges to a finite value. This feature is indicated by the solid lines, which represent the best fits to $1/x_n^2$ including the results of the second, third, and fourth KK-level sums. The dashed lines depict the $1/x_n$ behavior of the sum over a single fermion tower. The convergence of the total sum is guaranteed by cancellations between different modes of the same KK level.

The results for the KK sums ν_u and ν_d are shown in Figure 5.22 as functions of the KK scale for our set of 150 randomly chosen parameter points. The corresponding results for the coefficient ν_λ are almost identically to those of ν_d, and we do not show them explicitly. We see that the corrections to the effective hgg coupling that arise from triangle diagrams involving KK quarks are all strictly negative. In the up-type quark sector the corrections are almost a factor of 2 larger than those appearing in the down- and λ-type quark sectors. This feature can be traced back to the higher multiplicity of states in the former relative to the later sectors, which suggests that $\nu_u/\nu_{d,\lambda} = 15/9 \approx 1.7$. Numerically, we find that for $M_{\rm KK} = 2\,{\rm TeV}$ ($M_{\rm KK} = 3\,{\rm TeV}$) the average value of ν_u and $\nu_{d,\lambda}$ amounts to about -0.59 and -0.34 (-0.26 and -0.15) with the ratio of the values being quite close to the naive estimate. Since the leading KK-quark corrections to the effective hgg vertex decouple again as $v^2/M_{\rm KK}^2$, we parametrize the average values of $\nu_{u,d,\lambda}$ as $a_{u,d,\lambda}\,v^2/M_{\rm KK}^2$ and determine $a_{u,d,\lambda}$ from the best fit to the shown sample of points restricted to the range $M_{\rm KK} = [2, 10]\,{\rm TeV}$. The resulting numbers for the coefficients $a_{u,d,\lambda}$ are shown in Table 5.3. Points with a KK scale below $2\,{\rm TeV}$ have been excluded in the fit, since they depend sensitively on higher-order terms in $v/M_{\rm KK}$.
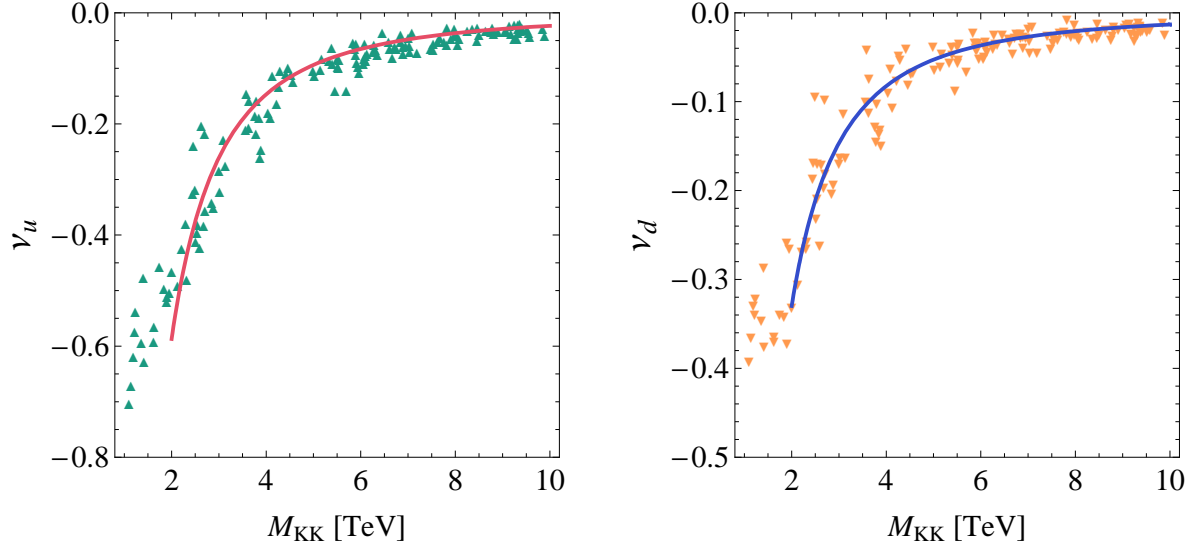
Figure 5.22:   Predictions for the coefficients ν_u and ν_d in the custodial RS model. The solid lines indicate the best fits to the shown sample of parameter points lying in the range $M_{\mathrm{KK}} = [2, 10]$ TeV. See [2] and text for details.

This feature is noticeable in the plots, which show that for very low KK scale the exact results for $\nu_{u,d}$ are typically above the solid lines indicating our fits. This should be kept in mind when using the parametrizations $a_{u,d,\lambda}\, v^2/M_{\mathrm{KK}}^2$ to calculate $\nu_{u,d,\lambda}$ for KK scales below 2 TeV.

Our results for the Higgs-boson production cross sections at the Tevatron and the LHC for center-of-mass energies $\sqrt{s} = 1.96$ TeV and $\sqrt{s} = 10$ TeV are shown in Figure 5.23. The SM results, on which also our RS predictions are based, correspond to those presented in Figure 1.6 and are depicted by red dashed lines. The solid red lines depict the RS results. The latter have been obtained by employing (5.125) and (5.126) using the fit formulae for $\kappa_{t,b}$ and $\nu_{u,d,\lambda}$ discussed before. The relevant values for $a_{t,b,u,d,\lambda}$ can be found in Table 5.3. All four panels show clearly that the Higgs production cross sections in gluon-gluon fusion experience a significant reduction in the custodial RS model. For the considered Higgs-boson masses, we find in the case of $M_{\mathrm{KK}} = 2$ TeV ($M_{\mathrm{KK}} = 3$ TeV) suppressions that range between -65% and -95% (-80% and -90%) at the Tevatron and from -45% to almost -100% (-45% to -90%) at the LHC, see also Figure 5.25. The found depletions survive even at $M_{\mathrm{KK}} = 5$ TeV, still reaching up to -40% at both colliders. Such a sensitivity to high scales is very interesting for the indirect search for new physics. Since both the theoretical accuracy [46, 47, 48, 49] and the expected experimental precision [339, 396] are at the level of 10%, the pronounced reductions in Higgs events from gluon-gluon fusion should be clearly visible at the LHC (for reasonably low KK scales). The non-trivial dependence of the RS corrections on the Higgs mass results form an interference of zero- and KK-mode contributions. The real part of the zero-mode amplitude increases until the $t\bar{t}$ threshold is reached. Above, it decreases quadratically with m_h, modulo logarithmic effects. It is positive for all values of the Higgs-boson mass. On the other hand, the real part of the amplitude associated to the virtual exchange of KK quarks is negative and a constant in the heavy-mass limit. Since for $M_{\mathrm{KK}} \lesssim 2$ TeV the latter contribution is always dominant, the correction arising from KK-quark triangle diagrams effectively flips the sign of
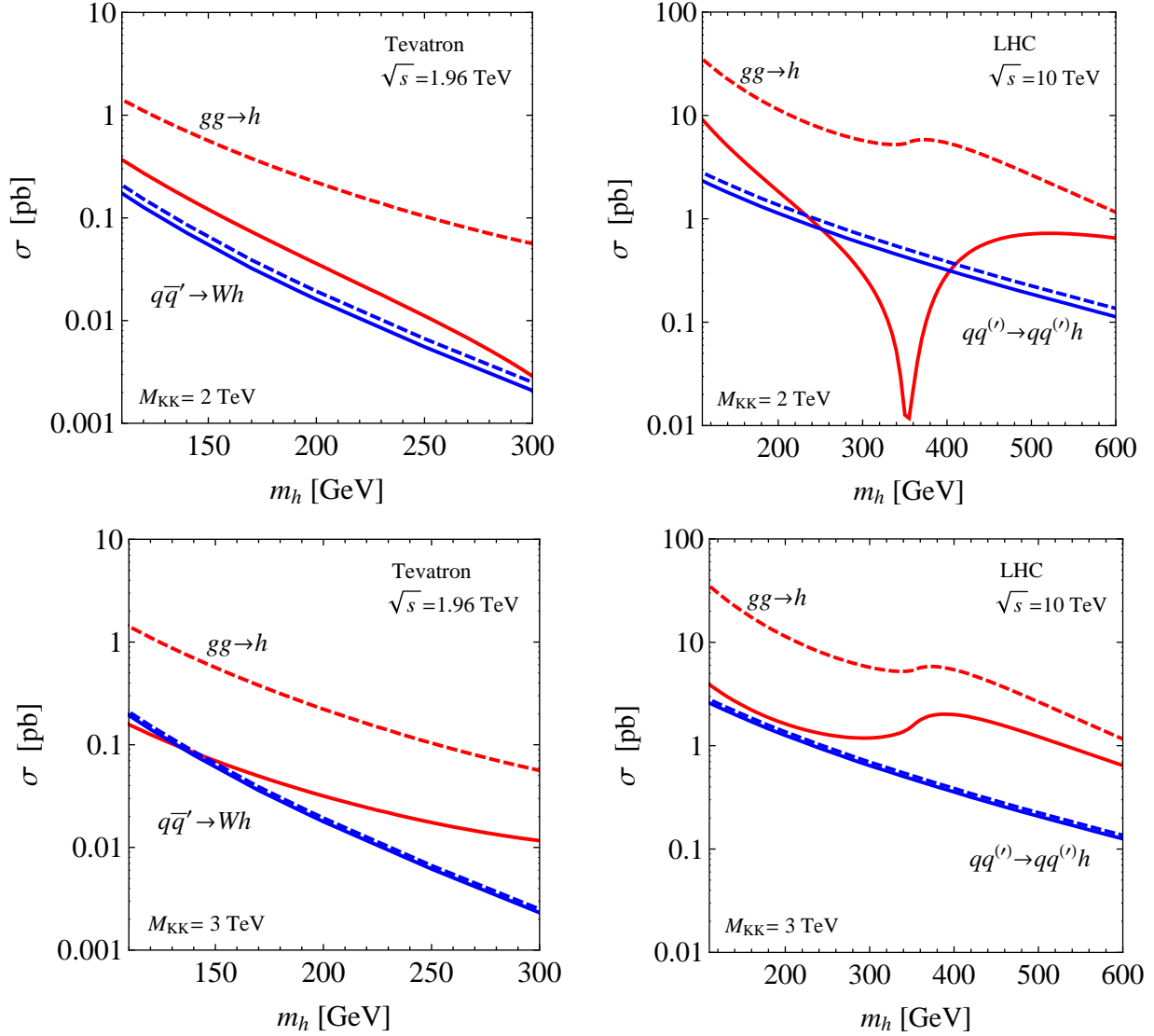
Figure 5.23: Main Higgs-boson production cross sections at the Tevatron (left) and the LHC (right) for center-of-mass energies of $\sqrt{s} = 1.96\,\text{TeV}$ and $\sqrt{s} = 10\,\text{TeV}$, employing $M_{\text{KK}} = 2\,\text{TeV}$ (upper row) and $M_{\text{KK}} = 3\,\text{TeV}$ (lower row). The dashed lines represent the SM predictions, while the solid lines correspond to the custodial RS model. In the case of the Tevatron the panels show gluon-gluon fusion (red) and associated $W^{\pm}$-boson production (blue), while for the LHC gluon-gluon (red) and weak gauge-boson fusion (blue) are presented. See [2] and text for details.

the real part of the total $gg \to h$ amplitude with respect to the SM expectation for small and high Higgs masses. However, in the threshold region where $m_h \approx 2m_t$, the destructive interference between the individual contributions can become almost perfect, leading to a strong suppression of Higgs production via gluon-gluon fusion. This feature can be observed clearly in the upper right panel of Figure 5.23. Because the RS contributions decouple rapidly for increasing KK scale, a complete extinction of the sum of individual amplitudes is not

a_t	a_b	a_t^V
15.08	9.08	3.63

a_u	a_d	a_λ	$a_{\gamma Z}^u$	$a_{\gamma Z}^d$	$a_{\gamma Z}^\lambda$	$a_{\gamma Z}^W$
−38.80	−21.80	−22.58	−46.46	17.98	−6.38	10.76

Table 5.3:   Fit coefficients entering the various contributions to Higgs-boson production and decay in units of v^2/M_{KK}^2. Corrections due to zero and KK modes are displayed in the upper and lower table, respectively.

possible for $M_{\mathrm{KK}} \gtrsim 2\,\mathrm{TeV}$. In this case, the zero-mode contribution to $gg \to h$ dominates, and the Higgs-mass dependence of the RS prediction is similar to the one of the SM result. It is important to stress that, in spite of the in principle many parameters in the fermion sector of the custodial RS model, the shown results for the Higgs-boson production cross section depend to first order only on the overall KK-mass scale. This claim is supported by the narrow spread of scatter points in Figure 5.22.

Let us now have a look on the subleading production mechanisms at the main hadron colliders. Here, the important LHC channel of weak gauge-boson fusion, $qq^{(\prime)} \to qq^{(\prime)}V^*V^* \to qq^{(\prime)}h$ with $V = W, Z$, receives only moderate corrections of around -10% (-5%) for $M_{\mathrm{KK}} = 2\,\mathrm{TeV}$ ($M_{\mathrm{KK}} = 3\,\mathrm{TeV}$). The same reduction will affect associated $W^\pm$-boson production, $q\bar{q}' \to W^* \to Wh$ at the Tevatron. The RS predictions for the corresponding production cross sections are illustrated by the solid blue lines in the right and left panels of Figure 5.23, respectively. The corresponding SM predictions, depicted by the blue dashed lines, are those of Figure 1.6. Finally, the cross section of associated top-quark pair production, $q\bar{q} \to t\bar{t}^* \to t\bar{t}h$, will also experience a reduction. For values of the KK scale in the ballpark of $2\,\mathrm{TeV}$, this suppression can amount up to -40%. Since all these processes happen at tree level, the RS predictions have all been obtained by a simple rescaling of the SM results. In that context, one has to consider the VEV shift (5.4) which partially cancels the depletion due to the mixing of the weak gauge bosons with their KK excitations. This effect has been included in deriving the numerical results above.

In summary, we find that the main Higgs-boson production modes at hadron colliders are suppressed in the custodial RS model relative to the SM. Clearly this affects Higgs searches, as we will detail below. Suppression effects in $gg \to h$ were also reported in [203, 249, 381]. In this context, see also [382] for a detailed analysis of Higgs-boson production cross sections and decay rates in a related general setup. A direct numerical comparison of the results of these publications with our findings is however not possible, since [203] only included zero-mode corrections, while [249, 381, 382] studied RS variants that differ from the set-up considered here. In [379], an enhancement of $gg \to h$ in a custodial RS variant has been found. However for a sufficiently IR-localized Higgs sector, this effect is caused by UV physics, above the cutoff Λ_{UV} of the RS EFT. Considering a Higgs profile with a finite width $\sim \eta$, the effect is driven by KK excitations with a mass of $m_n \sim 1/\eta$. It vanishes in the limit of a small width, if the KK sum is cutoff at $\Lambda_{\mathrm{UV}} < \infty$.

In [383] the authors studied corrections to gluon-gluon fusion arising from virtual exchange of very light fermionic KK modes. It has been found that for a heavy bottom-quark partner

with a mass $m_{b'}$ of a few hundred GeV the Higgs-boson production cross section via $gg \to h$ can be significantly enhanced. However, in order to achieve $m_{b'} \ll M_{\mathrm{KK}}$ with the embedding of quarks as chosen in (3.209), the P_{LR} symmetry has to be broken strongly via the bulk mass parameters of the $\mathcal{T}_1$ multiplets by choosing $c_{\mathcal{T}_{1i}}$ rather far away from $c_{\mathcal{T}_{2i}}$. While for $c_{\mathcal{T}_{1i}} > 1/2$ it is possible to achieve $\nu_d > 0$ and thus an enhancement of the $gg \to h$ cross section, such choices of parameters do not naturally reproduce the measured mass spectrum of the SM quarks for anarchic Yukawa couplings. If on the other hand $c_{\mathcal{T}_{1i}} < 1/2$, the correction ν_d remains strictly negative, and as a result the $gg \to h$ channel experiences a reduction. Moreover, choices for $c_{\mathcal{T}_{1i}}$, corresponding to a strong breaking of the P_{LR} symmetry, lead generically to a sizable negative shift in the $Zb_L\bar{b}_L$ coupling through (3.250), which is problematic in view of the stringent constraints arising from the $Z \to b\bar{b}$ pseudo observables.

5.3.2   Higgs-Boson Decay

We now move on to study the decay modes of the Higgs boson. In this context, we will consider all processes with quarks and gauge bosons in the final state that can receive important RS corrections and have a branching fraction larger than 10^{-4}. As we have not explicitly specified the embedding of the fermions in the lepton sector, we ignore decays into taus and muons, which we however expect to be SM-like, due to the rather UV localized profiles. Furthermore, we will not include loop contributions of KK leptons in our analysis of the $h \to \gamma\gamma$ and $h \to \gamma Z$ decay channels but rather estimate their impact.

In order to be able to calculate the decay rates of the Higgs boson into massive gauge bosons, we still need to give the RS corrections to the WWh, ZZh, and WWZ tree-level vertices. Due to the unbroken $U(1)_{\mathrm{EM}}$ gauge group, the $WW\gamma$ coupling is unchanged with respect to the SM to all orders in v^2/M_{KK}^2. The weak couplings involving the Higgs boson are derived from the cubic and quartic interactions given by (3.175). In unitary gauge, the relevant terms in the Lagrangian read

$$\mathcal{L}_{\mathrm{4D}} \ni \left(h^2 + 2\,h\,v_{\mathrm{RS_C}}\right) \left[\frac{g_L^2}{4} \left(1 - \Delta g_h^W\right) W_\mu^+ W^{-\mu} + \frac{g_L^2 + g_Y^2}{8} \left(1 - \Delta g_h^Z\right) Z_\mu Z^\mu \right], \quad (5.130)$$

where

$$\Delta g_h^V = x_V^2 \left[L \left(1 + \frac{s_V^2}{c_V^2}\right) - 1 + \frac{1}{2L} \right] + \mathcal{O}\left(x_V^4\right), \quad (5.131)$$

and $x_V \equiv m_V/M_{\mathrm{KK}}$ for $V = W, Z$. Due to the P_{LR} symmetry (3.234), one has $s_W^2/c_W^2 = 1$ and $s_Z^2/c_Z^2 = 1 - 2s_w^2$, which implies that the leading correction due to $\Delta g_h^{W,Z}$ takes the form $-2m_W^2/M_{\mathrm{KK}}^2\,L$. For $M_{\mathrm{KK}} = 2\,\mathrm{TeV}$ ($M_{\mathrm{KK}} = 3\,\mathrm{TeV}$) these terms amount to about -10% (-5%). However, when comparing the size of the WWh coupling to the value in the SM, one also has to take into account the fact that the VEV $v_{\mathrm{RS_C}}$ differs from v_{SM}.

The partial decay widths $\Gamma(h \to f)$ of the Higgs boson decaying to a final state f are again obtained by rescaling the SM decay widths. We use

$$\Gamma(h \to f)_{\mathrm{RS}} = |\kappa_f|^2\,\Gamma(h \to f)_{\mathrm{SM}}, \quad (5.132)$$

where the VEV shift enters the expressions

$$\kappa_W = \frac{v_{\mathrm{RS_C}}}{v_{\mathrm{SM}}} \left(1 - \Delta g_h^W\right) , \qquad \kappa_Z = \frac{v_{\mathrm{RS_C}}}{v_{\mathrm{SM}}} \left(1 - \Delta g_h^Z\right) , \tag{5.133}$$

for the decay of the Higgs boson into a pair of $W^\pm$ and Z bosons via the ratio $v_{\mathrm{RS_C}}/v_{\mathrm{SM}}$. This ratio can be obtained from (5.4). While the corresponding corrections coming with the subleading terms $\propto \Delta g_h^{W,Z}$ in the equation above are of $\mathcal{O}\left(x_V^4\right)$ and will be neglected in the following, the corrections to the leading terms have to be considered at $\mathcal{O}\left(x_V^2\right)$. We arrive at

$$\kappa_W = 1 - \frac{3}{4} x_W^2 \left[2L - 1 + \frac{1}{2L}\right] + \mathcal{O}\left(x_W^4\right) , \quad \kappa_Z = 1 - \frac{3}{4} x_W^2 \left[2L - \frac{4 - c_w^2}{3c_w^2}(1 - \frac{1}{2L})\right] + \mathcal{O}\left(x_Z^4\right) , \tag{5.134}$$

where we have used $g_L = g_R$. In consequence, the depletion due to the overlap of profiles is weakened by the VEV shift to the few per cent level.

Note that in the minimal RS model the expressions (5.131) hold in the limit $s_{W,Z} \to 0$. Our finding that the couplings WWh and ZZh experience a reduction from their SM expectations confirms the model-independent statements made in [386]. The parameters $\kappa_{g,t,b}$ for decays into two gluons, top or bottom quarks have already been given in (5.126) and (5.127).

In Figure 5.18 the diagrams inducing the decay into a pair of heavy quarks and massive gauge bosons are shown on the right in the top row. Apart from the change in the $ht\bar{t}$ coupling, we neglect RS corrections to the three-body decay $h \to tt^*\left(WW^*\right) \to tbW$. Relative to the two-body mode $h \to t\bar{t}$ this amounts to a correction of (far below) 1% in the SM. Given the smallness of this effect, the omission of possible new-physics effects in the Wtb coupling that would affect the $h \to tbW$ channel is well justified.

The RS correction entering the Higgs decay into two photons can be accounted for by employing

$$\kappa_\gamma = \frac{\sum_{i=t,b} N_c Q_i^2 \kappa_i A_q^h(\tau_i) + \kappa_W A_W^h(\tau_W) + \sum_{j=u,d,\lambda} N_c Q_j^2 \nu_j + \nu_\gamma^W}{\sum_{i=t,b} N_c Q_i^2 A_q^h(\tau_i) + A_W^h(\tau_W)} \tag{5.135}$$

in (5.132), where $N_c = 3$, $Q_{t,u} = 2/3$, $Q_{b,d} = -1/3$, $Q_\lambda = 5/3$, and $\tau_W \equiv 4m_W^2/m_h^2$. The explicit expression for the form factor $A_W^h(\tau_W)$, encoding the $W^\pm$-boson contribution, can be found in Appendix B.8. The first, second, and third terms in the numerator describe the effects of virtual heavy-quark, $W^\pm$-boson, and KK-quark exchange, respectively. The corresponding one-loop graphs are shown on the left in the bottom row of Figure 5.18 and in the center of Figure 5.19. Note that the amplitude $A_W^h(\tau_W)$ interferes destructively with the quark contribution $A_q^h(\tau_i)$, falling from $-21/4$ for $\tau_W \to \infty$ to $-15/4 - 9\pi^2/16$ at the WW threshold $\tau_W = 1$ and finally approaching $-3/2$ in the limit $\tau_W \to 0$. Within the SM, the $W^\pm$-boson contribution to the $h \to \gamma\gamma$ decay amplitude is always dominant below threshold.

Let us estimate the size of the leptonic contributions which have not been included in (5.135). While the precise impact of these effects depends on the exact realization of the lepton sector, which we have not specified, it is possible to predict their relative sign as well as their rough magnitude. Generalizing the result (5.135) to include contributions from triangle

diagrams with KK leptons only requires to perform the replacement

$$\sum_{j=u,d,\lambda} N_c Q_j^2 \nu_j \;\to\; \sum_{j=u,d,\lambda} N_c Q_j^2 \nu_j + Q_l^2 \nu_l \;=\; \frac{4\nu_u}{3} + \frac{\nu_d}{3} + \frac{25\nu_\lambda}{3} + \nu_l \,, \qquad (5.136)$$

where $\nu_u \approx 2\nu_d \approx 2\nu_\lambda$ and the parameter ν_l encodes the effects due to KK-lepton loops. Under the reasonable assumption that $\nu_l \approx \nu_u/2$, we conclude from (5.136) that the KK lepton contribution to the $h \to \gamma\gamma$ amplitude amounts to approximately 10% of the KK quark corrections and interferes constructively with the latter. In consequence, an omission of KK lepton effects in the calculation of κ_γ has only a minor numerical impact.

The sum entering the quantity ν_γ^W, representing the one-loop contribution due to $W^\pm$-boson KK modes, can be performed analytically in the decoupling limit. The corresponding Feynman diagram is displayed on the very right in Figure 5.19. Employing the results for the KK sums derived in Section 3.5, we obtain

$$\begin{aligned}
\nu_\gamma^W &= \frac{2\pi x_W^2 \, (g_L^2 + g_R^2)}{g_L^2} \sum_{n=1}^{\infty} \frac{\vec{d}_W^{\,T} \, \vec{\chi}_n^W(1) \, \vec{\chi}_n^{W\,T}(1) \, \vec{d}_W}{\left(x_n^W\right)^2} A_W^h(\tau_n^W) + \mathcal{O}(x_W^4) \\
&= \frac{2\pi x_W^2 \, (g_L^2 + g_R^2)}{g_L^2} \, \vec{d}_W^{\,T} \left[\mathbf{\Sigma}_W^{(1)}(1,1) - \mathbf{\Pi}_W(1,1) \right] \vec{d}_W \left(-\frac{21}{4} + \mathcal{O}\left(1/\tau_n^W\right) \right) \qquad (5.137) \\
&= -\frac{21}{8} \, \Delta g_h^W \left(1 + \mathcal{O}\left(1/\tau_n^W\right) \right),
\end{aligned}$$

where $\vec{d}_W = (c_W, -s_W)^T$ and $\tau_n^W \equiv 4\left(m_n^W\right)^2/m_h^2$. Since already $m_1^W \approx 2.5 M_{\mathrm{KK}} \gg m_h$, the terms suppressed by powers of τ_n^W in (5.137) can be ignored in practice. Note that in ν_γ^W, the VEV shift contributes only at $\mathcal{O}(x_W^4)$. The result for Δg_h^W has been given in (5.131).

The last missing ingredient that is needed to compute the branching fractions for all sought decay channels in the RS model is the rescaling factor for a decay into a photon and a Z boson. It reads

$$\kappa_{\gamma Z} = \frac{\sum_{i=t,b} N_c \dfrac{2\,Q_i v_i}{c_w} \kappa_i \kappa_i^V A_q^h(\tau_i, \lambda_i) + \kappa_W A_W^h(\tau_W, \lambda_W) + \sum_{j=u,d,\lambda} N_c \dfrac{2\,Q_j v_j}{c_w} \nu_{\gamma Z}^j + \nu_{\gamma Z}^W}{\sum_{i=t,b} N_c \dfrac{2\,Q_i v_i}{c_w} A_q^h(\tau_i, \lambda_i) + A_W^h(\tau_W, \lambda_W)} \,.$$

$$(5.138)$$

Here $v_i \equiv T_L^{3\,i} - 2s_w^2 Q_i$, and $\lambda_i \equiv 4m_i^2/m_Z^2$ for $i = t, b, W$. The amplitudes $A_{q,W}^h(\tau_i, \lambda_i)$ encoding the effects of virtual quarks and $W^\pm$ bosons in $h \to \gamma Z$ are collected in Appendix B.8. The corresponding Feynman diagrams are shown on the right in the bottom row of Figure 5.18. Like in the case of $h \to \gamma\gamma$, the SM decay rate for $h \to \gamma Z$ is in large parts of the parameter space dominated by the $W^\pm$-boson loop contribution. The function $A_W^h(\tau_W, \lambda_W)$ rises from around 4.6 to 9.8 between $\tau_W \to \infty$ and $\tau_W = 1$, and then falls to approximately 0.6 in the limit $\tau_W \to 0$. On the other hand, one has $A_q^h(\tau_i, \lambda_i) = -1/3$ for $\tau_i, \lambda_i \to \infty$ and $A_q^h(\tau_i, \lambda_i) = 0$ for $\tau_i, \lambda_i \to 0$.

The first term in the numerator of (5.138) depends on the ratios

$$\kappa_t^V = \frac{\left(g_L^u\right)_{33} + \left(g_R^u\right)_{33}}{v_t} \,, \qquad \kappa_b^V = \frac{\left(g_L^d\right)_{33} + \left(g_R^d\right)_{33}}{v_b} \,, \qquad (5.139)$$
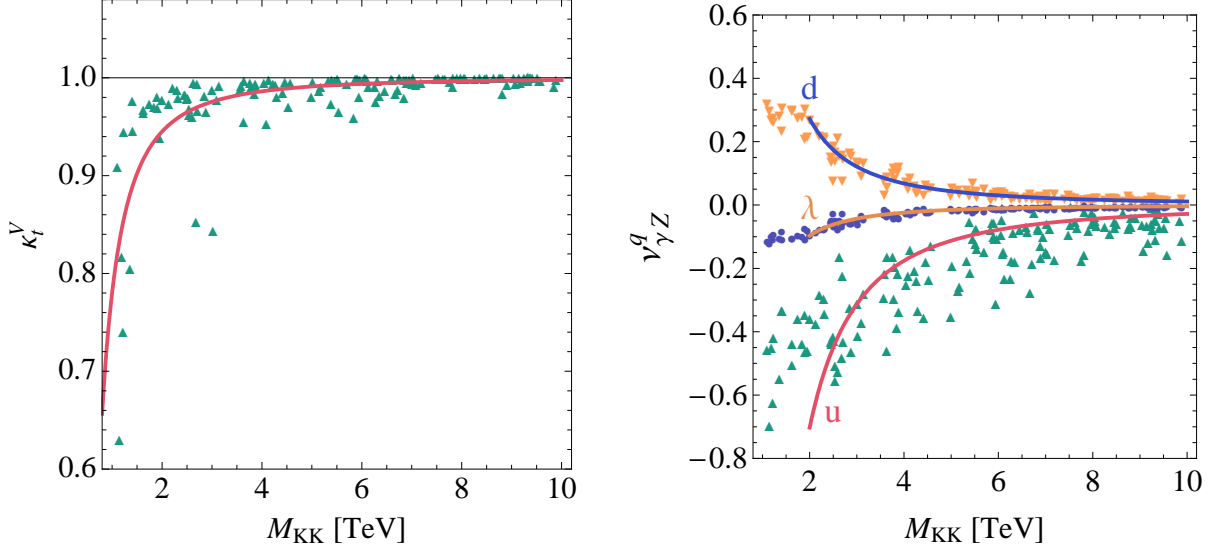
Figure 5.24:   Left: Predictions for the vector couplings of the Z boson to top and bottom quarks in the custodial RS model. Right: Different types of KK-quark contributions to the effective $h\gamma Z$ coupling. The solid lines show fits to the scatter points. See [2] and text for details.

which quantify the relative shift in the vector coupling of the Z boson to top and bottom quarks. In the left panel of Figure 5.24 we show the predictions for κ_t^V versus $M_{\rm KK}$ for our set of 150 parameter points. It is evident from the plot that the vector coupling of the Z boson to top quarks is always reduced in the custodial RS model relative to the SM. Numerically, the suppression amounts to a moderate effect of -5% (-2.5%) for $M_{\rm KK} = 2\,{\rm TeV}$ ($M_{\rm KK} = 3\,{\rm TeV}$). In contrast, the Z-boson coupling to bottom-quark pairs is larger than its SM value, but numerically the resulting effects turn out to be negligibly small due to the custodial protection mechanism. Consequently, we will set κ_b^V to 1 in our numerical analysis. Parametrizing the average value of the relative shift κ_t^V by $(1 - a_t^V\, v^2/M_{\rm KK}^2)$ the coefficient a_t^V can again be determined through a fit. Employing the shown set of parameter points, we obtain the value for a_t^V given in Table 5.3.

The second term in the numerator of (5.138) encodes the contribution arising from the $W^\pm$-boson triangle graph. The calculation of this zero-mode contribution is greatly simplified by the fact that at $\mathcal{O}(v^2/M_{\rm KK}^2)$ the triple gauge-boson vertex involving two $W^\pm$- and one Z-boson fields does not receive corrections in the RS model (regardless of the specific gauge group). This can be easily seen by employing that

$$\frac{2\pi}{L} \int_\epsilon^1 \frac{dt}{t}\, \chi_0^{(+)}(t) \,=\, \sqrt{2\pi} + \mathcal{O}\left(\frac{v^4}{M_{\rm KK}^4}\right), \tag{5.140}$$

and $\left[(\vec{A}_0^a)_2\, \chi_0^{(-)}(t)\right]^2 = \mathcal{O}(v^4/M_{\rm KK}^4)$. The expressions for $\chi_0^{(\pm)}(t)$ and $\vec{A}_0^a$ necessary to derive these results can be found in (3.207) and (3.208). By the same line of reasoning, it is also readily seen that all quartic gauge-boson vertices first differ at order $v^4/M_{\rm KK}^4$ from the corresponding SM expressions. In view of this extra suppression, we will set the triple gauge-boson couplings

of the zero modes to their SM values when evaluating the Higgs-boson branching fractions. In this approximation the effect of virtual $W^\pm$-boson exchange to (5.138) is simply given by the combination $\kappa_W A_W^h(\tau_W, \lambda_W)$, which up to the different form factor resembles the form of the corresponding term in (5.135).

The third term in the numerator of (5.138) describes the contribution to the $h \to \gamma Z$ amplitude stemming from the virtual exchange of KK quarks. The corresponding one-loop diagram is displayed in the middle of Figure 5.19. In the up-type quark sector we find

$$
\begin{aligned}
\nu_{\gamma Z}^u &= v_{\text{SM}} \sum_{n=4}^{\infty} \frac{\text{Re}\left[(g_h^u)_{nn}\right]}{m_n^u} \kappa_n^{u,V} A_q^h(\tau_n^u, \lambda_n^u) \\
&= \frac{2\pi}{\epsilon L} \frac{v_{\text{SM}}}{v_{\text{RS}_C}} \sum_{n=4}^{\infty} \frac{\text{Re}\left[\vec{a}_n^{U\dagger} \, \boldsymbol{C}_n^U(\pi^-) \left(\mathbf{1} - \frac{v_{\text{RS}_C}^2}{3\, M_{\text{KK}}^2} \tilde{\boldsymbol{Y}}_{\vec{u}} \bar{\boldsymbol{Y}}_{\vec{u}}^\dagger\right) \boldsymbol{S}_n^U(\pi^-) \, \vec{a}_n^U\right]}{x_n^u} \kappa_n^{u,V} A_q^h(\tau_n^u, \lambda_n^u),
\end{aligned}
$$

(5.141)

where $\kappa_n^{u,V}$ denotes the relative strength of vector coupling of the Z boson to the nth up-type quark KK mode defined in analogy to (5.139), and $\lambda_n^u \equiv 4(m_n^u)^2/m_Z^2$. Similar expressions apply in the case of down- and λ-type quark KK modes. Note again that the VEV shift $v_{\text{SM}}/v_{\text{RS}_C} \neq 1$ does not contribute to $\nu_{\gamma Z}^u$ at $\mathcal{O}(v^2/M_{\text{KK}}^2)$. The numerical results for $\nu_{\gamma Z}^u$, $\nu_{\gamma Z}^d$, and $\nu_{\gamma Z}^\lambda$, corresponding to our set of 150 random model parameter points, are depicted in the right panel of Figure 5.24. The solid lines indicate the best fit of the form $a_{\gamma Z}^{u,d,\lambda} v^2/M_{\text{KK}}^2$ to the sample of points with KK scales in the range $[2, 10]$ TeV. As before, points with $M_{\text{KK}} < 2$ TeV have been excluded in the fit, since they are subject to significant higher-order corrections. The corresponding coefficients $a_{\gamma Z}^{u,d,\lambda}$ can be found in Table 5.3. The average values of $\nu_{\gamma Z}^u$, $\nu_{\gamma Z}^d$, and $\nu_{\gamma Z}^\lambda$ obtained from the fit formulae are $-0.70\,(-0.31)$, $0.27\,(0.12)$, and $-0.10\,(-0.04)$ for $M_{\text{KK}} = 2$ TeV ($M_{\text{KK}} = 3$ TeV), respectively.

Denoting contributions from KK-lepton triangle graphs by $\nu_{\gamma Z}^l$, they can be included in (5.138) via the simple replacement

$$
\sum_{j=u,d,\lambda} N_c \frac{2 Q_j v_j}{c_w} \nu_{\gamma Z}^j \;\to\; \sum_{j=u,d,\lambda} N_c \frac{2 Q_j v_j}{c_w} \nu_{\gamma Z}^j + \frac{2 Q_l v_l}{c_w} \nu_{\gamma Z}^l.
$$

(5.142)

In order to estimate the typical size of $\nu_{\gamma Z}^l$ we need an analytic formula for the relative strength of the vector coupling between the Z boson and fermionic KK modes appearing in (5.141). We obtain

$$
\kappa_n^{f,V} = 1 - \frac{(\boldsymbol{\delta}_F)_{nn} - (\boldsymbol{\delta}_f)_{nn}}{v_f} + \mathcal{O}\left(\frac{m_Z^2}{M_{\text{KK}}^2}\right),
$$

(5.143)

where the expressions for $\boldsymbol{\delta}_{F,f}$ can be found in (3.239). In the case of the extended P_{LR} symmetry (3.252), it turns out that for down- and λ-type KK quarks the result for $\kappa_n^{f,V}$ can be expressed in terms of the electric charge and the third component of the weak isospin of the involved fermion, while no such formula can be derived for up-type quark KK modes. We get to excellent approximation ($f = d, \lambda$)

$$
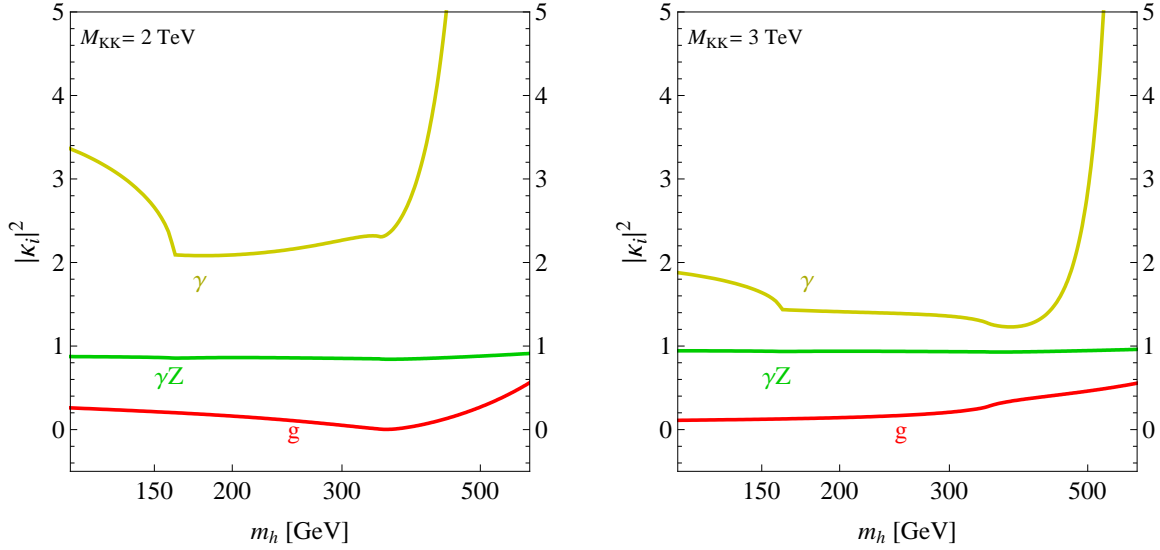\kappa_n^{f,V} = 1 + \frac{T_L^{3\,f_L}}{v_f},
$$

(5.144)

Figure 5.25:   RS-correction factors $|\kappa_g|^2$ (red line), $|\kappa_\gamma|^2$ (yellow line), and $|\kappa_{\gamma Z}|^2$ (green line) as functions of the Higgs-boson mass, employing $M_{\mathrm{KK}} = 2\,\mathrm{TeV}$ (left panel) and $M_{\mathrm{KK}} = 3\,\mathrm{TeV}$ (right panel). See [2] and text for details.

which implies that all down-type (λ-type) KK-quark modes couple with universal strength to the vector part of the Z-boson coupling. It follows that in the decoupling limit, $\tau_n^f, \lambda_n^f \to \infty$

$$\left(1 + \frac{T_L^{3\,f_L}}{v_f}\right) \frac{A_f^h(\tau_n^f, \lambda_n^f)}{A_f^h(\tau_n^f)} = \frac{a_{\gamma Z}^f}{a_f} \,. \tag{5.145}$$

From the numbers of the fit coefficients given in Table 5.3, we see that this relation is satisfied to an accuracy of around 1%. The KK-fermion effects in the down- and λ-type quark sectors that contribute to $h \to gg, \gamma\gamma, \gamma Z$ are thus universal, in the sense that they can be simply obtained from each other by an appropriate replacement of the vector couplings of the external fields.

Making now the plausible assumption that in the decoupling limit the sums $\nu_{\gamma Z}^d$ and $\nu_{\gamma Z}^l$ differ only by the presence of the vector couplings $\kappa_n^{d,V}$ and $\kappa_n^{l,V}$, we obtain the following estimate for the contribution to (5.142) from leptonic relative to down-type quark KK modes

$$\frac{Q_l v_l \nu_{\gamma Z}^l}{N_c Q_d v_d \nu_{\gamma Z}^d} \approx \frac{Q_l v_l \kappa_n^{l,V}}{N_c Q_d v_d \kappa_n^{d,V}} = \frac{3 - 6 s_w^2}{3 - 2 s_w^2} \approx 0.64\,. \tag{5.146}$$

In consequence, the sum (5.142) can be approximated as

$$\sum_{j=u,d,\lambda} N_c \frac{2 Q_j v_j}{c_w} \nu_{\gamma Z}^j + \frac{2 Q_l v_l}{c_w} \nu_{\gamma Z}^l \approx 0.88\,\nu_{\gamma Z}^u + 0.79\,\nu_{\gamma Z}^d - 3.04\,\nu_{\gamma Z}^\lambda + 0.50\,\nu_{\gamma Z}^d\,. \tag{5.147}$$

Note that the last term on the right-hand side encodes the effects due to KK leptons, and in order to obtain the numerical values we have inserted the relevant electroweak quantum numbers and used $s_w^2 \approx 0.23$. For $M_{\mathrm{KK}} = 2\,\mathrm{TeV}$, the sum above evaluates to $-0.11\,(0.03)$

if effects due to KK leptons are excluded (included). While these numbers imply that an omission of KK lepton effects can change the numerical value of the KK fermion contribution to $h \to \gamma Z$ notably, it is not difficult to see that the impact on (5.138) itself is limited, since the coefficient $\kappa_{\gamma Z}$ is dominated by the $W^{\pm}$-boson triangle contribution. We thus conclude that the absence of KK-lepton contributions in our prediction for $h \to \gamma Z$ will not change any of our conclusions.

The coefficient $\nu_{\gamma Z}^{W}$ in (5.138) incorporates the effects due to charged KK-boson excitations in the loop. The corresponding Feynman graph is displayed on the very right in Figure 5.19. This contribution reads explicitly

$$\nu_{\gamma Z}^{W} = \frac{2\pi x_W^2 \left(g_L^2 + g_R^2\right)}{g_L^2} \sum_{n=1}^{\infty} \frac{\vec{d}_W^{\,T} \vec{\chi}_n^{W}(1)\, \vec{\chi}_n^{W\,T}(1)\, \vec{d}_W}{\left(x_n^W\right)^2} \, \mathcal{I}_{nn0}^{WWZ} \, A_W^h(\tau_n^W, \lambda_n^W)\,, \qquad (5.148)$$

where

$$\mathcal{I}_{nn0}^{WWZ} = \frac{(2\pi)^{3/2}}{L} \int_{\epsilon}^{1} \frac{dt}{t} \left[\chi_0^{(+)Z}(\vec{A}_0^Z)_1 \left(\chi_n^{(+)W\,2}(\vec{A}_n^W)_1^2 + \frac{g_Y^2}{g_L^2} \chi_n^{(-)W\,2}(\vec{A}_n^W)_2^2 \right) \right. \\ \left. - \sqrt{1 - g_Y^4/g_L^4}\, \chi_0^{(-)Z}(\vec{A}_0^Z)_2\, \chi_n^{(-)W\,2}(\vec{A}_n^W)_2^2 \right]\,, \qquad (5.149)$$

and $\lambda_n^W \equiv 4\left(m_n^W\right)^2/m_Z^2$. Note that in the prefactor in the second line of the above formula we have set $g_L = g_R$. Since the first term in the sum of (5.148) is already suppressed by a factor of v^2/M_{KK}^2, the computation of $\nu_{\gamma Z}^{W}$ to this order only requires the knowledge of the overlap integral (5.149) to zeroth order in the ratio of the weak over the KK scale. We obtain

$$\mathcal{I}_{nn0}^{WWZ} = \frac{2\pi}{L} \int_{\epsilon}^{1} \frac{dt}{t} \left(\chi_n^{(+)W\,2}(\vec{A}_n^W)_1^2 + \frac{g_Y^2}{g_L^2} \chi_n^{(-)W\,2}(\vec{A}_n^W)_2^2 \right) + \mathcal{O}\left(\frac{v^2}{M_{\mathrm{KK}}^2}\right)\,. \qquad (5.150)$$

It is again an excellent approximation to evaluate the loop function $A_W^h(\tau_n^W, \lambda_n^W)$ in the infinite mass limit $\tau_W^h, \lambda_n^W \to \infty$, in which the form factor approaches $31\, c_w/6 - 11\, s_w^2/(6\, c_w) \approx 4.0$. We perform the sum in (5.148) numerically. In this way, we find $\nu_{\gamma Z}^{W} = 0.16$ ($\nu_{\gamma Z}^{W} = 0.07$) for $M_{\mathrm{KK}} = 2\,\mathrm{TeV}$ ($M_{\mathrm{KK}} = 3\,\mathrm{TeV}$). Values for $\nu_{\gamma Z}^{W}$ corresponding to different KK scales can be obtained by means of the fit formula $a_{\gamma Z}^{W}\, v^2/M_{\mathrm{KK}}^2$. The coefficient $a_{\gamma Z}^{W}$ is given in Table 5.3.

In Figure 5.25 we display the relative corrections $|\kappa_g|^2$, $|\kappa_\gamma|^2$, and $|\kappa_{\gamma Z}|^2$ for $M_{\mathrm{KK}} = 2\,\mathrm{TeV}$ (left) and $M_{\mathrm{KK}} = 3\,\mathrm{TeV}$ (right). The depicted curves represent the RS results obtained from (5.131) and (5.137) as well as from the relevant fit formulae with the values of the coefficients collected in Table 5.3. While the behavior of $|\kappa_g|^2$ has already been analyzed in Section 5.3.1, we see that $|\kappa_{\gamma Z}|^2$ is close to 1 and independent of the value of the Higgs-boson mass. This implies that the partial decay width $\Gamma(h \to \gamma Z)$ in the custodial RS model is essentially unchanged with respect to the SM. The relative correction $|\kappa_\gamma|^2$ is, on the other hand, a non-trivial function of m_h. Below the WW threshold, the $W^{\pm}$-boson amplitude dominates the SM $h \to \gamma\gamma$ decay rate and the contributions due to KK quarks and $W^{\pm}$ bosons both interfere constructively with the SM gauge-boson triangle graph. For $m_h = 130\,\mathrm{GeV}$, the new-physics contributions amount to around 70% (30%) of the total SM amplitude for $M_{\mathrm{KK}} = 2\,\mathrm{TeV}$ ($M_{\mathrm{KK}} = 3\,\mathrm{TeV}$), resulting in values $|\kappa_\gamma|^2 \approx 3$ ($|\kappa_\gamma|^2 \approx 1.7$). For $m_h \gtrsim 160\,\mathrm{GeV}$, the Higgs-mass dependence of the SM amplitude becomes less pronounced and the RS prediction stays
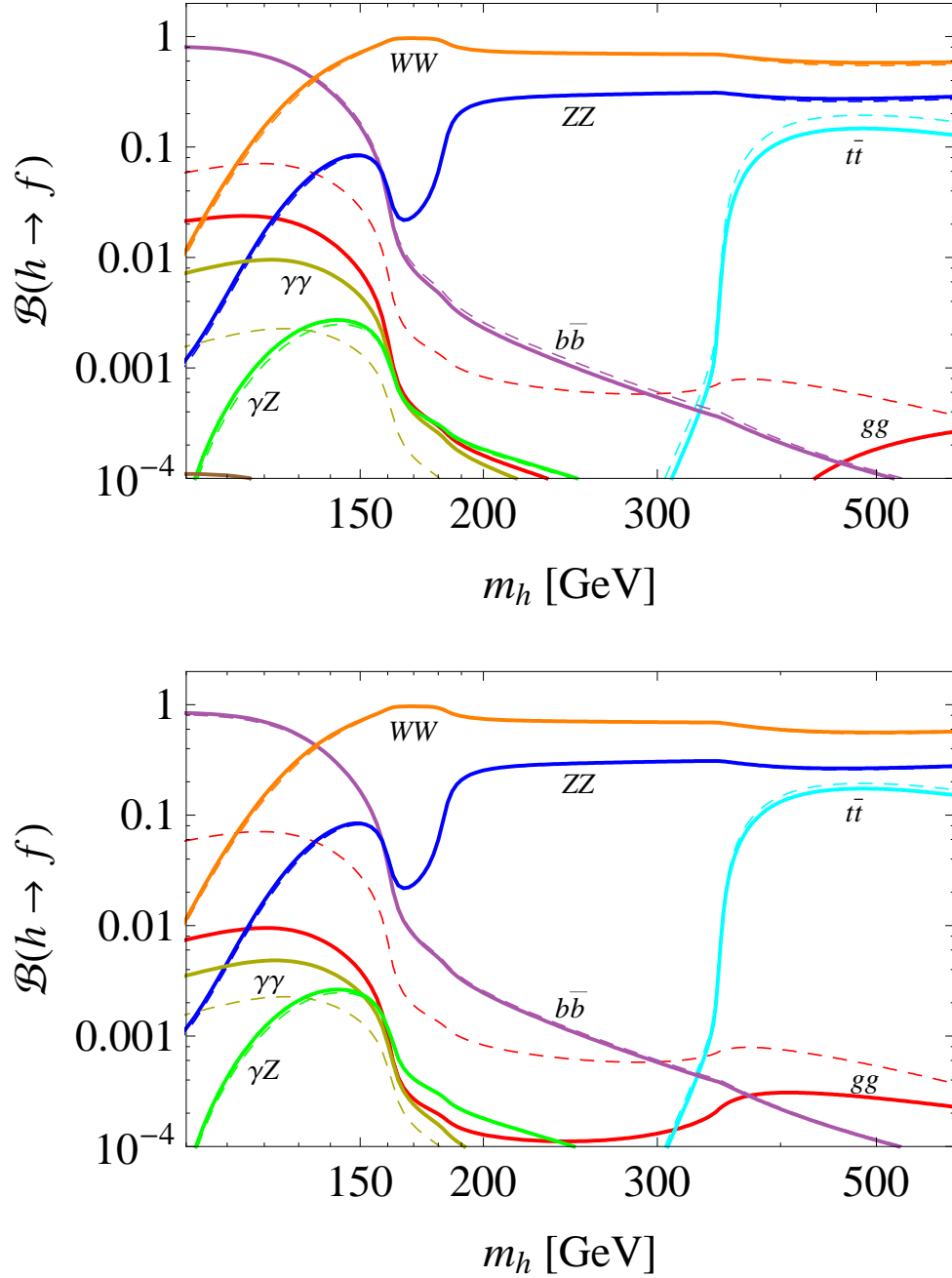
Figure 5.26:   Branching ratios for the decays $h \to f$ as functions of the Higgs-boson mass for $M_{\mathrm{KK}} = 2\,\mathrm{TeV}$ (upper panel) and $M_{\mathrm{KK}} = 3\,\mathrm{TeV}$ (lower panel).   The SM predictions are indicated by dashed lines, while the solid lines show the corresponding RS expectations. Branching fractions of less than 10^{-4} and decay channels into final states with muon, tau, charm-, and strange-quark pairs, which are all expected to remain SM-like, are not shown. See [2] and text for details.

almost constant. The strong rise of $|\kappa_\gamma|^2$, visible at higher values of the Higgs mass, is due to the fact that for $m_h \approx 650\,\text{GeV}$ the top-quark loop nearly cancels the $W^\pm$-boson contribution in the SM. As a result, for $m_h \gtrsim 500\,\text{GeV}$ the partial width $\Gamma(h \to \gamma\gamma)$ is almost entirely due to loops involving heavy KK modes, with the dominant contribution stemming from KK quarks.

Let us finally analyze the emerging picture of Higgs-boson decays, obtained using the above results. The various branching fractions in the custodial RS model are displayed by the solid lines in Figure 5.26, whereas the dashed lines illustrate the SM expectations calculated with the help of HDECAY [58]. The RS predictions are based on the results for $\kappa_{t,b,W,Z}$ quoted above and the curves for $|\kappa_{g,\gamma,\gamma Z}|^2$ displayed in Figure 5.25. It is evident that in the custodial RS model the branching ratios $h \to b\bar{b}$, $h \to WW$, and $h \to ZZ$ receive only insignificant corrections, not exceeding the level of $\pm 5\%$. For $m_h \gtrsim 180\,\text{GeV}$ the experimentally cleanest signature for the discovery of the Higgs boson at the LHC is the "golden" channel of a decay to four leptons, $h \to Z^{(*)}Z^{(*)} \to l^+l^-l^+l^-$. Since the $h \to ZZ$ branching fraction is essential SM-like, the reduction in the $gg \to h$ production cross section will make an observation of the Higgs boson in this channel more difficult.

Moderate effects occur in the non-discovery channels $h \to \gamma Z$ and $h \to t\bar{t}$. In the relevant ranges for the Higgs mass, the modifications in the branching ratios amount to around $+10\%$ $(+10\%)$ and -25% (-10%) for $M_{\text{KK}} = 2\,\text{TeV}$ $(M_{\text{KK}} = 3\,\text{TeV})$. The most pronounced effects are found for $h \to gg$ and $h \to \gamma\gamma$. For Higgs masses below the WW threshold, the branching fraction of the former mode is reduced by a factor of almost 4 (8), while the branching ratio of the latter transition is enhanced by a factor of around 4 (2). The corresponding maximal values of $\mathcal{B}(h \to \gamma\gamma)$ are $9.3 \cdot 10^{-3}$ $(4.8 \cdot 10^{-3})$ for $M_{\text{KK}} = 2\,\text{TeV}$ $(M_{\text{KK}} = 3\,\text{TeV})$ and arise at $m_h \approx 120\,\text{GeV}$. Calculating the rescaling factor $\varkappa = (\sigma_{\text{RS}}(gg \to h)\,\mathcal{B}(h \to \gamma\gamma)_{\text{RS}}) / (\sigma_{\text{SM}}(gg \to h)\,\mathcal{B}(h \to \gamma\gamma)_{\text{SM}})$ for $\sqrt{s} = 10\,\text{TeV}$ and the quoted maximal branching fractions, we obtain the values 1.03 (0.24). These numbers suggest that the statistical significance for a LHC discovery of the Higgs boson in $h \to \gamma\gamma$ can be slightly enhanced in the custodial RS model for low KK scales. Note that if the KK scale is lowered to 1 TeV, the branching ratio of $h \to tc$ can reach values above 10^{-4} for Higgs masses above $m_h \approx 180\,\text{GeV}$. In the limit of a vanishing charm-quark mass, $r_c = 0$, the corresponding decay rate is simply obtained from (5.73) by multiplying the branching fraction for $t \to ch$ with $g^2(1 - r_W^2)^2(1 + 2r_W^2)/(2r_W^2)\,m_h/(16\pi)$ and replacing r_h through r_t. For such a low KK scale, also the decay channel $h \to bs$ can open up below the WW threshold (whose rate obeys a similar formula), but typically stays below the level of 10^{-3}. Like for the case of the production cross sections, the value of the KK scale fixes the results for the Higgs-boson branching fractions to first approximation and leaves no space for large variations. RS predictions for the various branching fractions of the Higgs boson have been presented previously in [203]. Yet, a direct comparison with our results is difficult, as the latter work only includes RS corrections affecting the tree-level couplings of the Higgs boson to fermions.

The analysis performed in this section demonstrates that Higgs physics at the LHC could be very sensitive to warped extra dimensions, even for KK scales that are significantly too high for a direct production of KK modes and for suppressed FCNCs. It provides an example for a theory that features a SM Higgs sector which, depending on m_h, could be quite hard to discover with early LHC data, despite the absence of NP directly at ~ 1 TeV. This is mainly due to the depletion in the production cross section. Moreover, it could be possible

that we just find a single spin-0 Higgs-doublet with hypercharge 1/2 at the LHC, with however couplings that differ from the SM expectations. These modified couplings could be our only clear signal and hint for BSM physics. The analysis presented here demonstrates what to expect if warped extra dimensions are realized in nature.

Chapter 6

Conclusions and Outlook

Some pressing unresolved questions in particle physics might be addressed, if the world around us features more than four dimensions. The shortcomings, but also the successful features of the Standard Model of particle physics have finally lead to the construction of the custodial Randall-Sundrum model with bulk fields, an enlarged gauge symmetry group $SU(2)_L \times SU(2)_R \times U(1)_X \times P_{LR}$ and extended fermion representations. This model thus follows various directions to extend the SM which have been mentioned in the introduction of this thesis. We have discussed in detail the way to the custodial RS model, the solution to the gauge hierarchy problem and to the puzzle of fermion hierarchies.

A comprehensive discussion of the KK decomposition of RS models within the mass basis has been presented and exact expressions to all orders in $v^2/M_{\rm KK}^2$ for the masses of the SM fields and their KK excitations, as well as for the profiles of these fields in the extra dimension, have been derived. Special attention has been paid to the correct inclusion of Yukawa couplings involving Z_2-odd fermion fields, which would be naively lost in a perturbative approach. By demonstrating the analogy to the Froggatt-Nielsen mechanism, formulae for the hierarchical quark spectrum as well as for the CKM matrix in terms of $\mathcal{O}(1)$ localization parameters of the fermion fields have been derived. This anarchic approach to flavor improves the predictivity of the RS setup. We have performed a complete analysis of flavor changing effects at tree level, pointing out the importance of fermion mixing for neutral current interactions with the Z boson. We have also demonstrated how to perform infinite sums over KK towers in RS models. Beyond that, analytic expressions for five dimensional propagators for massive gauge bosons as well as for fermions have been presented. In the latter case, we have considered the complete Yukawa structure for the first time, mediating flavor off-diagonal transitions.

We have studied in detail the phenomenology of the minimal as well as of the custodial Randall-Sundrum proposal. Predictions for various observables have been presented. After an analysis of electroweak precision tests, we have shown that the minimal RS model, in combination with a heavy Higgs boson, could still furnish a viable setup. In fact, due to the RS scale of $\Lambda_{UV}(\pi) = \mathcal{O}(\text{TeV})$ at the IR brane, the natural assumption for the Higgs-boson mass in the RS framework would be $m_h \lesssim 1\,\text{TeV}$. Expanding our exact formulae in powers of $v^2/M_{\rm KK}^2$ has allowed to expose the dependence of observables on the input parameters of the model clearly. In particular, the exact approach has offered the possibility to decipher, which contributions to the $Z \to b\bar{b}$ pseudo observables can be removed in the custodial setup and which correspond to irreducible sources of P_{LR}-symmetry breaking.

Randall-Sundrum models have been used in the literature to address the enhancement in the $t\bar{t}$ forward-backward asymmetry measured at Tevatron. We have shown that it is not

possible to explain this anomaly in RS models with an anarchic approach to flavor. The leading order corrections to the charge-asymmetric cross section are strongly suppressed due to the UV localization and mostly vector-like couplings of light quarks. In this context we have taken into account the dominant next-to-leading order corrections for the first time. We have shown that they exceed the formally leading order corrections, and argued that this observation holds true for a broad class of new physics models. However, we still found a generic tension between generating large effects in the asymmetry and achieving a natural solution to the flavor hierarchy problem. We have investigated the rare decays $t \to cZ$ and $t \to ch$ as well as the non-unitarity of the quark mixing matrix. We demonstrated that among these, the most promising option to see signatures of the RS model is due to Higgs couplings. Moreover, we have calculated the anomalous magnetic moment of the muon in the RS setup, which was found to be orders of magnitude below the experimental bounds. The phenomenological survey has been continued with an analysis of B_s^0–$\bar{B}_s^0$ mixing. A calculation of the absorptive part of the mixing amplitude in the presence of new physics has been presented and the impact of the Randall-Sundrum setup on several CP-violating observables has been investigated. We have shown that an improved agreement of the theoretical values for A_{SL}^s, $S_{\psi\phi}$, and $\Delta\Gamma_s$ with experiment is possible.

A central purpose of the Large Hadron Collider is to explore the sector of electroweak symmetry breaking and to discover the Higgs boson. For the first time, we have presented a complete one-loop calculation of all relevant Higgs-boson production and decay channels in the custodial RS setup, incorporating the effects stemming from the extended electroweak gauge-boson and fermion sectors. We have shown that Higgs physics offers the possibility to test large scales at the LHC, that are significantly beyond the direct reach. Thus, RS models might show up first in modified Higgs-production cross-sections or branching fractions. Depending on its mass, the impact of the RS model could, on the other hand, make a discovery of the Higgs boson more difficult. It would be worthwhile studying the impact of the RS setup on Higgs searches and exclusion limits at the LHC and the Tevatron more detailed.

An ongoing issue is to understand RS models at the quantum level. A complete analytical calculation of loop mediated flavor-changing neutral currents such as $B \to X_s\gamma$ and of quantum corrections to flavor diagonal transitions like for a_μ, including bulk fermions, is still a desideratum. Since performing multiple infinite sums, accounting for the full RS flavor structure is not always feasible, the 5D propagators presented in this thesis will be useful to tackle these problems. Moreover, employing a proper regularization of the brane-Higgs sector, 5D fermion propagators at vanishing momentum transfer can be used to study loop mediated Higgs-production and -decay channels analytically.

Acknowledgments

First, I would like to owe my gratitude to my supervisor, Prof. Dr. Matthias Neubert who always supported me with his knowledge, guidance and encouragement. I had the opportunity to work on a highly interesting topic. Additionally, I would like to thank Prof. Dr. Hubert Spiesberger for his advice in many situations.

I was glad to write my thesis in an inspiring, encouraging environment and I want to thank the whole THEP. Especially, my officemates Torsten Pfoh, Michael Benzke and Alessandro Broggio for three cooperative years and Kaustubh Agashe, Valentin Ahrens, Volker Büscher, Marcela Carena, Sandro Casagrande, Hooman Davoudiasl, Uli Haisch, Nima Arkani-Hamed, Rainer Häußling, Gabriele Honecker, Barbara Jäger, Florian Jung, Daniel Litim, Lucia Massetti, Ben Pecjak, Martin Reuter, Christoph Schmell, Rainer Wanke, Stefan Weinzierl, Susanne Westhoff, Li Lin Yang and Omar Zanusso for helpful discussions. Special thanks goes to Martin Bauer and Raoul Malm for checking results, as well as to Martin Bauer, Stefan Berge, Alessandro Broggio, Tobias Hurth and Julia Seng for proof-reading! I also would like to thank Martin Bauer, Sandro Casagrande, Uli Haisch, Matthias Neubert, Torsten Pfoh and Susanne Westhoff for fruitful collaborations.

I owe my deepest gratitude to my family and my wife Julia.

Florian Goertz

The Feynman diagrams shown in this thesis have been produced with the help of `FeynArts` [397] and `Jaxodraw` [398].

Appendix A

Appendices Chapter 1

A.1 Pauli, Dirac, and Gell-Mann Matrices

The Pauli matrices are defined as

$$\sigma^1 = \begin{pmatrix} 0 & 1 \\ 1 & 0 \end{pmatrix}, \quad \sigma^2 = \begin{pmatrix} 0 & -i \\ i & 0 \end{pmatrix}, \quad \sigma^3 = \begin{pmatrix} 1 & 0 \\ 0 & -1 \end{pmatrix}. \tag{A.1}$$

The Dirac-gamma matrices fulfill the Clifford algebra

$$\{\gamma^\mu, \gamma^\nu\} = 2\,\eta^{\mu\nu}\mathbf{1}. \tag{A.2}$$

In the *Weyl representation* they read $(i = 1, 2, 3)$

$$\gamma^0 = \begin{pmatrix} 0 & \mathbf{1}_{2\times2} \\ \mathbf{1}_{2\times2} & 0 \end{pmatrix}, \quad \gamma^i = \begin{pmatrix} 0 & \sigma^i \\ -\sigma^i & 0 \end{pmatrix}. \tag{A.3}$$

The chirality matrix is defined as

$$\gamma^5 \equiv i\gamma^0\gamma^1\gamma^2\gamma^3 = \begin{pmatrix} -\mathbf{1}_{2\times2} & 0 \\ 0 & \mathbf{1}_{2\times2} \end{pmatrix}. \tag{A.4}$$

Finally, the Gell-Mann color matrices are

$$\lambda^1 = \begin{pmatrix} 0 & 1 & 0 \\ 1 & 0 & 0 \\ 0 & 0 & 0 \end{pmatrix}, \quad \lambda^2 = \begin{pmatrix} 0 & -i & 0 \\ i & 0 & 0 \\ 0 & 0 & 0 \end{pmatrix}, \quad \lambda^3 = \begin{pmatrix} 1 & 0 & 0 \\ 0 & -1 & 0 \\ 0 & 0 & 0 \end{pmatrix}, \quad \lambda^4 = \begin{pmatrix} 0 & 0 & 1 \\ 0 & 0 & 0 \\ 1 & 0 & 0 \end{pmatrix},$$

$$\lambda^5 = \begin{pmatrix} 0 & 0 & -i \\ 0 & 0 & 0 \\ i & 0 & 0 \end{pmatrix}, \quad \lambda^6 = \begin{pmatrix} 0 & 0 & 0 \\ 0 & 0 & 1 \\ 0 & 1 & 0 \end{pmatrix}, \quad \lambda^7 = \begin{pmatrix} 0 & 0 & 0 \\ 0 & 0 & -i \\ 0 & i & 0 \end{pmatrix}, \quad \lambda^8 = \frac{1}{\sqrt{3}} \begin{pmatrix} 1 & 0 & 0 \\ 0 & 1 & 0 \\ 0 & 0 & -2 \end{pmatrix}. \tag{A.5}$$

A.2 Custodial Symmetry

Starting from the general squared mass matrix (1.31) and demanding that one eigenvalue of the lower right block has to be zero (corresponding to the photon), while denoting the other

one by m_Z^2, leads to the conditions

$$\text{Det}\left[\begin{pmatrix} m_3^2 & m^2 \\ m^2 & m_0^2 \end{pmatrix}\right] = 0\,, \quad \text{Tr}\left[\begin{pmatrix} m_3^2 & m^2 \\ m^2 & m_0^2 \end{pmatrix}\right] = \text{m}_Z^2\,. \tag{A.6}$$

Identifying the eigenvector belonging to the vanishing eigenvalue as $(s_w, c_w)^T$ (forming a row of the matrix that rotates the vector fields to the mass basis) we get

$$\frac{s_w}{c_w} = -\frac{m^2}{m_3^2} = -\left|\frac{m_0}{m_3}\right|\,, \tag{A.7}$$

where we have used the first condition of (A.6). From the second relation we now derive

$$m_Z^2 = m_3^2 \left(1 + \frac{s_w^2}{c_w^2}\right)\,, \tag{A.8}$$

which results in

$$|m_3| = m_Z\, c_w\,. \tag{A.9}$$

We can use (A.7) to trade m_3 for m_0 which leads to $|m_0| = -m_Z\, s_w$. Applying the last relations we arrive at the most general (squared) mass matrix, compatible with the breaking pattern (1.18) of electroweak gauge symmetry

$$M^2 = \begin{pmatrix} m_W^2 & 0 & 0 & 0 \\ 0 & m_W^2 & 0 & 0 \\ 0 & 0 & m_z^2\, c_w^2 & -m_Z^2\, c_w s_w \\ 0 & 0 & -m_Z^2\, c_w s_w & m_Z^2\, s_w^2 \end{pmatrix}\,. \tag{A.10}$$

In order to fulfill the sought mass relation (1.29), one needs $m_3^2 = m_W^2$, as can be read off from (A.9). Thus, the mass matrix to start with (1.31), has to fulfill

$$m_1^2 = m_2^2 = m_3^2 = m_W^2 \tag{A.11}$$

in addition to the requirements following from the residual $U(1)_{EM}$ gauge invariance.

For the SM Higgs mechanism, this relation is fulfilled due to an accidental global symmetry in the Higgs Lagrangian. Writing the Higgs doublet as

$$\Phi = \begin{pmatrix} \phi_1 + i\,\phi_2 \\ \phi_3 + i\,\phi_4 \end{pmatrix}\,, \tag{A.12}$$

we see that terms of the form

$$\Phi^\dagger \Phi = \begin{pmatrix} \phi_1 \\ \phi_2 \\ \phi_3 \\ \phi_4 \end{pmatrix}^T \begin{pmatrix} \phi_1 \\ \phi_2 \\ \phi_3 \\ \phi_4 \end{pmatrix} \tag{A.13}$$

possess an $O(4)$ symmetry which is isomorphic to $SU(2)_L \times SU(2)_R$. As it is more convenient to work with the second form of the symmetry, we write the Higgs field as a 2×2 matrix,

composed of $\Phi^c \equiv i\sigma_2 \Phi^*$ and Φ (see (1.16))

$$\Phi = \begin{pmatrix} \phi^{0*} & \phi^+ \\ -\phi^- & \phi^0 \end{pmatrix}, \tag{A.14}$$

which transforms under $SU(2)_L \times SU(2)_R$ as

$$\Phi \to U_L \, \Phi \, U_R^\dagger. \tag{A.15}$$

Here, $U_{L,R}$ correspond to unitary $SU(2)_{L,R}$ transformation matrices. In Section 3.4 we also use such a form of the Higgs field, given a gauged version of the $SU(2)_L \times SU(2)_R$ symmetry. The Higgs potential (see (1.19)) now becomes

$$V(\Phi) = -\frac{\mu^2}{2}\mathrm{Tr}[\Phi^\dagger \Phi] + \frac{\lambda}{4}\mathrm{Tr}[\Phi^\dagger \Phi \, \Phi^\dagger \Phi]. \tag{A.16}$$

It is obviously invariant under the transformation (A.15). The same is true for the part containing the covariant derivatives, only if $g' = 0$, otherwise the coupling with B_μ breaks the global $SU(2)_R$ symmetry. Setting $g' = 0$, the Higgs Lagrangian (1.19) has the full global $SU(2)_L \times SU(2)_R$ symmetry, given that W_μ^i transforms as a triplet under $SU(2)_L$ and is a singlet under $SU(2)_R$. The vacuum expectation value of the Higgs field

$$\langle\Phi\rangle = \frac{v}{\sqrt{2}}\begin{pmatrix} 1 & 0 \\ 0 & 1 \end{pmatrix} \tag{A.17}$$

now breaks this global symmetry down according to

$$\begin{aligned} SU(2)_L \times SU(2)_R &\longrightarrow SU(2)_V\,, \qquad \langle\Phi\rangle \to U_V \, \langle\Phi\rangle \, U_V^\dagger\,, \\ \widehat{=} \quad O(4) &\longrightarrow O(3)\,. \end{aligned} \tag{A.18}$$

In the parametrization of (A.13), the residual $O(3)$ symmetry corresponds to a rotation among the components of Φ, which do not acquire a VEV. After EWSB, this symmetry requires the mass terms of the components of W_μ^i, transforming as a vector, to have the same coefficients (note that still $U(1)_{EM}$ is left unbroken)

$$m_1 = m_2 = m_3\,. \tag{A.19}$$

This relation remains valid (at the tree level) if we allow again for $g' \neq 0$ and leads to the mass relation (1.29). Thus we have identified a residual $O(3) \widehat{=} SU(2)_V$ symmetry, guaranteeing that this mass relation is fulfilled.

A.3   Unitarity, Triviality and Vacuum-Stability Bounds

Unitarity bound: To derive the unitarity bound on the Higgs-boson mass, it is useful to perform a partial wave analysis of the scattering amplitude

$$A(s,t) = 16\pi \sum_{l=0}^{\infty} (2l+1)a_l(s)P_l(\cos\theta)\,, \tag{A.20}$$

where $P_l(x)$ are Legendre Polynomials, $\cos\theta = 1+2t/s$ at high energies, and t is a Mandelstam variable, corresponding to the squared difference of an initial state momentum and a final state one, see Section 5.1.4. The total cross section for a $2 \to 2$ process becomes

$$\sigma = \frac{16\pi}{s} \sum_{l=0}^{\infty} (2l+1)|a_l(s)|^2\,. \tag{A.21}$$

Applying the optical theorem

$$\sigma = \frac{1}{s}\,\mathrm{Im}A(s,0)\,, \tag{A.22}$$

which follows from unitarity, it is easy to show that

$$|\mathrm{Re}\,a_l(s)| \le \frac{1}{2} \tag{A.23}$$

has to hold. Using the result for $W^{\pm}$-boson scattering at high energies $s \gg m_W^2$ (and for a heavy Higgs boson) [39]

$$A(s,t) = -\left[2\frac{m_h^2}{v^2} + \left(\frac{m_h^2}{v}\right)^2 \frac{1}{s-m_h^2} + \left(\frac{m_h^2}{v}\right)^2 \frac{1}{t-m_h^2} \right]\,, \tag{A.24}$$

we obtain from (A.23) (in the limit $s \gg m_h^2$) the s-wave (l=0) constraint

$$|\mathrm{Re}\,a_0| = \frac{m_h^2}{8\pi v^2} \le \frac{1}{2} \;\Rightarrow\; m_h \lesssim 870\,\mathrm{GeV}\,. \tag{A.25}$$

Triviality and vacuum-stability bounds: In the SM, the leading dependence of the Higgs-quartic coupling on the energy scale μ is given by the renormalization group equation [39]

$$\frac{d\lambda}{d\ln\mu^2} \simeq \frac{1}{16\pi^2}\left[6\lambda^2 + 6\lambda y_t^2 - 6y_t^4 - \frac{3}{2}\lambda(3g^2 + g'^2) + \frac{3}{8}(2g^4 + (g^2 + g'^2)^2) \right]\,, \tag{A.26}$$

where $y_t = \sqrt{2}/v\, m_t$ is the top-quark Yukawa coupling. The lighter-fermion contributions can be neglected to good approximation. For large λ only the first term on the right hand side of (A.26) contributes and the solution to this equation becomes

$$\lambda(\mu^2) = \lambda(\mu_0^2)\left(1 - \frac{3}{8\pi^2}\lambda(\mu_0^2)\ln\frac{\mu^2}{\mu_0^2} \right)^{-1}\,. \tag{A.27}$$

Looking at this equation we see that the Higgs quartic coupling blows up and hits a Landau pole at

$$\mu_c = v \, \exp\left[\frac{4\pi^2}{3\lambda(v^2)}\right] = v \exp\left[\frac{4\pi^2 v^2}{3m_h^2}\right]\,, \tag{A.28}$$

where we have chosen the electroweak symmetry breaking scale as the reference scale, $\mu_0 = v$, and used $\lambda(v^2)\, v^2 = m_h^2$. Requiring this pole not to appear until the Planck scale $\mu_c = M_{\rm Pl}$, which means that the Higgs sector of the SM is well behaved for the whole possible energy range of the theory, demands the Higgs boson to be light. However, a low Landau pole at around a TeV allows for a heavy Higgs boson

$$\begin{aligned} \mu_c &\gtrsim 10^{19}\,{\rm GeV} \;\Rightarrow\; m_h \lesssim 145\,{\rm GeV}\\ \mu_c &\gtrsim 1\,{\rm TeV} \;\Rightarrow\; m_h \lesssim 750\,{\rm GeV}\,. \end{aligned} \tag{A.29}$$

Note that, including the top Yukawa as well as the gauge couplings moderately modifies these results. A more exact perturbative constraint will be given below.

The vacuum stability bound on the Higgs-boson mass can be derived from requiring the Higgs potential to be bounded from below. This translates into $\lambda > 0$, see (1.19). Thus we have to study under which conditions (A.26) can drive the quartic coupling negative. To this end, we consider the renormalization group equation for small λ, which leads to the solution $(\mu_0 = v)$

$$\lambda(\mu^2) = \lambda(v^2) + \frac{1}{16\pi^2}\left[-24\frac{m_t^4}{v^4} + \frac{3}{8}(2g^4 + (g^2 + g'^2)^2)\right]\ln\frac{\mu^2}{v^2}\,. \tag{A.30}$$

Note that only the top Yukawa contribution can drive λ negative. If we do not want λ to become negative before the scale μ_c, we arrive at the condition

$$m_h^2 > \frac{v^2}{16\pi^2}\left[24\frac{m_t^4}{v^4} - \frac{3}{8}(2g^4 + (g^2 + g'^2)^2)\right]\ln\frac{\mu_c^2}{v^2}\,. \tag{A.31}$$

This leads to the bounds

$$\begin{aligned} \mu_c &\gtrsim 10^{19}\,{\rm GeV} \;\Rightarrow\; m_h \gtrsim 120\,{\rm GeV}\\ \mu_c &\gtrsim 1\,{\rm TeV} \;\Rightarrow\; m_h \gtrsim 70\,{\rm GeV}\,. \end{aligned} \tag{A.32}$$

Below the scale μ_c our theory is stable, whereas above, it would become unstable and has to be replaced by something new. The values quoted here all correspond to leading order results. The running of the top-quark Yukawa coupling is included. A proper two loop calculation, requiring perturbation theory to be valid and the Higgs potential to be stable below the cutoff μ_c leads to [39, 41]

$$\begin{aligned} \mu_c &\gtrsim 10^{16}\,{\rm GeV} \;\Rightarrow\; 130\,{\rm GeV} \lesssim m_h \lesssim 180\,{\rm GeV}\\ \mu_c &\gtrsim 1\,{\rm TeV} \;\Rightarrow\; 50\,{\rm GeV} \lesssim m_h \lesssim 800\,{\rm GeV}\,. \end{aligned} \tag{A.33}$$

A.4   Effective Field Theories

In this appendix we present the main concepts of effective field theories, which are used throughout this thesis. The fact that short-distance effects can be separated from long-distance effects, the concept on which EFTs are based, is crucial for a step-by-step progress in physics. Excellent introductions to the subject, on which part of the following is based, can be found in [76, 87, 399]. By making use of the renormalization group, EFTs are well suited to deal with multi scale problems which often appear in nature and they provide a modern notion of renormalization. Furthermore they allow for model-independent analyses. We will first describe the concept formally and then from a practical point of view with the help of an example.

Basically, the idea is the following. Consider a QFT with a certain fundamental scale M, which could be the mass of a heavy particle or some characteristic (euclidean) momentum transfer, and suppose we are only interested in predictions for energies $E \ll M$.[1] We can then construct an EFT, valid for this (low) energy range and to be UV completed by the full theory, in three steps:

1. Fix a cutoff $\Lambda < M$ and divide the fields ϕ of the QFT into low-energy Fourier modes ϕ_L and high-energy modes ϕ_H. One could for example use the absolute euclidean momentum $|k|$ after Wick rotation to distinguish these modes, such that

$$\phi_L(k) = \begin{cases} \phi(k), & |k| < \Lambda \\ 0, & |k| \geq \Lambda \end{cases}, \qquad \phi_H(k) = \begin{cases} 0, & |k| < \Lambda \\ \phi(k), & |k| \geq \Lambda \end{cases}, \qquad \phi = \phi_L + \phi_H .$$

$$(A.34)$$

   In the following we will leave the concrete method of dividing the fields into low- and high energy modes open, as it does not have to be specified for the upcoming discussion. S-matrix elements in our EFT, which we want to be the correct theory for low energies $E \ll \Lambda$, should now just depend on the fields ϕ_L. In the path integral formalism, they should be derived from vacuum correlation functions of the type

$$\langle 0|T\{\phi_L(x_1)\dots\phi_L(x_n)\}|0\rangle = \frac{(-i)^n}{Z[0]} \frac{\delta}{\delta J_L(x_1)} \cdots \frac{\delta}{\delta J_L(x_n)} Z[J_L]\bigg|_{J_L=0} . \qquad (A.35)$$

   We thus need source terms only for the low energy fields in the generating functional

$$Z[J_L] = \int \mathcal{D}\phi_L \mathcal{D}\phi_H \, e^{iS(\phi_L,\phi_H)+i\int d^dx J_L(x)\phi_L(x)} , \qquad (A.36)$$

   where $S(\phi_L, \phi_H) = \int d^dx \mathcal{L}(x)$ is the action of the QFT in d space-time dimensions.

2. Now we *integrate out* the high energy modes, which cannot be produced directly in experiments at energies $E < \Lambda$, by performing explicitly the corresponding path integral

$$e^{iS_\Lambda(\phi_L)} \equiv \int \mathcal{D}\phi_H \, e^{iS(\phi_L,\phi_H)} . \qquad (A.37)$$

---

[1]If a problem involves several scales, we can usually consider one at a time.

This leads to the new generating functional

$$Z[J_L] = \int \mathcal{D}\phi_L \, e^{iS_\Lambda(\phi_L) + i \int d^d x J_L(x)\phi_L(x)} \,, \tag{A.38}$$

where the high energy modes are removed as dynamical degrees of freedom from our theory. $S_\Lambda(\phi_L)$ is called the *Wilsonian effective action*. Note that, as modes with energies above Λ have been integrated out, this action is non local above this scale.

3. Finally we can expand this non-local action into a sum of local operators containing only low energy fields, by a so-called *Operator Product Expansion* (OPE), such that

$$S_\Lambda(\phi_L) = \int d^d x \, \mathcal{L}_{eff}^\Lambda(x) \,, \tag{A.39}$$

where the (local) effective Lagrangian

$$\mathcal{L}_{eff}^\Lambda(x) = \sum_{D,i} \frac{C_i^{(D)}}{M^{D-d}} \mathcal{Q}_i^{(D)}(\phi_L(x)) \tag{A.40}$$

consists of an infinite series of operators with mass dimensions D. The corresponding dimensionless coefficients $C_i^{(D)}$ have to appear with appropriate powers of M, the only scale present in the theory, in order to make the action dimensionless. The combined quantities $g_i^{(D)} \equiv C_i^{(D)} M^{d-D}$ are called *Wilson coefficients*. Note that for fixed D, just a finite number of operators can emerge ($i < \infty$), given that all fields have a strictly positive mass dimension. This is the case for the SM fields in $d \geq 3$. Furthermore, it is possible that for some values of D, the corresponding set of operators is empty. Since operators of mass dimension D are expected to scale like E^{D-d}, the expansion (A.40) features the order parameter $E/M \ll 1$.

Having obtained the local effective action, we have to address the question how to make use of a theory that contains apparently infinitely many parameters. The answer has already been sketched in Section 1.1.1 and is contained in the considerations before. As operators with increasing mass dimension are suppressed by bigger and bigger powers of M one can cut off the series at a certain level of precision (corresponding to a certain D), knowing that higher terms will at most give a contribution suppressed by E/M with respect to the contributions considered. In that sense, EFTs are automatically renormalizable and predictive (up to suppressed terms), since per definition only a finite number of parameters is present in the theory, after neglecting power suppressed corrections in (A.40) (assuming that $d \geq 3$). The argument of naturalness suggests that $C_i^{(D)} \sim \mathcal{O}(1)$, since besides M there is no other scale in the theory. Note that those coefficients now contain the information on the high energy modes which have been removed from the action. Thus, they will in principle depend on the scale Λ, providing a new paradigm of renormalization. From the dimensional analysis above, it is evident that operators with $D > 4$ will become less and less important at low energies. Thus they are named *irrelevant* (or non-renormalizable) operators, although they are very interesting, since they arise from integrating out heavy physics and tell us something about physics at the cutoff scale. Operators with $D < 4$ become more important at low energies and

are called *relevant* (or super-renormalizable), whereas those with $D = 4$ are called *marginal* (or renormalizable) operators. Relevant operators are problematic since they lead to a UV sensitivity, see Section 1.2.1.

In practice, it turns out that it is not always feasible to integrate out heavy modes formally as introduced before. It is often more practical to follow a procedure called *matching* which works in the following way. We know that (A.40) can only contain operators compatible with the symmetries of the theory. So we can turn the procedure around and write down all operators that are consistent with the given symmetries and depend just on the fields ϕ_L with so far *unknown* coefficients $C_i^{(D)}$, up to a certain mass dimension. This is now our EFT and we have already used such a procedure while constructing the SM Lagrangian in Section 1.1.1 (there with the complete field content observed so far). Now we know that, for energies below the cutoff, the amplitudes in the EFT, after integrating out certain modes, have to agree with those obtained in the full theory

$$A_m \equiv \langle f_m|\mathcal{L}_{\text{full}}|i_m\rangle \overset{!}{=} \sum_{D,i} \frac{C_i^{(D)}(\mu)}{M^{D-d}} \langle f_m|\mathcal{Q}_i^{(D)}(\mu)|i_m\rangle \,. \tag{A.41}$$

On the right hand side all insertions of operators contributing to a given matrix element up to a certain level of precision (mass dimension D) have to be considered. Note that in this equation, the full Lagrangian as well as the effective Lagrangian have been expanded up to first order in perturbation theory. However, it is possible to extend this matching to higher orders in the coupling constants. While not written out explicitly, at least the important higher order corrections in α_s are to be included implicitly on both sides. For processes mediated at leading order by $D = 6$ operators and for the case of the SM being the "full" theory we get at LO

$$A_m \equiv \langle f_m|\mathcal{L}_{\text{SM}}|i_m\rangle \overset{!}{=} \sum_i \frac{C_i^{(6)}(\mu)}{M^2} \langle f_m|\mathcal{Q}_i^{(6)}(\mu)|i_m\rangle + \text{higher } D \text{ operators.} \tag{A.42}$$

Here, we have used the scale μ instead of the hard cutoff Λ. This scale, being closer related to the more common approach of dimensional regularization, now takes the role of the cutoff. By calculating enough matrix elements A_m in the full theory, as well as in the EFT, and equating those with equal final and initial states, we can determine all Wilson coefficients present in the EFT, up to a sought level of precision. Note that in the following, we will use the term Wilson coefficient also for the dimensionless coefficients $C_i^{(D)}$. These coefficients have the important feature of being process independent, *i.e.*, they do not depend on the external states in (A.41). Thus they can be determined using a certain class of processes and then used for predictions in other processes via the EFT. If a process involves QCD at low scales, one usually has to resort to non-perturbative methods like lattice-QCD to calculate the corresponding matrix elements. However, note that the procedure of integrating out *high energy modes* via matching is independent of infrared (IR) physics. Thus, if one matches the theory at a scale where QCD is perturbative, it is possible to calculate the matrix elements in perturbation theory for the purpose of obtaining the corresponding Wilson coefficients.

We will now give an example of constructing an EFT from a "full" theory by studying Fermi's theory of weak interactions, valid for $E \ll m_W$. It is obtained by integrating out the heavy $W^\pm$-bosons of the SM, resulting in local effective $D = 6$ four-fermion vertices like the
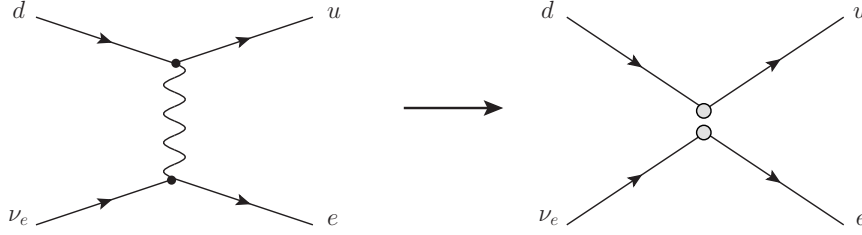
Figure A.1: Effective four-fermion interaction mediating β-decay, obtained by integrating out the heavy $W^{\pm}$ bosons of SM. The local four-quark vertex in the effective theory is denoted by the two gray circles in the second graph.

one mediating β-decay on the right hand side of Figure A.1. The lack of the exchange of the massive gauge bosons leads to a violation of unitarity within the Fermi theory above the scale of electroweak interactions $M_{\mathrm{EW}} \sim m_W$. However, as an effective theory with a cutoff at that scale, it is perfectly fine. The full SM gauge theory, including those fields, UV completes the Fermi theory at the electroweak scale. The diagram in the full theory (Figure A.1, left) leads to the amplitude

$$
\begin{aligned}
A &= -\frac{g^2}{8} V_{ud} \frac{1}{p^2 - m_W^2} (\bar{e}\,\nu_e)_{V-A} (\bar{u}\,d)_{V-A} \\
&= -\frac{g^2}{8m_W^2} V_{ud} \, (\bar{e}\,\nu_e)_{V-A} (\bar{u}\,d)_{V-A} + \mathcal{O}(\frac{p^2}{m_W^2}),
\end{aligned}
\tag{A.43}
$$

where $(\bar{e}\,\nu_e)_{V-A} \equiv \bar{e}\,(1 - \gamma^5)\nu_e$, *etc.*, and p^2 is the squared momentum transfer. Thus we immediately see that the corresponding effective Lagrangian, which gives the same result on the EFT side, has to take the form

$$
\mathcal{L}_{eff} = -\frac{G_F}{\sqrt{2}} V_{ud}\, C_1(\mu)(\bar{e}\,\nu_e)_{V-A}(\bar{u}\,d)_{V-A} + \text{higher } D \text{ operators,}
\tag{A.44}
$$

with $C_1 = 1$, working at tree level. Note that here we have pulled out a numerical factor times the weak coupling constant g^2, divided by the scale m_W^2, which are collected into the Fermi coupling constant of weak interactions $G_F/\sqrt{2} = g^2/(8m_W^2)$, as well as the CKM matrix element V_{ud}. This element is extracted exactly from the process discussed here. Furthermore we have not made explicit the color indices which are to be contracted between the adjacent quark fields. The higher D operators correspond to the higher powers of $\mathcal{O}(p^2/m_W^2)$ in the expansion (A.43). In the same way the Wilson coefficients for four-fermion operators involving other external states can be obtained. The result demonstrates that the reason for the apparent weakness of weak interactions compared to electromagnetism is not a substantially smaller coupling constant but merely the large mass of the $W^{\pm}$ bosons which suppresses the corresponding interaction at low energies, as mentioned in Section 1.1.2. Technically speaking, already the leading contribution corresponds to an irrelevant $D = 6$ operator. It was another

triumph of particle physics, that the $W^{\pm}$ bosons were discovered with a mass close to the scale of $(G_F/\sqrt{2})^{-1/2} \approx 110$ GeV that was indicated indirectly by low energy experiments. By expanding the $W^{\pm}$ propagator to zeroth order in the momentum transfer, we were able to match it on a $D = 6$ operator at the tree level. The same result can also be obtained by integrating out the $W^{\pm}$-bosons via the path integral formalism, as discussed before, since the corresponding integral is of Gaussian type. However, in more complicated situations, *e.g.* involving QCD, this is no more true. For QCD, another complication arises, because it is not perturbative at low energies, so in most cases one relies on the procedure of matching.

While for the operator studied above, QCD corrections do not alter the Wilson coefficient (they are the same in the full theory and in the EFT), this is not true for generic four-quark operators like $(\bar{s}^a c^a)_{V-A}(\bar{u}^b b^b)_{V-A}$ obtained by integrating out $W^{\pm}$ bosons and mediating for example the decay $b_L \to u_L \bar{c}_L s_L$. This partonic process is relevant for the hadronic decay $\bar{B}^0 \to \pi^+ D_s^-$ (similar processes will become relevant in Section 5.2.3). Here, QCD corrections generate a second operator $(\bar{s}^a c^b)_{V-A}(\bar{u}^b b^a)_{V-A}$ with interchanged color indices at $\mathcal{O}(\alpha_s)$. The corresponding Wilson coefficients at that order can be obtained by matching the matrix elements at the one-loop level, including gluon-corrections at $\mathcal{O}(\alpha_s)$ in the full theory as well as in the EFT. The coefficients now depend non-trivially on μ at that order, see [76, 87]. By lowering the cutoff of the EFT, one successively integrates out high energy modes (virtual gluon corrections). Their effects are absorbed into the Wilson coefficients which thus, as mentioned before, generically depend on the scale μ. Changing the scale corresponds to reshuffling contributions between the Wilson coefficient and the operator matrix element. We will now discuss the evolution of these coefficients with μ.

For this purpose we consider a generic operator basis of a given dimension D, *i.e.*, a complete set of operators of that mass dimension, allowed by the symmetries of a problem $\{\mathcal{Q}_i(\mu)\}$, $i = 1, \ldots, n$. Now we know that observables should not depend on the scale μ, separating high energy and low energy physics residing in the Wilson coefficients and matrix elements, respectively. Thus we conclude

$$\frac{d}{d\ln\mu} \sum_{i=1}^{n} C_i(\mu)\langle\mathcal{Q}_i(\mu)\rangle = 0. \tag{A.45}$$

As we started from a complete set of operators, it must be possible to expand the derivatives of the matrix elements on the left hand side of the equation above in terms of the operators contained in the basis

$$\frac{d}{d\ln\mu}\langle\mathcal{Q}_i(\mu)\rangle \equiv \sum_{j=1}^{n} -\gamma_{ij}(\mu)\langle\mathcal{Q}_j(\mu)\rangle. \tag{A.46}$$

The coefficients γ_{ij} measure the changes in the operator matrix elements under infinitesimal scale variations. They are called *anomalous dimensions* as they feature deviations from the naive scaling dimensions $(D - d)$ of the operators, due to quantum corrections. With this definition, we derive from (A.45) the famous *renormalization group equation*

$$\frac{d}{d\ln\mu} C_j(\mu) - \sum_{i=1}^{n} C_i(\mu)\gamma_{ij}(\mu) = 0, \tag{A.47}$$

where we have used that the $\mathcal{Q}_i$ are linearly independent from each other. In matrix notation

it reads

$$\frac{d}{d\ln\mu}\vec{C}(\mu) = \hat{\gamma}^T(\mu)\vec{C}(\mu). \tag{A.48}$$

Here, the anomalous dimension matrix (ADM) $\hat{\gamma}$ depends on the scale μ just through the running coupling $\alpha_s(\mu)$ in QCD. If it contains off-diagonal entries, the operators mix under renormalization. Before solving this equation we first switch variables from $\ln\mu$ to $\alpha_s(\mu)$ to arrive at

$$\frac{d}{d\alpha_s(\mu)}\vec{C}(\mu) = \beta^{-1}(\alpha_s(\mu))\,\hat{\gamma}^T(\alpha_s(\mu))\,\vec{C}(\mu), \tag{A.49}$$

where $\beta \equiv d\alpha_s(\mu)/d\ln\mu$ is the β-function of QCD. This renormalization group equation is now solved by

$$\vec{C}(\mu) = \hat{U}(\mu, m_W)\,\vec{C}(m_W)\,, \quad \hat{U}(\mu, m_W) \equiv T_\alpha \exp\left[\int_{\alpha_s(m_W)}^{\alpha_s(\mu)} d\alpha \frac{\hat{\gamma}^T(\alpha)}{\beta(\alpha)}\right], \tag{A.50}$$

which gives the evolution of the Wilson coefficients between one scale and another. Here, the initial condition has been chosen to be set by the values of the Wilson coefficients at the weak scale. The ADM can be calculated from the renormalization constants, appearing in the course of renormalizing the (effective) theory, see [76]. The corresponding exponential function in $U(\mu, m_W)$ is defined via its Taylor expansion. The ordering prescription T_α, which results in matrices $\hat{\gamma}^T(\alpha)$ with smaller α standing on the right of those with larger α is necessary since in general those matrices do not commute for different values of α. Clearly, if the evolution is to be performed between two scales with the threshold of a particle in between, which shall be integrated out, it can be performed in an iterative way. First in the EFT with this particle included and then, below the corresponding scale, in a theory without that particle as a dynamical degree of freedom. For example, an evolution could be performed first from a high mass scale $M > m_t$ down to m_t (where the top quark is integrated out) and then in a five-flavor theory further down to a lower scale μ by a two-step running

$$\vec{C}(\mu) = \hat{U}^{(5)}(\mu, m_t)\hat{U}^{(6)}(m_t, M)\vec{C}(M). \tag{A.51}$$

Let us stress a very important virtue of this process of integrating out high energy modes and absorbing their effects into running Wilson coefficients, described by a RG equation (A.50). If a problem involves several scales, one will generically encounter logarithms of ratios of these scales when calculating higher order corrections. For the time being, let us assume that we want to study a process involving a mass scale M at a second scale $\mu \ll M$, which could *e.g.* be set by the mass of another light particle present in the theory ($\mu \sim m$). If these scales are largely separated from each other, this can spoil the perturbative expansion in a small coupling constant since (for the case of QCD) now formally subleading corrections of the form

$$\frac{\alpha_s(\mu)}{4\pi}\ln\frac{M^2}{\mu^2}, \tag{A.52}$$

can easily become of $\mathcal{O}(1)$. Even if only weak couplings are involved, such logarithm terms can become important if one has for example $M = M_{\text{GUT}}$ and $\mu = m_W$. By integrating out physics related to the larger scale one can circumvent this problem. Matching the theory at

the large scale, one can avoid the presence of the problematic large logarithms involving the scale M (A.52). Remember that this matching procedure is independent of the low scale m. One can then evolve down the corresponding Wilson coefficients to the low scale by using the renormalization group evolution (A.50). This leads at leading order to a resummation of terms of the form $(\alpha_s(\mu)/(4\pi) \ln(M^2/\mu^2))^n$ (A.52), to all orders. These terms are now counted as $\mathcal{O}(1)$, avoiding the breakdown of the perturbative series. The matrix element in the EFT does not know about the large scale and thus, if one evaluates it (perturbatively) at the low scale it cannot feature large logarithms. The separation of high energy physics from low energy physics is a very important feature of EFTs. Processes involving low-energy QCD can thus be handled by integrating out the heavy physics and run down to a scale at which the resulting matrix element can be calculated on the lattice (or by means of other non-perturbative methods), while the high-energy contributions reside in the Wilson coefficients. This approach will be used in Section 5.2.3. Here we have assumed the existence of just two distinct scales. However, the application to problems with more scales is possible by an iterative procedure, as indicated before.

Finally, let us see how the resummation works schematically in the case of QCD corrections to the electroweak theory. For that purpose we expand the β-function as well as the ADM formally up to the LO in α_s, respectively

$$\beta(\alpha_s) = -2\alpha_s \left[\beta_0 \frac{\alpha_s}{4\pi} + \mathcal{O}(\alpha_s^2) \right] , \quad \hat{\gamma}(\alpha_s) = \hat{\gamma}_0 \frac{\alpha_s}{4\pi} + \mathcal{O}(\alpha_s^2). \tag{A.53}$$

Note that these quantities, as well as $\vec{C}(m_W)$ are free of large logarithms. The evolution matrix now takes the form

$$\hat{U}_0(\mu, m_W) = \left[\frac{\alpha_s(m_W)}{\alpha_s(\mu)} \right]^{\frac{\hat{\gamma}_0}{2\beta_0}} (1 + \mathcal{O}(\alpha_s)). \tag{A.54}$$

The matrix exponent can be evaluated via

$$\hat{U}_0(\mu, m_W) = \hat{V} \mathrm{diag} \left(\left[\frac{\alpha_s(m_W)}{\alpha_s(\mu)} \right]^{\frac{\vec{\gamma}_0}{2\beta_0}} \right) \hat{V}^{-1} \tag{A.55}$$

where $\hat{V}$ diagonalizes the ADM $\hat{\gamma}_0^T$

$$\hat{V}^{-1} \hat{\gamma}_0^T \hat{V} = \mathrm{diag}\left(\vec{\gamma}_0 \right). \tag{A.56}$$

Studying the case of a single operator for simplicity and expanding

$$U_0(\mu, m_W) = \left(1 + \beta_0 \frac{\alpha_s}{4\pi} \ln \frac{m_W^2}{\mu^2} + \cdots \right)^{-\frac{\gamma_0}{2\beta_0}} = 1 - \frac{\gamma_0}{2} \frac{\alpha_s}{4\pi} \ln \frac{m_W^2}{\mu^2} + \mathcal{O}\left(\alpha_s^2 \ln^2 \frac{m_W^2}{\mu^2} \right) + \cdots , \tag{A.57}$$

we see that all the logarithms of the form $(\alpha_s/(4\pi) \ln(M^2/\mu^2))^n$ (A.52) are present in $U_0(\mu, m_W)$, which can be calculated reliably in perturbation theory.

It is possible to generalize the concepts introduced here to more complicated processes and to include *e.g.* (loop-mediated) FCNCs relevant for meson mixing and decay. These processes

are interesting, because they are suppressed within the SM and thus very sensitive to BSM contributions. Here one integrates out internal states in *e.g.* box and penguin diagrams (for the case of the SM) and ends up with an effective weak Lagrangian mediating such processes. For details, we refer the reader to the literature [76, 87, 371] and to Section 5.2.3 where such effective Lagrangians are used to calculate amplitudes related to B-meson mixing and decay.

Let us stress again that EFTs are also well suited to match experiments with theory, without assuming a certain model. By writing down an OPE containing all fields up to a certain energy, consistent with the given symmetries, one can try to measure the various Wilson coefficients. Thus it is also possible to use the concept of EFTs without being able to integrate out certain modes explicitly (without knowing the underlying renormalizable model) and to learn something about nature. With the help of an OPE for the SM field content, one can try to collect information about its UV completion. Just like the $D = 6$ operators of Fermi theory arise from integrating out the heavy $W^{\pm}$ bosons within the SM, the SM probably has a UV completion that replaces it above a certain scale Λ_{UV}. This can be accounted for, by not truncating at the level of $D = 4$, see Section 1.1.6. The presence of this BSM theory leaves its imprints in higher dimensional operators containing the SM fields. By measuring the Wilson coefficients of these operators one can quantify possible deviations from the SM in terms of Lagrangian parameters. Below the threshold of NP, the SM, including $D > 4$ operators is an appropriate theory to describe nature. If one wants to be more specific and has a certain model in mind, one can calculate the Wilson coefficients in this model explicitly and compare them to the experimental results. By integrating out heavy fields of the model step by step one can resum large logarithms, arising when a theory contains several scales. These techniques will be used at several points in the phenomenology chapter (Chapter 5) of this thesis.

Appendix B

Appendices Chapter 5

B.1 Higgs-Boson Phase-Space Factors for A_{FB}^t

In this appendix we present the explicit analytical form of the phase-space factors, appearing in the Higgs-boson contribution to the charge-symmetric and -asymmetric part of the $t\bar{t}$ cross section, see (5.37) and (5.38). They read

$$
\begin{aligned}
f_S(z) &= -\frac{\beta\rho}{72}\left[1 + \frac{\rho\,(1-z)}{2} + \frac{\rho\left(4 + \rho\,(1-z)^2\right)}{8\beta}\,\ln\left(\frac{2\,(1+\beta) - \rho\,(1-z)}{2\,(1-\beta) - \rho\,(1-z)}\right)\right], \\
f_A(z) &= \frac{\rho}{144}\left[1 - \rho + \frac{\rho\left(4 + \rho\,(1-z)^2\right)}{4}\,\ln\left(\frac{\rho\left(4z + \rho\,(1-z)^2\right)}{(2 - \rho\,(1-z))^2}\right)\right],
\end{aligned}
\tag{B.1}
$$

where $z = m_h^2/m_t^2$, $\beta = \sqrt{1-\rho}$, and $\rho = 4m_t^2/\hat{s}$.

B.2 Tensor Integrals and Wilson Coefficients for A_{FB}^t in the ZMA

The non-factorizable products of overlaps $\widetilde{\boldsymbol{\Delta}}_A \otimes \widetilde{\boldsymbol{\Delta}}_B$ are defined as [213]

$$
\begin{aligned}
\left(\widetilde{\Delta}_F\right)_{mn} \otimes \left(\widetilde{\Delta}_{f'}\right)_{m'n'} &= \frac{2\pi^2}{L^2\epsilon^2}\int_\epsilon^1 dt \int_\epsilon^1 dt'\, t_<^2 \\
&\quad \times \left[a_m^{F\dagger}\,\boldsymbol{C}_m^Q(\phi)\,\boldsymbol{C}_n^Q(\phi)\,a_n^F + a_m^{f\dagger}\,\boldsymbol{S}_m^f(\phi)\,\boldsymbol{S}_n^f(\phi)\,a_n^f\right] \\
&\quad \times \left[a_{m'}^{f'\dagger}\,\boldsymbol{C}_{m'}^{f'}(\phi')\,\boldsymbol{C}_{n'}^{f'}(\phi')\,a_{n'}^{f'} + a_{m'}^{F'\dagger}\,\boldsymbol{S}_{m'}^Q(\phi')\,\boldsymbol{S}_{n'}^Q(\phi')\,a_{n'}^{F'}\right],
\end{aligned}
\tag{B.2}
$$

etc., where $F = U, D$ and $f = u, d$.

For the case of the up quark ($q = u$), the ZMA results for the Wilson coefficients appearing in (5.39) read

$$
C_{u\bar{u},\parallel}^{(V,8)} = -\frac{4\pi\alpha_s}{M_{\text{KK}}^2}\left[\frac{1}{2L} - \frac{F^2(c_{t_R})\,(2c_{t_R} + 5)}{4(2c_{t_R} + 3)^2} - \frac{F^2(c_{t_L})\,(2c_{t_L} + 5)}{4(2c_{t_L} + 3)^2}\right.
$$

$$- \frac{F^2(c_{u_R})}{4\,|(M_u)_{11}|^2} \sum_{i=1,2,3} \frac{(2c_{u_i}+5)\,|(M_u)_{1i}|^2}{(2c_{u_i}+3)^2} - \frac{F^2(c_{u_L})}{4\,|(M_u)_{11}|^2} \sum_{i=1,2,3} \frac{(2c_{Q_i}+5)\,|(M_u)_{i1}|^2}{(2c_{Q_i}+3)^2}$$

$$+ \frac{L}{2} \frac{F^2(c_{t_R})F^2(c_{u_R})}{(2c_{t_R}+3)\,|(M_u)_{11}|^2} \sum_{i=1,2,3} \frac{(c_{u_i}+c_{t_R}+3)\,|(M_u)_{1i}|^2}{(2c_{u_i}+3)(c_{u_i}+c_{t_R}+2)}$$

$$+ \frac{L}{2} \frac{F^2(c_{t_L})F^2(c_{u_L})}{(2c_{t_L}+3)\,|(M_u)_{11}|^2} \sum_{i=1,2,3} \frac{(c_{Q_i}+c_{t_L}+3)\,|(M_u)_{i1}|^2}{(2c_{Q_i}+3)(c_{Q_i}+c_{t_L}+2)} \Bigg] ,$$

$$C_{u\bar{u},\perp}^{(V,8)} = -\frac{4\pi\alpha_s}{M_{\mathrm{KK}}^2} \Bigg[\frac{1}{2L} - \frac{F^2(c_{t_R})\,(2c_{t_R}+5)}{4(2c_{t_R}+3)^2} - \frac{F^2(c_{t_L})\,(2c_{t_L}+5)}{4(2c_{t_L}+3)^2}$$

$$- \frac{F^2(c_{u_R})}{4\,|(M_u)_{11}|^2} \sum_{i=1,2,3} \frac{(2c_{u_i}+5)\,|(M_u)_{1i}|^2}{(2c_{u_i}+3)^2} - \frac{F^2(c_{u_L})}{4\,|(M_u)_{11}|^2} \sum_{i=1,2,3} \frac{(2c_{Q_i}+5)\,|(M_u)_{i1}|^2}{(2c_{Q_i}+3)^2}$$

$$+ \frac{L}{2} \frac{F^2(c_{t_L})F^2(c_{u_R})}{(2c_{t_L}+3)\,|(M_u)_{11}|^2} \sum_{i=1,2,3} \frac{(c_{u_i}+c_{t_L}+3)\,|(M_u)_{1i}|^2}{(2c_{u_i}+3)(c_{u_i}+c_{t_L}+2)}$$

$$+ \frac{L}{2} \frac{F^2(c_{t_R})F^2(c_{u_L})}{(2c_{t_R}+3)\,|(M_u)_{11}|^2} \sum_{i=1,2,3} \frac{(c_{Q_i}+c_{t_R}+3)\,|(M_u)_{i1}|^2}{(2c_{Q_i}+3)(c_{Q_i}+c_{t_R}+2)} \Bigg] . \tag{B.3}$$

Similar relations with obvious replacements hold in the case of the remaining light quarks $q = d, s, c$. For the t-channel Wilson coefficients in the vector channel, we get

$$C_{t\bar{u},\parallel}^{(V,8)} = -\frac{\pi\alpha_s}{M_{\mathrm{KK}}^2} L \left[\frac{F^2(c_{t_R})F^2(c_{u_R})\,|(M_u)_{13}|^2}{(2c_{t_R}+3)(c_{t_R}+1)\,|(M_u)_{11}|^2} + \frac{F^2(c_{t_L})F^2(c_{u_L})\,|(M_u)_{31}|^2}{(2c_{t_L}+3)(c_{t_L}+1)\,|(M_u)_{11}|^2} \right] ,$$

$$C_{t\bar{u},\parallel}^{(V,1)} = -\frac{\pi\alpha_e}{M_{\mathrm{KK}}^2} \frac{L}{s_w^2 c_w^2} \left[(T_3^u - Q_u s_w^2)^2 \frac{F^2(c_{t_L})F^2(c_{u_L})\,|(M_u)_{31}|^2}{(2c_{t_L}+3)(c_{t_L}+1)\,|(M_u)_{11}|^2} \right.$$

$$\left. + \left(s_w^2 Q_u \right)^2 \frac{F^2(c_{t_R})F^2(c_{u_R})\,|(M_u)_{13}|^2}{(2c_{t_R}+3)(c_{t_R}+1)\,|(M_u)_{11}|^2} \right] \tag{B.4}$$

$$- \frac{\pi\alpha_e Q_u^2}{M_{\mathrm{KK}}^2} L \left[\frac{F^2(c_{t_R})F^2(c_{u_R})\,|(M_u)_{13}|^2}{(2c_{t_R}+3)(c_{t_R}+1)\,|(M_u)_{11}|^2} + \frac{F^2(c_{t_L})F^2(c_{u_L})\,|(M_u)_{31}|^2}{(2c_{t_L}+3)(c_{t_L}+1)\,|(M_u)_{11}|^2} \right] .$$

The result for the Higgs-boson contribution to the t channel, which is of $\mathcal{O}(v^4/M_{\mathrm{KK}}^4)$, is given by

$$\tilde{C}_{t\bar{u}}^S = |(g_h^u)_{13}|^2 + |(g_h^u)_{31}|^2 , \tag{B.5}$$

where the ZMA expressions for the flavor off-diagonal Higgs couplings are given in (3.279).

B.3 RG Evolution of the Wilson Coefficients for A_{FB}^t

In this appendix we present analytic formulae relating the Wilson coefficients evaluated at the top-quark mass scale m_t to their initial conditions calculated at $M_{\text{KK}} \gg m_t$, see Appendix A.4. Since in the RS model the t-channel Wilson coefficients $\tilde{C}_{t\bar{u}}^V$ and $\tilde{C}_{t\bar{u}}^S$ are numerically irrelevant, we will not consider their running in the following. The RG evolution is performed at leading-logarithmic accuracy (*i.e.*, at one-loop order), neglecting tiny effects that arise from the mixing with QCD penguin operators. For the s-channel Wilson coefficients entering (5.48) and (5.49), one obtains for $P = V, A$ (*c.f.* (A.54)) [3]

$$\tilde{C}_{q\bar{q}}^P(m_t) = \left(\frac{2}{3\eta^{4/7}} + \frac{\eta^{2/7}}{3} \right) \tilde{C}_{q\bar{q}}^P(M_{\text{KK}}), \tag{B.6}$$

where $\eta \equiv \alpha_s(M_{\text{KK}})/\alpha_s(m_t)$ is the ratio of strong coupling constants evaluated at the relevant scales.

In order to judge the impact of RG effects, we evaluate (B.6) explicitly, using $\alpha_s(M_Z) = 0.139$, $M_{\text{KK}} = 1\,\text{TeV}$, and $m_t = 173.1\,\text{GeV}$, which leads to $\eta = 0.803$ at one-loop order. We obtain

$$\tilde{C}_{q\bar{q}}^P(m_t) = 1.07\,\tilde{C}_{q\bar{q}}^P(M_{\text{KK}}). \tag{B.7}$$

Thus, the RG evolution increases the Wilson coefficients $\tilde{C}_{q\bar{q}}^P$ by about 7% with respect to the values quoted in Table 5.1 which means that operator mixing represents only a numerically subdominant effect.

B.4 Wilson Coefficients of Penguin Operators

The Wilson coefficients of the penguin operators in (5.101), evaluated at the matching scale $\mu = M_{\text{KK}}$, read at $\mathcal{O}(v^2/M_{\text{KK}}^2)$ [213]

$$\begin{aligned}
C_3^{\text{RS}}(M_{\text{KK}}) &= \frac{\pi\alpha_s}{M_{\text{KK}}^2}\,\frac{(\boldsymbol{\Delta}_D')_{23}}{2N_c} - \frac{\pi\alpha}{6s_w^2 c_w^2\,M_{\text{KK}}^2}(\boldsymbol{\Sigma}_D)_{23}\,, \\
C_4^{\text{RS}}(M_{\text{KK}}) &= C_6^{\text{RS}}(M_{\text{KK}}) = -\frac{\pi\alpha_s}{2M_{\text{KK}}^2}\,(\boldsymbol{\Delta}_D')_{23}\,, \\
C_5^{\text{RS}}(M_{\text{KK}}) &= \frac{\pi\alpha_s}{M_{\text{KK}}^2}\,\frac{(\boldsymbol{\Delta}_D')_{23}}{2N_c}\,, \\
C_7^{\text{RS}}(M_{\text{KK}}) &= \frac{2\pi\alpha}{9M_{\text{KK}}^2}\,(\boldsymbol{\Delta}_D')_{23} - \frac{2\pi\alpha}{3c_w^2\,M_{\text{KK}}^2}(\boldsymbol{\Sigma}_D)_{23}\,, \\
C_8^{\text{RS}}(M_{\text{KK}}) &= C_{10}^{\text{RS}}(M_{\text{KK}}) = 0\,, \\
C_9^{\text{RS}}(M_{\text{KK}}) &= \frac{2\pi\alpha}{9M_{\text{KK}}^2}\,(\boldsymbol{\Delta}_D')_{23} + \frac{2\pi\alpha}{3s_w^2\,M_{\text{KK}}^2}(\boldsymbol{\Sigma}_D)_{23}\,,
\end{aligned} \tag{B.8}$$

where

$$\boldsymbol{\Sigma}_D \equiv \omega_Z^{d_L} L \left(\frac{1}{2} - \frac{s_w^2}{3} \right) \boldsymbol{\Delta}_D + \frac{M_{\text{KK}}^2}{m_Z^2}\,\boldsymbol{\delta}_D\,. \tag{B.9}$$

These results are valid for the minimal RS variant for $\omega_Z^{d_L} = 1$, whereas in the custodial RS model with P_{LR}-symmetry, one finds $\omega_Z^{d_L} = 0$, see (3.230) and below. Exact analytic expressions for $\boldsymbol{\Delta}_D$, $\boldsymbol{\Delta}'_D$, and $\boldsymbol{\delta}_D$, as well as the corresponding ZMA results are given in sections 3.2.4 and 3.4.3. The evolution of the penguin coefficients down to the mass of the bottom quark is treated in Appendix B.7.

B.5   Wilson Coefficients of Charged-Current Operators

In this appendix we derive ZMA expressions for the Wilson coefficients of the charged current operators in (5.101). The starting point is the (h.c. part of the) effective Hamiltonian as given in (3.269). Performing the overlap integrals with the corresponding fermion profiles in the ZMA, we arrive for the minimal RS model at

$$
\begin{aligned}
(\mathbf{V}_L^\dagger)_{mn} \otimes (\mathbf{V}_L)_{m'n'} ={}& (\boldsymbol{U}_d^\dagger \boldsymbol{U}_u)_{mn}(\boldsymbol{U}_u^\dagger \boldsymbol{U}_d)_{m'n'} \left[1 + \mathcal{O}\left(\frac{v^2}{M_{\mathrm{KK}}^2}\right)\right] \\
&+ \frac{m_W^2}{2M_{\mathrm{KK}}^2}\, L\, (\boldsymbol{U}_d^\dagger)_{mi}(\boldsymbol{U}_u)_{in}(\widetilde{\boldsymbol{\Delta}}_{QQ})_{ij}(\boldsymbol{U}_u^\dagger)_{m'j}(\boldsymbol{U}_d)_{jn'}\,,
\end{aligned}
\tag{B.10}
$$

with the non-factorizable correction [157]

$$
(\widetilde{\boldsymbol{\Delta}}_{QQ})_{ij} = \frac{F^2(c_{Q_i})}{3 + 2c_{Q_i}} \frac{3 + c_{Q_i} + c_{Q_j}}{2 + c_{Q_i} + c_{Q_j}} \frac{F^2(c_{Q_j})}{3 + 2c_{Q_j}}\,.
\tag{B.11}
$$

For B_s^0-meson decays, we need the element ($m = 2, n = 2, m' = 2, n' = 3$). Here, the leading term in (B.10), together with factorizable corrections of the form $v^2/M_{\mathrm{KK}}^2\,(...)_{mn} \cdot (...)_{m'n'}$, should be identified with λ_c^{bs}. In the custodial RS model, one would find additional factorizable terms, which also will be absorbed into CKM-matrix elements. Thus, we find at LO in v^2/M_{KK}^2

$$
C_2^{LL}(M_{\mathrm{KK}}) = \frac{m_W^2}{2M_{\mathrm{KK}}^2}\, L \frac{(\boldsymbol{U}_d^\dagger)_{2i}(\boldsymbol{U}_u)_{i2}}{(\boldsymbol{U}_d^\dagger \boldsymbol{U}_u)_{22}}\, (\widetilde{\boldsymbol{\Delta}}_{QQ})_{ij} \frac{(\boldsymbol{U}_u^\dagger)_{2j}(\boldsymbol{U}_d)_{j3}}{(\boldsymbol{U}_u^\dagger \boldsymbol{U}_d)_{23}}\,,
\tag{B.12}
$$

independent of the chosen scenario, and $C_1^{LL}(M_{\mathrm{KK}}) = 0$. For the mixed-chirality currents we arrive at

$$
\begin{aligned}
(\mathbf{V}_L^\dagger)_{mn} \otimes (\mathbf{V}_R)_{m'n'} ={}& (\boldsymbol{U}_d^\dagger \boldsymbol{U}_u)_{mn}(\boldsymbol{x}_u \boldsymbol{U}_u^\dagger)_{m'j}\, f(c_{Q_j})\, (\boldsymbol{U}_d\, \boldsymbol{x}_d)_{jn'}\,, \\
(\mathbf{V}_R^\dagger)_{mn} \otimes (\mathbf{V}_L)_{m'n'} ={}& (\boldsymbol{x}_d \boldsymbol{U}_d^\dagger)_{mi}\, f(c_{Q_i})\, (\boldsymbol{U}_u \boldsymbol{x}_u)_{in}(\boldsymbol{U}_u^\dagger \boldsymbol{U}_d)_{m'n'}\,,
\end{aligned}
\tag{B.13}
$$

where

$$
f(c) = \frac{1}{F^2(c)(1 - 2c)} - \frac{1}{1 - 2c} + \frac{F^2(c)}{(1 + 2c)^2}\left(\frac{1}{1 - 2c} - 1 + \frac{1}{3 + 2c}\right)\,.
\tag{B.14}
$$

Modifications due to the custodial model are of higher order. We find $C_1^{LR/RL}(M_{\mathrm{KK}}) = 0$ and

$$
\begin{aligned}
C_2^{LR}(M_{\mathrm{KK}}) &= \frac{(\boldsymbol{x}_u \boldsymbol{U}_u^\dagger)_{2i} \, f(c_{Q_i}) \, (\boldsymbol{U}_d \, \boldsymbol{x}_d)_{i3}}{(\boldsymbol{U}_u^\dagger \boldsymbol{U}_d)_{23}} \,, \\
C_2^{RL}(M_{\mathrm{KK}}) &= \frac{(\boldsymbol{x}_d \boldsymbol{U}_d^\dagger)_{2i} \, f(c_{Q_i}) \, (\boldsymbol{U}_u \, \boldsymbol{x}_u)_{i2}}{(\boldsymbol{U}_d^\dagger \boldsymbol{U}_u)_{22}} \,.
\end{aligned}
\tag{B.15}
$$

The running down to m_b is again treated in Appendix B.7.

B.6 Wilson Coefficients of $\Delta B = 2$ Operators

The $\Delta B = 2$ operators that contribute to the $\bar{B}_s^0$–B_s^0 mixing amplitude at tree-level are $\mathcal{Q}_1$, $\widetilde{\mathcal{Q}}_1$, $\mathcal{Q}_4$, and $\mathcal{Q}_5$. The operators $\mathcal{Q}_1$ and $\widetilde{\mathcal{Q}}_1$ do not mix under renormalization. The anomalous dimension for both is given by $\gamma_0^{\mathrm{VLL}} = 6 - 6/N_c$ [400]. The operators $\mathcal{Q}_{4,5}$ mix and the corresponding ADM can be taken from [400, 401]. The running of the coefficients is described by the general formula (B.18). Defining $\widetilde{\boldsymbol{\Delta}}_{dd}$ and $\widetilde{\boldsymbol{\Delta}}_{Qd}$ in analogy to (B.11), the RS coefficients in the ZMA, evaluated at the KK scale, are given by [213]

$$
C_1^{\mathrm{RS}}(M_{\mathrm{KK}}) = \frac{\pi L}{M_{\mathrm{KK}}^2} (\boldsymbol{U}_d^\dagger)_{2i}(\boldsymbol{U}_d)_{i3}(\widetilde{\boldsymbol{\Delta}}_{QQ})_{ij}(\boldsymbol{U}_d^\dagger)_{2j}(\boldsymbol{U}_d)_{j3}
\tag{B.16}
$$
$$
\times \left[\frac{\alpha_s}{2}\left(1 - \frac{1}{N_c}\right) + Q_d^2\,\alpha + (\omega_Z^{d_L d_L})\frac{(T_3^d - s_w^2\,Q_d)^2\,\alpha}{s_w^2 c_w^2} \right],
$$

$$
\widetilde{C}_1^{\mathrm{RS}}(M_{\mathrm{KK}}) = \frac{\pi L}{M_{\mathrm{KK}}^2} (\boldsymbol{W}_d^\dagger)_{2i}(\boldsymbol{W}_d)_{i3}(\widetilde{\boldsymbol{\Delta}}_{dd})_{ij}(\boldsymbol{W}_d^\dagger)_{2j}(\boldsymbol{W}_d)_{j3}
$$
$$
\times \left[\frac{\alpha_s}{2}\left(1 - \frac{1}{N_c}\right) + Q_d^2\,\alpha + (\omega_Z^{d_R d_R})\frac{(s_w^2\,Q_d)^2\,\alpha}{s_w^2 c_w^2} \right],
$$

$$
C_4^{\mathrm{RS}}(M_{\mathrm{KK}}) = -2\alpha_s \frac{\pi L}{M_{\mathrm{KK}}^2} (\boldsymbol{U}_d^\dagger)_{2i}(\boldsymbol{U}_d)_{i3}(\widetilde{\boldsymbol{\Delta}}_{Qd})_{ij}(\boldsymbol{W}_d^\dagger)_{2j}(\boldsymbol{W}_d)_{j3}
$$

$$
C_5^{\mathrm{RS}}(M_{\mathrm{KK}}) = \frac{\pi L}{M_{\mathrm{KK}}^2} (\boldsymbol{U}_d^\dagger)_{2i}(\boldsymbol{U}_d)_{i3}(\widetilde{\boldsymbol{\Delta}}_{Qd})_{ij}(\boldsymbol{W}_d^\dagger)_{2j}(\boldsymbol{W}_d)_{j3}
$$
$$
\times \left[\frac{2\alpha_s}{N_c} - 4Q_d^2\,\alpha + \omega_Z^{d_L d_R}\frac{4s_w^2\,Q_d\,(T_3^d - s_w^2\,Q_d)\,\alpha}{s_w^2 c_w^2} \right].
$$

Here we have introduced the correction factors $\omega_Z^{qq'}$, which are equal to 1 in the minimal RS model, and given by

$$
\omega_Z^{qq'} = 1 + \frac{1}{c_w^2 - s_w^2}\left(\frac{s_w^2(T_L^{3q} - Q^q) - c_w^2 T_R^{3q}}{T_L^{3q} - s_w^2 Q^q} \right)\left(\frac{s_w^2(T_L^{3q'} - Q^{q'}) - c_w^2 T_R^{3q'}}{T_L^{3q'} - s_w^2 Q^{q'}} \right)
\tag{B.17}
$$

in the custodial RS variant with P_{LR} symmetry. Numerically we find $\omega_Z^{d_L d_L} \approx 2.9$, $\omega_Z^{d_R d_R} \approx 150.9$, and $\omega_Z^{d_L d_R} \approx -15.7$. The quantum numbers $T_{L,R}^{3q}$ can be found in Section 3.4.3.

B.7   Running of the $\Delta B = 1$ Coefficients

The evolution of the RS Wilson coefficients of the $\Delta B = 1$ operators can again be performed along the lines as described in Appendix A.4. The ADM $\hat{\gamma}_0$ for the operator basis $\vec{Q} = (Q_1, Q_2, Q_{3..10})$, which is a function of N_c, n_f, n_u, and n_d (number of colors, flavors, up- and down-type quarks), can be found in [402, 403].

The evolution from M_{KK} to m_b is given by (*c.f.* (A.50) ff.)

$$\vec{C}(m_b) = \hat{U}^{(5)}(m_b, m_t)\,\hat{U}^{(6)}(m_t, M_{\mathrm{KK}})\,\vec{C}(M_{\mathrm{KK}})\,, \tag{B.18}$$

where, at LO in α_s,

$$\hat{U}^{(n_f)}(\mu_1, \mu_2) = \hat{V}\mathrm{diag}\left(\left[\frac{\alpha_s^{(n_f)}(\mu_2)}{\alpha_s^{(n_f)}(\mu_1)}\right]^{\frac{\vec{\gamma}_0}{2\beta_0(n_f)}}\right)\hat{V}^{-1}\,, \tag{B.19}$$

and $\hat{V}$ diagonalizes $\hat{\gamma}_0^T$ via $\mathrm{diag}(\vec{\gamma}_0) = \hat{V}^{-1}\hat{\gamma}_0^T\hat{V}$. The QCD β-function is given by $\beta_0(n_f) = (11N_c - 2\,n_f)/3$. The operators Q_1 and Q_2 will mix independently of n_f, n_u, and n_d. The evolution in the penguin sector receives a small admixture from charged current operators, however, the operators $Q_1^{LR/RL}$ and $Q_2^{LR/RL}$ do not mix into the penguin sector. Their internal mixing is identical to that of the LL operators. There is no mixing between charged currents of different chiralities. For the running of the LR/RL coefficients, one consequently uses

$$\gamma_0 = \begin{pmatrix} -\frac{6}{N_c} & 6 \\ 6 & -\frac{6}{N_c} \end{pmatrix} \tag{B.20}$$

in (B.18), which also describes the internal LL mixing.

B.8   Form Factors for Higgs-Boson Production and Decay

The form factors $A_{q,W}^h(\tau)$ and $A_{q,W}^h(\tau, \lambda)$ which describe the effects of quark and $W^\pm$-boson loops in the production and the decay of the Higgs boson are given by [39]

$$A_q^h(\tau) = \frac{3\tau}{2}\left[1 + (1 - \tau)\,f(\tau)\right]\,,$$

$$A_W^h(\tau) = -\frac{3}{4}\left[2 + 3\tau + 3\tau\,(2 - \tau)\,f(\tau)\right]\,,$$

$$A_q^h(\tau, \lambda) = -I(\tau, \lambda) + J(\tau, \lambda)\,,$$

$$A_W^h(\tau, \lambda) = c_w \left\{ 4 \left(3 - \frac{s_w^2}{c_w^2} \right) I(\tau, \lambda) + \left[\left(1 + \frac{2}{\tau} \right) \frac{s_w^2}{c_w^2} - \left(5 + \frac{2}{\tau} \right) \right] J(\tau, \lambda) \right\} . \qquad \text{(B.21)}$$

The functions $I(\tau, \lambda)$ and $J(\tau, \lambda)$ take the form

$$I(\tau, \lambda) = -\frac{\tau \lambda}{2(\tau - \lambda)} \left[f(\tau) - f(\lambda) \right] ,$$

$$J(\tau, \lambda) = \frac{\tau \lambda}{2 (\tau - \lambda)} + \frac{\tau^2 \lambda^2}{2 (\tau - \lambda)^2} \left[f(\tau) - f(\lambda) \right] + \frac{\tau^2 \lambda}{(\tau - \lambda)^2} \left[g(\tau) - g(\lambda) \right] , \qquad \text{(B.22)}$$

where the functions $f(\tau)$ and $g(\tau)$ read

$$f(\tau) = \begin{cases} -\dfrac{1}{4} \left[\ln \left(\dfrac{1 + \sqrt{1 - \tau}}{1 - \sqrt{1 - \tau}} \right) - i\pi \right]^2 , & \tau \le 1 , \\[2em] \arcsin^2 \left(\dfrac{1}{\sqrt{\tau}} \right) , & \tau > 1 , \end{cases} \qquad \text{(B.23)}$$

$$g(\tau) = \begin{cases} \sqrt{\tau - 1} \arcsin \left(\dfrac{1}{\sqrt{\tau}} \right) , & \tau \le 1 , \\[2em] \dfrac{1}{2} \sqrt{1 - \tau} \left[\ln \left(\dfrac{1 + \sqrt{1 - \tau}}{1 - \sqrt{1 - \tau}} \right) - i\pi \right] , & \tau > 1 . \end{cases} \qquad \text{(B.24)}$$

Appendix C

RS Parameter Points

In this appendix, we specify a set of three RS parameter points, *i.e.*, the bulk mass parameters of the quark fields and the Yukawa matrices, that are used in our numerical analysis. All the parameter sets given below have been obtained by random choice, as described at the beginning of Chapter 5.

Our first parameter point is specified by the following bulk mass parameters and Yukawa matrices[1]

$$
\begin{aligned}
c_{Q_1} &= -0.611\,, & c_{Q_2} &= -0.580\,, & c_{Q_3} &= -0.407\,, \\
c_{u_1} &= -0.688\,, & c_{u_2} &= -0.550\,, & c_{u_3} &= +0.091\,, \\
c_{d_1} &= -0.665\,, & c_{d_2} &= -0.627\,, & c_{d_3} &= -0.577\,,
\end{aligned}
\tag{C.1}
$$

$$
\begin{aligned}
\boldsymbol{Y}_u &= \begin{pmatrix} -1.303 - 0.364\,i & -1.215 + 0.089\,i & -1.121 - 1.679\,i \\ 1.857 + 1.199\,i & 2.038 + 1.105\,i & -0.484 - 0.193\,i \\ -1.052 + 0.546\,i & -2.833 + 0.191\,i & -1.287 - 1.141\,i \end{pmatrix}\,, \\
\boldsymbol{Y}_d &= \begin{pmatrix} -0.661 - 1.118\,i & -0.075 - 0.656\,i & 0.141 - 0.465\,i \\ -2.070 + 1.364\,i & -2.518 + 1.435\,i & 0.717 - 0.165\,i \\ 0.306 + 2.830\,i & 0.034 - 0.350\,i & -0.951 - 0.829\,i \end{pmatrix}\,.
\end{aligned}
\tag{C.2}
$$

Our second parameter point features

$$
\begin{aligned}
c_{Q_1} &= -0.646\,, & c_{Q_2} &= -0.573\,, & c_{Q_3} &= -0.449\,, \\
c_{u_1} &= -0.658\,, & c_{u_2} &= -0.513\,, & c_{u_3} &= +0.480\,, \\
c_{d_1} &= -0.645\,, & c_{d_2} &= -0.626\,, & c_{d_3} &= -0.578\,,
\end{aligned}
\tag{C.3}
$$

$$
\begin{aligned}
\boldsymbol{Y}_u &= \begin{pmatrix} 0.637 - 1.800\,i & 1.518 - 2.209\,i & 0.904 + 0.146\,i \\ 0.219 - 0.207\,i & -0.333 - 0.942\,i & 0.597 + 0.020\,i \\ 1.829 + 1.538\,i & -0.018 + 1.772\,i & -1.258 + 1.265\,i \end{pmatrix}\,, \\
\boldsymbol{Y}_d &= \begin{pmatrix} -2.835 - 0.946\,i & -0.404 + 0.746\,i & -1.135 + 0.060\,i \\ 0.724 - 0.350\,i & -2.214 - 0.555\,i & 0.610 - 0.051\,i \\ 0.701 - 0.101\,i & -0.154 + 0.104\,i & 1.514 + 0.919\,i \end{pmatrix}\,.
\end{aligned}
\tag{C.4}
$$

---

[1]The results are given to at least three significant digits.

Finally, the third parameter point reads

$$c_{Q_1} = -0.624 \,, \qquad c_{Q_2} = -0.563 \,, \qquad c_{Q_3} = -0.468 \,,$$
$$c_{u_1} = -0.712 \,, \qquad c_{u_2} = -0.560 \,, \qquad c_{u_3} = +0.899 \,, \tag{C.5}$$
$$c_{d_1} = -0.659 \,, \qquad c_{d_2} = -0.642 \,, \qquad c_{d_3} = -0.571 \,,$$

$$\boldsymbol{Y}_u = \begin{pmatrix} -0.541 + 1.517\,i & -1.083 + 1.857\,i & 1.718 - 2.057\,i \\ 0.359 - 1.713\,i & -2.208 + 1.404\,i & -1.160 + 0.886\,i \\ -1.172 - 0.543\,i & -0.116 - 0.238\,i & -0.669 - 1.688\,i \end{pmatrix} \,,$$

$$\boldsymbol{Y}_d = \begin{pmatrix} -0.878 - 1.677\,i & 0.190 + 0.573\,i & -0.817 + 2.663\,i \\ -1.792 + 0.861\,i & -2.880 + 0.132\,i & -0.070 - 1.151\,i \\ -1.679 + 1.588\,i & 0.972 + 0.615\,i & 1.421 + 0.981\,i \end{pmatrix} \,. \tag{C.6}$$

Note that for the custodial model $c_{d_i} \to c_{\mathcal{T}_{2i}}$ and $c_{u_i} \to c_{u_i^c}$.

Appendix D

Reference Values for the SM Parameters

The central values and errors of the $\overline{\text{MS}}$ quark masses, evaluated at the scale $M_{\text{KK}} = 1\,\text{TeV}$, that we use in our analysis are

$$
\begin{aligned}
m_u &= (1.5 \pm 1.0)\,\text{MeV}\,, & m_c &= (520 \pm 40)\,\text{MeV}\,, & m_t &= (144 \pm 5)\,\text{GeV}\,, \\
m_d &= (3.0 \pm 2.0)\,\text{MeV}\,, & m_s &= (50 \pm 15)\,\text{MeV}\,, & m_b &= (2.4 \pm 0.1)\,\text{GeV}\,.
\end{aligned}
\tag{D.1}
$$

They have been obtained by using the low-energy values as compiled in [12]. For the Wolfenstein parameters we use [404]

$$
\lambda = 0.2265 \pm 0.0008\,, \quad A = 0.807 \pm 0.018\,, \quad \bar{\rho} = 0.141\,^{+0.029}_{-0.017}\,, \quad \bar{\eta} = 0.343 \pm 0.016\,. \tag{D.2}
$$

If not stated otherwise, the remaining SM parameters entering our phenomenological analysis read [12, 36, 70]

$$
\begin{aligned}
\Delta\alpha^{(5)}_{\text{had}}(m_Z) &= 0.02758 \pm 0.00035\,, & \alpha_s(m_Z) &= 0.118 \pm 0.003\,, \\
m_W &= (80.399 \pm 0.023)\,\text{GeV}\,, & m_Z &= (91.1875 \pm 0.0021)\,\text{GeV}\,, \\
m_t &= (172.6 \pm 1.4)\,\text{GeV}\,.
\end{aligned}
\tag{D.3}
$$

We refer to the central values of these quantities as SM reference values. Unless noted otherwise, our reference value for the Higgs-boson mass is $m_h = 150\,\text{GeV}$.

Bibliography

[1] S. Casagrande, F. Goertz, U. Haisch, M. Neubert, T. Pfoh, JHEP **0810** (2008) 094. [arXiv:0807.4937 [hep-ph]].

[2] S. Casagrande, F. Goertz, U. Haisch, M. Neubert and T. Pfoh, JHEP **1009** (2010) 014. [arXiv:1005.4315 [hep-ph]].

[3] M. Bauer, F. Goertz, U. Haisch, T. Pfoh, S. Westhoff, JHEP **1011**, 039 (2010). [arXiv:1008.0742 [hep-ph]].

[4] F. Goertz and T. Pfoh, arXiv:1105.1507 [hep-ph]. Accepted for publication in Phys. Rev. D.

[5] S. L. Glashow, Nucl. Phys. **22** (1961) 579.

[6] S. Weinberg, Phys. Rev. Lett. **19** (1967) 1264.

[7] A. Salam, *In the Proceedings of 8th Nobel Symposium, Lerum, Sweden, 19-25 May 1968, pp 367-377.*

[8] D. J. Gross and F. Wilczek, Phys. Rev. Lett. **30** (1973) 1343.

[9] H. D. Politzer, Phys. Rev. Lett. **30**, 1346 (1973).

[10] D. J. Gross and F. Wilczek, Phys. Rev. D **8** (1973) 3633.

[11] G. 't Hooft, M. J. G. Veltman, Nucl. Phys. **B44** (1972) 189-213.

[12] K. Nakamura *et al.* [Particle Data Group], J. Phys. G **37**, 075021 (2010) and updated results available at: http://pdglive.lbl.gov/.

[13] R. Brandelik *et al.* [TASSO Collaboration], Phys. Lett. **B86** (1979) 243.

[14] M. Gell-Mann, Phys. Lett. **8** (1964) 214-215.

[15] G. Zweig, In *Lichtenberg, D. B. (Ed.), Rosen, S. P. (Ed.): Developments In The Quark Theory Of Hadrons, Vol. 1*, 22-101 and CERN-TH-401 + CERN-TH-412 (unpublished) (1964).

[16] M. E. Peskin, D. V. Schroeder, "An Introduction to quantum field theory," Reading, USA: Addison-Wesley (1995) 842 p.

[17] T. P. Cheng and L. F. Li, "Gauge theory of elementary particle physics," *Oxford, Uk: Clarendon (1984) 536 P. (Oxford Science Publications).*

[18] N. Arkani-Hamed, D. P. Finkbeiner, T. R. Slatyer and N. Weiner, Phys. Rev. D **79** (2009) 015014.

[19] S. Weinberg, "The Quantum theory of fields. Vol. 1: Foundations," *Cambridge, UK: Univ. Pr. (1995) 609 p.*

[20] S. Weinberg, "The quantum theory of fields. Vol. 2: Modern applications," *Cambridge, UK: Univ. Pr. (1996) 489 p.*

[21] A. Zee, "Quantum field theory in a nutshell," *Princeton, UK: Princeton Univ. Pr. (2010) 576 p.*

[22] R. D. Peccei, H. R. Quinn, Phys. Rev. Lett. **38**, 1440-1443 (1977).

[23] F. Englert and R. Brout, Phys. Rev. Lett. **13**, 321 (1964).

[24] P. W. Higgs, Phys. Rev. Lett. **13**, 508 (1964).

[25] G. S. Guralnik, C. R. Hagen and T. W. B. Kibble, Phys. Rev. Lett. **13**, 585 (1964).

[26] K. Kodama *et al.* [DONUT Collaboration], Phys. Lett. **B504** (2001) 218-224.

[27] H1prelim-10-141 , ZEUS-prel-10-017
`https://www.desy.de/h1zeus/combined_results/index.php?do=nc_cc`.

[28] G. Arnison *et al.* [UA1 Collaboration], Phys. Lett. B **122** (1983) 103.

[29] G. Arnison *et al.* [UA1 Collaboration], Phys. Lett. B **126** (1983) 398.

[30] M. Banner *et al.* [UA2 Collaboration], Phys. Lett. B **122** (1983) 476.

[31] P. Bagnaia *et al.* [UA2 Collaboration], Phys. Lett. B **129** (1983) 130.

[32] J. Alcaraz *et al.* [ALEPH Collaboration and DELPHI Collaboration and L3 Collaboration], arXiv:hep-ex/0612034, plots available at `http://lepewwg.web.cern.ch/LEPEWWG/`.

[33] J. M. Cornwall, D. N. Levin and G. Tiktopoulos, Phys. Rev. D **10**, 1145 (1974) [Erratum-ibid. D **11**, 972 (1975)].

[34] P. Sikivie, L. Susskind, M. B. Voloshin and V. I. Zakharov, Nucl. Phys. B **173** (1980) 189.

[35] C. Grojean, In *Particle Physics Beyond the Standard Model: Lecture Notes of the Les Houches Summer School 2005.*

[36] S. Schael *et al.* [ALEPH Collaboration], Phys. Rept. **427**, 257 (2006).

[37] D. Y. Bardin, P. Christova, M. Jack, L. Kalinovskaya, A. Olchevski, S. Riemann and T. Riemann, Comput. Phys. Commun. **133**, 229 (2001).

[38] A. B. Arbuzov *et al.*, Comput. Phys. Commun. **174**, 728 (2006).

[39] A. Djouadi, Phys. Rept. **457** (2008) 1.

[40] B. W. Lee, C. Quigg and H. B. Thacker, Phys. Rev. D **16** (1977) 1519.

[41] T. Hambye, K. Riesselmann, Phys. Rev. **D55** (1997) 7255-7262.

[42] A. Hasenfratz, *Quantum Fields on the Computer*, Ed. M. Creutz, (World Scientific, Singapore, 1992), p. 125.

[43] G. W. Anderson, Phys. Lett. **B243** (1990) 265-270.

[44] B. Grzadkowski and J. F. Gunion, arXiv:hep-ph/0610105.

[45] T. Plehn, arXiv:0910.4182 [hep-ph].

[46] V. Ahrens, T. Becher, M. Neubert and L. L. Yang, Eur. Phys. J. C **62**, 333 (2009).

[47] R. V. Harlander and W. B. Kilgore, Phys. Rev. Lett. **88**, 201801 (2002).

[48] C. Anastasiou and K. Melnikov, Nucl. Phys. B **646**, 220 (2002).

[49] V. Ravindran, J. Smith and W. L. van Neerven, Nucl. Phys. B **665**, 325 (2003).

[50] S. Moch and A. Vogt, Phys. Lett. B **631**, 48 (2005).

[51] E. Laenen and L. Magnea, Phys. Lett. B **632**, 270 (2006).

[52] A. Idilbi, X. d. Ji, J. P. Ma and F. Yuan, Phys. Rev. D **73**, 077501 (2006).

[53] V. Ravindran, Nucl. Phys. B **752**, 173 (2006).

[54] A. Idilbi, X. d. Ji and F. Yuan, Nucl. Phys. B **753**, 42 (2006).

[55] V. Ahrens, T. Becher, M. Neubert and L. L. Yang, Phys. Rev. D **79**, 033013 (2009).

[56] A. D. Martin, W. J. Stirling, R. S. Thorne and G. Watt, Phys. Lett. B **652**, 292 (2007).

[57] U. Aglietti *et al.*, arXiv:hep-ph/0612172 and `http://maltoni.home.cern.ch/maltoni/ TeV4LHC/SM.html`.

[58] A. Djouadi, J. Kalinowski and M. Spira, Comput. Phys. Commun. **108**, 56 (1998).

[59] R. Barate *et al.* [LEP Working Group for Higgs boson searches and ALEPH and DEL-PHI and L3 and OPAL Collaborations], Phys. Lett. **B565** (2003) 61-75.

[60] T. CDF, D. Collaborations, t. T. N. Phenomena and H. W. Group, arXiv:1107.5518 [hep-ex].

[61] The ATLAS collaboration, ATLAS-CONF-2011-135, August 22, 2011, Figure: ATLAS Experiment copyright 2011 CERN.

[62] ALEPH Collaboration, arXiv:1012.2367 [hep-ex], updated plots from `http://lepewwg.web.cern.ch/LEPEWWG/`.

[63] M. E. Peskin and T. Takeuchi, Phys. Rev. Lett. **65**, 964 (1990).

[64] M. E. Peskin and T. Takeuchi, Phys. Rev. D **46** (1992) 381.

[65] M. Golden and L. Randall, Nucl. Phys. B **361**, 3 (1991).

[66] B. Holdom and J. Terning, Phys. Lett. B **247**, 88 (1990).

[67] G. Altarelli and R. Barbieri, Phys. Lett. B **253**, 161 (1991).

[68] G. Altarelli, R. Barbieri and F. Caravaglios, Nucl. Phys. B **405**, 3 (1993).

[69] G. Altarelli, R. Barbieri and F. Caravaglios, Phys. Lett. B **314**, 357 (1993).

[70] The Tevatron Electroweak Working Group, arXiv:0803.1683 [hep-ex].

[71] D. Hanneke, S. Fogwell and G. Gabrielse, Phys. Rev. Lett. **100** (2008) 120801.

[72] R. Bouchendira, P. Cladé, S. Guellati-Khélifa, F. Nez and F. Biraben, Phys. Rev. Lett. **106** (2011) 080801.

[73] Y. Nir, arXiv:hep-ph/0109090.

[74] Y. Grossman, arXiv:1006.3534 [hep-ph].

[75] A. J. Buras, arXiv:hep-ph/0505175.

[76] A. J. Buras, arXiv:hep-ph/9806471.

[77] S. L. Glashow, J. Iliopoulos and L. Maiani, Phys. Rev. D **2** (1970) 1285.

[78] J. D. Bjorken, S. L. Glashow, Phys. Lett. **11** (1964) 255-257.

[79] G. Eilam, J. L. Hewett and A. Soni, Phys. Rev. D **44** (1991) 1473 [Erratum-ibid. D **59** (1999) 039901].

[80] J. A. Aguilar-Saavedra, Acta Phys. Polon. B **35** (2004) 2695.

[81] A. J. Buras, P. Gambino, M. Gorbahn, S. Jager and L. Silvestrini, Phys. Lett. B **500** (2001) 161.

[82] G. D'Ambrosio, G. F. Giudice, G. Isidori and A. Strumia, Nucl. Phys. B **645**, 155 (2002).

[83] M. Kobayashi and T. Maskawa, Prog. Theor. Phys. **49**, 652 (1973).

[84] C. Jarlskog, Phys. Rev. Lett. **55** (1985) 1039.

[85] A. D. Sakharov, Pisma Zh. Eksp. Teor. Fiz. **5**, 32 (1967) [JETP Lett. **5**, 24 (1967)] [Sov. Phys. Usp. **34**, 392 (1991)] [Usp. Fiz. Nauk **161**, 61 (1991)].

[86] W. Bernreuther, Lect. Notes Phys. **591** (2002) 237 [arXiv:hep-ph/0205279].

[87] M. Neubert, [hep-ph/0512222].

[88] A. J. Bevan *et al.* [UTfit Collaboration], PoS **ICHEP2010** (2010) 270.

[89] C. Becchi, A. Rouet and R. Stora, Annals Phys. **98** (1976) 287.

[90] M. Z. Iofa and I. V. Tyutin, Teor. Mat. Fiz. **27** (1976) 38.

[91] H. Nishino *et al.* [Super-Kamiokande Collaboration], Phys. Rev. Lett. **102** (2009) 141801.

[92] H. Georgi, S. L. Glashow, Phys. Rev. Lett. **32** (1974) 438-441.

[93] P. Langacker, arXiv:hep-ph/9411247.

[94] S. Weinberg, *Ultraviolet divergences in quantum theories of gravitation*, in *General Relativity: An Einstein centenary survey*, Eds. S.W. Hawking and W. Israel, Cambridge University Press (1979), p. 790.

[95] D. H. Lyth and A. Riotto, Phys. Rept. **314** (1999) 1.

[96] F. L. Bezrukov, M. Shaposhnikov, Phys. Lett. **B659** (2008) 703-706.

[97] F. Bezrukov and M. Shaposhnikov, JHEP **0907** (2009) 089.

[98] M. Nowakowski and A. Pilaftsis, Phys. Rev. D **48** (1993) 259.

[99] V. M. Abazov *et al.* [D0 Collaboration], [arXiv:1106.6308 [hep-ex]].

[100] T. Aaltonen *et al.* [CDF collaboration], CDF public note CDF/PHYS/BOTTOM/CDFR/9787, June, 2009.

[101] CDF public note CDF/ANAL/BOTTOM/PUBLIC/10206, November, 2010.

[102] `http://lhcb-public.web.cern.ch/lhcb-public/Images_2011/JpsiPhi.png`.

[103] T. Mannel, PoS **FPCP2010**, 029 (2010).

[104] A. Crivellin, Phys. Rev. **D81** (2010) 031301.

[105] G. Strycker *et al.* [CDF Collaboration], CDF/ANAL/TOP/PUBLIC/10224 Note, July 14, 2010, `http://www-cdf.fnal.gov/physics/new/top/2010/tprop/Afb/`.

[106] T. Aaltonen *et al.* [CDF Collaboration], Phys. Rev. D **83** (2011) 112003.

[107] CDF Collaboration, CDF Note 10436, March 10, 2011, `http://www-cdf.fnal.gov/physics/new/top/2011/DilAfb/`.

[108] M. Passera, W. J. Marciano and A. Sirlin, arXiv:1001.4528 [hep-ph].

[109] Z. Sullivan and A. Menon, Phys. Rev. D **83** (2011) 091504.

[110] T. Plehn and M. Takeuchi, J. Phys. G **38** (2011) 095006.

[111] G. Jungman, M. Kamionkowski, K. Griest, Phys. Rept. **267** (1996) 195-373.

[112] S. R. Coleman and J. Mandula, Phys. Rev. **159**, 1251 (1967).

[113] R. Haag, J. T. Lopuszanski, M. Sohnius, Nucl. Phys. **B88** (1975) 257.

[114] H. Georgi, Phys. Rev. Lett. **98** (2007) 221601.

[115] M. Neubert, Phys. Lett. **B660** (2008) 592-596.

[116] S. Weinberg, Phys. Rev. Lett. **43** (1979) 1566-1570.

[117] R. N. Mohapatra, A. Y. Smirnov, Ann. Rev. Nucl. Part. Sci. **56** (2006) 569-628.

[118] Y. Nir, Lectures given at *Cargese 2010: Physics at TeV colliders - From Tevatron to LHC.*

[119] A. Djouadi, Phys. Rept. **459** (2008) 1-241.

[120] S. R. Coleman, E. J. Weinberg, Phys. Rev. **D7** (1973) 1888-1910.

[121] M. Dine, "Supersymmetry and string theory: Beyond the standard model," *Cambridge, UK: Cambridge Univ. Pr. (2007) 515 p.*

[122] S. P. Martin, "A Supersymmetry primer," In *Kane, G.L. (ed.): Perspectives on supersymmetry* 1-98.*

[123] A. Signer, J. Phys. G **36**, 073002 (2009).

[124] J. Wess and J. Bagger, *Princeton, USA: Univ. Pr. (1992) 259 p.*

[125] U. Amaldi, W. de Boer and H. Furstenau, Phys. Lett. B **260** (1991) 447.

[126] W. de Boer and C. Sander, Phys. Lett. B **585** (2004) 276. Updated plot: W. de Boer, private communication.

[127] S. Weinberg, Phys. Rev. D **19** (1979) 1277.

[128] L. Susskind, Phys. Rev. **D20** (1979) 2619-2625.

[129] C. T. Hill and E. H. Simmons, Phys. Rept. **381** (2003) 235 [Erratum-ibid. **390** (2004) 553].

[130] H. Georgi, A. Pais, Phys. Rev. **D10** (1974) 539.

[131] H. Georgi, A. Pais, Phys. Rev. **D12** (1975) 508.

[132] N. Arkani-Hamed, A. G. Cohen and H. Georgi, Phys. Lett. B **513** (2001) 232.

[133] N. Arkani-Hamed, A. G. Cohen, E. Katz and A. E. Nelson, JHEP **0207**, 034 (2002).

[134] E. Katz, J. y. Lee, A. E. Nelson and D. G. E. Walker, JHEP **0510**, 088 (2005).

[135] R. Contino, Y. Nomura and A. Pomarol, Nucl. Phys. B **671** (2003) 148.

[136] K. Agashe, R. Contino, A. Pomarol, Nucl. Phys. **B719** (2005) 165-187.

[137] J. Thaler, I. Yavin, JHEP **0508** (2005) 022.

[138] G. Dvali, G. F. Giudice, C. Gomez, A. Kehagias, [arXiv:1010.1415 [hep-ph]].

[139] C. D. Froggatt and H. B. Nielsen, Nucl. Phys. B **147**, 277 (1979).

[140] T. Kaluza, Sitzungsber. Preuss. Akad. Wiss. Berlin (Math. Phys.) **1921** (1921) 966.

[141] O. Klein, Z. Phys. **37**, 895 (1926) [Surveys High Energ. Phys. **5**, 241 (1986)].

[142] H. Ooguri, Z. Yin, [hep-th/9612254].

[143] M. B. Green, J. H. Schwarz and E. Witten, *Cambridge, Uk: Univ. Pr. (1987) 469 P. (Cambridge Monographs On Mathematical Physics).*

[144] M. B. Green, J. H. Schwarz and E. Witten, *Cambridge, Uk: Univ. Pr. (1987) 596 P. (Cambridge Monographs On Mathematical Physics).*

[145] G. Veneziano, Nuovo Cim. **A57** (1968) 190-197.

[146] J.-F. Colonna, private communication, Illustration from *A Virtual Space-Time Travel Machine: A Gateway Between Art and Science with more than 3930 Still Pictures and Animations*, `http://www.lactamme.polytechnique.fr/`.

[147] N. Arkani-Hamed, S. Dimopoulos, G. R. Dvali, Phys. Lett. **B429** (1998) 263-272.

[148] D. J. Kapner, T. S. Cook, E. G. Adelberger, J. H. Gundlach, B. R. Heckel, C. D. Hoyle and H. E. Swanson, Phys. Rev. Lett. **98** (2007) 021101.

[149] I. Antoniadis, N. Arkani-Hamed, S. Dimopoulos, G. R. Dvali, Phys. Lett. **B436** (1998) 257-263.

[150] J. R. Ellis, G. Giudice, M. L. Mangano, I. Tkachev, U. Wiedemann, J. Phys. G **G35** (2008) 115004.

[151] N. Arkani-Hamed and M. Schmaltz, Phys. Rev. D **61**, 033005 (2000).

[152] K. R. Dienes, E. Dudas, T. Gherghetta, Phys. Lett. **B436** (1998) 55-65.

[153] N. Arkani-Hamed, S. Dimopoulos, G. R. Dvali, J. March-Russell, Phys. Rev. **D65** (2002) 024032.

[154] E. A. Mirabelli, M. Perelstein and M. E. Peskin, Phys. Rev. Lett. **82** (1999) 2236.

[155] S. Cullen, M. Perelstein, Phys. Rev. Lett. **83** (1999) 268-271.

[156] F. Goertz and T. Pfoh, JHEP **0810** (2008) 035.

[157] M. Bauer, S. Casagrande, L. Gründer, U. Haisch and M. Neubert, Phys. Rev. D **79** (2009) 076001.

[158] L. Randall and R. Sundrum, Phys. Rev. Lett. **83**, 3370 (1999).

[159] H. Davoudiasl, J. L. Hewett and T. G. Rizzo, Phys. Rev. Lett. **84** (2000) 2080.

[160] W. D. Goldberger, M. B. Wise, Phys. Rev. Lett. **83** (1999) 4922-4925.

[161] L. Randall and R. Sundrum, Phys. Rev. Lett. **83** (1999) 4690.

[162] L. Randall and M. D. Schwartz, JHEP **0111** (2001) 003.

[163] I. R. Klebanov and M. J. Strassler, JHEP **0008**, 052 (2000).

[164] S. B. Giddings, S. Kachru and J. Polchinski, Phys. Rev. D **66**, 106006 (2002).

[165] S. Kachru, R. Kallosh, A. Linde and S. P. Trivedi, Phys. Rev. D **68**, 046005 (2003).

[166] F. Brummer, A. Hebecker and E. Trincherini, Nucl. Phys. B **738**, 283 (2006).

[167] A. Lukas, B. A. Ovrut, K. S. Stelle and D. Waldram, Phys. Rev. D **59** (1999) 086001.

[168] H. L. Verlinde, Nucl. Phys. B **580**, 264 (2000).

[169] H. Davoudiasl, J. L. Hewett and T. G. Rizzo, Phys. Lett. B **473**, 43 (2000).

[170] A. Pomarol, Phys. Lett. B **486**, 153 (2000).

[171] S. Chang, J. Hisano, H. Nakano, N. Okada and M. Yamaguchi, Phys. Rev. D **62**, 084025 (2000).

[172] T. Gherghetta and A. Pomarol, Nucl. Phys. B **586**, 141 (2000).

[173] Y. Grossman and M. Neubert, Phys. Lett. B **474**, 361 (2000).

[174] S. J. Huber and Q. Shafi, Phys. Lett. B **498**, 256 (2001).

[175] S. J. Huber, Nucl. Phys. B **666**, 269 (2003).

[176] K. Agashe, G. Perez and A. Soni, Phys. Rev. Lett. **93**, 201804 (2004).

[177] K. Agashe, G. Perez and A. Soni, Phys. Rev. D **71**, 016002 (2005).

[178] S. J. Huber and Q. Shafi, Phys. Rev. D **63**, 045010 (2001).

[179] H. Davoudiasl, J. L. Hewett and T. G. Rizzo, Phys. Rev. D **63**, 075004 (2001).

[180] S. J. Huber, C. A. Lee and Q. Shafi, Phys. Lett. B **531**, 112 (2002).

[181] C. Csaki, C. Grojean, H. Murayama, L. Pilo and J. Terning, Phys. Rev. D **69** (2004) 055006.

[182] C. Csaki, C. Grojean, L. Pilo and J. Terning, Phys. Rev. Lett. **92** (2004) 101802.

[183] Y. Nomura, JHEP **0311** (2003) 050.

[184] R. Barbieri, A. Pomarol and R. Rattazzi, Phys. Lett. B **591** (2004) 141.

[185] C. Csaki, C. Grojean, J. Hubisz, Y. Shirman, J. Terning, Phys. Rev. **D70** (2004) 015012.

[186] N. S. Manton, Nucl. Phys. **B158** (1979) 141.

[187] C. Csaki, C. Grojean, H. Murayama, Phys. Rev. **D67** (2003) 085012.

[188] C. A. Scrucca, M. Serone, L. Silvestrini, Nucl. Phys. **B669** (2003) 128-158.

[189] C. A. Scrucca, M. Serone, L. Silvestrini, A. Wulzer, JHEP **0402** (2004) 049.

[190] J. M. Maldacena, Adv. Theor. Math. Phys. **2**, 231 (1998) [Int. J. Theor. Phys. **38**, 1113 (1999)].

[191] S. S. Gubser, I. R. Klebanov and A. M. Polyakov, Phys. Lett. B **428**, 105 (1998).

[192] E. Witten, Adv. Theor. Math. Phys. **2**, 253 (1998).

[193] N. Arkani-Hamed, M. Porrati and L. Randall, JHEP **0108**, 017 (2001).

[194] R. Rattazzi and A. Zaffaroni, JHEP **0104**, 021 (2001).

[195] R. Contino and A. Pomarol, JHEP **0411**, 058 (2004).

[196] T. Gherghetta, arXiv:1008.2570 [hep-ph].

[197] J. Erlich, PoS **CONFINEMENT8** (2008) 032.

[198] D. B. Kaplan and H. Georgi, Phys. Lett. B **136**, 183 (1984).

[199] D. B. Kaplan, H. Georgi and S. Dimopoulos, Phys. Lett. B **136**, 187 (1984).

[200] C. Bouchart, G. Moreau, Phys. Rev. **D80** (2009) 095022.

[201] C. Csaki, J. Hubisz and P. Meade, arXiv:hep-ph/0510275.

[202] C. Csaki, J. Erlich and J. Terning, Phys. Rev. D **66** (2002) 064021 .

[203] A. Azatov, M. Toharia, L. Zhu, Phys. Rev. **D80** (2009) 035016.

[204] J. A. Bagger, F. Feruglio and F. Zwirner, Phys. Rev. Lett. **88** (2002) 101601.

[205] J. Santiago, JHEP **0812** (2008) 046.

[206] A. L. Fitzpatrick, L. Randall and G. Perez, Phys. Rev. Lett. **100**, 171604 (2008).

[207] C. Cheung, A. L. Fitzpatrick and L. Randall, JHEP **0801**, 069 (2008).

[208] K. Agashe, T. Okui and R. Sundrum, Phys. Rev. Lett. **102** (2009) 101801.

[209] M. Carena, A. D. Medina, N. R. Shah, C. E. M. Wagner, Phys. Rev. **D79** (2009) 096010.

[210] S. J. Huber and Q. Shafi, Phys. Lett. B **512** (2001) 365.

[211] G. Burdman, Phys. Rev. D **66**, 076003 (2002).

[212] S. J. Huber and Q. Shafi, Phys. Lett. B **583** (2004) 293.

[213] M. Bauer, S. Casagrande, U. Haisch and M. Neubert, JHEP **1009** (2010) 017.

[214] F. del Aguila and J. Santiago, Phys. Lett. B **493**, 175 (2000).

[215] J. L. Hewett, F. J. Petriello and T. G. Rizzo, JHEP **0209**, 030 (2002).

[216] F. del Aguila, M. Perez-Victoria and J. Santiago, JHEP **0009**, 011 (2000).

[217] K. Agashe, M. Papucci, G. Perez and D. Pirjol, arXiv:hep-ph/0509117.

[218] K. Agashe, A. Delgado, M. J. May and R. Sundrum, JHEP **0308**, 050 (2003).

[219] A. Delgado and A. Falkowski, JHEP **0705**, 097 (2007).

[220] C. Csaki, A. Falkowski and A. Weiler, JHEP **0809**, 008 (2008).

[221] W. F. Chang, J. N. Ng and J. M. S. Wu, arXiv:0806.0667 [hep-ph].

[222] M. S. Carena, E. Ponton, J. Santiago and C. E. M. Wagner, Nucl. Phys. B **759** (2006) 202.

[223] M. S. Carena, E. Ponton, J. Santiago and C. E. M. Wagner, Phys. Rev. D **76** (2007) 035006.

[224] G. Burdman and L. Da Rold, JHEP **0811** (2008) 025.

[225] M. S. Carena, A. Delgado, E. Ponton, T. M. P. Tait and C. E. M. Wagner, Phys. Rev. D **68**, 035010 (2003).

[226] B. A. Dobrescu and C. T. Hill, Phys. Rev. Lett. **81**, 2634 (1998).

[227] R. S. Chivukula and N. J. Evans, Phys. Lett. B **464**, 244 (1999).

[228] M. E. Peskin and J. D. Wells, Phys. Rev. D **64**, 093003 (2001).

[229] D. Choudhury, T. M. P. Tait and C. E. M. Wagner, Phys. Rev. D **65**, 053002 (2002).

[230] R. Barbieri, L. J. Hall and V. S. Rychkov, Phys. Rev. D **74**, 015007 (2006).

[231] H. Davoudiasl, J. L. Hewett and T. G. Rizzo, Phys. Rev. D **68**, 045002 (2003).

[232] M. S. Carena, E. Ponton, T. M. P. Tait and C. E. M. Wagner, Phys. Rev. D **67**, 096006 (2003).

[233] H. Georgi, A. K. Grant and G. Hailu, Phys. Lett. B **506**, 207 (2001).

[234] H. C. Cheng, K. T. Matchev and M. Schmaltz, Phys. Rev. D **66**, 036005 (2002).

[235] J. A. Cabrer, G. von Gersdorff and M. Quiros, Phys. Lett. B **697** (2011) 208.

[236] J. A. Cabrer, G. von Gersdorff and M. Quiros, JHEP **1105** (2011) 083.

[237] J. A. Cabrer, G. von Gersdorff and M. Quiros, arXiv:1104.3149 [hep-ph].

[238] A. Carmona, E. Ponton and J. Santiago, arXiv:1107.1500 [hep-ph].

[239] K. Agashe, R. Contino, L. Da Rold and A. Pomarol, Phys. Lett. B **641**, 62 (2006).

[240] M. E. Albrecht, M. Blanke, A. J. Buras, B. Duling and K. Gemmler, JHEP **0909**, 064 (2009).

[241] M. Blanke, A. J. Buras, B. Duling, S. Gori and A. Weiler, JHEP **0903**, 001 (2009).

[242] A. J. Buras, B. Duling and S. Gori, JHEP **0909**, 076 (2009).

[243] J. Hirn and V. Sanz, Phys. Rev. D **76**, 044022 (2007).

[244] K. Agashe, G. Perez and A. Soni, Phys. Rev. D **75** (2007) 015002.

[245] K. Agashe and R. Contino, Phys. Rev. D **80**, 075016 (2009).

[246] B. Duling, arXiv:0912.4208 [hep-ph].

[247] M. Puchwein, Z. Kunszt, Annals Phys. **311** (2004) 288-313.

[248] M. S. Carena, A. Delgado, E. Ponton, T. M. P. Tait, C. E. M. Wagner, Phys. Rev. **D71** (2005) 015010.

[249] A. Falkowski, Phys. Rev. D **77**, 055018 (2008).

[250] C. Csaki, Y. Grossman, P. Tanedo, Y. Tsai, Phys. Rev. **D83** (2011) 073002.

[251] J. S. Schwinger, Phys. Rev. **73** (1948) 416.

[252] G. Burdman, Phys. Lett. B **590**, 86 (2004).

[253] S. Davidson, G. Isidori and S. Uhlig, Phys. Lett. B **663**, 73 (2008).

[254] S. Chang, C. S. Kim and J. Song, Phys. Rev. D **77**, 075001 (2008).

[255] M. Blanke, A. J. Buras, B. Duling, K. Gemmler and S. Gori, JHEP **0903**, 108 (2009).

[256] K. Agashe, A. Azatov and L. Zhu, Phys. Rev. D **79**, 056006 (2009).

[257] A. Azatov, M. Toharia and L. Zhu, Phys. Rev. D **80**, 031701 (2009).

[258] H. Davoudiasl and E. Ponton, Phys. Lett. B **680**, 247 (2009).

[259] M. Bona *et al.* [UT$_{fit}$ Collaboration], JHEP **0803**, 049 (2008).

[260] O. Gedalia, G. Isidori and G. Perez, Phys. Lett. B **682**, 200 (2009).

[261] C. Csaki, A. Falkowski and A. Weiler, Phys. Rev. D **80**, 016001 (2009).

[262] C. Csaki, G. Perez, Z. 'e. Surujon, A. Weiler, Phys. Rev. **D81** (2010) 075025.

[263] M. C. Chen, K. T. Mahanthappa and F. Yu, Phys. Rev. D **81** (2010) 036004.

[264] C. Delaunay, O. Gedalia, S. J. Lee, G. Perez, E. Ponton, Phys. Rev. **D83** (2011) 115003.

[265] G. Cacciapaglia, C. Csaki, J. Galloway, G. Marandella, J. Terning and A. Weiler, JHEP **0804**, 006 (2008).

[266] C. Csaki, D. Curtin, Phys. Rev. **D80** (2009) 015027.

[267] C. Delaunay, O. Gedalia, S. J. Lee, G. Perez and E. Ponton, arXiv:1101.2902 [hep-ph].

[268] K. Agashe, A. E. Blechman and F. Petriello, Phys. Rev. D **74** (2006) 053011.

[269] K. Agashe, Phys. Rev. D **80** (2009) 115020.

[270] M. -C. Chen, H. -B. Yu, Phys. Lett. **B672** (2009) 253-256.

[271] G. Perez, L. Randall, JHEP **0901** (2009) 077.

[272] C. Csaki, C. Delaunay, C. Grojean, Y. Grossman, JHEP **0810** (2008) 055.

[273] F. del Aguila, A. Carmona, J. Santiago, JHEP **1008** (2010) 127.

[274] L. Randall, M. D. Schwartz, Phys. Rev. Lett. **88** (2002) 081801.

[275] W. D. Goldberger and I. Z. Rothstein, Phys. Rev. D **68** (2003) 125011.

[276] K. Agashe, A. Delgado and R. Sundrum, Annals Phys. **304** (2003) 145.

[277] K. Agashe and G. Servant, Phys. Rev. Lett. **93** (2004) 231805.

[278] K. Agashe, G. Servant, JCAP **0502** (2005) 002.

[279] K. Kadota, Phys. Rev. **D77** (2008) 063509.

[280] K. Agashe, A. Falkowski, I. Low and G. Servant, JHEP **0804** (2008) 027.

[281] G. Panico, E. Ponton, J. Santiago and M. Serone, Phys. Rev. D **77** (2008) 115012.

[282] N. Haba, S. Matsumoto, N. Okada, T. Yamashita, JHEP **1003** (2010) 064.

[283] J. A. R. Cembranos, A. Dobado, A. L. Maroto, Phys. Rev. Lett. **90** (2003) 241301.

[284] G. R. Dvali, S. H. H. Tye, Phys. Lett. **B450** (1999) 72-82.

[285] S. Kachru, R. Kallosh, A. D. Linde, J. M. Maldacena, L. P. McAllister, S. P. Trivedi, JCAP **0310** (2003) 013.

[286] R. Sundrum and C. M. Wells, JHEP **1002** (2010) 097.

[287] J. H. Field, Mod. Phys. Lett. A **13**, 1937 (1998).

[288] A. Djouadi, G. Moreau and F. Richard, Nucl. Phys. B **773**, 43 (2007).

[289] C. Bouchart and G. Moreau, Nucl. Phys. B **810**, 66 (2009).

[290] The Tevatron Electroweak Working Group for the CDF and DØ Collaborations, arXiv:0903.2503 [hep-ex].

[291] E. Thomson *et al.* [CDF Collaboration], Conference Note 9913, October 19, 2009, `http://www-cdf.fnal.gov/physics/new/top/2009/xsection/ttbar_combined_46invfb/`.

[292] DØ Collaboration, Conference Note 5907-CONF, March 12, 2009, `http://www-d0.fnal.gov/Run2Physics/WWW/results/prelim/TOP/T79/`.

[293] T. Aaltonen *et al.* [CDF Collaboration], Phys. Rev. Lett. **100**, 231801 (2008).

[294] T. Aaltonen *et al.* [CDF Collaboration], Phys. Rev. D **77**, 051102 (2008).

[295] V. M. Abazov *et al.* [DØ Collaboration], Phys. Lett. B **668**, 98 (2008).

[296] A. Bridgeman, FERMILAB-THESIS-2008-50.

[297] T. Aaltonen *et al.* [CDF Collaboration], Phys. Rev. Lett. **102**, 222003 (2009).

[298] T. A. Schwarz, FERMILAB-THESIS-2006-51, UMI-32-38081.

[299] V. M. Abazov *et al.* [DØ Collaboration], Phys. Rev. Lett. **100**, 142002 (2008).

[300] T. Aaltonen *et al.* [CDF Collaboration], Phys. Rev. Lett. **101**, 202001 (2008).

[301] G. Strycker *et al.* [CDF Collaboration], CDF/ANAL/TOP/PUBLIC/9724 Note, March 17, 2009, `http://www-cdf.fnal.gov/physics/new/top/2009/tprop/Afb/`.

[302] J. H. Kühn and G. Rodrigo, Phys. Rev. Lett. **81**, 49 (1998).

[303] J. H. Kühn and G. Rodrigo, Phys. Rev. D **59**, 054017 (1999).

[304] O. Antunano, J. H. Kühn, and G. Rodrigo, Phys. Rev. D **77**, 014003 (2008).

[305] K. Melnikov and M. Schulze, Nucl. Phys. B **840**, 129 (2010).

[306] L. G. Almeida, G. Sterman and W. Vogelsang, Phys. Rev. D **78**, 014008 (2008).

[307] V. Ahrens, A. Ferroglia, M. Neubert, B. D. Pecjak and L. L. Yang, JHEP **1009**, 097 (2010).

[308] T. Schwarz *et al.*, CDF Note 10584, July 7, 2011 http://www-cdf.fnal.gov/physics/new/top/2011/AfbComb/Afb_combo_5invfb.pdf.

[309] V. M. Abazov *et al.* [D0 Collaboration], [arXiv:1107.4995 [hep-ex]].

[310] A. Djouadi, G. Moreau, F. Richard and R. K. Singh, Phys. Rev. D **82**, 071702 (2010).

[311] P. Ferrario and G. Rodrigo, Phys. Rev. D **80**, 051701 (2009).

[312] S. Jung, H. Murayama, A. Pierce and J. D. Wells, Phys. Rev. D **81**, 015004 (2010).

[313] K. Cheung, W. Y. Keung and T. C. Yuan, Phys. Lett. B **682**, 287 (2009).

[314] P. H. Frampton, J. Shu and K. Wang, Phys. Lett. B **683**, 294 (2010).

[315] J. Shu, T. M. P. Tait and K. Wang, Phys. Rev. D **81**, 034012 (2010).

[316] A. Arhrib, R. Benbrik and C. H. Chen, Phys. Rev. D **82**, 034034 (2010).

[317] I. Dorsner, S. Fajfer, J. F. Kamenik and N. Kosnik, Phys. Rev. D **81**, 055009 (2010).

[318] D. W. Jung, P. Ko, J. S. Lee and S. h. Nam, Phys. Lett. B **691**, 238 (2010).

[319] J. Cao, Z. Heng, L. Wu and J. M. Yang, Phys. Rev. D **81**, 014016 (2010).

[320] V. Barger, W. Y. Keung and C. T. Yu, Phys. Rev. D **81**, 113009 (2010).

[321] Q. H. Cao, D. McKeen, J. L. Rosner, G. Shaughnessy and C. E. M. Wagner, Phys. Rev. D **81**, 114004 (2010).

[322] B. Xiao, Y. k. Wang and S. h. Zhu, Phys. Rev. D **82**, 034026 (2010).

[323] R. S. Chivukula, E. H. Simmons and C. P. Yuan, arXiv:1007.0260 [hep-ph].

[324] B. Grinstein, A. L. Kagan, M. Trott and J. Zupan, Phys. Rev. Lett. **107** (2011) 012002.

[325] A. Djouadi, G. Moreau, F. Richard, Phys. Lett. **B701** (2011) 458-464.

[326] M. I. Gresham, I. W. Kim and K. M. Zurek, arXiv:1107.4364 [hep-ph].

[327] P. Ferrario and G. Rodrigo, Phys. Rev. D **78**, 094018 (2008).

[328] U. Haisch and S. Westhoff, arXiv:1106.0529 [hep-ph].

[329] P. Ferrario and G. Rodrigo, JHEP **1002**, 051 (2010).

[330] K. Agashe, A. Belyaev, T. Krupovnickas, G. Perez and J. Virzi, Phys. Rev. D **77**, 015003 (2008).

[331] F. A. Berends, K. J. F. Gaemers and R. Gastmans, Nucl. Phys. B **63**, 381 (1973).

[332] F. A. Berends, R. Kleiss, S. Jadach and Z. Was, Acta Phys. Polon. B **14**, 413 (1983).

[333] A. D. Martin, W. J. Stirling, R. S. Thorne and G. Watt, Eur. Phys. J. C **63**, 189 (2009).

[334] J. Campbell and R. K. Ellis, `http://mcfm.fnal.gov`.

[335] W. Bernreuther and Z. G. Si, Nucl. Phys. B **837**, 90 (2010).

[336] E. De Pree and M. Sher, Phys. Rev. D **73** (2006) 095006.

[337] T. Aaltonen *et al.* [CDF Collaboration], arXiv:0805.2109 [hep-ex].

[338] J. Carvalho *et al.* [ATLAS Collaboration], Eur. Phys. J. C **52**, 999 (2007).

[339] G. L. Bayatian *et al.* [CMS Collaboration], J. Phys. G **34**, 995 (2007).

[340] J. A. Aguilar-Saavedra and G. C. Branco, Phys. Lett. B **495**, 347 (2000).

[341] V. Weisskopf and E. P. Wigner, Z. Phys. **63** (1930) 54.

[342] V. Weisskopf and E. Wigner, Z. Phys. **65** (1930) 18.

[343] R.G. Sachs Annals Phys. **22** (1963) pp. 239-262.

[344] D. Buskulic *et al.* [ALEPH Collaboration], Phys. Lett. **B356** (1995) 409-422.

[345] A. J. Buras, W. Slominski and H. Steger, Nucl. Phys. B **245** (1984) 369.

[346] I. Dunietz, Annals Phys. **184** (1988) 350.

[347] A. Lenz and U. Nierste, JHEP **0706** (2007) 072.

[348] Z. Ligeti, M. Papucci and G. Perez, Phys. Rev. Lett. **97** (2006) 101801.

[349] A. Lenz and U. Nierste, arXiv:1102.4274 [hep-ph].

[350] D. Asner *et al.* [Heavy Flavor Averaging Group], arXiv:1010.1589 [hep-ex].

[351] Y. Grossman, Y. Nir and G. Raz, Phys. Rev. Lett. **97** (2006) 151801.

[352] A. Dighe, A. Kundu and S. Nandi, Phys. Rev. D **82** (2010) 031502.

[353] Y. Grossman, Phys. Lett. B **380** (1996) 99.

[354] I. Dunietz, R. Fleischer and U. Nierste, Phys. Rev. D **63**, 114015 (2001).

[355] A. Datta, M. Duraisamy and S. Khalil, Phys. Rev. D **83** (2011) 094501.

[356] M. Beneke, G. Buchalla and I. Dunietz, Phys. Rev. D **54**, 4419 (1996).

[357] M. Beneke, G. Buchalla, C. Greub, A. Lenz and U. Nierste, Phys. Lett. B **459** (1999) 631.

[358] A. S. Dighe, T. Hurth, C. S. Kim and T. Yoshikawa, Nucl. Phys. B **624** (2002) 377.

[359] M. Beneke, G. Buchalla, A. Lenz and U. Nierste, Phys. Lett. B **576**, 173 (2003).

[360] M. Ciuchini, E. Franco, V. Lubicz, F. Mescia and C. Tarantino, JHEP **0308** (2003) 031.

[361] A. Badin, F. Gabbiani and A. A. Petrov, Phys. Lett. B **653** (2007) 230.

[362] M. Neubert, Adv. Ser. Direct. High Energy Phys. **15** (1998) 239-293.

[363] C. W. Bauer and N. D. Dunn, Phys. Lett. B **696** (2011) 362.

[364] A. K. Alok, S. Baek and D. London, arXiv:1010.1333 [hep-ph].

[365] A. Dighe, A. Kundu and S. Nandi, Phys. Rev. D **76** (2007) 054005.

[366] C. Bobeth, U. Haisch, [arXiv:1109.1826 [hep-ph]].

[367] M. Fierz, Zeitschrift fur Physik 104 (1937) 553-565.

[368] C. C. Nishi, Am. J. Phys. **73** (2005) 1160.

[369] A. J. Buras, M. Jamin and P. H. Weisz, Nucl. Phys. B **347**, 491 (1990).

[370] J. Laiho, E. Lunghi and R. S. Van de Water, Phys. Rev. D **81** (2010) 034503.

[371] G. Buchalla, A. J. Buras and M. E. Lautenbacher, Rev. Mod. Phys. **68** (1996) 1125.

[372] D. Becirevic, V. Gimenez, G. Martinelli, M. Papinutto and J. Reyes, JHEP **0204** (2002) 025.

[373] A. Abulencia *et al.* [CDF Collaboration], Phys. Rev. Lett. **97** (2006) 242003.

[374] A. J. Buras and D. Guadagnoli, Phys. Rev. D **78** (2008) 033005.

[375] M. Blanke, A. J. Buras, D. Guadagnoli and C. Tarantino, JHEP **0610** (2006) 003.

[376] M. Bona *et al.* [UTfit Collaboration], PMC Phys. A **3** (2009) 6.

[377] `http://atlas.web.cern.ch/Atlas/GROUPS/PHYSICS/TDR/access.html`.

[378] B. Lillie, JHEP **0602** (2006) 019.

[379] A. Azatov, M. Toharia, L. Zhu, Phys. Rev. **D82** (2010) 056004.

[380] M. Frank, B. Korutlu and M. Toharia, arXiv:1107.5004 [hep-ph].

[381] G. Cacciapaglia, A. Deandrea and J. Llodra-Perez, JHEP **0906**, 054 (2009).

[382] J. R. Espinosa, C. Grojean and M. Mühlleitner, arXiv:1003.3251 [hep-ph].

[383] A. Djouadi and G. Moreau, Phys. Lett. B **660**, 67 (2008).

[384] F. Goertz, To appear in the proceedings of the 46th Rencontres de Moriond (Electroweak Session), [arXiv:1105.6070 [hep-ph]].

[385] M. Spira, arXiv:hep-ph/9510347 and references therein.

[386] I. Low, R. Rattazzi and A. Vichi, JHEP **1004**, 126 (2010).

[387] J. R. Ellis, M. K. Gaillard and D. V. Nanopoulos, Nucl. Phys. B **106**, 292 (1976).

[388] M. A. Shifman, A. I. Vainshtein, M. B. Voloshin and V. I. Zakharov, Sov. J. Nucl. Phys. **30**, 711 (1979) [Yad. Fiz. **30**, 1368 (1979)].

[389] B. A. Kniehl and M. Spira, Z. Phys. C **69**, 77 (1995).

[390] A. Pomarol, Phys. Rev. Lett. **85**, 4004 (2000).

[391] W. D. Goldberger and I. Z. Rothstein, Phys. Rev. Lett. **89**, 131601 (2002).

[392] K. Agashe, A. Delgado and R. Sundrum, Nucl. Phys. B **643**, 172 (2002).

[393] R. Contino, P. Creminelli and E. Trincherini, JHEP **0210**, 029 (2002).

[394] K. w. Choi and I. W. Kim, Phys. Rev. D **67**, 045005 (2003).

[395] W. D. Goldberger and I. Z. Rothstein, Phys. Rev. D **68**, 125012 (2003).

[396] G. Aad *et al.* [The ATLAS Collaboration], arXiv:0901.0512 [hep-ex].

[397] T. Hahn, Comput. Phys. Commun. **140**, 418 (2001).

[398] D. Binosi and L. Theussl, Comput. Phys. Commun. **161** (2004) 76.

[399] J. Polchinski, arXiv:hep-th/9210046.

[400] A. J. Buras, M. Misiak and J. Urban, Nucl. Phys. B **586** (2000) 397.

[401] J. A. Bagger, K. T. Matchev and R. J. Zhang, Phys. Lett. B **412** (1997) 77.

[402] A. J. Buras, M. Jamin, M. E. Lautenbacher and P. H. Weisz, Nucl. Phys. B **400** (1993) 37.

[403] M. Ciuchini, E. Franco, G. Martinelli and L. Reina, Nucl. Phys. B **415** (1994) 403.

[404] J. Charles *et al.* [CKMfitter Group], Eur. Phys. J. C **41**, 1 (2005) and updated results available at: `http://ckmfitter.in2p3.fr/`.